

Appendix A

Glossary and Definition of Terms

Event tree analysis is an inductive analysis process that utilizes an event tree graphical construct that shows the logical sequence of the occurrence of events in, or states of, a system following an initiating event.

A *failure mode* is a way that failure can occur, described by the means by which element or component failures must occur to cause loss of the sub-system or system function.

Fault tree analysis is a systems engineering method for representing the logical combinations of various system states and possible causes which can contribute to a specified event (called the top event).

A *fragility curve* is a function that defines the probability of failure as a function of an applied load level.

A *hazard* is condition, which may result from either an external cause (e.g. earthquake, flood, or human agency) or an internal vulnerability, with the potential to initiate a failure mode. It is a source of potential harm or a situation with a potential to cause loss.

The *performance* of a system or component can be defined as its ability to meet functional requirements. The performance of an item can be described by various elements, such as flood protection, reliability, capability, efficiency, and maintainability. The design and operation of system affects this performance.

A *system* is a deterministic entity comprising an interacting collection of discrete elements and commonly defined using deterministic models. The word *deterministic* implies that the system is identifiable and not uncertain in its architecture. The definition of the system is based on analyzing its functional and/or performance requirements. A description of a system may be a combination of functional and physical elements. Usually functional descriptions are used to identify high information levels on a system. A system can be divided into subsystems that interact. Additional details in the definition of the system lead to a description of the physical elements, components, and various aspects of

the system. Methods to address uncertainty in systems architecture are available and can be employed as provided by Ayyub and Klir (1996).

Reliability can be defined for a system or a component as its ability to fulfill its design functions under designated operating and/or environmental conditions for a specified time period. This ability is commonly measured using probabilities. Reliability is, therefore, the occurrence probability of the complementary event to failure.

Consequences for a failure event can be defined as the degree of damage or loss from some failure. Each failure of a system has some consequence(s). A failure could cause economic damage, environmental damage, injury or loss of human life, or other possible events. Consequences need to be quantified in terms of failure-consequence severities using relative or absolute measures for various consequence types to facilitate risk analysis.

Risk is the potential of losses for a system resulting from an uncertain exposure to a hazard or as a result of an uncertain event. Risk should be based on identified risk events or event scenarios. Risk can be viewed to be a multi-dimensional quantity that includes event-occurrence probability, event-occurrence consequences, consequence significance, and the population at risk; however, it is commonly measured as a pair of the probability of occurrence of an event, and the outcomes or consequences associated with the event's occurrence. Another common representation of risk is in the form of an exceedance probability function of consequences.

Probability is a measure of the likelihood, chance, odds, or degree of belief that a particular outcome will occur. A conditional probability is the probability of event occurrence based on the assumption that another event (or multiple events) has occurred.

Safety can be defined as the judgment of risk tolerance (or acceptability in the case of decision making) for the system. Safety is a relative term since the decision of risk acceptance may vary depending on the individual or the group of people making the judgment.

Risk analysis is the technical and scientific process to breakdown risk into its underlying components. Risk analysis provides the processes for identifying hazards, event-probability assessment, and consequence assessment. The risk analysis process answers three basic questions: (1) What can go wrong? (2) What is the likelihood that it will go wrong? (3) What are the consequences if it does go wrong? Also, risk analysis can include the impact of making any changes to a system to control risks.

Risk communication can be defined as an interactive process of exchange of information and opinion among stakeholders such as individuals, groups, and institutions. It often involves multiple messages about the nature of risk or expressing concerns, opinions, or reactions to risk managers or to legal and institutional arrangements for risk management. Risk communication greatly affects risk acceptance and defines the acceptance criteria for safety.

A *scenario* is a unique combination of states that lead to an outcome of interest. A scenario defines a suite of circumstances of interest in a risk assessment. Thus there may be loading scenarios, failure scenarios or downstream flooding scenarios.

Appendix B

IPET Public Website

In an effort to facilitate more efficient data searching, the taxonomy for the IPET Public Website has been reorganized according to Pre-Katrina and Post-Katrina data. While the Pre-Katrina data is still organized primarily according to New Orleans Hurricane Protection Projects and the type of data stored, the Post-Katrina data is currently organized as follows:

- (IPET) Interagency Performance Evaluation TaskForce
 - News Releases
 - Presentations
 - Reports
 - Soils
 - Structures
- Photographs
 - 17th Street 2005 Sep Oct Nov
 - 17th Street Slide Block Cores 2005 Oct Nov
 - 9th Ward
 - Bayou Bienvenue 2005.09(Sep)30 10(Oct)05 06
 - Bayou Dupree
 - Chef Menteur Hwy US 90
 - Entergy Plant – Paris Rd and GIWW 2005.09(Sep)
 - Helicopter Tour 2005.11(Nov)15
 - IHNC – Inner Harbor Navigation Canal
 - London Canal
 - MRGO
 - MRGO Air Product 2005.10(Oct)05
 - MRGO and GIWW Levee West Boh Bros Contr 2005 Sep and Oct
 - MS River Levee East Bank Vic Pointe A La Hache LA 2005Oct12
 - New Orleans Docks
 - Orleans Canal 2005.09(Sep)29 and 11(Nov)14
 - Orleans Canal Pumphouse 2005.09(Sep)30
 - Orleans Lakefront
 - Plaquemines Parish 2005 Nov

Users may view a list of the available documents, view a selected document in the website's view window or in a separate window, and download a specific file to their computer. Since most of the files posted on the site are in .pdf format,

a link to install the Adobe Acrobat Reader is provided. Also, a link to the New Orleans District Advertised Solicitations website is provided. A new feature was recently added to facilitate the collection of eyewitness account information via the public website.

As of 23 February, 2006, there were 2,344 documents/datasets posted to the IPET Public Website. Requests have been submitted for the approval to post additional documents/datasets to the Public Website. Since the Public website was opened on 2 November, 2005, the average daily number of hits to the Public Website is 91, while the average weekly number of hits is 612.

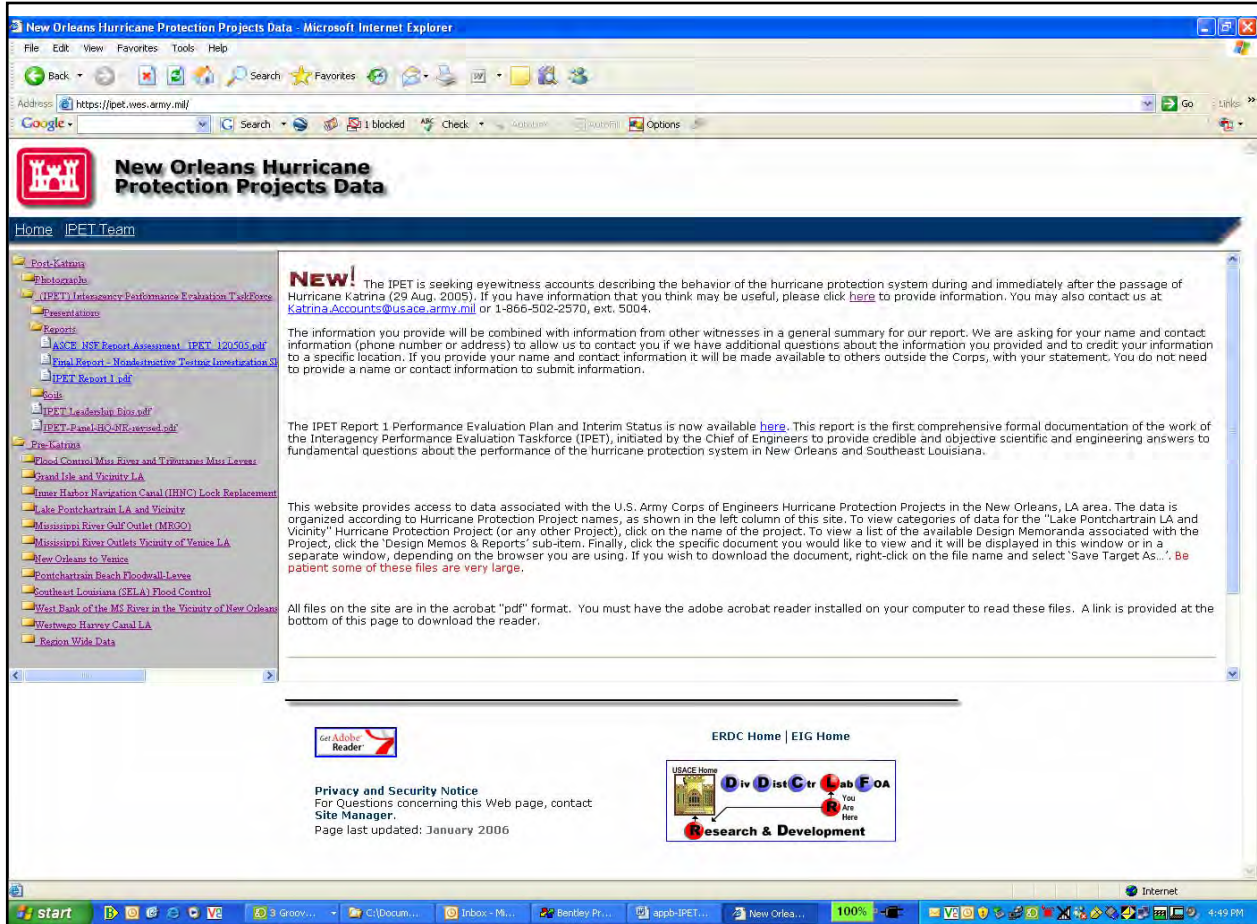


Figure B1. Screen capture of the frontpage of the New Orleans Hurricane Protection Projects Data website.

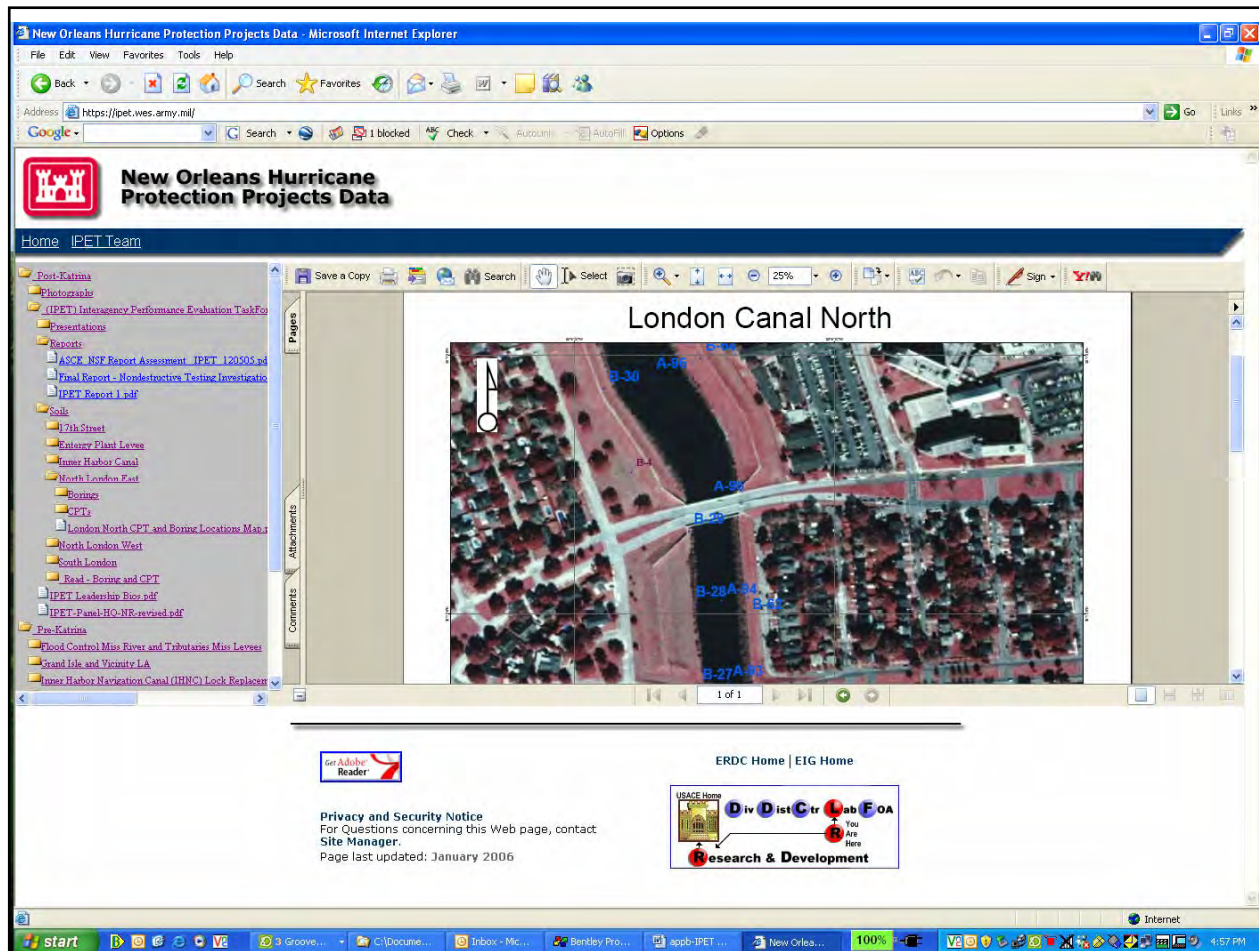


Figure B2. Screen capture of a document displayed in the view window of the New Orleans Hurricane Protection Projects Data website.

Users may view the date that a specific document was posted on the website by simply placing their mouse over the name of the document.

Metrics are collected daily on the number of hits to this website.

Appendix C

Data Repository – Organization and Content

In an effort to facilitate more efficient data searching, the taxonomy for the IPET Data Repository has been reorganized according to Pre-Katrina and Post-Katrina data. While the Pre-Katrina data is still organized primarily according to New Orleans Hurricane Protection Projects and the type of data stored (as shown in Report 1, Appendix G), the Post-Katrina data is currently organized as follows:

- (IPET) Interagency Performance Evaluation TaskForce
 - News Releases
 - Presentations
 - Reports
 - Soils
 - Structures
- Region Wide Data
 - Basemap
 - Presentations
 - Reports
- Photographs
 - 17th Street 2005 Sep Oct Nov
 - 17th Street Slide Block Cores 2005 Oct Nov
 - 9th Ward
 - Bayou Bienvenue 2005.09(Sep)30 10(Oct)05 06
 - Bayou Dupree
 - Chef Menteur Hwy US 90
 - Entergy Plant – Paris Rd and GIWW 2005.09(Sep)
 - Helicopter Tour 2005.11(Nov)15
 - IHNC – Inner Harbor Navigation Canal
 - London Canal
 - MRGO
 - MRGO Air Product 2005.10(Oct)05
 - MRGO and GIWW Levee West Boh Bros Contr 2005 Sep and Oct
 - MS River Levee East Bank Vic Pointe A La Hache LA 2005Oct12
 - New Orleans Docks

- Orleans Canal 2005.09(Sep)29 and 11(Nov)14
- Orleans Canal Pumphouse 2005.09(Sep)30
- Orleans Lakefront
- Plaquemines Parish 2005 Nov
- Project Information Reports
 - Lake Pontchartrain LA and Vicinity
 - New Orleans to Venice
- Structures
 - Floodwall Survey Profiles
 - Miscellaneous Surveys
 - Multi-Beam Channel Data
 - Single-Beam Channel Data
 - Topographic Surveys
- Videos - Aerial
 - New Orleans East
 - Plaquemines Parish Lower
 - Plaquemines Parish Upper
 - St. Bernard Parish

The architecture of the Data Repository, described in the Data Collection and Management section of IPET Report 1, is comprised of three main components: an unstructured data component, a GIS data component, and a large datasets component. An overall data manager integrates the data stored in the three components such that users may access all datasets from one central application without having to know which data is stored in which component. Following is a summary of data that is currently stored in each component of the Repository:

GIS Data Component

GIS is a computer technology that uses a geographic information system as an analytic framework for managing and integrating data, solving a problem, or understanding a past, present, or future situation. GIS provides an automated capability to link information to location data, such as people to addresses or buildings to parcels. The information can be graphically layered to provide a better understanding of how it all works together. A GIS is based on a structured database that describes features (buildings, streets, streams, monitoring wells, etc.) in geographic terms. The visualization component of GIS allows the geographic feature information to be displayed in a map view and supports queries, analysis, and editing of the data. The geoprocessing capabilities of GIS allow users to combine existing datasets, apply analytic rules, and create new derived datasets to support decision making. GIS is generally used as a decision support tool to map the location and description of features, to determine patterns of certain features, to determine what is near a specified feature, to map change in an area, or to perform ‘what-if’ analyses.

USACE enterprise standards have been defined to ensure that GIS is implemented and managed in a manner that facilitates data sharing and interoperability. An important feature of the enterprise GIS architecture is its scalability and repeatability across corporate, regional, district, and field office

levels. Scalable refers to its ability to accommodate a range in volumes of data and users, while repeatable means that this configuration can be replicated at corporate, regional, district, and field levels.

GIS is a fundamental component of this performance evaluation. GIS is being used to perform structural, hydrologic, economic, and risk analyses and visualizations. The Hurricane Protection System (levees, pumping stations, floodwalls), breach locations, roads, water bodies, parish boundaries, levee districts, digital elevations, and high water marks are just a few of the real-world objects represented as GIS features (Figure C-1).



Figure C-1. Example of GIS features displayed in ArcGIS.

To assure that we are maximizing the effectiveness and efficiency of our geospatial resources within IPET, TFG, TFH, TFX, MVD Forward and MVN, a Geographic Information System (GIS) working group was established. The working group consists of representatives from TFG, TFH, MVD Forward, MVN, and each IPET Task. This group conducts weekly conference calls to coordinate GIS efforts and to facilitate a smooth transition of IPET GIS data to MVN when the performance evaluation is concluded. The IPET GIS component was designed and implemented according to the Corps GIS Enterprise Architecture. Data are stored in an Oracle database on a USACE Central Processing Center server. Metadata is being collected and stored according to the FGDC metadata standard. Web Mapping Services are being developed to deliver some of the data layers and documents produced by the IPET. All USACE GIS users can request and receive access information to connect to this data. GIS data that is being developed by MVN, MVD Forward, TFG, and TFH will be sent to the IPET Data Manager for inclusion in this enterprise GIS database.

Once the IPET has completed their work, all raster products, vector data products and data sets will be replicated on MVN servers in Oracle databases. This will allow quick retrieval of large raster and vector products at MVN and

provide a mirrored back up system at MVD to protect against data loss from catastrophic events.

Large Datasets Component

Large Datasets, such as LIDAR, imagery, and Digital Elevation Model (DEM) data, are stored on a terabyte server, with metadata and geospatial extents of each dataset stored in an Oracle SDO database. Currently, the following datasets are available:

- LIDAR data for both pre-Katrina and post-Katrina timeframes at varying resolutions and spatial extents
- DEM datasets derived from LIDAR data
- Existing pre-Katrina DEM datasets provided by other organizations

Table C-1 lists the DEMs that have been adjusted to the new vertical datum (NAVD88 2004.65) as well as the source from which they were derived and other metadata about the source.

Table C-1					
DEM	Source	Collected by	Year Collected	Postings	Coverage
Pre-Katrina 1ft. Levee	LIDAR	John E. Chance Inc.	2000	Horizontal ~1ft.	Levees alignments surrounding East Orleans, Pontchartrain South Shore, St. Bernard Parish (MRGO, ICWW)
Post-Katrina 2ft. Levee	LIDAR	John E. Chance Inc.	2005	Horizontal ~2ft.	Levee alignments surrounding East Orleans, St. Bernard and Plaquemines
Post-Katrina 3ft. Levee	LIDAR	Joint Airborne Lidar Bathymetry Technical Center of Expertise	Jan-06	Horizontal ~3ft.	Levee alignment and back of levees for Pontchartrain South Shore, London Ave. Canal, 17th St. Canal, IHNC
Pre-Katrina 15ft. Interior	LIDAR (existing DEM from http://atlas.lsu.edu)	3001, Inc.	2003	Horizontal ~15ft.	All surface areas in Southern Louisiana

The following procedure was followed to adjust the data posted in NAVD88 elevation to the new NAVD88 (2004.65) elevation datum:

1. The location and elevation of the available NGS (National Geodetic Survey) control points for the New Orleans area were obtained from IPET Vertical Datum team. These points have both the old (date varies) and new elevation values obtained from NGS.

2. The deviations from the old elevation to the new elevations were computed for each point using the following equation: deviation = old_elevation – new_elevation. Since all new elevation data is lower than the old data, all deviation values were positive. The data was converted to feet using the

following conversion factor: 1 m = 3.28083333 ft. The values and associated computations were stored in a spreadsheet table.

3. The location and deviation values were converted into ESRI generate format. Only those control points where both old and new elevations were known were converted.

4. The deviation values at these control points were used to create a raster deviation surface with 1000' horizontal spacing using the following ArcInfo command:

```
idw0_100 = idw(adjust.gen, #, #, 2, SAMPLE, 12, #, 100,  
3227549.1114483, 181878.84143203, 3936932.6150204,  
733296.72876957)
```

5. The deviation surface was then rounded to three decimal places to reduce interpolation artifacts using the following ArcInfo command:

```
idw1_100 = (float(int( ( idw0_1000 * 1000) + .5)) / 1000)
```

6. The deviation surface was split into tiles to match the tiling of the DEMs and the spatial resolution changed to match the 1' horizontal spacing of the elevation data.

7. Each raster tile from the data set was then converted to the new datum by subtracting the deviation surface from the elevation data.

Following the datum adjustments, control data collected by the Vertical Datum team are used to validate the new DEMs. Currently, all four datasets listed in Table C-1 are undergoing validation.

These datasets are available for download as .zip files from the Basemap/Elevation folders in the Repository. USACE users may directly connect to an Internet portal that provides download capability, <https://erdcpw.erd.usace.army.mil/ldr>.

Unstructured Data Component

Unstructured data, such as .pdf files, .doc files, .jpg files, .txt files, .ppt files, etc., as well as engineering design files (.dgn) are stored in a Microsoft SQLServer database managed by Bentley ProjectWise Software. Currently, the following data are stored in this component:

- IPET News Releases
- IPET Presentations
- IPET Reports
- IPET Soil borings and cone penetrometer test data
- IPET Pump Station preliminary performance data for St. Bernard Parish
- USACE Operations Center briefing slides

- Post-Katrina reports
- Photographs of various New Orleans and Southeast La. Sites post-Katrina
- Project Information Reports for the rehabilitation efforts currently underway in New Orleans
- Post-Katrina surveys of the levees and floodwalls
- Aerial videos of the New Orleans and Southeast La. Area
- Annual inspection reports for the maintenance of completed flood control works in the New Orleans District
- NEXRAD hourly gridded multisensor precipitation data for 28,29,30 August 2005
- Pre-Katrina geodetic, geotechnical, hurricane, and miscellaneous reports
- Design Memoranda for the Hurricane Protection Projects within the IPET study area
- Periodic Inspection Reports for the Hurricane Protection Projects within the IPET study area
- Miscellaneous reports related to the Hurricane Protection Projects within the IPET study area
- Plans and Specifications for the some of the Hurricane Protection Projects within the IPET study area
- Contract documents for some of the Hurricane Protection Projects within the IPET study area
- Microstation design files (.dgn) of the Hurricane Protection Projects within the Lake Pontchartrain LA and Vicinity area.

As of 23 February 2006, there were 4,194 documents/datasets stored in the IPET Data Repository.

Appendix D

Summary of Key References

- Booij, N., Haagsma, IJ. G., Holthuijsen, L.H., Kieftenburg, A.T.M.M., Ris, R. C., van der Westhuysen, A. J., and Zijlema, M. 2004. "SWAN Cycle III Version 40.41 Users Manual," Delft University of Technology, Delft, The Netherlands, 118 p, <http://fluidmechanics.tudelft.nl/swan/index.htm>.
- Booij, N., Ris, R. C., and Holthuijsen, L.H. 1999. "A Third-Generation Wave Model for Coastal Regions, Part I: Model Description and Validation," *J. Geophys. Res.*, 104(C4), 7649-7666.
- Blain, C. A., J. J. Westerink, and R. A. Luettich, 1994. The influence of domain size on the response characteristics of a hurricane storm surge model. *J. Geophys. Res. - Oceans*, **99**, C9, 18467-18479.
- Blain, C. A., J. J. Westerink, and R. A. Luettich, 1998. Grid convergence studies for the prediction of hurricane storm surge. *Int. J. Num. Meth. Fluids*, **26**, 369-401.
- Cox, A. T., and V. J. Cardone, 2000. Operational system for the prediction of tropical cyclone generated winds and waves. *6th International Workshop on Wave Hindcasting and Forecasting*, November 6-10, 2000, Monterey, CA
- Cox, A. T., J. A. Greenwood, V. J. Cardone, and V. R. Swail, 1995. An interactive objective kinematic analysis system. Preprints, *Fourth International Workshop on Wave Hindcasting and Forecasting*, Banff, Alberta, Canada, Atmospheric Environment Service, 109-118.
- Feyen, J. C., J. J. Westerink, J. H. Atkinson, R. A. Luettich, C. Dawson, M. D. Powell, J. P. Dunion, H. J. Roberts, E. J. Kubatko, H. Pourtaheri, 2005. A Basin to Channel Scale Unstructured Grid Hurricane Storm Surge Model for Southern Louisiana , *Monthly Weather Review*, In Preparation.
- Holland, G. L., 1980. An analytical model of the wind and pressure profiles in hurricanes. *Mon. Wea. Rev.*, Vol 108, 1212-1218.

- Jelesnianski, C. P., and A. D. Taylor, 1973. A Preliminary View of Storm Surges Before and After Storm Modifications, *NOAA Technical Memorandum ERL WMPO-3*
- Kalany, E., M. Kanamitsu, R. Kistler, W. Collins, D. Deaven, L. Gandin, M. Iredell, S. Saha, G. White, J. Woollen, Y. Zhu, M. Chelliah, W. Ebisuzaki, W. Higgins, J. Janowiak, K.C. Mo, C. Ropelewski, J. Wang, A. Leetmaa, R. Reynolds, R. Jenne, and D. Joseph, 1996. The NCEP/NCAR 40-year reanalysis project. *Bull. American Met. Society*, Vol. 77, No. 3, 437-471.
- Knabb, R. D., J. R. Rhome, and D. P. Brown, 2005. Tropical Storm Report Hurricane Katrina 23-30 August 2005, National Hurricane Center, Dec 2005.
- Komen, G. J., L. Cavaleri, M. Donelan, K. Hasselmann, S. Hasselmann and P.A.E.M. Janssen, 1994. Dynamics and modelling of ocean waves. Cambridge University Press, Cambridge, UK, 560 pages.
- Powell, M. D., S. H. Houston, L. R. Amat, and N. Morisseau-Leroy, 1998. The HRD real-time hurricane wind analysis system. *J. Wind Engineer. Ind. Aerody.*, 77&78, 53-64.
- Smith, J. M., A. R. Sherlock, and D. T. Resio, 2001. "STWAVE: Steady-State spectral Wave Model User's manual for STWAVE, Version 3.0," ERDC/CHL SR-01-1, U.S. Army Corps of Engineers Engineer Research and Development Center, Vicksburg, MS.
- Thompson, E. F., and V. J. Cardone, 1996. Practical modeling of hurricane surface wind fields. *ASCE J. of Waterway, Port, Coastal and Ocean Engineering*, Vol 122, No. 4, 195-205.
- Tolman, H. L. 1998. A New Global Wave Forecast System at NCEP. In: *Ocean Wave Measurements and Analysis*, Vol. 2, (Ed: B. L. Edge and J. M. Helmsley), ASCE, 777-786.
- Tolman, H. L. 1999: User Manual and System Documentation of WAVEWATCH-III version 1.18. Technical Note, 110pp.
- Westerink, J. J., J. C. Feyen, J. H. Atkinson, R. A. Luetlich, C. N. Dawson, M. D. Powell, J. P. Dunion, H. J. Roberts, E. J. Kubatko, H. Pourtaheri, 2005. A New Generation Hurricane Storm Surge Model for Southern Louisiana, *Bulletin of the American Meteorological Society*, In Review, 2005.

Appendix E

Note on the Influence of the Mississippi River Gulf Outlet on Hurricane Induced Storm Surge in New Orleans and Vicinity

Joannes Westerink
Department of Civil Engineering and Geological Sciences
University of Notre Dame, Notre Dame IN 46556

Bruce Ebersole
Coastal and Hydraulics Laboratory
U.S. Army Engineer Research and Development Center
Vicksburg, MS 39180

Harley Winer
New Orleans District, U.S. Army Corps of Engineers
New Orleans, LA 70160

February 21, 2006

Concerns have been raised regarding the role of the Mississippi River Gulf Outlet (MRGO) on storm surge propagation into metropolitan New Orleans and vicinity. This note discusses hydrodynamic model simulations that evaluate the influence of the MRGO on flooding during major hurricane events. This note (whitepaper) is not intended as a final expression of the findings or conclusions of the United States Army Corps of Engineers, nor has it been adopted by the Corps as such. Rather, this note is a preliminary report summarizing data and interim conclusions compiled to date. As a preliminary report, this document and the information contained therein are subject to revisions and changes as additional information is obtained.

The physical system here is very complex, one comprised of a network of estuaries, lakes, rivers, channels, and low lying wetlands, with topographic major

relief defined by river banks and an extensive system of levees and raised roads. Water surface elevation response is driven by storm surge, tides, and wind-waves. Both storm surge and tides are characterized as forced very long wavelength inertial gravity waves, while wind-waves are gravity waves defined by their short period. All three types of waves propagate and experience various levels of local forcing which can further build amplitudes. In metropolitan New Orleans and vicinity, the amplitude of the tides is small; the maximum tide range is on the order of one half foot in Lake Pontchartrain and two feet in Chandeleur Sound. The amplitude of a storm surge can be much higher; for Hurricane Katrina, the peak storm surge along the MRGO adjacent to the St. Bernard Parish/Chalmette hurricane protection levee was computed to be as much as 18 ft. This note focuses on the relevant long period motion that dominates the circulation patterns in the area. In particular, the impact of the MRGO on large scale catastrophic storm surge development and propagation is examined.

The MRGO is a dredged channel that extends southeast to northwest from the Gulf of Mexico to a point where it first merges with the Gulf Intracoastal Waterway (GIWW), and then continues westward until it intersects the Inner Harbor Navigation Canal (IHNC) as shown in Figure 1. The first 9 miles, the bar channel, are in the open Gulf. The next 23 miles of the channel lie in the shallow open waters of Breton Sound. From there, the inland cut extends 14 miles to the northwest with open marsh on the northeast and a 4,000-ft wide dredged material placement bank on the southwest side. At this point the channel cuts across the ridge of a relict distributary of the Mississippi River, Bayou La Loutre. For nearly the next 24 miles, there is a hurricane protection levee atop a dredged material placement bank on the southwest side of the channel and Lake Borgne and open marsh lie to the northeast. A portion of the levee protecting St. Bernard Parish/Chalmette and the portion of the hurricane protection levee along the south side of Orleans East Parish, north of the GIWW, form the “funnel” that is often referenced. The point where the MRGO and GIWW channels merge is just to the east of the Paris Road Bridge (see Figure 1). From this point, the merged GIWW/MRGO channel continues west for about 6 miles to the point where it intersects the IHNC; this portion has hurricane protection levees on both banks. The IHNC extends from Lake Pontchartrain, to the north, to the Mississippi River to the south. The IHNC has levees or floodwalls along both banks. The IHNC Lock, which connects the IHNC to the Mississippi River, is located at the southern limit of the IHNC. The MRGO bar channel authorized depth is 38 ft; the authorized bottom width is 600 ft. The remainder of the channel has an authorized depth of 36 ft and an authorized bottom width of 400 or 450 ft, depending on location.

It is important to distinguish between two sections of the MRGO and the role each plays in tide and storm surge propagation. One is the east-west oriented section that runs between the IHNC and the confluence of the GIWW/MRGO near the Paris Road Bridge, labeled as the GIWW/MRGO in Figure 1, and hereafter referred to as Reach 1. The other is the much longer southeast-northwest section designated as the MRGO in Figure 1, and hereafter referred to as the Reach 2.

The critical section of the MRGO is Reach 1, the combined GIWW/MRGO. It is through this section of channel that Lake Pontchartrain and Lake Borgne are

hydraulically connected to one another via the IHNC. Reach 1 existed as the GIWW prior to the construction of the MRGO, although the maintained depth was lower. Because of this connectivity, the local storm surge and astronomical tide in the IHNC and in the section designated GIWW/MRGO is influenced by the tide and storm surge in both Lake Pontchartrain and Lake Borgne. The two Lakes are also connected to each other via the Rigolets and Chef Menteur Pass; the IHNC is the smallest of the three connections. The Reach 1 GIWW/MRGO section of channel is very important in determining the magnitude of storm surge that reaches the IHNC from Lake Borgne and Breton Sound. If the hydraulic connectivity between Lake Pontchartrain and Lake Borgne is eliminated at a point within this section of channel, tide or surge to the west of this point will become primarily influenced by conditions at the IHNC entrance to Lake Pontchartrain; and tide or storm surge to the east of this point will become primarily influenced by conditions in Lake Borgne.

Much concern seems to be focused on MRGO/Reach 2 that runs from the GIWW/MRGO confluence, just east of the Paris Road Bridge, to the southeast. Past work, McAnally and Berger (1997), Carillo et al. (2001), and Tate et al. (2002) for example, has shown that this section of the MRGO channel, along with the critical section, the GIWW/MRGO/Reach 1, plays an important role in the propagation of the astronomical tide wave and in the flux of more saline water from Lake Borgne/Breton Sound into Lake Pontchartrain via the IHNC. The significant role of the MRGO in the propagation of the low-amplitude tide has been established.

Three previous studies have been performed to examine the influence of MRGO/Reach 2 on flooding in New Orleans and vicinity. The first of these studies, Bretschneider and Collins (1966), was performed for the U.S. Army Corps of Engineers, New Orleans District (USACE-MVN). The primary objective of the study was to determine the effects of the MRGO channel, and dredged material placement banks, and associated works, on the hurricane surge environment of an area to the east of the Mississippi River from the southern end of the MRGO to the IHNC. The study looked at Hurricane Betsy and six synthetic storms. Based on simplified one-dimensional numerical computations and estimates of channel conveyance effects, the report concluded that Betsy would have produced essentially the same surge elevations with or without the MRGO.

The second study was also commissioned by the USACE-MVN and involved “closing” the MRGO/Reach 2 with a barrier placed across the MRGO extending out from state road 624 and the La Loutre Ridge (U.S. Army Corps of Engineers, New Orleans District, 2003). That closure was located just to the southeast of Shell Beach in Figure 1. The study examined 9 synthetic storms with a track to the west of the Mississippi River running parallel to the MRGO with input strengths varying from 65 to 124 knots and forward speeds ranging from 5 to 20 knots. In addition, Hurricane Betsy input winds were examined. Each of the 10 storms was simulated with and without the MRGO closure along the La Loutre Ridge. The study applied the S08 high resolution unstructured finite element grid with detailed refinement of the MRGO, GIWW, IHNC, the Rigolets Inlet and Chef Menteur Pass (Feyen et al. 2005, Westerink et al. 2006). Resolution and domain definition requirements have been verified for the S08 grid and the

resulting model has been validated (Blain et al. 1994, Blain et al. 1998, Westerink et al. 2000, Feyen et al. 2002, Feyen et al. 2005, Westerink et al. 2006). The S08 grid applies a larger approximation for the width of the MRGO/Reach 2 channel, thus leading to conservative estimates of the influence of the channel. A two dimensional depth integrated version of the ADCIRC model (Luettich et al. 1992, Luettich and Westerink 2004, Luettich and Westerink, 2005, Westerink et al. 2006), a finite element based shallow water equation code that is accurate, stable and robust, was used to perform the computations.

Results from this study showed that for low-amplitude storm surges (peak surge having a magnitude of 4 feet or less), the presence of MRGO/Reach 2 increased the storm surge by up to the following amounts: 0.5 ft at Shell Beach and Bayou Dupre, and 0.3 ft at Paris Road Bridge and the IHNC Lock. For nearly all situations that were examined (results for all ten storms at the four locations shown in Figure 1), the presence of the MRGO/Reach 2 either did not cause a significant change or the increase was less than 0.3 ft. In a few situations, notably a slow moving weak storm, the presence of the MRGO/Reach 2 channel actually led to a very small decrease in peak surge level at the four locations. For higher amplitude storm surges, peak surges on the order of 7 to 12 feet (which included Hurricane Betsy), changes induced by MRGO/Reach 2 were 0.3 ft or less for all situations. The MRGO did however considerably enhance drainage from Lake Pontchartrain through the IHNC/GIWW out to Breton Sound following passage of the storms.

A follow up study was commissioned by the State of Louisiana, Department of Natural Resources and implemented by URS Corporation (2006). This study applied the same unstructured S08 grid but filled in the MRGO/Reach 2 channel to surrounding topographic/bathymetric levels. This study also applied the ADCIRC code and the results were similar to the USACE-MVN study. Reach 2 of the MRGO had a very limited impact on increasing storm surge for large storms, including Hurricanes Betsy and Katrina. All changes were less than 0.6 ft and most changes were less than 0.3 ft, in the vicinity of New Orleans. Results also indicated that the MRGO enhanced post storm drainage from portions of the system.

In general, the studies cited above reached consistent conclusions. The change in storm surge induced by MRGO/Reach 2 (computed as a percentage of the peak surge magnitude) is greatest when the amplitude of the storm surge is low, on the order of a few feet or less. In these situations, changes induced by the MRGO are rather small, 0.5 ft or less, but this amount is as much as 25% of the peak surge amplitude. When the long wave amplitude is very low, the surge is more limited to propagation via the channels. Once the surge amplitude increases to the point where the wetlands become inundated, this section of the MRGO plays a diminishing role in influencing the amplitude of storm surge that reaches the vicinity of metropolitan New Orleans. For storm surges of the magnitude produced by Hurricanes Betsy and Katrina, which overwhelmed the wetland system, the influence of MRGO/Reach 2 on storm surge propagation is rather small. When the expansive wetland is inundated, the storm surge propagates primarily through the water column over this much larger flooded area, and the channels become a much smaller contributor to water conveyance.

The results of these studies can be readily understood by considering in more detail the evolution of storm surge for critical hurricane tracks passing to the west of the Mississippi River. These storms blow wind across the region first from the northeast, then from the east, then from the southeast and south and finally from the west. The sustained northeasterly and especially easterly winds push water onto the wide and shallow Mississippi-Alabama Shelf into Breton and Chandeleur Sounds, and Lake Borgne. These winds build surge up regionally on the shelf and in particular against the Mississippi River and hurricane protection levees in Plaquemines Parish, against the St. Bernard Parish/Chalmette hurricane protection levee system and into the so called funnel defined by the levees protecting St. Bernard Parish/Chalmette and New Orleans East along the confluence of the GIWW/MRGO. As winds become southerly, the significant surge that has built up along the Mississippi River levees in southern Plaquemines Parish starts to propagate north as a constrained wave up the Mississippi River and as an unconstrained wave through Breton Sound, both influenced by the strength and direction of the winds. Finally, westerly winds blow surge away from these levees.

We note that the surge driven by the sustained northeasterly and easterly winds is not influenced by the MRGO, since the direction of water movement is from east to west across Breton and Chandeleur Sounds and Lake Borgne. The brief southeasterly and southerly winds do guide the substantial surge wave that has built up in Plaquemines Parish north across Breton Sound. In the case of Hurricane Betsy, the surge propagated in a northerly direction along the Mississippi River levees and was stopped by river levees at English Turn. In the case of Hurricane Katrina, the surge propagated in a northeasterly direction perpendicular to the MRGO towards Gulfport, Mississippi. In either case, the northerly movement of water is not significantly influenced by the MRGO since the size of the surge is substantially larger than the increased cross sectional area for flow, or conveyance, offered by the MRGO. Furthermore the alignment of the MRGO does not coincide with the direction of propagation of the massive surge as it heads north and only briefly coincides with southeasterly winds which locally force flow.

We have simulated Hurricane Katrina both with the MRGO/Reach 2 in place as well as with the MRGO/Reach 2 filled to surrounding bathymetric and topographic levels. The hydrodynamic computations were performed with the TF01 ADCIRC model of Southern Louisiana which is a refinement of the earlier S08 model with added details and resolution for the coastal floodplains of the north shore of Lake Pontchartrain, Mississippi and Alabama (Interagency Performance Evaluation Task Force, 2006). We applied identical wind and pressure fields derived from a Planetary Boundary Layer (PBL) model to simulate the atmospheric forcing functions during the Katrina event (Thompson and Cardone, 1996). A sequence of hourly snapshots of water surface elevations with super-imposed winds (Figure 2) shows the evolution of storm surge with the MRGO in place. More detailed elevation values are given in corresponding labeled water elevation contour plots in Figure 3. Surge buildup starts with easterly winds blowing water from east to west against the Mississippi River levees in Plaquemines Parish as well against the hurricane protection levees of St. Bernard Parish/Chalmette in addition to driving water into the funnel defined by the levees protecting St. Bernard Parish/Chalmette and New Orleans East. When

winds become southerly, the massive surge that has built up in Breton Sound propagates north. We note that the northeasterly propagating storm surge has a crown of more than 16 ft above NGVD 29 extending out more than 12 miles and water levels in the entire Mississippi-Alabama Shelf exceed 10 ft above NGVD 29.

The simulation without the MRGO/Reach 2 results in very similar water levels in most of the domain for the Katrina event. Differences in the maximum Katrina event water levels with and without the MRGO in place are shown in Figures 4a and 4b. Notable differences with the MRGO Reach 2 channel in place are as follows: there is a reduction of water level of up to 0.2 ft at the entrance to the MRGO's inland cut; there is an increase of 0.3 to 0.4 ft in the marshes west of the MRGO in the region delineated by Pointe a la Hache, Carlisle, Stella, Caernarvon and Verret; a maximum increase of approximately 1.1 ft locally east of English Turn; in Lake Borgne along the MRGO there is a 0.1 to 0.2 ft increase; there is a 0.1 to 0.2 ft decrease along the St. Bernard Parish/Chalmette protection levee; and finally there is a 0.1 to 0.2 ft increase in a portion of the GIWW/MRGO/Reach 1. In all other regions, including in the IHNC, differences are less than 0.1 ft. In addition, the New Orleans and vicinity protection system is not impacted more than 0.2 ft. These results coincide with those from the earlier studies. We note that the small increases in surge due to the presence of MRGO/Reach 2 can be traced to the alignment of the local southeasterly winds that briefly occur later in the storm and that do in fact drive more water up the MRGO/Reach 2. These waters then feed into the northward-propagating surge wave and spread laterally relative to the propagation direction. However due to fact that the alignment between the wind and the MRGO/Reach 2 is brief and in light of the shelf-wide high water levels at this stage of the storm, the impact on channel conveyance is small. The largest difference and its associated pattern seen at English Turn is related to this mechanism as well as small differences in the northward propagating waves' phasing properties coupled with the winds turning at this point as the eye of the storm moves across this area. The small decreases in maximum water elevations occur due to a small reduction in the local resistance to water being pushed by local winds in a northwesterly direction at the entrance to the MRGO/Reach 2 inland cut and due to increased water depths reducing local set-up against the St. Bernard Parish/ Chalmette protection levee (local wind driven set-up is inversely proportional to the depth of the water).

The reasons for the very limited influence of the MRGO/Reach 2 in the vicinity of New Orleans for strong storm events are clear. First, the MRGO does not influence the important preliminary east-west movement of water that drives the significant build up of surge in the early parts of the storm. Second, the northerly propagation of surge during the later stages of the storm are only minimally influenced by the MRGO because the increased hydraulic conveyance associated with the channel is very limited for large storms due to the large surge magnitude and especially due to the very large lateral extent of the high waters on the Mississippi-Alabama shelf that build up early on from the east. In addition, the propagation direction of this surge wave does not typically align with the MRGO and furthermore the southeasterly winds which align with the MRGO occur only very briefly.

The fact that all studies show a larger proportional influence of the presence of the MRGO/Reach 2 for low intensity (low peak surge magnitude) events is related to the fact that the proportional increase in conveyance due to Reach 2 is greater when the surge is small and the water levels in Breton Sound and Lake Borgne are generally low. This also explains why we see a more rapid drop in post-storm Lake Pontchartrain levels for large-scale events with the MRGO in place. Waters typically withdraw relatively rapidly from Breton Sound and Lake Borgne due to the direct connection to open waters. The total combined conveyance of the Rigolets, Chef Menteur Pass and the IHNC/GIWW/MRGO system is increased with the MRGO in place under the lower post-storm levels on the Mississippi-Alabama shelf.

While the simulations clearly show that Reach 2 of the MRGO does not significantly influence the development of storm surge in the region for large storm events, Reach 1 (the combined GIWW/MRGO section) and the IHNC, together, provide a hydraulic connection between Lake Borgne and Lake Pontchartrain. As a result of this connection, the storm surge experienced within the IHNC and Reach 1 (GIWW/MRGO) is a function of storm surge in both Lakes; a water level gradient is established within the IHNC and Reach 1 that is dictated by the surge levels in the two lakes. This is true for both low and high storm surge conditions. To prevent storm surge in Lake Borgne from reaching the IHNC or GIWW/MRGO sections of waterway, flow through the Reach 1 channel must be dramatically reduced or eliminated, either by a permanent closure or some type of structure that temporarily serves to eliminate this hydraulic connectivity. The presence of an open channel is the key factor.

The hurricane protection levees along the south side of Orleans Parish and the eastern side of St. Bernard Parish along the MRGO, which together are referred to as a funnel, can locally collect and focus storm surge in this vicinity depending on wind speed and direction. This localized focusing effect can lead to a small local increase in surge amplitude. Strong winds from the east tend to maximize the local funneling effect.

References

- Blain, C.A., J.J. Westerink and R.A. Luettich, 1994: The Influence of Domain Size on the Response Characteristics of a Hurricane Storm Surge Model. *Journal of Geophysical Research - Oceans*, **99**, C9, 18467-18479.
- Blain, C.A., J.J. Westerink and R.A. Luettich, 1998: Grid Convergence Studies for the Prediction of Hurricane Storm Surge. *International Journal for Numerical Methods in Fluids*, **26**, 369-401.
- Bretschneider, C. L., and J.I. Collins, 1966: Storm Surge Effects of the Mississippi River-Gulf Outlet, Study A. NESCO Report SN-326-A, National Engineering Science Company, Pasadena, CA.
- Carillo, A. R., R.C. Berger, M.S. Sarruff, and B.J. Thibodeaux, 2001: Salinity Changes in Pontchartrain Basin Estuary, Louisiana, Resulting from Mississippi River-Gulf Outlet Partial Closure Plans. ERDC/CHL TR-01-04,

U.S. Army Corps of Engineers, Engineer Research and Development Center,
Vicksburg, MS.

- Feyen, J.C., J.H. Atkinson and J.J. Westerink, 2002: GWCE-Based Shallow Water Equation Simulations of the Lake Pontchartrain - Lake Borgne Tidal System. *Computational Methods in Water Resources XIV*, S.M. Hassanizadeh et al. Eds., Volume 2, *Developments in Water Science*, 47, Elsevier, Amsterdam, 1581-1588.
- Feyen, J.C., J.J. Westerink, R.A. Luettich, J.H. Atkinson, C.N. Dawson, M.D. Powell, J.P. Dunion, H.J. Roberts, E. J. Kubatko, H. Pourtaheri, 2005: A New Generation Hurricane Storm Surge Model for Southern Louisiana. *Bulletin of the American Meteorological Society*, In Review.
- Interagency Performance Evaluation Task Force, 2006: Performance Evaluation Plan and Interim Status, Report 1 of a Series; Performance Evaluation of the New Orleans and Southeast Louisiana Hurricane Protection System. Report MMTF 00038-06, U.S. Army Corps of Engineers, Washington D.C.
- Luettich, R.A., J.J. Westerink, and N.W. Scheffner, 1992: ADCIRC: An Advanced Three-Dimensional Circulation Model for Shelves, Coasts and Estuaries, Report 1: Theory and Methodology of ADCIRC-2DDI and ADCIRC-3DL. *Technical Report DRP-92-6*, Department of the Army, U.S. Army Corps of Engineers, Washington D.C.
- Luettich, R.A. and J.J. Westerink, 2004: Formulation and Numerical Implementation of the 2D/3D ADCIRC Finite Element Model Version 44.XX.
http://www.marine.unc.edu/C_CATS/adcirc/adcirc_theory_2004_12_08.pdf
- Luettich, R.A. and J.J. Westerink, 2005: ADCIRC: A Parallel Advanced Circulation Model for Oceanic, Coastal and Estuarine Waters; Users Manual for Version 45.08.
http://www.marine.unc.edu/C_CATS/adcirc/document/ADCIRC_title_page.html
- McAnally, W. H., and R.C. Berger, 1997: Salinity Changes in Pontchartrain Basin Estuary Resulting from Bonnet Carre Freshwater Diversion. Technical Report CHL-97-2, U.S. Army Engineer Waterways Experiment Station, Vicksburg, MS.
- Tate, J. N., A.R. Carillo, R.C. Berger, and B.J. Thibodeaux, 2002: Salinity Changes in Pontchartrain Estuary, Louisiana, Resulting from Mississippi River-Gulf Outlet Partial Closure Plans and Width Reduction. ERDC/CHL TR-02-12, U.S. Army Corps of Engineers, Engineer Research and Development Center, Vicksburg, MS.
- Thompson, E.F., and V.J. Cardone, 1996: Practical Modeling of Hurricane Surface Wind Fields. *Journal of Waterway, Port, and Coastal Engineering.*, **122**, 4, 195-205.

U.S. Army Corps of Engineers, New Orleans District, 2003: Numerical Modeling of Storm Surge Effect of MRGO Closure. New Orleans, LA.

URS Corporation, 2006: The Direct Impact of the Mississippi River Gulf Outlet on Hurricane Storm Surge. Performed under contract 2503-05-39, Prepared for State of Louisiana Department of Natural Resources, Baton Rouge, LA.

Westerink, J.J., R.A. Luetlich, H. Pourtaheri, 2000: Preliminary Sensitivity Studies of Tidal Response in the Lake Ponchartrain-Lake Borgne System. Contractors report prepared for the U.S. Army Corps of Engineers, New Orleans District, New Orleans, LA.

Westerink, J.J., R.A. Luetlich, J.C. Feyen, J.H. Atkinson, C. Dawson, M.D. Powell, J.P. Dunion, H.J. Roberts, E. J. Kubatko, H. Pourtaheri, 2006: A Basin to Channel Scale Unstructured Grid Hurricane Storm Surge Model for Southern Louisiana. *Monthly Weather Review*, To be submitted.

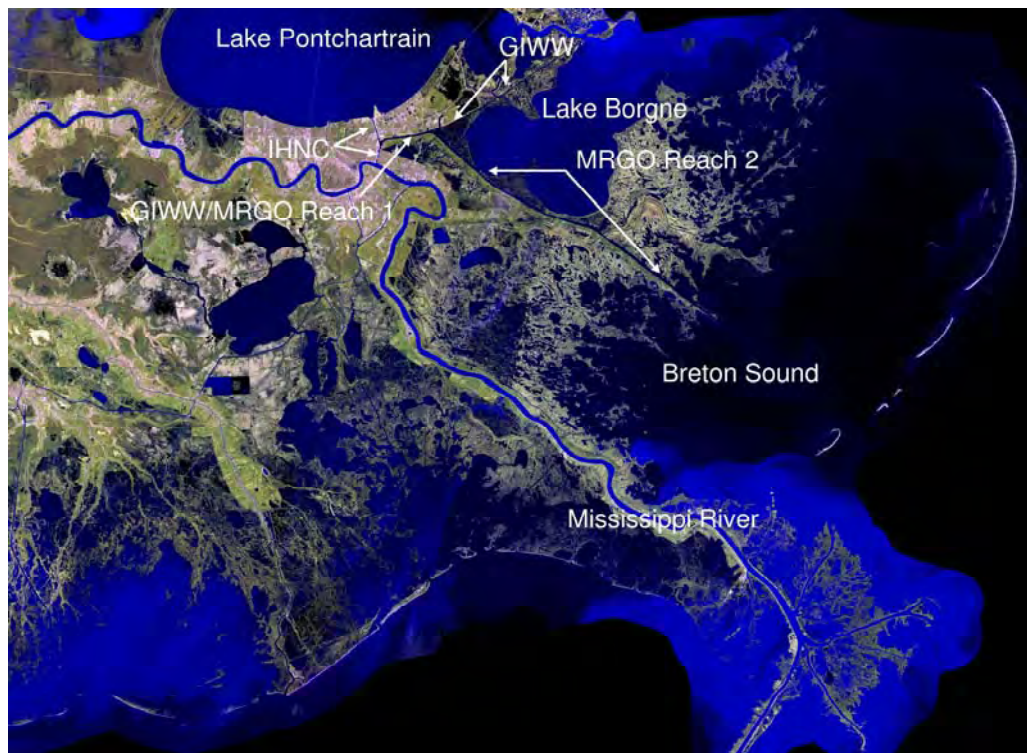


Figure 1a. Satellite image of Southeastern Louisiana.

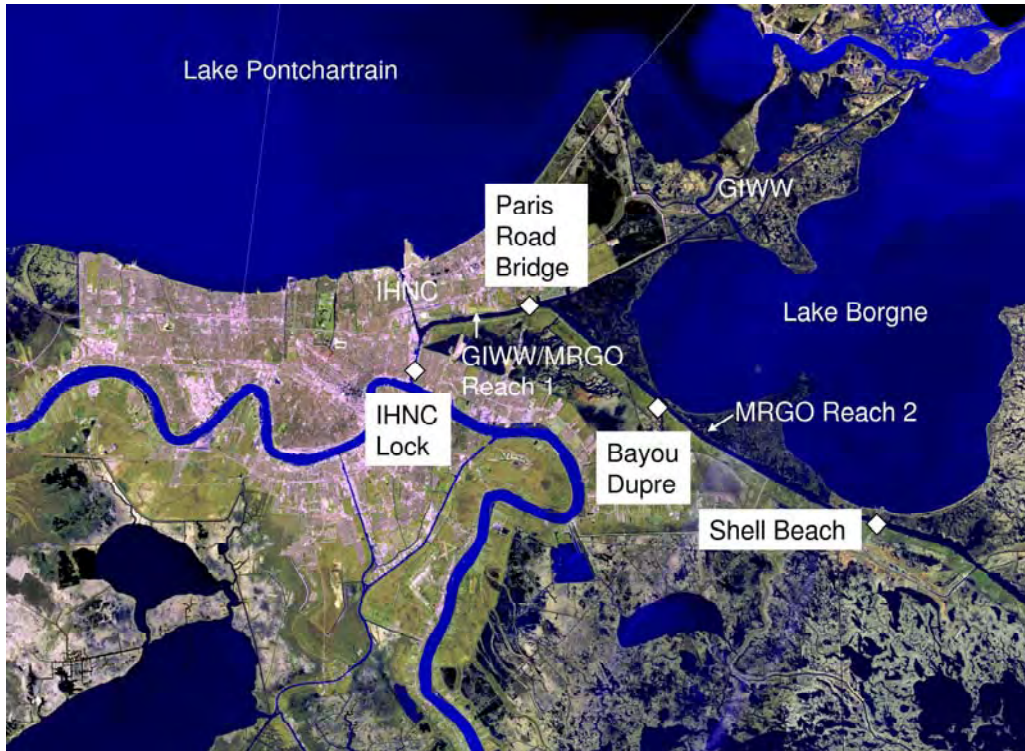


Figure 1b. Satellite image of metropolitan New Orleans and vicinity.

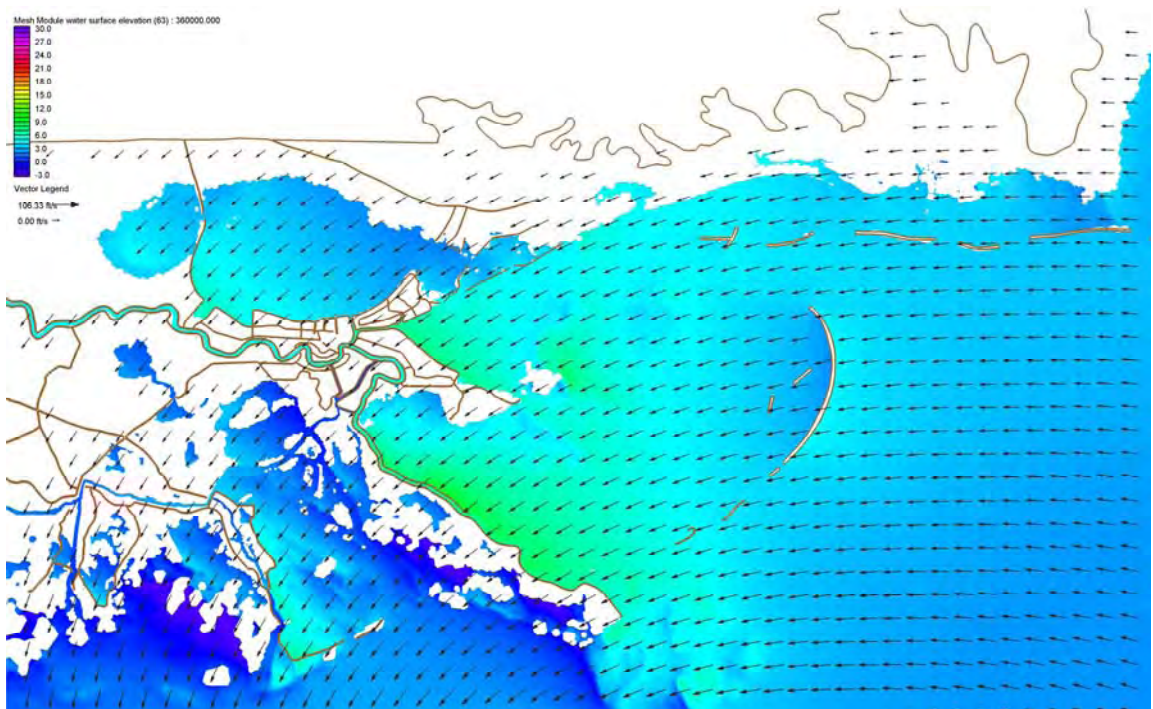


Figure 2a. Water surface elevation with respect to the NGVD29 (ft) with boundary layer adjusted wind velocity vectors (knots) during Hurricane Katrina on August 29, 2005 at 0700UTC.

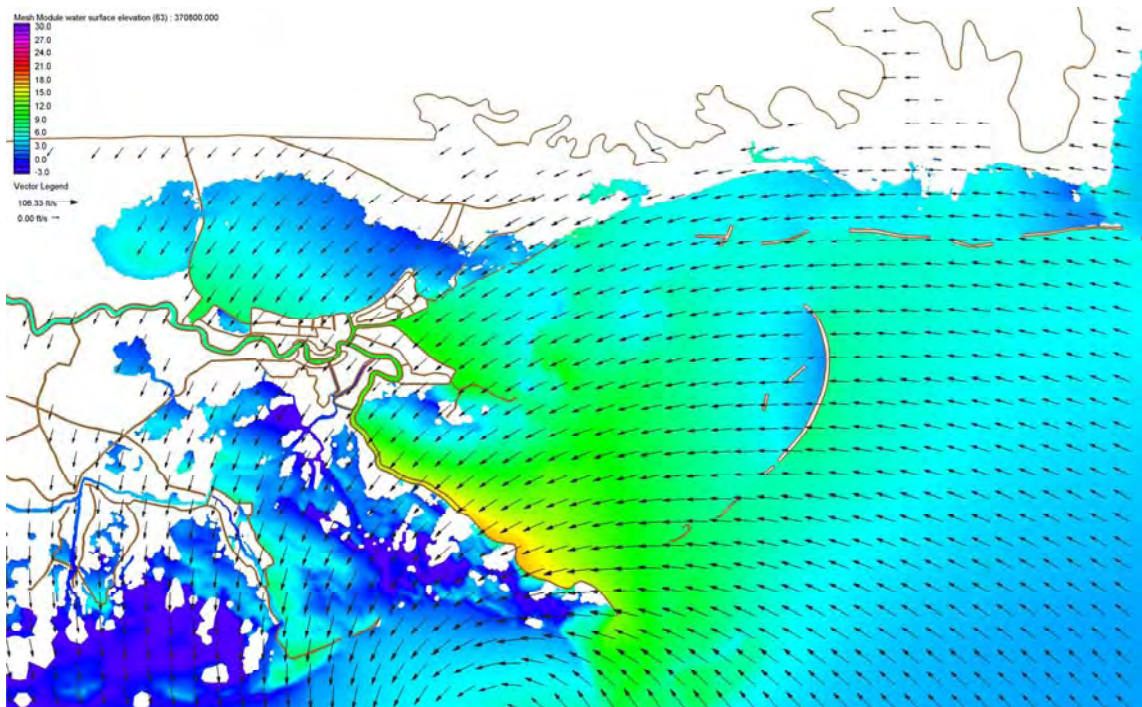


Figure 2b. Water surface elevation with respect to the NGVD 29 (ft) with boundary layer adjusted wind velocity vectors (knots) during Hurricane Katrina on August 29, 2005 at 1000UTC.

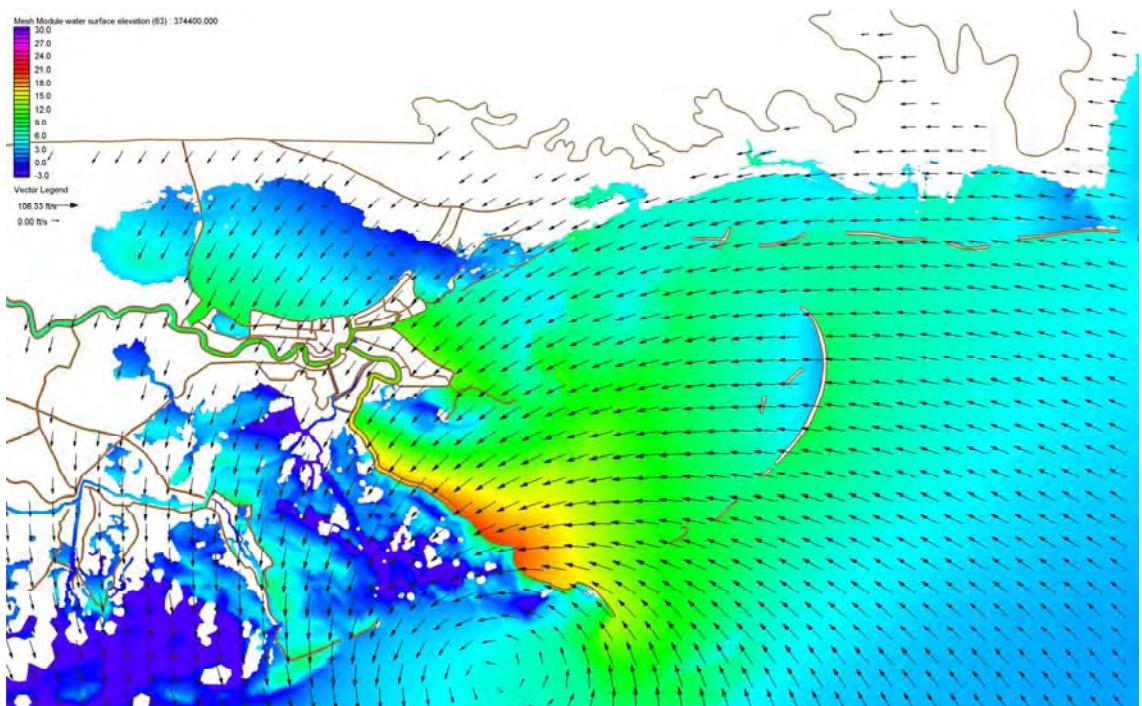


Figure 2c. Water surface elevation with respect to the NGVD 29 (ft) with boundary layer adjusted wind velocity vectors (knots) during Hurricane Katrina on August 29, 2005 at 1100UTC.

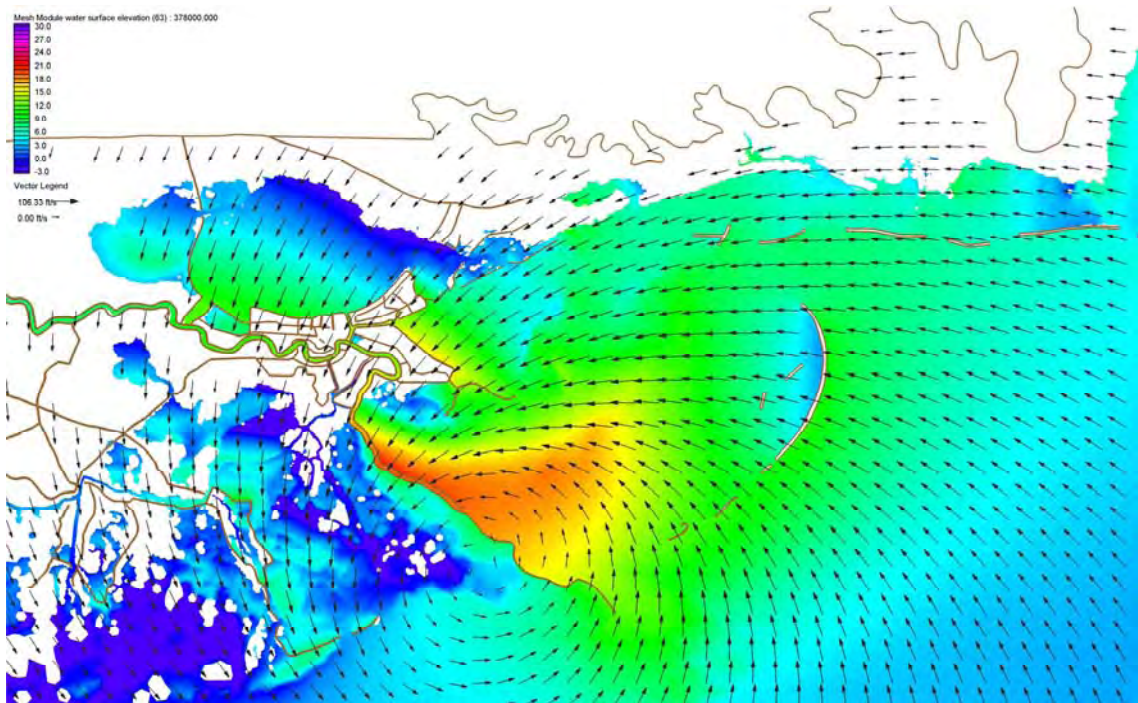


Figure 2d. Water surface elevation with respect to the NGVD 29 (ft) with boundary layer adjusted wind velocity vectors (knots) during Hurricane Katrina on August 29, 2005 at 1200UTC.

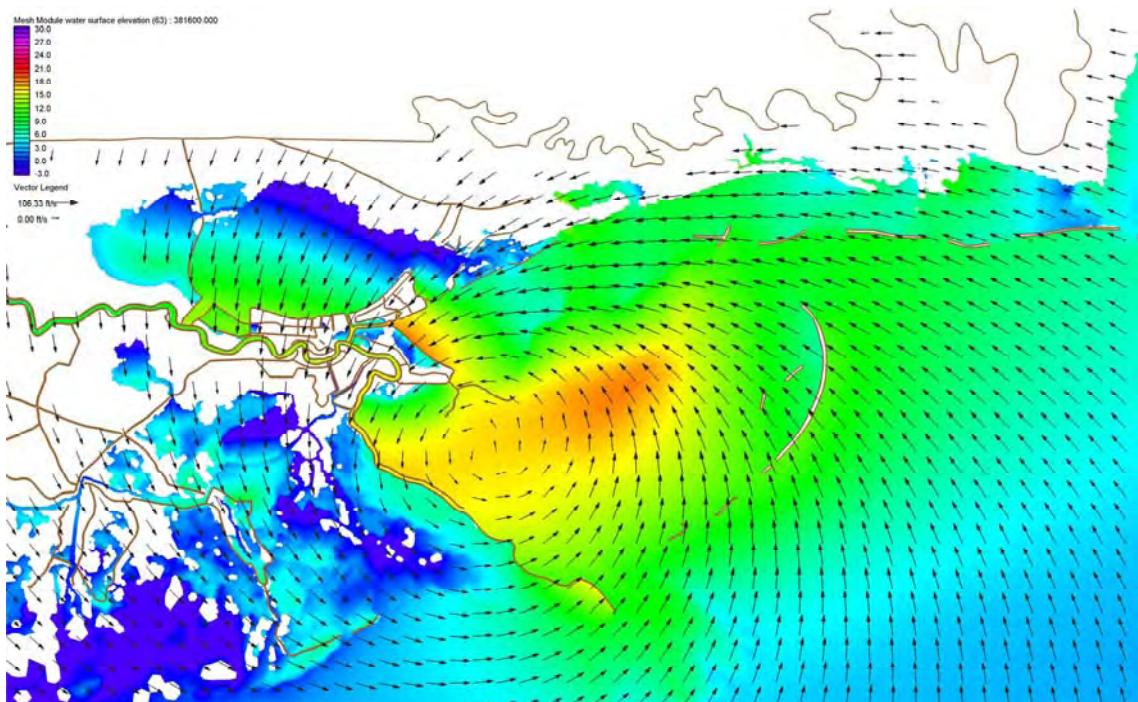


Figure 2e. Water surface elevation with respect to the NGVD 29 (ft) with boundary layer adjusted wind velocity vectors (knots) during Hurricane Katrina on August 29, 2005 at 1300UTC.

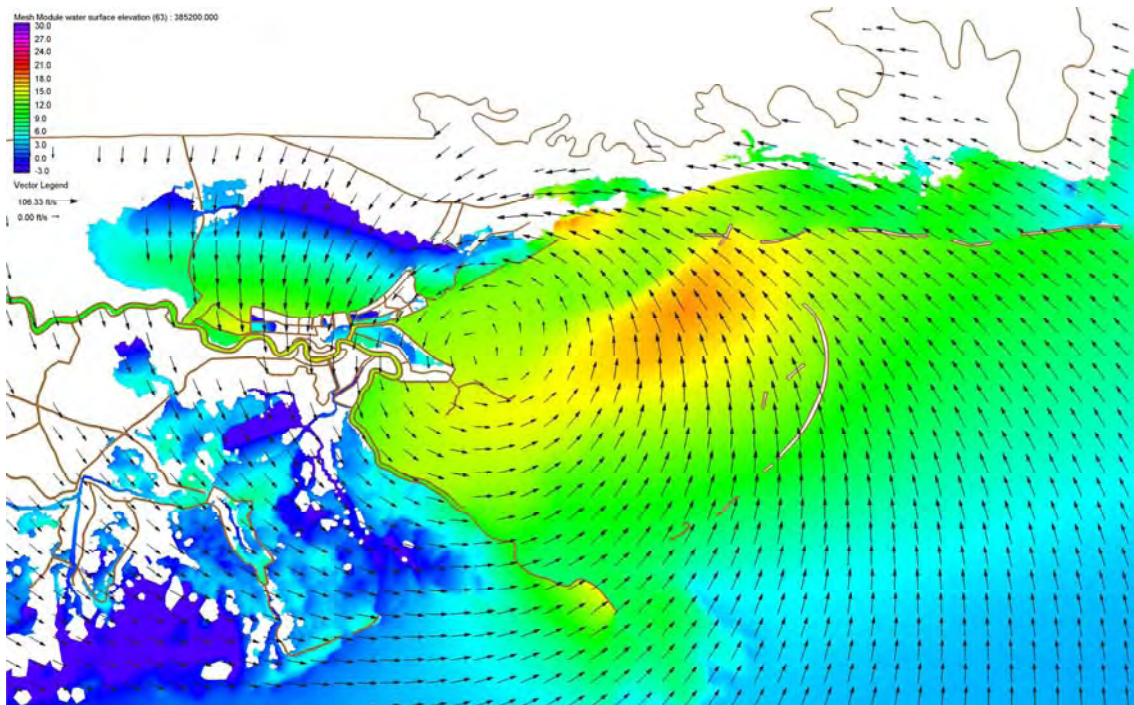


Figure 2f. Water surface elevation with respect to the NGVD 29 (ft) with boundary layer adjusted wind velocity vectors (knots) during Hurricane Katrina on August 29, 2005 at 1400UTC.

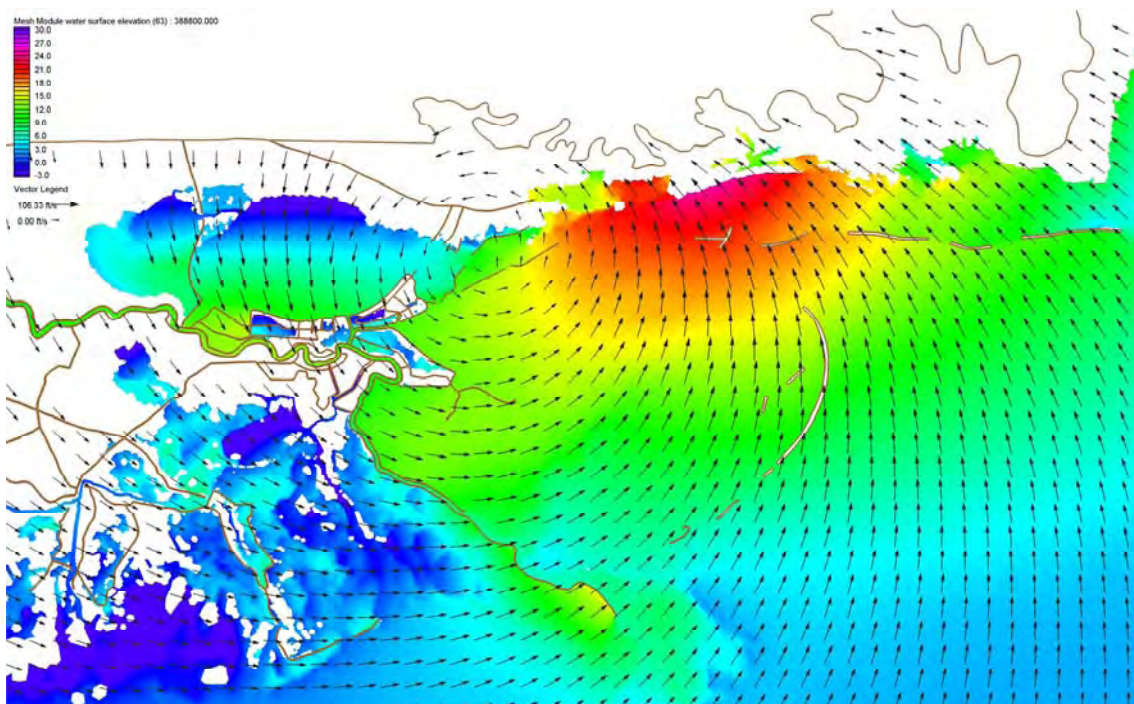


Figure 2g. Water surface elevation with respect to the NGVD 29 (ft) with boundary layer adjusted wind velocity vectors (knots) during Hurricane Katrina on August 29, 2005 at 1500UTC.

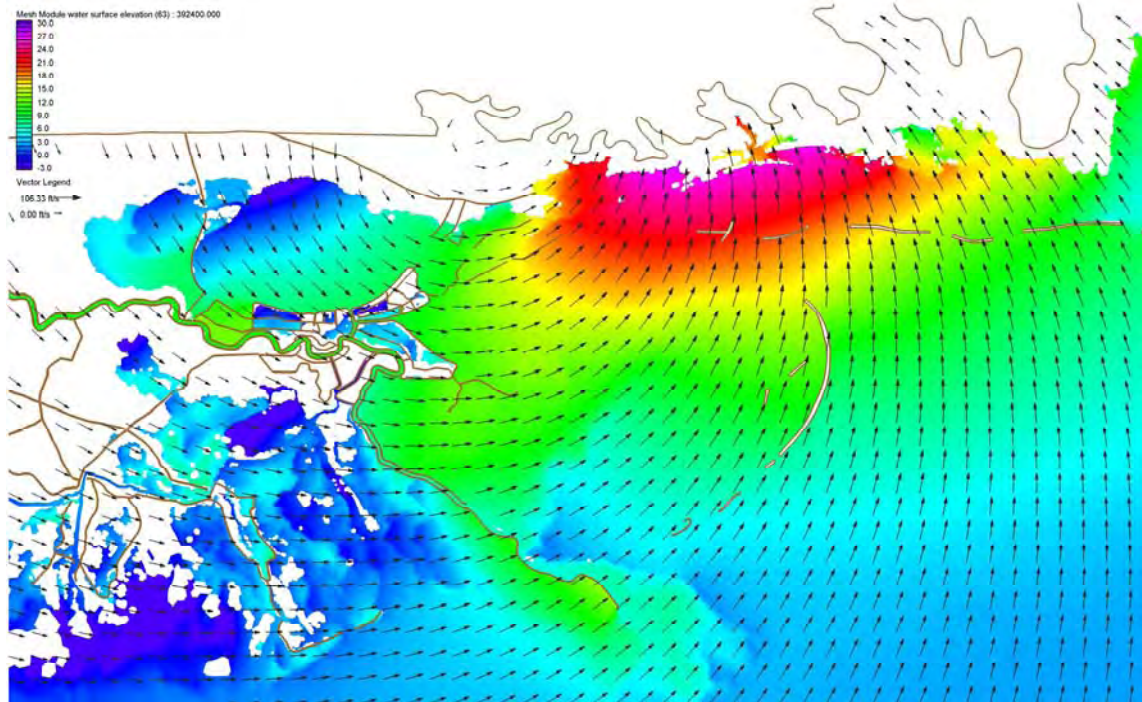


Figure 2h. Water surface elevation with respect to the NGVD 29 (ft) with boundary layer adjusted wind velocity vectors (knots) during Hurricane Katrina on August 29, 2005 at 1600UTC.

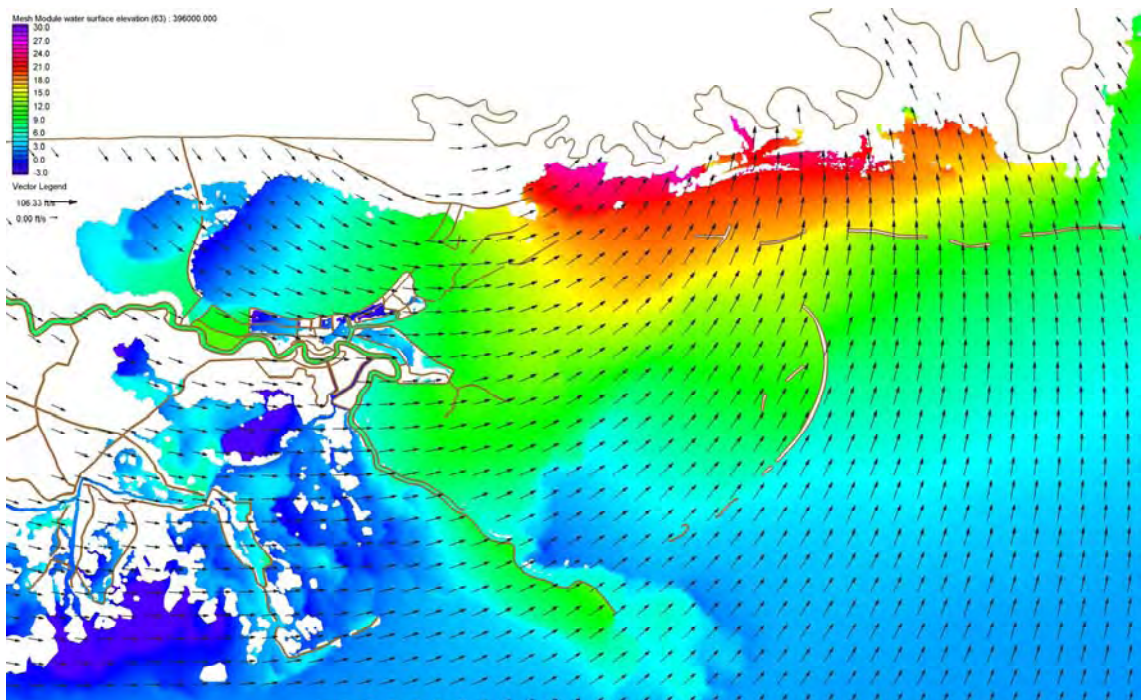


Figure 2i. Water surface elevation with respect to the NGVD 29 (ft) with boundary layer adjusted wind velocity vectors (knots) during Hurricane Katrina on August 29, 2005 at 1700UTC.

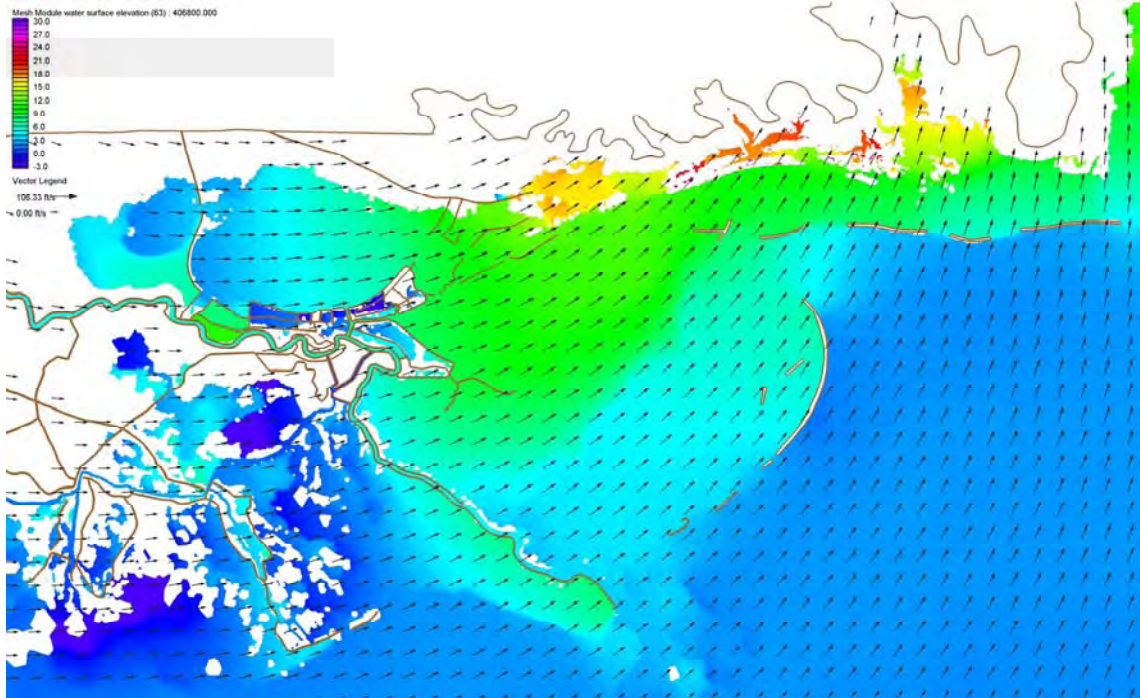


Figure 2j. Water surface elevation with respect to the NGVD 29 (ft) with boundary layer adjusted wind velocity vectors (knots) during Hurricane Katrina on August 29, 2005 at 2000UTC.

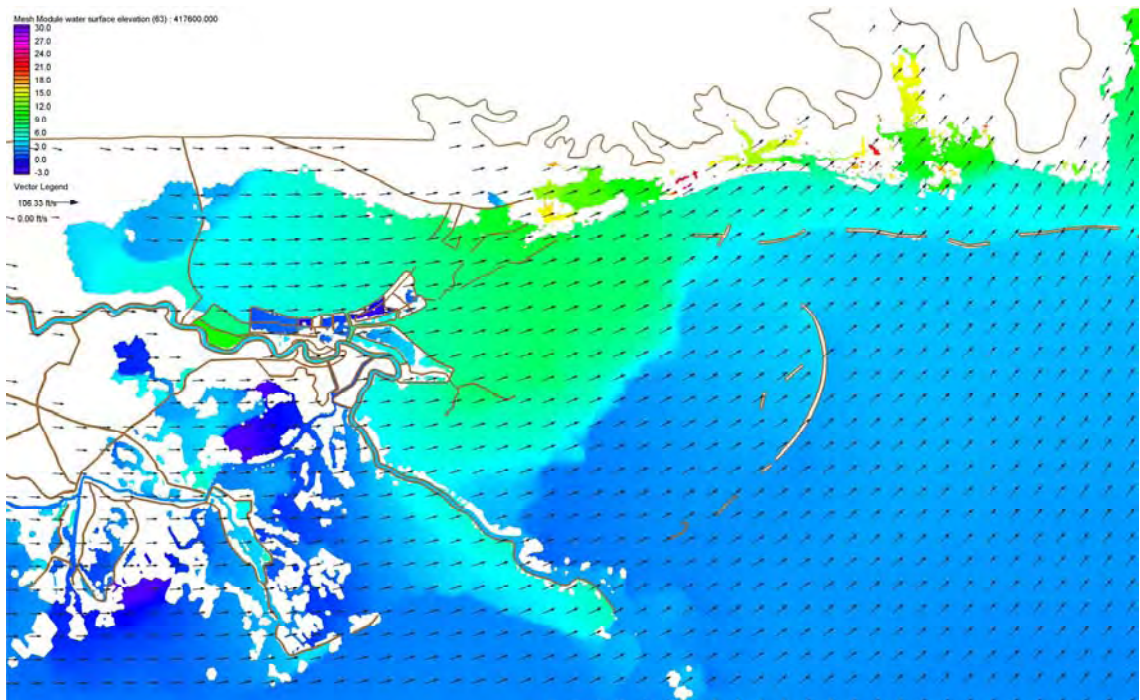


Figure 2k. Water surface elevation with respect to the NGVD 29 (ft) with boundary layer adjusted wind velocity vectors (knots) during Hurricane Katrina on August 29, 2005 at 2300UTC.

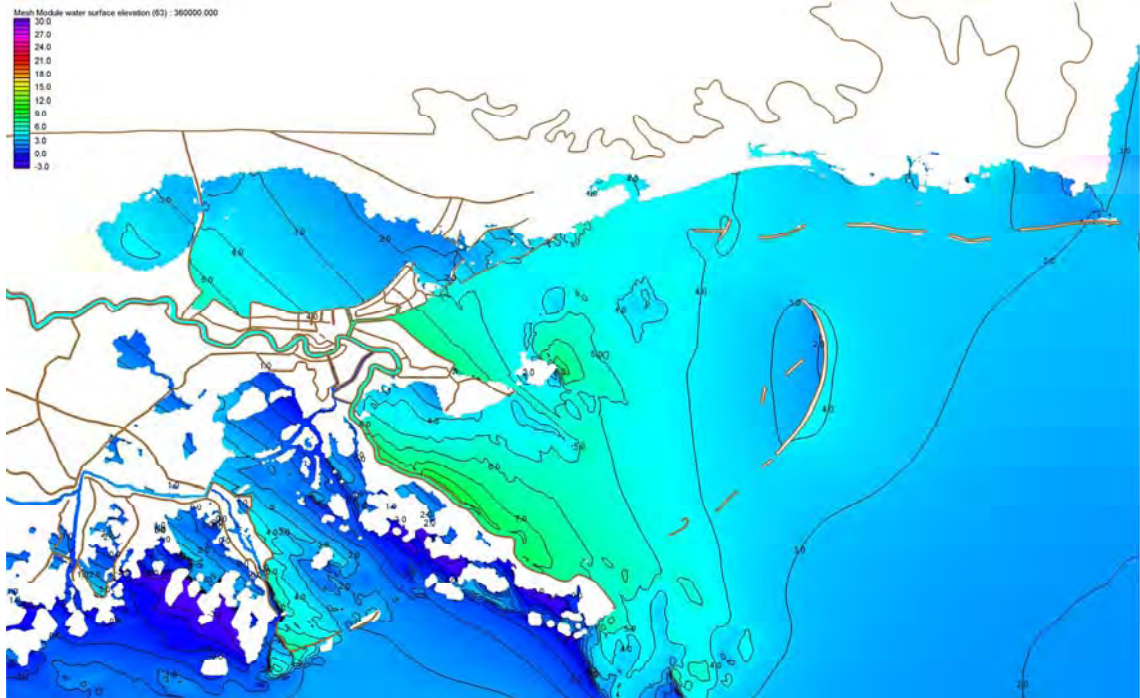


Figure 3a. Water surface elevation with respect to the NGVD 29 (ft) with labeled contours during Hurricane Katrina on August 29, 2005 at 0700UTC.

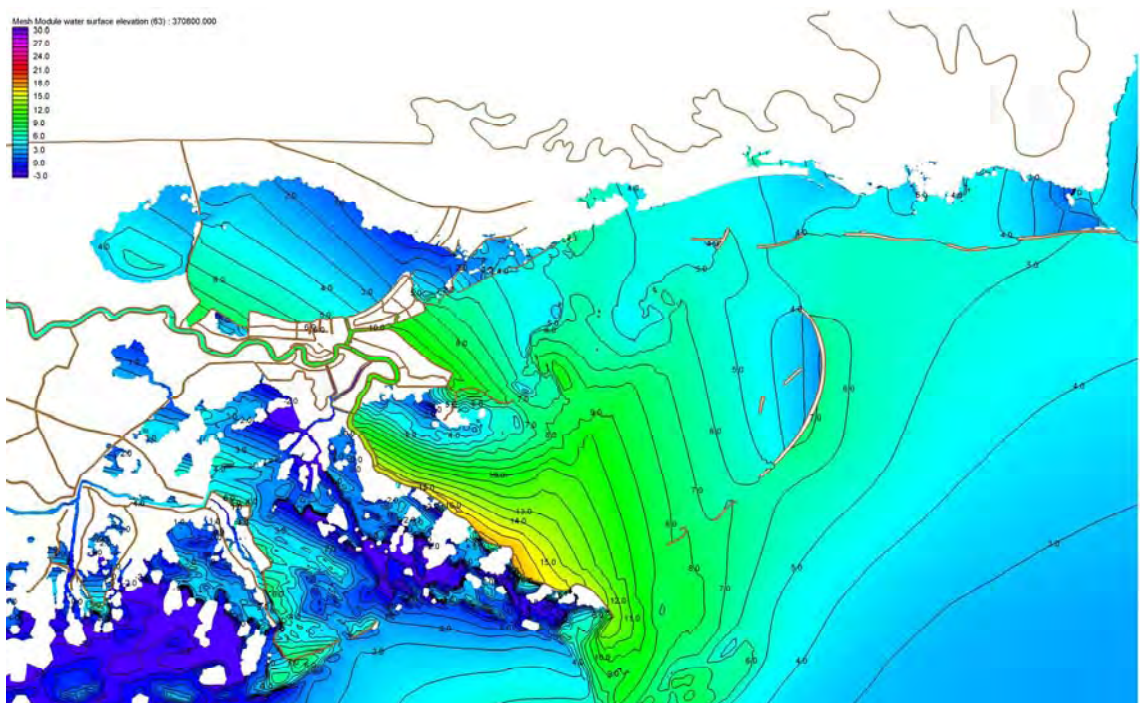


Figure 3b. Water surface elevation with respect to the NGVD 29 (ft) with labeled contours during Hurricane Katrina on August 29, 2005 at 1000UTC.

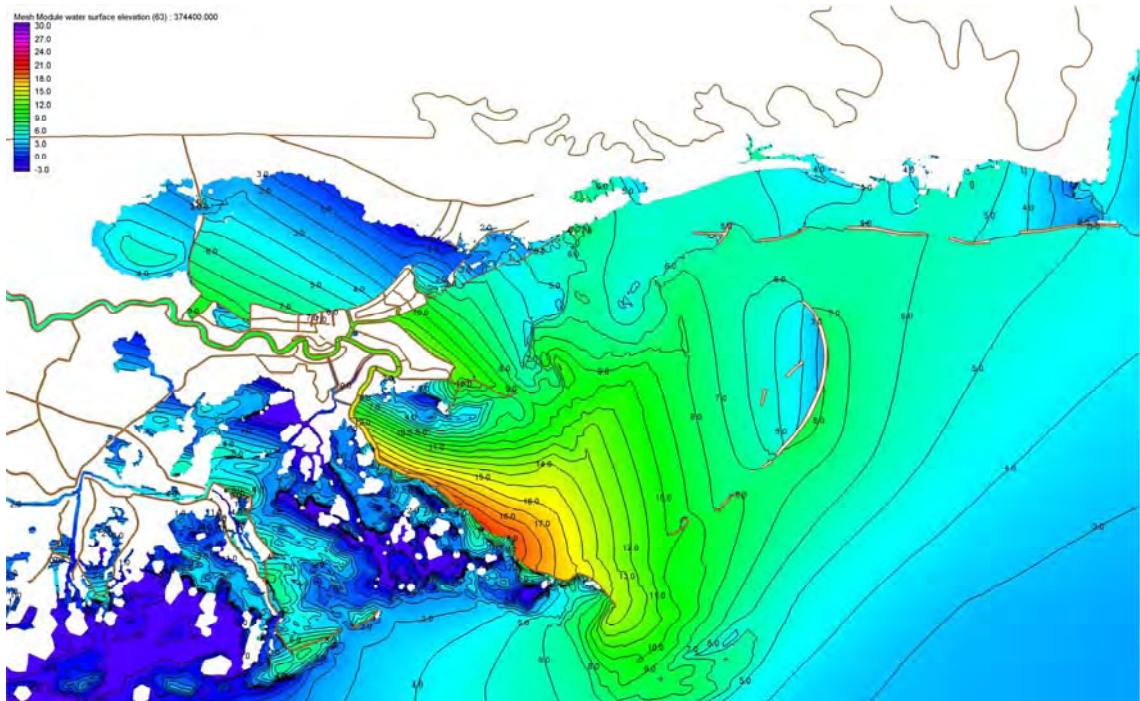


Figure 3c. Water surface elevation with respect to the NGVD 29 (ft) with labeled contours during Hurricane Katrina on August 29, 2005 at 1100UTC.

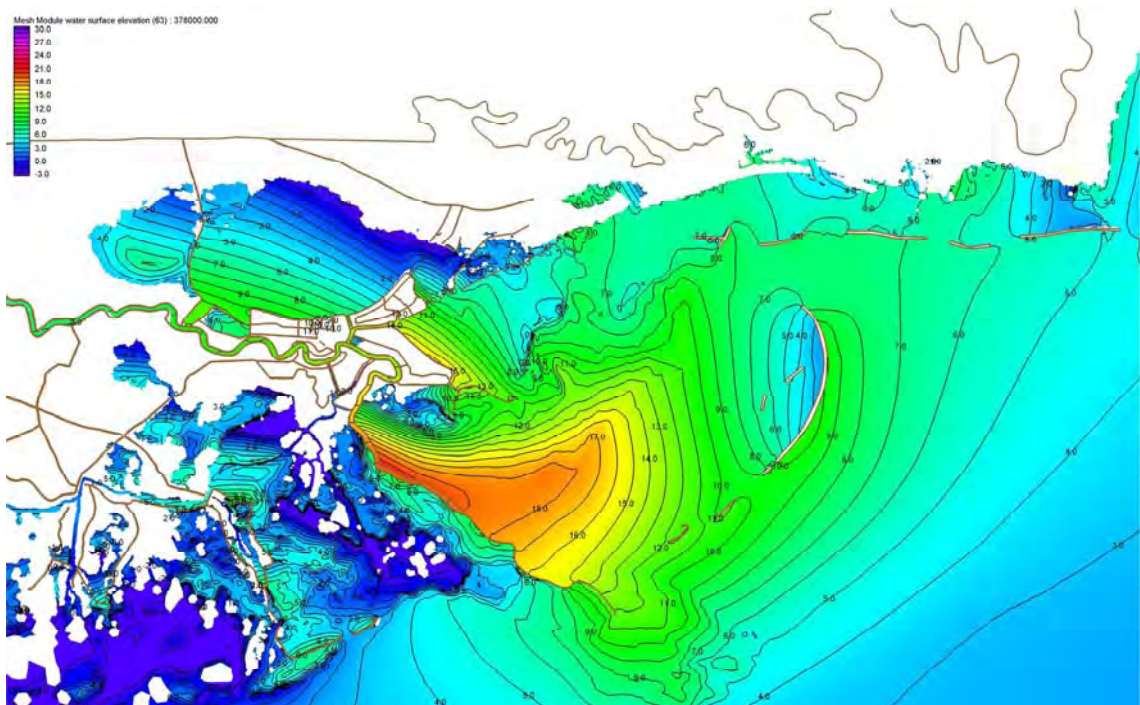


Figure 3d. Water surface elevation with respect to the NGVD 29 (ft) with labeled contours during Hurricane Katrina on August 29, 2005 at 1200UTC.

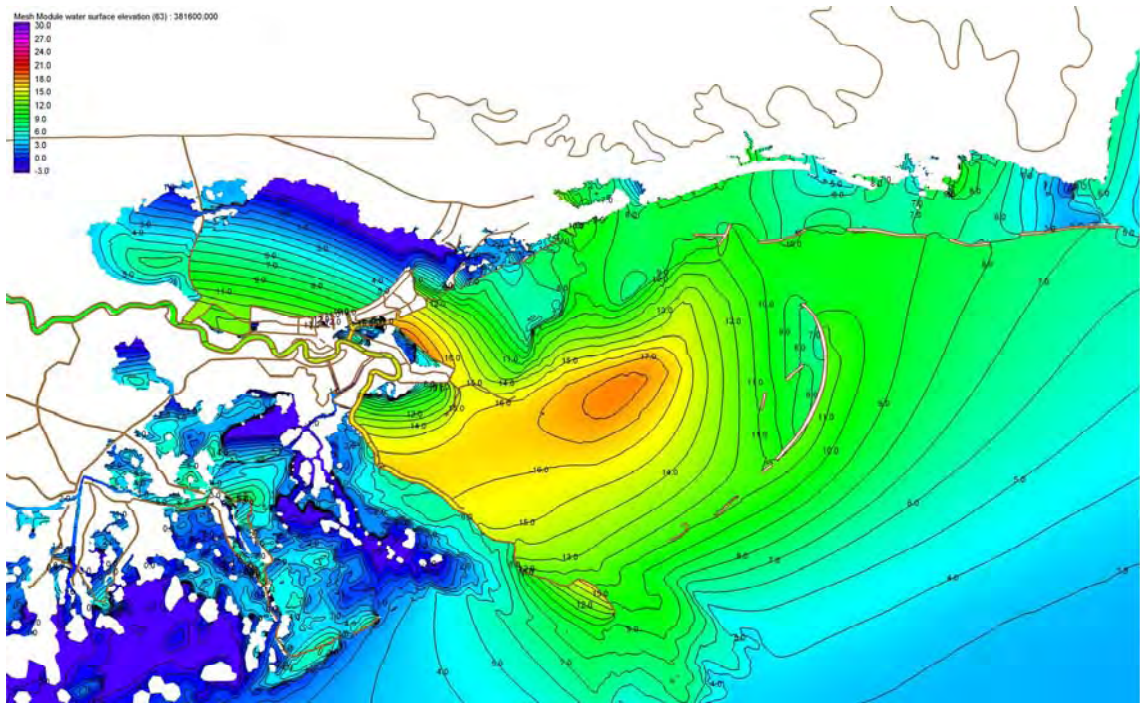


Figure 3e. Water surface elevation with respect to the NGVD 29 (ft) with labeled contours during Hurricane Katrina on August 29, 2005 at 1300UTC.

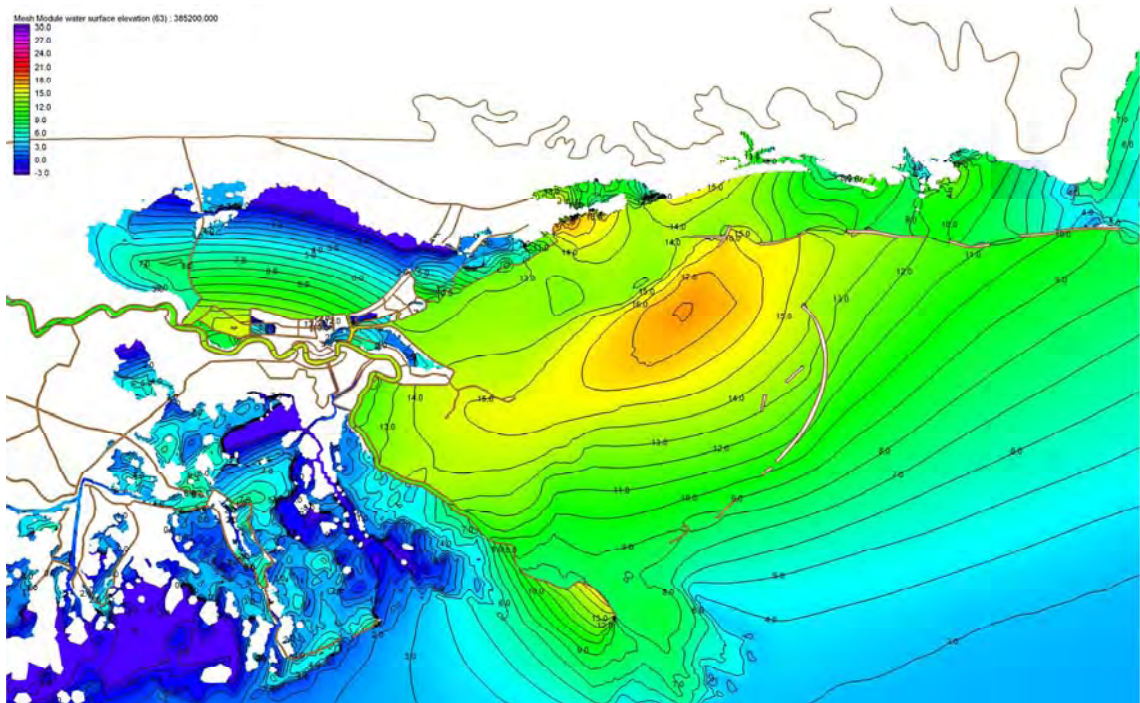


Figure 3f. Water surface elevation with respect to the NGVD 29 (ft) with labeled contours during Hurricane Katrina on August 29, 2005 at 1400UTC.

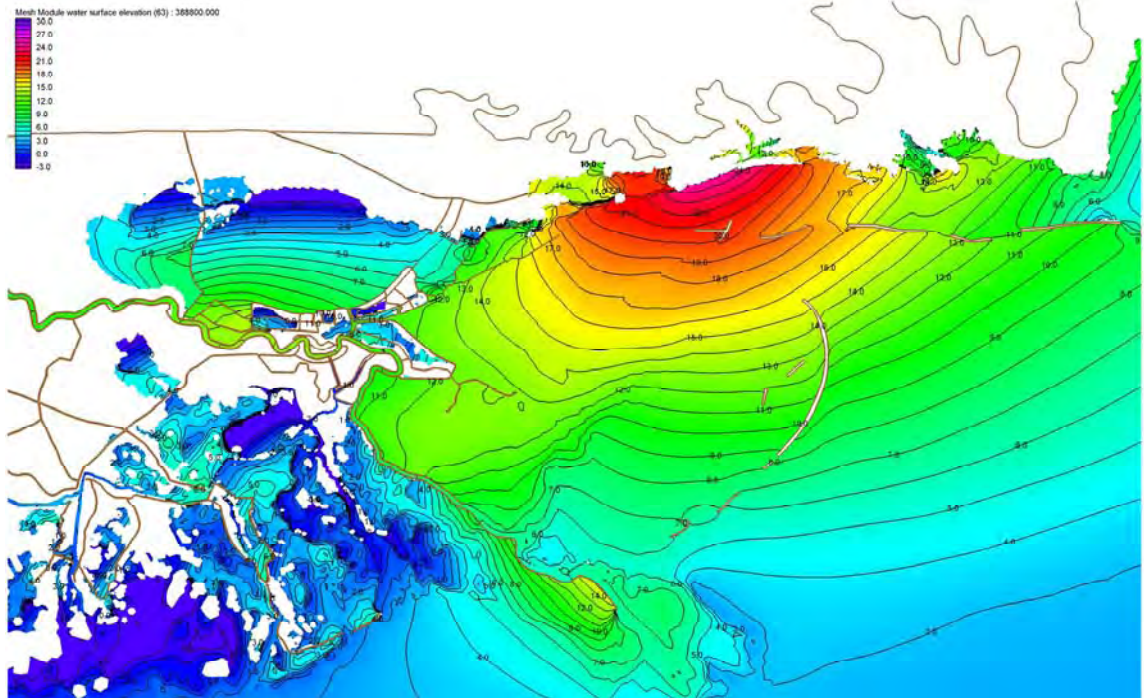


Figure 3g. Water surface elevation with respect to the NGVD 29 (ft) with labeled contours during Hurricane Katrina on August 29, 2005 at 1500UTC.

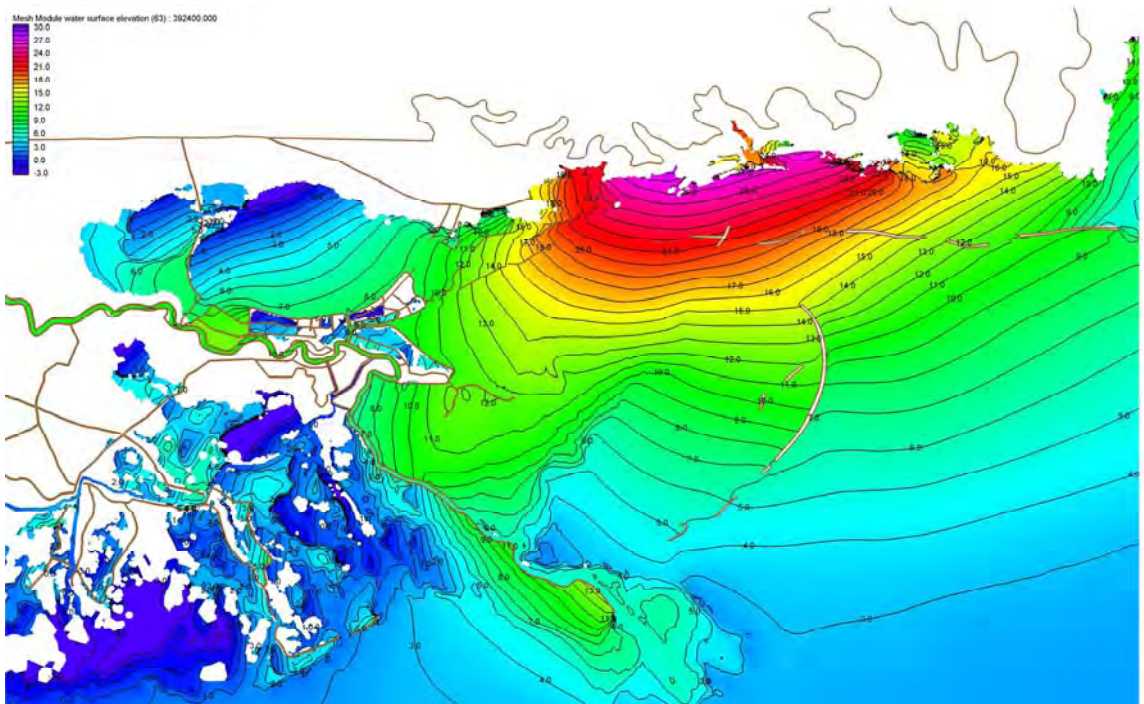


Figure 3h. Water surface elevation with respect to the NGVD 29 (ft) with labeled contours during Hurricane Katrina on August 29, 2005 at 1600UTC.

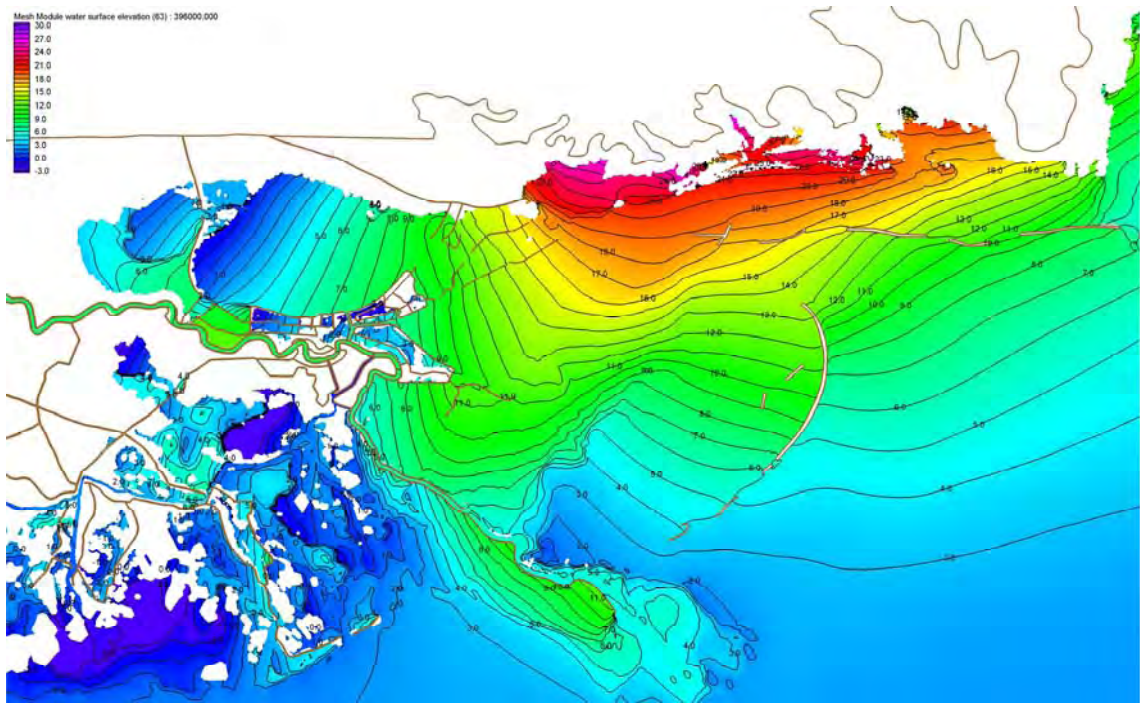


Figure 3i. Water surface elevation with respect to the NGVD 29 (ft) with labeled contours during Hurricane Katrina on August 29, 2005 at 1700UTC.

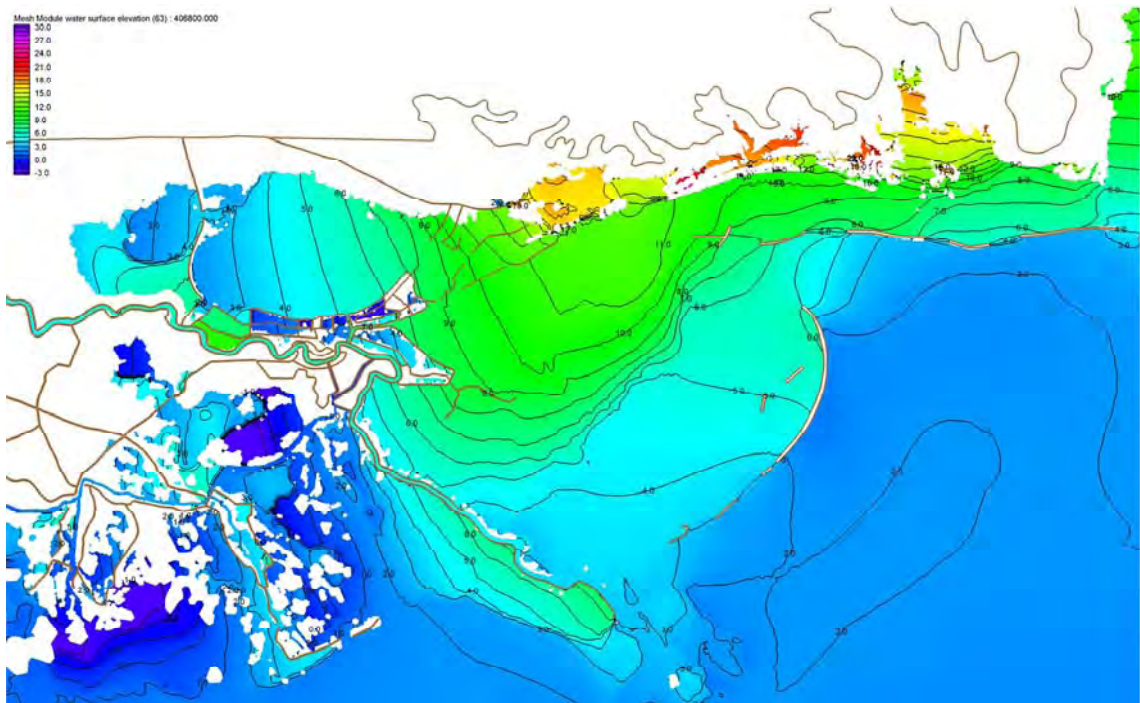


Figure 3j. Water surface elevation with respect to the NGVD 29 (ft) with labeled contours during Hurricane Katrina on August 29, 2005 at 2000UTC.

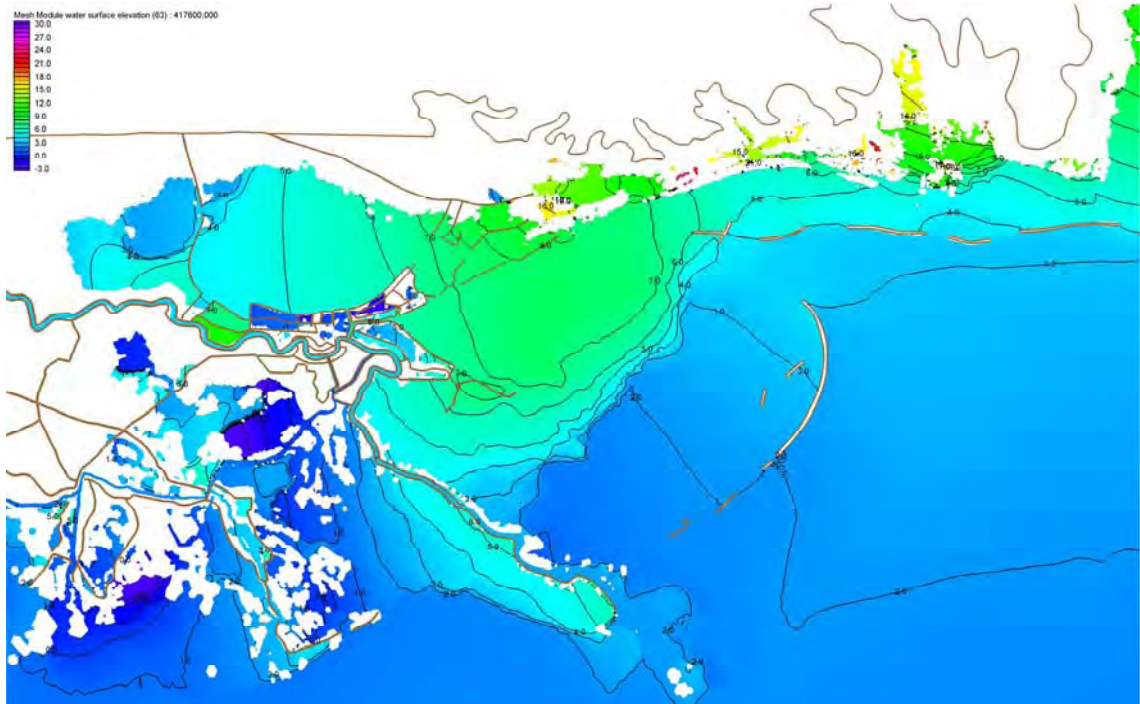


Figure 3k. Water surface elevation with respect to the NGVD 29 (ft) with labeled contours during Hurricane Katrina on August 29, 2005 at 2300UTC.

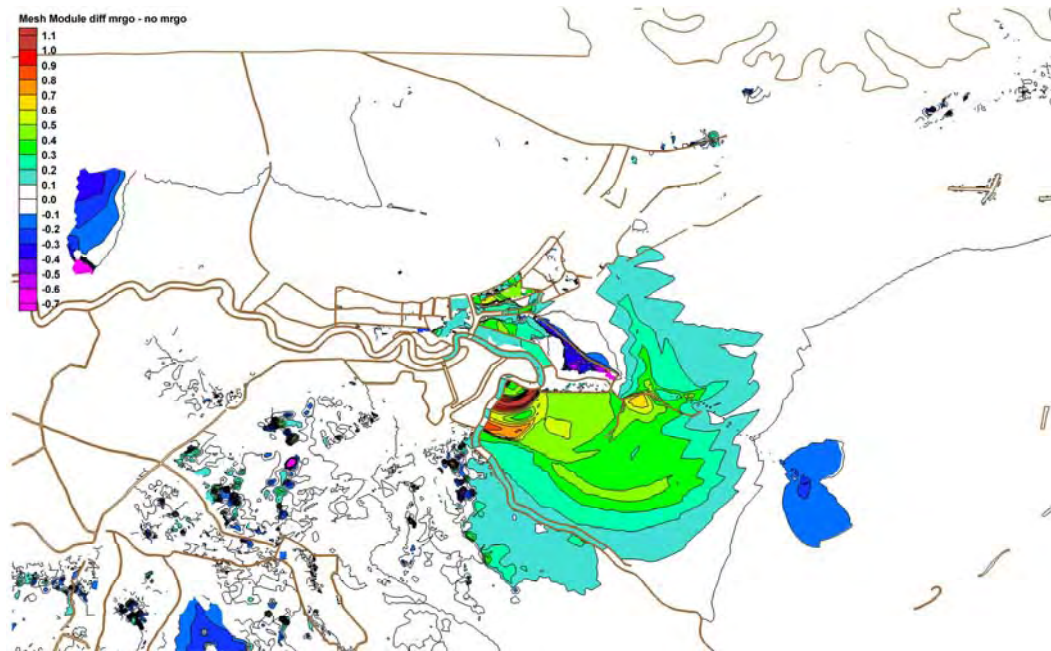


Figure 4a. Maximum Hurricane Katrina event differences in ft, for simulations with and without the MRGO in place. Positive differences indicate increased elevations with the MRGO in place while negative differences indicate decreased water levels with the MRGO in place.

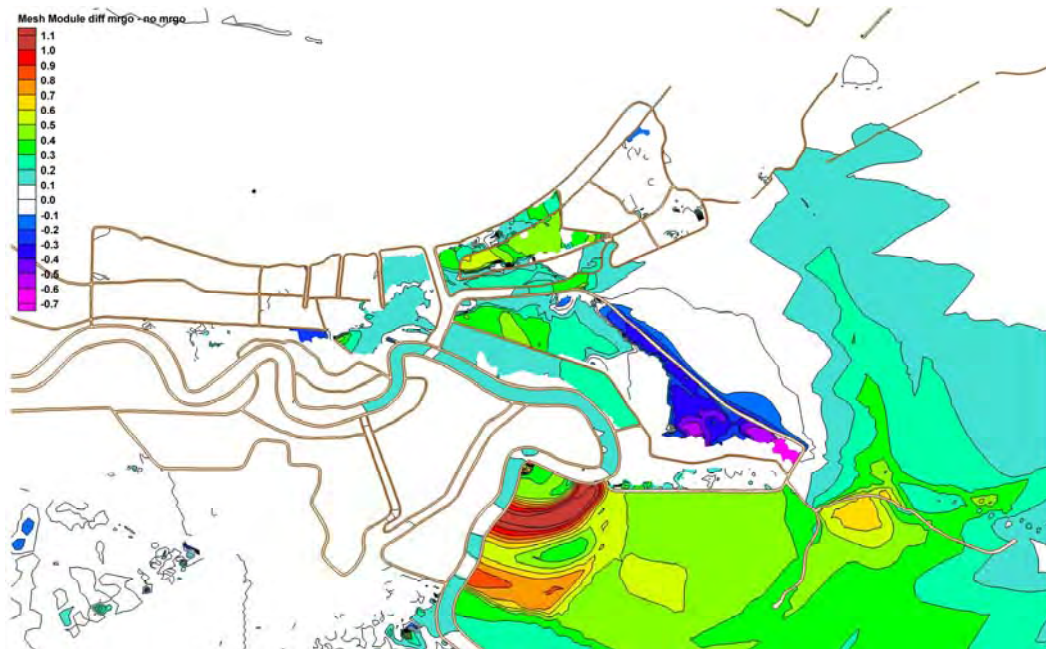


Figure 4b. Maximum Hurricane Katrina event differences in ft in metropolitan New Orleans and vicinity, for simulations with and without the MRGO in place. Positive differences indicate increased elevations with the MRGO in place while negative differences indicate decreased water levels with the MRGO in place.

Appendix F

Data Requirements for the IPET Study

Table F-1 below provides a listing of the data requirements based on input from the IPET Task Co-leaders. Each item is categorized as perishable, background, or new data. The color-coding in the table represents the data that has been posted to the Repository, where yellow represents partial or preliminary data and green represents complete data.

Table F-1		
Item #	Item	Perishable/Background/New
1	Post hurricane levee heights, profiles and alignments.	Perishable
2	Ground Surveys and Profiles of Ground and Structures(project/site, location, x,y,z, description, date, time, reference point for survey); pre- and post-storm canal cross-sections; GIS layer of canal centerlines and invert elevations	Perishable/ Background
3	Ground-based LIDAR of breaches (project/site, location, x,y,z, description, photos, date, time, reference point for survey)	Perishable
4	Breach configurations - locations, depth, width, descriptions, photos, erosion extents, date and time started and date and time fully developed.	Perishable
5	Land side scour locations	Perishable
6	High Water Marks	Perishable
7	Time history of events; Timeline of Katrina and Observed System Response - temporal hurricane track, observations: surge, flooding, wave heights, currents (direction, magnitude), pump operation, levee damage, debris in canals (quantity, composition), barges, boats, etc.; Eyewitness Accounts of the failures (project/site, location, x,y,z, description, date, time, reference point for survey); Interviews with USACE operators and emergency ops personnel concerning system performance;	Perishable
8	Geo-referenced photos of failure sites (x,y,z, project/site, description, measurement of erosion depth and breadth, date, time)	Perishable
9	Damage Survey Reports (project/site, location, x,y,z, description, photos, date, time, reference point for survey)	Perishable
10	Evidence of structural failure mechanisms (sheet pile depts, sheet pile embedment in concrete, concrete conditions)	Perishable

Table F-1		
Item #	Item	Perishable/Background/New
11	Repair records of emergency breach closures, photos of features buried during repairs	Perishable
12	; Bottom Profile of Canals, Bathymetric surveys, Scour Surveys (project/site, location, x,y,z, description, date, time, reference point for survey); Multi-beam sonar survey of bathymetry, sub-bottom characteristics (converted to x,y,z geo-referenced data and geo-referenced locations of scour and soil failures	Perishable/ New
13	Model results for Sequential Water Level (project/site, location, x,y,z, description, date, time, reference point for survey)	Perishable
14	Unwatering - Pump Flow rates and location of Discharge as a function of time	Perishable
15	combined TIN of land surface and detailed canals for each parish	New
16	DEM of all 5 parishes, pre-storm and post-storm DEM and structure/levee crest elevations	New
17	Top of floodwall and crest of levee surveys (project/site, location, x,y,z, description, date, time, reference point for survey); Survey of levee 'crest' elevations (perhaps DGPS on a 4-wheeler plus local surveys of tops of flood walls); Actual top and bottom of wall elevations (project/site, location, x,y,z, description, date, time); Levee and Flood Wall alignments and elevations (preferable in GIS)	Background/New
18	As-built cross-sections of levees (project/site, location, x,y,z, description, date, time, reference point for survey)	Background
19	Detailed surveys and/or as built plans for all Culverts (location, size, invert elevations of all culverts that bring flow into the canals from the land surface side)	Background
20	Detailed surveys and/or as built plans for all bridges in the study area	Background
21	Land use data (GIS layer)	Background
22	Soils data (STATSGO data)	Background
23	Drainage network GIS layer	Background
24	Digital Background maps and GIS layers (USGS digital quads, orthophotos, parcel data, streets and roads, etc...)	Background
25	Flood inundation maps resulting from hurricane Katrina (GIS layers showing flood boundaries of the event, with water surface elevations if possible)	New
26	Detailed project maps of the pre-Katrina system	Background
27	Historic precipitation data	Background
28	Historic stream gage data, high water marks, and pump station data for use in calibration of models; MVN Historical River Gage Records and associated benchmark reference data	Background
29	Tidal gage records and related analysis	Background
30	Geodetic Survey Archive Data (1960 to date)	Background
31	Storm surge histories	Background
32	System performance during past storm events	Background
33	Design Memos	Background
34	Plans and Specifications	Background
35	As Built Drawings	Background
36	Support Computations	Background
37	Construction QA Records	Background

Table F-1		
Item #	Item	Perishable/Background/New
38	Field Investigations	Background
39	Periodic Inspections	Background
40	A&E Reports	Background
41	Project modifications	Background
42	Construction reports	Background
43	Conference and Journal Articles	Background
44	Court records for Cases involving Levee Constructions	Background
45	Pump station data (location, number of pumps, pump capacity and efficiency curve for each pump, normal water surface elevation at which pump is turned on and off)	New
46	Pump station operation timeline, detailed	New
47	Pump stations performance output from Task 8	New
48	Stream gage information (time series of stages and flows at all possible locations) during Katrina	New
49	Hurricane Katrina Precipitation data (point data and NexRad radar data)	New
50	Lake Pontchartrain stage data	New
51	Models and Studies that have been performed by the District office and others	Background
52	Surge heights and hydrographs (pre, post, and during Katrina); measured water level hydrographs	New
53	Levee and floodwall failure modes (input data used to analyze floodwalls and levees, material strength distributions, uncertainty in sheet pile depth)	New
54	Soil Boring (project/site, location, x,y,z, description, graphs, date)	New
55	CPT Data (project/site, location, x,y,z, description, graphs, date)	New
56	Laboratory Logs (project/site, location, x,y,z, boring number, description, graphs, date)	New
57	Soil Test Data (project/site, location, x,y,z, boring number, description, graphs, date)	New
58	Soil Material Properties (project/site, location, x,y,z, description)	New
59	Sheet Pile Test Data (project/site, location, x,y,z, description, graphs, photos)	New
60	Concrete Test Data (project/site, location, x,y,z, description, graphs, photos)	New
61	Steel Reinforcement Test Data (project/site, location, x,y,z, description, graphs, photos)	New
62	Instrumentation (piezometer, slope inclinometers, wall deflection gages, etc.) (project/site, location, x,y,z, description, graphs, photos, date, time)	New
63	Reference Elevation/Datum (reference controlling benchmarks) for all LIDAR/DEM/Aerial mapping recently flown. Ensure all topographic DEM data is referenced to the same SE Louisiana Vertical Time-Dependent Reference framework and related water surface references	New
64	MVN Vertical Control/Topographic Surveys of Levees	New
65	vertical data survey of pump house monuments	New
66	Timeline of baseline water level data at station inlet and outlet - Task 2	New

Table F-1		
Item #	Item	Perishable/Background/New
67	Timeline of actual water level data at station inlet and outlet-Task 3	New
68	interpretation of pre-storm ground cover throughout the domain, or imagery to assess ground cover	New
69	Photos from historical hurricanes affecting these areas	Background
70	Aerial and Satellite Image (project/site, location, x,y,z, description, date, time)	New
71	Aerial videos (date, time, project/site, location, description)	New
72	Aerial photography of before flood and during flood	Background/New
73	Tasks 2, 3, 4, 8, 9 results	New
74	System models used by Task 5	New
75	Task 4 Wave/Water heights	New
76	Task 5a Physical Model Data	New
77	Surficial sediment concentration of contaminants in the canals and lake - value, location, time	Perishable
78	Total organic carbon concentration of bottom sediments in canals and lake - value, location, and time	Perishable
79	Analysis of benthos in sediments near pumps	Perishable
80	Wetland assessment and ground truthing in St. Bernard Parish	Perishable
81	Fish contaminant assessment	Background
82	Fish Health Assessment	Background
83	Endangered and Threatened fish assessment	Background

Appendix G

IPET Communications Efforts

The IPET communications efforts have followed the IPET charge to forward information to the public as quickly as possible through various methods. In all aspects, IPET has responded as quickly as possible, truthfully, and accurately to media requests and has proactively sought out media opportunities at all levels.

IPET media interaction has been on-going since the earliest data collection efforts immediately following Hurricane Katrina. To date, IPET has interacted with more than 100 media contacts, including national media such as the New York Times, Wall Street Journal, Los Angeles Times, National Public Radio, NBC News, CBS News, ABC News, CNN, etc. Special attention has been made to inform citizens in New Orleans and Southeast Louisiana who have a vested interest in IPET activities. Our communications efforts have included numerous repetitive contacts with the leading newspapers, radio stations and television stations in Louisiana.

IPET communication staff is also coordinating with the External Review Panel communications staff at the American Society of Civil Engineers (ASCE) and with the communications staff at the National Research Council (NRC) to effectively inform the public of our interaction and our responsibilities to our citizens. A news conference was held in conjunction with ASCE at the IPET Report 1 release on Jan. 10, and IPET supported media interviews at the NRC meeting in New Orleans on Jan. 18. Media opportunities will be scheduled for subsequent IPET report releases to ensure maximum dissemination of information to the public.

As a team, all IPET members have been made available for media interaction. This has included both Corps of Engineers and non-Corps members. Media support from both IPET team members, such as the Harris County Flood Control District, and IPET contractors, such as Rensselaer Polytechnic Institute, have been instrumental in informing the public of the activities of IPET.

IPET has also worked closely with other Corps of Engineers organizations in the affected areas of Southeast Louisiana, such as Task Force Guardian, the New Orleans District, and the Mississippi Valley Division to provide accurate and useful information to the public.

IPET information products (news releases, bios, etc.) have been posted on both the IPET public web site (<https://ipet.wes.army.mil>) and the Corps of Engineers public web site (www.usace.army.mil).

Communications efforts have also included professional videotaping of IPET modeling activities to share with documentary production companies, news crews and for historical purposes.

A USACE news release requesting relocated residents of the greater New Orleans area who stayed during Hurricane Katrina and personally witnessed flooding due to levee overtopping or floodwall breaching before relocating to provide information, photos, and any other related data to IPET was published on 16 February, 2006. Anyone with information may contact the IPET through the IPET web site (<https://ipet.wes.army.mil>). Information can also be e-mailed to Katrina.Accounts@usace.army.mil or eyewitnesses can call toll free 1-866-502-2570, extension 5004.

Appendix H

Task Force Guardian Inputs

IPET Products Provided to Task Force Guardian and Task Force Hope as of 10 March 2006

a. **Data Repository – 25 October 2005.** The IPET Data Repository was established as an entry point for collecting information pertaining to the New Orleans and Southeast Louisiana Hurricane Protection Projects that needs to be validated as factual. This repository supports both the IPET and TFH/TFG efforts by providing a database where information can be reviewed for accuracy and quality prior to posting the information on the IPET public website.

b. **Establishment of the IPET Public Website – 2 November 2005.** The IPET public website was established as a way to be fully transparent in effectively sharing factual information pertaining to the New Orleans and Southeast Louisiana Hurricane Protection Projects. The website provides a way to proactively communicate information that might otherwise require the public and TFG to process Freedom of Information Acts.

c. **Establishment of On-Line Team Workspace using Groove – 22 September 2005.** To enable IPET, ERP, and members of TFH/TFG with on-line workspaces to communicate and share information virtually, Groove software and technical support was provided by IPET. Through these virtual workspaces information can be effectively and efficiently shared. Groove is a primary tool used to bring the IPET, ERP, and TFH/TFG teams together in sharing knowledge and information required to accomplish their missions.

d. **Integration of the IPET Public Website and the TFH/TFG Electronic Bid Solicitation Websites – 15 November 2005.** As a way to more effectively enable public benefit from the historic and performance-related information on the IPET public website and the reconstruction plans and specifications on the TFH/TFG electronic bid solicitation website, electronic linkage was provided to facilitate integration of the two sites.

e. **“Summary of Field Observations Relevant to Flood Protection in New Orleans, LA” – 5 December 2005.** This IPET review provided Task Force Guardian with a simple statement of concurrence or nonconcurrence from the

IPET floodwall and levee sub team and additional relevant discussion for each of the major findings in the ASCE/NSF report's chapter eight, "Summary of Observations and Findings." The additional discussion relates to the analysis being conducted by the IPET or others that would assist in applying the ASCE/NSF findings to the reconstruction of hurricane protection in New Orleans.

f. **"Preliminary Wave and Water Level Results for Hurricane Katrina" – 23 November 2005.** This IPET report to TFH/TFG included observations from the IPET surge and wave sub team from a field trip and overflight of New Orleans and Southeast Louisiana.

g. **"Summary of IPET Numerical Model of Hurricane Katrina Surge and Wave Plans, Approach and Methods" – 19 December 2005.** This Power-Point presentation by the IPET surge and wave sub team provided TFH/TFG with an update on wave and water level results for Hurricane Katrina. Wave and water level results from fast-track simulations of upper Category 3 type storms on various storm tracks and a Standard Project Hurricane event were also provided.

h. **Review of Proposal to Float In and Sink a Barge to Close Canals by June 2006 – 28 December 2005.** The proposal included the use of existing large ship tunnel thrusters mounted on a barge with huge pumping capacities. Review determined that the closure plan does not have enough pumping capacity to match existing pumps during a hurricane.

i. **Technical Support to TFG on the Analysis and Design of the Reconstruction Plans and Specifications for the Breaches – Continuous Support as Needed.** Technical support continues to be provided to TFG on an as-needed basis. As a minimum, monthly face-to-face meetings take place in New Orleans. This support includes geotechnical and structural consultations. These discussions also include reviews of plans and specifications for reconstruction features such as T-walls, L-walls, I-walls, levees, and foundation investigations.

j. **Evaluation of Existing and As-Built Conditions at Canals – On-going.** This evaluation includes concrete and steel material properties for reinforcement and sheet piles on the I-walls, as-built length of sheet piles, surveys, and foundation material properties and boring logs.

k. **Life-cycle Documentation of the Hurricane Protection System – On-going.** This documentation includes a review of the design, construction, and operation and maintenance of the hurricane system.

l. **Verification of Current and Reconstructed Floodwall Elevations – November 2005.** Established a tidal gage in November 2005 at the 17th Street Canal to monitor current sea level relationships to the newest NAVD88 datum epoch (2004.65). Verified floodwall elevations on Lakefront outfall canals and IHNC relative to this latest tidal and vertical epoch.

- m. **LIDAR Ground Truthing – On-going.** Currently performing ground-truthing surveys throughout the region to calibrate various LIDAR-based elevation models used by Task Force Guardian.
- n. **Densification of Control Benchmarks – 31 December 2005.** IPET has established approximately 75 vertical benchmarks throughout the region. These control points are being used for Task Force Guardian construction activities.
- o. **Establishment of GIS Team – 2 February 2006.** The “GIS Team” was established to maximize the effectiveness and efficiency of the GIS resources within IPET, Task Force Guardian, Task Force Hope, and the New Orleans District. The GIS Team consists of members from each of the four teams and provides a way to integrate efforts and share information pertaining to the HPS. The GIS Team will also provide for a way to assure a smooth transition of IPET generated GIS information to the New Orleans District upon disbanding of IPET once its performance evaluation is completed. Significant IPET data sets shared with TFG in January and February 2006 include the digital elevation models, vertical datum survey data, geotechnical data, and photographs.
- p. **Insight into probable cause of breaching at 17th Street Canal – Continuous ending March 2006.** Information was shared with TFG on the probable cause of breaching at the 17th Street Canal. Recommendations were provided on considering the formation of a gap at the base of cantilever I-walls and shear strength variations between the centerline and inboard toe of levees used in combination with I-walls.
- q. **Storm Surge and Wave analysis results for Katrina and historical storms – December 2005.** Information pertaining to modeled Katrina storm surge and wave heights and periods for various locations along the HPS was provided to TFG. In addition, modeled surge and wave results from other historical storms were also provided.
- r. **Review comments on canal closure structures – December 2005 and January 2006.** IPET review comments for the outfall canal closure structures were provided to aid in development of high quality P&S for the closure structures.
- s. **Provided comments in IPET Report 2 regarding comparison of Hurricane Katrina wave and period conditions with design values – March 2006.** Design wave conditions, particularly wave period, should be re-evaluated for the east-facing levees in east Orleans, St. Bernard and Plaquemines Parishes.
- t. **Closure Structures Modeling – January – February 2006.** IPET members at MVN performed modeling analysis of the closure structures on 17th Street, Orleans and London Ave Canals.
- u. **MRGO White Paper – March 2006.** Input on analysis of MRGO effect on storm propagation into metropolitan New Orleans and vicinity.

Appendix I Pump Station Technical and Detailed Report

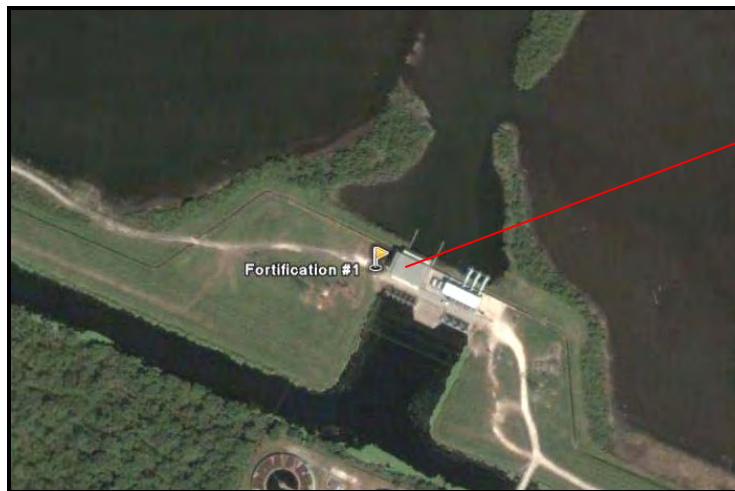




Pre-Hurricane Katrina – View from Inlet Canal

**4200 Jean Lafitte Pkwy.
Chalmette, LA 70043
504.512.6331**

Position: Latitude 29.966557° Longitude -89.975821°



Pre-Hurricane Katrina – Arial view of pump station

Pump Station Description

Fortification is 1 of 8 pumping stations in St Bernard Parish owned and operated by the Lake Borne Basin Levee District. The station contains three vertical pumps that were installed in 1972 with a total pumping capacity of 980 cubic feet per second (cfs)¹. Two of the pumps are driven by diesel engines and one by an electric motor. The drainage water is supplied to the pumps from the Florida Walk canal and discharges through the interior back levee to the marsh known as

¹ The Pump Information Table contains more details about the individual pump data and is located at the beginning of this section.

Bayou Bienvenue. The individual pump discharges have a tainter gate installed to cut off water flow in either direction.

Pump Station Operation

Pump station operators will turn the pumps on as they are required to reduce the water elevation in the canal. The pumps are normally turned on when the water in the canal reaches approximately -6 feet (NGVD) and turned off when the water level reaches -6.5 feet (NGVD). When heavy rainfall events are expected the station operators will pump the canal down to an elevation of -8.5 feet (NGVD). If the water elevation on the discharge side of the pump station is predicted to exceed 3.5 feet (NGVD) the station operator closes the discharge tainter gates.

Fuel Endurance Calculation

Assumptions :

- 1) #2 Diesel fuel is used with an HHV rating of 140,000 btu/gal
- 2) Burn rate of 35 gph @ 500 kW with above HHV rating
- 3) Diesel engines are running at rated capacity

PS 1 Fortification

3 pump drivers - 2 diesel and 1 electric. The diesels are rated at 1200 horsepower

The approximate burn rate for each diesel is then calculated:

$$R_{\text{burn}} := \left(35 \frac{\text{gal}}{\text{hr}} \right) \cdot \frac{1200\text{hp}}{500\text{kW}} \qquad R_{\text{burn}} = 62.639 \frac{\text{gal}}{\text{hr}}$$

Fuel Capacity

- 4 - 5000 gallon tanks
- 2 - 110 gallon day tanks

Fuel Endurance

The time the 5000 gallon tanks will last is calculated:

$$t_1 := \frac{4 \cdot 5000\text{gal}}{2R_{\text{burn}}} \qquad t_1 = 159.645 \text{ hr}$$

The time the 110 gallon tanks will last is calculated:

$$t_2 := \frac{2 \cdot 110\text{gal}}{2R_{\text{burn}}} \qquad t_2 = 1.756 \text{ hr}$$

The approximate total continuous run time for the pump station is:

$$T_t := t_1 + t_2 \qquad \boxed{T_t = 161.402 \text{ hr}}$$

$$\boxed{T_t = 6.725 \text{ day}}$$

Pump Curves

Pump capacity curves were obtained either from the parish or from the manufacturer of each pump. From these curves, a curve fit process was used to create new curves and equations.

Using drawings provided, assumptions were made regarding the dimensions of the pump station and the pump. Using these assumptions, the minor and friction losses were calculated in order to create the system curve. Two system curves were created due to the range of heads reported by the parish. The two curves represent the maximum and minimum operating heads reported.

Reverse Flow

The Engineering Hydraulics Design section of the US Army Corps of Engineers Portland District office performed analysis of reverse flow characteristics for each pump. The results are reverse flow rating curves that are attached to this section. The tables present the flow rates per individual pump. The detailed calculations, assumptions, and assumed dimensions are available upon request.

Katrina Event

8/28/05 -Operators pumped water in canal down to approximately 8.5 ft.

8/29/05 -Operators evacuated pump station at approximately 1:15 am.

8/30/05 -Operators returned to the station at 10:00 am. Water was the same elevation on both sides of pump station.

9/01/05 -Both pumps running.

9/11/05 -**Pump station back to normal operation.**

Damage Report

The following information was obtained from the Project Information Report (PIR) for New Orleans District:

Pump Station 1 sustained relatively minor damage because its operating floor elevation is 16 feet N.G.V.D. Flooding from the storm flooded the lower level of the station but the flood waters were approximately three feet below the concrete operating floor level. Pump station equipment that was damaged includes an electric pump motor, generator, trash rack bearing and gear box, and lighting. The building sustained damage to the metal siding and roof. Additionally, the diesel engine cooling system developed a leak. Auxiliary equipment damage included flooding of a bobcat used to remove debris from the trash racks.



Post-Hurricane Katrina – View from the Inlet Canal



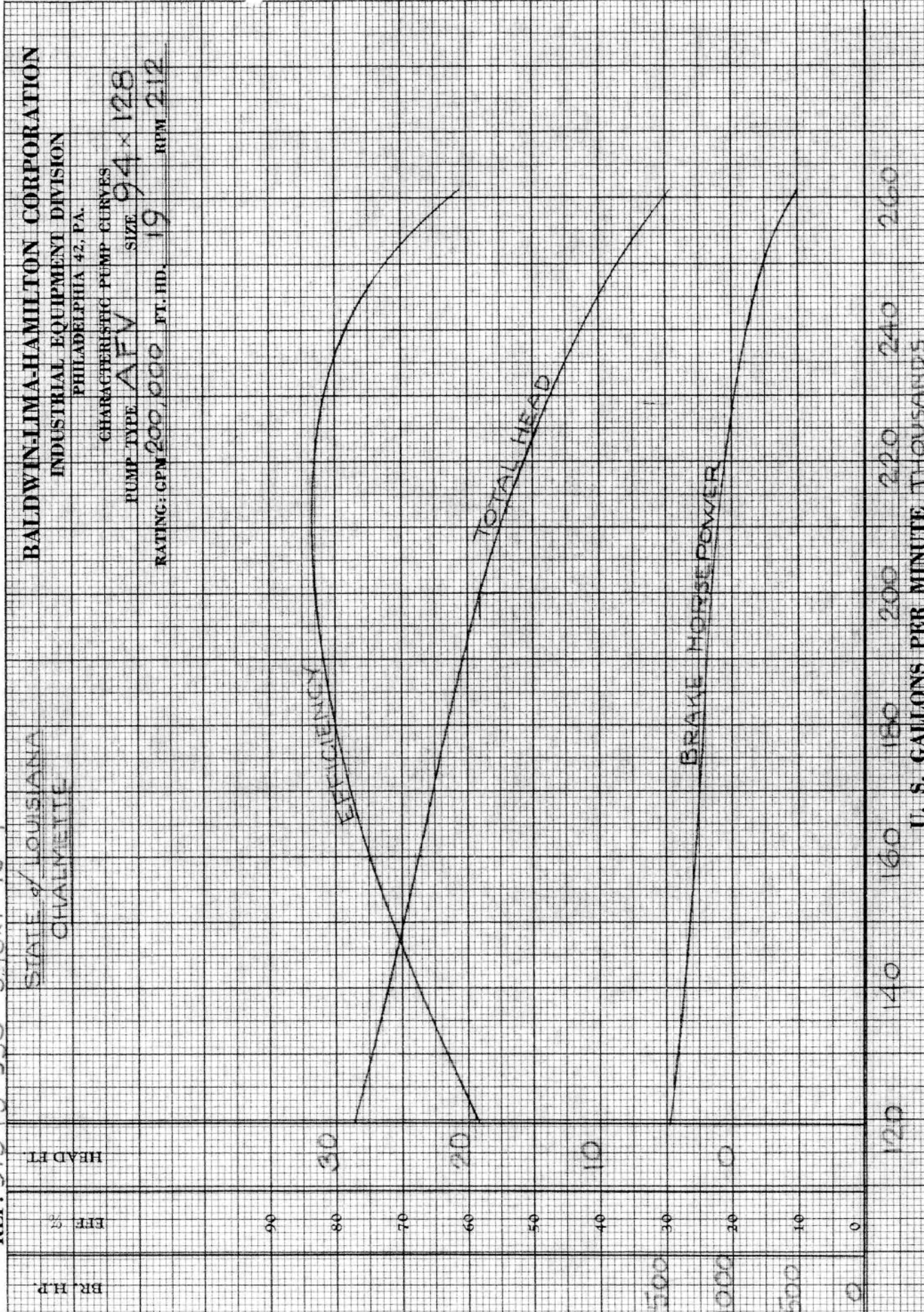
PS1 Fortification

Post-Hurricane Katrina – Aerial view of the pump station

CURVE NO.

F-15915

REF. 51343-550 548x1-15-4



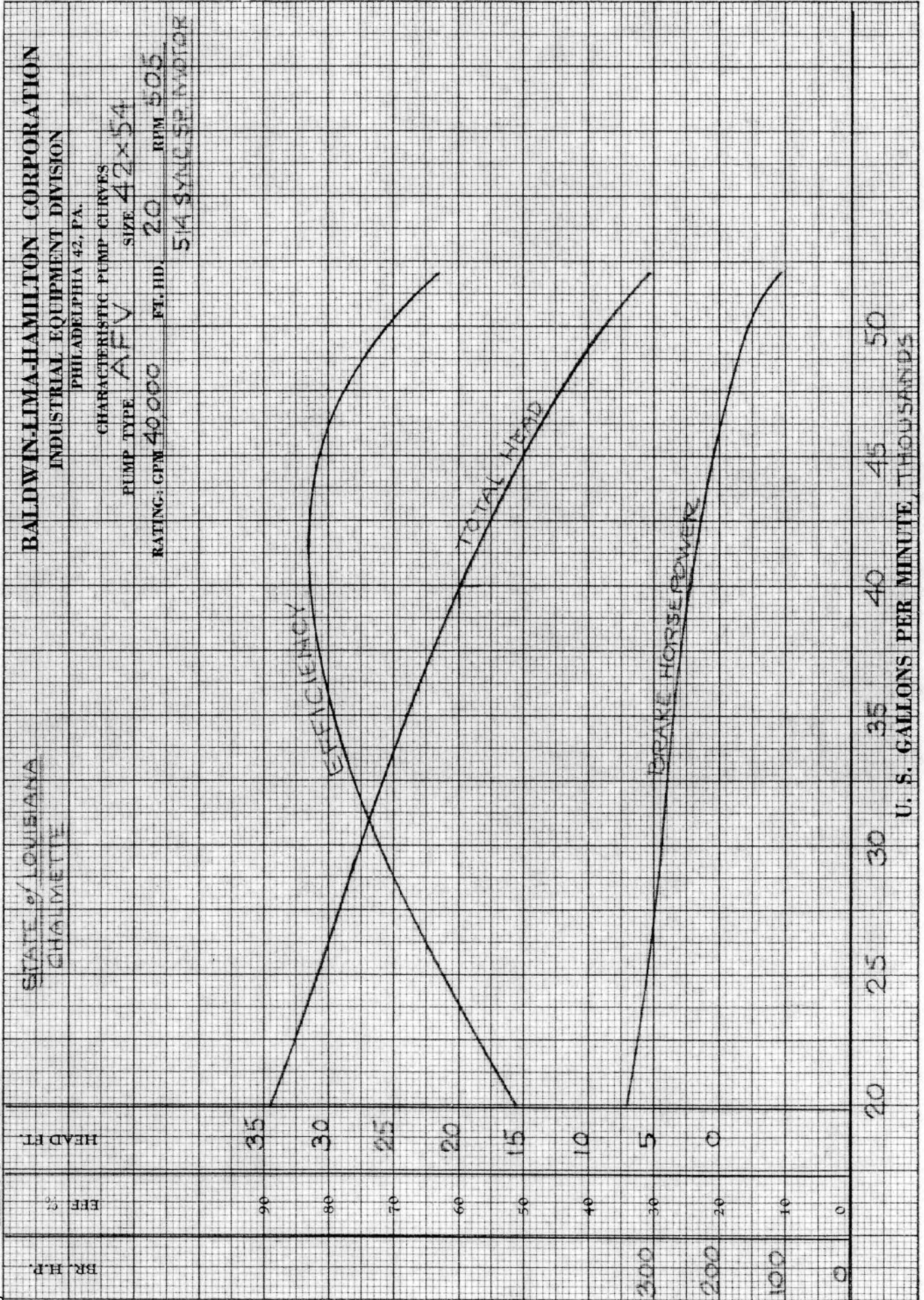
BALDWIN-LIMA-HAMILTON CORPORATION
 INDUSTRIAL EQUIPMENT DIVISION
 PHILADELPHIA 42, PA.
 CHARACTERISTIC PUMP CURVES
 PUMP TYPE **AFV** SIZE **94x128**
 RATING: GPM **200,000** FT. HD. **19** RPM **212**

STATE of LOUISIANA
 CHALMETTE

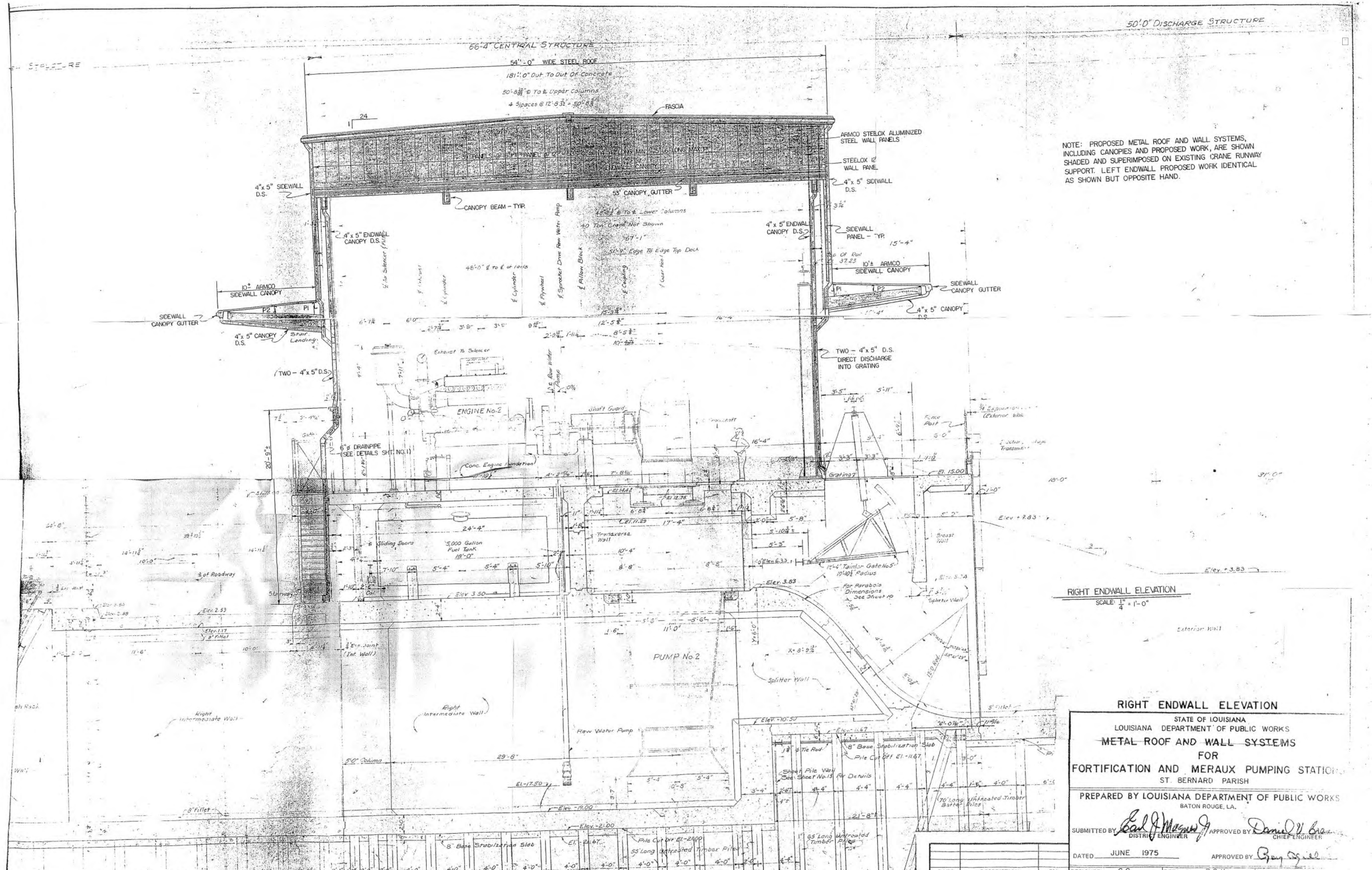
U. S. GALLONS PER MINUTE, THOUSANDS

CURVE NO. F 15915

REF. 51343-550



66'-4" CENTRAL STRUCTURE



NOTE: PROPOSED METAL ROOF AND WALL SYSTEMS, INCLUDING CANOPIES AND PROPOSED WORK, ARE SHOWN SHADED AND SUPERIMPOSED ON EXISTING CRANE RUNWAY SUPPORT. LEFT ENDWALL PROPOSED WORK IDENTICAL AS SHOWN BUT OPPOSITE HAND.

RIGHT ENDWALL ELEVATION
SCALE: 1/4" = 1'-0"

RIGHT ENDWALL ELEVATION

STATE OF LOUISIANA
LOUISIANA DEPARTMENT OF PUBLIC WORKS
METAL ROOF AND WALL SYSTEMS
FOR
FORTIFICATION AND MERAUX PUMPING STATION
ST. BERNARD PARISH

PREPARED BY LOUISIANA DEPARTMENT OF PUBLIC WORKS
BATON ROUGE, LA.

SUBMITTED BY *Carl J. Massey* DISTRICT ENGINEER APPROVED BY *Daniel V. Crain* CHIEF ENGINEER

DATED JUNE 1975 APPROVED BY *Ray Sigall*

DATE	DESCRIPTION	BY	DESIGNED	G.G.	DETAILED	P.G.K.	TRACED
	REVISIONS		CHECKED	A.E.S.	CHECKED	G.G.	CHECKED
			APPROVED				

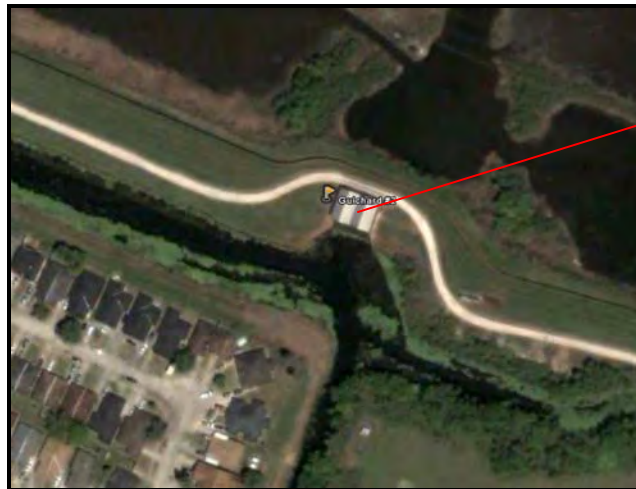
SHEET 3 OF 9 SHEETS



Pre-Hurricane Katrina – View from the south end

**4201 Jean Lafitte Pkwy.
Chalmette, LA 70043
504.512.6331**

Position: Latitude 29.961649° Longitude -89.964442°



PS2 Guichard

Pre-Hurricane Katrina – Aerial view of pump station

Pump Station Description

Guichard is 1 of 8 pumping stations in St Bernard Parish owned and operated by the Lake Borne Basin Levee District. The station contains four horizontal pumps that were installed in the 1950's with a total pumping capacity of approximately 755 cubic feet per second (cfs)¹. All four pumps are driven by diesel engines. The drainage water is supplied to the pumps from the Florida Walk canal and discharges through the interior back levee to the marsh known as Bayou Bienvenue.

¹ The Pump Information Table contains more details about the individual pump data and is located at the beginning of this section.

There was not enough information available to determine the rated capacity for pump 3. It was assumed it would be similar to the pump 1 (42") based on the available information.

Pump Station Operation

This pump station was available but not used in the days before Hurricane Katrina.

Fuel Endurance Calculation

Assumptions :

- 1) #2 Diesel fuel is used with an HHV rating of 140,000 btu/gal
- 2) Burn rate of 35 gph @ 500 kW with above HHV rating
- 3) Diesel engines are running at rated capacity

PS 2 Guichard

4 pump drivers - All diesels

2 diesels are 800 hp, 1 diesel is 335 hp, and 1 is approximately 300 hp

The approximate burn rate for each diesel is then calculated at:

$$R1_{\text{burn}} := \left(35 \frac{\text{gal}}{\text{hr}} \right) \cdot \frac{800\text{hp}}{500\text{kW}} \qquad R1_{\text{burn}} = 41.75 \frac{\text{gal}}{\text{hr}}$$

$$R2_{\text{burn}} := \left(35 \frac{\text{gal}}{\text{hr}} \right) \cdot \frac{335\text{hp}}{500\text{kW}} \qquad R2_{\text{burn}} = 17.48 \frac{\text{gal}}{\text{hr}}$$

$$R3_{\text{burn}} := \left(35 \frac{\text{gal}}{\text{hr}} \right) \cdot \frac{300\text{hp}}{500\text{kW}} \qquad R3_{\text{burn}} = 15.66 \frac{\text{gal}}{\text{hr}}$$

Fuel Capacity

1 - 5,000 gallon tank

4 - 60 gallon day tanks

Fuel Endurance

The time the 5,000 gallon tank will last is calculated:

$$t_1 := \frac{5000\text{gal}}{R1_{\text{burn}} + R2_{\text{burn}} + R3_{\text{burn}}} \qquad t_1 = 66.75 \text{ hr}$$

The time the 60 gallon tanks will last is calculated:

$$t_2 := \frac{4 \cdot 60\text{gal}}{R1_{\text{burn}} + R2_{\text{burn}} + R3_{\text{burn}}} \qquad t_2 = 3.204 \text{ hr}$$

The approximate total continuous run time for the station is:

$$T_t := t_1 + t_2 \qquad \boxed{T_t = 69.95 \text{ hr}}$$

$$\boxed{T_t = 2.915 \text{ day}}$$

Pump Curves

Pump curves were obtained from the manufacturer of the pumps. Serial numbers were unobtainable, and therefore only by making assumptions regarding the size and make of the pump as well as the similarity to that of PS 3 Bayou Villere and PS 5 E.J. Gore were any usable curves located. There was no usable information regarding pump 3, so it was assumed similar to

pump 1. From these curves, a curve fit process was used to create new curves and equations. From these curves, further assumptions were made regarding the dimensions of the pump station, pipe, and pumps so that friction and minor losses could be calculated. These calculations created the system curves. There are two curves using the maximum and minimum reported operating heads by the parish.

Reverse Flow

The Engineering Hydraulics Design section of the US Army Corps of Engineers Portland District office performed analysis of reverse flow characteristics for each pump. The results are reverse flow rating curves that are attached to this section. The tables present the flow rates per individual pump. The detailed calculations, assumptions, and assumed dimensions are available upon request.

Katrina Event

This station was designated as a backup and therefore was not used prior to Hurricane Katrina. After the hurricane the pump station could not be operated as the motors were overtopped with water.

Damage Report

The following information was obtained from the Project Information Report (PIR) for New Orleans District:

Pump Station 2 sustained substantial damage. With its operating floor at or near the natural ground elevation, the pump station was flooded to a depth of 6 to 7 feet. The four diesel engines were flooded along with control panels, compressors, motors, and vacuum pumps. The diesel fuel storage tank was moved off its concrete saddle foundation. All exterior and interior lighting was damaged. While the existing building was in poor condition prior to the storm, the wind and water caused additional damage to all four sides of the building and the building roof.



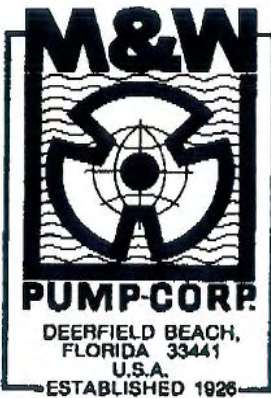
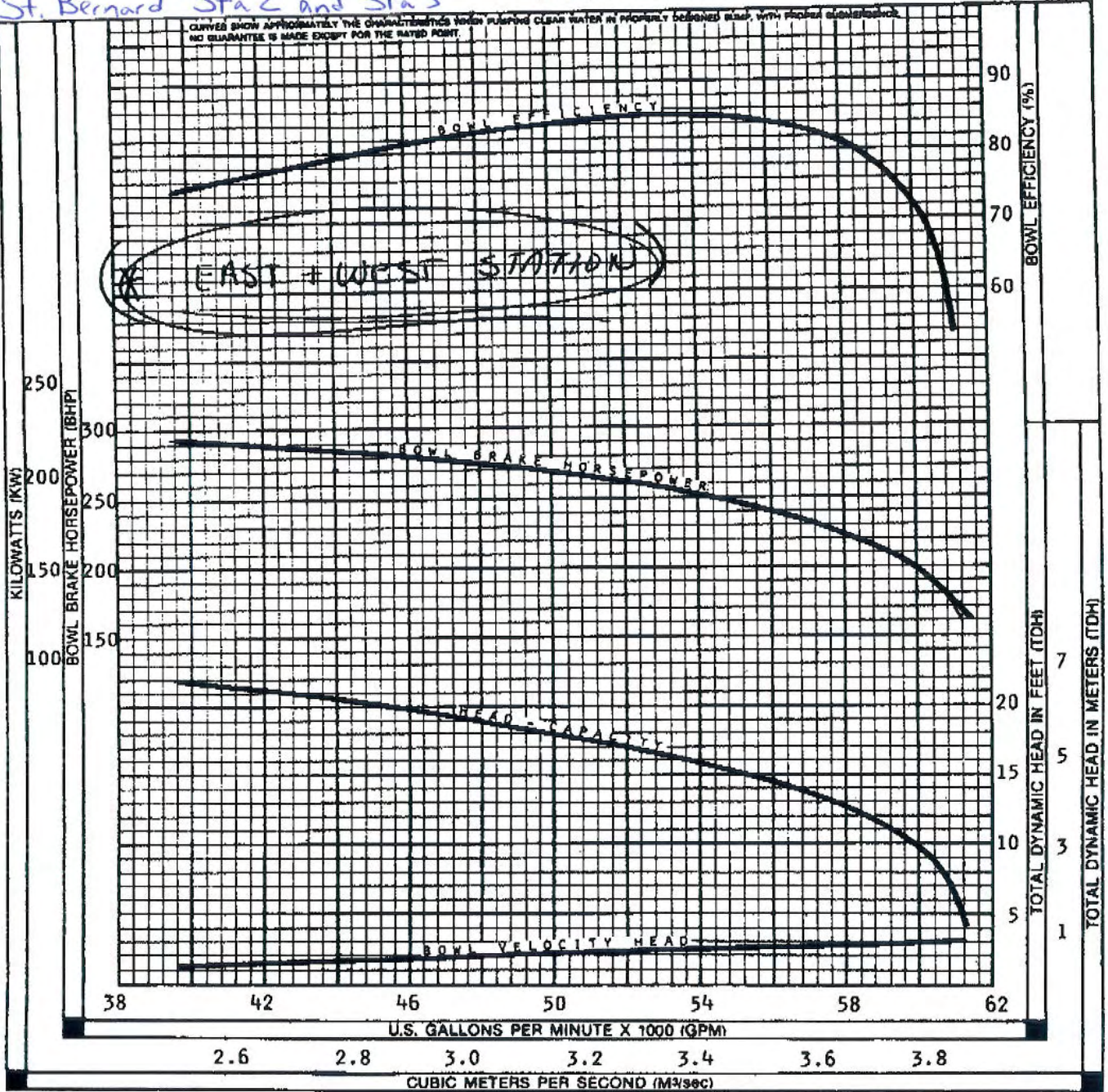
Post-Hurricane Katrina – View from the North



PS2 Guichard

Post-Hurricane Katrina – Aerial view of the pump station

St. Bernard Sta 2 and Sta 3



PUMP BOWL PERFORMANCE CURVE	
TYPE: AXIAL FLOW	PROPELLER DIA.: 42"
MODEL NO.: NC342P25	SPEED (RPM): 409
INTAKE DIA.: 63"	DISCHARGE COLUMN DIA.: 42"
CURVE NO.: CS4225	Ns: 12,050 CODE: 50
SINGLE STAGE FOR TWO STAGES MULTIPLY HEAD AND HORSEPOWER BY 2.0 AND EFFICIENCY BY 1.0	
PERFORMANCE BASED ON PUMPING CLEAR COLD NON-AERATED WATER, SPECIFIC GRAVITY 1.0, TEMPERATURE 65 DEGREES (FAHRENHEIT) OR LESS, AT SEA LEVEL. PERFORMANCE MAY BE AFFECTED BY HIGHER TEMPERATURES, SPECIFIC GRAVITIES, ALTITUDES, AND SUMP CONDITIONS.	

IT IS HEREBY CERTIFIED THAT THIS CURVE REPRESENTS THE TRUE PERFORMANCE CHARACTERISTICS OF THE M&W PUMP MODEL SHOWN AND WAS OBTAINED BY SCALE MODEL TEST AND CALCULATIONS IN ACCORDANCE WITH STANDARDS OF THE HYDRAULIC INSTITUTE.

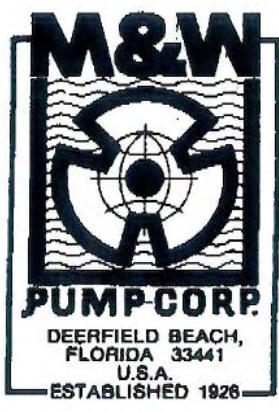
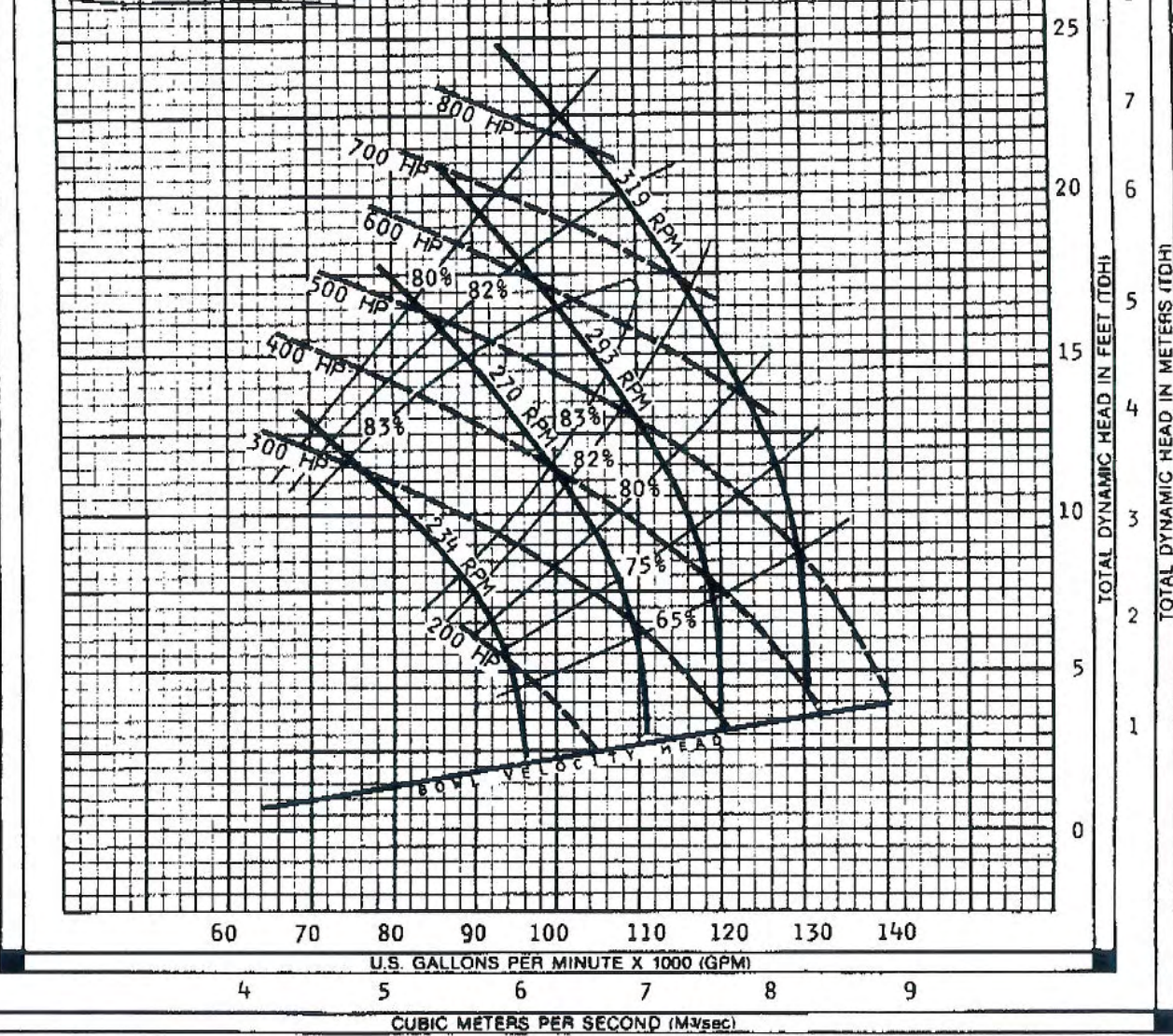


© All rights reserved, M&W PUMP CORPORATION 1985

PS#2 Pumps 2+4; PS#3 Pump

CURVES SHOW APPROXIMATELY THE CHARACTERISTICS WHEN PUMPING CLEAR WATER IN PROPERLY DESIGNED PUMP WITH PROPER SUBMERGENCE.
NO GUARANTEE IS MADE EXCEPT FOR THE RATED POINT.
HORSEPOWERS (HP) SHOWN REPRESENT NOMINAL RECOMMENDED ELECTRIC MOTOR SIZES.
PERCENTAGES (%) SHOWN REPRESENT BOWL EFFICIENCIES.

all 60" pumps

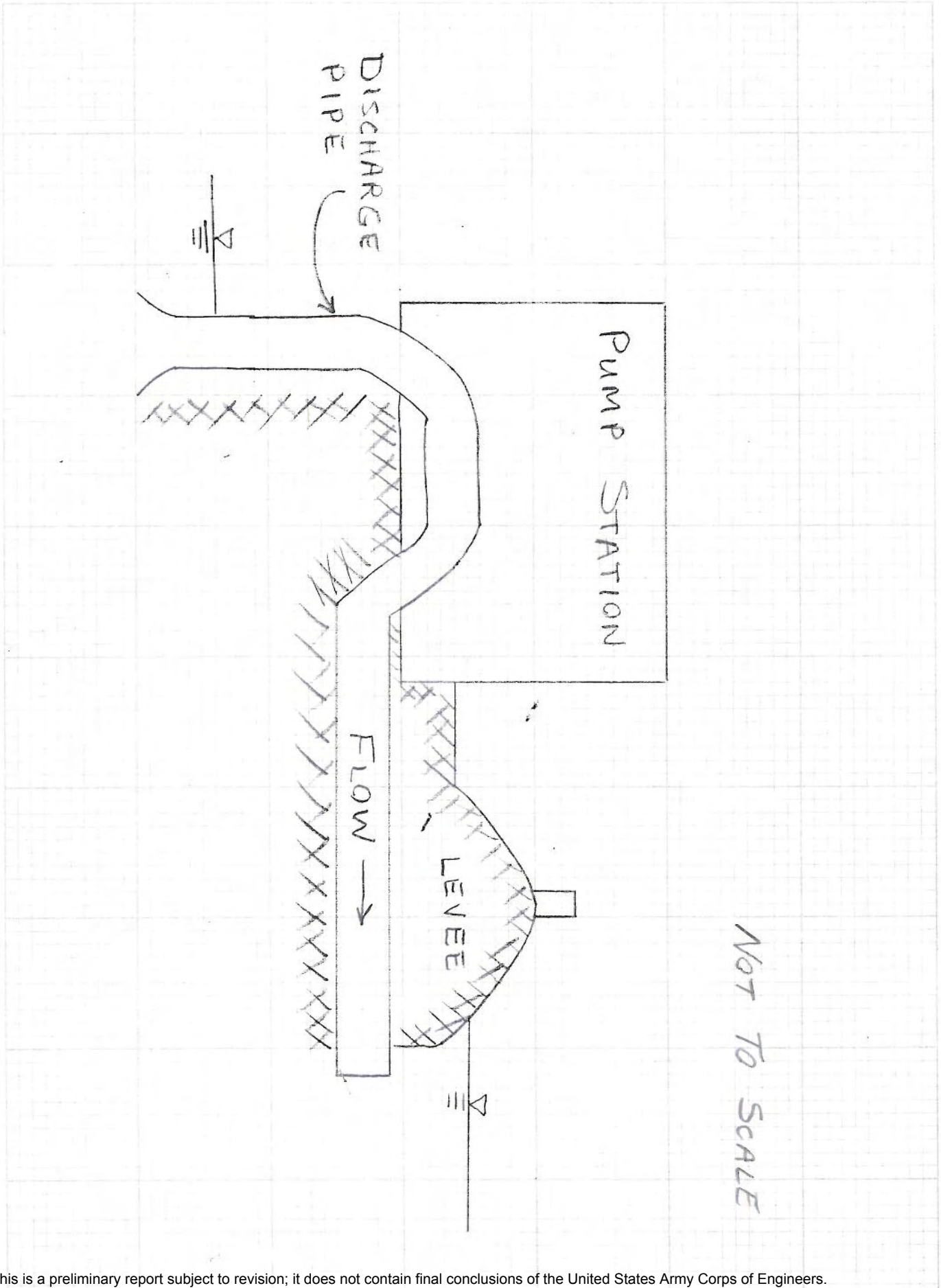


PUMP BOWL PERFORMANCE CURVE VARIABLE SPEED	
TYPE: AXIAL FLOW	PROPELLER DIA.: 60"
MODEL NO.: NC360P12	SPEED (RPM): AS NOTED
INTAKE DIA.: 90"	DISCHARGE COLUMN DIA.: 60"
CURVE NO.: VS60P12	Ng: 11,900 CODE: 50
SINGLE STAGE FOR TWO STAGES MULTIPLY HEAD AND HORSEPOWER BY 2.0 AND EFFICIENCY BY 1.0	
PERFORMANCE BASED ON PUMPING CLEAR COLD NON-AERATED WATER, SPECIFIC GRAVITY 1.0, TEMPERATURE 65 DEGREES (FAHRENHEIT) OR LESS, AT SEA LEVEL. PERFORMANCE MAY BE AFFECTED BY HIGHER TEMPERATURES, SPECIFIC GRAVITIES, ALTITUDES, AND PUMP CONDITIONS.	

IT IS HEREBY CERTIFIED THAT THIS CURVE REPRESENTS THE TRUE PERFORMANCE CHARACTERISTICS OF THE M&W PUMP MODEL SHOWN AND WAS OBTAINED BY SCALE MODEL TEST AND CALCULATIONS IN ACCORDANCE WITH STANDARDS OF THE HYDRAULIC INSTITUTE.



† All rights reserved, M&W PUMP CORPORATION 1985





Pre-Hurricane Katrina - View to the North

**3700 Bartolo
Meraux, LA 70075
504.512.6331**

Position: Latitude 29.951279° Longitude -89.934607°



PS3 Bayou Villere

Pre-Hurricane Katrina – Arial view of pump station

Pump Station Description

Bayou Villere is 1 of 8 pumping stations in St Bernard Parish owned and operated by the Lake Borne Basin Levee District. The station contains three horizontal pumps that were installed in the 1950's with a total pumping capacity of 800 cubic feet per second (cfs)¹. All three pumps are driven by diesel engines. The drainage water is supplied to the pumps from the Forty Arpent

¹ The Pump Information Table contains more details about the individual pump data and is located at the beginning of this section.

canal and discharges through the interior back levee to the marsh known as Bayou Villere. Pumps 1 and 2 have butterfly valves on the inlet piping leading to the pump to cut off water flow in either direction.

Pump Station Operation

This pump station is designated as a back up and therefore was not used in the days leading up to Hurricane Katrina.

Fuel Endurance Calculation

Assumptions:

- 1) #2 Diesel fuel is used with an HHV rating of 140,000 btu/gal
- 2) Burn rate of 35 gph @ 500 kW with above HHV rating
- 3) Diesel engines are running at rated capacity

PS 3 Bayou Villere

3 pump drivers - All diesels

Diesels are 800 hp

The approximate burn rate for each diesel is then calculated at:

$$R_{\text{burn}} := \left(35 \frac{\text{gal}}{\text{hr}} \right) \cdot \frac{800\text{hp}}{500\text{kW}} \qquad R_{\text{burn}} = 41.75 \frac{\text{gal}}{\text{hr}}$$

Fuel Capacity

1 - 2500 gallon tank

3 - 60 gallon day tanks

Fuel Endurance

The time the 2500 gallon tank will last is calculated:

$$t_1 := \frac{2500\text{gal}}{3R_{\text{burn}}} \qquad t_1 = 19.95\text{hr}$$

The time the 60 gallon tank will last is calculated:

$$t_2 := \frac{3 \cdot 60\text{gal}}{3R_{\text{burn}}} \qquad t_2 = 1.43\text{hr}$$

The approximate total continuous run time for the station is:

$$T_t := t_1 + t_2 \qquad T_t = 21.39\text{hr}$$

$$T_t = 0.89\text{day}$$

Pump Curves

Pump capacity curves were obtained. From these curves, a curve fit process was used to create new curves and equations. During the data collection, only one pump serial number was found, so the others were assumed to be similar. Using manufacturer data and making assumptions regarding the dimensions of the pump station and pump, as well as other necessary assumptions, the minor and friction losses were calculated so that system curves could be created. Two curves were made due to the range of operating heads reported from the parish. The two curves represent the maximum and minimum operating heads reported.

Reverse Flow

The Engineering Hydraulics Design section of the US Army Corps of Engineers Portland District office performed analysis of reverse flow characteristics for each pump. The results are reverse flow rating curves that are attached to this section. The tables present the flow rates per individual pump. The detailed calculations, assumptions, and assumed dimensions are available upon request.

Katrina Event

This station was designated as a backup and therefore was not used prior to Hurricane Katrina. After the hurricane the pump station could not be operated as the motors were overtopped with water.

Damage Report

The following information was obtained from the Project Information Report (PIR) for New Orleans District:

Pump Station 3 sustained substantial damage. With its operating floor at or near the natural ground elevation, the pump station was flooded to a depth of 8 feet. The three diesel engines and hydraulic drives were flooded along with the vacuum pump system and ancillary equipment. The diesel fuel storage tank was moved off its foundation. All exterior and interior lighting was damaged. While the existing building was in poor condition prior to the storm, the wind and water caused additional damage to all four sides of the building.



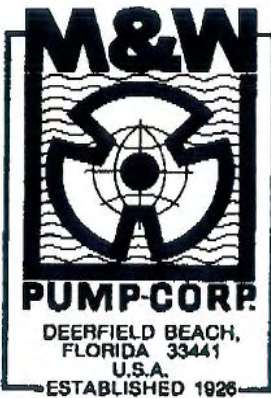
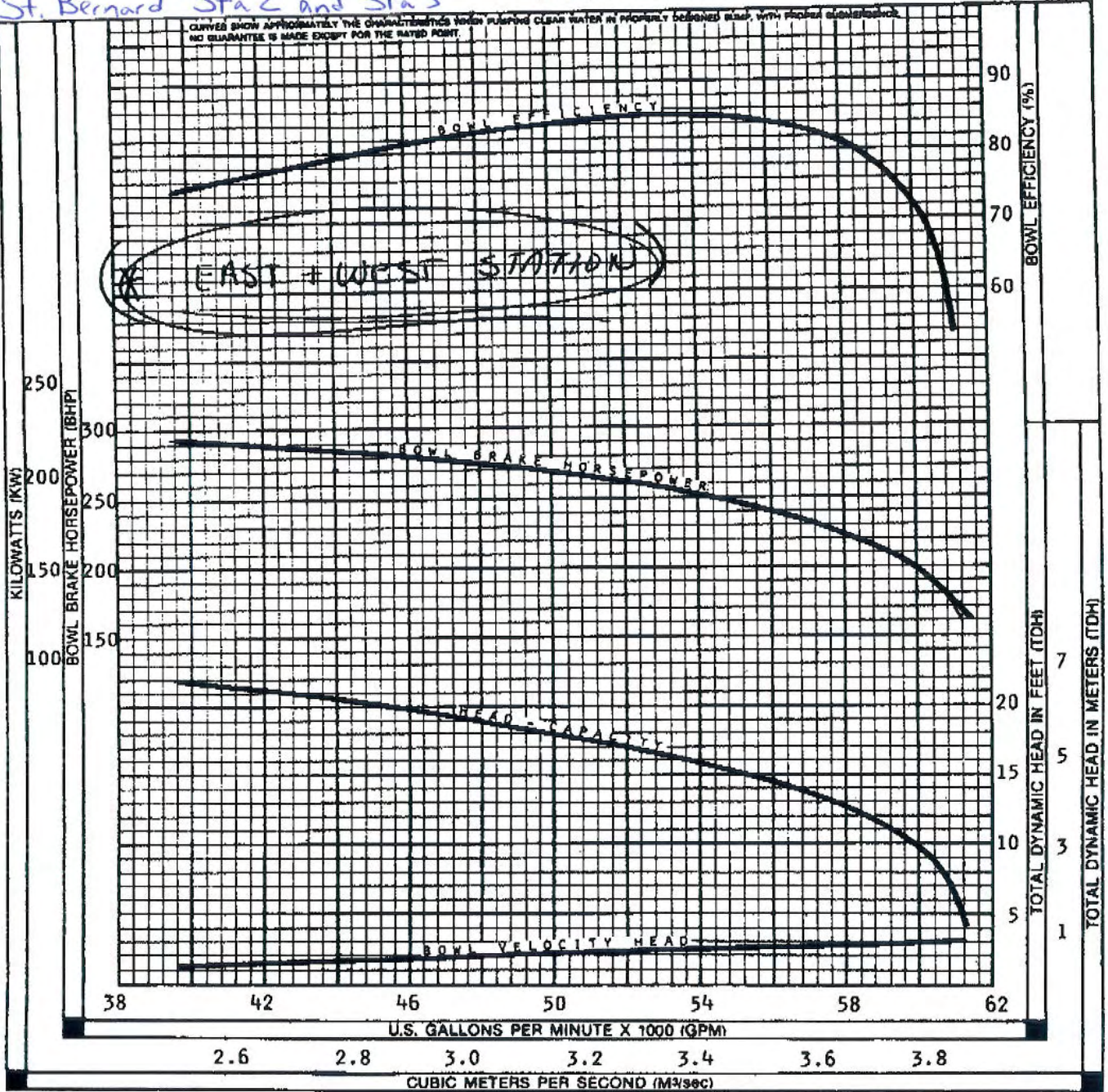
Post-Hurricane Katrina – View to the South



PS3 Bayou Villere

Post-Hurricane Katrina – Arial view of the pump station

St. Bernard Sta 2 and Sta 3



PUMP BOWL PERFORMANCE CURVE	
TYPE: AXIAL FLOW	PROPELLER DIA.: 42"
MODEL NO.: NC342P25	SPEED (RPM): 409
INTAKE DIA.: 63"	DISCHARGE COLUMN DIA.: 42"
CURVE NO.: CS4225	Ns: 12,050 CODE: 50
SINGLE STAGE FOR TWO STAGES MULTIPLY HEAD AND HORSEPOWER BY <u>2.0</u> AND EFFICIENCY BY <u>1.0</u>	
PERFORMANCE BASED ON PUMPING CLEAR COLD NON-AERATED WATER, SPECIFIC GRAVITY 1.0, TEMPERATURE 65 DEGREES (FAHRENHEIT) OR LESS, AT SEA LEVEL. PERFORMANCE MAY BE AFFECTED BY HIGHER TEMPERATURES, SPECIFIC GRAVITIES, ALTITUDES, AND SUMP CONDITIONS.	

IT IS HEREBY CERTIFIED THAT THIS CURVE REPRESENTS THE TRUE PERFORMANCE CHARACTERISTICS OF THE M&W PUMP MODEL SHOWN AND WAS OBTAINED BY SCALE MODEL TEST AND CALCULATIONS IN ACCORDANCE WITH STANDARDS OF THE HYDRAULIC INSTITUTE.

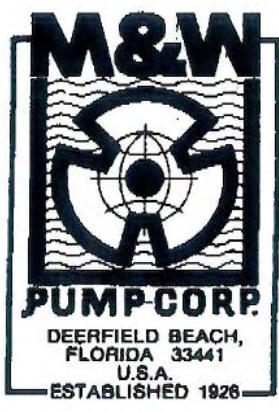
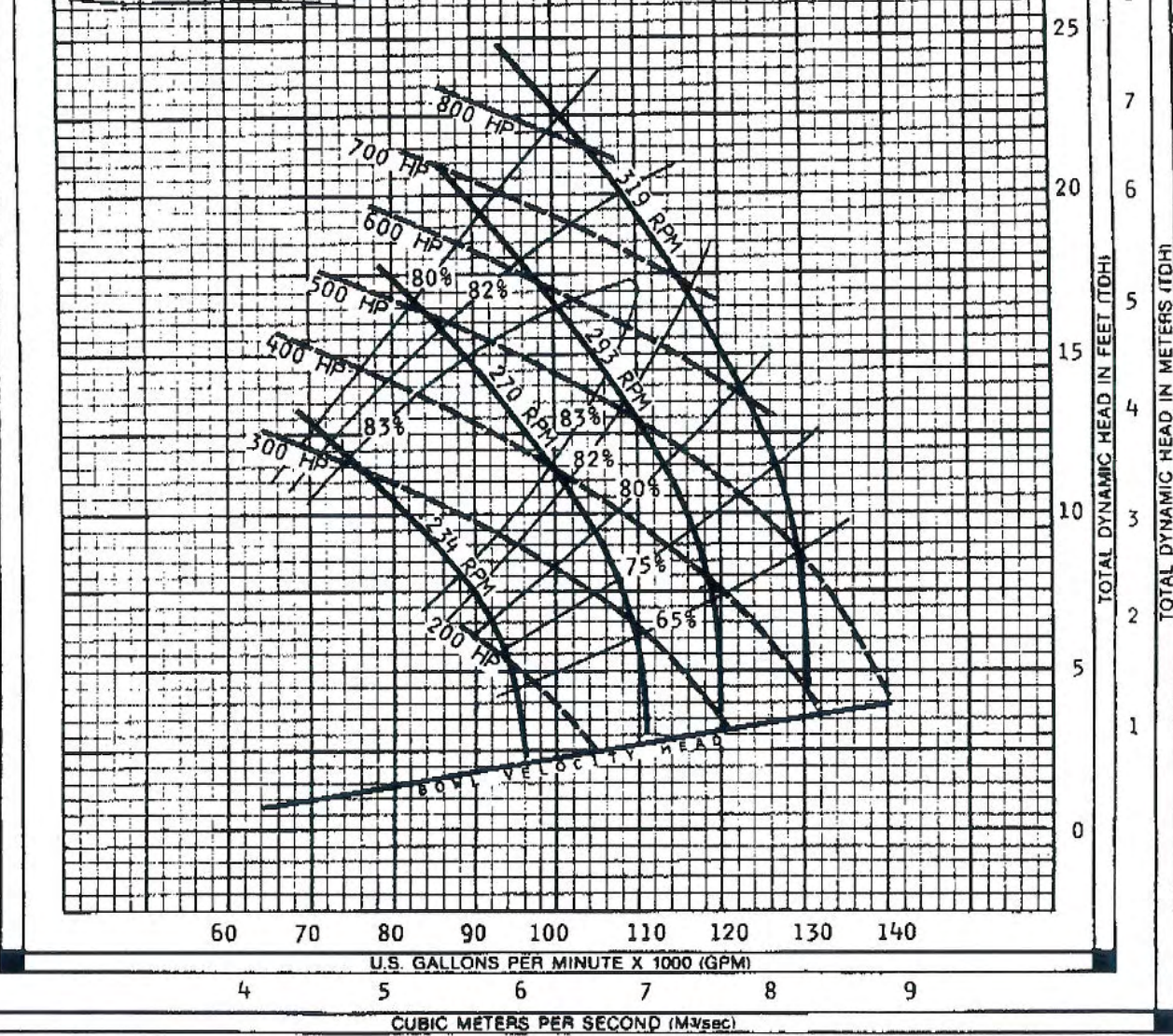


© All rights reserved, M&W PUMP CORPORATION 1985

PS#2 Pumps 2+4; PS#3 Pump

CURVES SHOW APPROXIMATELY THE CHARACTERISTICS WHEN PUMPING CLEAR WATER IN PROPERLY DESIGNED PUMP WITH PROPER SUBMERGENCE.
NO GUARANTEE IS MADE EXCEPT FOR THE RATED POINT.
HORSEPOWERS (HP) SHOWN REPRESENT NOMINAL RECOMMENDED ELECTRIC MOTOR SIZES.
PERCENTAGES (%) SHOWN REPRESENT BOWL EFFICIENCIES.

all 60" pumps

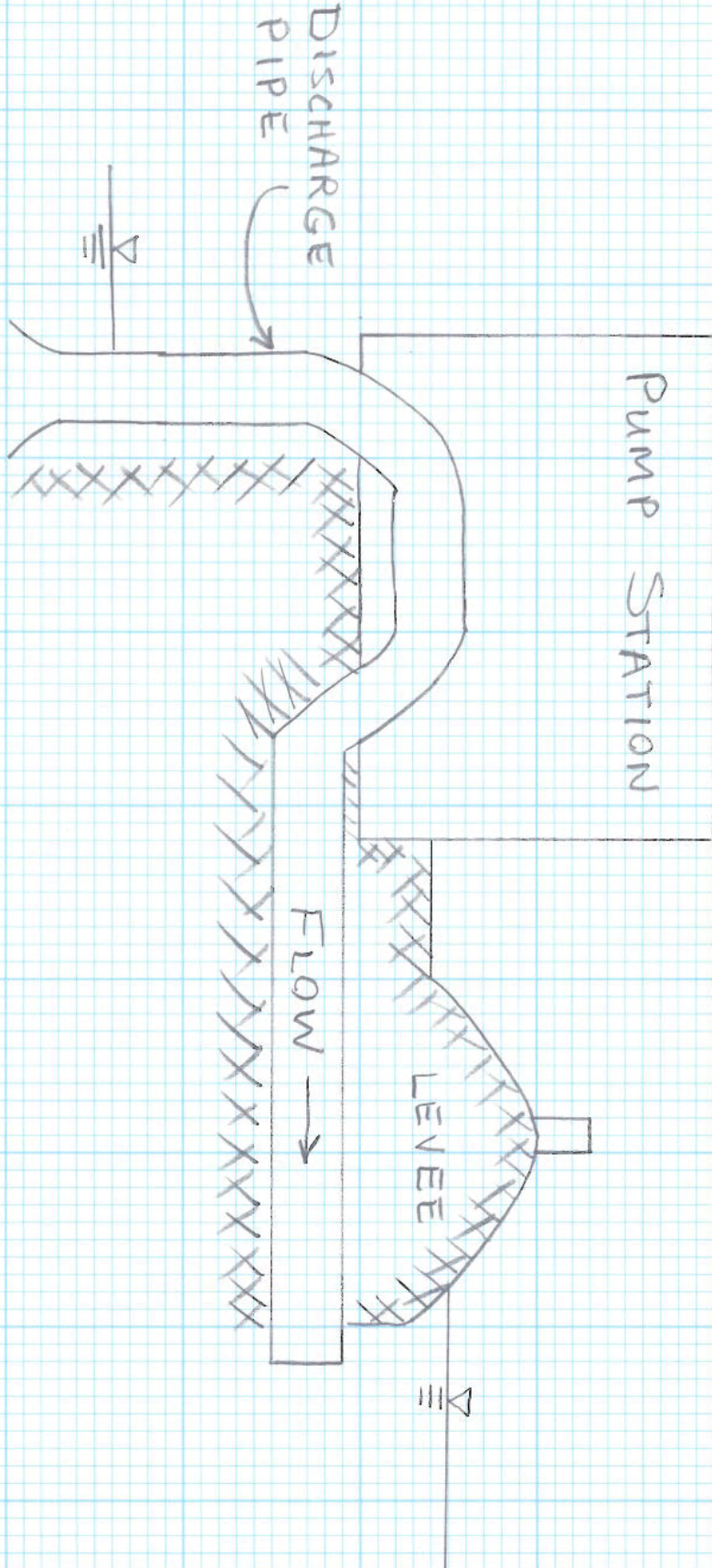


PUMP BOWL PERFORMANCE CURVE VARIABLE SPEED	
TYPE: AXIAL FLOW	PROPELLER DIA.: 60"
MODEL NO.: NC360P12	SPEED (RPM): AS NOTED
INTAKE DIA.: 90"	DISCHARGE COLUMN DIA.: 60"
CURVE NO.: VS60P12	Ng: 11,900 CODE: 50
SINGLE STAGE FOR TWO STAGES MULTIPLY HEAD AND HORSEPOWER BY 2.0 AND EFFICIENCY BY 1.0	
PERFORMANCE BASED ON PUMPING CLEAR COLD NON-AERATED WATER, SPECIFIC GRAVITY 1.0, TEMPERATURE 65 DEGREES (FAHRENHEIT) OR LESS, AT SEA LEVEL. PERFORMANCE MAY BE AFFECTED BY HIGHER TEMPERATURES, SPECIFIC GRAVITIES, ALTITUDES, AND PUMP CONDITIONS.	

IT IS HEREBY CERTIFIED THAT THIS CURVE REPRESENTS THE TRUE PERFORMANCE CHARACTERISTICS OF THE M&W PUMP MODEL SHOWN AND WAS OBTAINED BY SCALE MODEL TEST AND CALCULATIONS IN ACCORDANCE WITH STANDARDS OF THE HYDRAULIC INSTITUTE.



† All rights reserved, M&W PUMP CORPORATION 1985



NOT TO SCALE



Pre-Hurricane Katrina – View from Inlet Canal

**3200 Guerra Dr.
Violet, LA 70092
504.512.6331**

Position: Latitude 29.921331° Longitude -89.891292°



PS 4 - Meraux

Pre-Hurricane Katrina – Aerial view of pump station

Pump Station Description

Meraux is 1 of 8 pumping stations in St Bernard Parish owned and operated by the Lake Borne Basin Levee District. The station contains three vertical pumps that were installed in 1972 with a total pumping capacity of 980 cubic feet per second (cfs)¹. Two of the pumps are driven by diesel engines and one by an electric motor. The drainage water is supplied to the pumps from the Forty Arpent canal and discharges through the interior back levee to the marsh known as

¹ The Pump Information Table contains more details about the individual pump data and is located at the beginning of this section.

Bayou Dupre. The individual pump discharges have a tainter gates installed to cut off water flow in either direction.

Pump Station Operation

Pump station operators will turn the pumps on as they are required to reduce the water elevation in the canal. The pumps are normally turned on when the water in the canal reaches approximately -6 feet (NGVD) and turned off when the water level reaches -6.5 feet (NGVD). When heavy rainfall events are expected the station operators will pump the canal down to an elevation of -8.5 feet (NGVD). If the water elevation on the discharge side of the pump station is predicted to exceed 3.5 feet (NGVD) the station operator closes the discharge tainter gates.

Fuel Endurance Calculation

Assumptions :

- 1) #2 Diesel fuel is used with an HHV rating of 140,000 btu/gal
- 2) Burn rate of 35 gph @ 500 kW with above HHV rating
- 3) Diesel engines are running at rated capacity

PS 4 Meraux

3 pump drivers - 2 are diesels and 1 is electric

The 2 diesels are 1200 hp

The approximate burn rate for each diesel is then calculated at:

$$R_{\text{burn}} := \left(35 \frac{\text{gal}}{\text{hr}} \right) \cdot \frac{1200 \text{hp}}{500 \text{kW}} \qquad R_{\text{burn}} = 62.639 \frac{\text{gal}}{\text{hr}}$$

Fuel Capacity

4 - 5000 gallon tanks

2 - 110 gallon day tanks

Fuel Endurance

The time the 5000 gallon tanks will last is calculated:

$$t_1 := \frac{4 \cdot 5000 \text{gal}}{2 R_{\text{burn}}} \qquad t_1 = 159.64 \text{hr}$$

The time the 110 gallon tanks will last is calculated:

$$t_2 := \frac{2 \cdot 110 \text{gal}}{2 R_{\text{burn}}} \qquad t_2 = 1.75 \text{hr}$$

The approximate total continuous run time for the station is:

$$T_t := t_1 + t_2 \qquad T_t = 161.40 \text{hr}$$

$$T_t = 6.725 \text{day}$$

Pump Curves

Pump capacity curves were obtained either from the parish or from the manufacturer of each pump. From these curves, a curve fit process was used to create new curves and equations.

Using drawings provided, assumptions were made regarding the dimensions of the pump station and the pump. Using these assumptions, the minor and friction losses were calculated in order to create the system curve. Two system curves were created due to the range of heads reported by the parish. The two curves represent the maximum and minimum operating heads reported.

Reverse Flow

The Engineering Hydraulics Design section of the US Army Corps of Engineers Portland District office performed analysis of reverse flow characteristics for each pump. The results are reverse flow rating curves that are attached to this section. The tables present the flow rates per individual pump. The detailed calculations, assumptions, and assumed dimensions are available upon request.

Katrina Event

8/28/05 - Operators pumped water in canal down to approximately -8.5 feet (NGVD).

8/29/05 - Operators evacuated pump station at approximately 1:15 am.

9/03/05 - Operators returned to pump water down.

9/09/05 - **Pump Station back to normal operation.**

Damage Report

The following information was obtained from the Project Information Report (PIR) for New Orleans District:

Pump Station 4 sustained relatively minor damage because its operating floor elevation is 16 feet N.G.V.D. Flooding from the storm flooded the lower level of the station but the flood waters were approximately three feet below the concrete operating floor level. Pump station equipment that was damaged includes an air compressor, electromode heater, controller for compressed air dryer motor, and generator. The building sustained damage to metal siding and roof. Finally, one discharge flap gate was damaged and is not operational.



Post-Hurricane Katrina – View from the inlet canal



PS 4 - Meraux

Post-Hurricane Katrina – Aerial view of the pump station

CURVE NO. F-15915

F-15915

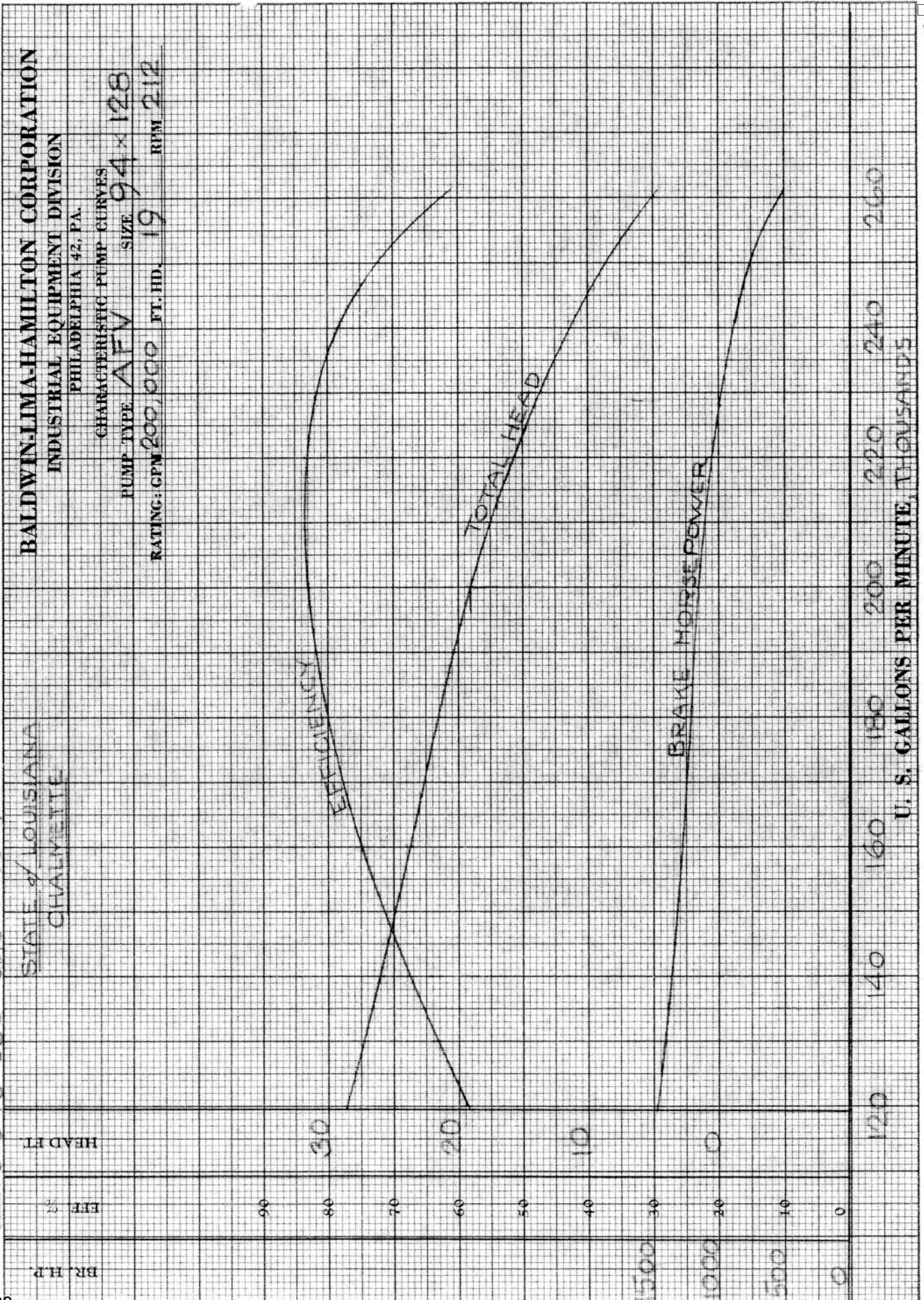
REF. 51343-550 548x1-15-4

STATE of LOUISIANA
CHALMETTE

BALDWIN-LIMA-HAMILTON CORPORATION
INDUSTRIAL EQUIPMENT DIVISION
PHILADELPHIA 42, PA.

CHARACTERISTIC PUMP CURVES

PUMP TYPE AFV SIZE 94x128
RATING: GPM 200,000 FT. HD. 19 RPM 212

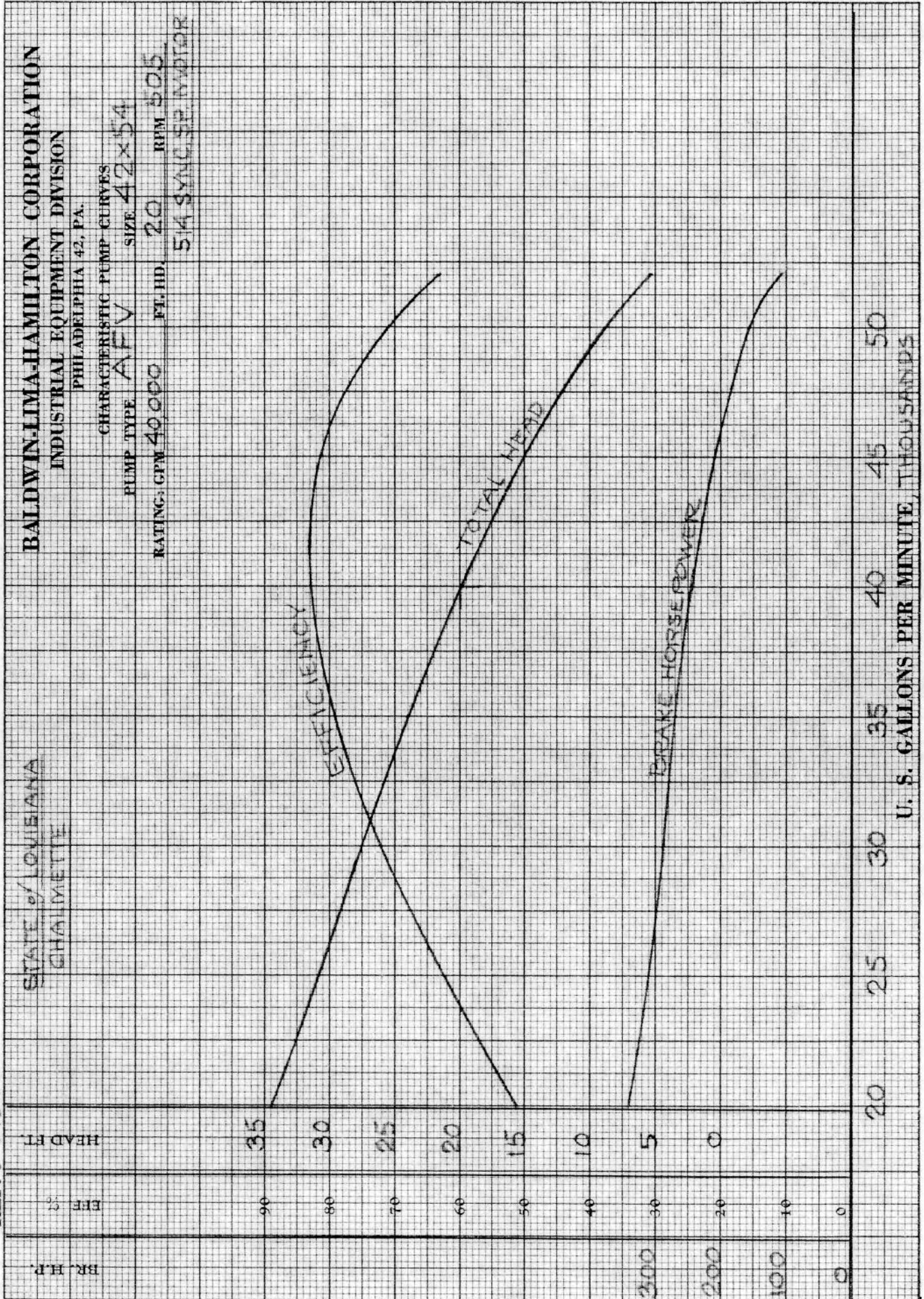


U. S. GALLONS PER MINUTE, THOUSANDS

CURVE NO. F 15915

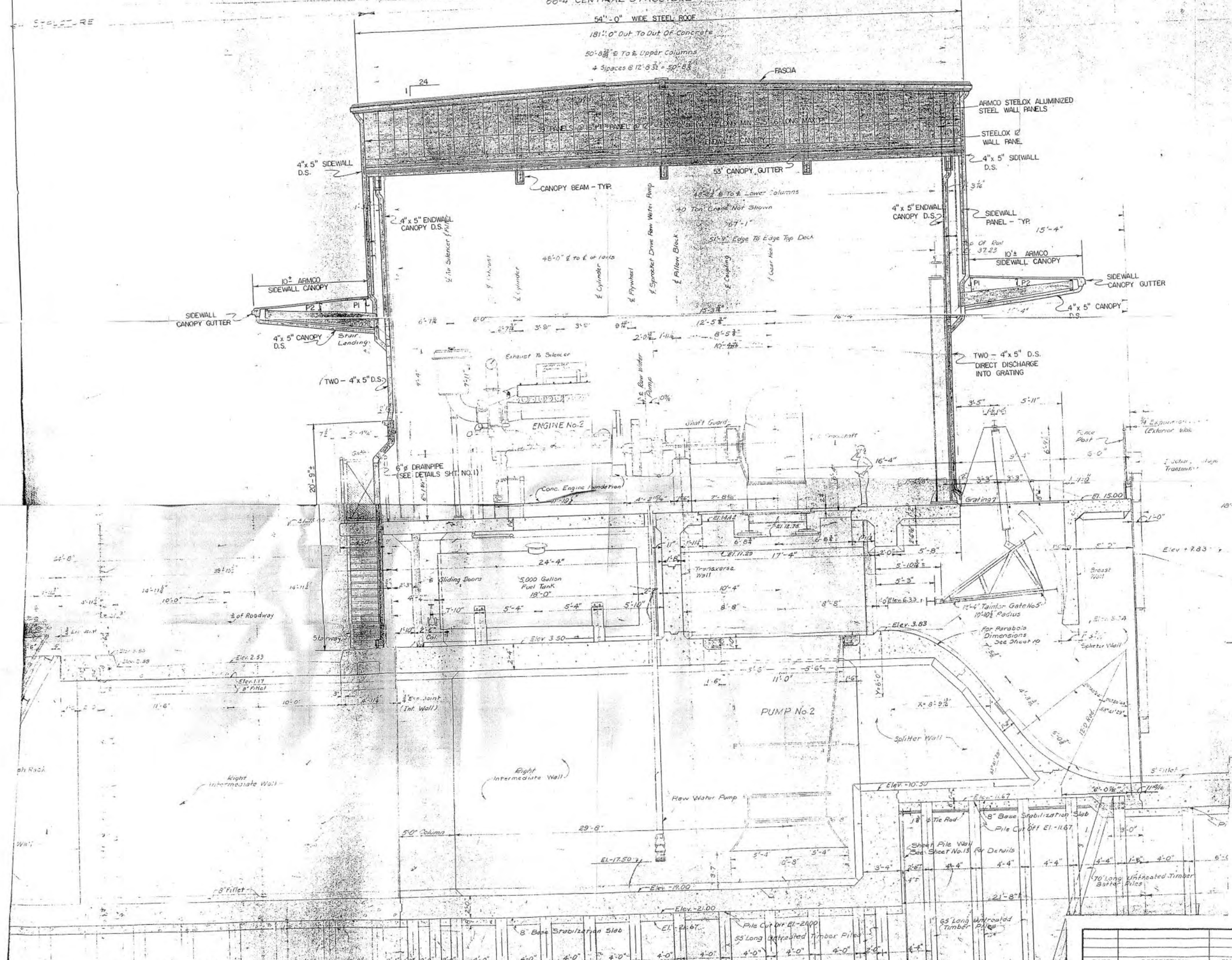
CURVE NO. F-15914

REF. 51243-550



CURVE NO. F-15914

66'-4" CENTRAL STRUCTURE



NOTE: PROPOSED METAL ROOF AND WALL SYSTEMS, INCLUDING CANOPIES AND PROPOSED WORK, ARE SHOWN SHADED AND SUPERIMPOSED ON EXISTING CRANE RUNWAY SUPPORT. LEFT ENDWALL PROPOSED WORK IDENTICAL AS SHOWN BUT OPPOSITE HAND.

RIGHT ENDWALL ELEVATION
SCALE: 1/4" = 1'-0"

RIGHT ENDWALL ELEVATION

STATE OF LOUISIANA
LOUISIANA DEPARTMENT OF PUBLIC WORKS
METAL ROOF AND WALL SYSTEMS
FOR
FORTIFICATION AND MERAUX PUMPING STATION
ST. BERNARD PARISH

PREPARED BY LOUISIANA DEPARTMENT OF PUBLIC WORKS
BATON ROUGE, LA.

SUBMITTED BY *Carl J. Massey* DISTRICT ENGINEER APPROVED BY *Daniel V. Crain* CHIEF ENGINEER

DATED JUNE 1975 APPROVED BY *Greg Sigall*

DATE	DESCRIPTION	BY
DESIGNED	G.G.	P.G.K.
CHECKED	A.E.S.	G.G.
APPROVED		

TRACED []
CHECKED []
SHEET 3 OF 9 SHEETS



Pre-Hurricane Katrina – View to the North

**7701 East Judge Perez Dr.
Violet, LA 70085
504.512.6331**

Position: Latitude 29.961649° Longitude -89.964442°



PS 5 – EJ Gore

Pre-Hurricane Katrina – Aerial view of the pump station

Pump Station Description

EJ Gore is 1 of 8 pumping stations in St Bernard Parish owned and operated by the Lake Borne Basin Levee District. The station contains six horizontal pumps that were installed in the 1980's with a total pumping capacity of 665 cubic feet per second (cfs)¹ and are driven by diesel engines. The drainage water is supplied to the pumps from the Forty Arpent canal and discharges through the interior back levee to the marsh known as Bayou Dupre. All pumps are equipped flap gates.

¹ The Pump Information Table contains more details about the individual pump data and is located at the beginning of this section.

Pump Station Operation

Pump station operators will turn the pumps on as they are required to reduce the water elevation in the canal. The pumps are normally turned on when the water in the canal reaches approximately 0.0 feet (NGVD) and turned off when the water level reaches -0.5 feet (NGVD). When heavy rainfall events are expected the station operators will pump the canal down to an elevation of -3.0 feet (NGVD).

Fuel Endurance Calculation

Assumptions :

- 1) #2 Diesel fuel is used with an HHV rating of 140,000 btu/gal
- 2) Burn rate of 35 gph @ 500 kW with above HHV rating
- 3) Diesel engines are running at rated capacity

PS 5 E.J. Gore

6 pump drivers - All diesels

Diesels are 335 hp

The approximate burn rate for each diesel is then calculated at:

$$R_{\text{burn}} := \left(35 \frac{\text{gal}}{\text{hr}} \right) \cdot \frac{335 \text{hp}}{500 \text{kW}} \quad R_{\text{burn}} = 17.48 \frac{\text{gal}}{\text{hr}}$$

Fuel Capacity

- 1 - 20,000 gallon tank
- 5 - 50 gallon day tanks
- 1 - 75 gallon tank

Fuel Endurance

The time the 20,000 gallon tank will last is calculated:

$$t_1 := \frac{20000 \text{gal}}{6R_{\text{burn}}} \quad t_1 = 190.62 \text{ hr}$$

The time the 50 gallon tanks will last is calculated:

$$t_2 := \frac{5 \cdot 50 \text{gal}}{6R_{\text{burn}}} \quad t_2 = 2.383 \text{ hr}$$

The time the 75 gallon tank will last is calculated:

$$t_3 := \frac{75 \text{gal}}{6R_{\text{burn}}} \quad t_3 = 0.715 \text{ hr}$$

The approximate total continuous run time for the station is:

$$T_t := t_1 + t_2 + t_3 \quad T_t = 193.719 \text{ hr}$$

$$T_t = 8.072 \text{ day}$$

Pump Curves

Pump curves were obtained from both the parish and the manufacturer. From these curves, a curve fit process was used to create new curves and equations. Using this data as well as making assumptions regarding the dimensions of the pump and the pump station, minor and friction losses were accounted for. These calculations led to the creation of the system curves. Two

curves were made due to the range of operating heads provided by the parish. The two curves represent the maximum and minimum operating heads reported.

Reverse Flow

The Engineering Hydraulics Design section of the US Army Corps of Engineers Portland District office performed analysis of reverse flow characteristics for each pump. The results are reverse flow rating curves that are attached to this section. The tables present the flow rates per individual pump. The detailed calculations, assumptions, and assumed dimensions are available upon request.

Katrina Event

8/28/05 - Operators pumped water in canal down to approximately -3.0ft.

8/29/05 - Operators evacuated station at approximately 1:15 am.

8/30/05 - **Motors were overtopped during storm. Pumps had not been repaired as of site visit.**

Damage Report



Post-Hurricane Katrina – View to the North

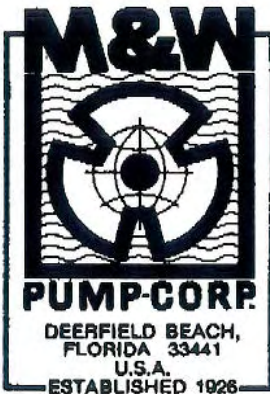
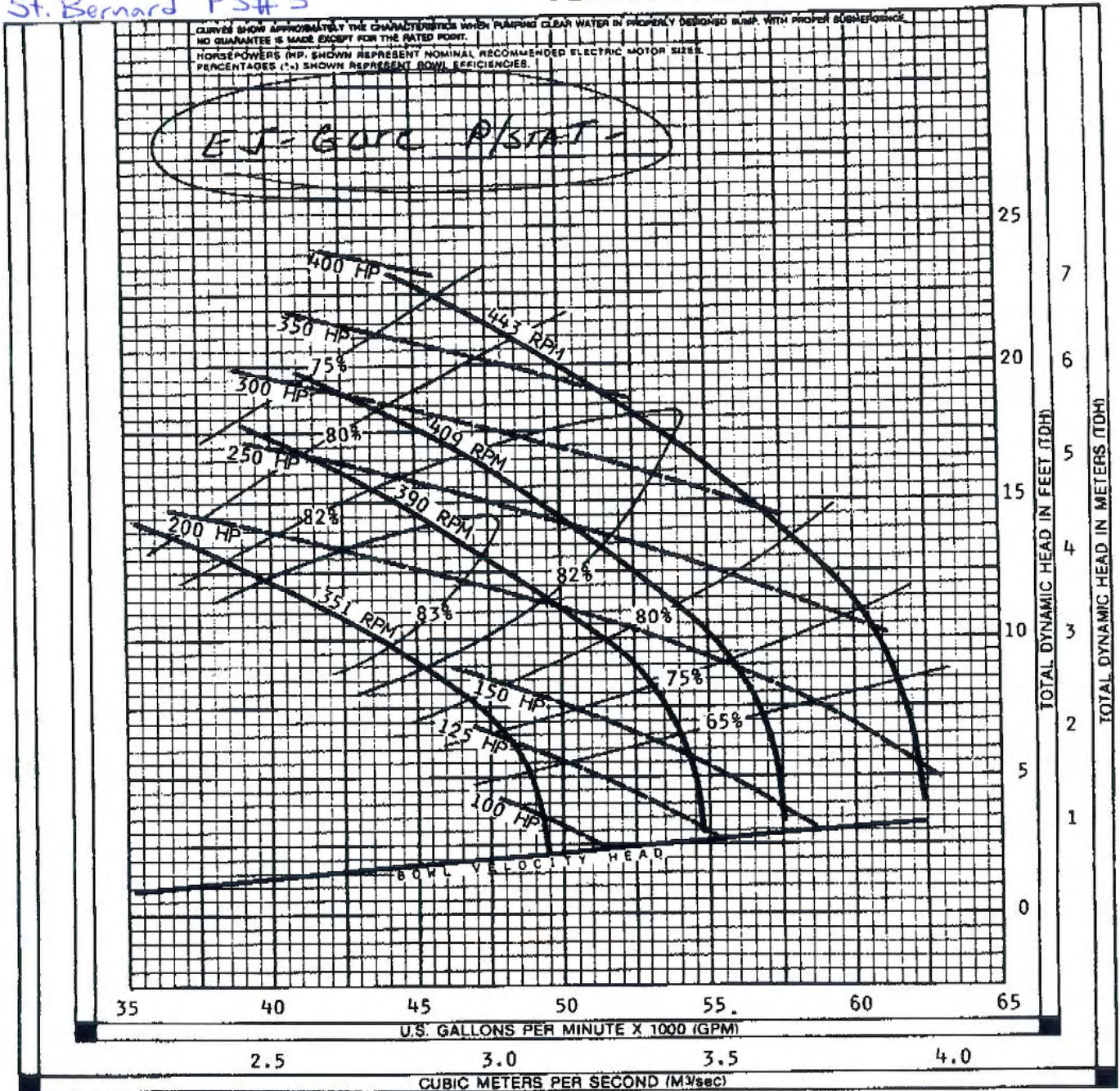
The following information was obtained from the Project Information Report (PIR) for New Orleans District:

Pump Station 5 sustained substantial damage. With the operating floor at approximately 2 feet N.G.V.D, flood waters within the building reached a height of 5 approximately 6 feet. The hydraulic driven pumps were damaged along with the six diesel engines. The generator and the electric pump motor and its controller were flooded. The hydraulic oil tank is not on its foundation and is contaminated with salt water along with the fuel system. The trash rack bar screens are damaged along with the slope pavement adjacent to the discharge pipes. Building damage includes damage to the rollup door, roof, and building office and restroom facility.

St. Bernard PS#5

AXIAL FLOW 42"

C166

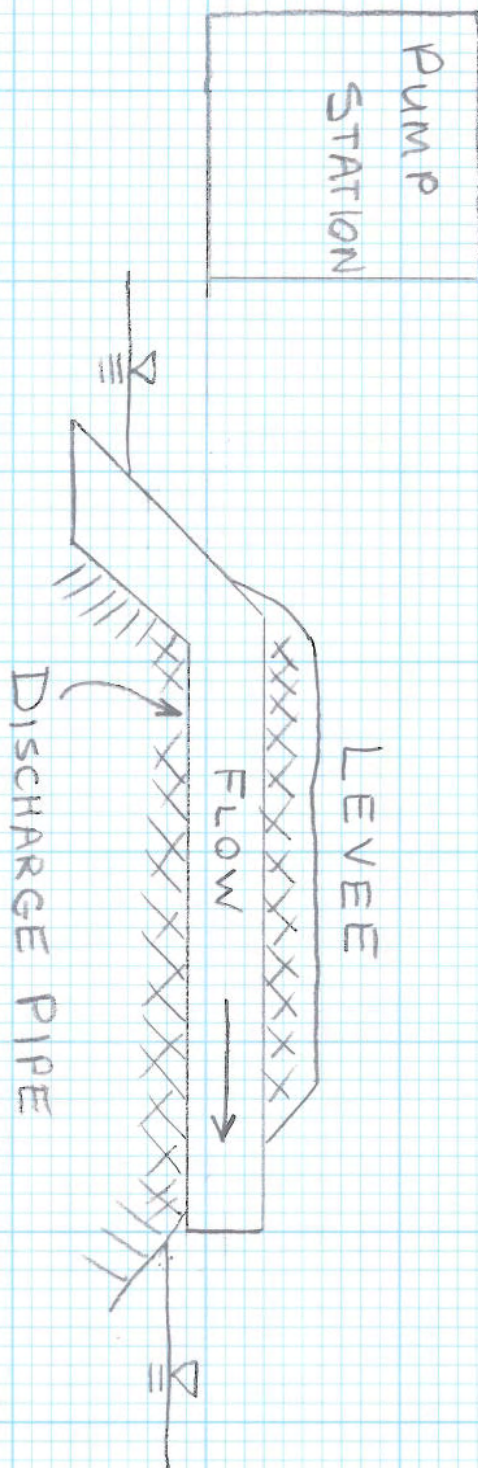


PUMP BOWL PERFORMANCE CURVE VARIABLE SPEED	
TYPE: AXIAL FLOW	PROPELLER DIA.: 42"
MODEL NO.: NC342P12	SPEED (RPM): AS NOTED
INTAKE DIA.: 63"	DISCHARGE COLUMN DIA.: 42"
CURVE NO.: VS42P12	Na: 11,800 CODE: .50
SINGLE STAGE FOR TWO STAGES MULTIPLY HEAD AND HORSEPOWER BY <u>2.0</u> AND EFFICIENCY BY <u>1.0</u>	
PERFORMANCE BASED ON PUMPING CLEAR COLD NON-AERATED WATER, SPECIFIC GRAVITY 1.0, TEMPERATURE 85 DEGREES (FAHRENHEIT) OR LESS, AT SEA LEVEL. PERFORMANCE MAY BE AFFECTED BY HIGHER TEMPERATURES, SPECIFIC GRAVITIES, ALTITUDES, AND SUMP CONDITIONS.	

IT IS HEREBY CERTIFIED THAT THIS CURVE REPRESENTS THE TRUE PERFORMANCE CHARACTERISTICS OF THE M&W PUMP MODEL SHOWN AND WAS OBTAINED BY SCALE MODEL TEST AND CALCULATIONS IN ACCORDANCE WITH STANDARDS OF THE HYDRAULIC INSTITUTE.

M&W PUMP CORPORATION
 CERTIFIED BY
 Available Upon Request

M&W PUMP CORPORATION
 Deerfield Beach, Florida



NOT TO SCALE



Pre-Hurricane Katrina – View from Inlet Canal

**4200 Jean Lafitte Pkwy.
Chalmette, LA 70043
504.512.6331**

Position: Latitude 29.966557° Longitude -89.975821°



PS 6 – Jean Lafitte

Pre-Hurricane Katrina – Aerial view of pump station

Pump Station Description

Jean Lafitte is 1 of 8 pumping stations in St Bernard Parish owned and operated by the Lake Borne Basin Levee District. The station contains three vertical pumps that were installed in 1990 with a total pumping capacity of 945 cubic feet per second (cfs)¹ and are driven by diesel engines. The drainage water is supplied to the pumps from the Florida Walk canal and discharges through the interior back levee to the marsh known as Bayou Bienvenue.

¹ The Pump Information Table contains more details about the individual pump data and is located at the beginning of this section.

Pump Station Operation

Pump station operators will turn the pumps on as they are required to reduce the water elevation in the canal. The pumps are normally turned on when the water in the canal reaches approximately -6 feet (NGVD) and turned off when the water level reaches -6.5 feet (NGVD). When heavy rainfall events are expected the station operators will pump the canal down to an elevation of -8.5 feet (NGVD).

Fuel Endurance Calculation

Assumptions :

- 1) #2 Diesel fuel is used with an HHV rating of 140,000 btu/gal
- 2) Burn rate of 35 gph @ 500 kW with above HHV rating
- 3) Diesel engines are running at rated capacity

PS 6 Jean Lafitte

3 pump drivers - All diesels

Diesels are 335 hp

The approximate burn rate for each diesel is then calculated at:

$$R_{\text{burn}} := \left(35 \frac{\text{gal}}{\text{hr}} \right) \cdot \frac{335 \text{hp}}{500 \text{kW}} \quad R_{\text{burn}} = 17.487 \frac{\text{gal}}{\text{hr}}$$

Fuel Capacity

- 1 - 20,000 gallon tank
- 5 - 50 gallon day tanks
- 1 - 75 gallon tank

Fuel Endurance

The time the 20,000 gallon tank will last is calculated:

$$t_1 := \frac{20000 \text{gal}}{6R_{\text{burn}}} \quad t_1 = 190.62 \text{hr}$$

The time the 50 gallon tanks will last is calculated:

$$t_2 := \frac{5 \cdot 50 \text{gal}}{6R_{\text{burn}}} \quad t_2 = 2.383 \text{hr}$$

The time the 75 gallon tank will last is calculated:

$$t_3 := \frac{75 \text{gal}}{6R_{\text{burn}}} \quad t_3 = 0.713 \text{hr}$$

The approximate total continuous run time for the station is:

$$T_t := t_1 + t_2 + t_3 \quad T_t = 193.719 \text{hr}$$

$$T_t = 8.072 \text{day}$$

Pump Curves

Pump capacity curves were obtained. From these curves, a curve fit process was used to create new curves and equations. Using this information and making assumptions about the pump and the pump station, friction and minor head losses were accounted for. These calculations led to the creation of the systems curves. Two curves were created due to the range of operation reported by the parish using only the maximum and minimum head required.

Reverse Flow

The Engineering Hydraulics Design section of the US Army Corps of Engineers Portland District office performed analysis of reverse flow characteristics for each pump. The results are reverse flow rating curves that are attached to this section. The tables present the flow rates per individual pump. The detailed calculations, assumptions, and assumed dimensions are available upon request.

Katrina Event

8/28/05 - Operators pumped water in canal down to approximately -8.5 feet (NGVD).

8/29/05 - Operators evacuated pump station at approximately 1:15 am.

8/30/05 - Operators returned to the station at 10:00 am. Water was the same elevation on both sides of pump station.

9/11/05 - **Pump station back to normal operation.**

Damage Report

The following information was obtained from the Project Information Report (PIR) for New Orleans District:

Pump Station 6 sustained relatively minor damage because its operating floor elevation is 16 feet N.G.V.D. Flooding from the storm flooded the lower level of the station but the flood waters were approximately three feet below the concrete operating floor level. The building damage consists of damaged roof panels. Mechanical damage includes damage to the trash rack gear boxes, trash removal equipment, engine exhaust flappers, and sanitation plant. Electrical damage consists of damage to lighting and the remote engine alarm panel.

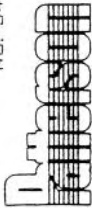


Post-Hurricane Katrina – View from the Inlet Canal



PS 6 – Jean Lafitte

Post-Hurricane Katrina – Aerial view of the pump station



PATTERSON PUMP COMPANY
A Subsidiary of Banner Industries, Inc.

CURVE NO. JC-576-94-01

REF.

BR. H.P.

EFF. %

HEAD FT.

CHARACTERISTIC CURVES

PUMP TYPE AFV SIZE 7.5 X 7.2

RATING: GPM _____ FT. HD. _____ RPM 272

JEAN LAFITTE P.S. (P.S. #6)

BAYOU DUCROS P.S. (P.S. #7)

PUMP EFFICIENCY

PUMP TDH VS Q, 272 RPM
POOL-TO-POOL HEAD VS Q

NPSHR

BHP VS. Q

TDH VS Q, 253 RPM

Q, U.S. GALLONS PER MINUTE / 1000

American blueprint 500228

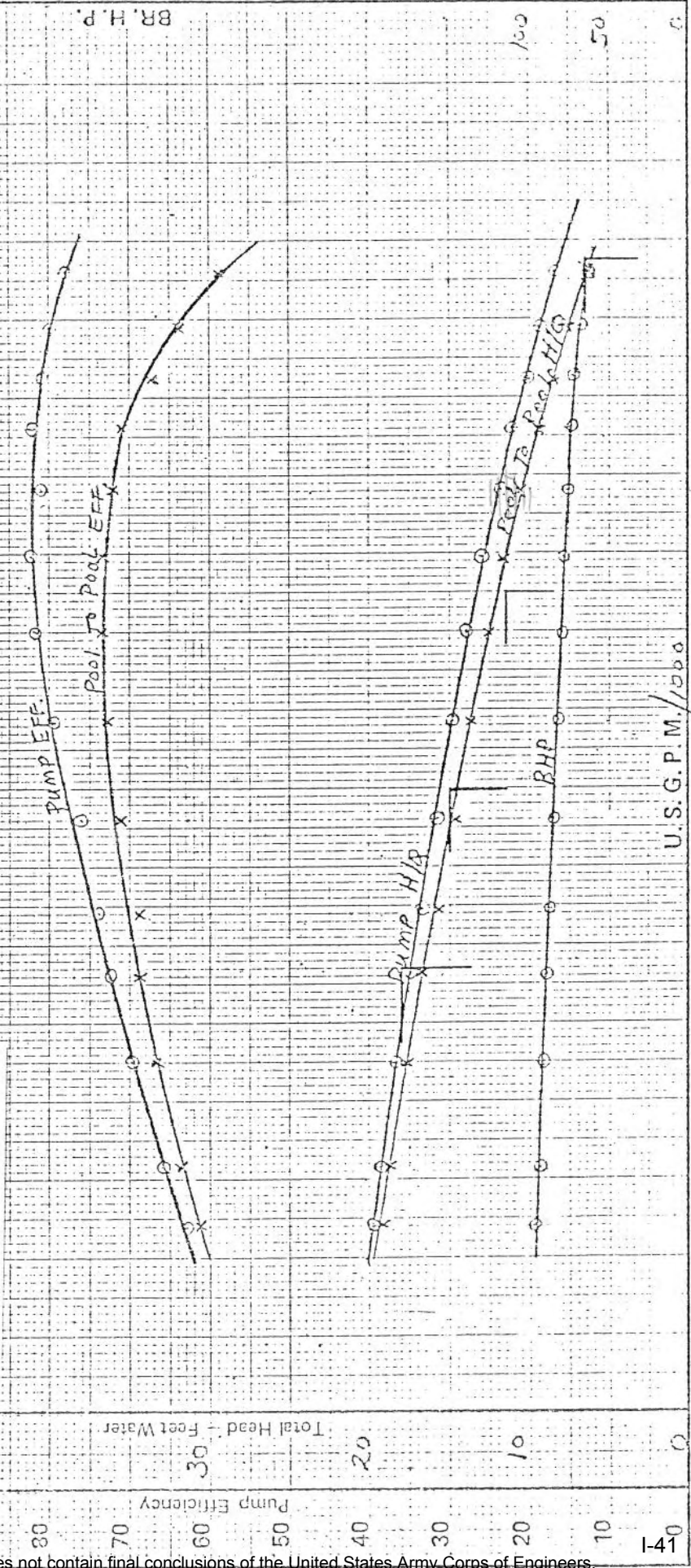
Sold To: _____ Date 10-4-83 Tested By BWJ Serial No. X-624

Job Driver:	HP	Motor Turbine Engine	GPM	Imp. Patt.	Imp. Type
Test Driver:	HP	Motor Dyn.	Ft. Hd.	No. Stages	Size
Motor Effy	Test Speed	Rated Speed	Test No.		

CERTIFIED TEST BY _____
 APPROVED BY _____
 WITNESSED BY _____

PATTERNS AVAILABLE FOR RATIOS:
 2.959
 3.23

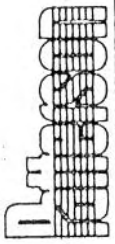
225 GPM
 19.1" @ 11.6"
 1957 FT



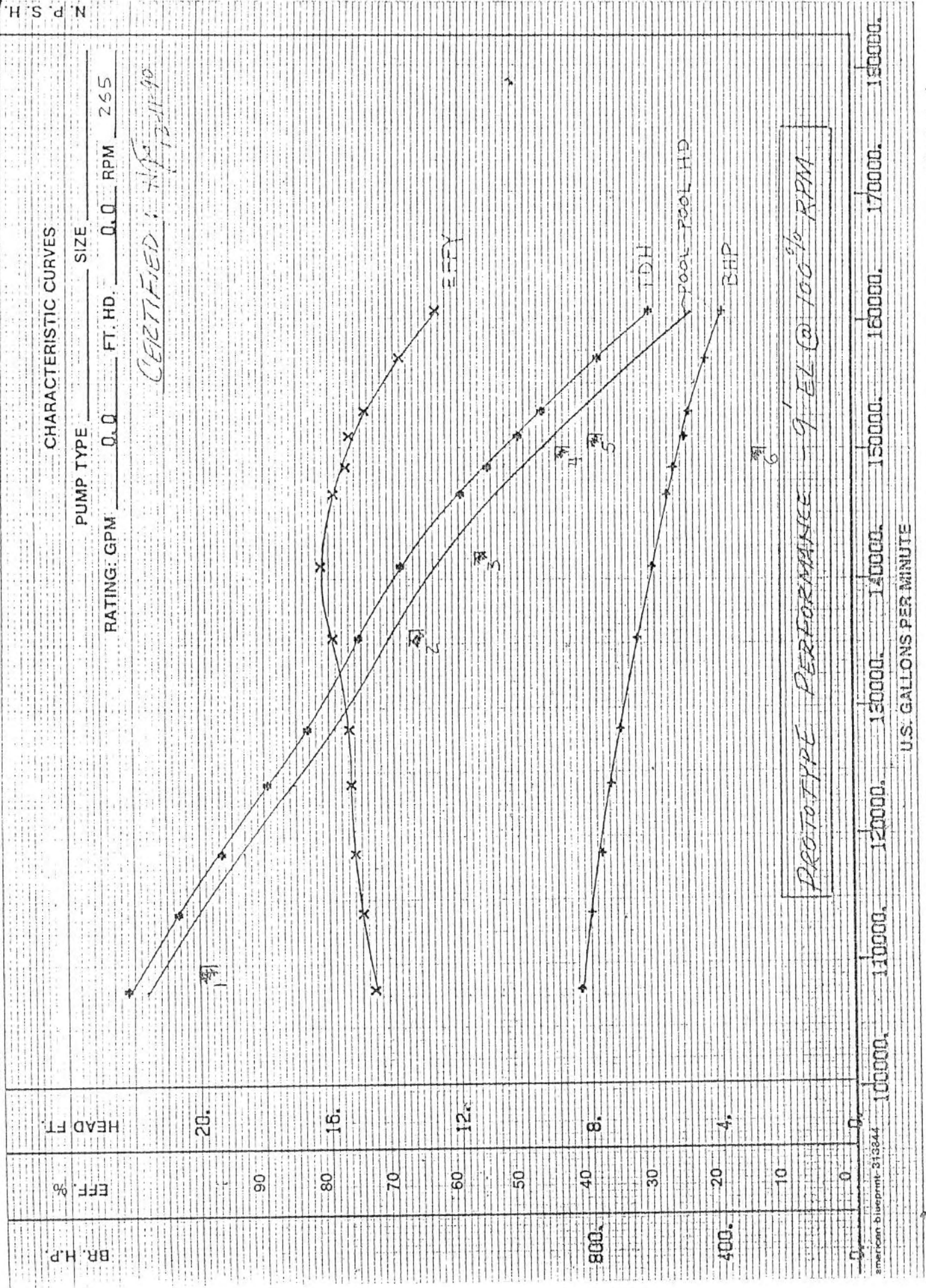
This is a preliminary report subject to revision; it does not contain final conclusions of the United States Army Corps of Engineers.

CURVE NO. 8544

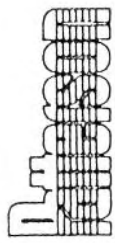
PROTOTYPE



PATTERSON PUMP COMPANY
A SUBSIDIARY OF THE GORMAN-RUPP CO



CURVE NO. 8544



PATTERSON PUMP COMPANY
A SUBSIDIARY OF THE GORMAN-RUFF CO.

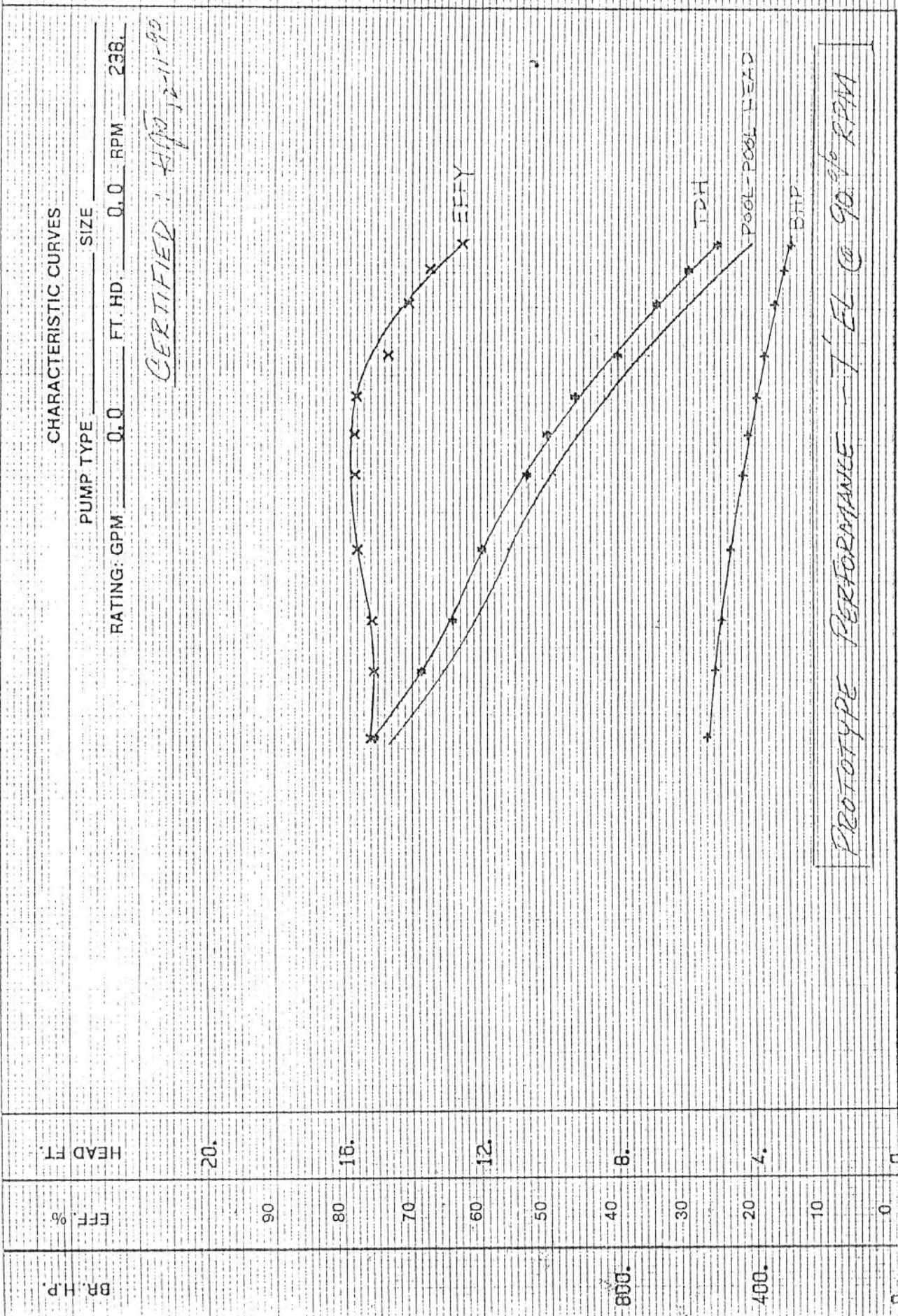
CURVE NO. 8532
PROTOTYPE

N. P. S. H.

CHARACTERISTIC CURVES

PUMP TYPE _____ SIZE _____
RATING: GPM 0.0 FT. HD. 0.0 RPM 238

CERTIFIED: HFD 12-11-99



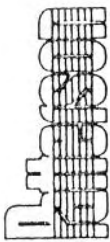
PROTOTYPE PERFORMANCE - 7' EL @ 90% RPM

0. 400. 800.
0. 20. 40. 60. 80. 90.
0. 80000. 90000. 100000. 110000. 120000. 130000. 140000. 150000. 160000.
U.S. GALLONS PER MINUTE

American blueprint 313844

This is a preliminary report subject to revision; it does not contain final conclusions of the United States Army Corps of Engineers.

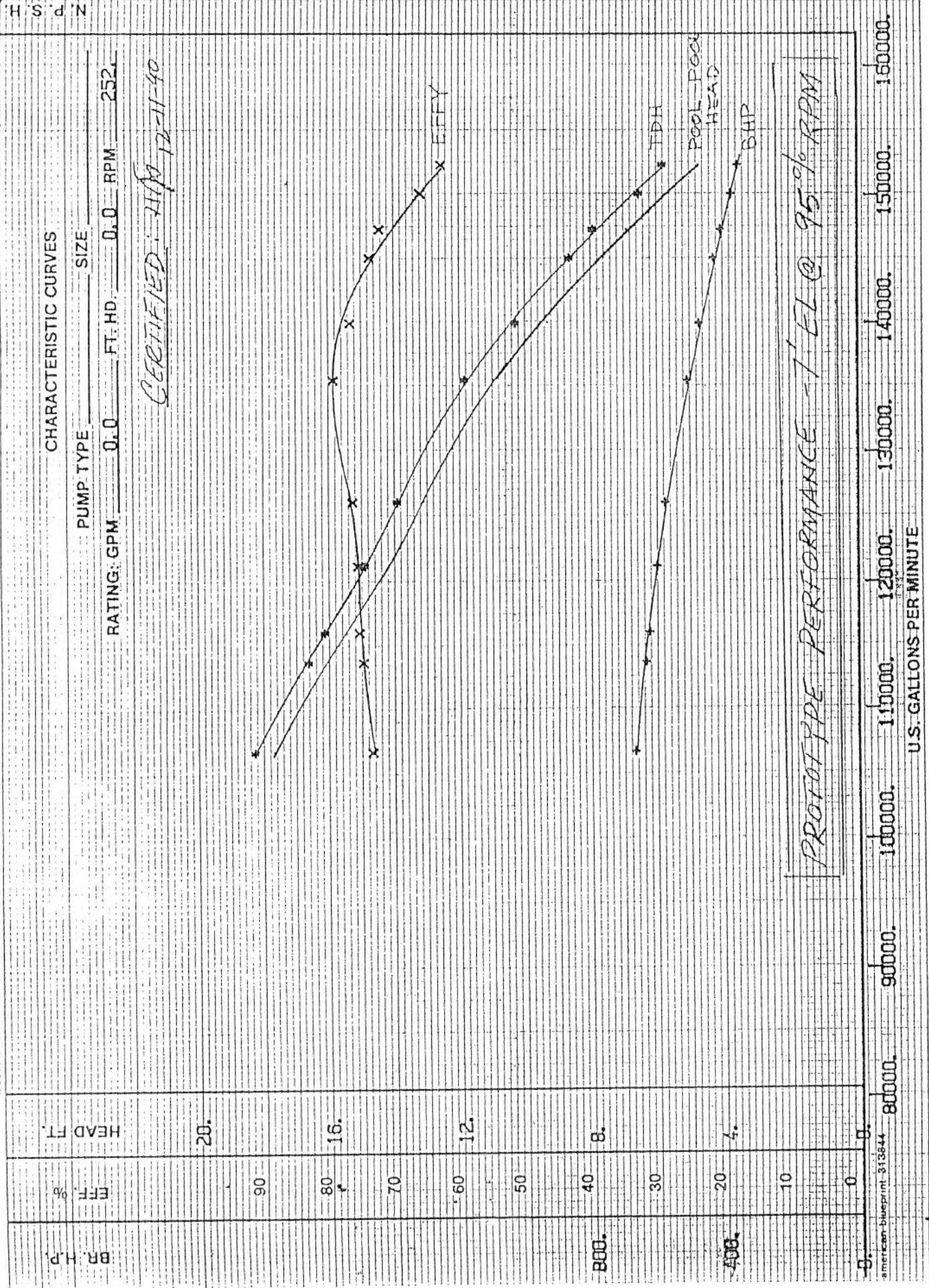
CURVE NO. 8533



PATERSON PUMP COMPANY
A SUBSIDIARY OF THE GORMAN-RUPP CO.

CURVE NO. 8522
PROTOTYPE

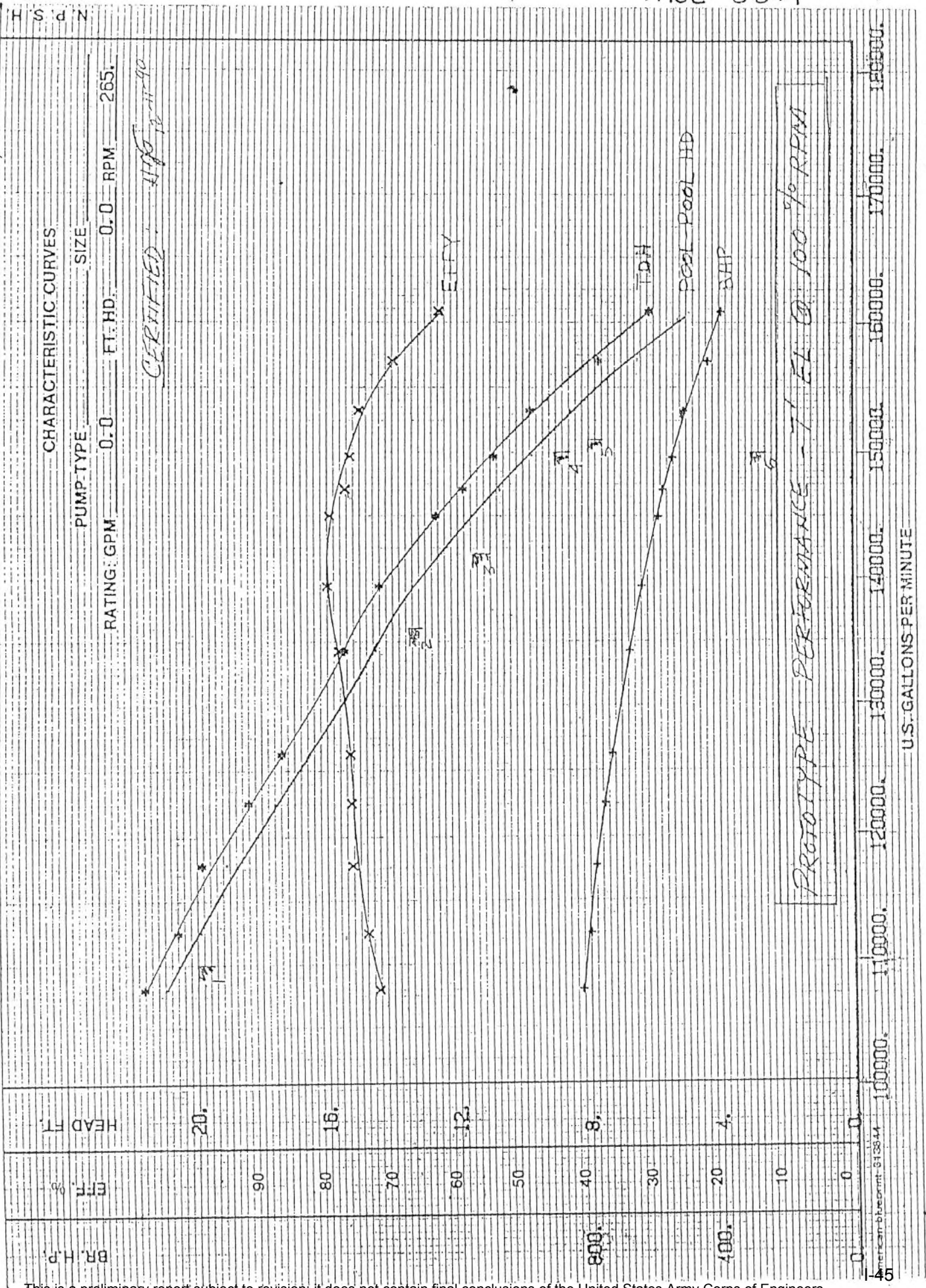
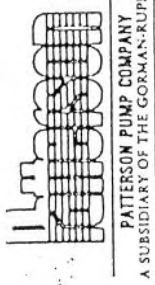
REF.



american blueprint 313844

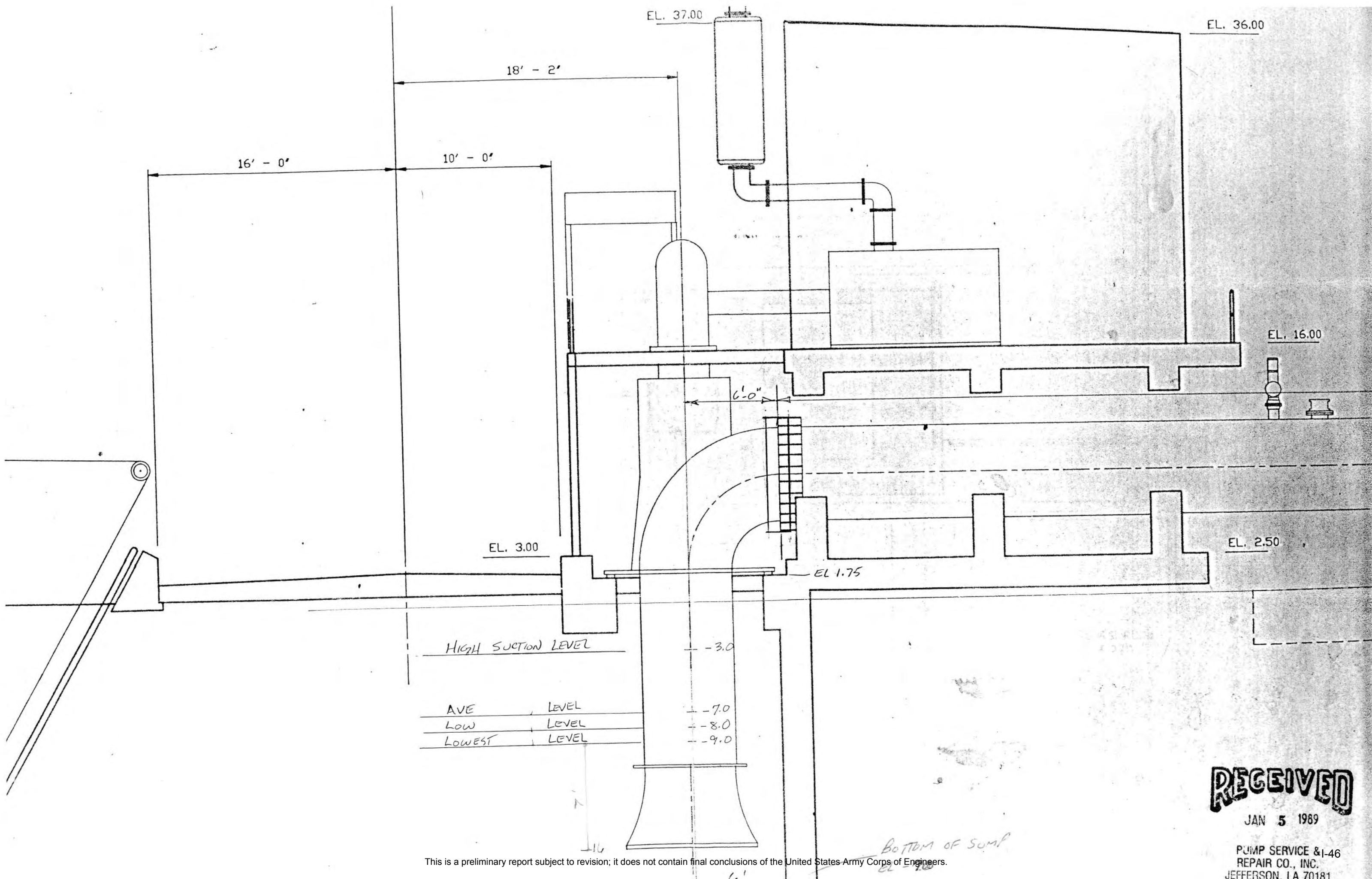
U.S. GALLONS PER MINUTE

CURVE NO. 8511
PROTOTYPE



This is a preliminary report subject to revision; it does not contain final conclusions of the United States Army Corps of Engineers.

CURVE NO. 8511



HIGH SUCTION LEVEL		
AVE	LEVEL	-7.0
LOW	LEVEL	-8.0
LOWEST	LEVEL	-9.0

RECEIVED

JAN 5 1989

PUMP SERVICE & I-46
REPAIR CO., INC.
JEFFERSON. LA 70181

This is a preliminary report subject to revision; it does not contain final conclusions of the United States Army Corps of Engineers.

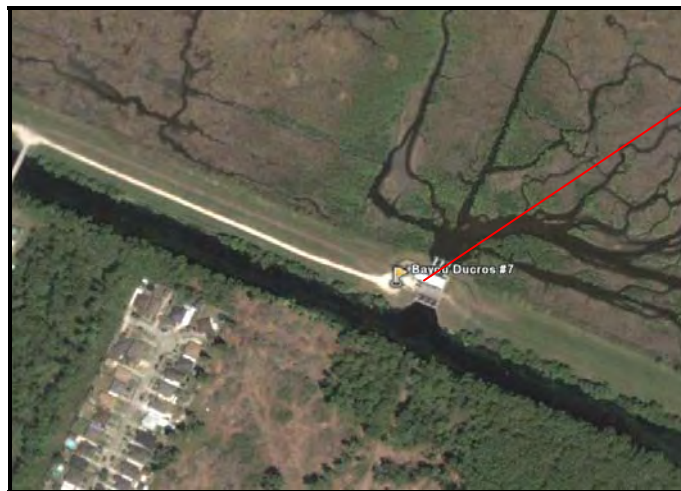
BOTTOM OF SUMP
EL - 9.0



Pre-Hurricane Katrina – View from Inlet Canal

**3701 Bartolo Dr.
Meraux, LA 70075
504.512.6331**

Position: Latitude 29.946969° Longitude -89.922244°



PS 7 – Bayou Ducros

Pre-Hurricane Katrina – Aerial view of pump station

Pump Station Description

Bayou Ducros is 1 of 8 pumping stations in St Bernard Parish owned and operated by the Lake Borne Basin Levee District. The station contains three vertical pumps that were installed in 1992 with a total pumping capacity of 1000 cubic feet per second (cfs)¹ and are driven by diesel engines. The drainage water is supplied to the pumps from the Forty Arpent canal and discharges through the interior back levee to the marsh known as Bayou Ducros.

¹ The Pump Information Table contains more details about the individual pump data and is located at the beginning of this section.

Pump Station Operation

Pump station operators will turn the pumps on as they are required to reduce the water elevation in the canal. The pumps are normally turned on when the water in the canal reaches approximately -6 feet (NGVD) and turned off when the water level reaches -6.5 feet (NGVD). When heavy rainfall events are expected the station operators will pump the canal down to an elevation of -8.5 feet (NGVD).

Fuel Endurance Calculation

Assumptions:

- 1) #2 Diesel fuel is used with an HHV rating of 140,000 btu/gal
- 2) Burn rate of 35 gph @ 500 kW with above HHV rating
- 3) Diesel engines are running at rated capacity

PS 7 Bayou Ducros

3 pump drivers - All diesels

Diesels are 1020 hp

The approximate burn rate for each diesel is then calculated at:

$$R_{\text{burn}} := \left(35 \frac{\text{gal}}{\text{hr}} \right) \cdot \frac{1020\text{hp}}{500\text{kW}} \qquad R_{\text{burn}} = 53.243 \frac{\text{ga}}{\text{hr}}$$

Fuel Capacity

- 2 - 10,000 gallon tanks
- 2 - 300 gallon day tanks

Fuel Endurance

The time the 10,000 gallon tank will last is calculated:

$$t_1 := \frac{2 \cdot 10000\text{gal}}{3R_{\text{burn}}} \qquad t_1 = 125.212\text{hr}$$

The time the 300 gallon tanks will last is calculated:

$$t_2 := \frac{2 \cdot 300\text{gal}}{3R_{\text{burn}}} \qquad t_2 = 3.756\text{hr}$$

The approximate total continuous run time for the station is:

$$T_t := t_1 + t_2 \qquad T_t = 128.969\text{hr}$$

$$T_t = 5.374\text{day}$$

Pump Curves

Pump capacity curves were obtained. From these curves, a curve fit process was used to create new curves and equations. Using drawings and manufacturer data, assumptions regarding the pump station and the pump were made in order to determine the minor and friction losses in the system. These calculations created the system curves. Two curves were created in order to

accommodate the range of operating heads provided by the parish. The maximum and minimum head values were used to generate these curves.

Reverse Flow

The Engineering Hydraulics Design section of the US Army Corps of Engineers Portland District office performed analysis of reverse flow characteristics for each pump. The results are reverse flow rating curves that are attached to this section. The tables present the flow rates per individual pump. The detailed calculations, assumptions, and assumed dimensions are available upon request.

Katrina Event

8/28/05 - Operators pumped water in canal down to approximately -8.5 feet (NGVD).

8/29/05 - Operators evacuated pump station at approximately 1:15 am.

8/30/05 - Operators returned to the station at 10:00 am. Water was the same elevation on both sides of pump station.

9/11/05 - **Pump station back to normal operation.**

Damage Report

The following information was obtained from the Project Information Report (PIR) for New Orleans District:

Pump Station 7 sustained relatively minor damage because its operating floor elevation is 16 feet N.G.V.D. Flooding from the storm flooded the lower level of the station but the flood waters were approximately three feet below the concrete operating floor level. Bearing and gears for the trash racks were damaged. Auxiliary equipment damage included flooding of a bobcat used to remove debris from the trash racks, fuel tank, and sanitation plant. Pump damage consists of a broken drain line. Engine damage consists of damage to an engine cooling motor, radiator leak and remote engine alarm panel. Two areas had some erosion including scour behind the station and near the west end stairs.

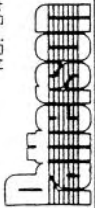


Post-Hurricane Katrina – Erosion



PS 7 – Bayou Ducros

Post-Hurricane Katrina – Aerial view of the pump station



PATTERSON PUMP COMPANY
A Subsidiary of Banner Industries, Inc.

REF.

HEAD FT.

EFF. %

BR. H.P.

90

80

70

60

50

40

30

20

10

0

1500

1000

500

0

30

20

10

0

American blueprint 500228

CURVE NO. JC-576-94-01

CHARACTERISTIC CURVES

PUMP TYPE AFV SIZE 7.5 X 7.2

RATING: GPM _____ FT. HD. _____ RPM 272

JEAN LAFITTE P.S. (P.S. #6)

BAYOU DUCROS P.S. (P.S. #7)

PUMP EFFICIENCY

PUMP TDH VS Q, 272 RPM
POOL-TO-POOL HEAD VS Q

NPSHR

BHP VS Q

TDH VS Q, 253 RPM

Q, U.S. GALLONS PER MINUTE / 1000

N.P.S.H.

30

20

10

0

180

170

160

150

140

130

120

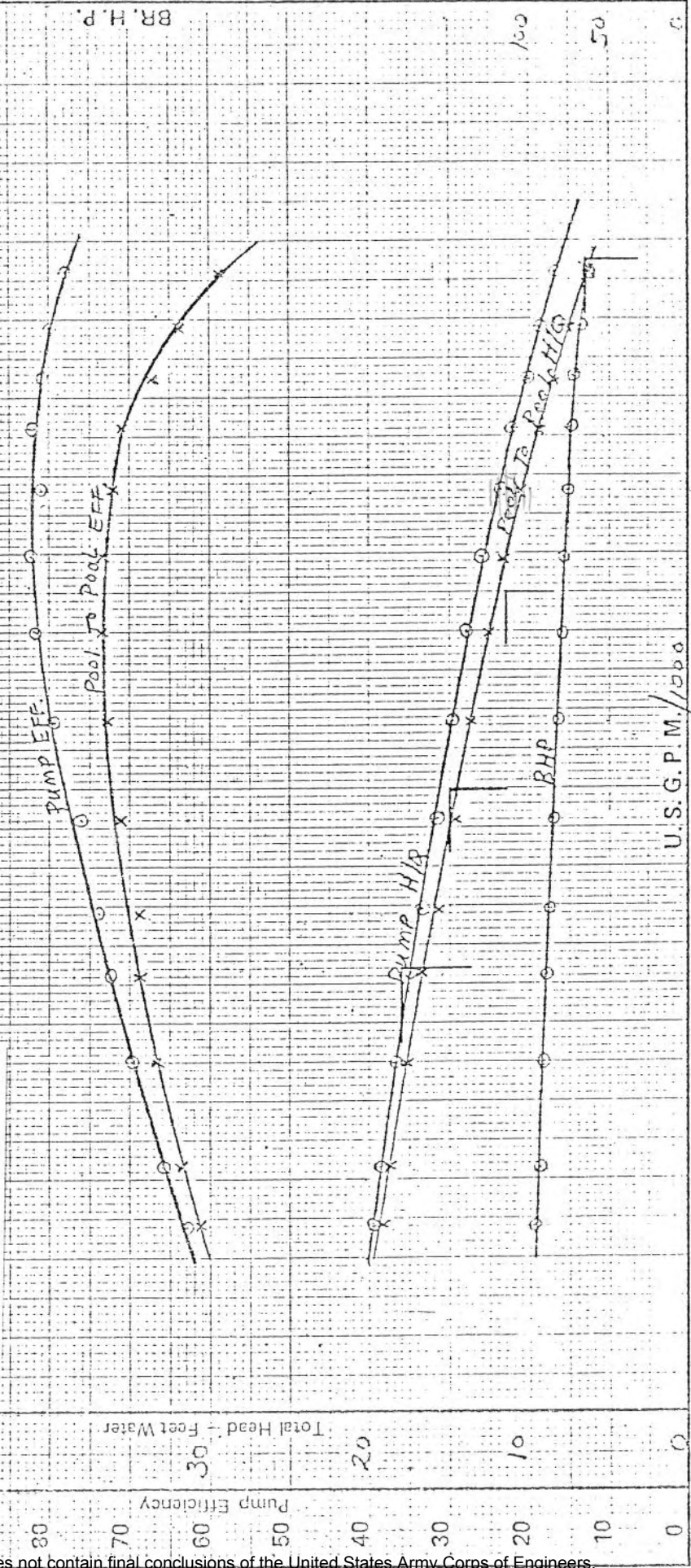
110

100

Serial No. X-624 Tested By BuJ Date 10-4-83

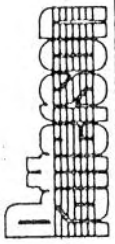
Job Driver:	HP	Motor Turbine Engine	GPM	Imp. Patt.	Imp. Type
Test Driver:	HP	Motor Dyn.	Ft. Hd.	No. Stages	Size
Motor Effy	Test Speed	Rated Speed	Test No.		

PATTERNS AVAILABLE FOR RATIOS:
 2.959
 3.23
 799
 799
 B-75248
 19.1" @ 11.6"
 24
 225 GPM
 1957 FT

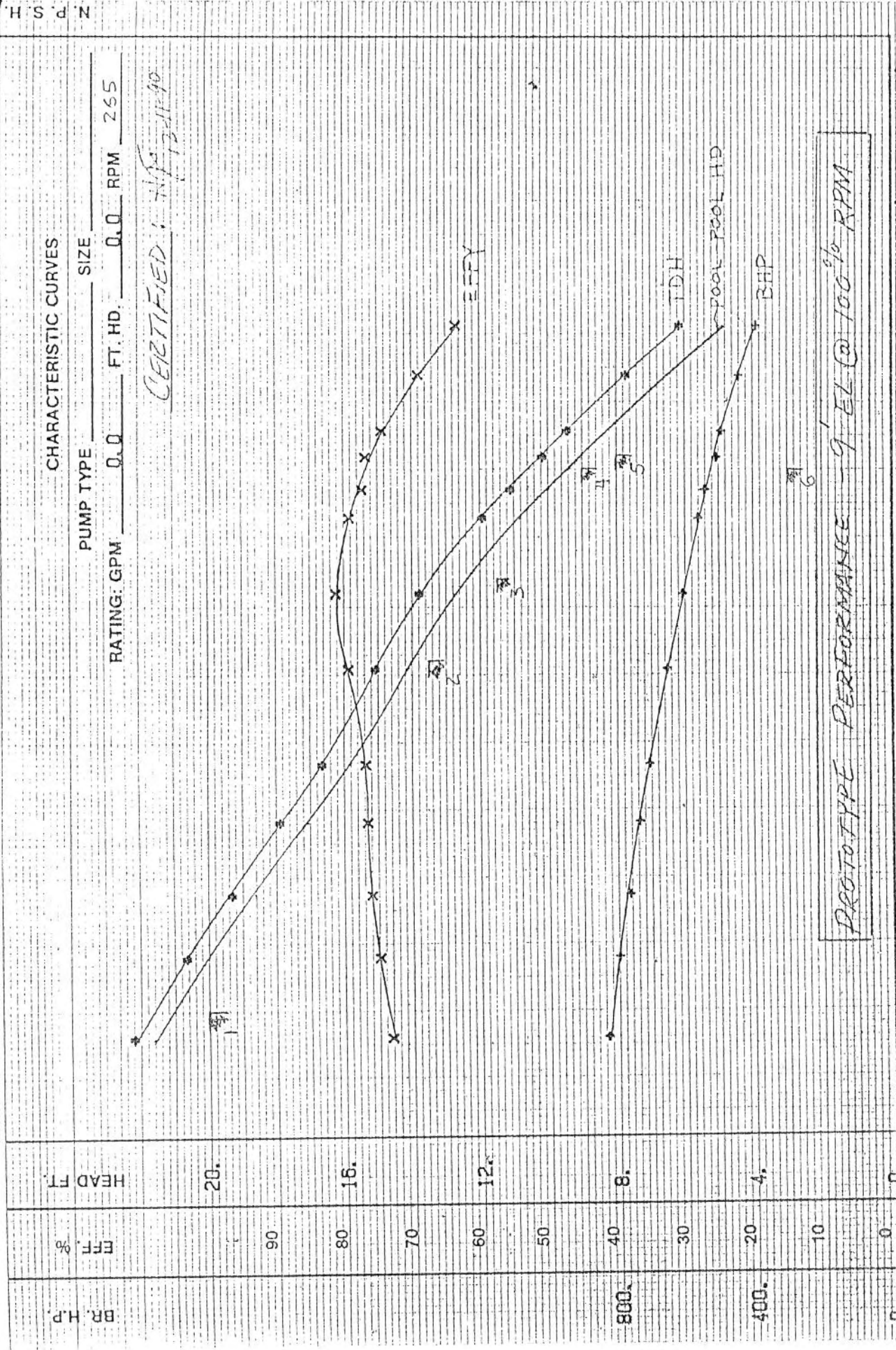


CURVE NO. 8544

PROTOTYPE



PATTERSON PUMP COMPANY
A SUBSIDIARY OF THE GORMAN-RUPP CO

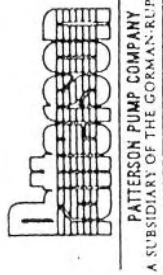


PROTOTYPE PERFORMANCE - 9' EL @ 100% RPM

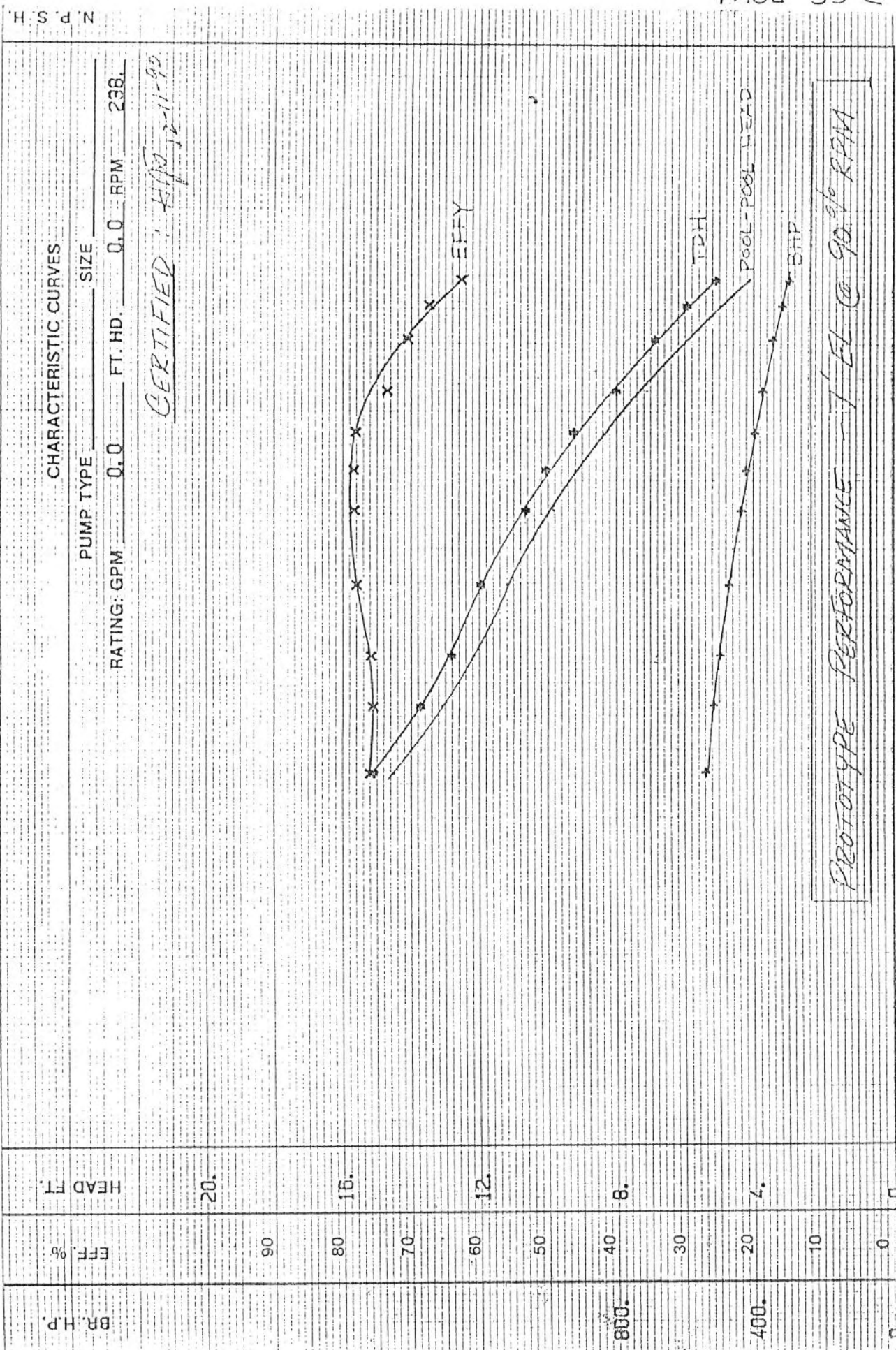
100000. 110000. 120000. 130000. 140000. 150000. 160000. 170000. 180000.

U.S. GALLONS PER MINUTE

CURVE NO. 8544



CURVE NO. 8532
PROTOTYPE



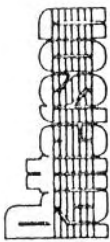
REF. HEAD FT. 20. 16. 12. 8. 4. 0.

EFF. % 90 80 70 60 50 40 30 20 10 0

BR. H.P. 800. 400. 0.

U.S. GALLONS PER MINUTE 0 10000 20000 30000 40000 50000 60000 70000 80000 90000 100000 110000 120000 130000 140000 150000 160000.

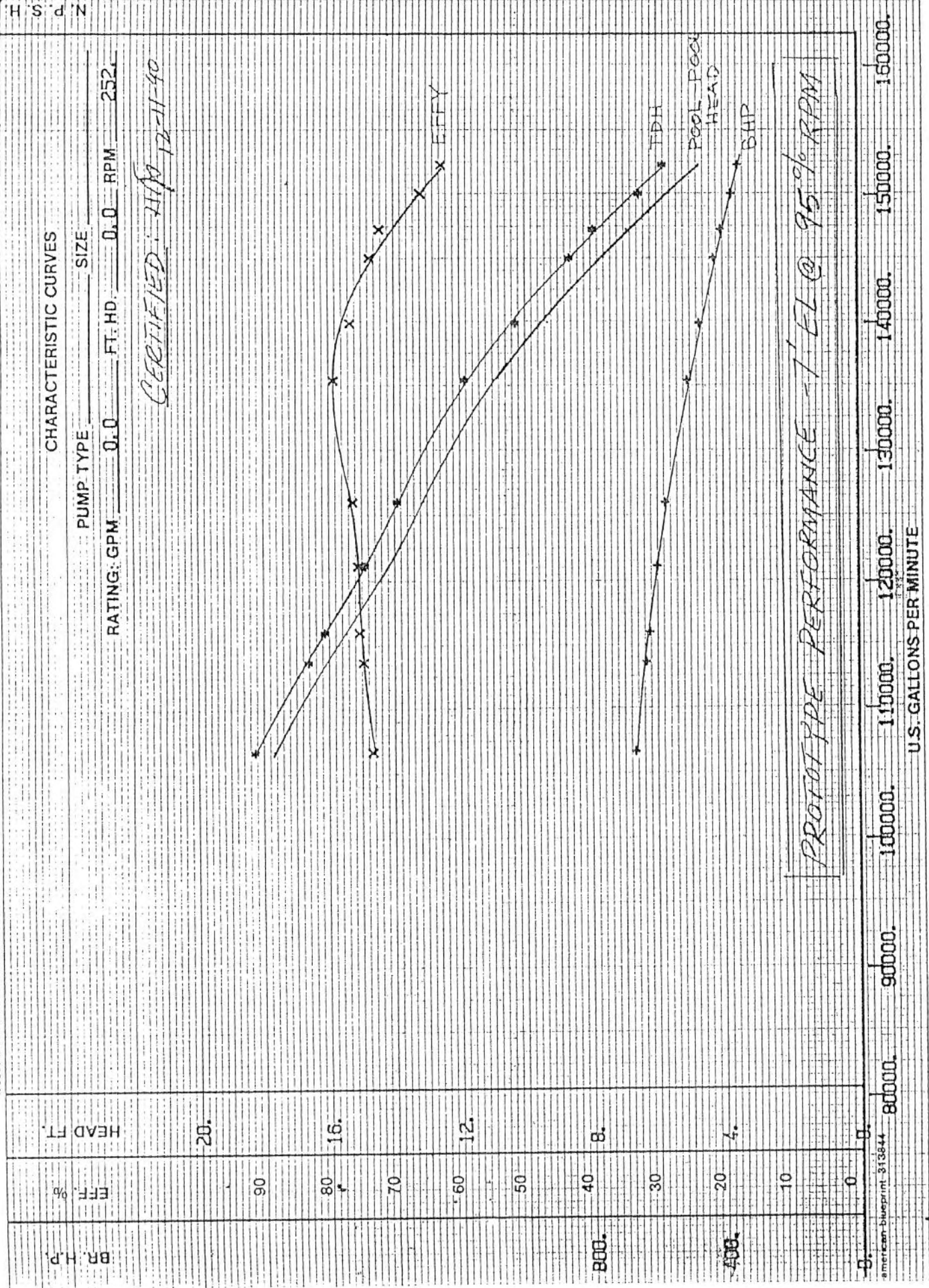
CURVE NO. 8533



PATERSON PUMP COMPANY
A SUBSIDIARY OF THE GORMAN-RUPP CO.

CURVE NO. 8522
PROTOTYPE

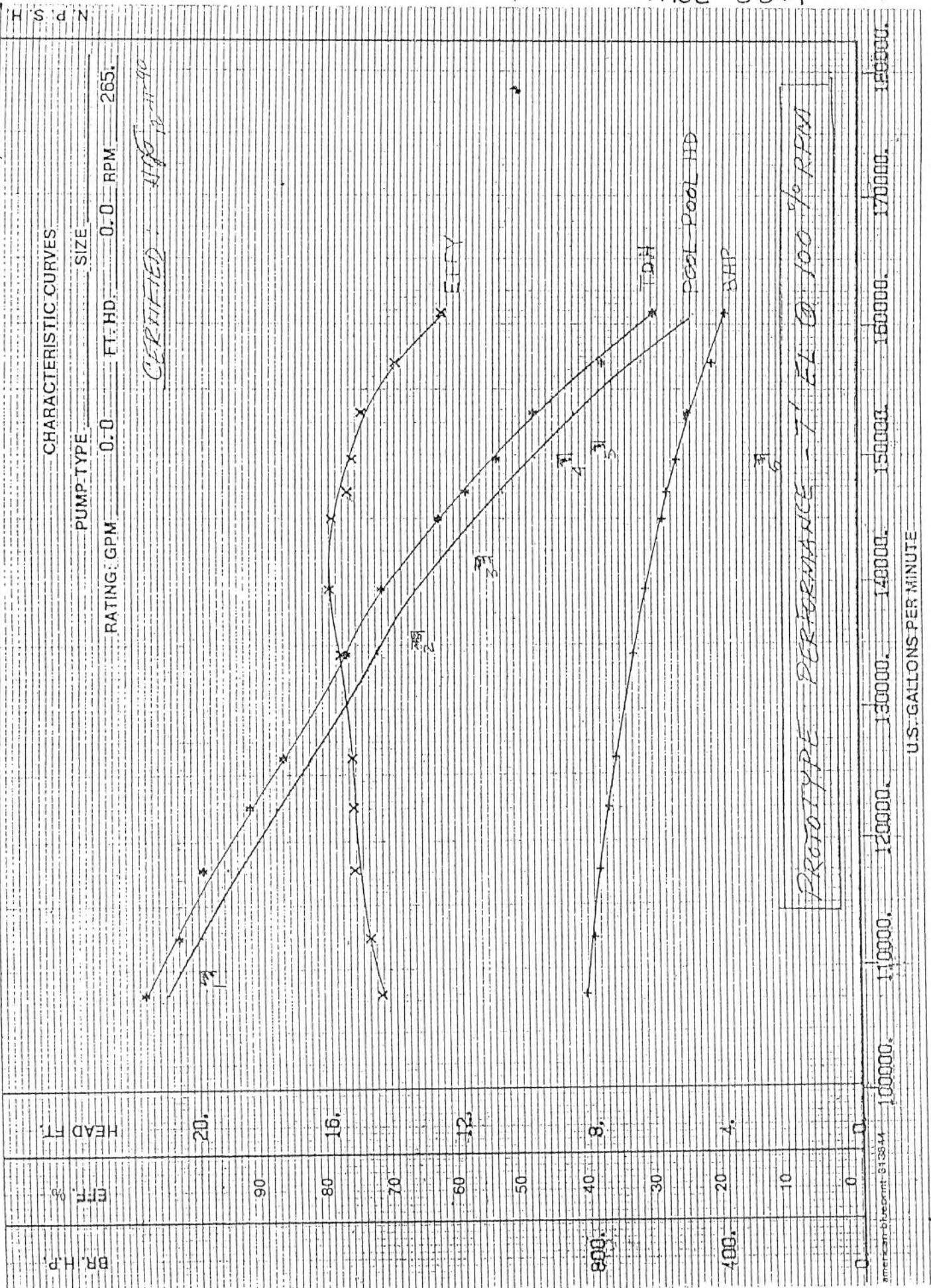
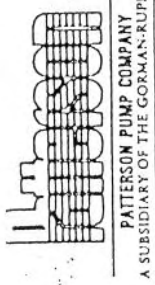
REF.



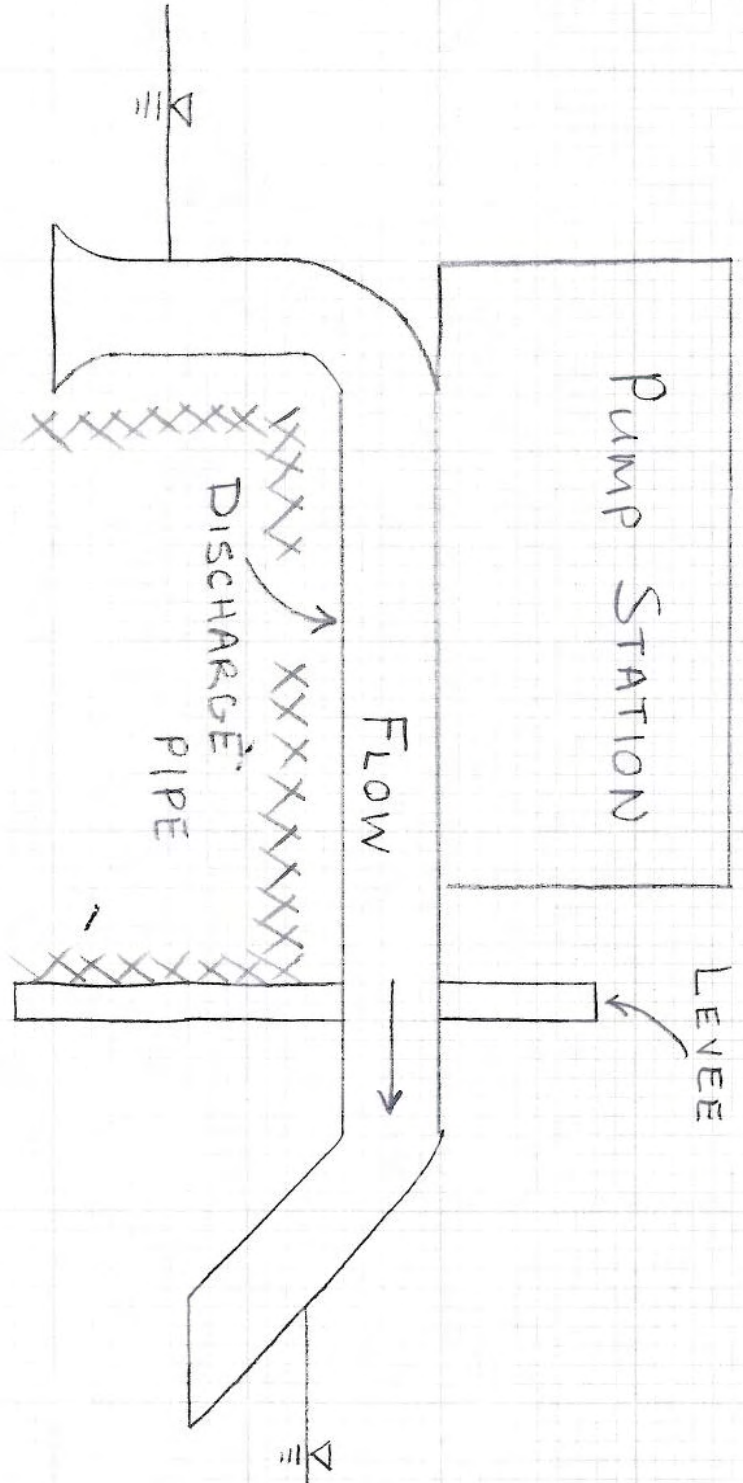
american blueprint 313844

U.S. GALLONS PER MINUTE

CURVE NO. 8511
PROTOTYPE



CURVE NO. 8511



NOT TO SCALE



Pre-Hurricane Katrina – View from Inlet Canal

**3616 Bayou Rd.
Verret, LA 70085
504-682-0591**

Position: Latitude 29.854064° Longitude -89.795715

Pump Station Description

St Mary is 1 of 8 pumping stations in St Bernard Parish owned and operated by the Lake Borne Basin Levee District. The station contains three vertical pumps that were installed in 1996 with a total pumping capacity of 835 cubic feet per second (cfs)¹ and are driven by diesel engines. The drainage water is supplied to the pumps from the Twenty Arpent canal and discharges through the hurricane protection levee to Lake Lery. The discharge pipes have check valves to prevent flow in the reverse direction.

Pump Station Operation

Pump station operators will turn the pumps on as they are required to reduce the water elevation in the canal. The pumps are normally turned on when the water in the canal reaches approximately 0.0 feet (NGVD) and turned off when the water level reaches -0.5 feet (NGVD). When heavy rainfall events are expected the station operators will pump the canal down to an elevation of -3.5 feet (NGVD).

Fuel Endurance Calculation

¹ The Pump Information Table contains more details about the individual pump data and is located at the beginning of this section.

Assumptions:

- 1) #2 Diesel fuel is used with an HHV rating of 140,000 btu/gal
- 2) Burn rate of 35 gph @ 500 kW with above HHV rating
- 3) Diesel engines are running at rated capacity

PS 8 St Mary

3 pump drivers - All diesels

Diesels are 1020 hp

The approximate burn rate for each diesel is then calculated at:

$$R_{\text{burn}} := \left(35 \frac{\text{gal}}{\text{hr}} \right) \cdot \frac{1020\text{hp}}{500\text{kW}} \qquad R_{\text{burn}} = 53.243 \frac{\text{gal}}{\text{hr}}$$

Fuel Capacity

- 2 - 10,000 gallon tanks
- 2 - 300 gallon day tanks

Fuel Endurance

The time the 10,000 gallon tank will last is calculated:

$$t_1 := \frac{2 \cdot 10000\text{gal}}{3R_{\text{burn}}} \qquad t_1 = 125.212\text{hr}$$

The time the 300 gallon tanks will last is calculated:

$$t_2 := \frac{2 \cdot 300\text{gal}}{3R_{\text{burn}}} \qquad t_2 = 3.756\text{hr}$$

The approximate total continuous run time for the station is:

$$T_t := t_1 + t_2 \qquad \boxed{T_t = 128.969\text{hr}}$$

$$\qquad \qquad \qquad \boxed{T_t = 5.374\text{day}}$$

Pump Curves

Pump capacity curves were obtained from the parish. These curves were recreated using a curve fit process. Analysis of the system necessitated the use of assumptions about the pump station and pump dimensions. These allowed for calculations regarding minor and friction losses. The system curves were created using these calculations. Two system curves were generated to accommodate the range of operation recorded by the parish, using maximum and minimum values of head.

Reverse Flow

The Engineering Hydraulics Design section of the US Army Corps of Engineers Portland District office performed analysis of reverse flow characteristics for each pump. The results are reverse flow rating curves that are attached to this section. The tables present the flow rates per individual pump. The detailed calculations, assumptions, and assumed dimensions are available upon request.

Katrina Event

8/28/05 - Operators pumped water in canal down to approximately -3.5 feet (NGVD).

8/29/05 - Operators evacuated pump station at approximately 1:15 am.

9/11/05 - **Pump station back to normal operation.**

Damage Report

The following information was obtained from the Project Information Report (PIR) for New Orleans District:

Pump Station 8 sustained relatively minor damage because its operating floor elevation is 16 feet N.G.V.D. Flooding from the storm flooded the lower level of the station but the flood waters were approximately eight feet below the concrete operating floor level. Building damage consists of loose roof panels, scour section near the discharge pipes, light fixtures, and the sewage aerator motor. Bearing and gears for the trash racks were damaged. Auxiliary equipment damage includes a front end loader used to remove debris from the trash racks.



Post-Hurricane Katrina – View from the Inlet Canal

CURVES SHOW APPROXIMATELY THE CHARACTERISTICS WHEN PUMPING CLEAR WATER. NO GUARANTEE IS MADE EXCEPT FOR THE RATED POINT.

CUSTOMER: ST. BERNARD PARISH
CAENARVON STATION NO. 8
CURVE NO. 840-70120-A
TYPE WCA X CENT. PUMP

CUST. P.O. NO.: PR07 716-44-0006 ITEM NO.: 125,000 G.P.M. 2.5 FT. HD. 230 R.P.M.
IMPELLER DWG. VANE-3

STEP-UP OF MODEL WITNESS
PERFORMANCE TEST NO. 1
MAX. SPHERE
IMP. DIA. 61.34 RMS

SUCT. POOL ELEV. = 0 FT. 100% SPEED

PUMP SERIAL NO.

SIGNED *M. R. ...* DATE 1-8-96

CERTIFIED FOR



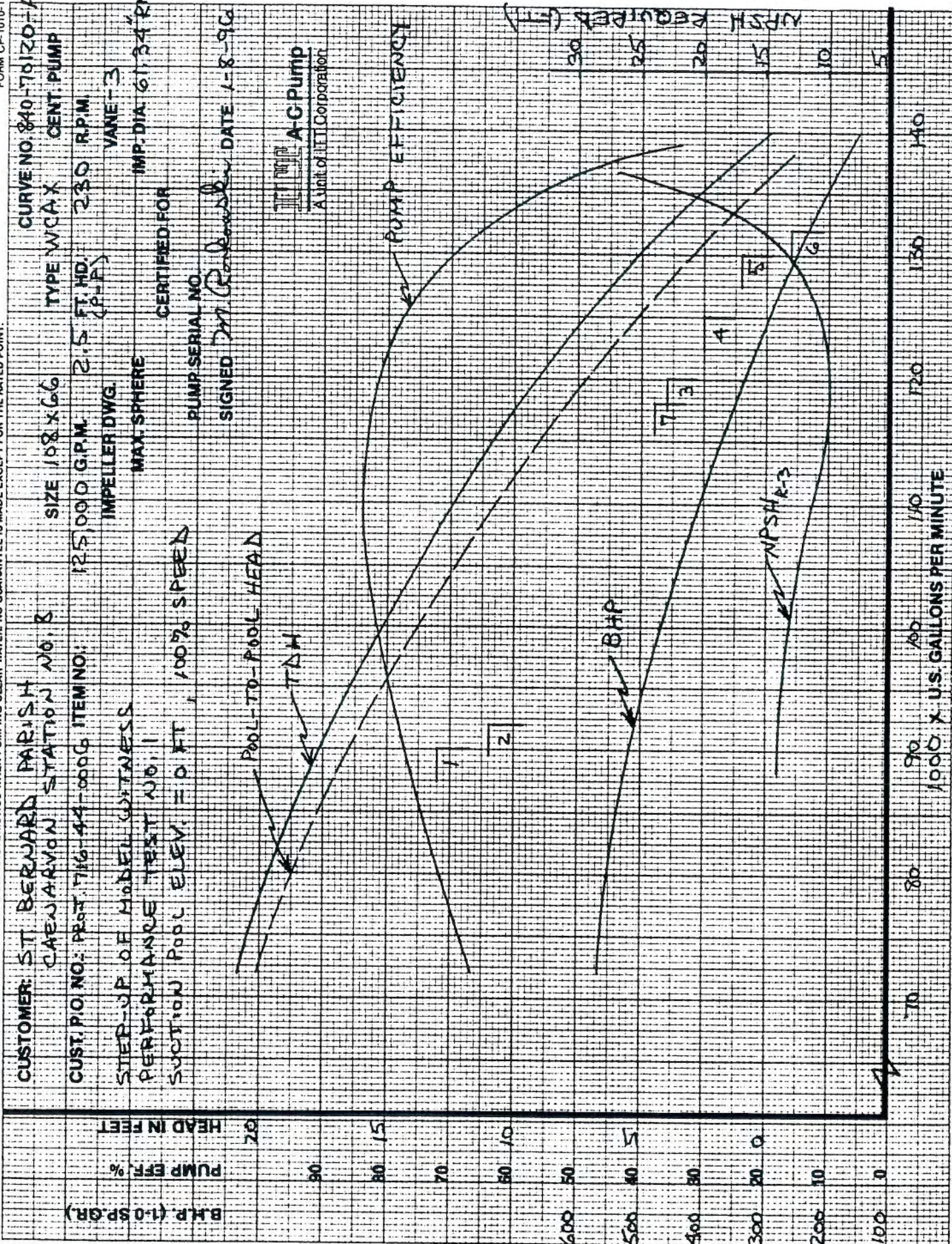
POOL-TO-POOL HEAD

TDM

BHP

PUMP EFFICIENCY

NPSH R-3



BHP (1-0 SPGR)
PUMP EFF. %
HEAD IN FEET

1000 X U.S. GALLONS PER MINUTE

CURVES SHOW APPROXIMATELY THE CHARACTERISTICS WHEN PUMPING CLEAR WATER. NO GUARANTEE IS MADE EXCEPT FOR THE RATED POINT.

CUSTOMER: ST. BERNARD PARISH
 CAENARVAN STATION NO. 8
 CUST. P.O. NO.: PROJ. 716-44-0006 ITEM NO.:
 STEP-UP OF MODEL WITNESS
 PERFORMANCE TEST NO. 2
 SUCTION POOL ELEV. = 0 FT., 95% SPEED

CURVE NO. 840-70120-B
 TYPE WCAX CENT. PUMP
 FT. HD. 218.5 R.P.M.
 VANE - 3
 IMP. DIA. 6 1/34 IN.

IMPELLER DWG. MAX. SPHERE
 CERTIFIED FOR
 PUMP SERIAL NO.
 SIGNED M. R. [Signature] DATE 1-8-96

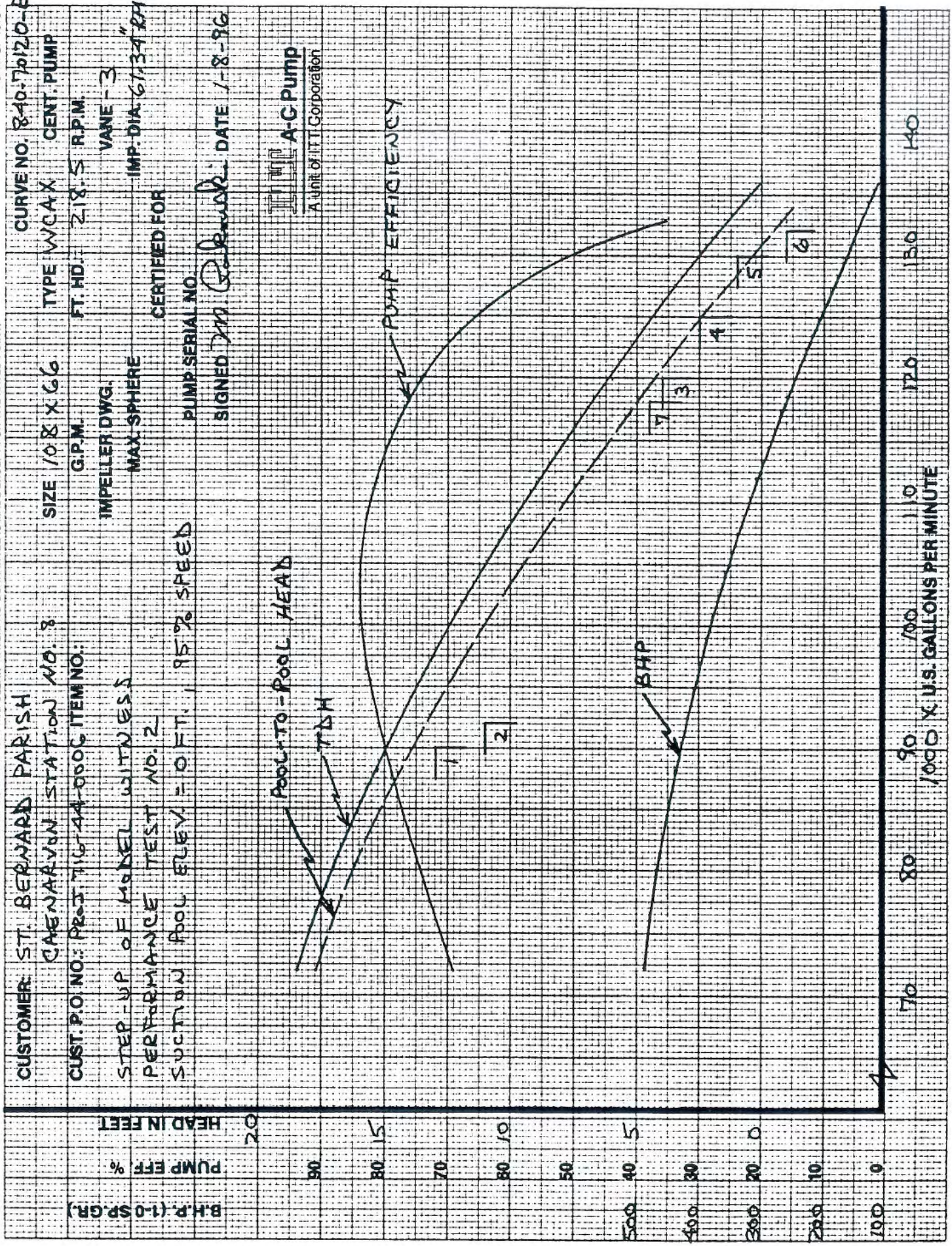


Pool-to-Pool HEAD

Pool-to-Pool HEAD

PUMP EFFICIENCY

BHP



CURVES SHOW APPROXIMATELY THE CHARACTERISTICS WHEN PUMPING CLEAR WATER. NO GUARANTEE IS MADE EXCEPT FOR THE RATED POINT.

FORM CP-1010-1

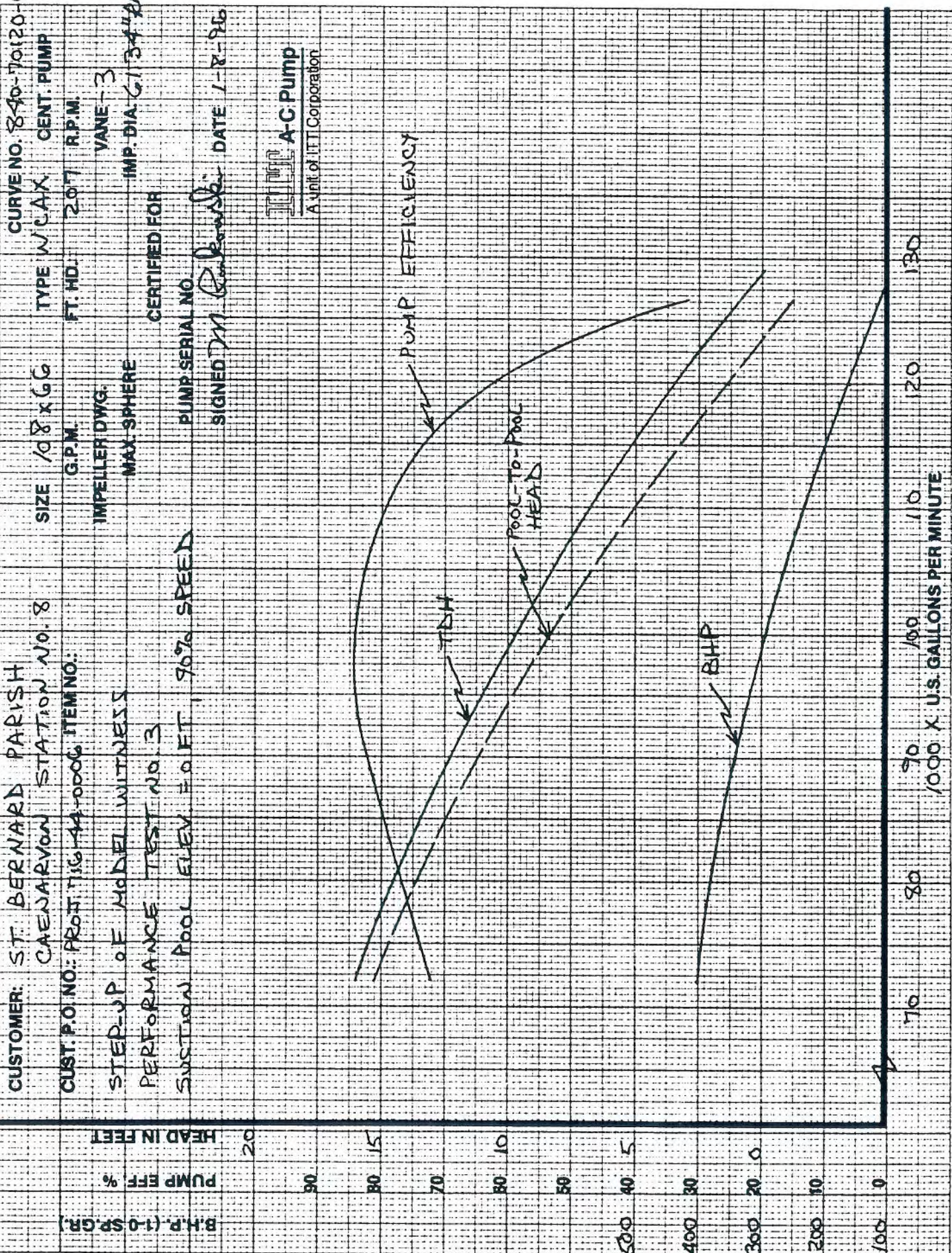
CUSTOMER: ST. BERNARD PARISH
 CAENARVON STATION NO. 8
 SIZE 108 X 66
 TYPE W/C AX
 CURVE NO. 840-70120-C

CUST. P.O. NO.: PROJ. T-16-44-0006 ITEM NO. 207
 G.P.M. 207
 FT. HD. 207
 R.P.M. 1734

STEP-UP OF MODEL WITNESS
 IMPELLER DWG. VANE-3
 IMP. DIA. 6 1/4"

PERFORMANCE TEST NO. 3
 MAX SPHERE
 CERTIFIED FOR

STATION POOL ELEV. 2.0 FT. 90% SPEED
 PUMP SERIAL NO.
 SIGNED *M. R. ...* DATE 1-8-96



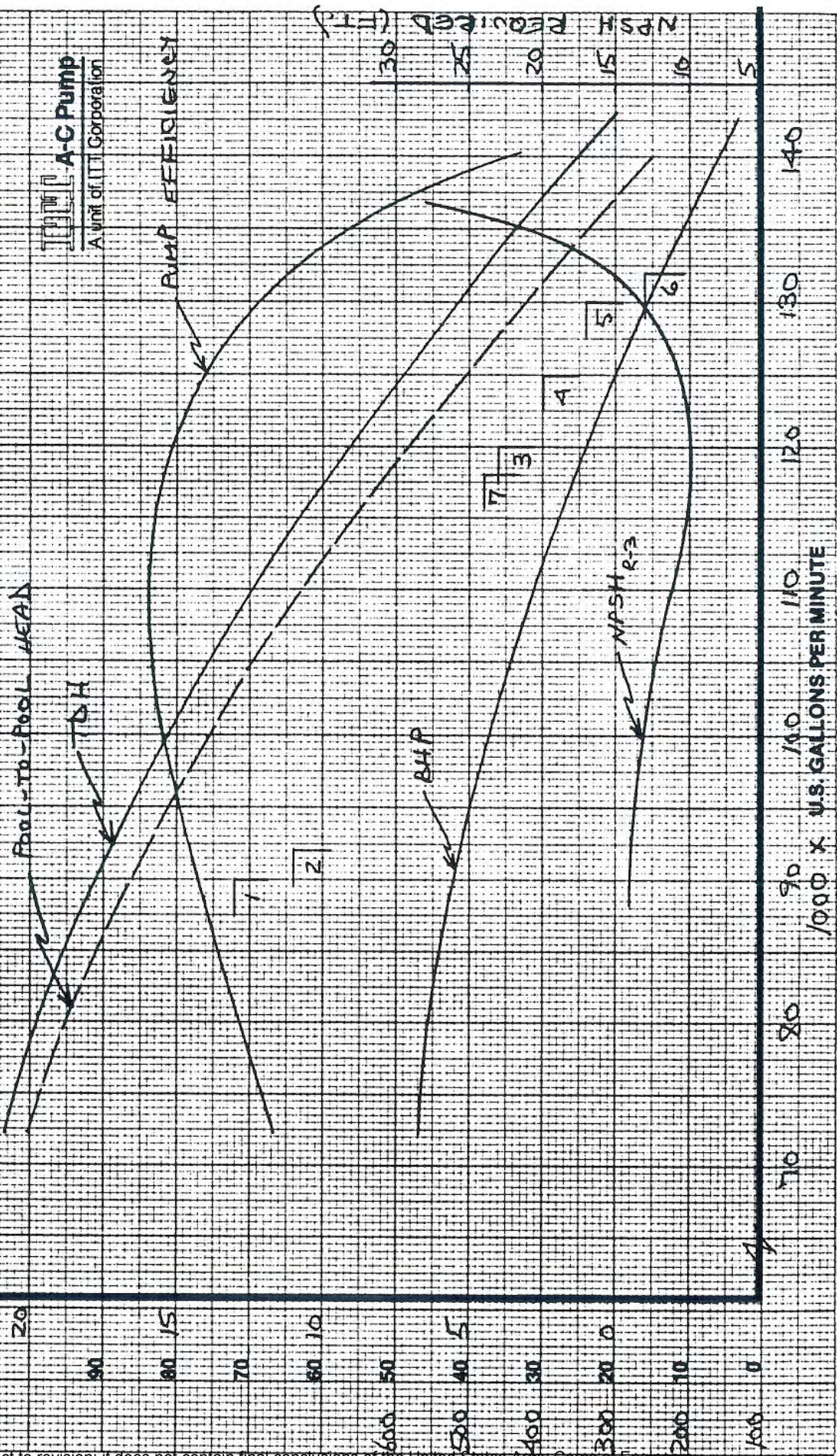
CURVES SHOW APPROXIMATELY THE CHARACTERISTICS WHEN PUMPING CLEAR WATER. NO GUARANTEE IS MADE EXCEPT FOR THE RATED POINT.

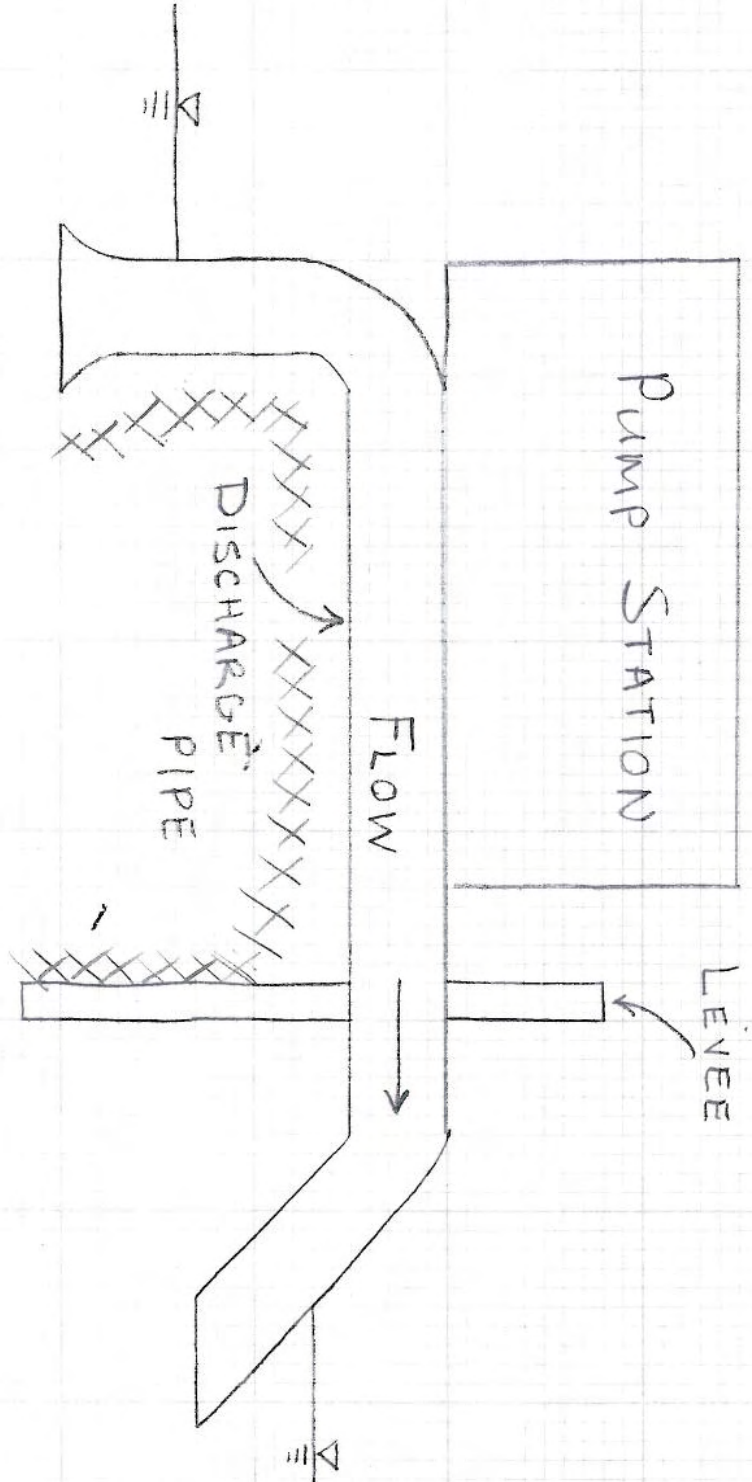
CUSTOMER: ST. BERNARD PARISH
 CAENARVON STATION NO. 8
 SIZE 108 X 66
 TYPE WCAX CENT. PUMP
 CURVE NO. 840-70120-D

CUST. P.O. NO.: PROJ. 76-44-0006 ITEM NO. 125000
 GPM. 2.5 FT. HD. 250 R.P.M.
 IMPELLER DWG. (P-P)
 VANE-3

STEP-UP OF MODEL WITNESS
 PERFORMANCE TEST NO. 4
 IMP. DIA. 61.34 INCHES

SUCTION POOL ELEV. = -2.0 FT., 100% SPEED
 PUMP SERIAL NO. _____
 SIGNED *M. R. ...* DATE 1-8-96





NOT TO SCALE

CENWP-EC-HD

DRAFT

24 February 2006

MEMORANDUM FOR RECORD

SUBJECT 60% Draft Submission of Estimated Backflow Rating Curves for St. Bernard Parish, LA

Problem Statement: A post Katrina flood study is being conducted for a watershed in Jefferson Parish in New Orleans District. During the flood event, the pumps stopped operating and reverse flow discharged backwards through the pump station conduits. The needs of the study include an approximate rating curve for reverse flow through the pump station.

Objectives: Develop rating curve for reverse flow rate versus head differential and provide documentation of rating and methods used.

Assumptions: Many assumptions needed to be made in order to complete the draft backflow rating curves associated with this document. Assumptions made in developing the backflow rating curve estimates are listed in the Excel file worksheets for each unique pump and configuration. The most significant assumptions have been included in the rating curve worksheets attached to this memorandum and are summarized below.

- **Data Assumptions:**
Many of the pump stations in St. Bernard Parish only had very sketchy information on pumps, intakes and discharge pipes with regard to: elevations, sizes, cross-sections, bends, diffusers, lengths, pump intake grates, discharge pipe baffles etc. In addition, elevations of the pump station and system were not always available or there appeared to be inconsistencies between collected questionnaire responses, sketches and photos. Lack of data may contribute to significant uncertainty in the backflow rating curves. For pump stations 1 and 4, all that was missing was the width of the discharge channel (assumed to be 10 feet from photos). The minimum error margin for all calculations is $\pm 30\%$. The error margin will naturally increase for those cases where station data is missing and pertinent dimensions must be estimated.
- **System Loss Assumptions:**
Intake, exit, bend, expansion, impeller and friction losses have been included for each unique pump and configuration. Some assumptions were made when system details were not available from the data (see above). The most significant loss was typically through the pump itself and is the largest cause of uncertainty. We currently estimate an error margin of $\pm 30\%$ related to the pump loss.
- **Flow Control Assumptions:**
Conditions that trigger variations in flow control were estimated using the following criteria:

- Backflow starts when the lake or reservoir head (H1 at intake of backflow condition) is greater than the controlling crest of the discharge pipe. The first trigger point is that H1 must exceed this crest elevation to start flow.
- Siphon flow starts with rising reservoir:
 - If there is no open air valve or vent, when H1 is greater than the controlling soffit of the discharge pipe. In this case the full flow rating curves (“If pipe primes, then full outlet control...”) are applied. The full flow curve table is provided in a matrix of H1 and H2 (downstream water level at normal pump intake). The second trigger point is this H1 value that initiates siphon flow condition.¹
 - If an open air vent is available, siphon does not develop. The critical flow control shown on the left side of the rating curve (“Assuming the pipe never primes”) controls. However, full flow will occur with an open air vent when certain H1 thresholds are exceeded (such that the soffit pressures exceed atmospheric pressure). The H1 thresholds are listed under respective tailwater levels in two rows beneath the full flow rating curve table.
- If siphon flow develops, then it will continue until either the pressure at the soffit of the crest pipe drops below -9.5 psi, or when H1 falls below with 1 foot of the top of the outlet to the lake (which acts as the intake in reverse flow conditions). The third trigger point is the estimated elevation at which the siphon breaks. If the siphon breaks, then critical flow controls.

Conclusions: Modifications could be made to the estimates if and when more detailed information becomes available to make more conclusive backflow rating curve assumptions. The CENWP-EC-HD will continue to seek data on pump loss coefficients.

The 60% reverse flow rating curves are attached in order of pump stations. The tables present the flow rates per individual pump. The detailed calculations, assumptions, and assumed dimensions are available upon request.

Steve Schlenker
 Karen Kuhn
 Hydraulic Engineers
 CENWP-EC-HD

¹ The threshold for which siphon flow develops is unpredictable and is dependent on conditions and system geometry. A momentary abrupt rise in the lake water surface could send a pulse that primes the conduit. On the other hand, minor cracks or air leaks in the conduit could also prevent or break the siphon before it would normally give way (3rd trigger point). The current H1 threshold values are based on EC-HD judgment—however the values are subject to change as more information is obtained.

St. Bernard Parish, #1 Fortifications Canal Pumping Station: 42 x 54 inches

<p>ENGINEERING DESIGN SHEET</p> <p>PROJECT: St. Bernard Parish Pump Stations #1/ Foundation Canal Pumping Station-42x54" pump 40,000 gpm (1 pump this size, 3 total in station)</p> <p>SUBJECT: Backflow Rating Curves</p>		<p>OFFICE SYMBOL: CENWP-EC-HD COMPUTED BY: KK/SS DATE: 22 Feb 2006 WORKSHEET: Rating Curve</p> <p>CHECKED BY: SJS/KAK</p>						
<p>Crest Elevation (ft) = 3.83</p> <p>Trigger Points: Flow starts when H1 > is greater than 3.83 ft crest of intake</p> <p>Assume Tainter Gate Left Open</p> <p>DRAFT Rating Curves for Approx 40,000 gpm Pump (42 X 54" diam propeller) (assumed Pump #1 for #1 Fortification Canal Pumping Station)</p> <p>Discharge in CFS for H1 & H2</p>								
<p>Rating Curve Per Pump: Flow Rate for H1 versus H2</p>								
		Elevation (H2) at Backflow Outlet C3						
		-6	-4	-2	0	2	4	6
H1 U/s Reservoir Elevation (ft)	Level Above Discharge Pipe Crest (ft)	H2 = -6 (ft)	H2 = -4 (ft)	H2 = -2 (ft)	H2 = 0 (ft)	H2 = 2 (ft)	H2 = 4 (ft)	H2 = 6 (ft)
3.00	-0.83	0	0	0	0	0	0	0
3.50	-0.33	0	0	0	0	0	0	0
4.00	0.17	2	2	2	2	2	0	-88
4.50	0.67	17	17	17	17	17	17	-76
5.00	1.17	39	39	39	39	39	39	-62
5.50	1.67	66	66	66	66	66	66	-44
6.00	2.17	98	98	98	98	98	98	0
6.50	2.67	134	134	134	134	132	98	44
7.00	3.17	173	173	173	164	139	107	62
7.50	3.67	215	210	191	170	145	116	76
8.00	4.17	232	215	196	175	152	124	88
8.50	4.67	236	219	201	181	158	132	98
9.00	5.17	240	224	206	186	164	139	107
9.50	5.67	244	228	210	191	170	145	116
10.00	6.17	248	232	215	196	175	152	124
10.50	6.67	252	236	219	201	181	158	132
11.00	7.17	256	240	224	206	186	164	139
11.50	7.67	259	244	228	210	191	170	145
12.00	8.17	263	248	232	215	196	175	152
12.50	8.67	267	252	236	219	201	181	158
13.00	9.17	270	256	240	224	206	186	164

NOTES:

- 1 Rating curve is accurate within ± 30% due uncertainty of pump curve loss coefficient and unknown width of discharge channel
- 2 Loss and Trigger Point Assumptions:
 - Pump loss coefficient = 3.00
 - Siphon flow does not start till H1 > soffit of pipe at crest(Zt)
 - Intake loss = 0.5
 - Exit Loss = 1.2 (grating effect)
 - Bend and expansion losses also incorporated
- 3 Data Assumptions:
 - Tainter Gate Left open
 - Discharge Channel width = 10 feet
- 4 Data Needs:
 - Discharge Channel width
- 5 Backflow prevention:
 - Available: Tainter Gate for closure

St. Bernard Parish, #1 Fortifications Canal Pumping Station: 94 x 128 inches

<p>ENGINEERING DESIGN SHEET PROJECT: St. Bernard Parish Pump Stations #4 Meraux Pump Station-94x128" pumps 200,000 gpm (2 pumps this size, 3 total in station) SUBJECT: Backflow Rating Curves</p>		<p>OFFICE SYMBOL: CENWP-EC-HD COMPUTED BY: KK/SS DATE: 22 Feb 2006 WORKSHEET: Rating Curve CHECKED BY: SJS/KAK</p>						
<p>Crest Elevation (ft) = 3.83 Trigger Points: Flow starts when H1 > is greater than 3.83 ft crest of weir</p> <p>Assume Tainter Gate Left Open</p> <p>DRAFT Rating Curves for Approx 200,000 gpm Pump (94X128" diam propeller) (assumed Pump #2&3 for #4 Meraux Pumping Station)</p> <p>Discharge in CFS for H1 & H2</p>								
<p>Rating Curve per Pump: Flow Rate for H1 versus H2 Elevation (H2) at Backflow Outlet C3</p>								
		-6	-4	-2	0	2	4	6
H1 U/s Reservoir Elevation (ft)	Level Above Weir Crest (ft)	H2 = -6 (ft)	H2 = -4 (ft)	H2 = -2 (ft)	H2 = 0 (ft)	H2 = 2 (ft)	H2 = 4 (ft)	H2 = 6 (ft)
3.00	-0.83	0	0	0	0	0	0	0
3.50	-0.33	0	0	0	0	0	0	0
4.00	0.17	2	2	2	2	2	0	-361
4.50	0.67	17	17	17	17	17	17	-312
5.00	1.17	39	39	39	39	39	39	-255
5.50	1.67	66	66	66	66	66	66	-180
6.00	2.17	98	98	98	98	98	98	0
6.50	2.67	134	134	134	134	134	134	134
7.00	3.17	173	173	173	173	173	173	173
7.50	3.67	215	215	215	215	215	215	215
8.00	4.17	259	259	259	259	259	259	259
8.50	4.67	306	306	306	306	306	306	306
9.00	5.17	355	355	355	355	355	355	355
9.50	5.67	405	405	405	405	405	405	405
10.00	6.17	458	458	458	458	458	458	458
10.50	6.67	512	512	512	512	512	512	512
11.00	7.17	567	567	567	567	567	567	567
11.50	7.67	624	624	624	624	624	624	598
12.00	8.17	682	682	682	682	682	682	625
12.50	8.67	741	741	741	741	741	741	650
13.00	9.17	800	800	800	800	800	765	675

NOTES:

- 1 Full flow Rating curve is accurate within $\pm 30\%$ due uncertainty of pump curve loss coefficient and timing and degree of siphoning developed
- 2 Loss and Trigger Point Assumptions:
 Pump loss coefficient = 3.00
 Siphon flow does not start till H1 > soffit of pipe at crest(Zt)
 Intake loss = 0.5
 Exit Loss = 1.2
 Bend and expansion losses also incorporated
- 3 Data Assumptions:
 Tainter Gate Left open
 Discharge gate width = 10 feet
- 4 Data Needs:
 Discharge gate width
- 5 Backflow prevention:
 Available: Tainter Gate for Closure

St. Bernard Parish, #2 Guichard and #3 Bayou Villere: 42 inch Pumps

ENGINEERING DESIGN SHEET			OFFICE SYMBOL: CENWP-EC-HD			
PROJECT: St. Bernard Parish Pump Stations			COMPUTED BY: KK/SS		DATE: 22 Feb 2006	
Guichard #2/ Bayou Villere #3 -42" pumps approx 50,000 gpm					WORKSHEET: Rating Curve	
SUBJECT: Backflow Rating Curves			CHECKED BY: SJS/KAK			

Crest Elevation (ft) = 11

Trigger Points:
 Flow starts when H1 > is greater than 11 ft crest of conduit
 Siphon Flow starts with rising H1 when:
 If no open air valve or vent, when H1 > Soffit = 14.5 ft assume siphon starts when H1 = Zt
 If open vent; see bottom of table for when full flow occurs
 If siphon flow develops, flow stops (approx.) when H1 < 2 ft assume drawdown at intake ≈1 ft.

DRAFT Rating Curves for Approx 50,000 gpm Pump (42" propeller)
 (assumed Pump #1 for Guichard PS#2 and possible pump(s) for Bayou Villere PS#3)

Discharge in CFS for H1 & H2

Assuming Pipe never primes:

H1 U/s Reservoir Elevation (ft)	Level Above Discharge Pipe Crest (ft)	Q Flow Rate (cfs)
8.00	-3.00	0
8.50	-2.50	0
9.00	-2.00	0
9.50	-1.50	0
10.00	-1.00	0
10.50	-0.50	0
11.00	0.00	0
11.50	0.50	2
12.00	1.00	6
12.50	1.50	13
13.00	2.00	21
13.50	2.50	30
14.00	3.00	39
14.50	3.50	48
15.00	4.00	56
15.50	4.50	65
16.00	5.00	73
16.50	5.50	80
17.00	6.00	87
17.50	6.50	94
18.00	7.00	101

If Pipe primes then full flow outlet control as siphon:
 Primed Flow (full Outlet Control) as function of H2
 Elevation (H2) at Backflow Outlet C3

-6	-3.16667	-0.333333	2.5	5.333333	8.166667	11
Primed Conduit, H2 =-6 (ft)	Primed Conduit, H2 =-3 (ft)	Primed Conduit, H2 =0 (ft)	Primed Conduit, H2 =3 (ft)	Primed Conduit, H2 =5 (ft)	Primed Conduit, H2 =8 (ft)	Primed Conduit, H2 =11 (ft)
113	101	87	71	49	-12	-52
115	103	90	74	54	17	-48
117	105	92	77	58	28	-43
119	107	95	80	62	35	-37
121	109	97	83	65	41	-30
123	112	99	85	69	46	-21
124	114	102	88	72	51	0
126	116	104	91	75	55	21
128	118	106	93	78	59	30
130	119	108	95	81	63	37
132	121	110	98	84	66	43
133	123	112	100	86	70	48
135	125	114	102	89	73	52
137	127	116	105	91	76	56
138	129	118	107	94	79	60
140	130	120	109	96	82	64
142	132	122	111	99	84	67
143	134	124	113	101	87	71
145	136	126	115	103	90	74
146	137	127	117	105	92	77
148	139	129	119	107	95	80

Estimated H1 required for full flow if Open Air Valve or vent:
 TW=-6 TW=-3 TW=0 TW=3 TW=5 TW=8 TW=11
 If Open Air Valve H1 > 19 18 17 15 14 12 #NUM!

NOTES:

- 1 Full flow Rating curve is accurate within ± 30% due uncertainty of pump curve loss coefficient and timing and degree of siphoning developed
- 2 Loss and Trigger Point Assumptions:
 Pump loss coefficient = 3.00
 Siphon flow does not start till H1 > soffit of pipe at crest(Zt)
 Intake loss = 0.5
 Exit Loss = 1
 Bend and expansion losses also incorporated
- 3 Data Assumptions:
 Shape/length/angle of: bends, pipes, outlet, intake assumed from Pump info in questionnaire and photos.
 Elevations assumed from information on questionnaire sheets for PS#2 & assumed similarity to PS#6.
 NOTE: Information regarding elevations for PS#2 and PS#3 are not consistent (varies by about 10 feet)
- 4 Data Needs:
 Shape/length/angle of: bends, pipes, outlet, intake.
 Elevations for bends, pipes, pump, outlet, intake etc.
 Pump info for Pump #3 at Guichard PS#2; and for Pumps #1, #2, #3 for Bayou Villere PS#3
 Cover sheet for PS#2 indicates pump #3 is 75,000 gpm pump. No other usable info given.
 Need pump diam for pump #3 to estimate backflow curve.
 Cover sheet for PS#3 indicates 3 pumps @ 50,000 & 75,000 & 100,000 gpm
 Questionnaire responses indicate 3 pumps @ 60" propeller, 90" intake, 60" discharge column.
 More information needed to determine if curves given are usable for PS#3.
- 5 Backflow prevention:
 Available: PS#2 No floodgates; No backflow valves
 PS#3 Intake pipes to pumps 1 and 2 have butterfly valves
 Installed/used: PS#2 n/a
 PS#3 No backstops/brakes installed to prevent reverse rotation

St. Bernard Parish, #2 Guichard and #3 Bayou Villere: 60 inch Pumps

ENGINEERING DESIGN SHEET			OFFICE SYMBOL: CENWP-EC-HD			
PROJECT: St. Bernard Parish Pump Stations			COMPUTED BY: KK/SS		DATE: 22 Feb 2006	
Guichard #2/ Bayou Villere #3-60" pumps appr 100,000 gpm					WORKSHEET: Rating Curve	
SUBJECT: Backflow Rating Curves			CHECKED BY: SJS/KAK			

Crest Elevation (ft) = 11

Trigger Points:
 Flow starts when H1 > is greater than 11 ft crest of conduit
 Siphon Flow starts with rising H1 when:
 If no open air valve or vent, when H1 > Soffit = 16.0 ft assume siphon starts when H1 = Zt
 If open vent; see bottom of table for when full flow occurs
 If siphon flow develops, flow stops (approx.) when H1 < 3 ft assume drawdown at intake ≈1 ft.

DRAFT Rating Curves for Approx 100,000 gpm Pump (60" diam propeller)
(assumed Pump #2 & #4 for Guichard PS#2 and possible pump(s) for Bayou Villere PS#3)

Discharge in CFS for H1 & H2

Assuming Pipe never primes:

H1 U/s Reservoir Elevation (ft)	Level Above Discharge Pipe Crest (ft)	Q Flow Rate (cfs)
8.00	-3.00	0
8.50	-2.50	0
9.00	-2.00	0
9.50	-1.50	0
10.00	-1.00	0
10.50	-0.50	0
11.00	0.00	0
11.50	0.50	2
12.00	1.00	7
12.50	1.50	16
13.00	2.00	27
13.50	2.50	41
14.00	3.00	55
14.50	3.50	70
15.00	4.00	86
15.50	4.50	102
16.00	5.00	118
16.50	5.50	133
17.00	6.00	148
17.50	6.50	162
18.00	7.00	176

If Pipe primes then full flow outlet control as siphon:
 Primed Flow (full Outlet Control) as function of H2
 Elevation (H2) at Backflow Outlet C3

-6	-3.16667	-0.33333	2.5	5.33333	8.16667	11
Primed Conduit, H2 = -6 (ft)	Primed Conduit, H2 = -3 (ft)	Primed Conduit, H2 = 0 (ft)	Primed Conduit, H2 = 3 (ft)	Primed Conduit, H2 = 5 (ft)	Primed Conduit, H2 = 8 (ft)	Primed Conduit, H2 = 11 (ft)
233	208	180	146	102	-25	-108
237	212	185	152	111	36	-98
241	217	190	159	119	57	-88
245	221	195	165	127	72	-76
249	226	200	170	134	84	-62
253	230	205	176	141	95	-44
256	234	209	181	148	105	0
260	238	214	187	154	114	44
264	242	218	192	161	122	62
268	246	223	197	167	129	76
271	250	227	202	172	137	88
275	254	231	206	178	144	98
278	258	236	211	183	150	108
282	261	240	215	188	157	116
285	265	244	220	193	163	124
288	269	248	224	198	168	132
292	272	251	229	203	174	139
295	276	255	233	208	180	146
298	279	259	237	212	185	152
302	283	263	241	217	190	159
305	286	266	245	221	195	165

Estimated H1 required for full flow if Open Air Valve or vent:
 TW=-6 TW=-3 TW=0 TW=3 TW=5 TW=8 TW=11
 If Open Air Valve H1 > 19 18 16 15 14 12 #NUM!

NOTES:

- Full flow Rating curve is accurate within ± 30% due uncertainty of pump curve loss coefficient and timing and degree of siphoning developed
- Loss and Trigger Point Assumptions:
 Pump loss coefficient = 3.00
 Siphon flow does not start till H1 > soffit of pipe at crest(Zt)
 Intake loss = 0.5
 Exit Loss = 1
 Bend and expansion losses also incorporated
- Data Assumptions:
 Shape/length/angle of: bends, pipes, outlet, intake assumed from Pump info in questionnaire and photos.
 Elevations assumed from information on questionnaire sheets for PS#2 & assumed similarity to PS#6.
 NOTE: Information regarding elevations for PS#2 and PS#3 are not consistent (varies by about 10 feet)
- Data Needs:
 Shape/length/angle of: bends, pipes, outlet, intake.
 Elevations for bends, pipes, pump, outlet, intake etc.
 Pump info for Pump #3 at Guichard PS#2; and for Pumps #1, #2, #3 for Bayou Villere PS#3
 Cover sheet for PS#2 indicates pump #3 is 75,000 gpm pump. No other usable info given.
 Need pump diam for pump #3 to estimate backflow curve.
 Cover sheet for PS#3 indicates 3 pumps @ 50,000 & 75,000 & 100,000 gpm
 Questionnaire responses indicate 3 pumps @ 60" propeller, 90" intake, 60" discharge column
 More information needed to determine if curves given are usable for PS#3.
- Backflow prevention:
 Available: PS#2 No floodgates; No backflow valves
 PS#3 Intake pipes to pumps 1 and 2 have butterfly valves
 Installed/used: PS#2 n/a
 PS#3 No backstops/brakes installed to prevent reverse rotation

St. Bernard Parish, #4 Meraux Pumping Station: 42 x 54 inches

ENGINEERING DESIGN SHEET		OFFICE SYMBOL: CENWP-EC-HD	
PROJECT: St. Bernard Parish Pump Stations #4 Meraux Pumping Station-42x54" pump 40,000 gpm (1 pump this size, 3 total in station)		COMPUTED BY: KK/SS	DATE: 22 Feb 2006
SUBJECT: Backflow Rating Curves		CHECKED BY: SJS/KAK	WORKSHEET: Rating Curve

Crest Elevation (ft) = 3.83
 Trigger Points:
 Flow starts when H1 > is greater than 3.83 ft crest of intake

Assume Tainter Gate Left Open

DRAFT Rating Curves for Approx 40,000 gpm Pump (42 X 54" diam propeller)
(assumed Pump #1 for #4 Meraux Pumping Station)

Discharge in CFS for H1 & H2

Rating Curve Per Pump: Flow Rate for H1 versus H2

		Elevation (H2) at Backflow Outlet C3						
		-6	-4	-2	0	2	4	6
H1 U/s Reservoir Elevation (ft)	Level Above Discharge Pipe Crest (ft)	H2 = -6 (ft)	H2 = -4 (ft)	H2 = -2 (ft)	H2 = 0 (ft)	H2 = 2 (ft)	H2 = 4 (ft)	H2 = 6 (ft)
3.00	-0.83	0	0	0	0	0	0	0
3.50	-0.33	0	0	0	0	0	0	0
4.00	0.17	2	2	2	2	2	0	-88
4.50	0.67	17	17	17	17	17	17	-76
5.00	1.17	39	39	39	39	39	39	-62
5.50	1.67	66	66	66	66	66	66	-44
6.00	2.17	98	98	98	98	98	88	0
6.50	2.67	134	134	134	134	132	98	44
7.00	3.17	173	173	173	164	139	107	62
7.50	3.67	215	210	191	170	145	116	76
8.00	4.17	232	215	196	175	152	124	88
8.50	4.67	236	219	201	181	158	132	98
9.00	5.17	240	224	206	186	164	139	107
9.50	5.67	244	228	210	191	170	145	116
10.00	6.17	248	232	215	196	175	152	124
10.50	6.67	252	236	219	201	181	158	132
11.00	7.17	256	240	224	206	186	164	139
11.50	7.67	259	244	228	210	191	170	145
12.00	8.17	263	248	232	215	196	175	152
12.50	8.67	267	252	236	219	201	181	158
13.00	9.17	270	256	240	224	206	186	164

NOTES:

- 1 Rating curve is accurate within $\pm 30\%$ due uncertainty of pump curve loss coefficient and unknown width of discharge channel
- 2 Loss and Trigger Point Assumptions:
 Pump loss coefficient = 3.00
 Siphon flow does not start till H1 > soffit of pipe at crest(Zt)
 Intake loss = 0.5
 Exit Loss = 1.2 (grating effect)
 Bend and expansion losses also incorporated
- 3 Data Assumptions:
 Tainter Gate Left open
 Discharge Channel width = 10 feet
- 4 Data Needs:
 Discharge Channel width
- 5 Backflow prevention:
 Available: Tainter Gate for closure

St. Bernard Parish, #4 Meraux Pumping Station: 94 x 128 inches

ENGINEERING DESIGN SHEET		OFFICE SYMBOL: CENWP-EC-HD						
PROJECT: St. Bernard Parish Pump Stations		COMPUTED BY: KK/SS	DATE: 22 Feb 2006					
#4 Meraux Pumping Station-94x128" pumps		WORKSHEET: Rating Curve						
200,000 gpm (2 pumps this size, 3 total in station)		CHECKED BY: SJS/KAK						
SUBJECT: Backflow Rating Curves								
Crest Elevation (ft) = 3.83								
Trigger Points:								
Flow starts when H1 > is greater than		3.83 ft	crest of weir					
Assume Tainter Gate Left Open								
DRAFT Rating Curves for Approx 200,000 gpm Pump (94X128" diam propeller)								
(assumed Pump #2&3 for #4 Meraux Pumping Station)								
Discharge in CFS for H1 & H2								
Rating Curve per Pump: Flow Rate for H1 versus H2								
Elevation (H2) at Backflow Outlet C3								
		-6	-4	-2	0	2	4	6
H1 U/s Reservoir Elevation (ft)	Level Above Weir Crest (ft)	H2 = -6 (ft)	H2 = -4 (ft)	H2 = -2 (ft)	H2 = 0 (ft)	H2 = 2 (ft)	H2 = 4 (ft)	H2 = 6 (ft)
3.00	-0.83	0	0	0	0	0	0	0
3.50	-0.33	0	0	0	0	0	0	0
4.00	0.17	2	2	2	2	2	0	-361
4.50	0.67	17	17	17	17	17	17	-312
5.00	1.17	39	39	39	39	39	39	-255
5.50	1.67	66	66	66	66	66	66	-180
6.00	2.17	98	98	98	98	98	98	0
6.50	2.67	134	134	134	134	134	134	134
7.00	3.17	173	173	173	173	173	173	173
7.50	3.67	215	215	215	215	215	215	215
8.00	4.17	259	259	259	259	259	259	259
8.50	4.67	306	306	306	306	306	306	306
9.00	5.17	355	355	355	355	355	355	355
9.50	5.67	405	405	405	405	405	405	405
10.00	6.17	458	458	458	458	458	458	458
10.50	6.67	512	512	512	512	512	512	512
11.00	7.17	567	567	567	567	567	567	567
11.50	7.67	624	624	624	624	624	624	598
12.00	8.17	682	682	682	682	682	682	625
12.50	8.67	741	741	741	741	741	741	650
13.00	9.17	800	800	800	800	800	765	675

NOTES:

- 1 Full flow Rating curve is accurate within $\pm 30\%$ due uncertainty of pump curve loss coefficient and timing and degree of siphoning developed
- 2 Loss and Trigger Point Assumptions:
 - Pump loss coefficient = 3.00
 - Siphon flow does not start till H1 > soffit of pipe at crest(Zt)
 - Intake loss = 0.5
 - Exit Loss = 1.2
 - Bend and expansion losses also incorporated
- 3 Data Assumptions:
 - Tainter Gate Left open
 - Discharge gate width = 10 feet
- 4 Data Needs:
 - Discharge gate width
- 5 Backflow prevention:
 - Available: Tainter Gate for Closure

St. Bernard Parish, #5 E.J. Gore Pump Station

Flap gates on pipe exits prevent reverse flow through pumps.

St. Bernard Parish, #6 Jean Laffitte and #7 Bayou Ducros pumps

ENGINEERING DESIGN SHEET

PROJECT: St. Bernard Parish Pump Stations
Jean Laffitte #6 & Bayou Ducros #7

SUBJECT: Backflow Rating Curves

OFFICE SYMBOL: CENWP-EC-HD

COMPUTED BY: KK/SS DATE: 22 Feb 2006

WORKSHEET: Rating Curve

CHECKED BY: SJS/KAK

Crest Elevation (ft) = 5

Trigger Points:

Flow starts when H1 > is greater than 5 ft crest of conduit

Siphon Flow starts with rising H1 when:

If no open air valve or vent, when H1 > Soffit = 11.0 ft assume siphon starts when H1 = Zt

If open vent; see bottom of table for when full flow occurs

If siphon flow develops, flow stops (approx.) when H1 < 4 ft assume drawdown at intake ?1 ft.

DRAFT Rating Curves for Each Pump (3 total for each pump station)

Discharge in CFS for H1 & H2

Assuming Pipe never primes:

H1 U/s Reservoir Elevation (ft)	Level Above Discharge Pipe Crest (ft)	Q Flow Rate (cfs)
5.00	0.00	0
5.45	0.45	2
5.90	0.90	7
6.35	1.35	14
6.80	1.80	25
7.25	2.25	37
7.70	2.70	51
8.15	3.15	65
8.60	3.60	80
9.05	4.05	95
9.50	4.50	110
9.95	4.95	125
10.40	5.40	139
10.85	5.85	154
11.30	6.30	167
11.75	6.75	181
12.20	7.20	194
12.65	7.65	206
13.10	8.10	219
13.55	8.55	231
14.00	9.00	242

If Pipe primes then full flow outlet control as siphon:

Primed Flow (full Outlet Control) as function of H2

Elevation (H2) at Backflow Outlet C3						
-7.0	-5.0	-3.0	-1.0	1.0	3.0	5.0
Primed Conduit, H2 = -7 (ft)	Primed Conduit, H2 = -5 (ft)	Primed Conduit, H2 = -3 (ft)	Primed Conduit, H2 = -1 (ft)	Primed Conduit, H2 = 1 (ft)	Primed Conduit, H2 = 3 (ft)	Primed Conduit, H2 = 5 (ft)
301	274	245	213	174	123	0
306	280	252	220	183	136	58
312	286	259	228	192	148	82
317	292	265	235	201	159	101
322	298	272	242	209	169	116
328	304	278	249	217	179	130
333	309	284	256	225	188	143
338	315	290	262	232	197	154
343	320	295	269	239	205	165
348	325	301	275	246	213	175
352	330	307	281	253	221	184
357	335	312	287	260	229	193
362	340	318	293	266	236	202
367	345	323	299	272	243	210
371	350	328	304	278	250	218
376	355	333	310	284	257	225
380	360	338	315	290	263	233
385	364	343	321	296	270	240
389	369	348	326	302	276	247
393	374	353	331	307	282	254
398	378	358	336	313	288	260

Estimated H1 required for full flow if Open Air Valve or vent:

TW=-7 TW=-5 TW=-3 TW=-1 TW=1 TW=3 TW=5

If Open Air Valve H1 > 17 15 13 11 9 7 5

NOTES:

1 Full flow Rating curve is accurate within ± 30% due uncertainty of pump curve loss coefficient and timing and degree of siphoning developed

2 Loss and Trigger Point Assumptions:

Pump loss coefficient = 3.00

Siphon flow does not start till H1 > soffit of pipe at crest(Zt)

Intake loss = 2 (diffusion chamber at normal exit)

Exit Loss = 1

Bend and expansion losses also incorporated

3 Data Assumptions:

Shape/length/angle of diffuser/baffle based on photos

Shape/length/angle of 2nd bend based on sketch and photos

Pipe lengths estimated from photos and 1988 Design Worksheet.

Elevations in msl and NGVD are same

4 Data Needs:

Shape/length/angle of diffuser & detail of baffle

Detail of pumps incl bend to discharge pipe, impeller

St. Bernard Parish, #8 St Mary pumps

ENGINEERING DESIGN SHEET

PROJECT: St. Bernard Parish Pump Stations
St. Mary #8

SUBJECT: Backflow Rating Curves

OFFICE SYMBOL: CENWP-EC-HD

COMPUTED BY: KK/SS DATE: 22 Feb 2006

WORKSHEET: Rating Curve

CHECKED BY: SJS/KAK

Crest Elevation (ft) = 4.75

Trigger Points:

Flow starts when H1 > is greater than 4.75 ft crest of conduit

Siphon Flow starts with rising H1 when:

If no open air valve or vent, when H1 > Soffit = 10.3 ft assume siphon starts when H1 = Zt

If open vent; see bottom of table for when full flow occurs

If siphon flow develops, flow stops (approx.) when H1 < 4 ft assume drawdown at intake ?1 ft.

DRAFT Rating Curves for Each Pump, 108x66 Centrifugal, approx 125,000 gpm, No. of Identical Pumps = 3

Discharge in CFS for H1 & H2

If Pipe primes then full flow outlet control as siphon:

Primed Flow (full Outlet Control) as function of H2

Elevation (H2) at Backflow Outlet C3

Assuming Pipe never primes:

H1 U/s Reservoir Elevation (ft)	Level Above Discharge Pipe Crest (ft)	Q Flow Rate (cfs)
3.00	-1.75	0
3.50	-1.25	0
4.00	-0.75	0
4.50	-0.25	0
5.00	0.25	1
5.50	0.75	4
6.00	1.25	12
6.50	1.75	22
7.00	2.25	35
7.50	2.75	49
8.00	3.25	63
8.50	3.75	78
9.00	4.25	92
9.50	4.75	107
10.00	5.25	120
10.50	5.75	134
11.00	6.25	147
11.50	6.75	159
12.00	7.25	172
12.50	7.75	183
13.00	8.25	195

-7	-5	-3	-1	1	3	5
Primed Conduit, H2 = -7 (ft)	Primed Conduit, H2 = -5 (ft)	Primed Conduit, H2 = -3 (ft)	Primed Conduit, H2 = -1 (ft)	Primed Conduit, H2 = 1 (ft)	Primed Conduit, H2 = 3 (ft)	Primed Conduit, H2 = 5 (ft)
228	204	176	144	102	0	-102
233	210	184	153	114	51	-88
239	216	191	161	125	72	-72
244	222	197	169	135	88	-51
249	228	204	176	144	102	0
255	233	210	184	153	114	51
260	239	216	191	161	125	72
265	244	222	197	169	135	88
269	249	228	204	176	144	102
274	255	233	210	184	153	114
279	260	239	216	191	161	125
283	265	244	222	197	169	135
288	269	249	228	204	176	144
292	274	255	233	210	184	153
297	279	260	239	216	191	161
301	283	265	244	222	197	169
306	288	269	249	228	204	176
310	292	274	255	233	210	184
314	297	279	260	239	216	191
318	301	283	265	244	222	197
322	306	288	269	249	228	204

Estimated H1 required for full flow if Open Air Valve or vent:

TW=-7 TW=-5 TW=-3 TW=-1 TW=1 TW=3 TW=5

If Open Air Valve H1 > 16 14 12 10 8 6 #NUM!

NOTES:

1 Full flow Rating curve is accurate within ± 30% due uncertainty of pump curve loss coefficient and timing and degree of siphoning developed

2 Loss and Trigger Point Assumptions:

Pump loss coefficient = 3.00
Siphon flow does not start till H1 > soffit of pipe at crest(Zt)
Intake loss = 2
Exit Loss = 1
Bend and expansion losses also incorporated

3 Data Assumptions:

Shape/length/angle of diffuser/baffle based on photos for PS#6 and PS#8 (similar to PS#6 but longer pipe)
Shape/length/angle of 2nd bend based on 1/2 dwg and photos (assumed similar to PS#6/7)
Pipe lengths estimated from photos and 1988 Design Worksheet for PS#6 and photos for PS#8.

4 Data Needs:

Shape/length/angle of diffuser & detail of baffle
Detail of pumps incl bend to discharge pipe, impeller

Name	Pump	Capacity	Manufacture	Size	Model Number	Serial Number	Installed	Driver	Rated Pump Speed	Pump Type	Pump Elevation*	Pump Curve	Discharge Gates	Rated Head	Track Rack Design Head	Intake Location	Discharge Location	Intake water elevation at Start	Intake water elevation at Stop	Intake water elevation range	Water elevations that effects station	Bearing Lubrication	Backstops or brakes
		(cfs)		(in)			(year)	Electric /Diesel	(rpm)	(Vertical/Horizontal)	(NGVD)	(yes/no)	(type)	(ft)	(ft)			(NGVD)	(NGVD)	(NGVD)	(NGVD)	(oil/water)	(yes/no)
Fortification #1	1	445	Baldwin-Lima-Hamilton (Patterson)	94 x 128	AFV	?	1972	Diesel	212	Vertical	-1.5	yes	tainter gates	19	n/a	Florida Walk Canal	Bayou Bienvenue	-6.0	-6.5	0.5	8	Oil	No
	2	90	Baldwin-Lima-Hamilton (Patterson)	42 x 54	AFV	?	1972	Electric 60 Hz	505	Vertical	-1.5	yes	tainter gates	20	n/a	Florida Walk Canal	Bayou Bienvenue	-6.0	-6.5	0.5	8	Oil	No
	3	445	Baldwin-Lima-Hamilton (Patterson)	94 x 128	AFV	?	1972	Diesel	212	Vertical	-1.5	yes	tainter gates	19	n/a	Florida Walk Canal	Bayou Bienvenue	-6.0	-6.5	0.5	8	Oil	No
	Total	980																					
Guichard #2	1**	111	M&W (MWI)	42	NC342P12	?	1950's	Diesel	n/a	Horizontal	-8	yes	none	n/a	n/a	Florida Walk Canal	Bayou Bienvenue	-6.0	-6.5	0.5	4	Oil	No
	2**	267	M&W (MWI)	60	NC360P12	?	1950's	Diesel	n/a	Horizontal	-8	yes	none	n/a	n/a	Florida Walk Canal	Bayou Bienvenue	-6.0	-6.5	0.5	4	Oil	No
	3**	110	?	?	?	1950's	Diesel	n/a	Horizontal	-8	yes	none	n/a	n/a	Florida Walk Canal	Bayou Bienvenue	-6.0	-6.5	0.5	4	Oil	No	
	4**	267	M&W (MWI)	60	NC360P12	?	1950's	Diesel	n/a	Horizontal	-8	yes	none	n/a	n/a	Florida Walk Canal	Bayou Bienvenue	-6.0	-6.5	0.5	4	Oil	No
Total	755																						
Bayou Villere #3	1**	266	M&W (MWI)	60	NC360P12	?	1950's	Diesel	n/a	Horizontal	-8	yes	butterfly valve	n/a	n/a	Forty Arpent Canal	Bayou Villere	-6.0	-6.5	0.5	12	Oil	Yes
	2**	267	M&W (MWI)	60	NC360P12	?	1950's	Diesel	n/a	Horizontal	-8	yes	butterfly valve	n/a	n/a	Forty Arpent Canal	Bayou Villere	-6.0	-6.5	0.5	12	Oil	Yes
	3***	267	M&W (MWI)	60	NC360P12	?	1950's	Diesel	n/a	Horizontal	-8	yes	none	n/a	n/a	Forty Arpent Canal	Bayou Villere	-6.0	-6.5	0.5	12	Oil	No
	Total	800																					
Meraux #4	1	445	Baldwin-Lima-Hamilton (Patterson)	94 x 128	AFV	?	1972	Diesel	212	Vertical	-1.5	yes	floodgate	n/a	n/a	Forty Arpent Canal	Bayou Dupre	-6.0	-6.5	0.5	16	Grease	No
	2	90	Baldwin-Lima-Hamilton (Patterson)	42 x 54	AFV	?	1972	Electric 60 Hz	505	Vertical	-1.5	yes	floodgate	n/a	n/a	Forty Arpent Canal	Bayou Dupre	-6.0	-6.5	0.5	16	Grease	No
	3	445	Baldwin-Lima-Hamilton (Patterson)	94 x 128	AFV	?	1972	Diesel	212	Vertical	-1.5	yes	floodgate	n/a	n/a	Forty Arpent Canal	Bayou Dupre	-6.0	-6.5	0.5	16	Grease	No
	Total	980																					
E.J. Gore #5	1	111	M&W (MWI)	42	NC342P12	?	1980's	Diesel	n/a	Horizontal	-8	yes	flap gates	n/a	n/a	Forty Arpent Canal	Bayou Dupre	0.0	-0.5	0.5	2	Oil	No
	2	111	M&W (MWI)	42	NC342P13	?	1980's	Diesel	n/a	Horizontal	-8	yes	flap gates	n/a	n/a	Forty Arpent Canal	Bayou Dupre	0.0	-0.5	0.5	2	Oil	No
	3	111	M&W (MWI)	42	NC342P14	?	1980's	Diesel	n/a	Horizontal	-8	yes	flap gates	n/a	n/a	Forty Arpent Canal	Bayou Dupre	0.0	-0.5	0.5	2	Oil	No
	4	111	M&W (MWI)	42	NC342P15	?	1980's	Diesel	n/a	Horizontal	-8	yes	flap gates	n/a	n/a	Forty Arpent Canal	Bayou Dupre	0.0	-0.5	0.5	2	Oil	No
	5	111	M&W (MWI)	42	NC342P16	?	1980's	Diesel	n/a	Horizontal	-8	yes	flap gates	n/a	n/a	Forty Arpent Canal	Bayou Dupre	0.0	-0.5	0.5	2	Oil	No
	6	110	M&W (MWI)	42	NC342P17	?	1980's	Diesel	n/a	Horizontal	-8	yes	flap gates	n/a	n/a	Forty Arpent Canal	Bayou Dupre	0.0	-0.5	0.5	2	Oil	No
Total	665																						
Jean Lafitte #6	1	315	Patterson Pump Co.	75 x 72	AFV	90PT-14688-90-G72	1990	Diesel	272	Vertical	-8	yes	none	10.5	n/a	Florida Walk Canal	Bayou Bienvenue	-6.0	-6.5	0.5	9	Grease	Yes
	2	315	Patterson Pump Co.	75 x 72	AFV	90PT-14688-90-G72	1990	Diesel	272	Vertical	-8	yes	none	10.5	n/a	Florida Walk Canal	Bayou Bienvenue	-6.0	-6.5	0.5	9	Grease	Yes
	3	315	Patterson Pump Co.	75 x 72	AFV	90PT-14688-90-G73	1990	Diesel	272	Vertical	-8	yes	none	10.5	n/a	Florida Walk Canal	Bayou Bienvenue	-6.0	-6.5	0.5	9	Grease	Yes
	Total	945																					
Bayou Ducros #7	1	333	Patterson Pump Co.	75 x 72	AFV	90PT-14688-90-G73	1992	Diesel	272	Vertical	-8	yes	none	10.5	n/a	Forty Arpent Canal	Bayou Ducros	-6.0	-6.5	0.5	16	Grease	Yes
	2	333	Patterson Pump Co.	75 x 72	AFV	90PT-14688-90-G73	1992	Diesel	272	Vertical	-8	yes	none	10.5	n/a	Forty Arpent Canal	Bayou Ducros	-6.0	-6.5	0.5	16	Grease	Yes
	3	334	Patterson Pump Co.	75 x 72	AFV	90PT-14688-90-G73	1992	Diesel	272	Vertical	-8	yes	none	10.5	n/a	Forty Arpent Canal	Bayou Ducros	-6.0	-6.5	0.5	16	Grease	Yes
	Total	1000																					
St. Mary #8	1	278	ITT-AC	108 x 66	115-143543	1-0840-70720-02	1996	Diesel	230	Vertical	-9 (intake)	yes	none	2.5	n/a	Twenty Arpent Canal	Lake Lery	0.0	-0.5	0.5	8	Grease	Yes
	2	278	ITT-AC	108 x 66	115-143543	1-0840-70720-01	1996	Diesel	230	Vertical	-9 (intake)	yes	none	2.5	n/a	Twenty Arpent Canal	Lake Lery	0.0	-0.5	0.5	8	Grease	Yes
	3	279	ITT-AC	108 x 66	115-143543	1-0840-70720-03	1996	Diesel	230	Vertical	-9 (intake)	yes	none	2.5	n/a	Twenty Arpent Canal	Lake Lery	0.0	-0.5	0.5	8	Grease	Yes
	Total	835																					

* Elevations estimated by Bob Turner/Lake Borgne Levee District and from engineering plans (when available)

Pump Station	Pump	Capacity (cfs)	8/28/2005 Start Stop	8/29/2005 Start Stop	8/30/2005 Start Stop	8/31/2005 Start Stop	9/1/2005 Start Stop	9/2/2005 Start Stop	9/3/2005 Start Stop	9/4/2005 Start Stop	9/5/2005 Start Stop	9/6/2005 Start Stop	9/7/2005 Start Stop	9/8/2005 Start Stop	9/9/2005 Start Stop	9/10/2005 Start Stop	9/11/2005 Start Stop	9/12/2005 Start Stop	9/13/2005 Start Stop	9/14/2005 Start Stop	9/15/2005 Start Stop	
Fortification #1	1 (East)	577					NA	NR	NR	NR	NR	NR	NR	NR	NR	NR	NR	NR				
	2 (Center)	100					NR	NR	NR	NR	NR	NR	NR	NR	NR	NR	NR	NR				
	3 (West)	577					20:00 Run	Run 11:30	9:00 16:00	9:00 22:00	NR	NR	NR	NR	NR	NR	NR	NR				
	Total	1254																				
Guichard #2	1	111	NR	NR	NA	NA	NA	NA	NA	NA	NA	NA	NA	NA	NA	NA	NA	NA	NA	NA	NA	
	2	223	NR	NR	NA	NA	NA	NA	NA	NA	NA	NA	NA	NA	NA	NA	NA	NA	NA	NA	NA	
	3	167	NR	NR	NA	NA	NA	NA	NA	NA	NA	NA	NA	NA	NA	NA	NA	NA	NA	NA	NA	
	4	223	NR	NR	NA	NA	NA	NA	NA	NA	NA	NA	NA	NA	NA	NA	NA	NA	NA	NA	NA	
Total	724																					
Bayou Villere #3	1	n/a	NR	NR	NA	NA	NA	NA	NA	NA	NA	NA	NA	NA	NA	NA	NA	NA	NA	NA	NA	
	2	n/a	NR	NR	NA	NA	NA	NA	NA	NA	NA	NA	NA	NA	NA	NA	NA	NA	NA	NA	NA	
	3	n/a	NR	NR	NA	NA	NA	NA	NA	NA	NA	NA	NA	NA	NA	NA	NA	NA	NA	NA	NA	
Total	500																					
Meraux #4	1 (East)	557	19:05 20:25						9:20 16:20													
	2 (Electric)	89	NR						NR													
	3 (West)	557	NR						NR													
Total	1203																					
E.J. Gore #5	1	110			NA	NA	NA	NA	NA	NA	NA	NA	NA	NA	NA	NA	NA	NA	NA	NA	NA	
	2	110			NA	NA	NA	NA	NA	NA	NA	NA	NA	NA	NA	NA	NA	NA	NA	NA	NA	
	3	110			NA	NA	NA	NA	NA	NA	NA	NA	NA	NA	NA	NA	NA	NA	NA	NA	NA	
	4	110			NA	NA	NA	NA	NA	NA	NA	NA	NA	NA	NA	NA	NA	NA	NA	NA	NA	
	5	110			NA	NA	NA	NA	NA	NA	NA	NA	NA	NA	NA	NA	NA	NA	NA	NA	NA	
	6	110			NA	NA	NA	NA	NA	NA	NA	NA	NA	NA	NA	NA	NA	NA	NA	NA	NA	
Total	660																					
Jean Lafitte #6	1	334	16:00 16:45		14:45 22:00	6:00 20:00	6:00 Run	Run 6:00	8:00 19:30 20:30 Run	Run 14:00	7:30 22:00	22:00 Run	Run 1:00 22:00 Run	Run Run	Run Run	Run Run	Run 9:00 11:30 13:30 16:30 18:30 22:30 0:00	3:30 5:00				
	2	334	16:00 16:45		14:45 22:00	6:00 20:00	6:00 Run	Run 6:00	8:00 19:30 20:30 Run	Run 14:00	7:30 22:00	22:00 Run	Run 1:00 22:00 Run	Run Run	Run Run	Run Run	Run 9:00 11:30 13:30 16:30 18:30 22:30 0:00	3:30 5:00				
	3	334	16:00 16:45		14:45 22:00	6:00 20:00	6:00 Run	Run 6:00	8:00 19:30 20:30 Run	Run 14:00	7:30 22:00	22:00 Run	Run 1:00 22:00 Run	Run Run	Run Run	Run Run	Run 9:00 11:30 13:30 16:30 18:30 22:30 0:00	3:30 5:00				
Total	1002																					
Bayou Ducros #7	1	334	7:40 9:10 17:00 17:45 19:35 20:05							8:00 Run	Run 16:00 18:00 Run	Run Run	Run Run	Run Run	Run Run	Run 0:00	8:30 12:00					
	2	334	7:40 9:10 17:00 17:45 19:35 20:05							8:00 Run	Run 16:00 18:00 Run	Run Run	Run Run	Run Run	Run Run	Run 0:00	8:30 12:00					
	3	334	7:40 9:10 17:00 17:45 19:35 20:05							8:00 Run	Run 16:00 18:00 Run	Run Run	Run Run	Run Run	Run Run	Run 0:00	8:30 12:00					
Total	1002																					
St. Mary #8	1	279					15:45 Run	Run Run	Run Run	Run Run	Run Run	Run Run	Run Run	Run Run	Run 20:00		15:00 Run	Run 17:30	14:00 19:30	7:00 Run	Run Run	Run 1:00
	2	279	9:15 0:00				15:45 Run	Run Run	Run Run	Run Run	Run Run	Run Run	Run Run	Run Run	Run Run	Run 14:00	6:00 Run	Run 21:30	14:00 16:30	7:15 Run	Run Run	Run 3:00
	3	279								11:45 Run	Run Run	Run Run	Run Run	Run Run	Run Run	Run Run	Run Run	Run Run	Run Run	Run Run	Run Run	Run 6:00
Total	837																					

Time in Local CST Day Light Savings
Pumps Not Available NA
No Reported Run Times NR
Continued to Run Run
Damaged/ Lost/ Unavailable Record
Information was not obtained (Area considered Unwatered)



St Bernard Parish Canal and Tide Level Readings

Pump Stations	28-Aug-05		29-Aug-05		30-Aug-05		31-Aug-05		1-Sep-05		2-Sep-05		3-Sep-05		4-Sep-05		5-Sep-05		6-Sep-05		7-Sep-05		8-Sep-05		9-Sep-05		10-Sep-05		11-Sep-05		12-Sep-05		13-Sep-05		14-Sep-05		15-Sep-05						
	Time	Gage	Time	Gage	Time	Gage	Time	Gage	Time	Gage	Time	Gage	Time	Gage	Time	Gage	Time	Gage	Time	Gage	Time	Gage	Time	Gage	Time	Gage	Time	Gage	Time	Gage	Time	Gage	Time	Gage	Time	Gage	Time	Gage					
PS 1 - Fortication	Canal	2:00		2:00		2:00		2:00		2:00		2:00		2:00		2:00		2:00		2:00		2:00		2:00		2:00		2:00		2:00		2:00		2:00		2:00		2:00					
	Canal	6:00		6:00		6:00		6:00		6:00		6:00		6:00		6:00		6:00		6:00		6:00		6:00		6:00		6:00		6:00		6:00		6:00		6:00		6:00					
	Canal	10:00		10:00		10:00		10:00		10:00		10:00		10:00		10:00		10:00		10:00		10:00		10:00		10:00		10:00		10:00		10:00		10:00		10:00		10:00		10:00			
	Tide	2:00		2:00		2:00		2:00		2:00		2:00		2:00		2:00		2:00		2:00		2:00		2:00		2:00		2:00		2:00		2:00		2:00		2:00		2:00		2:00			
PS 2 - Guichard	Canal	2:00		2:00		2:00		2:00		2:00		2:00		2:00		2:00		2:00		2:00		2:00		2:00		2:00		2:00		2:00		2:00		2:00		2:00		2:00		2:00			
	Canal	6:00		6:00		6:00		6:00		6:00		6:00		6:00		6:00		6:00		6:00		6:00		6:00		6:00		6:00		6:00		6:00		6:00		6:00		6:00		6:00			
	Canal	10:00		10:00		10:00		10:00		10:00		10:00		10:00		10:00		10:00		10:00		10:00		10:00		10:00		10:00		10:00		10:00		10:00		10:00		10:00		10:00		10:00	
	Tide	2:00		2:00		2:00		2:00		2:00		2:00		2:00		2:00		2:00		2:00		2:00		2:00		2:00		2:00		2:00		2:00		2:00		2:00		2:00		2:00		2:00	
PS 3 - Bayou Villere	Canal	2:00		2:00		2:00		2:00		2:00		2:00		2:00		2:00		2:00		2:00		2:00		2:00		2:00		2:00		2:00		2:00		2:00		2:00		2:00		2:00			
	Canal	6:00		6:00		6:00		6:00		6:00		6:00		6:00		6:00		6:00		6:00		6:00		6:00		6:00		6:00		6:00		6:00		6:00		6:00		6:00		6:00			
	Canal	10:00		10:00		10:00		10:00		10:00		10:00		10:00		10:00		10:00		10:00		10:00		10:00		10:00		10:00		10:00		10:00		10:00		10:00		10:00		10:00		10:00	
	Tide	2:00		2:00		2:00		2:00		2:00		2:00		2:00		2:00		2:00		2:00		2:00		2:00		2:00		2:00		2:00		2:00		2:00		2:00		2:00		2:00		2:00	
PS 4 - Meraux	Canal	2:00		2:00		2:00		2:00		2:00		2:00		2:00		2:00		2:00		2:00		2:00		2:00		2:00		2:00		2:00		2:00		2:00		2:00		2:00		2:00			
	Canal	6:00		6:00		6:00		6:00		6:00		6:00		6:00		6:00		6:00		6:00		6:00		6:00		6:00		6:00		6:00		6:00		6:00		6:00		6:00		6:00			
	Canal	10:00		10:00		10:00		10:00		10:00		10:00		10:00		10:00		10:00		10:00		10:00		10:00		10:00		10:00		10:00		10:00		10:00		10:00		10:00		10:00		10:00	
	Tide	2:00		2:00		2:00		2:00		2:00		2:00		2:00		2:00		2:00		2:00		2:00		2:00		2:00		2:00		2:00		2:00		2:00		2:00		2:00		2:00		2:00	
PS 5 - E.J. Gore	Canal	2:00		2:00		2:00		2:00		2:00		2:00		2:00		2:00		2:00		2:00		2:00		2:00		2:00		2:00		2:00		2:00		2:00		2:00		2:00		2:00			
	Canal	6:00		6:00		6:00		6:00		6:00		6:00		6:00		6:00		6:00		6:00		6:00		6:00		6:00		6:00		6:00		6:00		6:00		6:00		6:00		6:00			
	Canal	10:00		10:00		10:00		10:00		10:00		10:00		10:00		10:00		10:00		10:00		10:00		10:00		10:00		10:00		10:00		10:00		10:00		10:00		10:00		10:00		10:00	
	Tide	2:00		2:00		2:00		2:00		2:00		2:00		2:00		2:00		2:00		2:00		2:00		2:00		2:00		2:00		2:00		2:00		2:00		2:00		2:00		2:00		2:00	
PS 6 - Jean Lafitte	Canal	2:00		2:00	8.4	2:00		2:00		2:00		2:00		2:00		2:00		2:00		2:00		2:00		2:00		2:00		2:00		2:00		2:00		2:00		2:00		2:00		2:00			
	Canal	6:00		6:00		6:00		6:00		6:00		6:00		6:00		6:00		6:00		6:00		6:00		6:00		6:00		6:00		6:00		6:00		6:00		6:00		6:00		6:00			
	Canal	10:00		10:00		10:00		10:00		10:00		10:00		10:00		10:00		10:00		10:00		10:00		10:00		10:00		10:00		10:00		10:00		10:00		10:00		10:00		10:00		10:00	
	Tide	2:00		2:00	2.0	2:00		2:00		2:00		2:00		2:00		2:00		2:00		2:00		2:00		2:00		2:00		2:00		2:00		2:00		2:00		2:00		2:00		2:00			
PS 7 - Bayou Ducros	Canal	2:00		2:00		2:00		2:00		2:00		2:00		2:00		2:00		2:00		2:00		2:00		2:00		2:00		2:00		2:00		2:00		2:00		2:00		2:00		2:00			
	Canal	6:00		6:00		6:00		6:00		6:00		6:00		6:00		6:00		6:00		6:00		6:00		6:00		6:00		6:00		6:00		6:00		6:00		6:00		6:00		6:00			
	Canal	10:00		10:00		10:00		10:00		10:00		10:00		10:00		10:00		10:00		10:00		10:00		10:00		10:00		10:00		10:00		10:00		10:00		10:00		10:00		10:00		10:00	
	Tide	2:00		2:00		2:00		2:00		2:00		2:00		2:00		2:00		2:00		2:00		2:00		2:00		2:00		2:00		2:00		2:00		2:00		2:00		2:00		2:00		2:00	
PS 8 - St. Mary	Canal	2:00		2:00		2:00		2:00		2:00		2:00		2:00		2:00		2:00		2:00		2:00		2:00		2:00		2:00		2:00		2:00		2:00		2:00		2:00		2:00			
	Canal	6:00		6:00		6:00		6:00		6:00		6:00		6:00		6:00		6:00		6:00		6:00		6:00		6:00		6:00		6:00		6:00		6:00		6:00		6:00		6:00			
	Canal	10:00		10:00		10:00		10:00		10:00		10:00		10:00		10:00		10:00		10:00		10:00		10:00		10:00		10:00		10:00		10:00		10:00		10:00		10:00		10:00			
	Tide	2:00		2:00		2:00		2:00		2:00		2:00		2:00		2:00		2:00		2:00		2:00		2:00		2:00		2:00		2:00		2:00		2:00		2:00		2:00		2:00		2:00	

Readings were extracted from Operations Logs acquired by IPET Task 8 for each pump station where available.

Appendix J

Engineering and Operational Risk and Reliability Analysis

Table of Contents

Executive Summary	2
Background	5
Analysis Boundaries.....	6
<i>Study Region and Hurricane Protection System</i>	7
<i>Analysis Assumptions and Constraints</i>	8
Risk Analysis Methodology	8
<i>Overview</i>	8
<i>Contributing Factors and Their Relationships</i>	8
<i>Hurricane Protection System</i>	11
<i>Probabilistic Risk Model</i>	11
<i>Conceptual Event Tree</i>	13
<i>Risk Quantification</i>	14
Hazard Analysis and Initiating Events	33
<i>Historic Methods</i>	33
<i>Joint Probability (JP) Methods</i>	34
<i>Monte Carlo Simulation Methods</i>	34
<i>Choice of a Method</i>	35
<i>Hurricane Recurrence at Landfall</i>	36
<i>Pre- and Post-Landfall Parameter Variation</i>	40
<i>Parameter Discretization for Risk Analysis</i>	45
<i>Assessment of Hurricane Loads $L(\Theta)$</i>	46
<i>Mid-resolution model runs</i>	49
<i>Calibration and Extension of the MR Results Using the HR Runs</i>	49
<i>Rainfall Intensity</i>	51
<i>Epistemic Uncertainty</i>	53
<i>Climatic Effects and Their Contribution to Epistemic Uncertainty</i>	54
Reliability Analysis	55

<i>Summary approach</i>	56
<i>Structures, components, and systems constituting the HPS</i>	57
<i>Failure definitions and limiting states</i>	57
<i>Methodological approach</i>	59
<i>Fragility curves and failure probabilities</i>	61
Consequences	68
<i>Liaison with Louisiana State University Hurricane Center</i>	70
Risk Profiles and Summaries.....	71
Uncertainty Analysis	71
References	75
<i>Risk methodology</i>	75
<i>Hurricane Methodology</i>	75
Appendix A. Terminology	78
Appendix B. New Orleans East Polder	80
<i>NOE – Background</i>	80
<i>NOE – Design Memorandums</i>	81
<i>NOE – Layout of Reaches for Risk Model by Physical Feature</i>	82
<i>NOE – Elevations Along the Defined Reaches</i>	95
Appendix C - Jefferson Polder	97
Appendix D - St. Charles Polder	97
Appendix E - Plaquemines Polder.....	97
Appendix F - St. Bernards Polder	97
Appendix G - Evaluation of Loss Exceedance Probabilities.....	97

Executive Summary

The mission of the IPET risk and reliability analysis is to examine the risks to life and property posed by the New Orleans hurricane protection system that was in place prior to Katrina and by the system as it is expected to exist at the start of the next hurricane season (1 June 2006). The risk analysis will consider the expected performance of the various elements of the system and the consequences associated with that performance. All engineered systems impose risks that result from humans using technology to create conditions or activities that are not produced by nature. For instance, the hurricane protection system in New Orleans has been designed to control interior flooding within New Orleans and protection to the city from storm induced surges and waves. The hurricane protection system (HPS) project is designed to perform this function without imposing unacceptable risks to public safety, property and welfare.

The risk analysis covers four states that represent the condition of the New Orleans hurricane protection system.

- The system as it existed before the arrival of Hurricane Katrina. Knowledge gained from IPET studies will be considered in the analysis.

- After Hurricane Katrina with repairs that have been completed prior to the 2006 hurricane season. Some projects may be ongoing after 1 June 2006.
- After Hurricane Katrina with all repair and improvement projects complete, but prior to longer-term increases in the authorized level of protection.
- The system as authorized before the arrival of Hurricane Katrina. All authorized components of the HPS are constructed and knowledge gained from IPET studies will be considered in the analysis.

The difference in relative risks among the three states will be a unified measure for fully evaluating the performance of the integrated system before Hurricane Katrina, after Hurricane Katrina, and during the interim recovery period.

Two groups of questions concerning the performance of the hurricane protection system (HPS) are addressed by the risk and reliability analyses:

Pre-Katrina: The system as it existed before the arrival of Hurricane Katrina. This state is the baseline for estimating risk, and includes the following:

1. What was the reliability of the hurricane protection system to prevent flooding of protected areas of the HPS that was in existence before the arrival of Katrina, for the standard project hurricane? Note that some components of the authorized projects had not been constructed prior to Katrina.
2. What was the reliability of the hurricane protection system to prevent flooding of protected areas with all of the authorization projects completed, for the standard project hurricane?
3. What is the estimated annual rate of occurrence of system failure due to hurricane events?
4. What are the probability distributions and annual rates of consequences that would result from failure of the hurricane protection system as defined in terms of life loss and economic impact?
5. What is the uncertainty in these estimates?

The pre-Katrina analysis does not attempt to recreate the design intent or knowledge that the designers used to determine the configuration of the HPS. Engineering parameters, foundation conditions and operational information gained by IPET through exploration and testing since the hurricane are used. This allows for an assessment of the actual risks that existed pre-Katrina. An additional analysis was conducted on the authorized HPS that includes all features in the original design that were not completed prior to Katrina.

Post-Katrina: After Hurricane Katrina with repairs made prior to the 2006 hurricane season, and during the interim recovery period after the hurricane protection system has been strengthened and improved, but prior

to longer-term increases in the authorized level of protection. This group includes:

1. What is the reliability of the HPS to prevent flooding of protected areas for the authorized standard project hurricane with the system repairs and improvements in place as of June 1, 2006?
2. What is the frequency of flooding due to the range of expected hurricane events with the system repairs and improvements in place as of June 1, 2006?
3. What are the probability distributions and annual rates of consequences that would result from failure of the hurricane protection system as defined in terms of life loss and economic impact?
4. What is the uncertainty in these estimates?

The condition of the system has been degraded by the effects of hurricane Katrina. Flood walls and levees may have been overtopped, damaged by impacts from debris, saturated, submerged and/or breached. Permanent repairs on these elements have been accomplished since the hurricane that may have different material strength parameters than the original feature. This difference in strengths is considered in the analyses of component reliability. The pumping system was also damaged and shut down or submerged. The post Katrina reliability of the levees, flood walls and pumping stations will be considered in the risk assessment. The reliability of the various elements of the protection system will be determined using analytical and expert elicitation methods.

The term reliability is intended to mean the conditional probability of a component or system performing intended function. This result can also be used to determine the conditional probability of failure. System failure refers to the failure of the HPS to provide protection from flooding in one or more protected areas and can also be thought of as the occurrence of flood inundation. The effectiveness of the protection system is also dependent upon how well the operational elements of the system performed. Elements such as road closure structures, gate operations and pumping plants, etc. that requires human operation and proper installation during a flood fight can dramatically impact flood levels. The lessons learned concerning the performance of these elements during Katrina will be considered in the analysis.

The changed demographics of the local areas protected by the system will be considered when determining the consequences. In some areas, many homes and much of the infrastructure were destroyed by the hurricane and some may not be rebuilt. Therefore the pre-Katrina populations and property values will be impacted and must be considered in the post-Katrina analysis.

Risk is generally calculated by combining the probability of system failure with the consequences associated with that failure. For New Orleans, the post Katrina risks will be lower primarily due to reduced population and economic activity. In order to better compare the adequacy of pre and post Katrina HPS, probability of failure and inundation mapping will be used as the primary metric by which to measure the effectiveness of repairs and improvements.

Background

Decisions about natural hazards are best made by explicitly and quantitatively considering risks. Implementation of risk analysis to the hurricane protection system (HPS) of New Orleans and S.E. Louisiana is difficult because the system serves a large geographical region and our capability to accurately model hurricanes in regions as complex as the Mississippi delta is limited. Nonetheless, modeling capabilities have improved enough in recent years to make risk analysis an important tool for decision making as the New Orleans HPS is restored.

It is important to note that detailed knowledge of the New Orleans HPS and the engineering parameters that influence its performance or of the hurricane characteristics is limited. For example, we do not know with certainty the properties of foundation soils underlying the extensive levee system, or even the frequency with which hurricanes occur. Hurricane models can predict winds, waves and surges only with limited precision, and reliability models of levee performance when subjected to hurricane forces are similarly limited. Hence, the risks of hurricane-induced flooding cannot be established with certainty. Therefore a risk analysis must include not just a best estimate of risk, but also an estimate of the uncertainty in that best estimate.

The reliability and risk analyses relate the performance of individual features (floodwalls, levees, pumps, levee closures, etc.) located throughout the hurricane protection system to the overall performance of the integrated system and the impact of that performance on economics and public safety. The reliability of all structural features also considers the varying foundation conditions that exist throughout the hurricane protection system. The risk analysis covers three states that represent the condition of the hurricane protection system.

- The system as it existed before the arrival of Hurricane Katrina. This state is the baseline for estimating risk.
- After Hurricane Katrina with repairs made prior to the 2006 hurricane season.
- During the interim recovery period after the hurricane protection system has been strengthened and improved, but prior to longer-term increases in the authorized level of protection.

Risk analysis examines potential life and property losses posed by the as-built hurricane protection system prior to Katrina and by the system after Katrina in its repaired or improved condition. Reliability analysis examines the engineering performance of various elements of the system. The reliability results are used in conjunction with the consequences associated with that performance to estimate the corresponding risks. The reliability of the various elements of the protection system is determined using analytical and expert elicitation methods.

During the risk studies several key issues were considered:

- Defining the physical features of the system required an accurate inventory of all components that provide protection against storm surge and waves. It was important to model not only the cross sections and strength parameters of these components but also transitions between elements, differences in the top elevation along a reach of similar components and varying foundation conditions. The characterization of the physical features of the protection system was, however, limited by the available information and the resources available to process that information under IPET. These limitations are expressed in the analyses as uncertainties that are characterized and communicated so that they can be accounted for in decisions making.

- At many locations, the hurricane protection system has been degraded by Hurricane Katrina. Levees and floodwalls may have been overtopped or otherwise damaged. The impacts of these events upon the condition of the features is not necessarily apparent by visual inspection. The possibility of such weakening has been considered in the current condition of features of the system that survived Katrina in order to estimate the risk for the 2006 hurricane season.

- Emergency repairs of breached elements were accomplished after Hurricane Katrina, and permanent repairs have subsequently been completed. The structural/geotechnical strength of the repairs have been considered.

- The pumping system is an important element that controls flooding during and after a storm. Pumping plant reliability and capacity have therefore been considered.

- The consequences of pre- and post-Katrina flooding are different due to changes in population and economic activity. Task 10 has relied on the Task 9 Team to define post-Katrina exposure scenarios and to quantify the consequences of HPS failures.

- The effectiveness of the protection system depends on human factors as well as engineered systems (e.g., timely road and railroad closures, gate operations, functioning of pumping stations, and so on). Lessons learned from Katrina and other natural disasters will be used in modeling human performance.

Appendix A lists key terminology and definitions used in this report.

Analysis Boundaries

An important initial step in the analysis is to clearly define the bounds of the study. These bounds included defining the geographic bounds of the study region and the elements of the hurricane protection system, the resolution of information and analyses to be performed, and analysis constraints or assumptions associated with the IPET analysis. These areas are defined in the following subsections and in detail in the Appendices.

Study Region and Hurricane Protection System

At a macro scale, this analysis examines risks to New Orleans and the South East Louisiana area associated with the performance of the hurricane protection system (HPS). Figure J-1 identifies the region to be considered and the major features of the hurricane protection system.

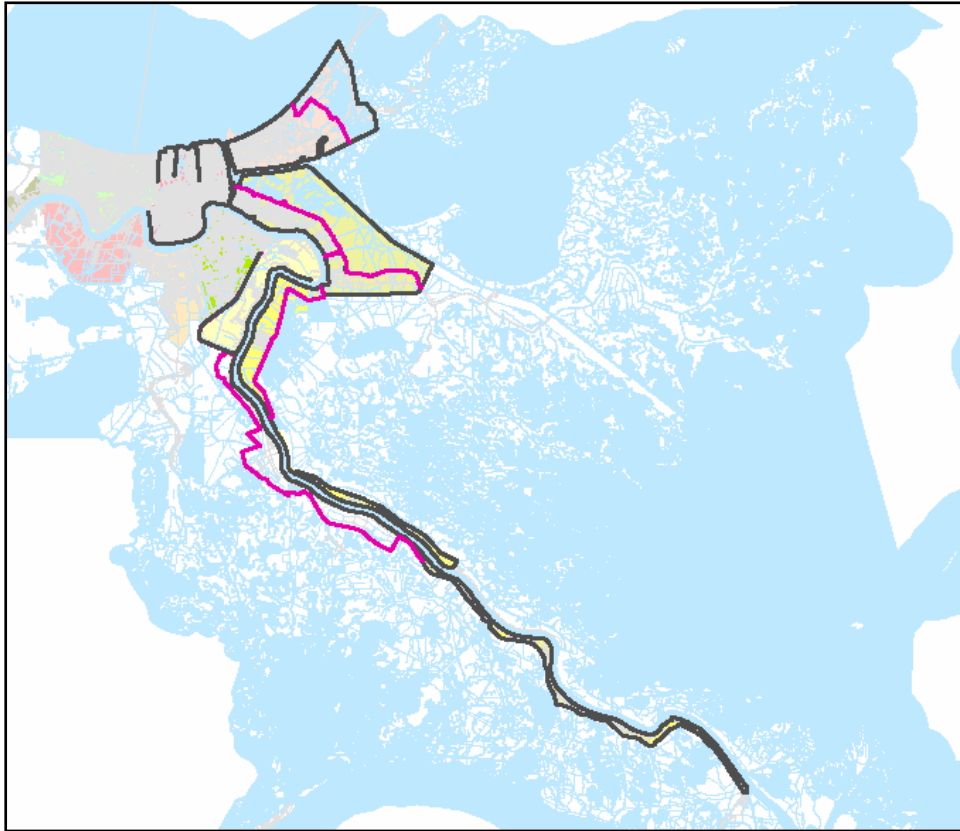


Figure J-1. Map of the New Orleans and the south east Louisiana area, the geographic bounds of the study region considered in the risk analysis and the primary features of the hurricane protection system

The hurricane protection system is comprised of a variety of subsystems, structures and components which include: earthen levees, floodwalls, foundation conditions, pumping stations, canals, wall closures, power supply systems, operations personnel. The system is also a combination of several sub-systems (polders) which are independently maintained and operated by local parishes and levee boards. Data collected by Teams 1 and 6, and during a site visit is used to define characteristics of the polders and their interdependence for use in the risk model.

Appendices B through F contain a complete inventory of the structures, systems and components that were considered in the risk analysis. The information provided in the appendices was obtained from a number of the IPET teams. The reader should note that all of the structures, systems and components listed may not have been included in the risk analysis model. Some items may

have been screened out of the analysis, whereas others may not have been included since they do not play a role in the performance of the hurricane protection system or the consequences that result in the event of a failure.

Analysis Assumptions and Constraints

As part of the process of developing the risk analysis model, it was necessary to identify key assumptions and analysis constraints. Constraints refer to events or factors that were not modeled or considered explicitly in the analysis. The assumptions and constraints are provided at the appropriate location in subsequent sections.

The following table lists the analysis limitations or constraints of the risk analysis.

No.	Limitation or Constraint
1.	Model procedures that existed prior to Katrina
2.	Geographic area limited to elements of the hurricane protection system in the 5 parishes
3.	Hazards and thus consequences not considered in the risk analysis are: a. Wind Damage to buildings b. Fire c. Civil unrest d. Effect of a release of hazardous materials
4.	The performance of the evacuation system in New Orleans was not explicitly modeled in the risk analysis. Its consideration was limited to a parametric consideration of the variation of the sensitivity of the risk analysis results to the relative effectiveness of evacuation.

Risk Analysis Methodology

Overview

The following sections describe the overall risk analysis methodology of the hurricane protection system. Sections that follow discuss individual parts of the analysis (hurricane hazard analysis, levee and floodwall vulnerability or fragility analysis) as they relate to the overall risk analysis methodology. The basic elements of the risk analysis methodology are illustrated in Figure J-2. The analysis is represented in terms of a series of modules which interface to provide a risk model for the New Orleans HPS.

Contributing Factors and Their Relationships

The development of a risk analysis model was facilitated by the preparation of an influence diagram. The process of creating an influence diagram helped establish a basic understanding of the elements of the hurricane protection system and their relationship to the overall system performance during a hurricane event and the analysis of consequences and risks.

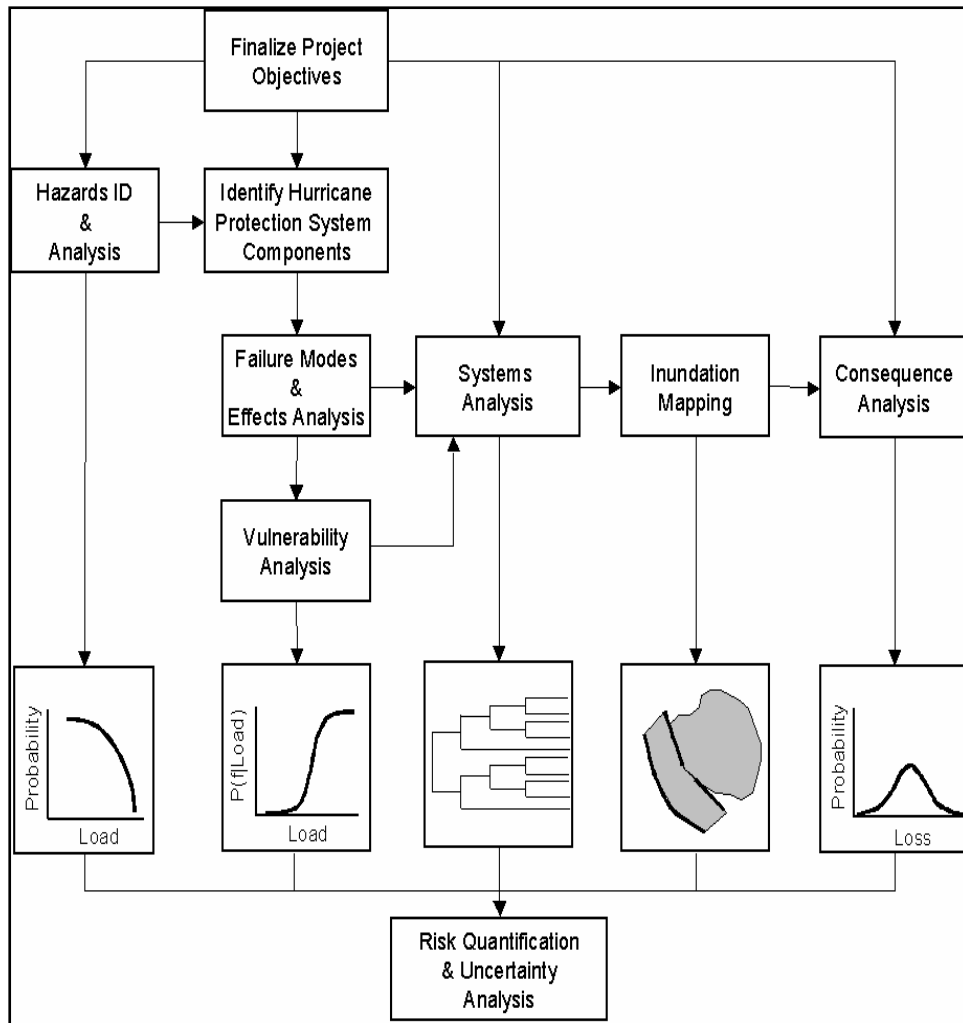


Figure J-2. Risk analysis logic diagram

Figure J-3 shows the influence diagram for the hurricane protection system and the analysis of consequences. There are four parts to the diagram influence diagram:

- Value nodes (rounded-corner box)
- Chance nodes (circular areas)
- Decision nodes (square-corner boxes)
- Factors and dependencies in the form of arrows.

The influence diagram shown in Figure J-3 was used to develop an event (or probability) tree for the hurricane protection system. Figure J-4 shows an initial probability tree derived from the influence diagram in Figure J-3. The top events across the tree identify the random events whose state following the occurrence of the hurricane could contribute to flooding in a protected area. The tree begins with the initiating event, a hurricane that generates a storm surge, winds and rainfall in the region.

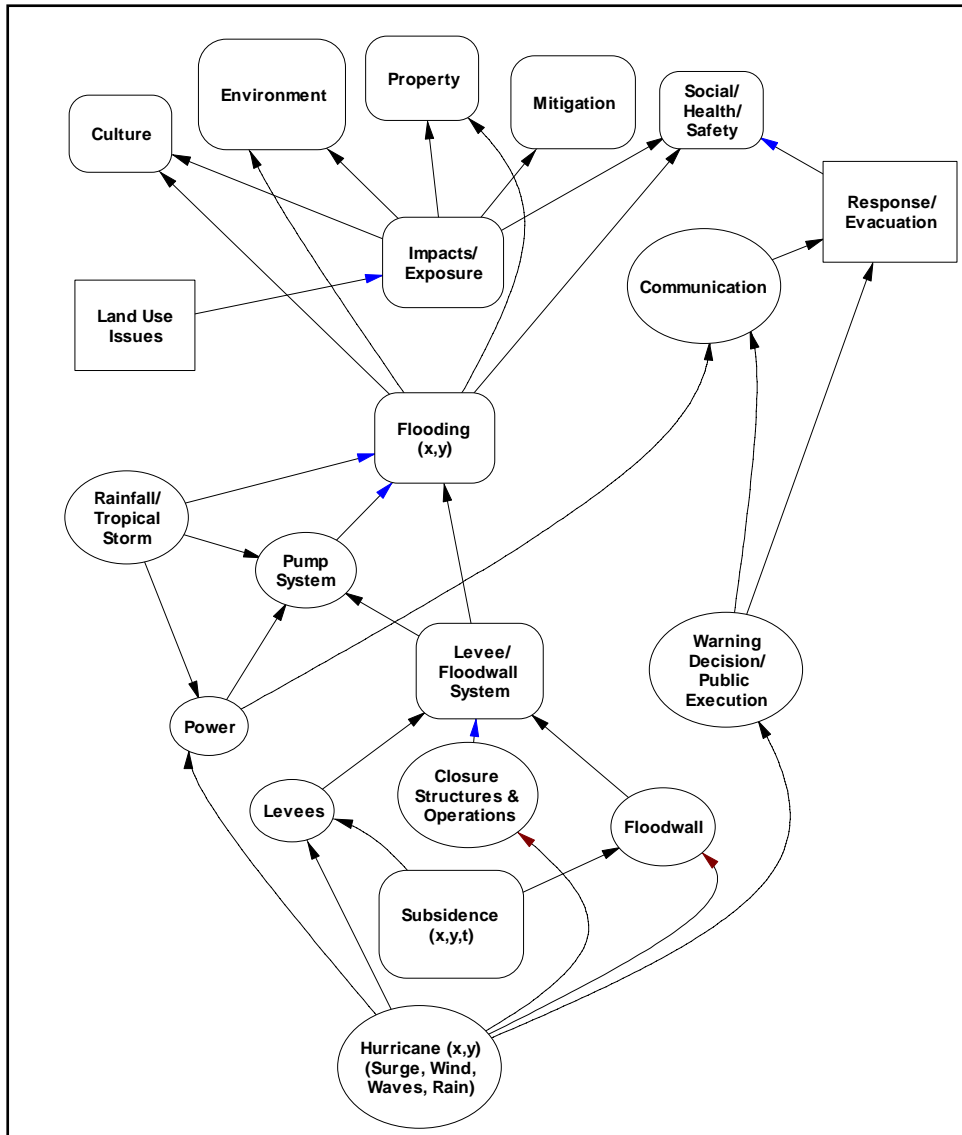


Figure J-3. Influence Diagrams for Risk Analysis

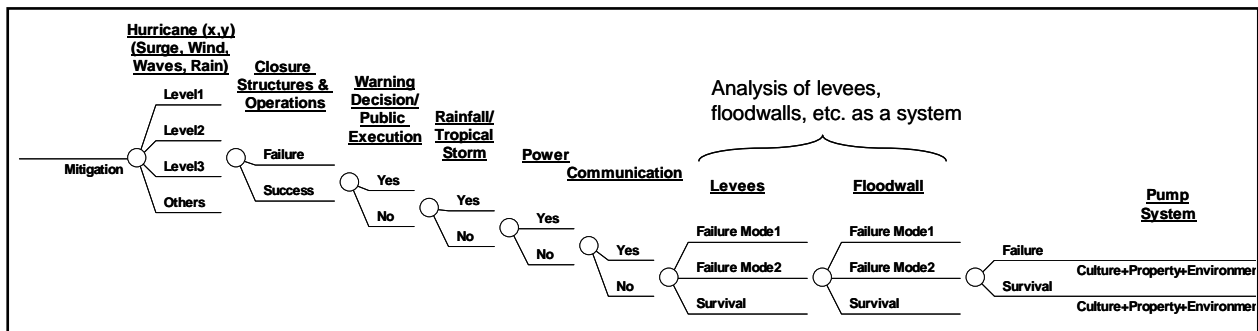


Figure J-4. Probability Tree for the Hurricane Protection System

Hurricane Protection System

The entire hurricane protection system is provided in Figure J-1. The hurricane protection system (HPS) considered in the reliability and risk analysis task is schematically shown in Figure J-5. The system consists of polders, sub-polders and reaches. The definition of these polders, sub-polders and reaches are based on the following considerations:

- Local jurisdiction,
- Floodwall type and cross section,
- Levee type and cross section,
- Engineering parameters defining structural performance,
- Soil strength parameters,
- Foundations parameters, and
- Surge and wave levels.

Reaches (*R*) of each polder is uniquely identified using sequential numbers as shown in the figure. The figure also shows the approximate locations of pumping stations.

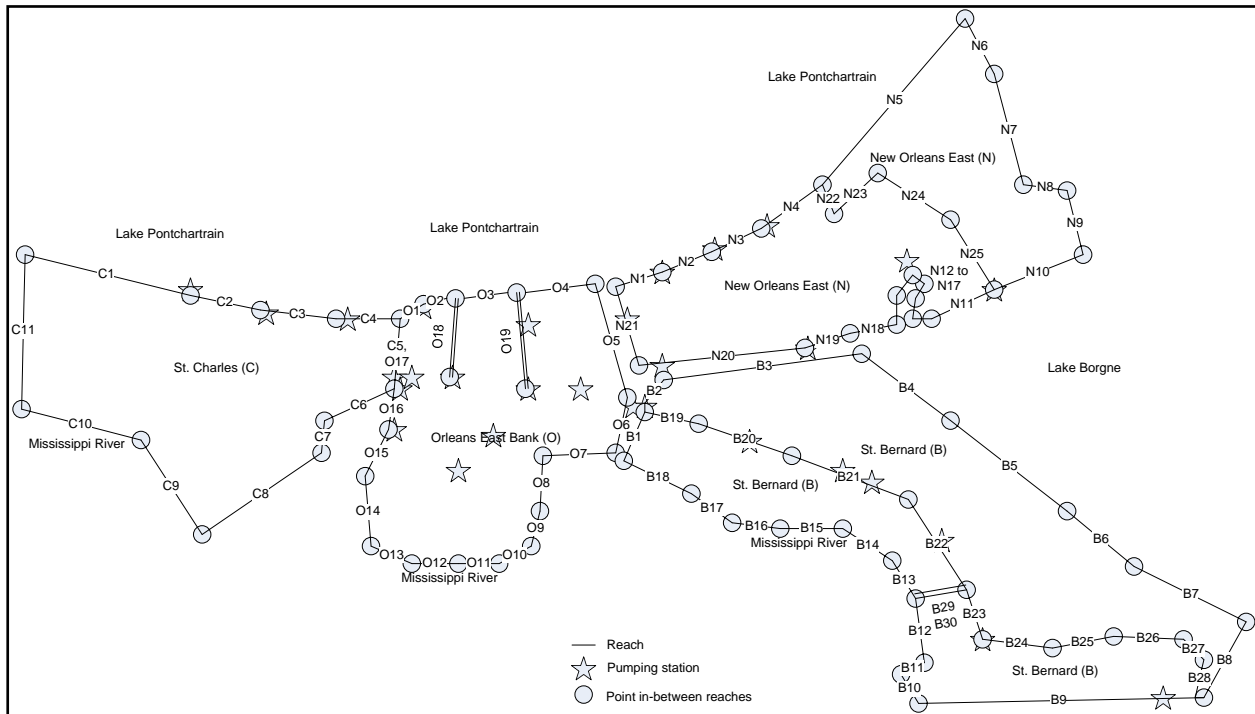


Figure J-5. Hurricane Protection System Defined by Polders and Reaches

Probabilistic Risk Model

Risk associated with the hurricane protection system is quantified through the hurricane rate (λ) and the probability $P(C > c)$ with which a consequence

measure C exceeds different levels c . The loss exceedance probability per event is evaluated as

$$P(C > c) = \sum_i \sum_j P(h_i) P(S_j | h_i) P(C > c | h_i, S_j) \quad (\text{J-1})$$

An annual loss exceedance rate can be estimated as follows

$$\lambda(C > c) = \sum_i \sum_j \lambda P(h_i) P(S_j | h_i) \times P(C > c | h_i, S_j) \quad (\text{J-2})$$

where $P(h_i)$ is the probability of hurricane events of type i , $P(S_j | h_i)$ is the probability that the system is left in state j from the occurrence of h_i , and $P(C > c | h_i, S_j)$ is the probability that the consequence C exceeds level c under (h_i, S_j) . Summation is over all hurricane types i and all system states j in a suitable discretization. Simulation studies of hurricanes for risk analysis require the use of representative combinations of hurricane parameters and their respective probabilities. The outcome of this process is a set of hurricane simulation cases and their respective conditional probabilities $P(h_i)$.

Evaluation of the hurricane rate λ and the probability $P(h_i)$, the conditional probabilities $P(S_j | h_i)$, and the conditional probabilities $P(C > c | h_i, S_j)$ is the main objective of the hurricane model, the system model, and the consequence model, respectively. The probability $P(S_j | h_i)$ should cover the states of the components of the HPS, such as closure structure and operations, precipitation levels, electric power availability, failures modes of levees and floodwalls, and pumping station reliability. To assess the state of the HPS given a hurricane event requires an evaluation of the reliability of individual structures, systems and components (e.g., levees, floodwalls, pump systems) when they are exposed to the loads and effects of the hurricane (e.g., the peak surge, wave action) and the relationship of these elements to the overall function of the system to prevent flooding in protected areas.

If point estimates of consequences (i.e., $(c | h_i, S_j)$) are available instead of $P(C > c | h_i, S_j)$, order statistics can be used to construct the exceedance probability $P(C > c | h_i, S_j)$ as provided in Appendix G.

The hurricane loss provided by Eq. J-1 can be used to compute a cumulative distribution function (CDF) $F_S(s)$ as $1 - P(C > c)$. The CDF of the accumulated damage (loss) during a non-random time interval $[0, t]$ is given by

$$F(s; t, \lambda) = \sum_{n=0}^{\infty} e^{-\lambda t} \frac{(\lambda t)^n}{n!} F_S^{(n)}(s) \quad (\text{J-3})$$

where $F_S^{(n)}(s)$ is the n -fold convolution of $F_S(s)$.

Conceptual Event Tree

The probability tree of Figure J-4 can be simplified by determining the frequency of flooding levels and displaying the results as contours within the polders. Consequences were determined with Task 9 and are simplified by grouping communication, warning decision and public execution into an *exposure factor* parameter applied to lives and property at risk. The resulting event tree appropriately branched out is shown in Figure J-6. This tree is used as a basis for developing the risk analysis methodology. The events of the tree are defined in Table J-1.

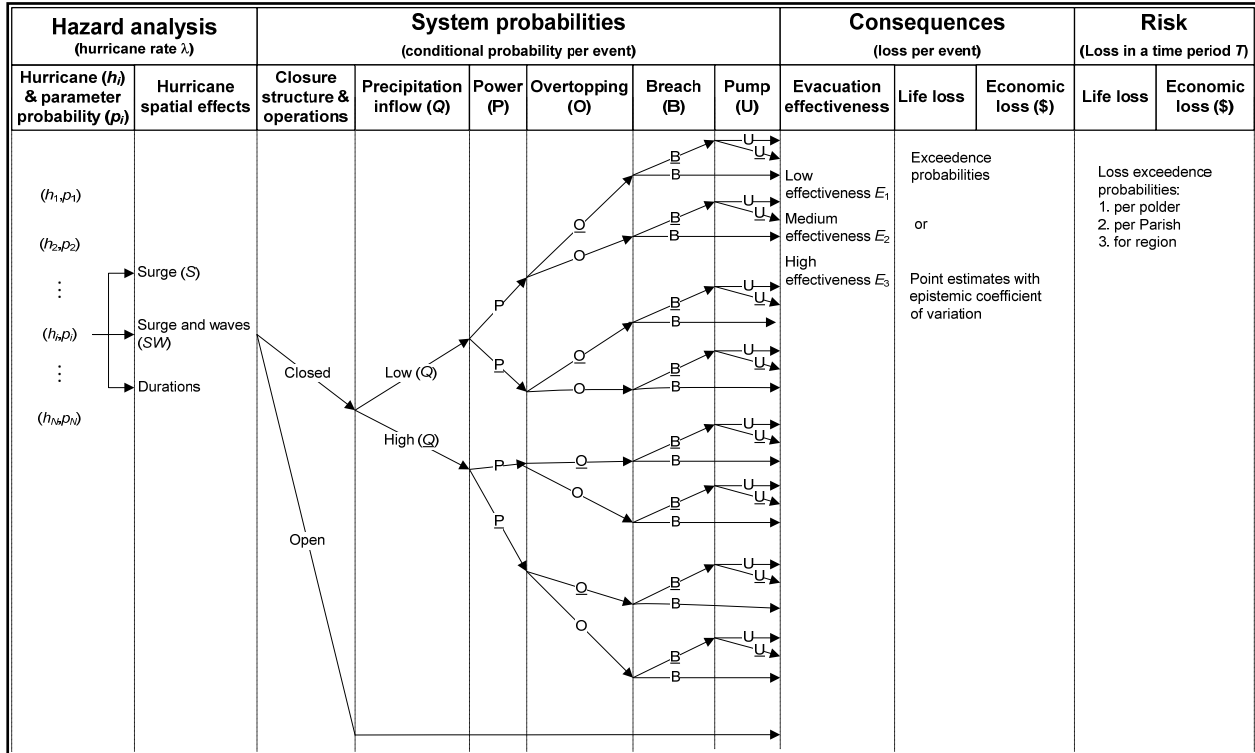


Figure J-6. Conceptual Event Tree for Risk Analysis Underlined events (i.e., \underline{Q} , \underline{P} , \underline{O} , \underline{B} , and \underline{U}) are the complements of the respective events (i.e., Q , P , O , B , and U).

Table J-1. Summary of the Event Tree Top Events	
Top Event	Description
Hurricane initiating event	The hurricane initiating event is mapping of the peak flood surge with waves in the study area with a hurricane rate λ . This event can be denoted, $h(x,y)$, and has a probability of occurrence, $P(h(x,y))$ and a rate of occurrence of $\lambda P(h(x,y))$.
Closure structure and operations	This event models whether the hurricane protection system closures have been sealed prior to the hurricane. This event depends on a number of factors as illustrated in the influence diagram. The closure structures are treated in groups in terms of probability of being closed in preparation for the arrival of a hurricane.
Precipitation inflow (Q)	This event corresponds to the rainfall that occurs during a hurricane event.
Power (P)	This event models the availability of power (normal) power for the pump systems. This event is modeled in the event tree to represent a common mode of failure for the pump systems, and is included in developing a model for drainage and pumping efficiency or lack thereof including backflow through pumps.
Overtopping (O)	This event models the failure of the enclosure/protection system due to overtopping, given that failure has not occurred by some other (non-overtopping) failure mode. If failure (breach) does not occur, some flooding due to overtopping could result.
Breach (B)	This event models the failure of the enclosure/protection system (e.g., levees/floodwalls, closures) during the hurricane, exclusive of overtopping failures). This event includes all other failures and it models all 'independent' levee/floodwall sections.
Pump System (U)	This event models the availability of the pump system and its ability to handle a particular floodwater volume. This event is treated in aggregate with drainage effectiveness and power reliability including backflow through pumps.

Risk Quantification

Functional Modeling and Computational Considerations. A hurricane protection system (HPS) has the primary function of keeping water away from protected areas. The HPS breaks down the protected areas into polders. Some polders are divided internally into sub-polders. This partitioning is based on the internal drainage and pumping system within each polder. Figure J-5 illustrates the New Orleans East polder and the two sub-polders for illustration purposes. Polders and sub-polders are divided into sections, or reaches, that have similar cross-sections, material strength parameters and foundation conditions. Table J-2 shows a table constructed for a reach belonging to a polder. For each reach, the following items are defined:

1. start and end stations
2. reach length
3. protection height
4. polder and sub-polder membership designation

The table shows other items that are needed and referenced in subsequent sections.

The quantification of risk associated with a hurricane protection system requires quantifying its performance or lack thereof. A measure of the lack of performance is the amount of water that is expected to reach the protected areas for a particular hurricane, i.e., a given hurricane run. The water enters protected areas as a result of one or more of the following two cases:

1. overtopping volumes and associated probabilities and epistemic uncertainties

2. breach elevations and associated probabilities and epistemic uncertainties

The risk quantification framework has, therefore, the objective of obtaining these estimates.

The conceptual event tree presented in Figure J-6 can be reconfigured to facilitate the computations of overtopping volume and breach elevation with associated probabilities and epistemic uncertainties as provided in Figure J-7. The figure shows the two quantities of interest in boxes as the post-surge elevation that would result in cases of breach, and the water volume that results in cases of overtopping (OT), precipitation, open closures, leaks from joints, and backflow from pumping stations.

The subsequent sections describe the computational details needed to quantify risk. They are presenting in a manner that correspond to the events shown in Figure J-7, and a level of details needed to construct a spreadsheet to perform the computations. The sections that follow provide the background information and basis behind the approaches used for these computations.

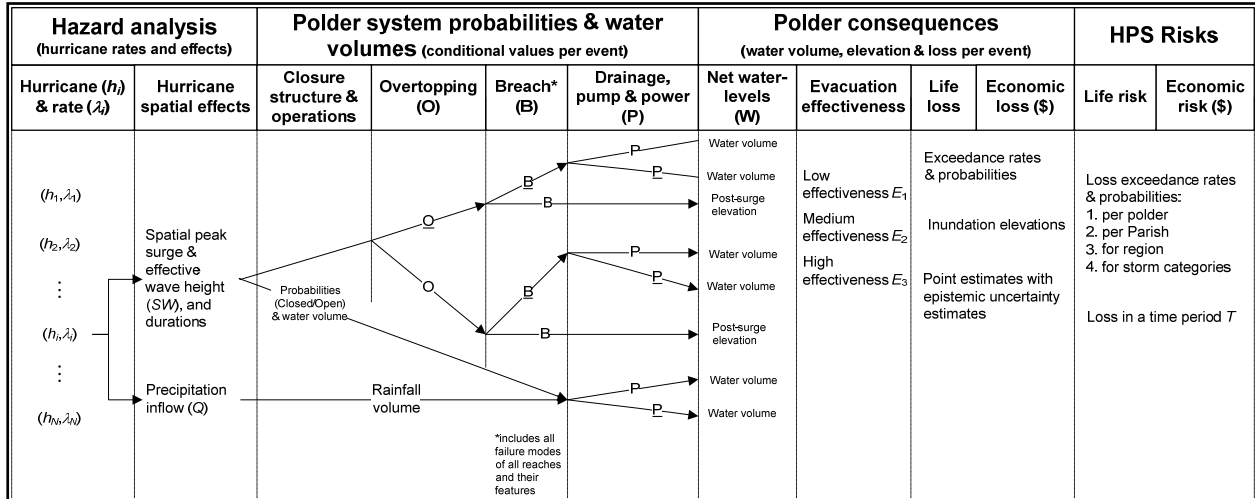


Figure J-7. Event Tree for Quantifying Risk. Underlined events (i.e., P, O, and B) are the complements of the respective events (i.e., P , O , and B).

Table J-2. System Definition, Hurricane Hazard, and Overtopping (OT) Results

Reach			Reach 1										
Reach start-end stations			To be provided										
Reach coordinates			To be provided										
Equal allocation to Sub-Polder(s)			1										
Reach length (ft)			2000										
Reach elevation (ft)			16										
Mean (Weir Coeff.)			3.33										
COV (Weir Coeff.)			0.15										
*Not used (needed for breaches)													
Hurricane Runs			Reach 1										
Run	Rate (R)		Surge+Waves		Duration		Post-surge elevation*		OT Length		OT Probability	OT Volume (Weir Eq)	
i	Mean	StD	Hs		T		Hps		L		P(OT)	V OT	
			Mean	StD	Mean	StD	Mean	StD	Mean	StD		Mean	StD
ID	event/yr	event/yr	ft	ft	sec	sec	ft	ft	ft	ft		ft^3	ft^3
1	5.00E-04	1.00E-04	25	1	3600	720	8	1	2000	0	1.00E+00	6.549E+08	1.637E+08
2	5.00E-04	1.00E-04	24	1	3600	720	8	1	2000	0	1.00E+00	5.311E+08	1.328E+08
3	7.50E-04	1.50E-04	23	1	4320	864	8	1	2000	0	1.00E+00	5.107E+08	1.277E+08
4	1.00E-03	2.00E-04	22	1	3600	720	8	1	2000	0	1.00E+00	3.365E+08	8.412E+07
5	1.00E-03	2.00E-04	21	1	5400	1080	8	1	2000	0	1.00E+00	3.930E+08	9.825E+07
6	1.50E-03	3.00E-04	20	1	5400	1080	8	1	2000	0	1.00E+00	3.008E+08	7.520E+07
7	2.00E-03	4.00E-04	19	1	3600	720	8	1	2000	0	9.99E-01	1.505E+08	3.762E+07
8	2.00E-03	4.00E-04	18	1	3600	720	8	1	2000	0	9.82E-01	1.103E+08	2.758E+07
9	2.00E-03	4.00E-04	17	1	5400	1080	8	1	1000	200	8.42E-01	5.906E+07	1.891E+07
10	2.00E-03	4.00E-04	16	1	5400	1080	8	1	1000	200	4.88E-01	4.082E+07	1.307E+07
11	3.50E-03	7.00E-04	15	1	5400	1080	8	1	1000	200	1.58E-01	2.714E+07	8.688E+06
12	5.00E-03	1.00E-03	14	1	5400	1080	8	1	1000	200	2.82E-02	1.719E+07	5.504E+06
13	5.00E-03	1.00E-03	13	1	5400	1080	8	1	1000	200	3.06E-03	1.025E+07	3.280E+06
14	5.00E-03	1.00E-03	12	1	5400	1080	8	1	1000	200	2.33E-04	5.637E+06	1.805E+06
15	5.00E-03	1.00E-03	11	1	5400	1080	8	1	1000	200	1.49E-05	2.781E+06	8.903E+05
16	5.00E-03	1.00E-03	10	1	5400	1080	8	1	1000	200	9.60E-07	1.171E+06	3.749E+05
17	5.00E-03	1.00E-03	9	1	5400	1080	8	1	1000	200	7.62E-08	3.840E+05	1.229E+05

Hurricane Hazard Analysis. The joint probability (JP) of hurricane parameters is used for the purpose of generating hurricane runs. This method parameterizes hurricanes using a vector θ of characteristics at landfall (central pressure drop, radius of maximum wind, etc.). From the values of θ for historic events, one estimates the recurrence rate density $\lambda(\theta) = \lambda f(\theta)$ where λ is the rate of hurricane events in a neighborhood of the region of interest and $f(\theta)$ is the joint probability density function of θ in that neighborhood. These runs produce combined wind, surge and wave M that are computationally demanding. To reduce the number of runs of M , a response surface approach can be used. In this approach one selects a relatively small number m of vectors θ_i and uses M to calculate the corresponding surge and wave levels at the sites of interest. Then one fits a response surface model to each response variable (surge or wave level at a specific site) in terms of θ . Finally, one uses a refined discretization $\{\theta_i\}$ of parameter space with the response surface as a proxy model in place of M to represent the hurricane hazard. The outcomes of these computations are combined surge and effective wave values (called surge/wave values) at particular locations of interest along the hurricane protection system, e.g., representative values at the reaches. These values are denoted as h_i in Figure 3-6.

The water elevation need for the risk analysis as a loading can be taken as the surge elevation plus the effective wave height if waves are present, called the surge/wave elevation. Surge only, therefore, need not to be considered as a separate loading condition.

Hurricane rate modeling and prediction methods are then used to compute the corresponding exceedance rates to h_i values, and are denoted as λ_i in Figure J-7. Also, surge duration and post-surge elevation, i.e., applicable lake or river water level, are needed. The epistemic uncertainties in both the surge/wave elevation and the rates are represented in the form of standard deviation of respective biases in prediction methods and practices. Table J-2 shows a summary of such results as they appear in a spreadsheet under development for this purpose. The values provided in this table are for illustration purposes, and are shown in Figure J-8.

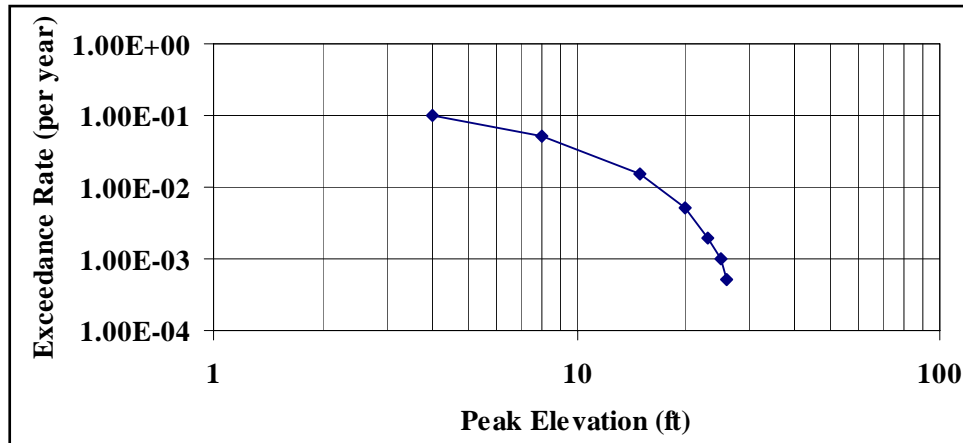


Figure J-8. Surge and wave Exceedance Curve Corresponding to Table J-2

Overtopping Flow Rate and Volume Models, and Probabilities.

Deterministic Models. The overtopping rate can be computed using the rectangular weir formulae (Daugherty, et al. 1985). The overtopping water flow has the elevation H and width L . If the water is assumed to be the ideal liquid, it can be shown using the energy conservation law that the flow rate Q (L^3/T) is given by the following equation:

$$Q = \frac{2}{3}(2g)^{1/2} LH^{3/2} \quad (J-4)$$

where g is the acceleration of gravity. The actual flow over the weir is known to be less than ideal (Daugherty, et al. 1985) because the effective flow area is considerably smaller than the product LH .

The model can be enhanced further for engineering applications by replacing the term $\frac{2}{3}(2g)^{1/2}$ in Eq. J-4 by the empirical coefficient, known as the weir coefficient C_w , so that Eq. J-4 takes on the following form:

$$Q = C_w LH^{3/2} \quad (J-5)$$

where

$$C_w = \begin{cases} 3.33 & \text{if } L \text{ and } H \text{ are given in English units} \\ 1.84 & \text{if } L \text{ and } H \text{ are given in SI units} \end{cases} \quad (\text{J-6})$$

Note that the C_w for the ideal fluid case is $\frac{2}{3}(2g)^{1/2}$ which is equal to 2.95 m/s^2 . This coefficient is assumed to have a coefficient of variation (COV) of 0.15.

For the application considered, the volume of the overtopping (OT) water V for a given reach can be calculated as

$$V(L, T, H_s, H_p) = C_w LT(H_s - H_p)^{3/2} \quad (\text{J-7})$$

where L is OT length taken as a fraction of the reach length, H_s is surge elevation, H_p is the top the protection for a reach elevation, T is surge duration, and the evaluation is constrained by the inequality that $H_s > H_p$. The resulting volume is the conditional volume *given* overtopping.

Uncertainty Analysis. For a particular hurricane run, the values of L , H_s , and T can be estimated. These point estimates involve epistemic uncertainty. The OT volume as given by Eq. J-7 is, therefore, a random variable that is a function of the following random variables: L , H_s , and T , assuming H_p deterministic. For specified probabilistic characteristics of L , H_s , and T , the probabilistic characteristics of V can be evaluated. Assuming L , H_s , and T , to be non-correlated, the mean value and the standard deviation of V can be evaluated using Monte Carlo simulation and nonlinear curve fitting based on least squares.

The uncertainty analysis of the OT flow rate can be assessed using Monte Carlo simulation based on a normally distributed epistemic uncertainty of the H_s at a reach for a particular hurricane run. Using Eq. J-5, the OT rate for a unit width (i.e., $L = 1$) is

$$q = 3.33H^{3/2} \quad (\text{J-8})$$

where $H = H_s - H_p$ with the constraint that $H_s > H_p$, which reflects the deterministic nature of Eq. J-8. A truncated distribution resulting from such a formulation requires the use of Monte Carlo simulation. The simulation was performed using 100 cycles for mean H values incremented from -6 to 10 ft using an increment of 0.01 ft, and standard deviation (S) values of 0, 1, and 2 ft as shown in Figure J-9a. Figure J-9b shows the differential increase in flow rate due to the standard deviation of water Head. Regression analysis was performed to obtain the mean and standard deviation of the conditional OT rate as follows:

$$\bar{q} = (\bar{H} + 10)^{3.87577} \exp(0.01916S_H - 6.92066) \quad (\text{J-9a})$$

$$S_q^2 = 80.65(\bar{H} + 10) + 165.67S_H^2 - 1344.26 \quad \text{if } \geq 0; \quad \text{otherwise } S_q^2 = 0 \quad (\text{J-9b})$$

The respective multiple correlation coefficients are 0.996 and 0.870. The respective plots of simulated and predicted values are shown in Figures J-10 and J-11. The coefficient of variation of the flow rate ($COV(q)$) can be computed as $COV(q) = S_q / \bar{q}$. Equations J-9a and J-9b can be adjusted to account for various weir coefficients, such as 2.6 for levees and 3.0 for floodwalls. Similar models can be used for flow through open closures.

Equation J-9a is a substitute of Eq. J-8 in the case of random water elevation, which at least assumes that it is applicable for $S_H > 0$. Physically, Eq. J-9a shows that water overtopping is possible even when $H_s < H_p$, i.e., when the water elevation is negative.

The coefficient of variation of the OT volume as given by Eq. J-7 can be evaluated using first-order approximation of a Taylor series expansion at the mean to produce the following estimate:

$$COV_V \cong \sqrt{COV_{C_w}^2 + COV_T^2 + COV_q^2 + COV_L^2} \quad (\text{J-10})$$

The above equation is based on the assumption of independence for the random variables representing the epistemic uncertainty, and the $COV(H_p)=0$.

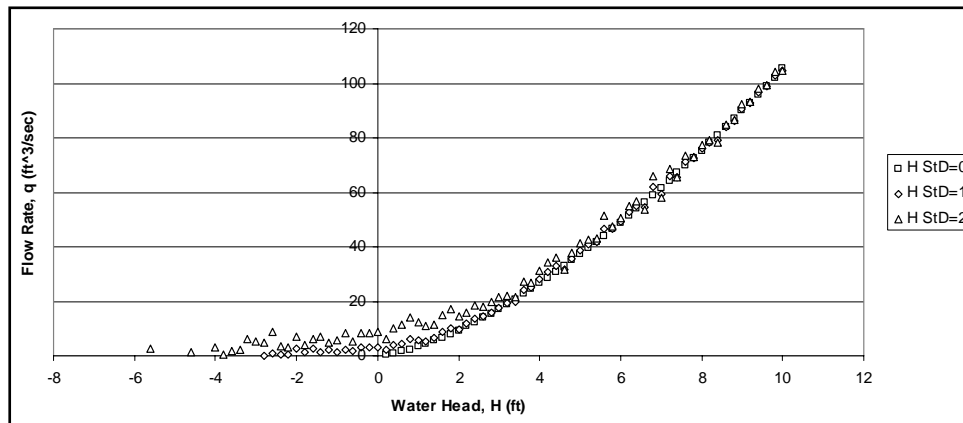


Figure J-9a. Simulated Flow Rate

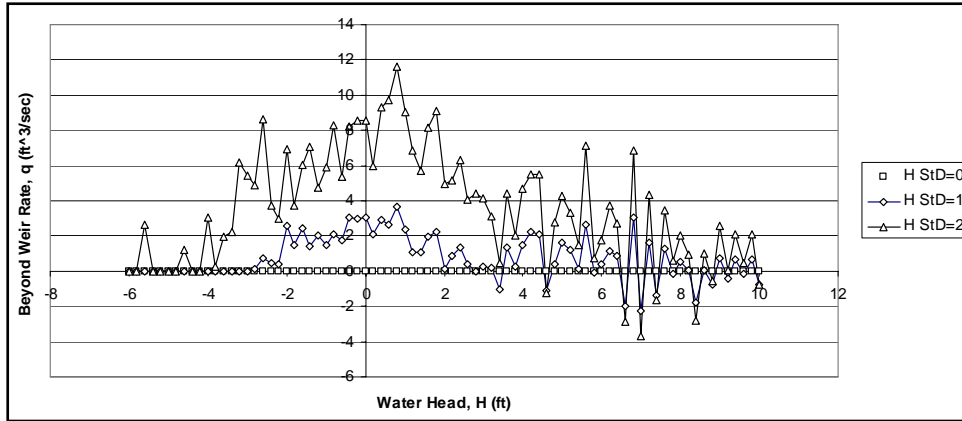


Figure J-9b. Differential Increase in Flow Rate Due to Standard Deviation of Water Head

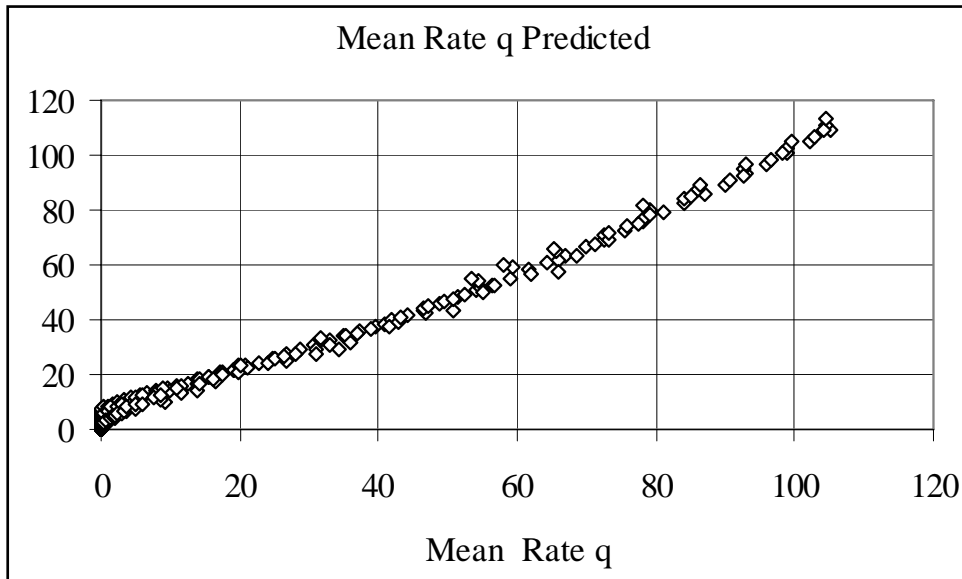


Figure J-10. Mean Rate

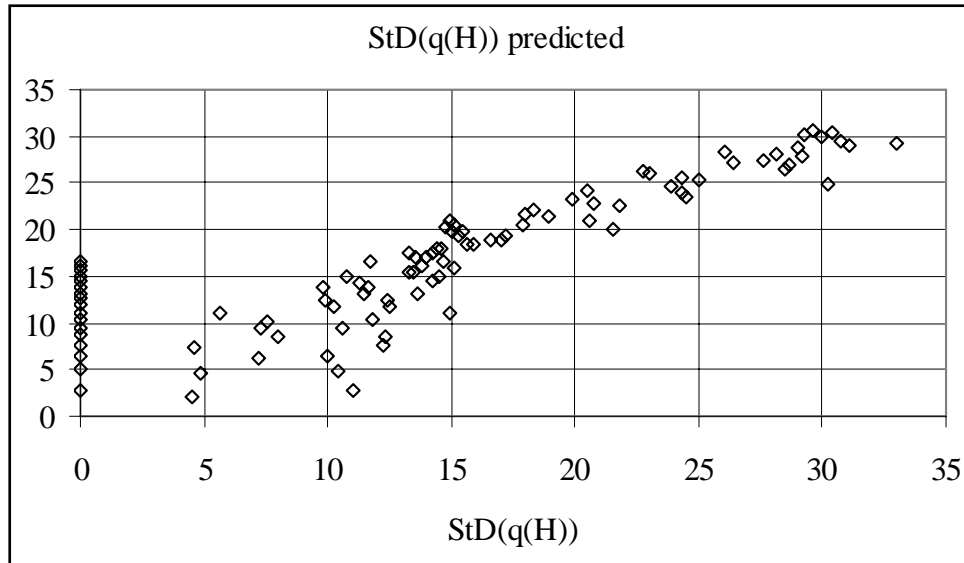


Figure J-11. Standard Deviation of Rate

Overtopping Probability. Probabilities of overtopping can be computed based on a performance function as commonly used in structural reliability assessment (see for example Ayyub 2003; Ayyub and McCuen 2003) as given by

$$Z = R - L \quad (J-11)$$

where Z = performance function, R = strength (resistance) and L = loading in the structure. In this case the resistance is provided by the hurricane protection elevation, and the loading is provided by the surge/wave elevation. The non-performance probability can be computed as

$$P = \text{Prob} (g < 0) \quad (J-12)$$

The reliability index for normally distributed random variables is

$$\beta = \frac{\mu_R - \mu_L}{\sqrt{\sigma_R^2 + \sigma_L^2}} \quad (J-13a)$$

where μ_R = mean value of strength R , μ_L = mean value of the load effect L , σ_R = standard deviation of strength R , and σ_L = standard deviation of the load effect L .

The reliability index for lognormally distributed random variables is

$$\beta = \frac{\ln\left(\frac{\mu_R}{\mu_L} \sqrt{\frac{\delta_L^2 + 1}{\delta_R^2 + 1}}\right) - \mu_L}{\sqrt{\ln\left((\delta_R^2 + 1)(\delta_L^2 + 1)\right)}} \quad (\text{J-13b})$$

where d = coefficient of variation. Equation J-13b is used in this study. The relationship between the reliability index β and the probability of failure is given by

$$P_f = 1 - \Phi(\beta) \quad (\text{J-14})$$

where $\Phi(\cdot)$ = cumulative probability distribution function of the standard normal distribution. Additional information on reliability assessment methods including non-normal and correlated random variables is provided by Ayyub (2003), and Ayyub and McCuen (2003).

The cumulative distribution function (CDF) of the total volume for a polder of n reaches can be computed as follows:

$$F_V = \sum_{i=1}^n p_i F_{V_i} \quad (\text{J-15})$$

where p_i = a branch probability in an event tree, and F = CDF. In case of point estimates of flooding per reach, computations can be based on order statistics. Once the total volume is obtained from all overtopping and breach cases, the net volume (as a random variable) needed for consequence analysis can be computed as follows:

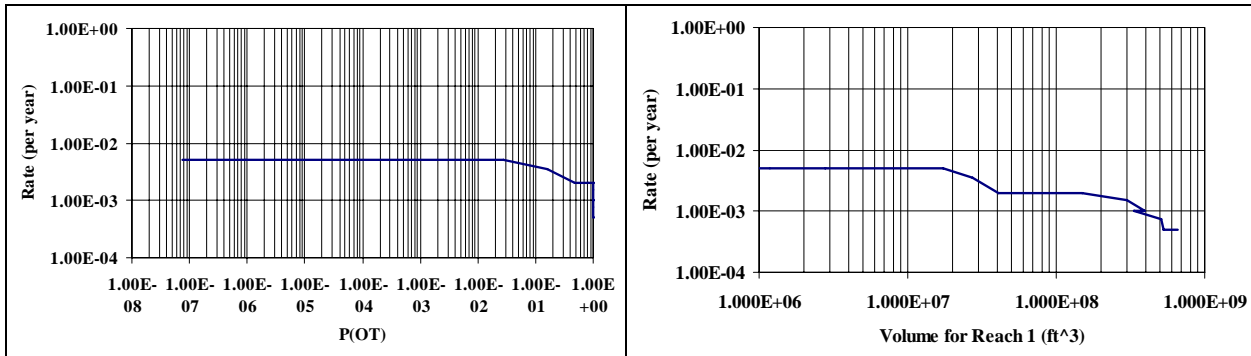
$$\begin{aligned} \text{Net Volume} &= \text{Total Volume} + \text{Precipitation} - \text{Pumping Volume} \\ &\quad + \text{Pumping Backflow} \end{aligned} \quad (\text{J-16})$$

The pumping volume and backflow are considered as a multiplier called the pumping factor.

Illustrations. As was stated previously, Table J-2 provides typical results for a reach. Four hypothetical reaches were used to construct overtopping results that were aggregated by sub-polders as illustrated in Table J-3. In this example, the polder is assumed to contain only one sub-polder. The overtopping results for this polder include the overtopping (OT) probability, i.e., $P(\text{OT})$, and the overtopping volume based on an overtopping condition, i.e., $V|\text{OT}$. The epistemic uncertainty for the $V|\text{OT}$ is also provided. The epistemic uncertainty for the $P(\text{OT})$ is not provided and might not be necessary. Figures J-12 and J-13 show the exceedance rate curves of the $P(\text{OT})$ and $V|\text{OT}$ for reach 1 and sub-polder 1, respectively.

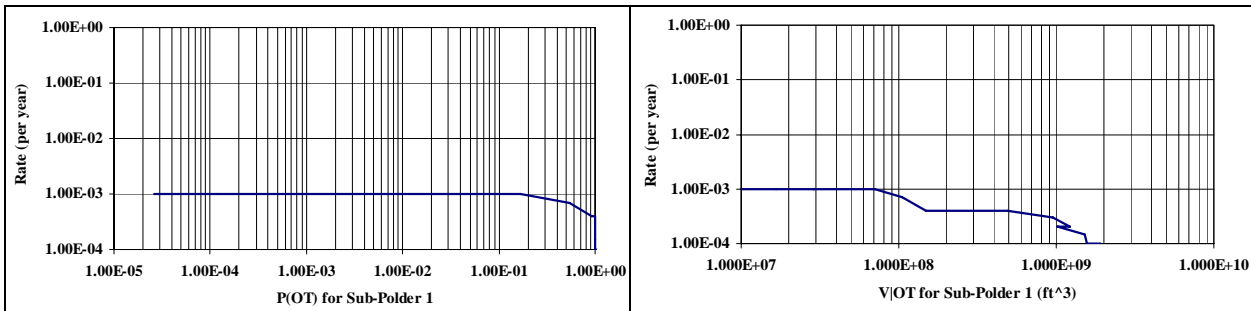
Table J-3
Aggregation of Overtopping Volume by Sub-polders and Polders

Summary by Sub-Polders											
1				2				3			
Sub-Polder		1		Sub-Polder		2		Sub-Polder		3	
OT Probability		OT Volume (Weir Eq)		OT Probability		OT Volume (Weir Eq)		OT Probability		OT Volume (Weir Eq)	
P(OT)		V OT		P(OT)		V OT		P(OT)		V OT	
Mean	StD	Mean	StD	Prob.	Prob.	Mean	StD	Prob.	Prob.	Mean	StD
Prob.	Prob.	ft ³	ft ³	Prob.	Prob.	ft ³	ft ³	Prob.	Prob.	ft ³	ft ³
1.00E+00	NA	1.893E+09	2.484E+08		TBD		TBD		TBD		TBD
1.00E+00	NA	1.557E+09	2.038E+08		TBD		TBD		TBD		TBD
1.00E+00	NA	1.521E+09	1.985E+08		TBD		TBD		TBD		TBD
1.00E+00	NA	1.020E+09	1.328E+08		TBD		TBD		TBD		TBD
1.00E+00	NA	1.216E+09	1.578E+08		TBD		TBD		TBD		TBD
1.00E+00	NA	9.522E+08	1.232E+08		TBD		TBD		TBD		TBD
1.00E+00	NA	4.893E+08	6.311E+07		TBD		TBD		TBD		TBD
1.00E+00	NA	3.430E+08	4.644E+07		TBD		TBD		TBD		TBD
9.98E-01	NA	2.647E+08	4.066E+07		TBD		TBD		TBD		TBD
9.14E-01	NA	1.488E+08	2.434E+07		TBD		TBD		TBD		TBD
5.39E-01	NA	1.045E+08	1.705E+07		TBD		TBD		TBD		TBD
1.67E-01	NA	7.094E+07	1.156E+07		TBD		TBD		TBD		TBD
3.24E-02	NA	4.622E+07	7.531E+06		TBD		TBD		TBD		TBD
4.95E-03	NA	2.864E+07	4.680E+06		TBD		TBD		TBD		TBD
7.25E-04	NA	1.667E+07	2.746E+06		TBD		TBD		TBD		TBD
1.20E-04	NA	8.957E+06	1.500E+06		TBD		TBD		TBD		TBD
2.60E-05	NA	4.340E+06	7.475E+05		TBD		TBD		TBD		TBD



(a) Overtopping Probability (P(OT)) (b) Overtopping Volume (V|OT)

Figure J-12. Exceedance Rate Curves for Reach 1



(a) Overtopping Probability (P(OT)) (b) Overtopping Volume (V|OT)

Figure J-13. Exceedance Rate Curve for Sub-Polder 1

Water Volumes from Other Features of the Protection System. The hurricane protection system includes other features that could contribute to water volume making its way to the protected areas during a hurricane. These features include:

1. closure structures that are left open or failed to close
2. localized changes in levee or floodwall elevations that create a gap in the HPS

These features are identified within each reach and assigned to sub-polders in case of nonperformance. For the closure structures case, the water volume resulting from the closure structure for a given hurricane can be computed based on respective closure closing probabilities, width of the closure structure, elevation of the bottom of the structure, and Eqs. J-9a and J-9b. The water volume associated with the localized changes in levee or floodwall elevations requires identifying the changes in elevation and the lengths over which the elevation varies. Sample computations are shown in Table J-4.

Table J-4. Water Volumes from Other Features

Feature		Closures including gates				Feature		Water-tight joints				
Reach number	1	2				Reach number	1					
Sub-Polder allocation	1	1				Sub-Polder allocation	1					
Feature number(s)	1, 2	3, 4, 5				Count	100					
Total width (ft)	100	200										
Feature bottom elevation (ft)	15	14										
Open probability*	0.1	0.5				Failure probability*	0.01					
*COV = 0.15						*COV = 0.15						
Hurricane Runs		Expected Water Volume from Open Closures						Expected Water Volume from Failed Joints				
Run	Rate (R)		Water Volume(Open)				Closure Water Volume		Joint Water Volume			
i	Mean	StD	Water Volume(Open)		Water Volume(Open)		V(C)		V(J)		V(J)	
ID	event/yr	event/yr	Mean	StD	Mean	StD	ft^3	ft^3	Mean	StD	Mean	StD
											ft^3	ft^3
1	5.00E-04	1.00E-04	3.99E+07	9.99E+06	5.91E+07	1.48E+07	3.353E+07	8.688E+06			3.000E+07	6.000E+06
2	5.00E-04	1.00E-04	3.27E+07	8.19E+06	4.87E+07	1.22E+07	2.762E+07	7.161E+06			3.000E+07	6.000E+06
3	7.50E-04	1.50E-04	3.19E+07	7.97E+06	4.77E+07	1.19E+07	2.702E+07	7.010E+06			3.000E+07	6.000E+06
4	1.00E-03	2.00E-04	2.13E+07	5.32E+06	3.20E+07	8.01E+06	1.815E+07	4.712E+06			3.000E+07	6.000E+06
5	1.00E-03	2.00E-04	2.52E+07	6.31E+06	3.83E+07	9.57E+06	2.167E+07	5.631E+06			3.000E+07	6.000E+06
6	1.50E-03	3.00E-04	1.97E+07	4.91E+06	3.01E+07	7.52E+06	1.700E+07	4.422E+06			3.000E+07	6.000E+06
7	2.00E-03	4.00E-04	1.00E+07	2.51E+06	1.55E+07	3.88E+06	8.753E+06	2.278E+06			3.000E+07	6.000E+06
8	2.00E-03	4.00E-04	7.52E+06	1.88E+06	1.18E+07	2.94E+06	6.634E+06	1.729E+06			3.000E+07	6.000E+06
9	2.00E-03	4.00E-04	8.28E+06	2.65E+06	1.31E+07	3.28E+06	7.383E+06	1.933E+06			3.000E+07	6.000E+06
10	2.00E-03	4.00E-04	5.91E+06	1.89E+06	9.50E+06	3.04E+06	5.343E+06	1.693E+06			3.000E+07	6.000E+06
11	3.50E-03	7.00E-04	4.08E+06	1.31E+06	6.69E+06	2.14E+06	3.754E+06	1.192E+06			3.000E+07	6.000E+06
12	5.00E-03	1.00E-03	2.71E+06	8.69E+05	4.55E+06	1.46E+06	2.547E+06	8.101E+05			3.000E+07	6.000E+06
13	5.00E-03	1.00E-03	1.72E+06	5.50E+05	2.96E+06	9.49E+05	1.654E+06	5.276E+05			3.000E+07	6.000E+06
14	5.00E-03	1.00E-03	1.02E+06	3.28E+05	1.83E+06	5.86E+05	1.018E+06	3.257E+05			3.000E+07	6.000E+06
15	5.00E-03	1.00E-03	5.64E+05	1.80E+05	1.06E+06	3.38E+05	5.845E+05	1.878E+05			3.000E+07	6.000E+06
16	5.00E-03	1.00E-03	2.78E+05	8.90E+04	5.56E+05	1.78E+05	3.059E+05	9.880E+04			3.000E+07	6.000E+06
17	5.00E-03	1.00E-03	1.17E+05	3.75E+04	2.58E+05	8.25E+04	1.406E+05	4.575E+04			3.000E+07	6.000E+06

Breach Elevation and Volume Models.

Three Cases of Breach Failure of Reaches. The risk quantification can be effectively performed by examining three cases of breach failure that correspond to branches presented in the event tree of Figure J-7. The three cases are:

1. breach given overtopping
2. breach given no overtopping
3. breach due to feature failures

The first case of breach given overtopping is primarily driven by erosion resulting from overtopping water flow. The computations of breach failure probability for this case can be performed using Eqs. J-13 and J-14 by considering *R* as *time to breach* and *L* as the *duration of overtopping* provided in

Table J-2. The time to breach is a random variable that can be quantified by its mean and standard deviation, and is a function of water flow and speed, and characteristics of the protection side of the hurricane protection system. Sample computations are shown in Table J-5. The water level in this case is the post-surge level in an adjacent water body. The results should be aggregated by sub-polder using system reliability modeling as discussed in the subsequent sections.

The second case of breach given no overtopping is driven by all applicable failure modes of the levees and walls as discussed in Chapter 5. Sample computations are shown in Table J-6. The water level in this case is the post-surge level in an adjacent water body. The results should be aggregated by sub-polder using system reliability modeling as discussed in the subsequent sections. All failure modes were considered, and exclusions are justified and reported in the reliability analysis chapter. All failure modes for a reach are aggregated into one failure probability as a function of water elevation (i.e., a fragility curve) that accounts for correlations associated with the length of the reach. Therefore, failure probabilities of the reaches can be treated as corresponding to independent events. The epistemic uncertainty in these failure probabilities can be computed that accounts for all the epistemic uncertainties on the strength parameters and modeling aspect of the reliability models.

The third case of breach due to failed features requires computing additional breach probabilities associated with instability of drainage structures and failure of transitions due to erosion. The resulting water levels from these breaches are the post-surge water elevations determined by an adjacent water body on the unprotected side.

Table J-5. Computations Relating to Breach given Overtopping

Reach		Reach 1				Reach 2				Reach 3				Reach 4					
Reach start-end stations		To be provided				To be provided				To be provided				To be provided					
Reach coordinates		To be provided				To be provided				To be provided				To be provided					
Equal allocation to Sub-Polder(s)		1				1				1				1					
Reach length (ft)		2000				1800				2200				2200					
Reach elevation (ft)		16				14				13				13					
Time to breach (sec)*		7200				10800				10800				6000					
COV(time to breach) =		0.5																	
Hurricane Runs		Reach 1				Reach 2				Reach 3				Reach 4					
Run	Rate (R)		Surge+Waves		Post-surge elevation		Surge+Waves		Post-surge elevation		Surge+Waves		Post-surge elevation		Surge+Waves		Post-surge elevation		
	Mean	StD	P(B OT)	Hps	P(B OT)	Hps	P(B OT)	Hps	P(B OT)	Hps	P(B OT)	Hps	P(B OT)	Hps	P(B OT)	Hps	P(B OT)	Hps	
ID	event/yr	event/yr	Mean	StD	ft	ft	Mean	StD	ft	ft	Mean	StD	ft	ft	Mean	StD	ft	ft	
1	5.00E-04	1.00E-04	0.12026	0.02405	8	8	1	0.0247	0.00494	8	8	1	0.0247	0.00494	8	8	1	0.2067	0.04135
2	5.00E-04	1.00E-04	0.12026	0.02405	8	8	1	0.0247	0.00494	8	8	1	0.0247	0.00494	8	8	1	0.2067	0.04135
3	7.50E-04	1.50E-04	0.20675	0.04135	8	8	1	0.0538	0.01075	8	8	1	0.0538	0.01075	8	8	1	0.3221	0.06442
4	1.00E-03	2.00E-04	0.12026	0.02405	8	8	1	0.0247	0.00494	8	8	1	0.0247	0.00494	8	8	1	0.2067	0.04135
5	1.00E-03	2.00E-04	0.35119	0.07024	8	8	1	0.1203	0.02405	8	8	1	0.1203	0.02405	8	8	1	0.4896	0.09791
6	1.50E-03	3.00E-04	0.35119	0.07024	8	8	1	0.1203	0.02405	8	8	1	0.1203	0.02405	8	8	1	0.4896	0.09791
7	2.00E-03	4.00E-04	0.12026	0.02405	8	8	1	0.0247	0.00494	8	8	1	0.0247	0.00494	8	8	1	0.2067	0.04135
8	2.00E-03	4.00E-04	0.12026	0.02405	8	8	1	0.0247	0.00494	8	8	1	0.0247	0.00494	8	8	1	0.2067	0.04135
9	2.00E-03	4.00E-04	0.35119	0.07024	8	8	1	0.1203	0.02405	8	8	1	0.1203	0.02405	8	8	1	0.4896	0.09791
10	2.00E-03	4.00E-04	0.35119	0.07024	8	8	1	0.1203	0.02405	8	8	1	0.1203	0.02405	8	8	1	0.4896	0.09791
11	3.50E-03	7.00E-04	0.35119	0.07024	8	8	1	0.1203	0.02405	8	8	1	0.1203	0.02405	8	8	1	0.4896	0.09791
12	5.00E-03	1.00E-03	0.35119	0.07024	8	8	1	0.1203	0.02405	8	8	1	0.1203	0.02405	8	8	1	0.4896	0.09791
13	5.00E-03	1.00E-03	0.35119	0.07024	8	8	1	0.1203	0.02405	8	8	1	0.1203	0.02405	8	8	1	0.4896	0.09791
14	5.00E-03	1.00E-03	0.35119	0.07024	8	8	1	0.1203	0.02405	8	8	1	0.1203	0.02405	8	8	1	0.4896	0.09791
15	5.00E-03	1.00E-03	0.35119	0.07024	8	8	1	0.1203	0.02405	8	8	1	0.1203	0.02405	8	8	1	0.4896	0.09791
16	5.00E-03	1.00E-03	0.35119	0.07024	8	8	1	0.1203	0.02405	8	8	1	0.1203	0.02405	8	8	1	0.4896	0.09791
17	5.00E-03	1.00E-03	0.35119	0.07024	8	8	1	0.1203	0.02405	8	8	1	0.1203	0.02405	8	8	1	0.4896	0.09791

Table J-6. Computations Relating to Breach given No Overtopping

Reach		Reach 1				Reach 2				Reach 3				Reach 4			
Reach start-end stations		To be provided				To be provided				To be provided				To be provided			
Reach coordinates		To be provided				To be provided				To be provided				To be provided			
Equal allocation to Sub-Polder(s)		1				1				1				1			
Reach length (ft)		2000				1800				2200				2200			
Reach elevation (ft)		16				14				13				13			
Additional parameter		To be provided				To be provided				To be provided				To be provided			

Hurricane Runs		Reach 1						Reach 2						Reach 3						Reach 4					
Run	Rate (R)	Surge		Post-surge elevation		Surge		Post-surge elevation		Surge		Post-surge elevation		Surge		Post-surge elevation		Surge		Post-surge elevation					
i	Mean	StD	P(B NOT)	Hps	Mean	StD	P(B NOT)	Hps	Mean	StD	P(B NOT)	Hps	Mean	StD	P(B NOT)	Hps	Mean	StD	P(B NOT)	Hps					
ID	event/yr	event/yr	All Modes	ft	ft	All Modes	ft	ft	All Modes	ft	ft	All Modes	ft	ft	All Modes	ft	ft	All Modes	ft	ft					
1	5.00E-04	1.00E-04	0.1	0.05	8	1	0.1	0.05	8	1	0.1	0.05	8	1	0.1	0.05	8	1	0.1	0.05	8	1			
2	5.00E-04	1.00E-04	0.2	0.1	8	1	0.2	0.1	8	1	0.2	0.1	8	1	0.2	0.1	8	1	0.2	0.1	8	1			
3	7.50E-04	1.50E-04	0.1	0.05	8	1	0.1	0.05	8	1	0.1	0.05	8	1	0.1	0.05	8	1	0.1	0.05	8	1			
4	1.00E-03	2.00E-04	0.1	0.1	8	1	0.1	0.1	8	1	0.1	0.1	8	1	0.1	0.1	8	1	0.1	0.1	8	1			
5	1.00E-03	2.00E-04	0.1	0.1	8	1	0.1	0.1	8	1	0.1	0.1	8	1	0.1	0.1	8	1	0.1	0.1	8	1			
6	1.50E-03	3.00E-04	0.05	0.1	8	1	0.05	0.1	8	1	0.05	0.1	8	1	0.05	0.1	8	1	0.05	0.1	8	1			
7	2.00E-03	4.00E-04	0.2	0.1	8	1	0.2	0.1	8	1	0.2	0.1	8	1	0.2	0.1	8	1	0.2	0.1	8	1			
8	2.00E-03	4.00E-04	0.2	0.1	8	1	0.2	0.1	8	1	0.2	0.1	8	1	0.2	0.1	8	1	0.2	0.1	8	1			
9	2.00E-03	4.00E-04	0.2	0.2	8	1	0.2	0.2	8	1	0.2	0.2	8	1	0.2	0.2	8	1	0.2	0.2	8	1			
10	2.00E-03	4.00E-04	0.2	0.05	8	1	0.2	0.05	8	1	0.2	0.05	8	1	0.2	0.05	8	1	0.2	0.05	8	1			
11	3.50E-03	7.00E-04	0.2	0.05	8	1	0.2	0.05	8	1	0.2	0.05	8	1	0.2	0.05	8	1	0.2	0.05	8	1			
12	5.00E-03	1.00E-03	0.2	0.05	8	1	0.2	0.05	8	1	0.2	0.05	8	1	0.2	0.05	8	1	0.2	0.05	8	1			
13	5.00E-03	1.00E-03	0.2	0.05	8	1	0.2	0.05	8	1	0.2	0.05	8	1	0.2	0.05	8	1	0.2	0.05	8	1			
14	5.00E-03	1.00E-03	0.2	0.05	8	1	0.2	0.05	8	1	0.2	0.05	8	1	0.2	0.05	8	1	0.2	0.05	8	1			
15	5.00E-03	1.00E-03	0.2	0.05	8	1	0.2	0.05	8	1	0.2	0.05	8	1	0.2	0.05	8	1	0.2	0.05	8	1			
16	5.00E-03	1.00E-03	0.2	0.05	8	1	0.2	0.05	8	1	0.2	0.05	8	1	0.2	0.05	8	1	0.2	0.05	8	1			
17	5.00E-03	1.00E-03	0.2	0.05	8	1	0.2	0.05	8	1	0.2	0.05	8	1	0.2	0.05	8	1	0.2	0.05	8	1			

Polder Reliability Analysis. Failure modes, performance functions, basic random variables, and computational procedures of failure probability are provided in the reliability analysis chapter. The failure probabilities of n failure modes for all reaches in a polder are denoted as p_1, p_2, \dots, p_n . The breach failure probability for a polder (P_B) can be computed as

$$P_B(Polder) = 1 - \prod_{i=1}^n (1 - p_i) \tag{J-17}$$

Equation J-17 can be used for the cases of probability of breach given overtopping, the probability of breach given non-overtopping, and the probability of breach of features.

Water Elevation and Volume. The hurricane runs are expected to produce the level of flood inundation within a polder after a hurricane surge. The surge hydrograph produced by a hurricane is used to compute the water volume entering a polder during levee overtopping or breaching, and the post-surge water elevation (H_{ps}) within the polder. In the case of levee overtopping, H_{ps} within a polder is based on a water volume computed using the duration of overtopping. If a breach occurs and the invert of the breach is below the final elevation of the adjacent body of water, H_{ps} is the elevation of that body of water. If the breach invert is above the final elevation of the adjacent body of water, H_{ps} is based on a water volume entering the polder computed using the duration that the surge is above the breach invert. The topography of the polder, and the drainage and pumping models provided by Tasks 2,3 and 8 are used to construct such a relationship. An example of this relationship was provided in the 2000

unwatering plan of the greater metropolitan area of New Orleans, LA prepared the District which has figures that relate stage elevation to storage. Figure J-14 shows such a stage-storage plot for the New Orleans East (Citrus). Regression analysis was used to fit a model for this plot. The resulting model with a multiple correlation coefficient of 0.998 is

$$V = 1.8690 \times 10^7 (E + 7.5)^2 + 2.9492 \times 10^8 (E + 7.5) \quad (J-18)$$

where V = storage volume (ft^3), E = stage elevation (ft), and E domain of -7.5 to 15 ft. These relationships were provided by Tasks 2 and 3 for the risk analysis.

These computations become more complicated when a polder has two or more sub-polders in which flooding is controlled by separate pumping and drainage systems. For the two sub-polder case as an example, the computations of the final volumes can be assessed as follows:

Let

V_1 inflow to sub-polder 1

V_2 inflow to sub-polder 2

V_{1f} final water volume in sub-polder 1

V_{2f} final water volume in sub-polder 2

V_{12f} final water volume for combined sub-polders 1 and 2

C_{12} capacity of sub-polder 1 for water flowing from sub-polder 1 to sub-polder 2

C_{21} capacity of sub-polder 2 for water flowing from sub-polder 2 to sub-polder 1



Figure J-14. Stage-Storage Relationship of New Orleans (Citrus)

The final volumes can be computed as shown in Table J-7.

Table J-7. Polder Inflow Volumes		
Condition	Model	Comments
Case 1 $V_1 < C_{12}$ and $V_2 < C_{21}$	$V_{1f} = V_1$ and $V_{2f} = V_2$	Provide elevations
Case 2 $V_1 \geq C_{12}$ and $V_2 \geq C_{21}$	Develop and use V_{12f}	Provide elevations
Case 3 $V_1 \geq C_{12}$ and $V_2 < C_{21}$		
Case 3.1 $\Delta V_1 = V_1 - C_{12}$ $\Delta V_1 + V_2 < C_{21}$	Use $V_{1f} = C_{12}$ and $V_{2f} = V_2 + \Delta V_1$	Provide elevations
Case 3.2 $\Delta V_1 = V_1 - C_{12}$ $\Delta V_1 + V_2 \geq C_{21}$	Use V_{12f}	Provide elevations
Case 4 $V_1 < C_{12}$ and $V_2 \geq C_{21}$		
Case 4.1 $\Delta V_2 = V_2 - C_{21}$ $\Delta V_2 + V_1 < C_{12}$	Use $V_{2f} = C_{21}$ and $V_{1f} = V_1 + \Delta V_2$	Provide elevations
Case 4.2 $\Delta V_2 = V_2 - C_{21}$ $\Delta V_2 + V_1 \geq C_{12}$	Use V_{12f}	Provide elevations

Water Level and Probability Aggregation Prior to Drainage, Pumping and Backflow. The results from overtopping and breach analysis can be aggregated and summarized in terms of water volume, post-surge elevation, associated probabilities, and epistemic uncertainties. A sample summary is shown in Table J-8.

Table J-8a. Illustrative Water Level and Probability Aggregation for Overtopping Failures

Parameters		Polder X																																	
Sub-Polder Name		Polder X	1																																
Sub-Polder number		xxxxx																																	
Sub-Polder Population at Risk																																			
Additional parameter																																			
Additional parameter																																			
Additional parameter																																			
Hurricane Runs				Water Volume (ft ³)																															
Run i	Rate (R)		Probability P(OT)	Overtopping Volume (V OT)			Precipitation Rainfall volume			Water from Closures&Joints Water volume			NOT Subtotal water volume Water volume			OT Subtotal water volume Water volume																			
	Mean	StD		Mean	StD	StD	Mean	StD	StD	Mean	StD	StD	Mean	StD	StD	Mean	StD	StD																	
ID	event/yr	event/yr	ft ³	ft ³	ft ³	ft ³	ft ³	ft ³	ft ³	ft ³	ft ³	ft ³	ft ³	ft ³	ft ³	ft ³	ft ³	ft ³																	
1	5.00E-04	1.00E-04	1.000E+00	1.893E+09	2.484E+08	5.000E+07	1.500E+07	6.353E+07	1.056E+07	1.135E+08	1.834E+08	2.006E+09	2.491E+08	5.00E-04	1.00E-04	1.000E+00	1.557E+09	2.038E+08	6.000E+06	1.800E+06	5.762E+07	9.342E+06	6.362E+07	9.514E+06	1.620E+09	2.040E+08									
2	5.00E-04	1.00E-04	1.000E+00	1.521E+09	1.985E+08	6.000E+06	1.800E+06	5.702E+07	9.227E+06	6.302E+07	9.401E+06	1.584E+09	1.988E+08	5.00E-04	1.00E-04	1.000E+00	1.020E+09	1.328E+08	6.000E+06	1.800E+06	4.815E+07	7.839E+06	5.415E+07	7.839E+06	1.074E+09	1.330E+08									
3	7.50E-04	1.50E-04	1.000E+00	1.216E+09	1.578E+08	6.000E+06	1.800E+06	5.167E+07	8.228E+06	5.767E+07	8.423E+06	1.273E+09	1.580E+08	1.00E-03	3.00E-04	1.000E+00	9.522E+08	1.232E+08	6.000E+06	1.800E+06	4.700E+07	7.453E+06	5.300E+07	7.668E+06	1.005E+09	1.235E+08									
4	1.00E-03	2.00E-04	1.000E+00	4.893E+08	6.311E+07	6.000E+06	1.800E+06	3.875E+07	6.418E+06	4.475E+07	6.666E+06	5.340E+08	6.346E+07	1.00E-03	4.00E-04	1.000E+00	3.430E+08	4.644E+07	6.000E+06	1.800E+06	4.263E+07	6.498E+06	3.856E+08	4.689E+07	2.00E-03	4.00E-04	1.000E+00	9.977E-01	2.647E+08	4.066E+07	1.800E+05	3.798E+07	6.306E+06	3.027E+08	4.115E+07
5	2.00E-03	4.00E-04	1.000E+00	1.488E+08	2.434E+07	6.000E+05	1.800E+05	3.375E+07	6.234E+06	3.594E+07	6.237E+06	1.847E+08	2.512E+07	2.00E-03	4.00E-04	1.000E+00	2.647E+08	4.066E+07	6.000E+06	1.800E+06	4.263E+07	6.498E+06	3.856E+08	4.689E+07	2.00E-03	4.00E-04	1.000E+00	9.977E-01	2.647E+08	4.066E+07	1.800E+05	3.798E+07	6.306E+06	3.027E+08	4.115E+07
6	3.00E-03	6.00E-04	1.000E+00	1.045E+08	1.705E+07	6.000E+05	1.800E+05	3.375E+07	6.117E+06	3.435E+07	6.120E+06	1.388E+08	1.812E+07	3.00E-03	6.00E-04	1.000E+00	7.094E+07	1.156E+07	6.000E+05	1.800E+05	3.315E+07	6.057E+06	1.041E+08	1.305E+07	5.00E-03	1.00E-03	1.000E+00	4.622E+07	7.531E+06	6.000E+05	1.800E+05	3.165E+07	6.023E+06	7.848E+07	9.645E+06
7	5.00E-03	1.00E-03	1.000E+00	2.864E+07	4.680E+06	6.000E+05	1.800E+05	3.102E+07	6.009E+06	3.162E+07	6.012E+06	6.026E+07	7.619E+06	5.00E-03	1.00E-03	1.000E+00	2.864E+07	4.680E+06	6.000E+05	1.800E+05	3.102E+07	6.009E+06	6.026E+07	7.619E+06	5.00E-03	1.00E-03	1.000E+00	2.864E+07	4.680E+06	6.000E+05	1.800E+05	3.162E+07	6.012E+06	6.026E+07	7.619E+06
8	5.00E-03	1.00E-03	1.000E+00	8.957E+06	1.667E+07	6.000E+05	1.800E+05	3.058E+07	6.003E+06	3.118E+07	6.006E+06	4.785E+07	6.804E+06	5.00E-03	1.00E-03	1.000E+00	1.204E+04	1.500E+06	6.000E+05	1.800E+05	3.091E+07	6.004E+06	3.986E+07	6.188E+06	5.00E-03	1.00E-03	1.000E+00	1.204E+04	1.500E+06	6.000E+05	1.800E+05	3.091E+07	6.004E+06	3.986E+07	6.188E+06
9	5.00E-03	1.00E-03	1.000E+00	4.340E+06	7.475E+05	6.000E+05	1.800E+05	3.014E+07	6.001E+06	3.074E+07	6.003E+06	3.508E+07	6.049E+06	5.00E-03	1.00E-03	1.000E+00	4.340E+06	7.475E+05	6.000E+05	1.800E+05	3.014E+07	6.003E+06	3.508E+07	6.049E+06	5.00E-03	1.00E-03	1.000E+00	4.340E+06	7.475E+05	6.000E+05	1.800E+05	3.074E+07	6.003E+06	3.508E+07	6.049E+06

Table J-8b. Illustrative Water Level and Probability Aggregation for Breach Failures

Parameters		Breaches																					
Run i	Rate (R) Mean	Reaches P(B QT)				Reaches P(B NOT)				Drainage Structures P(DS)				Transitions P(Transition)				Breach Probability P(B)				Post-surge Elevation	
		Mean	Std	Prob.	Prob.	Mean	Std	Prob.	Prob.	Mean	Std	Prob.	Prob.	Mean	Std	Prob.	Prob.	Mean	Std	ft	ft		
		event/yr	event/yr	event/yr	event/yr	event/yr	event/yr	event/yr	event/yr	event/yr	event/yr	event/yr	event/yr	event/yr	event/yr	event/yr	event/yr	event/yr	event/yr	event/yr	event/yr	event/yr	
1	5.00E-04	1.00E-04	3.362E-01	4.834E-02	3.439E-01	1.000E-01	1.000E-04	2.000E-05	1.000E-04	1.000E-04	2.000E-05	1.000E-04	2.000E-04	1.000E-05	1.000E-04	2.000E-05	3.36E-01	1.11E-01	1.11E-01	8	1		
2	5.00E-04	1.00E-04	3.362E-01	4.834E-02	5.904E-01	2.000E-01	1.000E-04	2.000E-05	1.000E-04	1.000E-04	2.000E-05	1.000E-04	2.000E-04	1.000E-05	1.000E-04	2.000E-05	3.36E-01	2.06E-01	2.06E-01	8	1		
3	7.50E-04	1.50E-04	5.185E-01	7.805E-02	3.439E-01	1.000E-01	1.000E-04	2.000E-05	1.000E-04	1.000E-04	2.000E-05	1.000E-04	2.000E-04	1.000E-05	1.000E-04	2.000E-05	5.19E-01	1.27E-01	1.27E-01	8	1		
4	1.00E-03	2.00E-04	3.362E-01	4.834E-02	3.439E-01	2.000E-01	1.000E-04	2.000E-05	1.000E-04	1.000E-04	2.000E-05	1.000E-04	2.000E-04	1.000E-05	1.000E-04	2.000E-05	3.36E-01	2.06E-01	2.06E-01	8	1		
5	1.00E-03	2.00E-04	7.437E-01	1.252E-01	3.439E-01	2.000E-01	1.000E-04	2.000E-05	1.000E-04	1.000E-04	2.000E-05	1.000E-04	2.000E-04	1.000E-05	1.000E-04	2.000E-05	7.44E-01	2.36E-01	2.36E-01	8	1		
6	1.50E-03	3.00E-04	7.437E-01	1.252E-01	1.855E-01	2.000E-01	1.000E-04	2.000E-05	1.000E-04	1.000E-04	2.000E-05	1.000E-04	2.000E-04	1.000E-05	1.000E-04	2.000E-05	7.44E-01	2.36E-01	2.36E-01	8	1		
7	2.00E-03	4.00E-04	3.362E-01	4.834E-02	5.904E-01	2.000E-01	1.000E-04	2.000E-05	1.000E-04	1.000E-04	2.000E-05	1.000E-04	2.000E-04	1.000E-05	1.000E-04	2.000E-05	3.36E-01	2.06E-01	2.06E-01	8	1		
8	2.00E-03	4.00E-04	3.362E-01	4.834E-02	5.904E-01	2.000E-01	1.000E-04	2.000E-05	1.000E-04	1.000E-04	2.000E-05	1.000E-04	2.000E-04	1.000E-05	1.000E-04	2.000E-05	3.36E-01	2.06E-01	2.06E-01	8	1		
9	2.00E-03	4.00E-04	7.437E-01	1.252E-01	5.904E-01	4.000E-01	1.000E-04	2.000E-05	1.000E-04	1.000E-04	2.000E-05	1.000E-04	2.000E-04	1.000E-05	1.000E-04	2.000E-05	7.44E-01	4.19E-01	4.19E-01	8	1		
10	2.00E-03	4.00E-04	7.437E-01	1.252E-01	5.904E-01	1.000E-01	1.000E-04	2.000E-05	1.000E-04	1.000E-04	2.000E-05	1.000E-04	2.000E-04	1.000E-05	1.000E-04	2.000E-05	7.31E-01	1.60E-01	1.60E-01	8	1		
11	3.50E-03	7.00E-04	7.437E-01	1.252E-01	5.904E-01	1.000E-01	1.000E-04	2.000E-05	1.000E-04	1.000E-04	2.000E-05	1.000E-04	2.000E-04	1.000E-05	1.000E-04	2.000E-05	6.73E-01	1.60E-01	1.60E-01	8	1		
12	5.00E-03	1.00E-03	7.437E-01	1.252E-01	5.904E-01	1.000E-01	1.000E-04	2.000E-05	1.000E-04	1.000E-04	2.000E-05	1.000E-04	2.000E-04	1.000E-05	1.000E-04	2.000E-05	6.16E-01	1.60E-01	1.60E-01	8	1		
13	5.00E-03	1.00E-03	7.437E-01	1.252E-01	5.904E-01	1.000E-01	1.000E-04	2.000E-05	1.000E-04	1.000E-04	2.000E-05	1.000E-04	2.000E-04	1.000E-05	1.000E-04	2.000E-05	5.96E-01	1.60E-01	1.60E-01	8	1		
14	5.00E-03	1.00E-03	7.437E-01	1.252E-01	5.904E-01	1.000E-01	1.000E-04	2.000E-05	1.000E-04	1.000E-04	2.000E-05	1.000E-04	2.000E-04	1.000E-05	1.000E-04	2.000E-05	5.91E-01	1.60E-01	1.60E-01	8	1		
15	5.00E-03	1.00E-03	7.437E-01	1.252E-01	5.904E-01	1.000E-01	1.000E-04	2.000E-05	1.000E-04	1.000E-04	2.000E-05	1.000E-04	2.000E-04	1.000E-05	1.000E-04	2.000E-05	5.91E-01	1.60E-01	1.60E-01	8	1		
16	5.00E-03	1.00E-03	7.437E-01	1.252E-01	5.904E-01	1.000E-01	1.000E-04	2.000E-05	1.000E-04	1.000E-04	2.000E-05	1.000E-04	2.000E-04	1.000E-05	1.000E-04	2.000E-05	5.91E-01	1.60E-01	1.60E-01	8	1		
17	5.00E-03	1.00E-03	7.437E-01	1.252E-01	5.904E-01	1.000E-01	1.000E-04	2.000E-05	1.000E-04	1.000E-04	2.000E-05	1.000E-04	2.000E-04	1.000E-05	1.000E-04	2.000E-05	5.91E-01	1.60E-01	1.60E-01	8	1		

Net Water Level Due to Drainage, Pumping and Backflow. The summary results from Table J-8 can be used in conjunctions with drainage and pumping efficiency, and any backflow potential through the pumps that are functions of water volume and elevations to compute net water volumes. A sample summary is shown in Table J-9.

Table J-9. Illustrative Net Water Level Computations

Parameters		Polder X						Polder X					
Polder Name		1						2					
Sub-Polder number		xxxxx						xxxxx					
Sub-Polder Population at Risk													
Additional parameter		0.2						0.2					
Pumping factor COV		??						??					
Mean capacity of sub-Polder (ft ³)													
Std Capacity of Sub-Polder (ft ³)													

Hurricane Runs		Water Volume (ft ³)						Water Volume (ft ³)						
Run	Rate (R)		Overtopping	OT Subtotal water volume		Pumping	Net water volume		Overtopping	OT Subtotal water volume		Pumping	Net water volume	
i	Mean	Std	Probability	Mean	Std	Factor	Mean	Std	Probability	Mean	Std	Factor	Mean	Std
ID	event/yr	event/yr	P(OT)	ft ³	ft ³	(including backflow)	ft ³	ft ³	P(OT)	ft ³	ft ³	(including backflow)	ft ³	ft ³
1	5.00E-04	1.00E-04	1.000E+00	2.006E+09	2.491E+08	8.000E-01	1.605E+09	3.778E+08	0.000E+00	0.000E+00	0.000E+00	8.000E-01	0.000E+00	TBD
2	5.00E-04	1.00E-04	1.000E+00	1.620E+09	2.040E+08	1.200E+00	1.944E+09	4.595E+08	0.000E+00	0.000E+00	0.000E+00	1.200E+00	0.000E+00	TBD
3	7.50E-04	1.50E-04	1.000E+00	1.584E+09	1.988E+08	1.000E+00	1.584E+09	3.739E+08	0.000E+00	0.000E+00	0.000E+00	1.000E+00	0.000E+00	TBD
4	1.00E-03	2.00E-04	1.000E+00	1.074E+09	1.330E+08	6.000E-01	6.444E+08	1.516E+08	0.000E+00	0.000E+00	0.000E+00	6.000E-01	0.000E+00	TBD
5	1.00E-03	2.00E-04	1.000E+00	1.273E+09	1.580E+08	6.000E-01	7.639E+08	1.798E+08	0.000E+00	0.000E+00	0.000E+00	6.000E-01	0.000E+00	TBD
6	1.50E-03	3.00E-04	1.000E+00	1.005E+09	1.235E+08	6.000E-01	6.031E+08	1.416E+08	0.000E+00	0.000E+00	0.000E+00	6.000E-01	0.000E+00	TBD
7	2.00E-03	4.00E-04	1.000E+00	5.340E+08	6.346E+07	6.000E-01	3.204E+08	7.454E+07	0.000E+00	0.000E+00	0.000E+00	6.000E-01	0.000E+00	TBD
8	2.00E-03	4.00E-04	1.000E+00	3.856E+08	4.689E+07	6.000E-01	2.314E+08	5.415E+07	0.000E+00	0.000E+00	0.000E+00	6.000E-01	0.000E+00	TBD
9	2.00E-03	4.00E-04	9.977E-01	3.027E+08	4.115E+07	6.000E-01	1.816E+08	4.392E+07	0.000E+00	0.000E+00	0.000E+00	6.000E-01	0.000E+00	TBD
10	2.00E-03	4.00E-04	9.142E-01	1.847E+08	2.512E+07	6.000E-01	1.108E+08	2.680E+07	0.000E+00	0.000E+00	0.000E+00	6.000E-01	0.000E+00	TBD
11	3.50E-03	7.00E-04	5.390E-01	1.388E+08	1.812E+07	6.000E-01	8.331E+07	1.989E+07	0.000E+00	0.000E+00	0.000E+00	6.000E-01	0.000E+00	TBD
12	5.00E-03	1.00E-03	1.670E-01	1.041E+08	1.305E+07	6.000E-01	6.245E+07	1.474E+07	0.000E+00	0.000E+00	0.000E+00	6.000E-01	0.000E+00	TBD
13	5.00E-03	1.00E-03	3.237E-02	7.848E+07	9.645E+06	6.000E-01	4.709E+07	1.105E+07	0.000E+00	0.000E+00	0.000E+00	6.000E-01	0.000E+00	TBD
14	5.00E-03	1.00E-03	4.949E-03	6.026E+07	7.619E+06	6.000E-01	3.616E+07	8.555E+06	0.000E+00	0.000E+00	0.000E+00	6.000E-01	0.000E+00	TBD
15	5.00E-03	1.00E-03	7.246E-04	4.785E+07	6.604E+06	6.000E-01	2.871E+07	6.977E+06	0.000E+00	0.000E+00	0.000E+00	6.000E-01	0.000E+00	TBD
16	5.00E-03	1.00E-03	1.204E-04	3.986E+07	6.188E+06	6.000E-01	2.392E+07	6.055E+06	0.000E+00	0.000E+00	0.000E+00	6.000E-01	0.000E+00	TBD
17	5.00E-03	1.00E-03	2.597E-05	3.508E+07	6.049E+06	6.000E-01	2.105E+07	5.588E+06	0.000E+00	0.000E+00	0.000E+00	6.000E-01	0.000E+00	TBD

Sub-Polder and Polder Event Trees. The event tree according to Figure J-7 can be evaluated as shown in Table J-10 for the sub-polders. The water volume and elevation capacities of sub-polders should be determined in order to develop logic rules for water flow among sub-polders. Figures J-15 and J-16 illustrate the resulting risk profiles. Epistemic uncertainty propagation is presently under development and will provide bounds on the results. Non-parametric methods for uncertainty propagation will also be examined.

Table J-10. Risk Profiles of Sub-polders and Polders

Parameters		Polder X													
Polder Name		1													
Sub-Polder number		xxxxx													
Sub-Polder Population at Risk															
Additional parameter															
Additional parameter															
Additional parameter															
Additional parameter															

Hurricane Runs		Water Volume (ft ³)				Breach		Post-surge Elevation		Evacuation Effectiveness		Life Risk		Economic Risk	
Run	Rate (R)	Overtopping Rate		Net water volume		Breach Rate $\lambda P(B)=\lambda(P(B OT)+P(B NOT))$		Mean	StD	Mean	StD	Mean	StD	Mean	StD
i	Mean	StD	$\lambda(1-P(B))P(OT)$	Mean	StD	Mean	StD	ft	ft						
ID	event/yr	event/yr	ft ³	ft ³	ft ³	ft ³	ft ³	ft	ft			Mean	StD	Mean	StD
1	5.00E-04	1.00E-04	3.318E-04	1.605E+09	3.778E+08	1.68E-04	6.49E-05	8	1	TBD	TBD	TBD	TBD	TBD	TBD
2	5.00E-04	1.00E-04	3.318E-04	1.944E+09	4.595E+08	1.68E-04	1.08E-04	8	1	TBD	TBD	TBD	TBD	TBD	TBD
3	7.50E-04	1.50E-04	3.609E-04	1.584E+09	3.739E+08	3.89E-04	1.23E-04	8	1	TBD	TBD	TBD	TBD	TBD	TBD
4	1.00E-03	2.00E-04	6.636E-04	6.444E+08	1.516E+08	3.36E-04	2.16E-04	8	1	TBD	TBD	TBD	TBD	TBD	TBD
5	1.00E-03	2.00E-04	2.561E-04	7.639E+08	1.798E+08	7.44E-04	2.79E-04	8	1	TBD	TBD	TBD	TBD	TBD	TBD
6	1.50E-03	3.00E-04	3.842E-04	6.031E+08	1.416E+08	1.12E-03	4.18E-04	8	1	TBD	TBD	TBD	TBD	TBD	TBD
7	2.00E-03	4.00E-04	1.327E-03	3.204E+08	7.454E+07	6.73E-04	4.33E-04	8	1	TBD	TBD	TBD	TBD	TBD	TBD
8	2.00E-03	4.00E-04	1.327E-03	2.314E+08	5.415E+07	6.73E-04	4.33E-04	8	1	TBD	TBD	TBD	TBD	TBD	TBD
9	2.00E-03	4.00E-04	5.118E-04	1.816E+08	4.392E+07	1.49E-03	8.89E-04	8	1	TBD	TBD	TBD	TBD	TBD	TBD
10	2.00E-03	4.00E-04	4.923E-04	1.108E+08	2.680E+07	1.46E-03	4.34E-04	8	1	TBD	TBD	TBD	TBD	TBD	TBD
11	3.50E-03	7.00E-04	6.164E-04	8.331E+07	1.989E+07	2.36E-03	7.33E-04	8	1	TBD	TBD	TBD	TBD	TBD	TBD
12	5.00E-03	1.00E-03	0.000E+00	6.245E+07	1.474E+07	3.08E-03	1.01E-03	8	1	TBD	TBD	TBD	TBD	TBD	TBD
13	5.00E-03	1.00E-03	0.000E+00	4.709E+07	1.105E+07	2.98E-03	9.98E-04	8	1	TBD	TBD	TBD	TBD	TBD	TBD
14	5.00E-03	1.00E-03	0.000E+00	3.616E+07	8.555E+06	2.96E-03	9.96E-04	8	1	TBD	TBD	TBD	TBD	TBD	TBD
15	5.00E-03	1.00E-03	0.000E+00	2.871E+07	6.977E+06	2.95E-03	9.95E-04	8	1	TBD	TBD	TBD	TBD	TBD	TBD
16	5.00E-03	1.00E-03	0.000E+00	2.392E+07	6.055E+06	2.95E-03	9.95E-04	8	1	TBD	TBD	TBD	TBD	TBD	TBD
17	5.00E-03	1.00E-03	0.000E+00	2.105E+07	5.558E+06	2.95E-03	9.95E-04	8	1	TBD	TBD	TBD	TBD	TBD	TBD

Risk Profile by Polders, Storm Categories, and for the region. The risk profiles for polders, storm categories and the region can be evaluated by performing the corresponding aggregation similar to what is done for the sub-polders, and results can be displayed using similar curves to the ones provided in Figures J-15 and J-16.

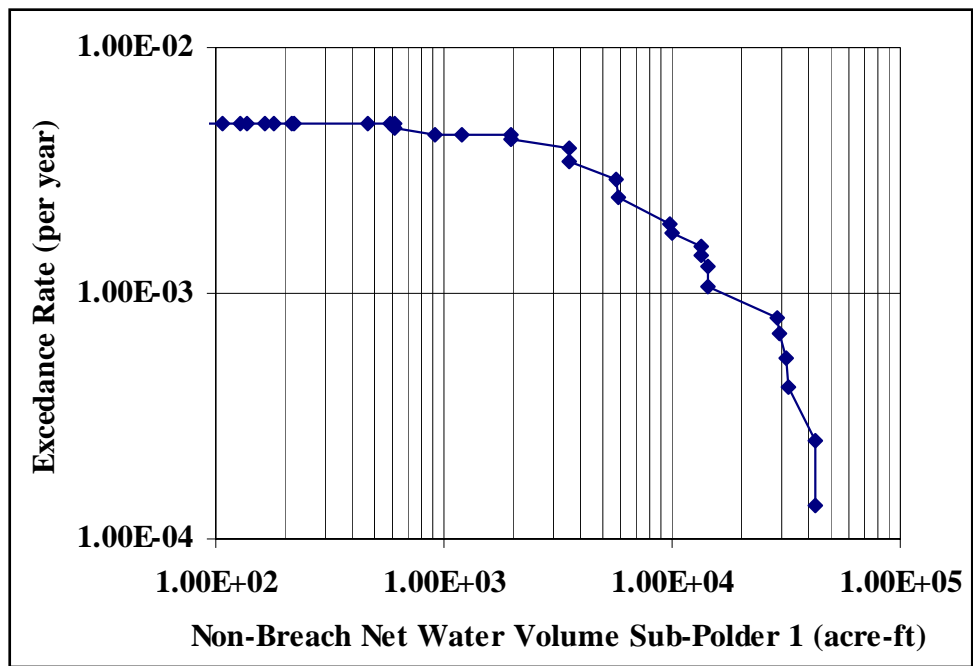


Figure J-15. Overtopping Risk Profile for Sub-Polder 1

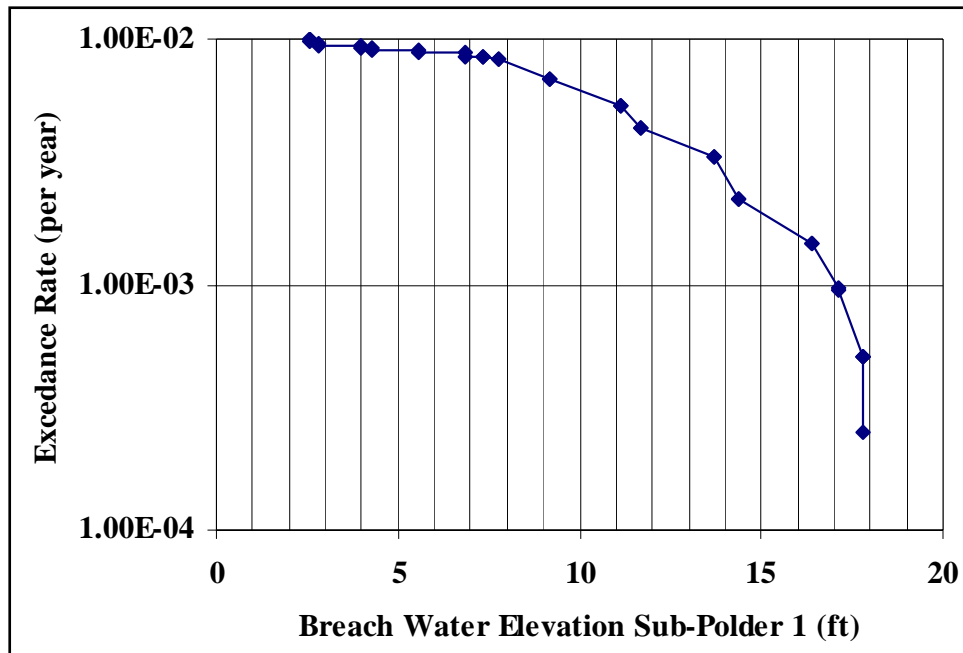


Figure J-16. Breach Risk Profile for Sub-Polder 1

Hazard Analysis and Initiating Events

Several methods have been developed to quantify hurricane hazard, typically in the context of wind-related risk. These methods are classified into three main types: historic (HI), joint-probability (JP), and Monte Carlo simulation (MC) methods.

Historic Methods

Historic (HI) methods quantify the hazard based on the rate at which the effect of interest, L , (e.g. L = wind speed or surge or loss) has occurred in the historical record. These methods are fundamentally nonparametric, i.e. they do not assume a parametric form for the recurrence rate of the hurricanes or their effects. One problem with purely nonparametric historic approaches is the “granularity” of the results that reflects the small number of significant events in the historical record and the sensitivity of the results to unusual occurrences (“outliers”) during the observation period. To reduce these effects, some HI approaches include smoothing procedures. For example, the empirical simulation technique (EST) of Sheffner et al. (1996) “smears” the influential historical hurricanes by replacing them with a sweep of hypothetical events with somewhat different characteristics, typically with different landfall locations. Other smoothing methods fit a parametric distribution to the hurricane effects L_i calculated from the historic events. An example of the latter type is the 1987 version of the National Hurricane Center Risk Analysis Program HURISK (Neumann, 1987). The EST method has been extensively used by the USACE and FEMA to identify design events with relatively low return periods, up to

100 years. Confidence intervals on the results are usually obtained through bootstrapping (resampling) techniques.

Joint Probability (JP) Methods

Joint probability (JP) methods make a parametric representation of hurricanes, typically based on their characteristics $\underline{\theta}$ at landfall and the filling rate after landfall. For example, $\underline{\theta}$ might include the location and velocity vector, the central pressure deficit, the radius to maximum winds and possibly a few other parameters at landfall. The historic record is used to estimate the recurrence rate $\lambda(\underline{\theta})$. One then calculates the effects of interest, say $L(\underline{\theta})$, for a suitable set of $\underline{\theta}$ values and, by combining $\lambda(\underline{\theta})$ and $L(\underline{\theta})$, one obtains the recurrence rate $\lambda(L)$.

The values of $\underline{\theta}$ for which $L(\underline{\theta})$ is calculated may form a regular (factorial) discretization of a critical region in parameter space. Alternatively, one may use Monte Carlo simulation or importance sampling to generate a set of values $\{\underline{\theta}_i\}$ from that region. Factorial discretization and importance sampling are generally preferred when interest is in the tail distribution of L , whereas straight MC simulation is more efficient for short return periods. The MC and importance sampling versions of the JP method may be seen as procedures that replace the actual historical catalog with a much larger synthetic catalog. The JP approach with MC simulation is perhaps the most frequently used method for hurricane wind hazard; see for example Russell (1971), Batts et al. (1980), Georgiou et al. (1983), and Vickery and Twisdale (1995a). If the number of events $\underline{\theta}_i$ is too large to evaluate the responses L_i with high accuracy, one may use coarser analysis procedures to rank the events or to interpolate the results for a subset of events.

Monte Carlo Simulation Methods

Monte Carlo (MC) simulation methods use a stochastic representation of the origin and temporal evolution of hurricanes in the general region of interest, in this case the North Atlantic region. The random trajectory and parameter evolution are typically represented through Markov processes of suitable order, discrete in time but continuous in state. The state-transition parameters vary spatially and are estimated from the historical record. A large number of hurricane events are simulated using this random dynamic model. The sample is trimmed to retain only the events that are significant to the region and the effects of interest and the retained events are treated like the historical sample in the HI methods. As in the JP method, when the number of retained events is too large to evaluate the responses L_i with high accuracy, one must use parsimonious high-accuracy runs in combination with less accurate methods. The MC simulation method was first proposed by Vickery et al. (2000). More recent studies that use MC simulation are Huang et al. (2001) and Powell et al. (2005).

Choice of a Method

The attractiveness of a method depends in general on the amount of data and computational resources available as well as the objective of the analysis. Regarding the latter, it matters whether (1) interest is in frequent or rare events, (2) the objective is to identify design events with given return periods (return-period analysis) or find the rate at which certain consequences are exceeded (risk analysis), and (3), in the case risk analysis, whether the losses occur in a small geographical region that may be considered uniformly impacted by any given hurricane or over an extended region where spatial homogeneity of the hurricane loads cannot be assumed. For flood hazard, return-period analysis is generally easier than risk analysis because hurricane severity may be ranked using surrogate quantities (such as a rough estimate of maximum surge) that are much easier to calculate than the flooding conditions themselves.

Since medium to long return periods are of interest, historical methods are discarded. Both JP and MC methods can handle such return periods. MC approaches face the problem of sorting out the potentially damaging events from large suites of simulated hurricane scenarios. This is not a trivial problem for the geographically extended and differently vulnerable system we are considering. For these reasons, the joint probability approach has been selected. This approach is further described in the following few sections.

To implement a JP method for hurricane hazard, it is convenient to describe hurricanes at landfall through the parameter vector $\underline{\theta} = [\Delta P, R_{\max}, X, \theta, V, B]$, where

- ΔP (mB) = central pressure deficit at landfall
- R_{\max} (km) = radius to maximum winds at landfall
- X (km) = longitudinal landfall location relative to downtown New Orleans (positive if east of New Orleans)
- θ (degrees) = direction of storm motion at landfall, ($\theta = 0$ for tracks pointing north, increasing clockwise)
- V (m/s) = storm translation speed at landfall
- B = Holland's radial pressure profile parameter at landfall (Holland, 1980)

While the variation of these parameters before and after landfall is also of interest, our primary characterization of hurricanes is in terms of their properties at landfall. Hence the main tasks of hazard quantification are the estimation of the recurrence rate $\lambda(\underline{\theta})$ and the evaluation of the environmental loads $L(\underline{\theta})$ over a suitable range of $\underline{\theta}$ values. These tasks are described below, together with other issues such as the discretization of $\underline{\theta}$ space for risk analysis, the treatment of pre- and post-landfall conditions, the use of strategies to reduce the computational effort, and the assessment of epistemic uncertainty.

Hurricane Recurrence at Landfall

The recurrence law for $\underline{\Theta}$ may be written as

$$\lambda(\underline{\Theta}) = \lambda_o f(\underline{\Theta}) \quad (\text{J-19})$$

where $\lambda(\underline{\Theta})$ is the rate density function for $\underline{\Theta}$, meaning that $\lambda(\underline{\Theta})dV$ is the rate of hurricanes with parameters in an infinitesimal volume dV around $\underline{\Theta}$, λ_o is the total occurrence rate in a suitable region of parameter space, and $f(\underline{\Theta})$ is the joint PDF of $\underline{\Theta}$ inside that region.

Information used to estimate λ_o and $f(\underline{\Theta})$ includes historical data sets (mainly NOAA's HURDAT data for λ_o , ΔP , X , θ and V and data on R_{\max} from Ho et al., 1987) as well as published distribution results. The HURDAT data set (Jarvinen et al., 1984, and recent updates) has been used to extract values of (ΔP , X , θ , V) at landfall over the stretch of coastline between longitudes 85W and 95W. For recurrence analysis, we have considered only storms of hurricane strength at landfall (defined as those having measured or estimated $\Delta P \geq 25$ mb) since 1890. Earlier events have been neglected because prior to 1890 the historical record is severely incomplete and less accurate. The HURDAT data set has been used also to analyze pre-landfall conditions.

Information on the structure and parameterization of $f(\underline{\Theta})$ is provided in various references, including Holland (1980), Ho et al. (1987), Vickery and Twisdale (1995a,b), Chouinard et al. (1997), Vickery et al. (2000), Huang et al. (2001), Willoughby and Rahn (2004), and Powell et al. (2005). For the coastal area of interest here, the main findings of these studies are:

- The distribution of ΔP may be assumed to be either lognormal or Weibull. The Weibull distribution tends to give better fits to the data when all tropical storms not just hurricanes are included, whereas the lognormal model is appropriate when only hurricanes are considered; see Vickery and Twisdale (1995a). Using the lognormal model and a locally weighted maximum-likelihood procedure, Chouinard et al. (1997) found that along the Louisiana Coast the standard deviation of ΔP is almost constant at 21 mb, whereas the mean value of ΔP increases eastward from about 32 mb near the Texas border to about 38 mb near the Mississippi border. This trend is attributed to the sea temperature anomaly of the Loop Current.
- Depending on coastal location, the distribution of θ is generally found to be normal or a mixture of two normal distributions, one for easterly storms and the other for westerly storms (Vickery and Twisdale, 1995a; Huang et al., 2001).
- Vickery et al. (2000) found that V may be taken to be lognormally distributed, with mean value about 6 m/s and standard deviation about 2.5 m/s. V has a mild dependence on θ , increasing as θ increases (Vickery and Twisdale, 1995a).

- R_{\max} decreases with increasing hurricane intensity ΔP and its conditional distribution given ΔP may be taken to be lognormal (Vickery and Twisdale, 1995a; Powell et al., 2005). Using data from Ho et al. (1987), Vickery et al. (2000) fitted several linear and quadratic models to $\ln R_{\max}$ against ΔP and latitude. A simple one, with coefficient of determination $R^2 = 0.28$, is $\ln R_{\max} = 2.636 - 0.00005086\Delta P^2 + 0.03949Lat$. Willoughby and Rahn (2004) obtained qualitatively similar results when regressing $\ln R_{\max}$ against latitude and maximum wind speed. Their logarithmic standard deviation is 0.66.

- B varies with R_{\max} and possibly ΔP or maximum wind speed V_{\max} and latitude (Holland, 1980, Vickery et al., 2000, Willoughby and Rahn, 2004, Powell et al., 2005). For storms of hurricane strength, Vickery et al. fitted several relations using data from different flight height ranges. Their recommended mean value relation is $B = 1.38 + 0.00184\Delta P - 0.00309R_{\max}$. Willoughby and Rahn (2004) studied the dependence of B on R_{\max} , V_{\max} , and latitude. These found that the distribution of B is nearly symmetrical and somewhat flatter and shorter-tailed than a normal distribution (in part because their estimation algorithm searches for optimal values between 0.5 and 2.5). Although Willoughby and Rahn estimate a linear dependence of B on $\ln R_{\max}$, the slope coefficient is only marginally significant. The regression residual has standard deviation 0.36. The data analyzed by Powell et al. (2005) is a subset of that of Willoughby and Rahn. The Powell et al. subset uses selection criteria (high winds, low-level flights, and geographical location) that are relevant also to the present study. Powell et al. find that a good fit for $(B|R_{\max}, Lat)$ is given by a truncated normal distribution with mean value $1.881 - 0.0109Lat - 0.00557R_{\max}$, standard deviation 0.286 (before truncation), and range between 0.8 and 2.2.

The above observations have been used in the modeling of $\lambda(\underline{\theta})$. However, dependencies, distribution types and parameter values have been sometimes modified based on further data analyses. Two data sets are used: a broad longitude (BL) data set, which includes HURDAT data at landfall for all hurricanes at landfall ($\Delta P \geq 25$ mb) since 1890 that made landfall between longitudes 85W and 95W. The narrow longitude (NL) data set is the subset with landfall locations between 87.5W and 92.5W. The BL and NL data sets include 62 and 32 events, respectively.

- **Location X and recurrence rate λ_o .** Within both latitude ranges, landfall is approximately uniformly distributed (the uniform distribution easily passes various statistical tests). Using the BL data sets one obtains $\lambda_o = 5.7 \times 10^{-4}$ per longitude-km per year, with a coefficient of variation of 0.18.

- **Approach angle θ .** The distribution of θ for both longitude ranges is very nearly normal (tests of normality pass with P around 0.5 with no evidence of bimodality). For the BL data set, which is preferred for statistical accuracy, the normal distribution fit is shown in Figure J-17.

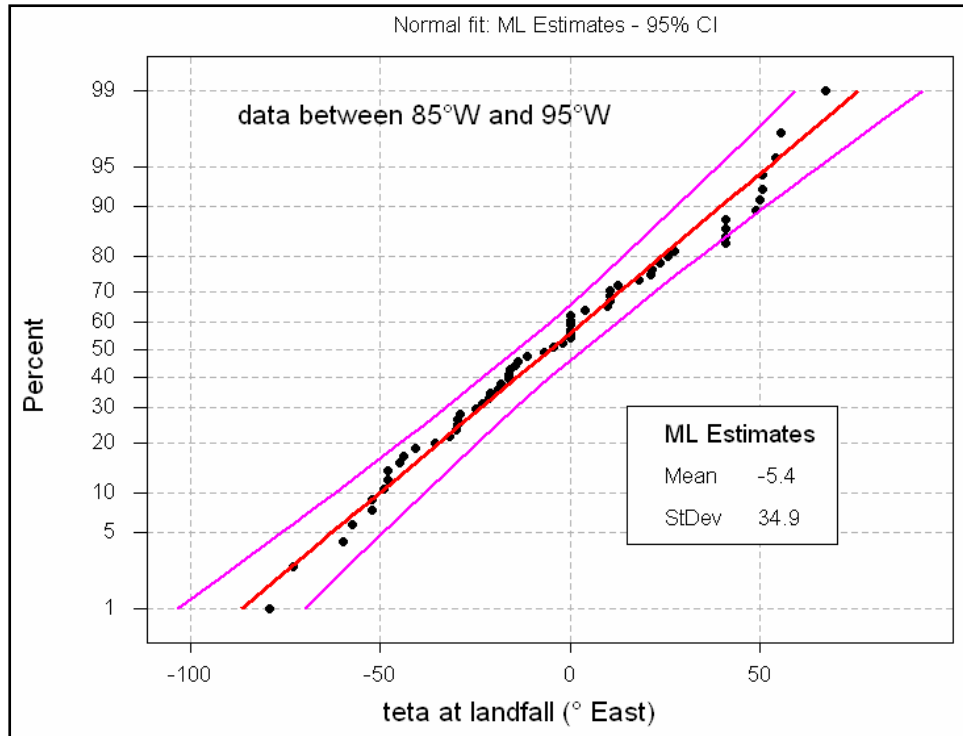


Figure J-17. Normal distribution fit for the approach angle θ

- **Central pressure deficit ΔP .** For $\Delta P > 34$ mb, which is the range of interest to us, the BL and NL data are fitted well by nearly identical shifted lognormal distributions, with shift parameter 18 mb, i.e. $(\Delta P - 18)$ has lognormal distribution for $\Delta P > 34$ mb. The four largest values of ΔP in the data set are associated with hurricanes Camilla, Katrina, Carmen, and Betsy. All four hurricanes have occurred inside the narrow longitude range. The slightly more conservative fit obtained from the NL data set, which is the one we prefer, is shown in Figure J-18. The local trend in the mean value of ΔP observed by Chouinard et al. (1997) is small and statistically not significant; hence it is ignored.

- **Translational speed V .** The often-used lognormal model is not well supported by our data. Better fits are obtained with a Weibull distribution model. The Weibull fit to the NL data is shown in Figure J-19.

- **R_{\max} .** For R_{\max} we use the model in Eq. 9 of Vickery et al. (2000), which for $\text{Lat} = 30N$ gives

$$\ln(R_{\max}) = 3.962 - 0.00567\Delta P + \varepsilon_R \quad (\text{J-20})$$

where ε_R is a normal variable with zero mean and standard deviation 0.313.

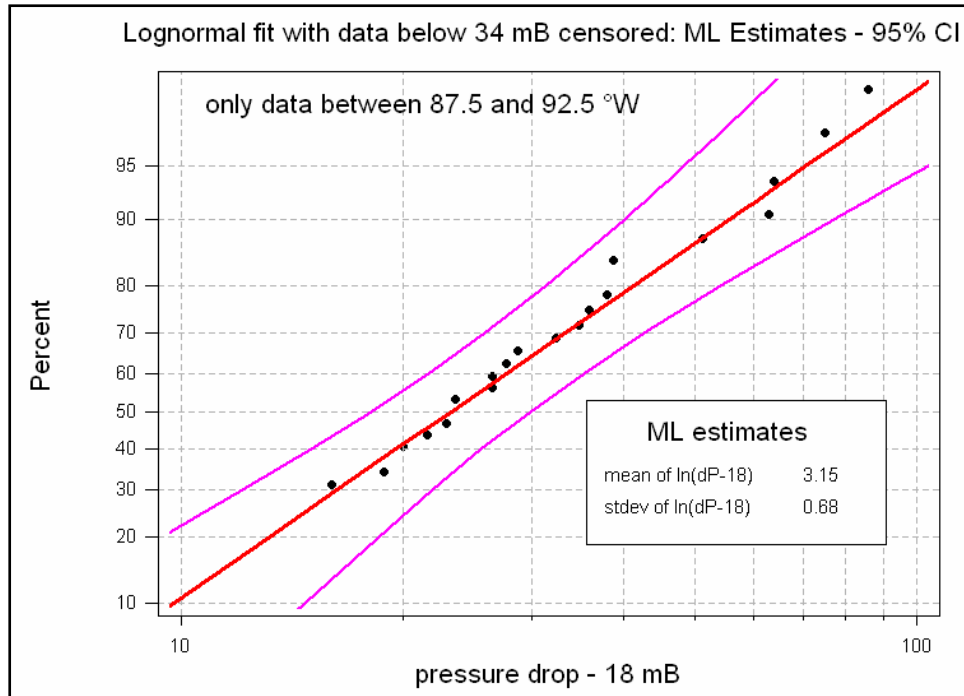


Figure J-18. Lognormal distribution of $(\Delta P - 18)$ fitted to ΔP values above 34 mb in the narrow longitude range

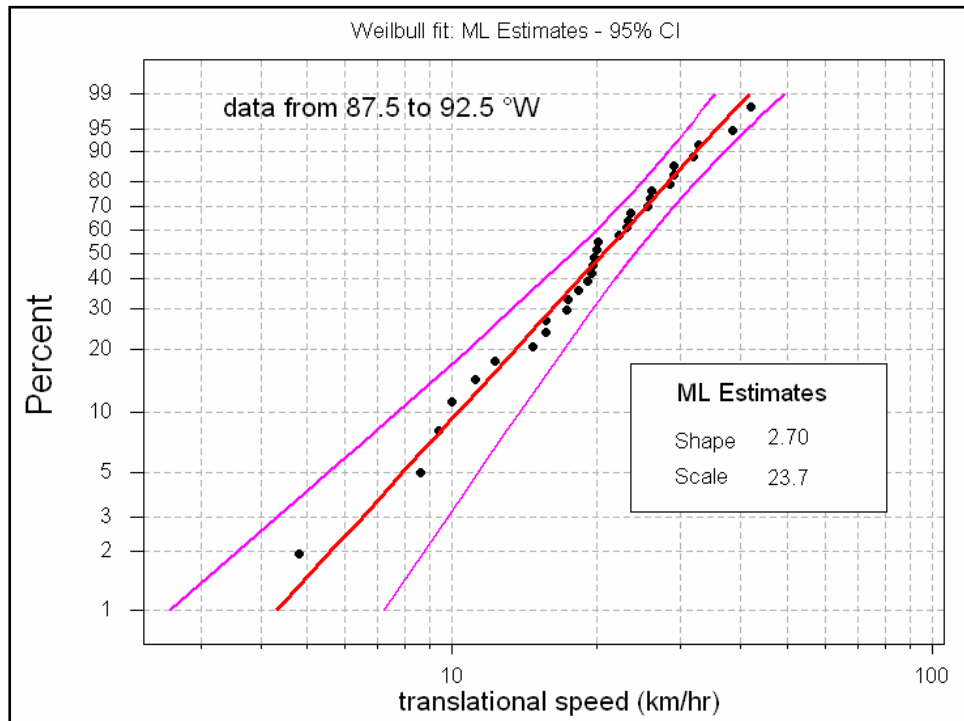


Figure J-19. Weibull fit to storm speed data in the WL data set

- **Holland's B .** For B Powell et al.'s (2005) model is used, which for Lat = 30N gives

$$B = 1.554 - 0.00557R_{\max} + \varepsilon_B \quad (\text{J-21})$$

where ε_B is a normal variable with zero mean and standard deviation 0.286.

Pre- and Post-Landfall Parameter Variation

The θ parameterization concerns exclusively the hurricane characteristics at landfall. One possibility, which has often been used in hurricane hazard analysis, is to assume straight paths and constant values of ΔP , R_{\max} , V and B prior to landfall; see for example Russell (1971), Batts et al. (1980), Georgiou et al. (1983), Neumann (1991), and Vickery and Twisdale (1995a). A more refined approach is used for the hurricane path and the pre-landfall variability of these parameters, as described in the following sections.

Pre-Landfall Parameter Variation. All tropical storms (not just hurricanes) after 1890 in the HURDAT record that made landfall within latitudes 85W and 95W are used to estimate the mean hurricane path for landfall angles θ around -60° , -30° , 0 , 30° , 60° . Results are shown in Figure J-20, where the dots represent average locations at 12 hour intervals relative to the time of landfall. These θ -dependent paths are used in all the hurricane analyses.

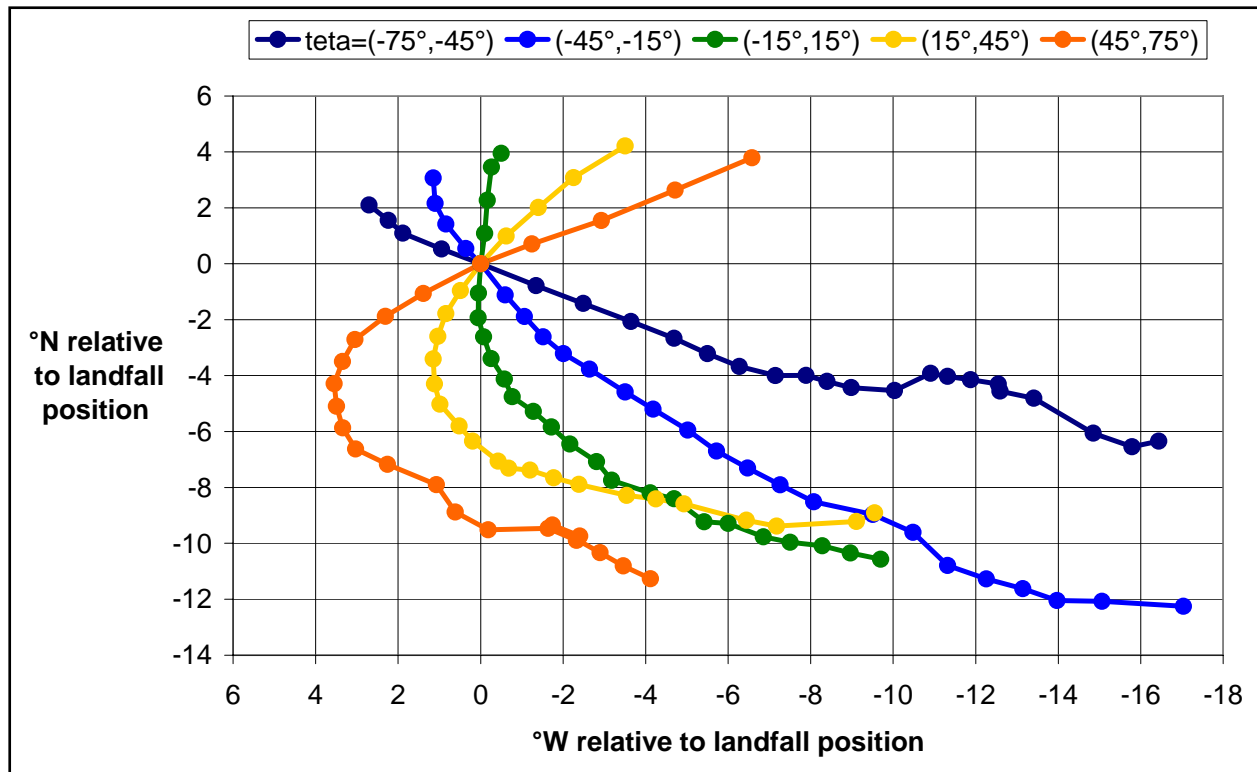


Figure J-20. Mean hurricane path depending on landfall angle θ

The temporal variation of ΔP and V is considered through the ratios

$$\Delta P_R(t) = \frac{\Delta P(t)}{\Delta P} \tag{J-22}$$

$$V_R(t) = \frac{V(t)}{V}$$

where t is time before landfall and ΔP and V are the values at landfall (the values for $t = 0$). Dependence of $\Delta P_R(t)$ and $V_R(t)$ on the parameters θ at landfall has been investigated. While the statistics of $\Delta P_R(t)$ may be taken to be independent of θ , $V_R(t)$ varies significantly with V (and to a negligible extent on the storm direction at landfall, θ). Since the ratios in Eq. J-22 have significant temporal correlation, one may represent their uncertain evolution in time by assuming perfect dependence. Under perfect dependence, one may connect the P -quantile values of $\Delta P_R(t)$ and $V_R(t)$ at different times t to produce single time series, $\Delta P_{R,P}(t)$ and $V_{R,P}(t)$, for each probability P . Figure J-21 shows empirical and smoothed estimates of $\Delta P_{R,P}(t)$ for $P = 0.25, 0.5$ and 0.75 . Notice the tendency for ΔP to decrease during the 12 hours prior to landfall. This decrease is likely due to temperature gradients in the Gulf due to the Loop Current and its eddies and perhaps more importantly to the effect of land on the peripheral hurricane winds prior to landfall. In some cases (including hurricane Katrina), this intensity decay is rather pronounced, whereas in others (like

hurricane Camille), it is not. The $\Delta P_R(t)$ profile for Katrina, which is shown in Figure J-21 for comparison, lies within the inter-quartile range and is close to the upper 75% profile during the 18 hours prior to landfall.

Figure J-22 shows similar results for $V_{R,P}(t)$. Since $V_{R,P}(t)$ depends significantly on V at landfall, results are shown separately for $V < 15$ km/h, V between 15 and 25 km/h, and $V > 25$ km/h (the empirical mean values of V within these ranges are close to the values of V used in the analysis; see Section 4).

The temporal profiles of translational speed in Figure J-22 reflect the fact that $V(t)$ is close to a stationary process (with ergodicity in the mean). This is why, for large t , $V(t)$ loses memory of its value at landfall and $V_R(t)$ is small (large) for V large (small).

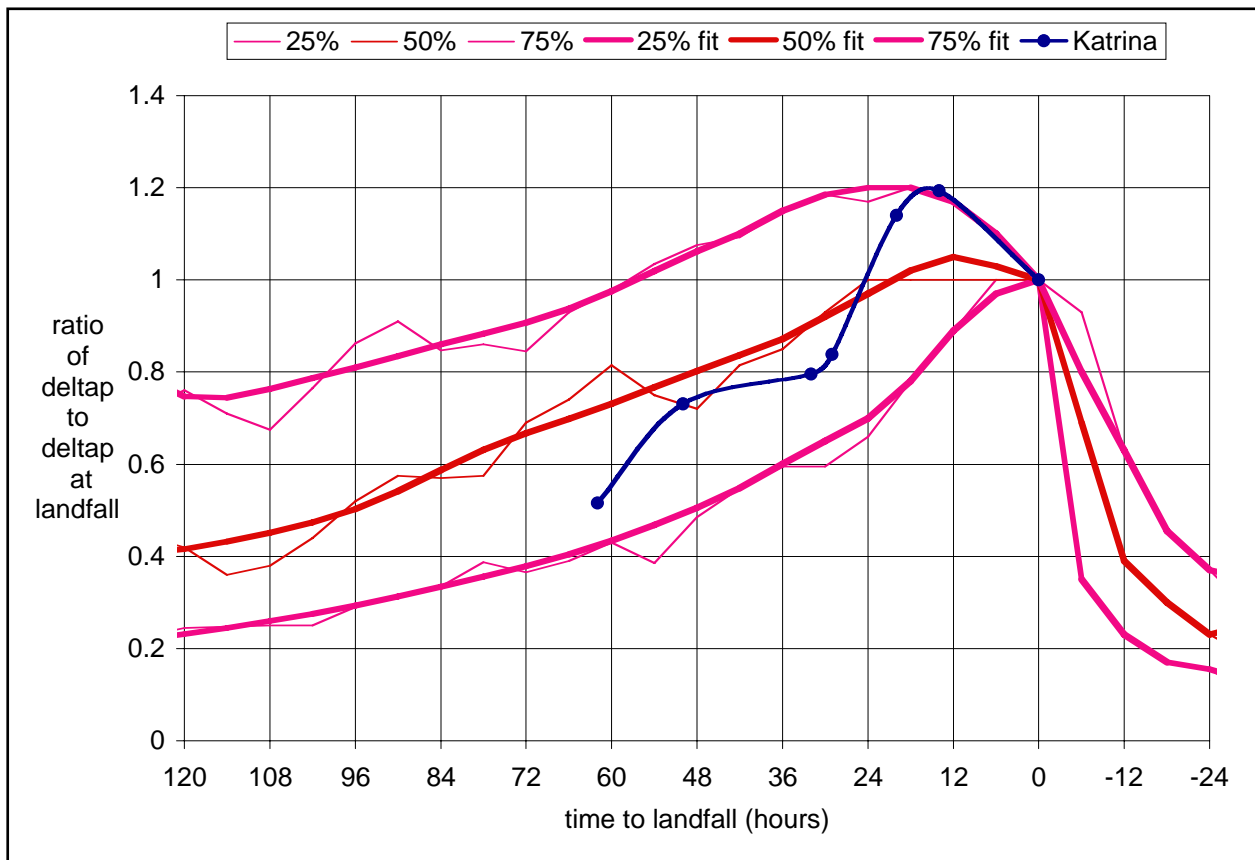


Figure J-21. Pressure deficit ratios $\Delta P_{R,P}(t)$ for $P = 0.25, 0.5$ and 0.75

HURDAT does not include information on R_{\max} and B . For R_{\max} , we use the model in Eq. 7 of Vickery et al. (2000), which gives

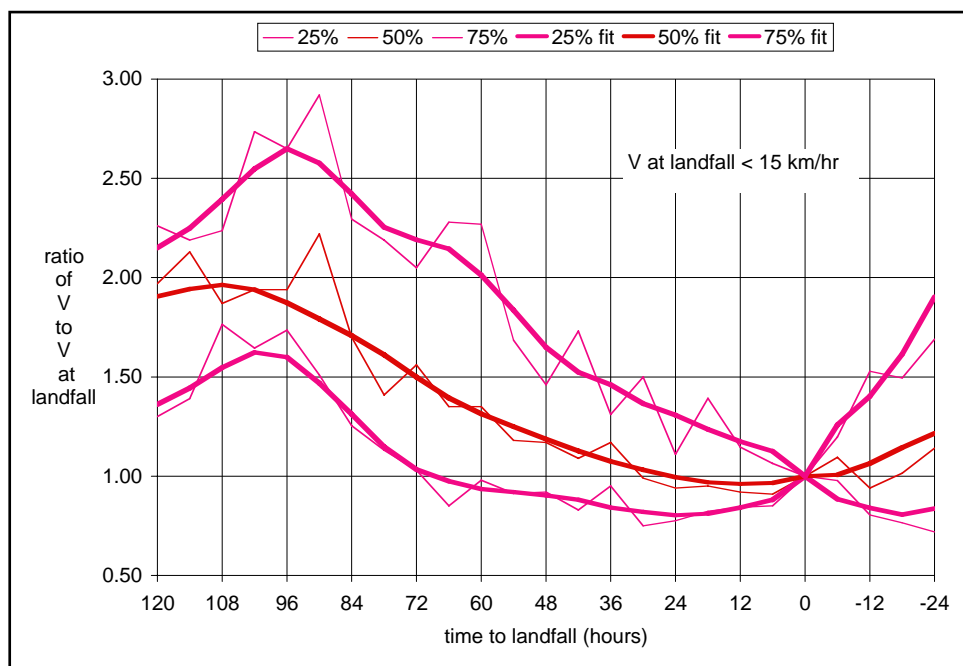
$$R_{\max}(t) \propto e^{-0.00005086 \Delta P(t)^2 + 0.03949 Lat(t)} \quad (J-23)$$

as a first-order adjustment to the value at landfall using $\Delta P(t)$ and $Lat(t)$ along the track.

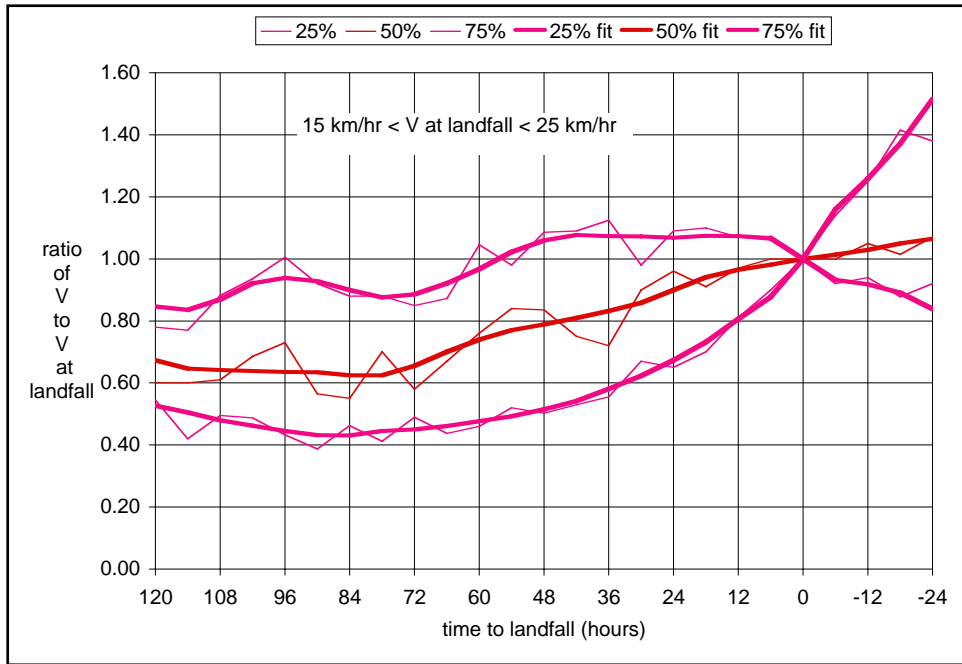
For B , Powell et al.'s (2005) model is used, which gives the dependence of $B(t)$ on $R_{max}(t)$ and $Lat(t)$ as

$$B(t) = const. - 0.0109Lat(t) - 0.00557 R_{max}(t) \quad (J-24)$$

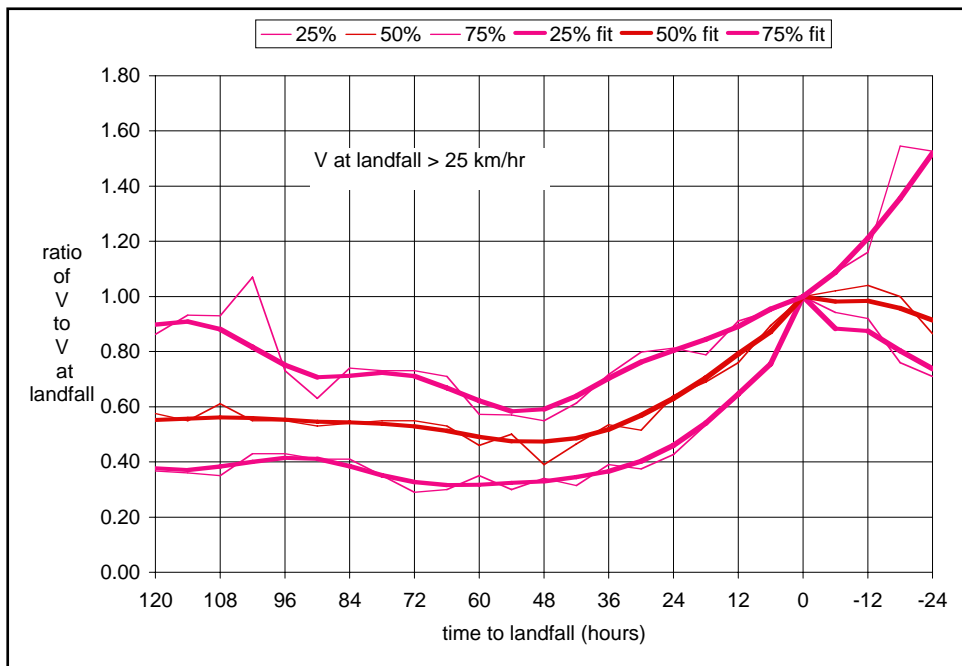
The factor in Eq. J-23 and the constant in Eq. J-24 are adjusted to reproduce the values of R_{max} and B at landfall. Both equations give a mean-trend corrections along the track. No random temporal fluctuation of R_{max} or B is considered.



(a) $V < 15$ km/h



(b) $15 \text{ km/hr} < V < 25 \text{ km/hr}$



(c) $V > 25 \text{ km/h}$

Figure J-22. Storm speed ratios $V_{R,P}(t)$ for $P = 0.25, 0.5$ and 0.75 and (a) $V < 15 \text{ km/h}$, (b) V between 15 and 25 km/h , and (c) $V > 25 \text{ km/h}$

All of the analyses described below in Sections 4.6.2 and 4.6.3 are performed using the mean tracks in Figure J-20, the median ratios $\Delta P_{R,0.5}(t)$ and $V_{R,0.5}(t)$ in Figures J-20 and J-21, and the mean temporal evolutions of R_{\max} and B in

Eqs. J-23 and J-24. The ratios $\Delta P_{R,P}(t)$ and $V_{R,P}(t)$ for $P = 0.25$ and 0.75 in Figures J-21 and J-22 are used to assess uncertainty on the environmental loads due to variability in the pre-landfall values of ΔP and V .

Post-landfall Conditions. After landfall, several hurricane parameters undergo significant changes. For example, the pressure deficit ΔP decreases in an approximately exponential way and the radius of maximum winds R_{\max} tends to increase. The only change that may have significant effect on surges and waves is the temporal decay of ΔP , which generally has the form

$$\Delta P(t) = \Delta P e^{-\alpha t} \quad (\text{J-25})$$

where t is time after landfall, ΔP is pressure deficit at landfall, and α is a decay parameter. For t in hours and ΔP in mb, Vickery and Twisdale (1995b) found that for the Gulf of Mexico α has mean value $0.035 + 0.0005 \Delta P$ and standard deviation 0.0355 . These statistics are consistent with data in our narrower longitude range; see quantile plots in Figure J-21 for $t < 0$. Since α is not a sensitive parameter for waves and surges, we use this mean value expression in Eq. J-25 and neglect the variability.

Parameter Discretization for Risk Analysis

Hurricane risk is evaluated by considering a large number of possible scenario hurricanes, each associated with one value of Θ . These scenario events are selected considering the joint density $f(\Theta)$ as well as the potential for induced damage.

For the parameters X and ΔP , which have a generally monotonic effect on the environmental loads, ranges have been that produce moderate to intense effects at the polders. Specifically, for the quantity $X \cos(\theta)$, which measures the minimum distance of the hurricane track from downtown New Orleans, the range $[-130, +110]$ km is used. This choice is based on preliminary sensitivity runs, which indicate that hurricanes at greater distances from New Orleans do not dominate the risk. For the pressure deficit ΔP , we have used the range $[41, 130]$ mb, where 41 mb is a representative value for Cat-2 hurricanes and 130 mb is well into the high Cat-5 range.

The other parameters have effects the sign and magnitude of which depends on location. We have generally varied them within their central 80% or 90% confidence intervals (i.e. the intervals that contain the value of the parameter with probability 0.8 or 0.9), obtained from the recurrence model. For parameters that depend significantly on other parameters, conditional rather than marginal ranges have been used.

The above ranges define a region in parameter space. A possible discretization of this region is given by all combinations of the parameter values listed in Table J-11.

The parameters above the dashed line in Table J-11 refer to conditions at landfall and those below the dashed line are for conditions before or after landfall. The first 3 values of ΔP in Table J-10 are representative of hurricane Categories 2, 3 and 4 whereas the last 3 values represent various levels within Category 5. The values of V approximate the 5%, 25%, 50%, 75%, 95% Weibull quantiles in Figure J-19. Finally notice that smooth $V_{R,0.5}(t)$ curves are shown in Figure J-22 only for some ranges of V . Curves for specific values of V are obtained by first finding the average value of V for each range in Figure J-19 (these average values are close to 8, 21, and 36 km/h) and then interpolating the curves for other values of V of interest.

Table J-11 Parameter levels that may be considered for risk analysis	
Parameter	Levels for risk analysis
ΔP (mb)	41, 59, 80, 100, 115, 130
V (km/h)	8, 15, 21, 27, 36
$X_{\cos}(\theta)$ (km)	-130, -90, -50, -10, 30, 70, 110
θ	-60, -30, 0, 30, 60
R_{\max}	10%, 50%, 90% quantiles from Eq. J-20
B	5%, 25%, 50%, 75%, 95% quantiles from Eq. J-21

$\Delta P_R(t)$	smooth $\Delta P_{R,0.5}(t)$ curve in Figure J-21
$V_R(t)$	smooth $V_{R,0.5}(t)$ curves in Figure J-22 depending on V
$R_{\max}(t)$	from R_{\max} , $\Delta P(t)$ and $Lat(t)$; see Eq. J-23
$B(t)$	from B , R_{\max} and $Lat(t)$; see Eq. J-24
α	$0.035 + 0.0005 \Delta P$
No. of cases	26,250

Not all the 26,250 hurricane scenarios in Table J-11 need be considered for risk assessment: some may be excluded because they are exceedingly rare and others because they are unlikely to cause significant losses. For example, hurricanes with small R_{\max} and large $|X|$ do not threaten the New Orleans region. Also, depending on the sensitivity of the loads L to each parameter, the number of parameter levels may be reduced. Conversely, if a better representation of a parameter or a more accurate decomposition of risk is required, then the number of levels may be increased. This is especially true for ΔP .

Assessment of Hurricane Loads $L(\Theta)$

Finding the environmental loads L for each parameter vector Θ of interest is the most challenging task of hurricane hazard characterization. Following is a description of how this is done for still water levels, waves, and rainfall intensity.

Still Water Levels and Waves. It is well known that surge and waves interact (surge affects waves and vice-versa). Therefore, one should ideally assess these loads using a coupled formulation. Sophisticated coupled programs

are currently being developed, but at the present time such programs are not at a stage that they can be routinely used.

An alternative is to follow an iterative approach, whereby one first calculates the surge $H(x,y,t)$ without waves, then estimates the wave field $W(x,y,t)$ given the preliminary estimate of the surge, and finally re-runs the surge code considering the calculated wave field. While the treatment of waves has not been finalized yet, the plan is use a simple wave parameterization scheme based on results obtained in previous detailed analyses. This parameterization approach should produce rather accurate results and greatly streamlines computations (Robert Dean, personal communication). Surges are calculated using the ADCIRC code (Luettich et al., 1992).

ADCIRC uses a triangular grid with spatially varying resolution, which for our application covers the entire Gulf of Mexico. The resolution increases in coastal areas, in particular near the Louisiana Coast. High-resolution grids may include millions of nodes and must be run with time steps on the order of 1 second to avoid numerical problems. Such dense grids produce accurate results and can adequately resolve topographic effects on horizontal scales of tens of meters along the coast.

Since it is not feasible to use such dense computational grids for all the parameter combinations in Table J-11, a different strategy must be adopted, in which one avoids running all cases and those that are run use computational grids at lower resolutions.

Reduction in the Number of ADCIRC Runs. To reduce the number of runs, one can take advantage of two conditions: 1. If dependence of H on a parameter A is smooth, then one may calculate H for a subset of levels of A and use interpolation for the other levels, and 2. If two parameters A and B do not interact (additively or multiplicatively), then the (additive or multiplicative) effect of varying one of them is the same irrespective of the level of the other parameter. In this case one can infer H for all combinations of A and B by varying each parameter while keeping the other parameter constant. Determination of whether either condition applies can be made using a low-resolution (LR) grid with only a few thousand nodes. Moreover, for this purpose one may run ADCIRC just once, ignoring the effect of waves.

These considerations reduce the number of needed ADCIRC runs from about 26,000 in Table J-11 to about 1,000. However, even 1,000 hurricane scenarios are too many to be run with a high-density grid. The strategy selected is to run these cases with a medium-resolution (MR) grid with approximately 90,000 nodes and use the high-resolution (HR) grid for only about 40 cases. The HR runs are then used to calibrate the MR results.

The spatial pattern of surge and waves depends primarily on $[R_{\max}, X, \theta]$. Since the effect of these parameters at a given geographic location is generally non-monotonic, interpolation involving these parameters would not produce accurate results. In addition, these parameters interact among themselves. Hence, all combinations of $[R_{\max}, X, \theta]$ in Table J-11 must be run using the MR model.

The use of only 3 levels of R_{\max} in Table J-11 reduces the computational effort in the MR runs.

The LR runs have shown that, for given [R_{\max} , X , θ], the water level H at each geographical location depends smoothly on ΔP , V , and B . Hence one may consider a smaller number of levels of these parameters and calculate H for the other levels through interpolation. This has led to the MR run plan in Table J-12.

Table J-12	
Parameter levels for mid-resolution runs	
Parameter	Levels for mid-resolution analysis
ΔP (mb)	41, 80, 115
V (km/h)	8, 21, 36
$X \cos(\theta)$ (km)	-130, -90, -50, -10, 30, 70, 110
θ	-60, -30, 0, 30, 60
R_{\max}	10%, 50%, 90% quantiles from Eq. J-20
B	5%, 50%, 95% quantiles from Eq. J-21

$\Delta P_R(t)$	smooth $\Delta P_{R,0.5}(t)$ curve in Figure J-21
$V_R(t)$	smooth $V_{R,0.5}(t)$ curves in Figure J-22 depending on V
$R_{\max}(t)$	from R_{\max} , $\Delta P(t)$ and $Lat(t)$; see Eq. J-23
$B(t)$	from B , R_{\max} and $Lat(t)$; see Eq. J-24
α	$0.035 + 0.0005 \Delta P$
No. of cases	2835

One may reduce the number of MR runs even further. From the LR runs, it was determined that the multiplicative effect of Holland's B on the surge depends mildly on ΔP and V . Therefore there is no need to run different values of B with each combination of ΔP and V . This produces the MR plan in Table J-13, which comprises two sub-factorials of the levels in Table J-12, with a total of only 1155 runs.

Table J-13		
Final plan for the mid-resolution runs		
	Mid-resolution model runs	
Parameter	Factorial 1	Factorial 2
ΔP (mb)	41, 80, 115	80
V (km/h)	8, 21, 36	21
$X_{cos}(\)$ (km)	-130, -90, -50, -10, 30, 70, 110	-130, -90, -50, -10, 30, 70, 110
R_{max}	-60, -30, 0, 30, 60	-60, -30, 0, 30, 60
B	10%, 50%, 90% quantile from Eq. J-20	10%, 50%, 90% quantile from Eq. J-20
	50% quantile from Eq. J-21	5%, 95% quantiles from Eq. J-21
-----	-----	-----
$\Delta P_R(t)$	$\Delta P_{R,0.5}(t)$ from Figure J-21	$\Delta P_{R,0.5}(t)$ from Figure J-21
$V_R(t)$	$V_{R,0.5}(t)$ from Figure J-22	$V_{R,0.5}(t)$ from Figure J-22
$R_{max}(t)$	from Eq. J-23	from Eq. J-23
$B(t)$	from Eq. J-24	from Eq. J-24
	$0.035 + 0.0005 \Delta P$	$0.035 + 0.0005 \Delta P$
No. of runs	945	210
Total runs	1155	

For the HR runs, the subset of 36 hurricanes in Table J-14 is retained. In general, the levels in Table J-14 have been chosen to maximize the accuracy of calibration of the MR results.

Table J-14	
Factorial plan for the high-resolution runs	
Parameter	High-resolution model runs
ΔP (mb)	80, 115
V (km/h)	21
$X_{cos}(\)$ (km)	-90, -10, 70
R_{max}	-60, 0, 60
B	10%, 90% quantiles from Eq. J-20
	50% quantile from Eq. J-21
-----	-----
$\Delta P_R(t)$	$\Delta P_{R,0.5}(t)$ from Figure J-21
$V_R(t)$	$V_{R,0.5}(t)$ from Figure J-22
$R_{max}(t)$	from R_{max} , $\Delta P(t)$ and $Lat(t)$; see Eq. J-23
$B(t)$	from B , R_{max} and $Lat(t)$; see Eq. J-24
	$0.035 + 0.0005 \Delta P$
No. of cases	36

Calibration and Extension of the MR Results Using the HR Runs

For the 36 cases in Table J-14, the water levels H and the wave characteristics W are directly extracted from the HR runs. For the remainder of the cases in Table J-13, which are run only with the MR grid, corrections must be made to

reflect the bias of that coarser discretization. The bias is site-specific, as it depends on the local geometry of the coast, the topography, and the different local land coverage of the MR and HR grids. The correction further depends on the hurricane parameters $\underline{\theta}$. For example, the correction at a given location generally depends on landfall position X , direction θ , and possibly storm intensity ΔP . Finally, one must consider that our focus is on high water and wave values. The approach that follows reflects these considerations.

Let Y be a generic response of interest, e.g. Y = water level or significant wave height. At each location of interest $k = (x_k, y_k)$ and for each of the 36 events in Table J-14, we calculate $Y_{\max,MR,kj}$ and $Y_{\max,HR,kj}$, the maximum values of Y at k from the MR and HR runs, and the calibration factor

$$\gamma_{Y_{kj}} = \frac{Y_{\max,HR,kj}}{Y_{\max,MR,kj}} \quad (\text{J-26})$$

If $Y_{\max,MR,kj}$ and $Y_{\max,HR,kj}$ fall below some minimum value, the ratio $\gamma_{Y_{kj}}$ is considered “undefined.”

Next a distance d_{ij} between any pair of parameter vectors $(\underline{\theta}_i, \underline{\theta}_j)$ is defined where $\underline{\theta}_i$ is the vector for MR case i in Table J-13 and $\underline{\theta}_j$ is the vector for HR case j in Table J-14. The distance function should reflect the sensitivity of $\gamma_{Y_{kj}}$ in Eq. J-26 to different parameters (if the loads are insensitive to a parameter, differences in that parameter level should be contributing little to d_{ij}).

Finally, the time history $Y_{MR,ki}(t)$ for hurricane i in Table J-13 is corrected using a square-distance weighting scheme. The corrected values, $\hat{Y}_{ki}(t)$, are given by

$$\hat{Y}_{ki}(t) = \left(\frac{\sum_j \gamma_{Y_{kj}} / d_{ij}^2}{\sum_j 1 / d_{ij}^2} \right) Y_{MR,ki}(t) \quad (\text{J-27})$$

where the two summations extend over the values of j for which $\gamma_{Y_{kj}}$ is defined.

The previous calibration procedure applies to locations k at which the MR grid produces realistic results. At locations where this is not so, for example along narrow canals where the MR values are not reliable or may not even exist (because the MR grid does not extend to those locations), one must use a different strategy. HR results are used to fit regression relations in terms of values along the coast where the MR solution is available. Then one uses those fitted regressions to extrapolate the estimates from Eq. J-27.

Rainfall Intensity

Rainfall is among the variables that affect the inundation of the polders. While rainfall is not of primary concern for the hurricane protection system, it is a contributor to the frequency of low-level flood losses. Hence it was decided that a relatively coarse model of hurricane-induced rainfall would suffice.

Prior to NASA's Tropical Rainfall Measuring Mission (TRMM) (Simpson et al., 1988), information on hurricane rainfall was scanty. The TRMM mission, which started in November 1997, produced vast amounts of rainfall estimates for tropical storms and hurricanes at a spatial scale of about 5 km in various tropical regions, including the Atlantic basin. These rainfall products have been analyzed statistically by Lonfat et al. (2004) and Chen et al. (2006). The model proposed below is based primarily on these two studies and on discussions with Dr. Shuyi Chen at the University of Miami.

Mean Rainfall Intensity. Hurricane rainfall intensity I (mm/h) varies with distance r from the hurricane center and azimuth β relative to the direction of motion. Moreover, the mean intensity field $m_I(r, \beta)$ varies with the central pressure deficit ΔP , the radius of maximum winds R_{\max} , the storm velocity V , and the vertical wind shear S (in the above quoted references, S is measured as the difference between the horizontal wind fields at the 200 and 850 hPa levels). Finally, rainfall intensity displays strong fluctuations at different scales around the mean value $m_I(r, \beta)$.

The azimuthal average of $m_I(r, \beta)$, $m_I(r)$, gives the symmetrical component of the mean rainfall field. This component has a maximum at a distance from the hurricane center close to R_{\max} and decays in an approximately exponential way at larger distances. This decay is contributed by the approximately exponential decay of both the fraction of rainy area and the mean rainfall intensity at the rainy locations. The rate of exponential decay $m_I(r)$ is inversely proportional to the size of the hurricane; hence in good approximation it is inversely proportional to R_{\max} .

The value of $m_I(r)$ for $r = R_{\max}$ increases with increasing ΔP , approximately doubling from a Cat2 to a Cat4-5 event. Considering the Cat12 and CAT3-5 results in Lonfat et al. (2004) as representative of the Cat1-2 boundary and of Cat4, respectively, assuming linear dependence of the mean rainfall intensity at R_{\max} on Δp , and fitting an exponential decay with distance as mentioned above, one obtains

$$m_I(r) = \begin{cases} 1.14 + 0.12\Delta P, & \text{for } r \leq R_{\max} \\ (1.14 + 0.12\Delta P)e^{-0.3\left(\frac{r-R_{\max}}{R_{\max}}\right)}, & \text{for } r > R_{\max} \end{cases} \quad (\text{J-28})$$

where m_I is in mm/h and ΔP is in mb.

The asymmetric component of the mean rainfall field, i.e. the way $m_I(r, \beta)$ depends on the azimuth β , is affected mainly by the storm velocity V and the vertical wind shear S . This influence is complex, as the asymmetric pattern and its strength vary with the absolute and relative values of V and S , the relative direction of wind shear and storm motion, the distance r from the center, and the geographic location. For hurricanes in the Atlantic region, there is a general tendency for rainfall to intensify in the front-east quadrant relative to the direction of storm motion and de-intensify in the rear-west quadrant. This tendency is especially evident for fast-moving storms and away from the hurricane center, reaching about 30-40% of $m_I(r)$ for $r \approx 3R_{\max}$. The effect is stronger over land than over water.

Variability of Rainfall Intensity. For each TRMM observation of each hurricane, Lonfat et al. (2004) extracted the average rainfall intensity $\bar{I}^+(r, r+10)$ at rainy locations inside annular regions of 10 km width. Using these values, they found the empirical distribution of $\bar{I}^+(r, r+10)$ for different r and different storm intensity classes. A consistent result is that $\bar{I}^+(r, r+10)$ varies by a factor of about 7 above and below the median value. The standard deviation of $\log(\bar{I}^+(r, r+10))$ corresponds to a factor of about 2-2.5. Hence the variability of this average rainfall intensity is very large.

In addition, there is variability in the fraction of rainy area. The latter variability is not given in Lonfat et al. (2004), but it can be bounded and roughly estimated as follows. The mean fraction of rainy area, m_{F^+} , is given by Lonfat et al. as a function of r and storm intensity range. Given m_{F^+} , an upper bound to the variance of F^+ is obtained by assuming that F^+ is either 0 (no rain in the region) or 1 (it rains everywhere in the region). In this case

$Var[F^+] = m_{F^+}(1 - m_{F^+})$, with a coefficient of variation $V_{F^+} = \sqrt{\frac{1}{m_{F^+}} - 1}$. A more

realistic estimate of the coefficient of variation is perhaps one half of this theoretical upper bound, or

$$V_{F^+} \approx 0.5 \sqrt{\frac{1}{m_{F^+}} - 1} \quad (\text{J-29})$$

For distances r up to 150 km, which are those that contribute the most to intense rainfall, m_{F^+} is around 0.9 irrespective of hurricane intensity and Eq. J-29 gives $V_{F^+} \approx 0.17$. This coefficient of variation is much smaller than the coefficient of variation of rainfall intensity inside the rainy area, which is on the order of 1.0. Therefore, the variability of the rainy area may be neglected.

Assessment of Rainfall Intensity Inside the Polders. Based on the above considerations, the following simplified model of rainfall inside the polders is suggested. First the mean rainfall contribution from the symmetric component of

the mean rain field, $m_I(r)$ is selected, then asymmetric component and finally the variability of rainfall around the mean is assessed.

Denote by $m_{I_k}(r,t)$ the temporal variation of $m_I(r)$ for hurricane k (in our model, temporal variation is due to the variations of ΔP). The contribution of $m_{I_k}(r,t)$ to the mean rainfall intensity in polder j is evaluated as $m_{I_k}(r_{jk}(t),t)$, where $r_{jk}(t)$ is the distance of a representative point of polder j from the center of hurricane k at time t .

For hurricanes that pass to the right or near the polder, the azimuthal dependence of the rainfall field is neglected. For hurricanes that pass to the left of a polder, one may account for the asymmetric component by multiplying the above symmetric mean rainfall values by 1.5. This factor includes intensification due to land effects.

Uncertainty may be expressed by a lognormal random variable with mean value 1 and log standard deviation 0.69, which corresponds to an uncertainty factor of 2. This random factor should be applied to the entire mean rainfall time history. In reality, rainfall intensity inside a polder would display significant fluctuations in time and space, which locally could far exceed a factor of 2. However, the above random factor should adequately reflect uncertainty on the total precipitation in a polder during the passage of a hurricane.

Epistemic Uncertainty

Epistemic uncertainty (uncertainty due to limited information and knowledge) affects all aspects of the hazard characterization. While a thorough assessment of these uncertainties is beyond the scope of this project, a rough quantification of uncertainty on the hurricane rates $\lambda(\Theta)$ and the loads $L(\Theta)$ will be made.

General Considerations. The hurricane rates $\lambda(\Theta)$ are uncertain due to the limited historical sample size, possible errors in the assumed form of marginal and conditional distributions (especially in the tail regions), and the uncertain near-future hurricane activity due to fluctuations and trends associated with climate changes and multi-decadal cycles. A first-order assessment of uncertainty on $\lambda(\Theta)$ is based on the hurricane effects of global warming and shorter-term climatic fluctuations in the North Atlantic.

Causes of epistemic uncertainty on $L(\Theta)$ are hurricane model errors, for example the wind field idealization, the coefficient of friction with the water surface, the effects of waves on water level, etc. One can estimate the size of these errors from the skill at hindcasting historical events or by comparing results from different modeling assumptions.

Other epistemic uncertainties are associated with the imperfect calibration of the MR model using the sparse HR results. One may estimate the magnitude of these errors by considering the variability of the calibration factors $\gamma_{Y_{kj}}$ in

Eq. J-26 in hurricane parameter space. Finally, there are interpolation errors when estimating water heights and waves for parameters θ not used in the MR plan.

Climatic Effects and Their Contribution to Epistemic Uncertainty

The potential effect of global warming on the frequency, size and intensity of tropical cyclones is a hotly debated issue in the technical literature; see Pielke et al. (2005), Emanuel (2005b), and Elsner (2005) for recent reviews. Theoretical analysis, numerical modeling and historical data analysis have all been used to study the effects of climate variations on various features of tropical cyclones. The main results on hurricane frequency and intensity are summarized below. What determines hurricane size is poorly understood; hence the possible dependence of R_{\max} on global warming and other climatic factors is not considered.

Frequency of Tropical Cyclones. It is possible to argue theoretically that global warming could produce either a decrease or an increase in hurricane activity; an ambiguity that is also reflected in the contradictory results produced by different global circulation models (Broccoli and Manabe, 1990; Haarsma et al., 1992; Henderson-Sellers et al., 1998; Houghton et al., 2001).

From an observational viewpoint, the frequency of tropical cyclones worldwide has remained remarkably constant during the past 100 years or more (Elsner and Kocher, 2000; Webster et al., 2005; Emanuel, 2005b). Since during this period the planet has undergone global warming and cooling, one may conclude that climatic changes of this type and magnitude have small effects on the rate of tropical cyclones at the planetary scale.

On the other hand, significant fluctuations in tropical cyclone activity at decadal and multi-decadal scales have occurred in various parts of the world. For example, hurricane activity in the North Atlantic was low in the 1970s, 1980s, and early 1990s compared with the 1940s, 1950s and early 1960s or with the decade since 1995. Changes in hurricane frequency between active and quiescent periods have been by factors of 2 or more (Goldenberg et al., 2001). The current rate in the North Atlantic is about 50% higher than the historical average rate and will likely persist at least over the next 5 years (Elsner, 2005). These fluctuations are due to well-known cycles like the El-Nino-Southern Oscillation (ENSO), which by increasing the wind shear dampens the rate and intensity of hurricanes, the tropical Atlantic sea-surface temperature (SST), with warmer temperatures usually producing higher hurricane rates, and the Atlantic multi-decadal oscillation (AMO), which is the difference in air pressure between Iceland and the Azores and is thought to affect mainly the hurricane tracks (Elsner, 2005).

Intensity of Tropical Cyclones. The effect of global warming on tropical cyclone intensity is somewhat more controversial. It has been argued that an increase in sea surface temperature would make the atmosphere more thermodynamically unstable and increase the maximum potential intensity (PI) of hurricanes (Emanuel, 1987; Lighthill et al., 1994; Henderson-Sellers et al.,

1998). In turn, PI has been shown to be highly correlated with the average intensity of hurricanes (Emanuel, 2000). Following this argument, increases in intensity under a warmer climate may be expected (Emanuel, 2005a).

On the other hand, it may also be argued that an increase in sea surface temperature would increase the vertical wind shear, which tends to disrupt the symmetry of tropical cyclones and reduces their intensity.

Empirical evidence of higher hurricane intensity during the past 50 years, when the sea surface temperature has increased by about 0.2 degree centigrade, is weak (Landsea et al., 1999; Bister and Emanuel, 2002; Free et al., 2004; Chan and Liu, 2004). This is in agreement with findings based on global circulation models. For example, Knutson and Tuleya (2004) and Michaels et al. (2005) predict increases in wind speed of 5% or less by the year 2080. Therefore, while future variations in intensity due to global warming are considered possible, it is generally expected that such variations will be modest and overshadowed by the multi-decadal fluctuations.

Results that contrast with this general consensus are reported in Emanuel (2005a). Using data worldwide, Emanuel found that the energy released by hurricanes has increased by about 70% over the past 30 years and attributes the phenomenon to global warming. This phenomenon is contributed by an increase of 15% in the maximum wind speed and an increase of 60% in storm duration. These findings have been contested by other researchers and must be considered preliminary pending further validation.

Epistemic Uncertainty on Future Hurricane Climate. From the preceding discussion, uncertainty on the hurricane statistics in the Gulf of Mexico during the next 50-100 years is dominated by multi-decadal oscillations. Specifically, considering that the North Atlantic is now experiencing a 50% higher-than normal activity and that this elevated activity may persist over a number of years and possibly decades, it is reasonable for the next 50-100 years to increase the average historical rate of hurricanes by 20% and allow for an additional 25% uncertainty factor around this corrected rate. The latter factor includes uncertainty on the historical rate due to the finite observation period (16%) as well as uncertainty on the future evolution of the hurricane frequency (judgmentally assessed).

Considering the general consensus and dissenting views on the effect of global warming on hurricane intensity, the historical mean pressure deficit is increased by 3% and in addition apply a 5% uncertainty factor on the increased mean value. Since the effects of different factors on hurricane frequency and intensity are poorly correlated, these components of epistemic uncertainty may be treated as independent.

Reliability Analysis

As part of the risk and reliability analysis, an evaluation must be made of the conditional probability of failure (i.e., reliability) of structures, systems and

components when they are exposed to the effects (loads) of a hurricane. The analysis has three steps:

1. Specify the structures, components, and systems constituting the hurricane protection system for each polder.
2. Define *failure* and identify failure modes for each structure, system and component; and define a limit or failure state for each failure mode.
3. Assign conditional probabilities (fragilities) of those failure states given hurricane effects.

Two conditions are being analyzed for the reliability of levees, flood walls and pumping stations: (1) pre-Katrina, and (2) post-reconstruction and repair as projected for June.

Summary approach

The reliability of the hurricane protection system (HPS) under potential water surge and wave loadings is quantified using structural and geotechnical reliability models integrated within a larger systems description of each polder. The reliability models for the HPS components are being developed based on design and construction information, and on the results of the Team Seven and Team Eight studies.

Standard reliability models are being used that combine uncertainties in structural material properties, geotechnical engineering properties, subsurface soil profile conditions, and engineering performance models of levees, floodwalls, and transition points. Uncertainties due to spatial and temporal variation (aleatory uncertainty) and due to limited knowledge (epistemic uncertainty) are tracked separately in the analysis, to provide a best estimate of frequency of failures along with a measure of the uncertainty in that frequency.

To date, the reliability model has been developed for the Orleans East (NOE) polder as a means of exercising the approach. The perimeter protection system comprises levees, flood walls, levees with floodwalls on top, and various points of transition or localized facilities such as pumping stations, drainage works, pipes penetrating the HPS, or gates. This perimeter has been divided into reaches that are deemed to be homogeneous in three aspects: structural cross-section, elevation, and geotechnical cross-section. Approximately 20 such reaches have been identified for NOE.

Geometric and engineering properties have been identified for each reach of NOE and summarized in flat-file data tables. Structural cross-sections were initially identified by review of as-build drawings, aerial photographs, and GIS overlays; and were confirmed by on-the-ground reconnaissance by Team 10 members. Elevations were initially assessed in the same reconnaissance, and were later supplemented by LIDAR data and field surveys provided to the Team. Geotechnical cross-sections and corresponding soil engineering properties were derived from the original Design Memoranda for the respective project areas of

the polder, supplemented by site characterization data collected post-Katrina at levee flood wall failure sites (cone penetrometer and laboratory measurements).

Reliability assessments are performed for individual reaches of the HPS for given water levels and loadings. This results in fragility curves for each reach by mode of failure. For each reach and mode of failure, the fragility curve gives the conditional frequency at which a failure state is exceeded. As a first step, engineering performance models and calculations have been adapted from original Design Memoranda. Engineering parameter and model uncertainties are propagated through those calculations to obtain approximate fragility curves as a function of water height on the HPS. These results will later be calibrated against the ongoing work by Task 7, which is applying more sophisticated analysis techniques to similar structural and geotechnical profiles in the vicinity of failures. Failure modes identified by Task 7 will be incorporated into the reliability analyses as those results become available.

Systems risk model. The reliability assessments for individual reaches of the polder perimeter (and possibly of interior levees or walls) are combined in a systems model which brings together the uncertainties in hurricane hazard and HPS fragility to calculate frequencies of volume and duration of flooding within the polder. The systems risk model, embedded in a software application, is structured around an event-tree description of the occurrence of hurricane events, corresponding water and wave heights, and resulting response of the HPS. This model separately tracks aleatory and epistemic uncertainties from both the hurricane hazard and the structural and geotechnical response, producing a best estimate of frequency and duration of flooding, along with measures of uncertainty in those frequencies.

Structures, components, and systems constituting the HPS

Appendices B through F contain a complete inventory of the structures, systems and components that were considered as part of the risk analysis. A list of subsystems and components of the HPS is shown in Table J-15. This is not intended to be exhaustive, but representative.

Failure definitions and limiting states

The HPS for each polder comprises four components: (1) levees, (2) I-walls (which may be atop levees), (3) T-walls (which may be atop levees), and (4) transitions and closures. The reliability analysis examines the performance of the each of these components, separately and in combination.

The following structures in the HPS were not independently evaluated for their failure modes: (1) concrete apron with some I-walls, and (2) sheetpiles with a 3 to 4 ft concrete cap. Either can be addressed with failure modes developed for I-walls.

Table J-15 Components in the Hurricane Protection System.	
No.	Sub-system/Components
1	Pump System
	a. Pump and motors
	b. Power – Grid
	c. Emergency Power – Diesel Generator
	d. Diesel Fuel
	e. Pump House Structure
	f. Operators
	g. Intakes
2	Closure
	a. Closure Support Structure
	b. Closure Stop-Logs, Gate or...
	c. Crew Operations
3	Levee Sections
	a. Embankment Section - A levee section must be divided into a series of independent segments. These segments are defined on the basis of physical discontinuities (geometric, physical (e.g., at the closure-embankment juncture)), embankment material/construction characteristics (e.g., correlation lengths either inferred or measured).
	b. Foundation (could be modeled similar to the levee embankment or separate.)
4	Floodwall (Note, as with the case of levee embankments, we will have to consider whether individual wall sections are independent or correlated.)
	a. Wall Structure
	b. Wall-Wall Joint/Interface
	c. Wall Foundation (Embankment Interface)
	d. Wall-Embankment Interface
	e. Sheetpile
	f. Sheetpile-Sheetpile Joint

The following failure modes or contributing factors were not considered in the reliability analysis: (1) On-going settlement of levees or walls due to subsurface consolidation. Existing and planned elevations were used in the analysis. (2) Internal erosion (piping) of levees due to seepage. While sand boils were reported following Katrina, failures did not occur at the same locations. Available geotechnical data for levee designs, and that obtained under IPET, are insufficiently detailed to determine localized weaknesses in the soil (i.e. local sand lenses) that may exist under levees. Internal erosion may be reconsidered in later studies. (3) The effects of maintenance on the HPS capacity over time. Improper maintenance or neglect can lead to reduced capacity of the levees in particular; gates and other moving components also require maintenance. Trees, landscaping, and pools were observed on the protected (landside) embankments after Hurricane Katrina, indicating a lack of enforcement and maintenance of the levees. However, there is insufficient information at present to include maintenance considerations. (4) Impact by a barge or floating tree, or other large object, on the floodwalls or levees. (5) Failure of 3-bulb waterstop.

Component Failure. For each structure, system and component, a performance level is defined such that its occurrence corresponds to a failure to perform an intended function. The critical structures and components within the

HPS, as above, are the levees, I-walls, T-walls, and transitions and closures. These structures and components can fail in a variety of modes. For each mode of failure a limit state is defined, which, if it were to occur would result in a failure to prevent flooding. Limit states differ across the failure modes associated with levee performance and floodwall performance.

From a practical perspective, engineering models of the mechanics of structure or component performance are limited in their ability to explicitly model a 'failure' state. As a result, an analysis is usually carried out for 'incipient' failure (limiting stability). If this state is equaled or exceeded, the structure or component is expected to fail to perform as intended.

System Failure. Depending on the performance of individual structures, systems and components in the HPS, various outcomes may result. For purposes of evaluating the performance of the HPS, the outcome of most interest is whether a protected area is flooded or not.

The HPS is assumed to fail if flooding occurs in a protected area beyond that expected from rainfall and runoff. Given this definition, a failure of the HPS can occur even if the structures or components making up the system do not fail, for example, if levees or wall are overtopped but not breached.

Flooding can occur as a result of a number of different chains of events that occur individually or in combination. Chains of events that can result in flooding are:

- Levee or floodwall breaching.
- Inflow to an area due to levee or flood wall overtopping (that does not result in breaching) and which exceeds the capacity of the pump system to discharge this inflow.
- Inflow to an area that occurs as a result of rainfall.
- Inflow to an area that occurs when the capacity of the pump system is exceeded as a result of the surge elevation in the canals, resulting in backflow through pumphouses.

From a practical perspective, the events of interest have to do with whether flooding occurs at all and if the flooding is a result of a levee breach. Flooding that occurs as a result of rainfall or overtopping in most cases will not be as consequential and may be mitigated by the pumping system (e.g., failed or not).

Methodological approach

The failure modes that lead to breach of the polder perimeters are associated with four principal failure modes:

1. levee or levee foundation failure
2. levee erosion from overtopping
3. floodwall failure

4. failure modes associated with *point* features such as transitions, junctions and closures

In the case when the perimeter of a polder is breached, it is important to understand whether the number of breaches and their location matter. The losses near a breach may be high due to the sudden release of water, but this damage may be small relative to that which occurs in the entire area inundated by the breach. The location of the breach may, however, be important if there are critical facilities near the breach. At the parish aggregation level, it may matter little how many breaches occur and where except that life loss may be highest at the breach.

A similar consideration concerns the mitigating effects of the pumping system. If the capacity of the pumping system can be exceeded by the inflow volume from a single breach then the number and location of the breaches may not matter and the pumping system can be ignored in the risk analysis.

The nature of uncertainty in reliability analysis. The uncertainties dealt with in the risk analysis are of two types:

Natural variability is associated with the “inherent” randomness of natural processes, manifesting as variability over time for phenomena that take place at a single location (temporal variability), or as variability over space for phenomena that take place at different locations but at a single time (spatial variability), or as variability over both time and space. This is aleatory uncertainty.

Knowledge uncertainty is attributed to lack of data, lack of information about events and processes, or lack of understanding of physical laws that limits our ability to model the real world. This is epistemic uncertainty.

The adverse performance of elements of mechanical, electrical, and human elements of the HPS, such as pumps, the availability of power, and the closure of gates, is predominantly treated as random (i.e., aleatory) events.

Fragility Curves. Fragility curves summarize the probability of structures, components, or systems reaching their respective limit states (i.e., failure), conditioned on levels of hurricane loading. For example, the fragility curve of Figure J-23 schematically represents the probability of failure by deep-sliding instability of a levee section as a function of water height.

Once the fragility curve for each structure and component failure mode has been determined, an event tree can be quantified in a similar manner. For each sequence in the event tree, a ‘sequence’ fragility curve is determined by simply evaluating the event tree logic at each successive elevation level. Once each sequence has been evaluated, the composite or total fragility for system failure can be determined for each system performance state of interest, e.g., no flooding has occurred in any area protected by the HPS or flooding as a result of levee/floodwall failure or flooding as a result of rainfall and/or overtopping, by simply summing the fragility curves for the sequences that result in the same state.

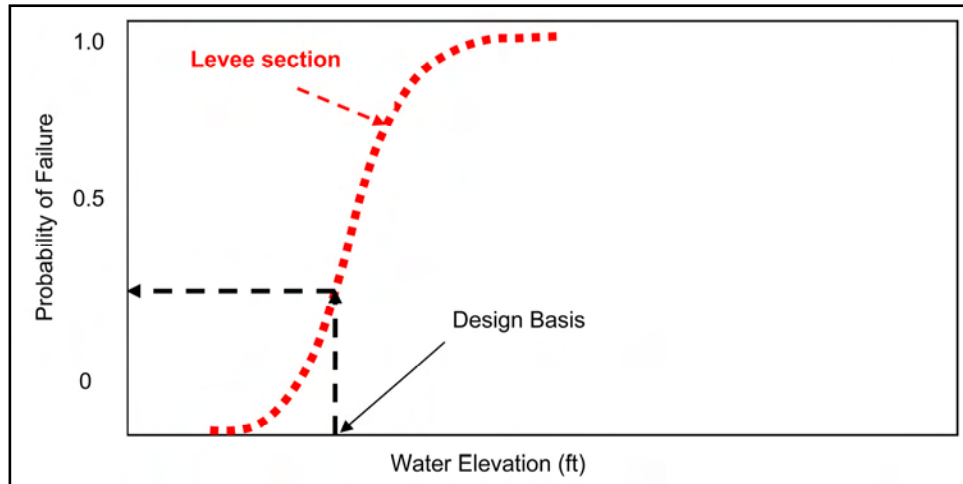


Figure J-23. Illustration of the fragility of a levee section, showing conditional probability of failure by deep-sliding within the foundation soils, as a function of the height of water on the exterior of the levee. Design basis water elevation indicates probability of failure at authorized level.

The total fragility for hurricane protection system, that is the fragility for system failure of any type provides a measure of the reliability of the entire system as a function of peak flood depth.

Fragility curves and failure probabilities

The failure modes included in the reliability analyses to model component performance in the risk analyses of the hurricane protection system (HPS) are defined for use in the appropriate branch segments of the event tree that models the HPS. The events of interest that have been selected to predict component performance are overtopping (O), breach (B), and pumping (U). Shown below are the branch segments analyzed. Where an event is underline, the event is the complement of the even, i.e., O indicates a non-overtopping event. The branch segments from the event tree are: { O, B, U ; O, B, U; O, B, U; O, B, U; O, B; O, B }.

In branches where breaching occurs, it has been assumed that the flow rate of water into the polder exceeds the capacity of the pumping stations (U). The probability of failure for the levees and floodwalls when subjected combinations of overtopping and breaching (O, B; O, B; O, B) are evaluated separately from the performance of the pumping stations.

Failure of a component has been defined as an event where flood waters enter the polder. Only a complete breach of a levee or floodwall is considered; partial breaching is not included. The expression for determining the probability of failure has been included where known in order to identify the information required. All probabilities are conditional upon the flood elevation (and associated hazards, such as wave forces, where applicable).

The following hazards are considered as component loads in the risk analysis: (1) flood elevation - storm surge plus wave setup, (2) breaking waves, (3) flood flow rate and duration for scour and erosion

Levee Failure Modes. Reliability assessments are performed for individual reaches of approximately homogeneous structural type, elevation, geotechnical conditions, and water levels and loadings. This results in fragility curves for each reach by mode of failure. Engineering performance models are adapted from the USACE original Design Memoranda. Engineering parameter and model uncertainties are propagated through those calculations to obtain approximate fragility curves as a function of water height. The geotechnical models used in the DM will be calibrated against the ongoing work by Task 7. Additional failure modes identified by Task 7 will be incorporated into the reliability analyses as they become available.

Shear sliding failure (both shallow and deep). Deep soil failure due to shear capacity of the foundation or levee material being exceeded. The shear resistance of the soils are reduce as seepage occurs until the flood-induced loads exceeds the soil shear capacity. Reliability is based on the probability that shear capacity of the saturated soils is exceeded by the loads on the levee for a given hurricane. A failure along the wedge lines of least resistance (or factor of safety) due to excess pore pressure leading to a shear failure in the soil. Reliability is based on the probability that shear resistance of a wedge is exceeded by the loads on the levee for a given hurricane.

Levee overtopped and erosion breaching. Reliability is based on the probability of overtopping causing erosion of a levee that leads to a breach. Two approaches are considered: The first approach considers flow velocities over the levee. The second approach considers flood elevation, which is an indirect parameter of flow velocity, but is estimated by the storm surge modeling.

The combinations of critical flow velocity and critical duration required to initiate erosion on the protected side of the levee and to continue for a sufficient duration to cause a breach of the levee. Possible approaches for estimating the flow velocity are (1) use of a dam spillway erosion method, or (2) a weir equation coupled with the surge inflow velocity (obtained from the storm surge analysis). Reliability is based on the probability that flow velocities experienced during overtopping exceed the erosion resistance of the soil.

$$P_{E(x)} = P[\text{flood velocity } (x) - \text{critical velocity for soil erosion } (x) > 0]$$

$$\text{And/or } P[\text{flood velocity duration } (x) > \text{critical duration } (x)] P_{OT(x)}$$

$$P_{E(x)} = \text{Probability of erosion failure.}$$

I-Wall Failure Modes. The two modes of failure due to soil or foundation failure are correlated because each mode relies on the same soil profile. A single P_f will be provided for the first mode of failure at each reach along with an estimate of the epistemic uncertainty for the soil properties and P_f .

Wall pressures failure. Deep soil failure due to shear capacity of the foundation or levee material supporting the I-wall being exceeded. Possible contributing factors: dredging canals to new depths; failure of cut-off barrier

(sheetpile) to prevent seepage under levee. The shear resistance of the soils are reduce as seepage occurs until the flood-induced loads exceeds shear capacity of the soils supporting the I-wall and/or sheetpile. Reliability is based on the probability that shear capacity of the saturated soils is exceeded by the loads on the floodwall for a given hurricane.

$$P_f = P[S_{\text{flood level}} - S_{\text{capacity}} > 0] P[\text{flood level}]$$

Where: P_f = probability of failure

Deep shear failure (wedge failure beneath sheetpile). Soil separations develop in front of the sheetpile or the levee resulting in increased hydrostatic forces on the flood side of the I-wall and the levee. If the separation is of sufficient depth, the hydrostatic forces on the wall may exceed the shear strength of the supporting soil and cause failure along wedge lines of least resistance behind the sheetpile. Reliability is based on the probability that shear resistance of a wedge is exceeded by the loads on the levee and floodwall for a given hurricane.

$$P_f = P[S_{\text{flood level}} - S_{\text{wedge capacity}} > 0] P[\text{flood level}]$$

Where: P_f = probability of failure

I-wall overtopped and erosion breaching.

Failure Mode B4a. Failure by rotation of I-wall, reducing I-wall elevation. This failure mode occurs after significant erosion of the protected (landside) side of the levee due to overtopping by one of the following mechanisms: Either the erosion of excess pore pressure could lead to a failure of the passive wedge behind the I-wall and sheetpile, resulting in a rotation toward the protected side and a crest elevation reduced to ground level (assuming erosion continues once flow increases over rotated I-wall).

$$P_f = P[S_{\text{flood level}} - S_{\text{wedge capacity}} > 0] P[\text{flood level}]$$

Where: P_f = probability of failure

Failure Mode B4b. Failure of the I-wall and/or sheetpile. A single P_f will be provided for the first mode of failure out of the three modes listed here at each reach along with an estimate of the epistemic uncertainty for the P_f .

Failure Mode B4b-1. Flexural failure of the sheetpile, induced by flood level, dynamic wave forces, and land-side erosion as cantilever length increases as shear and moment capacity are reduced. Reliability is based on the probability that the flexural strength of the sheetpile is exceeded by the moments exerted on it by the flood forces.

$$P_f = P[M_{\text{flood level}} - M_{\text{sheetpile}} > 0] P[\text{flood level}]$$

Where: P_f = probability of failure

Failure Mode B4b-2 Flexural failure of the concrete at the sheetpile interface, induced by flood level, dynamic wave forces, and land-side erosion. Reliability is based on the probability that the flexural strength of the concrete is exceeded by the moments exerted on it by the flood forces.

$$P_f = P[M_{\text{flood level}} - M_{\text{concrete section}} > 0] P[\text{flood level}]$$

Where: P_f = probability of failure

Failure Mode B4b-3. Failure of 3-bulb waterstop at I-wall panel junction, caused by differential loading and displacement between panels, developing tensile, T, and shear, S, forces in the water stop and I-wall panels. This may be due to levee erosion on flood side or dynamic flood and wave forces modifying the rotation point between I-wall panels, or to lateral displacement of the levee from a foundation shear failure. Three-bulb rubber waterstop between panels can fail in 3 modes:

1. Waterstop failure in the rubber material due to tensile or shear load
2. Waterstop pulls out of concrete due to tensile load
3. Concrete fails in tension around waterstop due to tensile or shear load

Reliability is based on the probability that the tensile or shear strength of the waterstop is exceeded by the forces exerted on it by the flood.

$$P_{fS} = P[S_{\text{flood level}} - S_{\text{capacity}} > 0] P[\text{flood level}]$$

Where: P_{fS} = probability of shear failure

$$P_{fT} = P[T_{\text{flood level}} - T_{\text{capacity}} > 0] P[\text{flood level}]$$

Where: P_{fT} = probability of tensile failure

T-wall with a Levee. T-walls are incorporated into the design for the HPS at locations where structures such as gates or drainage structures require additional foundation support. These T-walls are constructed using a reinforced concrete stem sections founded on battered prestressed concrete pile supports with a sheet pile wall cutoff to depth. These walls are designed to have much lower lateral deflections than I-walls under dynamic flood and wave forces. The T-walls were designed to handle five load conditions including varying conditions of uplift on the base. Overall, these structures performed well during Katrina and were expected to have a lower probability of failure than I-wall structures. A typical T-wall section for the INHC is shown in Figure J-24.

Failure Modes for T-walls. The T-walls were designed based on both pile forces (in both compression and tension) and deflection based on varying subgrade modulus. The design utilized the methods for battered piles presented by Hrennikoff (ASCE, 1950) and Davidson and Gill (ASCE 1963). The base and stem were designed for flexural failure using traditional reinforced concrete design techniques. Flexural failure within the T-wall (between wall and base) could be induced by flood level, dynamic wave forces, and flood-side erosion. The sections were not analyzed using a global stability analysis of the section.

Significant overtopping and erosion around both the flood and protected side of the T-walls did occur Katrina. This will be addressed in the reliability model through uplift calculation. The limit states considered for reliability purposes in this report will be the allowable pile loads (combined axial and bending), allowable deflection of the prestressed concrete piles and flexure failure in the base/stem.

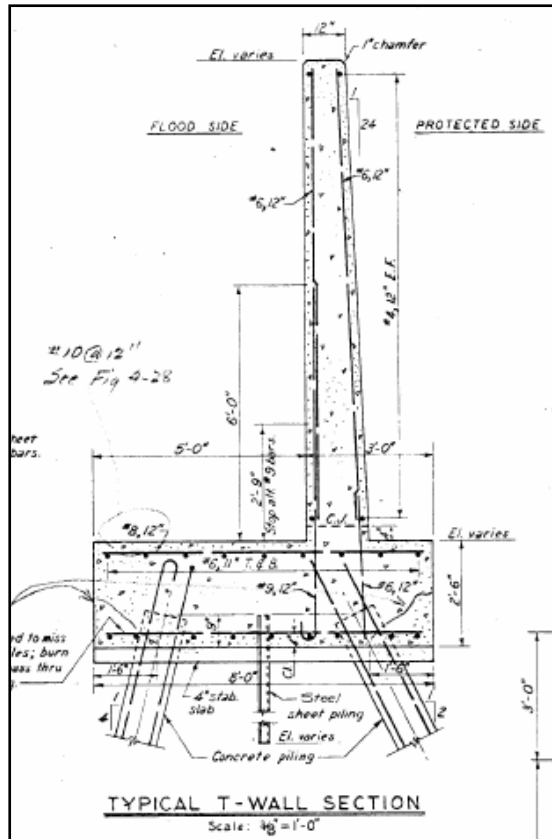


Figure J-24. Typical T-wall Section for INHC

Limit State 1 - Combined pile loads (tension and compression) – The probability of failure is based on the combined axial and bending effects in the concrete piles exceeding unity and would be based on varying pool elevations to determine the fragility curves

$$P_f = P\left[\frac{f_a}{F_a} + \frac{f_b}{F_b} > 1\right]$$

where,

f_a = axial load

F_a = allowable axial load

f_b = bending stress

F_b = allowable bending stress

Limit State 2 - Deflection at top of T-wall – The probability of failure is based in the exceedence of a set allowable deflection for the wall and would be based on varying pool elevations to determine the fragility curve. The equation for the probability of failure would be:

$$P_f = P[Y_a - y < 0]$$

where,

Y_a = allowable deflection

y = deflection

Limit State 3 - Flexural Failure – The probability of failure is based on the probability that the flexural strength of the T-wall is exceeded by the moments exerted on it by the flood forces and would be based on varying pool elevations to determine the fragility curves.

$$P_f = P[M_{\text{flood level}} - M_{\text{T-wall-in}} > 0]$$

HPS Transitions and Point Structures. A number of HPS breaches were observed at transitions between HPS components. These breaches were typically at levee/I-wall, levee/T-wall or I-wall/T-wall transitions. Many of the HPS breaches were at point structures such as gates (road and railroad), pump stations, or around drainage control structures. These transitions indicate a weak link in the HPS due to the differing stiffness of the components which permit them to become areas of significant erosion during a hurricane event.

Many of these transition zones that failed utilize a “wrap-in” levee section to a more rigid wall structure. These levee sections slope quickly away from the transition to expose the I- or T-wall. These steep slopes permit a concentrated zone for the erosion of the levee that will eventually expose the I-wall or T-wall structure to additional loading and continued eroding. This dynamic process will eventually lead to instability and collapse or damage to that transitional section of the wall. An example of a levee transition for a gate section on the east bank of the INHC is shown in Figure J-25 below.

The failure modes for these transition zones are highly complex and dynamic. The failure modes will utilize the qualitative erosion parameters being developed by IPET Team 7 as the basis for change in the stability of components at the transition zones. Reliability models will be developed based on point structures (gates, control structures, pump stations) as determined from the system definition for each polder.

Failure Mode 1- Scour and erosion causing point structure instability - A levee breach may occur due to loss of the supporting I- or T-walls at a point structure and scour could create instability and collapse of the structure creating a breached area. This change in stability is due to erosion and scour around the drainage structure and the fragility curve will be based on varying the water elevation. The probability of failure is based on driving and resisting forces as:

$$P_f = P[\text{Resisting Forces} - \text{Driving Forces} < 0]$$

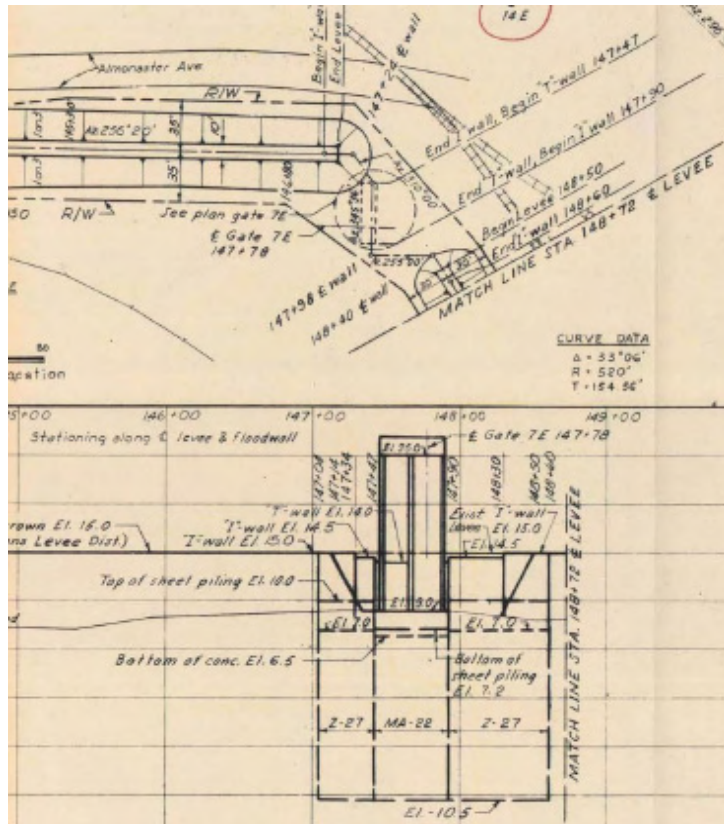


Figure J-25. Example of Transition Zone for East Bank of INHC

Failure Mode 2 - Breach at the water stop between the I-wall and T-wall panel junction - This failure mode may be caused by differential displacement between panels develops tensile, T, and shear, S, forces in the water stop and panels. This may be due to levee erosion on the flood side or different rotation point between panels, or to lateral displacement of the levee from a foundation shear failure. Water stops between panels can fail in 3 modes:

1. Waterstop failure in the rubber material due to tensile or shear load
2. Waterstop pulls out of concrete due to tensile load
3. Concrete fails in tension around waterstop due to tensile or shear load

The fragility curve will be based on varying the water elevation and the probability of failure is tensile and shear forces in the water stops as:

$$P_{fs} = P[S_{\text{flood level}} - S_{\text{capacity}} > 0]$$

$$P_{ft} = P[T_{\text{flood level}} - T_{\text{capacity}} > 0]$$

Failure Mode 3 - Breach at the levee and I-wall transition - This failure mode may occur due to levee erosion on the protected side, where the erosion starts at the end of the levee transition and progresses back toward the I-wall, until the I-wall rotates toward the protected side. Either the erosion of excess pore pressure could lead to a failure of the passive wedge behind the I-wall and sheetpile, resulting in a rotation toward the protected side and a crest elevation

reduced to ground level (assuming erosion continues once flow increases over rotated I-wall).

$$P_f = P[S_{\text{flood level}} - S_{\text{wedge capacity}} > 0]$$

Pumping Stations. The pumping stations are critical HPS system components because they maintain the flood levels on the protected side. Unfortunately, many of the pumping stations during Katrina reached and exceeded their pumping capacity shortly into the storm. Their reliability during Katrina was not exceedingly high as the stations primarily failed due to rising waters at the plants, a lack of external or backup power source, or were shut down due to inefficient pumping. These systems are designed to handle specific level of rainfall and are easily overwhelmed when the levees are overtopped by a hurricane event.

The following failure modes are possible for the pumping stations:

- a. Interior flooding of station
- b. Loss of power
 1. No commercial power
 2. Back up generator fails
 - (a) Mechanical
 - (b) Fuel unavailability
- c. Pumps not functioning at time of incident
- d. Mechanical failure of components
- e. Operator unavailability
- f. Debris blocking intakes
- g. Reversed or back flow through outfall pipes

The reliability of the pumping stations will be included into the risk model as point sources. The reliability will be based on data collected on the pumping stations, performance data maintained by Task Force Hope, and information from the dewatering plan for New Orleans developed by the New Orleans District. The fragility curves for each pumping stations will need to be limited to a specific elevation or volume of water within the polder. These fragility curves will vary for each pumping station and will reflect the interior drainage areas and back flow potential.

Consequences

The primary output of the risk and reliability modeling of Team 10 will be an estimate of the probability of life loss and physical damage relating to the performance of the hurricane protection system in southeastern Louisiana. The three scenario cases which are being considered: 1) the pre-Katrina (August 28, 2005) risk, 2) the actual Katrina experience, and 3) the risk associated with conditions as of June 1, 2006. A probabilistic estimate of losses (life and property) will be provided.

Team 10 is working in close collaboration with Team 9 (Consequences) to ascertain appropriate relationships of inundation, impact and life and property loss. Team 9 is considering consequences in four areas: 1) economic consequences, including direct damage and indirect losses, at local, regional and national level; 2) environmental consequences; 3) social, cultural and historical consequences, and; 4) life safety and health consequences.

As of mid-February, the work of Team 9 has been initiated, but limited data has been collected and no firm inputs are available to the modeling effort of Team 10. Team 10 members providing liaison with Team 9 have contributed to the refinement of the flood life loss model (lifesim) and have established contact with the Louisiana State University Hurricane Center and Team Louisiana which have been tasked with the State of Louisiana to carry out forensic evaluation of the Katrina event.

Issues of interface between team activities remain a major concern. Attempts are underway to clarify the necessary input to model consequences in the categories mentioned above. It had earlier been assumed that a maximum flood elevation in each sub-folder would provide sufficient characterization of the event to generate consequence estimates. In further discussion with subgroups of Team 9, it is evident that for the case of life loss several factors are considered of critical importance including rate of inundation, duration of inundation, and velocity of flow. These factors relate to the feasibility of evacuation and rescue to prevent life loss. For physical damage, it is also possible that these characteristics will be desirable for the refinement of loss estimates. Social and demographic data is also required for the life loss estimation. This data is currently being collected but has not been analyzed to develop useful relationships for the risk model. Detailed analysis of fatality data is still required to relate socio-economic demographic information to specific risk factors for fatality. The application of the flood life loss model (lifesim) requires more detailed consideration of both evacuation and rescue procedures. That evaluation will be carried out by the Consequences team.

The Risk team is developing risk and reliability models which will be calibrated by earlier events including Katrina, but will be useful in evaluating potential variation in design, management and other risk-related factors for future events and future modification of the hurricane protection system. The establishment of valid general relationships between measurable event impacts and measurable event consequences is critical to the completion of the risk model. Currently, the Consequences team has committed to focusing its attention on two specific quantitative characterizations of consequences: 1) life loss (rather than injury, health status, mental health, etc.) and, 2) the dollar value of direct physical damage to buildings and infrastructure (rather than indirect costs such as business interruption, loss of revenue, etc.). These simplifications are necessary because of difficulties in data collection and because of time limitations imposed on the preparation of the IPET report. It should be borne in mind, that these are only representative consequences and not comprehensive. The full social, economic and culture impact of the event will be considerably greater than that represented than the two selected factors.

Liaison with Louisiana State University Hurricane Center

Team 10 liaison with the Louisiana State University Hurricane Center has provided valuable input to the understanding of Katrina consequences. The Hurricane Center at LSU has been deeply involved in assessment of previous hurricane losses and modeling of expected losses due to future hurricanes for a number of years. Of specific relevance to the consequences evaluation, the LSU hurricane center is now working with the Louisiana State Coroner's Office to analyze fatality data on the roughly 1200 confirmed fatalities (bodies recovered). Of these, approximately 700 have been identified, and circumstances and location of death have been established. LSU is currently carrying out detailed studies of fatality circumstances and has developed a GIS for the location of victims recovered and their home addresses. This material is not currently available to IPET because of privacy concerns and further negotiation will be necessary to obtain data relevant to the IPET consequences study. The LSU Hurricane Center has collaborated with the FEMA mitigation assessment team which has carried out an analysis of building damage in the affected area and this data will be available from FEMA. The work is carried out under a FEMA contract with URS. The LSU Hurricane Center includes LSU faculty members with experience and expertise in a range of relevant areas: evacuation, experts in transportation, planning and traffic management have been directly involved in the development of state evacuation policy and have played a major role in the successful evacuation of over 1 million people from New Orleans. Members of the Sociology Faculty have worked on the analysis of behavioral aspects of warning and evacuation response in various neighborhoods and populations of New Orleans. Regional economists from LSU have developed input-output modeling for the region which will provide perspective on indirect losses at the regional level. The Hurricane Center also participated in the PAM exercise organized by FEMA in advance of Katrina and documentation of the PAM exercise should provide a useful input for the consequence calculation. The FEMA contractor for the PAM exercise was Innovative Emergency Management of Louisiana.

The Hurricane Center has developed its own models for the impact of hurricanes in the New Orleans region. It has calibrated ADCIRC for Betsy (1965) experience and it provided model results of Katrina impact to the Louisiana Department of Emergency Preparedness and the Times-Picayune in advance of Katrina landfall (these model results did not include breaching of the levee and floodwall system). Data sources identified by the LSU Hurricane Center have been communicated to the Consequences team for follow-up. The clarification of required inputs and expected outputs of the Consequences team represent a major step forward. It is now necessary to communicate those input needs to other relevant IPET teams and to incorporate those expected outputs into the risk model.

Risk Profiles and Summaries

The reliability and risk analysis will relate the performance of individual features (floodwalls, levees, pumps, etc.) located throughout the hurricane protection system to the overall performance of operating the integrated system.

Storm and system performance scenarios will be studied in the risk model to determine the economic and life risks of the New Orleans hurricane protection system:

- As authorized, as a state constituting the baseline for estimating risk;
- As built, before the arrival of Hurricane Katrina;
- June 1, 2006: After Hurricane Katrina repairs have been accomplished prior to the 2006 hurricane season, nominally on June 1 2006; and
- Longer-term options for providing a greater level of protection through a strengthened and improved hurricane protection features.

The difference in relative risks among the three states will be a unified measure for fully evaluating the performance of the integrated system before Hurricane Katrina, after Hurricane Katrina, and during the interim recovery period.

The results of the risk and reliability analyses can be portrayed in various ways in order to facilitate risk communication to inform decision makers and with different public audiences. These will include narratives describing hurricane and system performance scenarios, inundation mapping based on the scenarios studied and graphic displays to portray critical components and identify significant failure modes. Also, Figure J-26 illustrates a typical risk result for economic consequences (in this case the mean frequency of exceedance for economic consequences).

Uncertainty Analysis

One of the objectives of the risk analysis is to quantitatively assess the uncertainties associated with modeling the performance of the HPS, likelihood of failure and the associated consequences of flooding. There are two fundamentally different sources of uncertainty that affect an estimation of the likelihood of future events. The first is attributed to the inherent randomness of events in nature. These events are predicted in terms of their likelihood of occurring (e.g., the chance of heads in a coin flip). This source of uncertainty is known as aleatory uncertainty and is, in principle, irreducible.

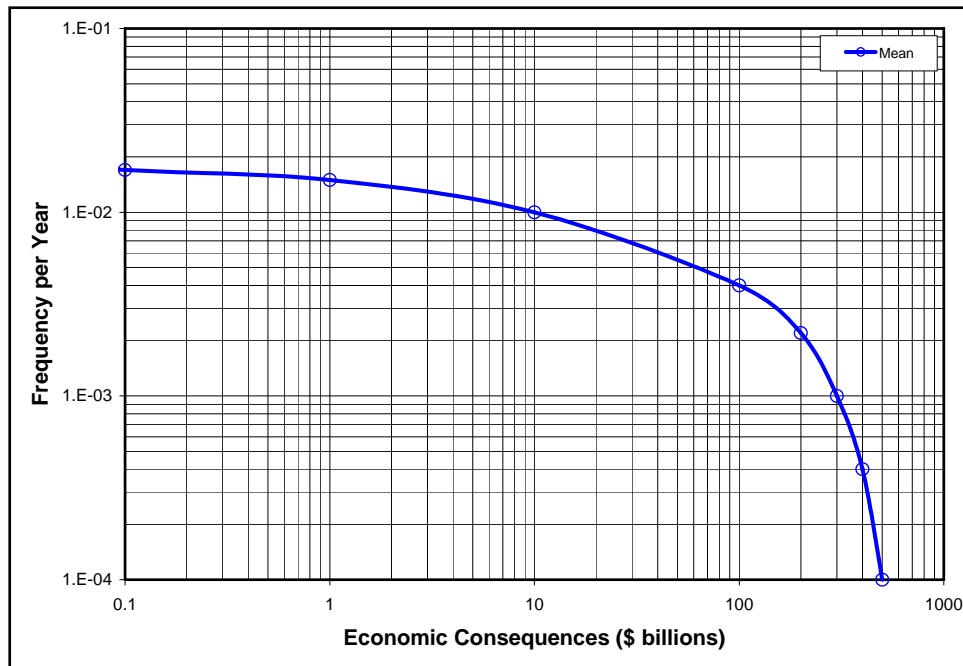


Figure J-26. Illustration of Typical Risk Analysis Results for Economic Consequences

The second source of uncertainty is attributed to our lack of knowledge or data. For example, the ability to determine the likelihood of an event (i.e., its rate of occurrence) requires that certain data be available. Depending on the volume of data that is available, the *accuracy* of the estimate of the rate of occurrence will vary. If limited data are available, the estimated rate may be quite uncertain (i.e., statistical confidence intervals on parameter estimates will be large). A second type of knowledge uncertainty is attributed to our lack of understanding (e.g., knowledge) about the physical processes that must be modeled (e.g., the meteorological processes that generate hurricane events). Often scientists and engineers have interpretations of existing data and models of physical processes of interest that often competing in the sense they lead to different results, while at the same time are consistent with observations. In these instances expert evaluations are often required to assess the current state of knowledge and to quantitatively evaluate the level of uncertainty. These sources of uncertainty are referred to as epistemic (knowledge-based) uncertainty.

The distinction between what is aleatory and what is epistemic uncertainty can often seem arbitrary. For example, the distinction depends on the models that are used in a particular analysis. In addition, their estimates can change in time. Nonetheless, making a distinction between the sources of uncertainty in logical manner helps insure that all uncertainties are quantified and those that can be reduced with additional data or knowledge are identified.

In principle, epistemic uncertainties are reducible with the collection of additional data or the use/development of improved models. However, in a given project, it is typically not possible to reduce these uncertainties.

Figure J-27 shows an example of where the epistemic uncertainty is manifested in the results of the HPS risk analysis. Shown is the probability density function on the estimate frequency of HPS failure (where failure is simple used here as the occurrence of inundation in one or more protected areas). The uncertainty in the estimate of the frequency of failure is an aggregation of the uncertainties in the estimate of the frequency and magnitude of hurricane storm surge and in the estimate of the reliability (or fragility) of the structures, systems and components that comprise the HPS.

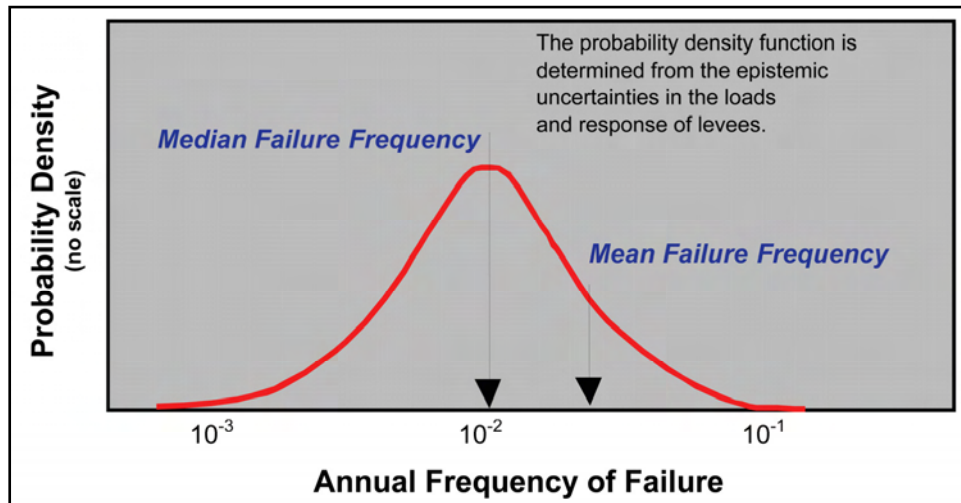


Figure J-27. Illustration of the Uncertainty in the Estimate of the Frequency HPS Failure due to Hurricane Events

In the HPS risk and reliability analysis, there will be uncertainties associated with each of the inputs to the risk model developed by other IPET teams. Sensitivity studies of the parameters used in the drainage model, failure mode models and pumping station performance models are used in order to identify critical sources of uncertainty. In addition, sensitivity studies are conducted during the development of the risk model to identify uncertainties in the input parameters synthesized by Team 10 and to identify data or analyses that could reduce uncertainties.

The effectiveness of the protection system is also dependent upon how well the operational elements of the system performed. Elements such as road closure structures, gate operations and pumping plants, etc. that requires human operation and proper installation during a flood fight can dramatically impact flood levels. The lessons learned concerning the performance of these elements during Katrina will be considered in the uncertainty analysis using parametric analysis.

Figure J-28 shows the fragility for the HPS including uncertainty and its effect on the estimate of the reliability at the authorization basis.

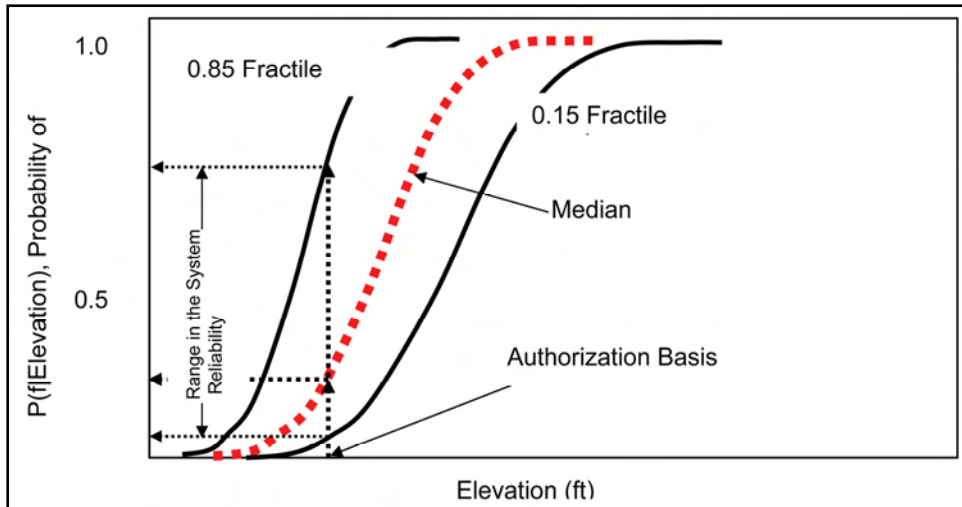


Figure J-28. Illustration of the Fragility for the HPS Including Modeling Uncertainty and the Effect at the Authorization Basis

The epistemic uncertainties in each part of the analysis lead to uncertainty in the final risk results. Propagating the uncertainties of the individual parts of the analysis through to the final result, produces a probability distribution on the frequency of exceedance of consequence metrics (e.g., economic consequences). This result is shown in Figure J-29.

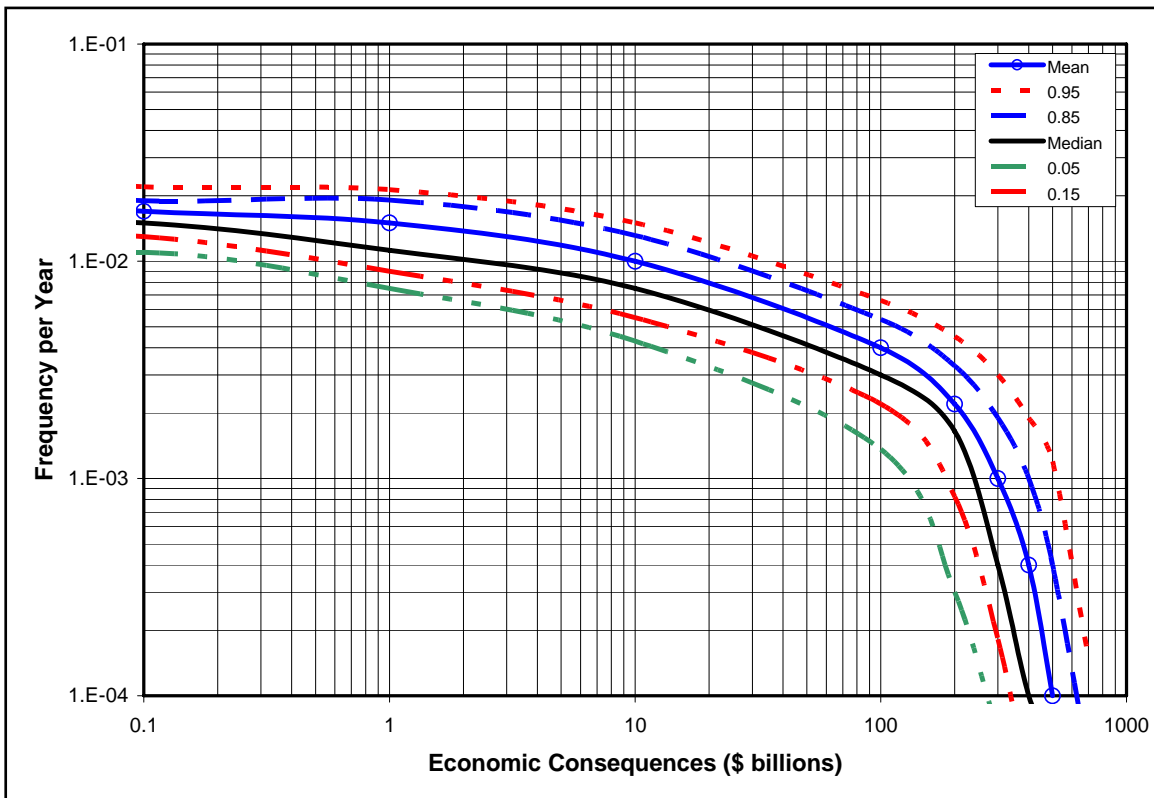


Figure J-29. Illustration of Typical Risk Analysis Results for Economic Consequences Including Uncertainty

References

Risk methodology

- Ayyub, B. M., 2003. Risk Analysis in Engineering and Economics, Chapman & Hall/CRC Press, FL.
- Ayyub, B. M., and McUen, R. H., 2003. Probability, Statistics and Reliability for Engineers and Scientists, Chapman & Hall/CRC Press, FL.
- Daugherty, R., Franzini, J., and Finnemore E., 1985, Fluid Mechanics with Engineering Applications, 598 p., McGraw-Hill Book Co., NY.
- Kumamoto, H., and Henley, E.J., 1996, Probabilistic Risk Assessment and Management for Engineers and Scientists, Second Edition, IEEE Press, New York.
- Modarres, M., Kaminskiy, M., Krivstov, V., 1999. Reliability Engineering and Risk Analysis: A Practical Guide, Marcel Decker Inc., New York, NY.
- USACE, 2000, Unwatering Plan of the Greater Metropolitan Area of New Orleans, LA, USACE New Orleans District.

Hurricane Methodology

- Batts, M. E., Cordes, M. R., Russell, L. R., Shaver, J. R., and Simiu, E. (1980), "Hurricane Wind Speeds in the United States," *Rep. No. BSS-124*, Nat. Bureau of Standards, U.S. Department of Commerce, Washington, D.C.
- Bister, M. and K. A. Emanuel (2002), "Low Frequency Variability of Tropical Cyclone Potential Intensity. 1: Interannual to Interdecadal Variability," *J. Geoph. Res.* **107**: 4801.
- Broccoli, A. J. and S. Manabe (1990), "Can Existing Climate Models Be Used to Study Anthropogenic Changes in Tropical Cyclone Climate?" *Geophys. Res. Lett.* **17**: 1917-1920.
- Chan, J. C. L. and S. L. Liu (2004), "Global Warming and Western North Pacific Typhoon Activity from an Observational Perspective," *J. Climate* **17**: 4590-4602.
- Chen, S., M. Lonfat, J. A. Knaff, and F. D. Marks, Jr. (2006), "Effects of Vertical Wind Shear and Storm Motion on Tropical Cyclone Rainfall Asymmetries Deduced from TRMM," submitted to *Monthly Weather Review*.
- Chouinard, L. E., C. Liu, and C. K. Cooper (1997), "Model for Severity of Hurricanes in Gulf of Mexico," *J. of Waterway, Port, Coastal and Ocean Engineering*, **123**(3): 120-129.

- Elsner, J. B. (2005), "Hurricane Science Review: The Next 5 Years?" Dept. of Geography, Florida State University, <http://garnet.fsu.edu/~jelsner/www>.
- Elsner, J. B. and B. Kocher (2000), "Global Tropical Cyclone Activity: A Link to the North Atlantic Oscillation," *Geophys. Res. Lett.* **27**: 129-132.
- Emanuel, K. A. (1987), "The Dependence of Hurricane Intensity on Climate," *Nature* **326**: 483-485.
- Emanuel, K. A. (2000), "A Statistical Analysis of Tropical Cyclone Intensity," *Mon. Wea. Rev.* **128**: 1139-1152.
- Emanuel, K. A. (2005a), "Increasing Destructiveness of Tropical Cyclones Over the Past 30 Years," *Nature* **436**: 686-688.
- Emanuel, K. A. (2005b), "Anthropogenic Effects on Tropical Cyclone Activity," Dept. of Earth and Planetary Sciences, MIT, <http://wind.mit.edu/~emanuel/anthro2.htm>.
- Free, M., M. Bister, and K. A. Emanuel (2004), "Potential Intensity of Tropical Cyclones: Comparison of Results from Radiosonde and Reanalysis Data," *J. Climate* **17**: 1722-1727.
- Georgiou, P. N., Davenport, A. G., and Vickery, B. J. (1983), "Design Wind Speed in Regions Dominated by Tropical Cyclones," *J. Wind Engrg. And Industrial Aerodynamics*, **13**(1): 139-152.
- Goldenberg, S. B., C. W. Landsea, A. M. Mestas-Nunez, and W. M. Gray (2001), "The Recent Increase in Atlantic Hurricane Activity: Causes and Implications," *Science* **293**: 474-479.
- Haarsma, R. J., J. F. B. Mitchell, and C. A. Senior (1992), "Tropical Disturbances in a GCM," *Climate Dyn.* **8**: 247-257.
- Henderson-Sellers, A. H. Zhang, G. Berz, K. A. Emanuel, W. Gray, C. Landsea, G. Holland, J. Lighthill, S-L. Shieh, P. Webster, and K. McGuffie (1998): "Tropical Cyclones and Global Climate Change: A Post-IPCC Assessment," *Bull. Amer. Meteor. Soc.* **79**: 9-38.
- Ho, F. P., J. C. Su, J. L. Hanevich, R. J. Smith, and F. P. Richards (1987), "Hurricane Climatology for the Atlantic and Gulf Coasts of the United States," *NOAA Technical Report NWS 38*, U.S. Department of Commerce, Washington, D.C.
- Holland, G. J. (1980), "An Analytic Model of the Wind and Pressure Profiles in Hurricanes," *Monthly Weather Review*, **108**: 1212-1218.

- Houghton, J. T., Y. Ding, D. J. Griggs, M. Noguer, P. J. van der Linden, and D. Xiaosu, Eds. (2001), *Climate Change 2001: The Scientific Basis: Contributions of Working Group I to the Third Assessment Report of the Intergovernmental Panel on Climate Change*, Cambridge University Press, 881 pp.
- Jarvinen, B. R., Neumann, C. J., and Davis, M. A. S. (1984), "A Tropical Cyclone Data Tape for the North Atlantic Basin 1886-1893: Contents, Limitations and Uses," *NOAA Tech. Memo. NWS-NHC-22*, U.S. Department of Commerce, Washington, D.C.
- Knutson, T. R. and R. E. Tuleya (2004), "Impact of CO₂-induced Warming on Simulated Hurricane Intensity and Precipitation: Sensitivity to the Choice of Climate Model and Convective Parameterization," *J. Climate* **17**: 3477-3495.
- Landsea, C. W., R. A. Pielke Jr., A. M. Mestas-Nunez, and J. A. Knaff (1999), "Atlantic Basin Hurricanes: Indices of Climatic Changes," *Climatic Change* **42**: 89-129.
- Lighthill, J., G. J. Holland, W. M. Gray, C. Landsea, K. A. Emanuel, G. Craig, J. Evans, Y. Kurihara, and C. P. Guard (1994), "Global Climate Change and Tropical Cyclones," *Bull. Amer. Meteor. Soc.* **75**: 2147-2157.
- Lonfat, M., F. D. Marks, Jr., and S. S. Chen (2004), "Precipitation Distribution in Tropical Cyclones Using the Tropical Rainfall Measuring Mission (TRMM) Microwave Imager: A Global Perspective," *Mon. Wea. Rev.*, **132**: 1645-1660.
- Luettich, R. A., J. J. Westerink, and N. W. Sheffner (1992), "ADCIRC: An Advanced Three-dimensional Circulation Model for Shelves, Coasts and Estuaries; Report 1: Theory and Methodology of ADCIRC-2DDI and ADCIRC-3DL," *Coastal Engineering Research Center, U. S. Army Engineer Waterways Experiment Station*, Technical Report DRP-92-6, Vicksburg, MS.
- Michaels, P. J., P. C. Knappenberger, and C. W. Landsea (2005), "Comments on 'Impact of CO₂-induced Warming on Simulated Hurricane Intensity and Precipitation: Sensitivity to the Choice of Climate Model and Convective Parameterization'," *J. Climate*, in press.
- Neumann, C. J. (1991), "The National Hurricane Center Risk Analysis Program (HURISK)," *NOAA Tech. Memo. NWS-NHC-38*, U.S. Department of Commerce, Washington, D.C.
- Pielke, R. A. Jr., C. W. Landsea, M. Mayfield, J. Laver, and R. Pasch (2005), "Hurricanes and Global Warming," *Bull. Amer. Meteor. Soc.*, November, 2005: 1571-1575.
- Powell, M., G. Soukup, S. Cocke, S. Gulati, N. Morisseau-Leroy, S. Hamid, N. Dorst, and L. Axe (2005), "State of Florida Hurricane Loss Projection Model: Atmospheric Science Component," *J. Wind Engineering and Industrial Aerodynamics*, **93**: 651-674.

- Russell, L. R. (1971), "Probability Distribution for Hurricane Effects," *J. Wtrwy., Harb. And Coast. Engrg. Div., ASCE*, **97**(1): 139-154.
- Scheffner, N. W., L. E. Borgman, and D. J. Mark (1996), "Empirical Simulation Technique Based Storm Surge Frequency Analyses," *J. Wtrwy., Port, Coast., and Oc. Engrg.* **122**(2): 93-101.
- Vickery, P. J. and L. A. Twisdale (1995a), "Prediction of Hurricane Wind Speeds in the United States," *J. of Structural Engineering*, **121**(11): 1691-1699.
- Vickery, P. J. and L. A. Twisdale (1995b), "Wind-Field and Filling Models for Hurricane Wind-Speed Predictions," *J. of Structural Engineering*, **121**(11): 1700-1709.
- Vickery, P. J., P. F. Skerlj, and L. A. Twisdale (2000), "Simulation of Hurricane Risk in the U.S. Using Empirical Track Model," *J. of Structural Engineering*, **126**(10): 1222-1237.
- Webster, P. J., G. J. Holland, J. A. Curry, and H.-R. Chang (2005), "Changes in Tropical Cyclone Number, Duration, and Intensity in a Warming Environment," *Science* **309**: 1844-1846.
- Willoughby, H. E. and M. E. Rahn (2004), "Parametric Representation of the Primary Hurricane Vortex. Part I: Observations and Evaluation of the Holland (1980) Model," *Monthly Weather Review*, **132**: 3033-3048.

Appendix A. Terminology

Event tree analysis is an inductive analysis process that utilizes an event tree graphical construct that shows the logical sequence of the occurrence of events in, or states of, a system following an initiating event.

A *failure mode* is a way that failure can occur, described by the means by which element or component failures must occur to cause loss of the sub-system or system function.

Fault tree analysis is a systems engineering method for representing the logical combinations of various system states and possible causes which can contribute to a specified event (called the top event).

A *fragility curve* is a function that defines the probability of failure as a function of an applied load level.

A *hazard* is condition, which may result from either an external cause (e.g. earthquake, flood, or human agency) or an internal vulnerability, with the potential to initiate a failure mode. It is a source of potential harm or a situation with a potential to cause loss.

The *performance* of a system or component can be defined as its ability to meet functional requirements. The performance of an item can be described by

various elements, such as flood protection, reliability, capability, efficiency, and maintainability. The design and operation of system affects this performance.

A *system* is a deterministic entity comprising an interacting collection of discrete elements and commonly defined using deterministic models. The word *deterministic* implies that the system is identifiable and not uncertain in its architecture. The definition of the system is based on analyzing its functional and/or performance requirements. A description of a system may be a combination of functional and physical elements. Usually functional descriptions are used to identify high information levels on a system. A system can be divided into subsystems that interact. Additional details in the definition of the system lead to a description of the physical elements, components, and various aspects of the system. Methods to address uncertainty in systems architecture are available and can be employed as provided by Ayyub and Klir (1996).

Reliability can be defined for a system or a component as its ability to fulfill its design functions under designated operating and/or environmental conditions for a specified time period. This ability is commonly measured using probabilities. Reliability is, therefore, the occurrence probability of the complementary event to failure.

Consequences for a failure event, can be defined as the degree of damage or loss from some failure. Each failure of a system has some consequence(s). A failure could cause economic damage, environmental damage, injury or loss of human life, or other possible events. Consequences need to be quantified in terms of failure-consequence severities using relative or absolute measures for various consequence types to facilitate risk analysis.

Risk is the potential of losses for a system resulting from an uncertain exposure to a hazard or as a result of an uncertain event. Risk should be based on identified risk events or event scenarios. Risk can be viewed to be a multi-dimensional quantity that includes event-occurrence probability, event-occurrence consequences, consequence significance, and the population at risk; however, it is commonly measured as a pair of the probability of occurrence of an event, and the outcomes or consequences associated with the event's occurrence. Another common representation of risk is in the form of an exceedance probability function of consequences.

Probability is a measure of the likelihood, chance, odds, or degree of belief that a particular outcome will occur. A conditional probability is the probability of event occurrence based on the assumption that another event (or multiple events) has occurred.

Safety can be defined as the judgment of risk tolerance (or acceptability in the case of decision making) for the system. Safety is a relative term since the decision of risk acceptance may vary depending on the individual or the group of people making the judgment.

Risk analysis is the technical and scientific process to breakdown risk into its underlying components. Risk analysis provides the processes for identifying hazards, event-probability assessment, and consequence assessment. The risk

analysis process answers three basic questions: (1) What can go wrong? (2) What is the likelihood that it will go wrong? (3) What are the consequences if it does go wrong? Also, risk analysis can include the impact of making any changes to a system to control risks.

Risk communication can be defined as an interactive process of exchange of information and opinion among stakeholders such as individuals, groups, and institutions. It often involves multiple messages about the nature of risk or expressing concerns, opinions, or reactions to risk managers or to legal and institutional arrangements for risk management. Risk communication greatly affects risk acceptance and defines the acceptance criteria for safety.

A *scenario* is a unique combination of states that lead to an outcome of interest. A scenario defines a suite of circumstances of interest in a risk assessment. Thus there may be loading scenarios, failure scenarios or downstream flooding scenarios.

Appendix B. New Orleans East Polder

New Orleans East (NOE) Polder

NOE – Background

The New Orleans East hurricane protection system was designed as part of the Lake Pontchartrain, LA and Vicinity Hurricane Protection Project. The New Orleans East (NOE) portion of the project protects 45,000 acres of urban, industrial, commercial, and ecological lands. As designed, the levees were generally constructed with a 10-foot crown width with side slopes of 1 on 3. The height of the levees varies but was in the range of 12 - 19 feet depending upon location and design characteristics. There are also floodwall segments along the line of protection that consists of sheet-pile walls or concrete I-walls constructed on the top of sheet-pile. The line of protection was designed to provide protection from the Standard Project Hurricane (approximately a fast moving Category 3 storm). As designed, there is a total of approximately 206,000 linear feet of levees and floodwalls, 8 pump stations, 3 U.S. Fish and Wildlife Service (USFWS) pump stations, a multitude of culverts through/over the levee/floodwall, and multiple gate closures for road and rail crossings. The NOE polder is essentially broken into two major sections, as shown in Figure J-B1. The west side of the polder is primarily residential and the east side is essentially a wetlands area. These two areas are separated by a small levee. The west side of the polder is further divided into residential and industrial areas. The area along the GIWW and IHNC is primarily industrial while the remainder of the western portion is residential in nature.

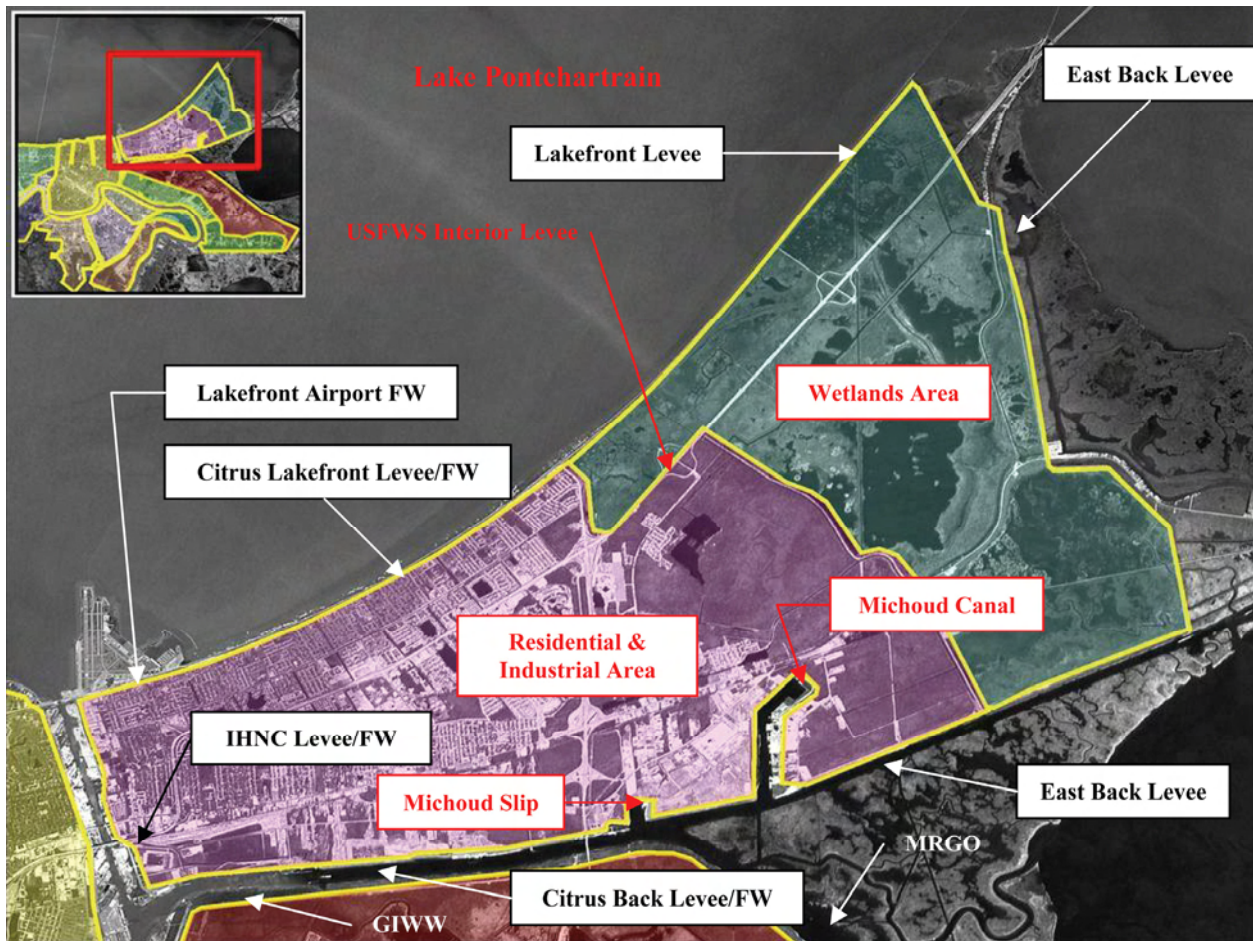


Figure J-B1. New Orleans East Polder – Major Stretches by DM

NOE – Design Memorandums

For the purposes of the IPET risk assessment, each polder must be broken into “reaches” that are defined by a combination of physical characteristics, major elevation changes, and potential consequences. Many of the basic reaches were defined initially by when individual design memorandums (DM) were completed and then constructed since different stretches of the levee/floodwall were raised at different times throughout the life of the structure. There are a total of 7 levee/floodwall major stretches separated by different DM’s within NOE. These 7 are defined below and illustrated in Figure J-B1.

Lakefront Airport Floodwall

Beginning Point: Northwest corner of polder below Ted Hickey Bridge

Ending Point: End of floodwall just south of Hayne Blvd closure gate

Citrus Lakefront Levee/Floodwall

Beginning Point: Begin transition levee just south of Hayne Blvd closure

Ending Point: Levee height transition at Paris Road and USFWS levee

Lakefront Levee

Beginning Point: Levee transition at Paris Road and USFWS interior levee

Ending Point: South Point at northeast end of polder

East Levee

Beginning Point: South Point at northeast corner of polder

Ending Point: GIWW at southeast corner of polder

East Back Levee

Beginning Point: GIWW at southeast corner of polder

Ending Point: Northeast end of Michoud Canal floodwall

Citrus Back Levee/Floodwall

Beginning Point: Northeast end of Michoud Canal floodwall

Ending Point: Southwest corner of polder at IHNC

IHNC East Levee/Floodwall

Beginning Point: Southwest corner of polder at IHNC

Ending Point: Northwest corner of polder under Ted Hickey Bridge

NOE – Layout of Reaches for Risk Model by Physical Feature

Within these major stretches defined by the DM's there are reaches, which are defined by physical changes in the protection system, i.e. switching from floodwall to levee, etc..., or by changes in geotechnical parameters. Within each reach, there are specific "key points" whose reliability needs to be determined in order to calculate the effect on the overall reach being evaluated. An example of a "key point" would be a closure gate at a road or rail line crossing along a floodwall. IPET engineers reviewed existing plans, damage survey reports, and conducted field verification inspections to ensure each polder was accurately defined within the system. As a part of the field verification inspections, GPS coordinates were obtained and stationing from DM's and "as-built" plans was verified. For each polder, this information was transformed into a spread sheet and then a system map for each polder, as shown in Figure J-B2. Finally, digital photographs with incorporated notes were developed to compliment the spread sheets and system map for further clarification. This collection of information was then categorized to get a clear picture of how the polder should be defined for risk assessment purposes. A summary of the reach and point definitions for NOE is provided in Figure J-B2 with a brief supporting narrative on each reach. Polder definition starts at the northwest corner of the polder where the floodwall along the IHNC intersects the floodwall along the Lakefront Airport (NOE1). This occurs at Sta. 4+02 B/L, which is equal to the DM stationing of 10+13 W/L. The end of the physical definition of the NOE polder occurs at the same point since it is self enclosed.

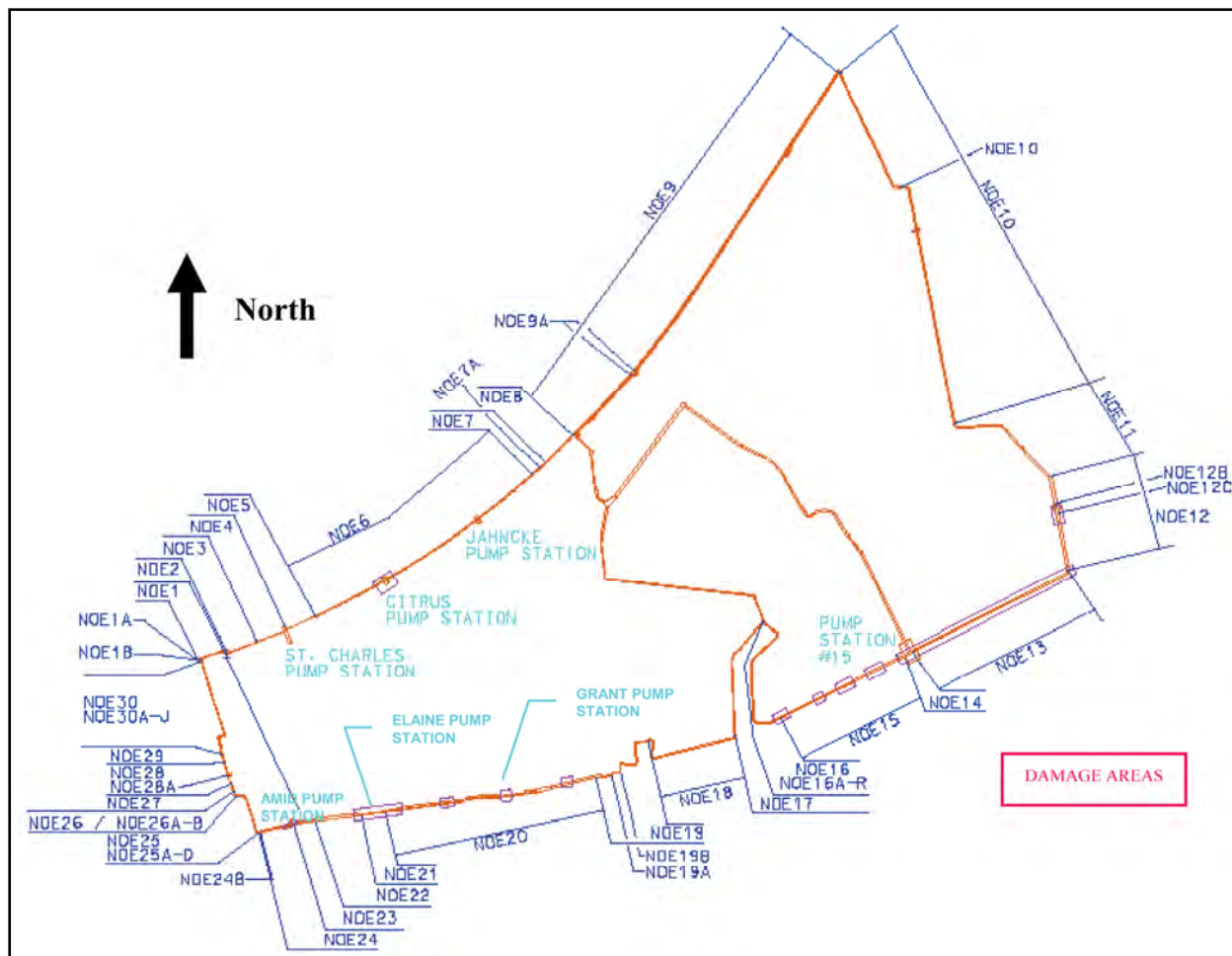


Figure J-B2. New Orleans East Polder – Reaches Defined

The details of each reach and key point is detailed in the spread sheet for the individual polders. The NOE is summarized by reach as follows:

Reach NOE1 (Lakefront Airport DM). This reach is defined by 2,326 linear feet of floodwall at the Lakefront Airport. It is located at the northwest end of the polder. There are two key points (NOE1a and NOE1b) within this reach, both closure gates, located near the end of this reach. The reach ends just after the second closure gate for Hayne Boulevard. There was significant scour from overtopping along this section of i-wall, as shown in Figure J-B3, but the wall performed well with no noticeable deformation.



Figure J-B3. Scour Behind Lakefront Airport FW from Overtopping

Reach NOE2 (Citrus Lakefront DM). This reach is defined by a short 97' transition levee between the end of the Lakefront Airport floodwall and the beginning of the Stars and Stripes Floodwall. There are no key points within this reach.

Reach NOE3 (Citrus Lakefront DM). This reach is defined by 2,325 linear feet of floodwall. There are two basic types of floodwall along this reach each consisting of about ½ the length of this reach. The first type is a short concrete capped i-wall with levee high on both sides and the second is a taller i-wall section where the protected side has a concrete sidewalk adjacent to a road.

Reach NOE4 (Citrus Lakefront DM). This reach is defined by 2,330 linear feet of the Stars and Stripes Levee. A small concrete i-wall for the discharge pipes at the St. Charles Pump Station is located near the end of this reach.

Reach NOE5 (Citrus Lakefront DM). This reach is defined by 2,270 linear feet of the Stars and Stripes floodwall. There are no key points within this reach.

Reach NOE6 (Citrus Lakefront DM). This reach is defined by a 19,112 linear feet segment of levee. It begins at the end of the Stars and Stripes floodwall and ends at the west side of the Lincoln Beach floodwall. There are two “key” points within this segment: two small floodwall sections embedded within the levee for the discharge pipes of the Citrus and Jahncke Pump Stations. There was some minor scouring and overtopping of this levee at various locations, as indicated in Figure J-B4, but no failures.



Figure J-B4. Minor Scour from Overtopping at Jahncke Pump Station

Reach NOE7 (Citrus Lakefront DM). This reach is defined by a 1,474 linear feet segment of floodwall near Lincoln Beach. There is one “key point” located in the flood wall, which is a closure gate, shown as NOE7a.

Reach NOE8 (Citrus Lakefront DM). This reach of levee, 2,724 linear feet, ends the Citrus Lakefront section at the intersection of Paris Road, the interior local levee, and the west side of the Lakefront Levee. There are no key points within this reach, although the levee height is considerably different as it proceeds to the Lakefront Levee section, as shown in Figure J-B5.



Figure J-B5. Begin Lakefront Levee at Citrus Lakefront and Paris Road
(Lakefront Levee @ El. 19.0 +/- and Citrus Lakefront Levee @
13.5+/-)

Reach NOE9 (Lakefront Levee DM). This reach covers 33,165 feet of levee along Lake Pontchartrain from Paris Road to South Point, which is the extreme northeast corner of the polder. There is 368' long i-wall around the Exxon/Mobil pipeline crossing that is the only “key point” within the reach, depicted at NOE9a in Figure J-B2.

Reach NOE10 (East Levee DM). This reach is defined by a 27,665 linear feet segment of levee from South Point to where Highway 90 crosses the levee. There are several “key points” within this stretch including 4 culverts through the levee (3 gravity structures and 1 USFWS pump station) and 1 gated closure at Highway 11. For clarity, these are not illustrated in Figure J-B2. Reference the spread sheet in the appendix for further details regarding their location and description.

Reach NOE11 (East Levee DM). This levee is 8,942' long and goes from Highway 11 and serves as a transition section where the design changes. There are no “key points” located within this reach.

Reach NOE12 (East Levee DM). The final reach of levee along the East section is 7,190' long and extends to the GIWW. There are 4 key points along the levee (3 culverts thru the levee and a gated closure at the railroad crossing). The railroad closure structure, shown as NOE12c in Figure J-B2, experienced severe damage during Katrina from overtopping. An aerial view of that damage is shown in Figure J-B6.



Figure J-B6. Aerial View of Damage at RR Closure Along East Levee (Point NOE12c on System Map)

Reach NOE13 (East Back Levee DM). This section of levee, measuring 22,257 linear feet, was heavily damaged during Katrina from overtopping. It begins at the east end where it ties into the East Levee and continues to the east end of the floodwall around the Orleans Parish Pump Station #15. There are no key points within this reach. Much of this levee was destroyed, as shown in Figure J-B7, and is in the process of being rebuilt.



Figure J-B7. Failure of Levee by Overtopping East of PS #15 (East Back Levee)

Reach NOE14 (East Back DM). This reach is defined by the floodwall around Pump Station #15. There are two types of walls within this reach, sheet pile walls at the edges and concrete i-walls around the discharge pipes. The total length of wall is 493 feet. Portions of the transition sheet pile sections were heavily damaged during Katrina from overtopping, as shown in Figure J-B8. There are no key points within this short reach.



Figure J-B8. Floodwall Failure Near Orleans Pump Station #15

Reach NOE15 (East Back DM). This 10,120 ft section of levee extends from the east end of the Orleans Parish #15 floodwall to the start of the floodwall on the east side of the Michoud Canal at the GIWW. There is one key point within this reach for a utility pipe crossing.

Reach NOE16 (East Back DM). This reach consists of the east floodwall around the Michoud Canal. It is approximately 10,757 feet long. It starts at the GIWW and continues along the Michoud Canal where it joins with the Citrus Back floodwall. There are 18 key points along this reach for gated closures at industry and road crossings. However, from site inspections, it appears as if 5 of these gates are placed in the permanently closed position. As shown in Figure J-B9, the transition sheet pile floodwall at the beginning of this reach failed during Katrina.

Reach NOE17 (Citrus Back DM). The beginning of the Citrus Back stretch starts with this reach at the northwest end of the Michoud Canal and ends at the southwest side of the Michoud Canal at the GIWW. This reach consists of 9,318 feet of floodwall with no key points within this reach.

Reach NOE18 (Citrus Back DM). This reach represents the 7,905' segment of levee between the Michoud Canal and Michoud Slip. There are no key points within this reach of levee.



Figure J-B9. Floodwall Failure at East End of Michoud Canal FW

Reach NOE19 (Citrus Back DM). The reach represents the 6,155 ft of floodwall around the Michoud Slip. There are 2 gates closures and 2 ramps within this reach.

Reach NOE20 (Citrus Back DM). This reach contains 15,940 ft of levee between the west end of the Michoud Slip and the east end of the combination floodwall for the bulk loading facility. There are three key points within this reach for culverts crossing the levee, including the discharge pipes for Grant Pump Station, as reference in Figure J-B2.

Reach NOE21 (Citrus Back DM). This reach is defined by the 1,820 ft combination floodwall built for the bulk loading facility and Elaine Pump Station, whose relative location is shown on the system map in Figure J-B2. This wall was heavily damaged during Katrina, as shown in Figure J-B10, and is currently being repaired.



Figure J-B10. Floodwall Failure at Bulk Loading Facility/Elaine PS

Reach NOE22 (Citrus Back DM). This reach is for the levee (3,453 ft long) between the floodwalls at the bulk loading facility/Elaine PS (east side) and Amid PS (west side). There are no key points within this reach.

Reach NOE23 (Citrus Back DM). This reach is the 1,587 ft section of floodwall located just east of the Amid Pump Station. This wall did suffer minor overtopping, but no major damage. There are no key points within this reach.

Reach NOE24 (Citrus Back DM). The final reach of this DM is 2,348 feet of levee extending from the end of the floodwall just east of the Amid Pump Station to its tie in with the Inner Harbor Navigation Canal (IHNC) east levee. There are two key points located within this reach including the discharge pipes over the levee at Amid PS and the railroad closure gate structure just east of the tie in with the IHNC levee. This structure was overtopped and sustained serious erosion problems, but no major structural damage, as indicated by the eroded areas in Figure J-B11.



Figure J-B11. Erosion Damage Around RR Closure (Citrus Back Levee)

Reach NOE25 (IHNC DM). This reach is 3,803 ft long and consists of levee. There are 4 closure gates within this reach each of which suffered erosion damage from overtopping during Katrina. Structural damage was minimal to these closure structures. The very end of this reach suffered a major washout area where the levee serves as a ramp just near the I-10 overpass. A photograph of this washout damage is shown in Figure J-B12.

Reach NOE26 (IHNC DM). This short reach of floodwall (537 ft) starts near the end of the washout area and extends just under the I-10 overpass. This section is considered a reach because it faces several different directions and contains two key points, both closure gates.



Figure J-B12. Major Washout Area from Overtopping Near I-10 Overpass (Citrus Back Levee)

Reach NOE27 (IHNC DM). This reach consists of a short transition levee (526 ft) between floodwalls. There are no key points within this short reach.

Reach NOE28 (IHNC DM). This section of floodwall (1,876 ft) starts between the I-10 and Highway 90 overpasses and ends where it serves as the foundation for the Dupuy Storage Facility (see Figure J-B12). There is one key point in this section which is the old Highway 90 overpass location. It does not appear as if remedial repairs were made this transition section when the overpass was relocated.

Reach NOE29 (IHNC DM). This short section of floodwall (643 ft) serves as the Dupuy Storage Building foundation, as shown in Figure J-B13. This section was deemed an individual reach because overtopping issues along this short reach may not be of major concern with the building.



Figure J-B13. Floodwall Serves as Building Foundation (Dupuy Storage Facility – IHNC East)

Reach NOE30 (IHNC DM). The last reach of the polder consists of 8,168 ft of floodwall. There are several key points within this reach including the Dwyer PS discharge pipes and several closure gates. Portions of this wall were overtopped as indicated by the erosion behind the floodwall adjacent to closure gate E-13 and shown in Figure J-B14. This erosion, which measures approximately 8' wide by 2.5' deep, did not cause major structural problems with the wall at this location.



Figure J-B14. Erosion Behind Floodwall Adjacent to Gate E-13 (IHNC East)

In summary, the NOE polder is divided into 30 reaches for the purposes of the risk analysis. There are a total of 14 floodwall reaches (49,749 linear feet) and 16 levee reaches (167,577 linear feet). Thus, the polder is roughly 23% floodwall and 77% levee for evaluation purposes. Approximately 6,700 feet of levee, primarily the East Back Levee section, was damaged or destroyed from overtopping during Katrina. An additional 24,600 feet of floodwall was damaged to some extent from overtopping. This was spread out across different sections of the polder. Some of the damage to the floodwalls will only require that landside fill be placed back where scouring took some of the resisting, passive wedge away. Other shorter sections of wall are being totally rebuilt as a result of the overtopping causing their failure.

NOE – Elevations Along the Defined Reaches

One of the critical inputs to completing the risk assessment for the hurricane protection system is a clear understanding of the elevations along each polder both pre-Katrina and as a result of any fixes from Task Force Guardian. There are different ways this can be addressed when conducting the risk assessment, but in order to get the best information, “average” lengths of elevations to the nearest ½ foot increment were developed. A variety of survey information was required to develop this information for NOE. Four different sources of data were required to obtain the best estimate of levee/floodwall elevations at the time of Katrina. A September 2005 LIDAR survey was used to establish elevations for most non-failed sections of levees. For the Citrus Back Levee, September 2000

Plan and Profile sheets were provided by TFG. For levee sections that had major failures (East Back Levee), October 2001 survey data was available and provided by TFG. Finally, LIDAR survey data is collected by aerial means and it did not pick up the top of floodwalls. In November 2005, a field survey was done using NAVD88 datum to determine top of floodwall elevations at the various locations along NOE.

The survey information for NOE was collected and categorized along each reach. The elevations vary considerably, but were developed where “average” ½ foot elevation changes occurred and then stations were matched to these locations. This information is provided in the NOE spread sheet. In summary, the weighted average of levee/floodwall height coupled with the range is provided in Table J-B1.

Table J-B1. Elevation Information by Reach for NOE Polder					
Reach	DM	Weighted Average Elevation	Maximum Elevation in Reach	Minimum Elevation in Reach	Source
NOE1	Lakefront Airport	11.6	11.7	11.6	Nov05 Survey
NOE2	Citrus Lakefront	13.0	13.0	13.0	Sep05 LIDAR
NOE3	Citrus Lkfrt	need data	need data	need data	???
NOE4	Citrus Lakefront	13.2	13.5	11.5	Sep05 LIDAR
NOE5	Citrus Lakefront	14.3	14.6	14.1	Nov05 Survey
NOE6	Citrus Lakefront	13.0	13.5	12.0	Sep05 LIDAR
NOE7	Citrus Lakefront	12.5	12.7	12.2	Nov05 Survey
NOE8	Citrus Lakefront	12.9	13.0	12.5	Sep05 LIDAR
NOE9	Lakefront Levee	18.4	20.0	18.0	Sep05 LIDAR
NOE10	East Levee	15.1	15.5	12.5	Sep05 LIDAR
NOE11	East Levee	16.8	17.5	16.5	Sep05 LIDAR
NOE12	East Levee	17.8	19.0	13.5	Sep05 LIDAR
NOE13	East Back Levee	15.5	16.5	15.0	Oct01 Survey
NOE14	East Back Levee	19.9	22.2	17.5	Nov05 Survey
NOE15	East Back Levee	16.8	17.0	16.5	Oct01 Survey
NOE16	East Back Floodwall	17.9	18.0	17.5	Nov05 Survey
NOE17	Citrus Back Floodwall	20.7	21.0	20.5	Nov05 Survey
NOE18	Citrus Back Levee	17.4	17.5	17.0	Nov05 Survey
NOE19	Citrus Back Floodwall	17.2	17.1	17.8	Nov05 Survey
NOE20	Citrus Back Levee	14.6	15.0	14.0	Sep00 Plan & Profile
NOE21	Citrus Back Floodwall	need data	need data	need data	???
NOE22	Citrus Back Levee	14.0	14.0	14.0	Sep00 Plan & Profile
NOE23	Citrus Back Floodwall	14.5	15.1	14.4	Nov05 Survey
NOE24	Citrus Back Levee	13.6	14.0	13.0	Nov05 Survey
NOE25	IHNC East	12.0	12.5	11.5	Nov05 Survey
NOE26	IHNC East	12.5	12.5	12.5	Nov05 Survey

NOE27	IHNC East	12.5	12.5	12.5	Nov05 Survey
NOE28	IHNC East	13.2	13.5	12.0	Nov05 Survey
NOE29	IHNC East	13.5	13.5	13.5	Nov05 Survey
NOE30	IHNCE East	12.4	13.0	11.5	Nov05 Survey

Appendix C - Jefferson Polder

Appendix D - St. Charles Polder

Appendix E - Plaquemines Polder

Appendix F - St. Bernards Polder

Appendix G - Evaluation of Loss Exceedance Probabilities

In the case of using point estimates of probabilities, the results should be summarized as provided in Table J-G1, and the loss exceedance probabilities can be then computed. The events in Table J-G1 are assumed to be independent Bernoulli random variables with the following probability mass functions:

$$P(E_i \text{ occurs}) = p_i \quad (\text{J-G1})$$

$$P(E_i \text{ does not occur}) = 1 - p_i \quad (\text{J-G2})$$

If the events are indexed in reverse order of their losses (i.e., $L_i \geq L_{i+1}$), the mean (expected) exceedance probability for a given loss $EP(L_i)$, can be found as

$$\begin{aligned} EP(L_i) &= P(L > L_i) = 1 - P(L \leq L_i) \\ &= 1 - \prod_{j=1}^i (1 - p_j) \end{aligned} \quad (\text{J-G3})$$

The exceedance probability (EP) curve based on the data from Table J-G1 is shown in Figure J-G1.

If prediction capabilities are needed, a model can be that is simple and concave upward (i.e., similar to Figure J-G1). Such function should be positive and limited from the above by unity. These requirements are satisfied for the survivor function of Pareto distribution, which (for the random variable L) can be written as

$$P(L) = \left(1 + \frac{L}{d}\right)^{-c} \quad (\text{J-G4})$$

Table J-G1. Loss Exceedance Probabilities (Hypothetical Values).				
Event (E_i)	Annual Probability of Occurrence (p_i)	Loss (L_i)	Exceedance Probability (EP(L_i))	E(L) = (p_iL_i)
Event ₁	0.002	25,000,000	0.0020	50,000
Event ₂	0.005	15,000,000	0.0070	75,000
Event ₃	0.010	10,000,000	0.0169	100,000
Event ₄	0.020	5,000,000	0.0366	100,000
Event ₅	0.030	3,000,000	0.0655	90,000
Event ₆	0.040	2,000,000	0.1029	80,000
Event ₇	0.050	1,000,000	0.1477	50,000
Event ₈	0.050	800,000	0.1903	40,000
Event ₉	0.050	700,000	0.2308	35,000
Event ₁₀	0.070	500,000	0.2847	35,000
Event ₁₁	0.090	500,000	0.3490	45,000
Event ₁₂	0.100	300,000	0.4141	30,000
Event ₁₃	0.100	200,000	0.4727	20,000
Event ₁₄	0.100	100,000	0.5255	10,000
Event ₁₅	0.283	0	0.6597	0

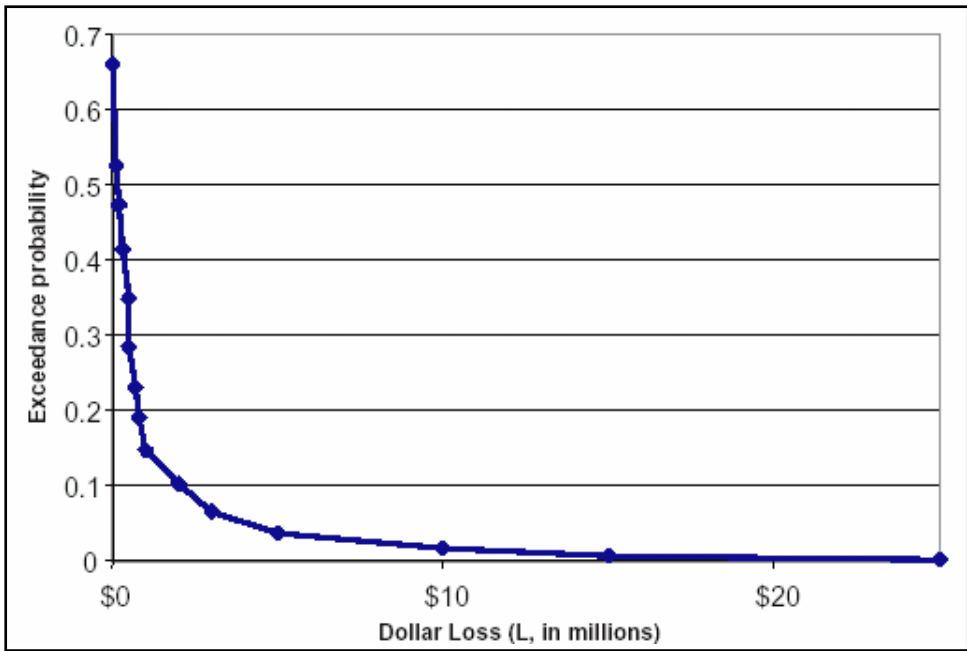


Figure J-G1. Mean Exceedance Probability Curve Based on Data from Table J-G1

Appendix K The Performance – Flood Wall and Levee Performance Analysis

K1 Soil Data Report – 17th Street Canal

Introduction

This is an interim data report detailing the data collected by the Interagency Performance Evaluation Task Force (IPET) to support the analysis of the I-wall section that breached at the 17th Street canal as a result of Hurricane Katrina on August 29, 2005. The location of the 17th Street canal is shown in Figure K1-1. The site of the breach, located on the east bank near the north end of the canal, is also noted on Figure K1-1.

The data will be used in the Floodwall and Levee Performance Analysis task as part of its effort to determine how the flood protection structures performed in the face of the forces to which they were subjected by Hurricane Katrina, and to compare this performance with the design intent, the actual as-built condition, and observed performance. This effort includes understanding why certain structures failed catastrophically and why others did not. The effort will determine, in detail, how the levees and floodwalls performed during Hurricane Katrina. The studies being conducted under this effort involve compiling available information concerning the as-built conditions of the levees and floodwalls, and eye-witness accounts of their performance during the hurricane to establish the underlying set of facts; performing field investigations, including mapping and soil borings to determine post-failure conditions; performing laboratory tests to determine properties of soils and structural materials for use in analyses of performance; developing analytical models in the form of cross sections at areas where breaches occurred and areas where the levees and floodwalls were stable; and performing limit equilibrium and soil-structure interaction analyses to develop a full understanding of the performance of the levees and floodwalls and to provide guidance for future design analyses. These studies will be documented in a series of reports. The series of reports will start with data reports detailing the data collected on the site conditions at 17th Street canal, London Avenue canal, Orleans canal, and Inner Harbor Navigation canal, as noted on Figure K1-1.

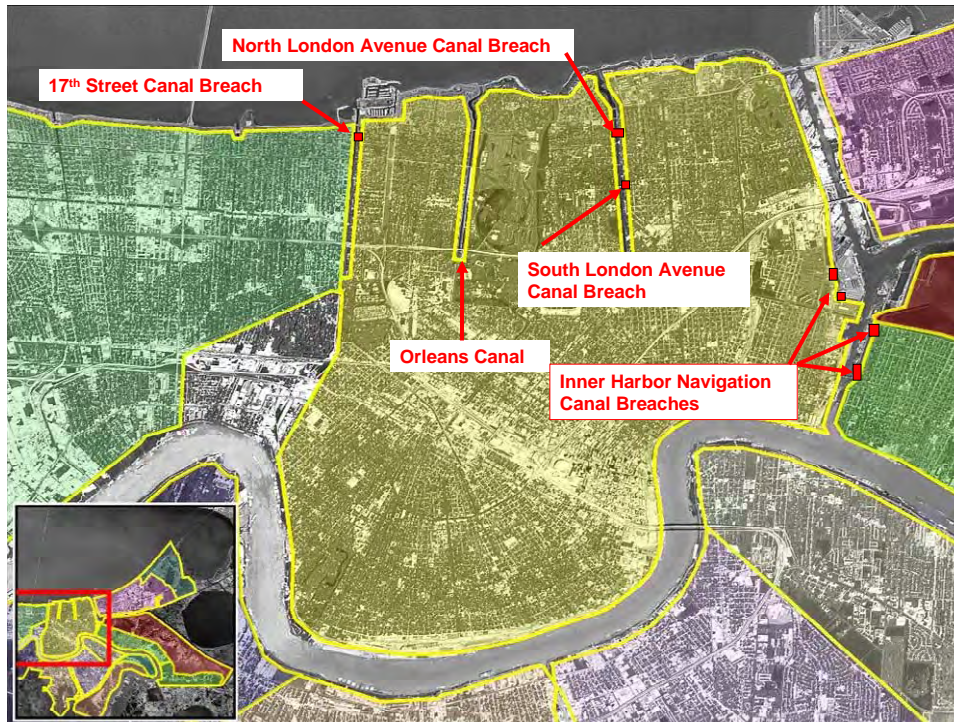


Figure K1-1. Location of Orleans Parish canals.

The key data obtained for the breach site and documented as part of this report include:

- a. Geology of the area.
- b. Description of soil stratigraphy.
- c. Representative pre-Katrina cross section through the breach area.
- d. Soil undrained shear strength profiles.

These data were obtained from a variety of sources, including the project's General Design Memorandum, design documents, and surveys prepared prior to Katrina. In addition, this report contains information obtained from field and laboratory investigations and surveys conducted after the Hurricane Katrina event. This report was prepared with the intent to provide numerical and physical modelers with the information needed to build their models.

Geology

Introduction

Before examining the individual failure areas at the 17th Street canal, a review of the geology is presented to familiarize the reader with the broader context of the geology of the delta plain, its stratigraphy, and the soils comprising the foundations at the different failure areas. For comparison purposes, the general geology of the 17th Street, Orleans, and London Avenue canals levee breaches is reviewed. The geology of the New Orleans area has been determined from detailed mapping studies of the Louisiana Coastal Plain (LCP), from a review of the published literature, from data collection activities at each of the failure sites by an IPET study team, and from an evaluation of preexisting and recently drilled engineering borings from each of the failure areas.

Previous Studies

A review of the past geologic literature from the New Orleans area identifies the US Army Corps of Engineers (USACE) as being actively involved with much of the regional and focused geologic studies that have been performed in the eastern LCP or deltaic plain (Dunbar and others, 1994 and 1995; Dunbar, Torrey, and Wakeley, 1999; Fisk, 1944; Kemp and Michel, 1967; Kolb, Smith, and Silva, 1975; Kolb, 1964; Kolb and Van Lopik, 1958a and 1958b; Kolb and Schultz, 1954; Kolb and Saucier, 1982; May and others, 1984; Michel, 1967; Saucier, 1963, 1984, and 1994; and Schultz and Kolb, 1950). Many of these studies and associated geologic maps are available from a USACE-sponsored website on the geology of the Lower Mississippi Valley that is accessible to the public at lmvmapping.erdc.usace.army.mil.

Geologic History and Principal Physiographic Features of the New Orleans Area

To better understand the soils beneath the 17th Street, Orleans, and London Avenue canals, and the engineering properties of these soils, a brief summary of the geologic history of the New Orleans area is presented. Detailed descriptions of the geologic history are presented in Saucier (1964 and 1994); Kolb, Smith, and Silva (1975); Kolb and Saucier (1982); and Kolb and Van Lopik (1958).

The geology and stratigraphy of the New Orleans area are young in terms of its age. Generally, sediments comprising the New Orleans area are less than 7,000 years old. Formation of the present day New Orleans began with the rise in global sea level, beginning about 12,000 to 15,000 years before the present. The rise in sea level was caused by melting of continental glaciers in the Northern Hemisphere and the release of ice-bound water to the oceans. At the maximum extent of continental glaciation, eustatic sea level was approximately 300 ft (~100 m) lower than the present level. In addition, the ancestral coastal shoreline was much farther south of its current location, probably near the edge of the continental shelf.

The underlying Pleistocene surface throughout much of coastal Louisiana was subaerial, and exposed to oxidation, weathering, and erosion. These conditions led to the development of a well-developed drainage network across its surface, and created a distinct soil horizon in terms of its engineering properties. The Pleistocene horizon is easily recognizable in borings because of its distinct physical properties as compared to the overlying Holocene fill (i.e., oxidized color, stiffer consistency, higher shear strength, lower water content, and other physical properties.). The axis of the main valley or entrenchment of the Mississippi River was located west of New Orleans, in the vicinity of present day Morgan City, LA (Figure K1-2). Consequently, development of the early Holocene deltas was concentrated near the axis of Mississippi entrenchment when sea level rise began to stabilize sometime between 5,000 to 7,000 years before the present. New Orleans is located on the eastern edge of this buried entrenchment or alluvial valley.

The Pleistocene surface in the New Orleans area is variable, but generally ranges between 50 and 75 ft below sea level as determined from detailed mapping and examination of boring data (Kolb and Van Lopik 1958; Kolb, Smith, and Silva 1974; Saucier 1994; and Dunbar and others 1994 and 1995). Various sea level curves for the Louisiana coast are presented and discussed in Kolb, Smith, and Silva (1975) and Tornquist and Gonzalez (2002). These curves generally indicate that sea level transgression in the New Orleans area generally occurred between 6,000 to 9,000 years before the present, based on the mapped depths to the top of the Pleistocene surface.

As the rate of the sea level rise declined and stabilized, it led to the development of five, short-lived delta complexes across the Louisiana coast by deposition of Mississippi River sediments (Figure K1-2). Individual delta complexes are composed of numerous, branching distributary channels. These channels transport and deposit fluvial sediments along the margin of the delta and build land seaward into shallow coastal water. Distributary channels from the St. Bernard delta are responsible for filling the shallow Gulf waters in the greater New Orleans area (Frazier 1967).

Bayou Sauvage is a major distributary involved in the filling of the shallow Gulf waters in the New Orleans area (Figure K1-3). This channel extends eastward from the Mississippi River and is composed of Bayous Metairie, Gentilly (or Gentilly Ridge), and Sauvage. Natural levees of this distributary channel form a pronounced physiographic feature in the northern New Orleans area (Figure K1-3). Similarly, Mississippi River's natural levees are some of the highest land elevations found in New Orleans, and these were the first areas to be settled by the early inhabitants in the 1700s. Distributary channels in New Orleans are pronounced physiographic features, and are associated with the St. Bernard delta complex as determined from radiocarbon dating of organic sediments (Frazier, 1967; Kolb and Van Lopik 1958; McFarlan 1961; Britsch and Dunbar 1999; and Smith, Dunbar, and Britsch 1986).

Equally important to the development and filling history of the New Orleans area is the presence of a buried, barrier beach ridge which formed approximately 4,500 to 5,000 years before the present. This beach extends northeast in the subsurface along the southern shore of Lake Ponchartrain (Figure K1-4). Sea

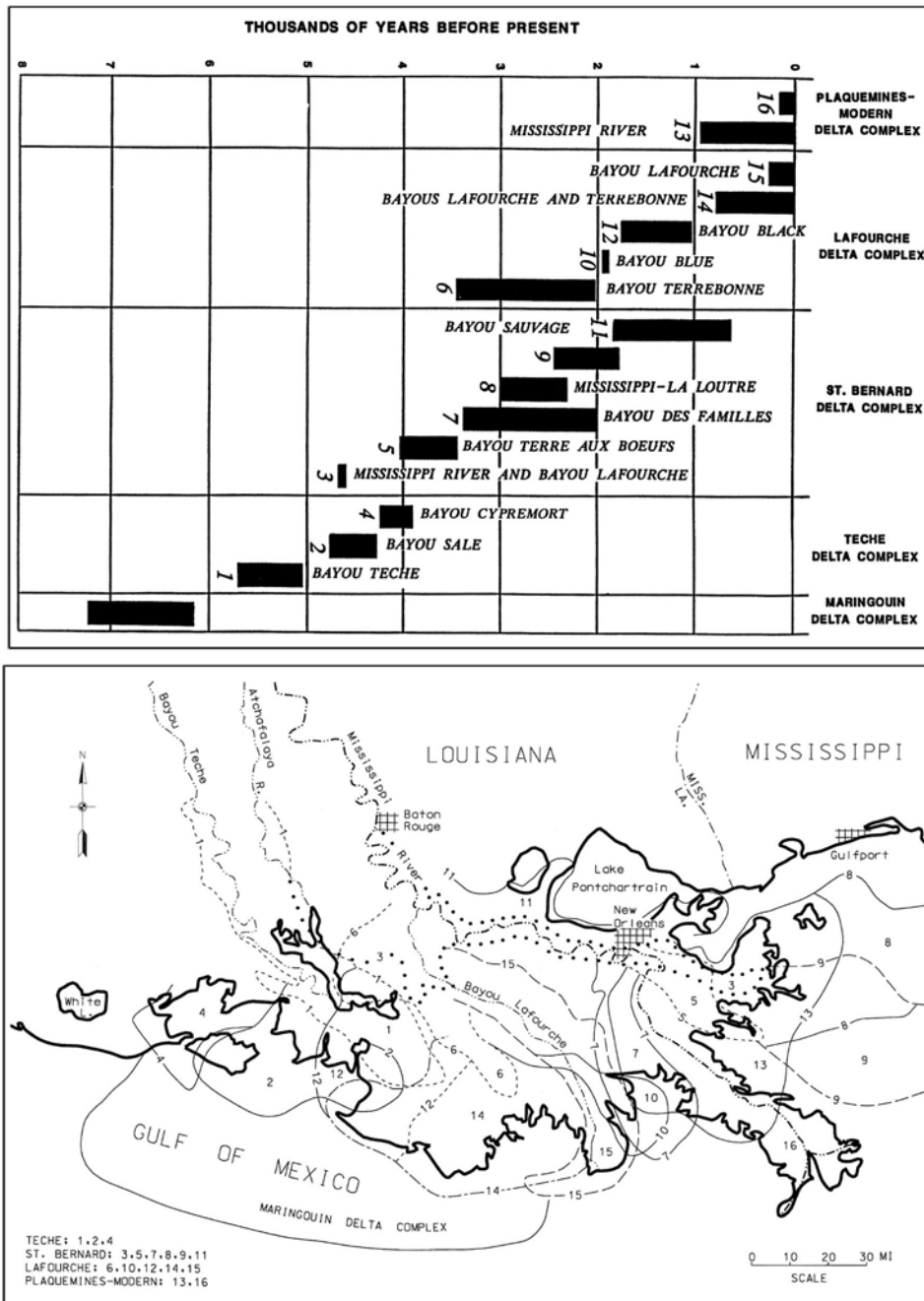


Figure K1-2. Location and approximate chronology of the Mississippi River Deltas, major distributary channels are numbered, note Bayou Sauvage (No. 11) which extends across the New Orleans area and forms the Bayou Metairie/Gentilly Ridge (after Frazier, 1967). Morgan City, LA, located along axis of maximum Mississippi River entrenchment.

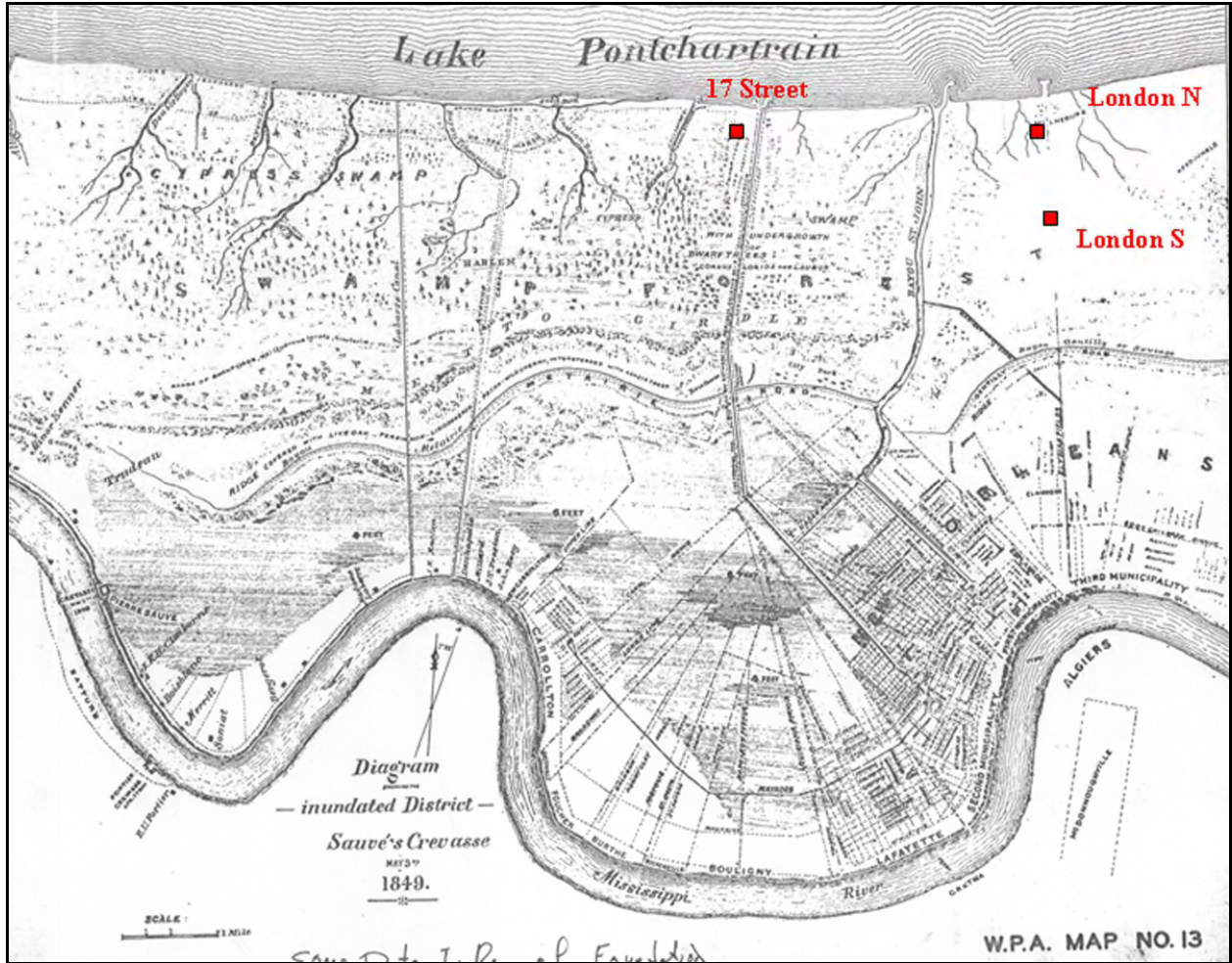


Figure K1-3. New Orleans area map from 1849 showing city limits and topography. Note the location of Bayous Metairie and Gentilly (i.e., Bayou Sauvage) and the identified cypress swamp north of the city at this time (Work Projects Administration 1943).

level was 10 to 15 ft lower than the current level when the beach ridge formed. A stable sea level permitted sandy sediments from the Pearl River to the east to be concentrated by longshore drift, and formed a sandy spit or barrier beach complex in the New Orleans area as shown by Figure K1-3 (Saucier 1994).

The presence of the barrier beach affected sedimentation patterns and the subsequent locations for advancing distributary channels in the New Orleans area. The beach complex likely prevented the Mississippi River and later St. Bernard distributaries from completely filling Lake Pontchartrain with sediment. Consequently, foundation soils beneath the 17th Street, Orleans, and London Avenue canal breaches are affected by their proximity to the buried beach complex. As shown by Figure K1-4, the breach at the 17th Street canal is located on the protected or land side of the beach ridge, while both of the London canal breaches are located over the thickest part or axis of this ridge complex. The beach ridge cuts across the Orleans canal with the north portion on the landside and south portion over the axis of this ridge complex.

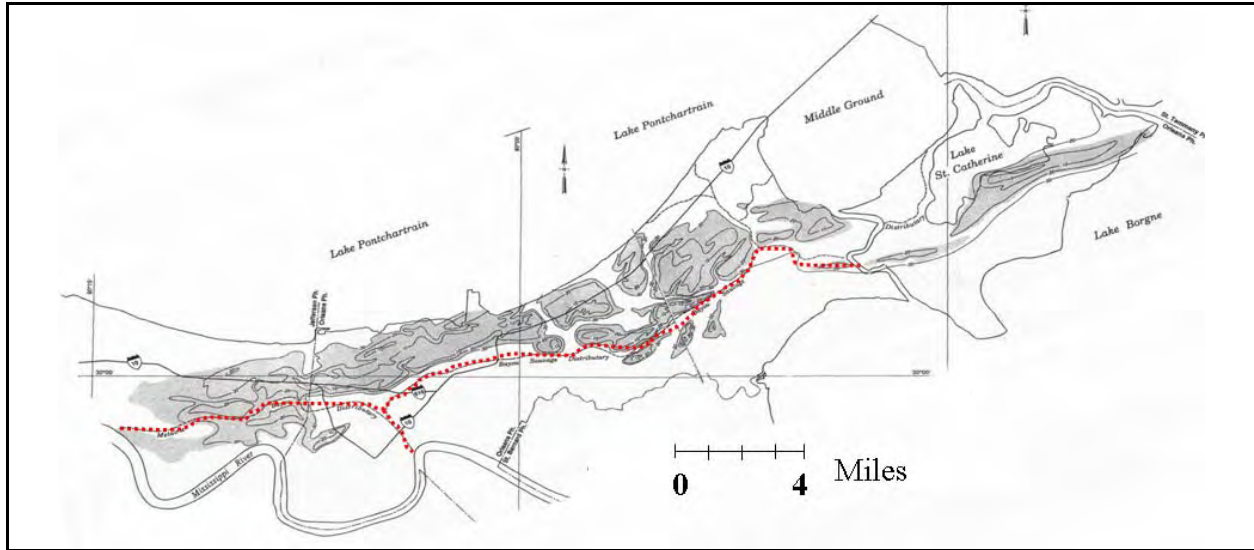


Figure K1-4a. Pine Island buried beach complex in the New Orleans Area (from Saucier 1994). Course of Bayou Sauvage (i.e., Bayous Metairie and Gentilly) identified in red. Note the presence of the barrier beach prevented this distributary course from extending northward into present day Lake Ponchartrain and filling the lake. Canal breaches are identified in blue with 17th Street breach behind the thickest part of the beach ridge, while both the London North and South breaches are on the axis of the barrier. See Figure K1-3b for close-up of canal areas.

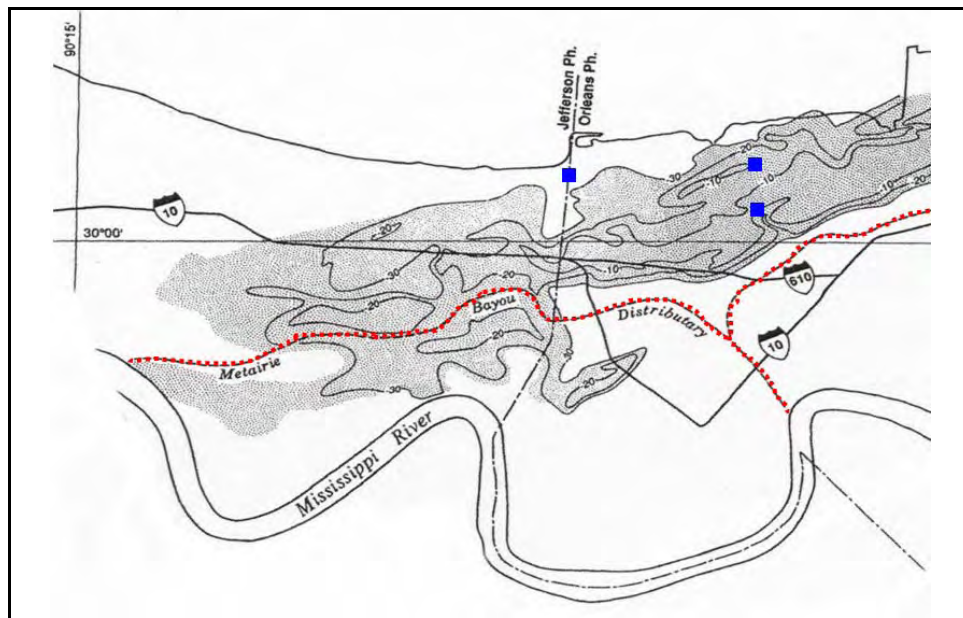


Figure K1-4b. Close-up view of the buried beach ridge, and the locations of the canal breaches to the buried beach (after Saucier 1994). The 17th Street breach is located behind the axis of the beach ridge while the London Canal breaches are located on the axis of the ridge. Bayou Metairie is identified in red and forms the Bayou Sauvage distributary course (No. 11) in Figure K1-2

Surface and Subsurface Geology of the New Orleans Area

A geologic map of the New Orleans area is presented in Figure K1-5 and identifies the major environments of deposition at the surface in the vicinity of the 17th Street, Orleans, and London Avenue canals. Located on the surface of the New Orleans area are natural levee and point bar deposits adjacent to the Mississippi River, abandoned distributary courses (Bayou Sauvage-Metairie north of the Mississippi River and Bayou des Familles south of the Mississippi River, respectively), and extensive marsh-swamp deposits at the surface (see also Figure K1-3). Land reclamation occurred in the 1920's along the shore of Lake Ponchartrain by dredging, and this area is identified as spoil deposits.

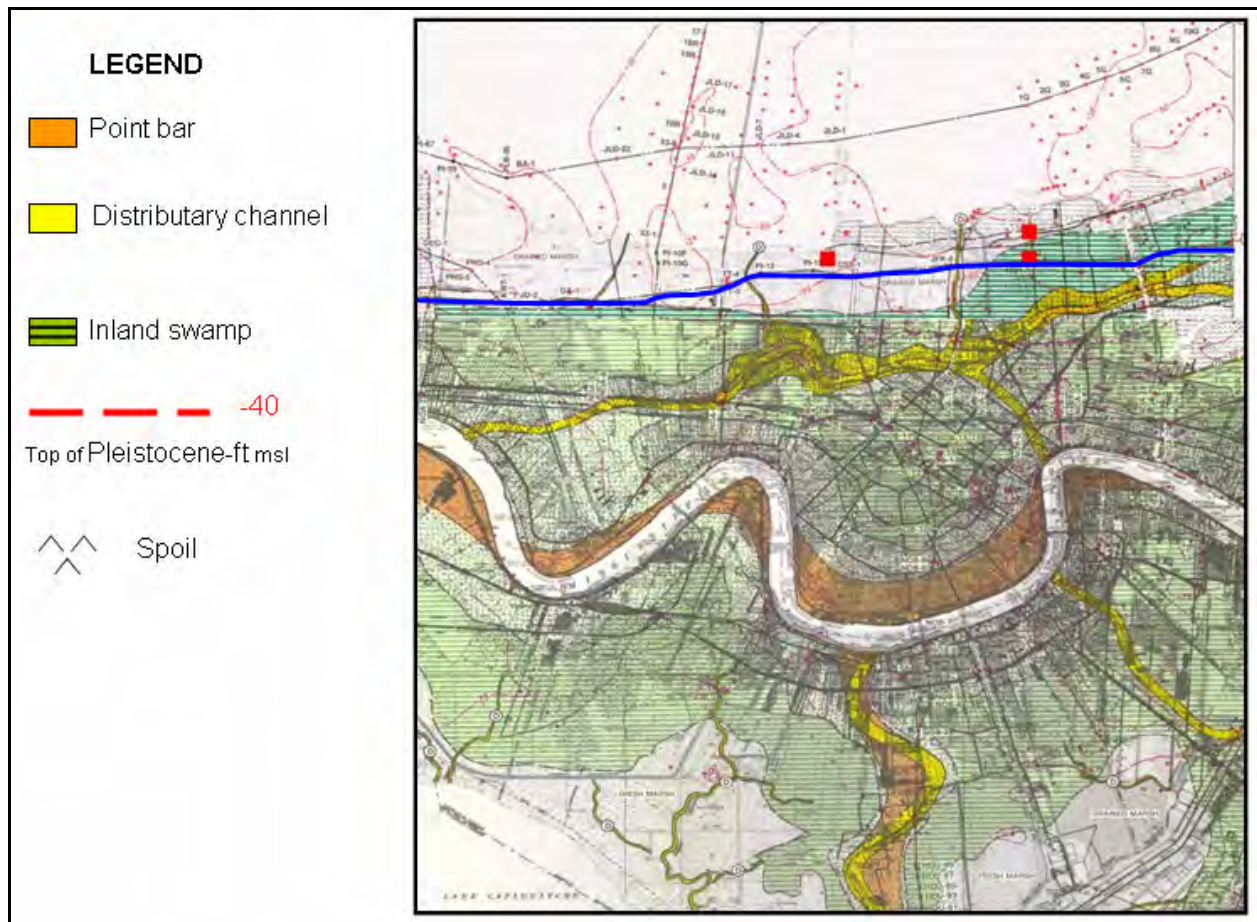


Figure K1-5. Geology map of the New Orleans and Spanish Fort Quadrangles showing the distribution of environments at surface. Elevation of the Pleistocene surface shown in red along with borings used to map this surface. Cross-section C-C' in blue extends through 17th Street and London Canal Areas (areas identified in red). See website lmvmapping.erd.c.usace.army.mil for nearby maps and other cross-sections identified. Portion of cross-section C-C' above is presented as Figure K1-6 (from Dunbar and others 1994 and 1995)

A portion of cross-section C-C from the Spanish Fort Quadrangle is presented as Figure K1-6 to identify the general subsurface stratigraphy beneath the 17th Street and London canal breaches. Boring data from this section

identify distinct depositional environments in the subsurface that are stacked vertically and form a stratigraphic record of the filling history during the Holocene period. Major stratigraphic units in the subsurface, beginning with the oldest, include the Pleistocene (older fluvial and deltaic deposits), bay sound/estuarine, relic beach (Pine Island Beach ridge) lacustrine/interdistributary, and marsh/swamp deposits. A summary description of the different depositional environments in the New Orleans area is presented in Appendix A (from Dunbar, Torrey, and Wakeley, 1999). Additionally, detailed descriptions of the different depositional environments are contained in Saucier (1994), Kolb (1962), and Kolb and Van Lopik (1958).

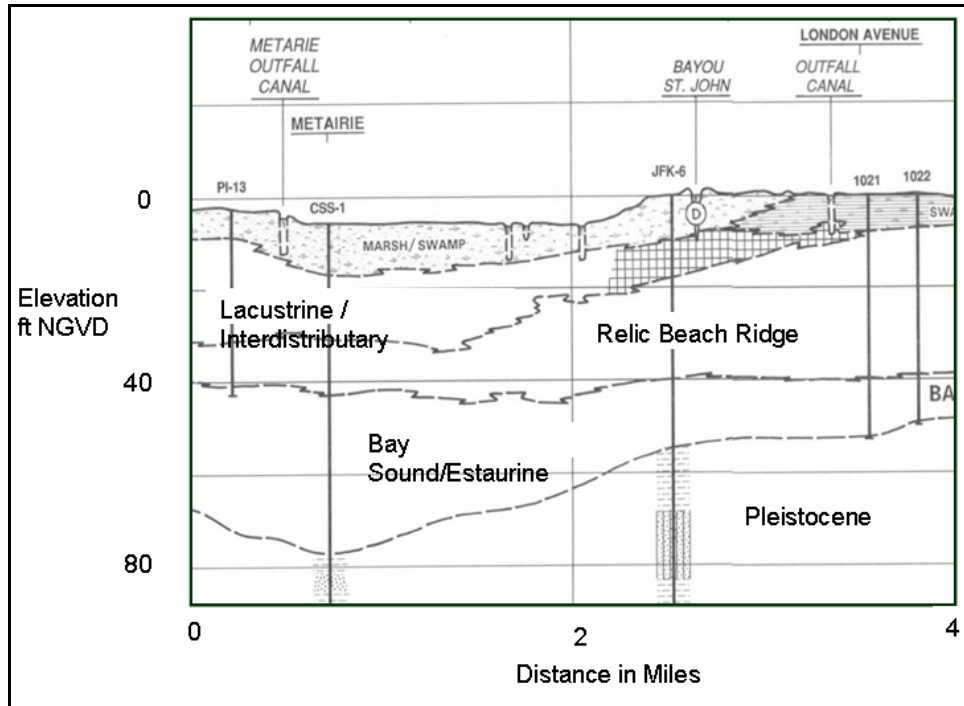


Figure K1-6. Portion of cross section C-C" from the Spanish Fort Quadrangle which extends through the 17th and London Canal breaches and identifies the stratigraphic environments in the subsurface (from Dunbar and others 1995)

Besides mapping the horizontal and vertical limits of the various environments of deposition, relationships between these environments and key engineering properties of the respective soils have been developed. These relationships have been tabulated and are published in Kolb (1962), Montgomery (1974), and Saucier (1994). A summary of these engineering relationships is presented in Appendix A. Similarly, relationships have been developed from the engineering properties and laboratory soil test data from 17th Street, Orleans, and London Avenue canals. These data are presented in later sections of this summary as related to discussions of their engineering significance.

Geologic information from the New Orleans area helped the IPET focus its investigation and collection of data for the 17th Street, Orleans, and London Avenue canal breaches. An understanding of the geology was an important first

step to systematically collecting and evaluating stratigraphic and engineering data from these breach areas.

Development of Cross Sections

Pre-Katrina Sections

A significant amount of information was obtained from General Design Memorandum No. 20 – 17th Street Outfall Canal – Volume 1 (GDM No. 20) in the development of pre-Katrina cross sections. This document was completed in March 1990 in preparation for upgrading the New Orleans levee system to provide increased flood protection against a stronger revised design hurricane.

Figures K1-7 and K1-8 show longitudinal profiles of the east and west bank levees of the northern half of the 17th Street Outfall canal, respectively. These figures, obtained from GDM No. 20, show boring locations and the soil types obtained during the explorations for the project upgrade. It is noted that odd numbered borings are located on the west bank, and even numbered borings are located on the east bank. Noted on the figures is the location of the breach site which is situated on the east bank of the canal between Stations 560+50 and 564+50.

A more detailed representation of the soil stratigraphy profile along the centerline in the breach area is shown in Figure K1-9. This profile was constructed using additional soil data acquired during the post-Katrina soil exploration conducted during September through October 2006. The additional borings included B1, B2, B3, B4, B5, NO-1-05U, and NO-2-05U. A plan view showing the locations of both old and new borings is shown in Figure K1-10. The new borings were needed because only the two old borings, B62 and B64 (reported in GDM No. 20), were in the immediate vicinity of the breach. The new borings extended the depth of the investigation in this area from approximately Elevation -50 ft NGVD to Elevation -115 ft NGVD. Additionally, data from cone penetration testing, from the new exploration program, were used to supplement soil data from the old and new borings and refine the stratigraphy in the breach area. Since the levee was destroyed in the breach area during the storm, the new borings, B1 through B4, were drilled from a barge in the canal and were offset from the centerline. Data acquired from these borings were projected back to the centerline in an effort to improve the interpretation of the stratigraphy.

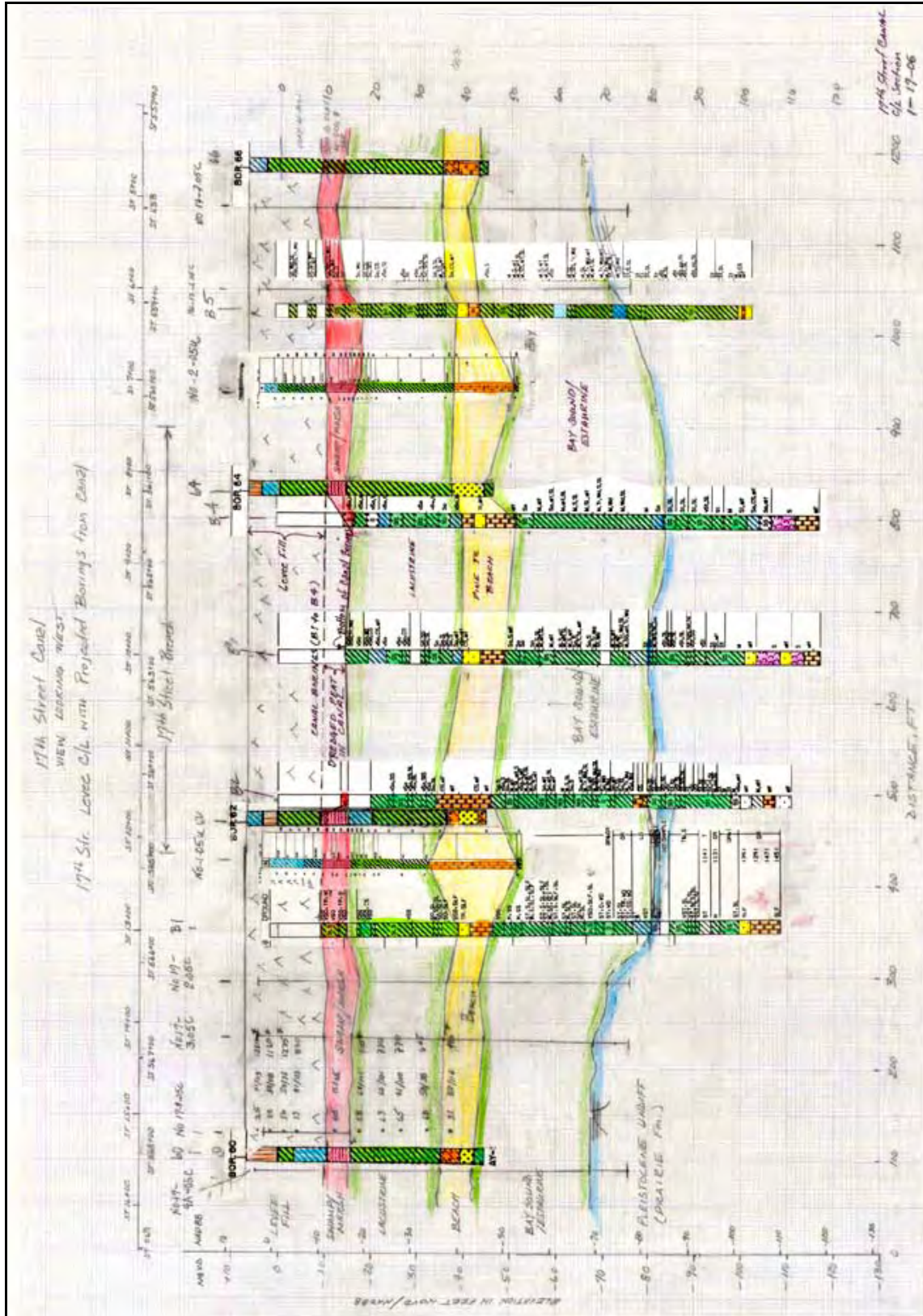


Figure K1-9. Centerline (CL) Cross-section of Breach



Figure K1-10. Boring and CPT Location Map

The information presented on Figure K1-9 yielded the following interpretation of the subsurface stratigraphy in the breach area. The subsurface in the breach area was simplified into six basic groups of soil types over the depth of the investigation:

Layer	Approximate Elevation of Top of Layer, ft (NGVD)	Approximate Elevation of Bottom of Layer (NGVD)	Soil Type	Consistency
Embankment	6.5	-10	Clayey (CL's and CH)	Stiff
Marsh	-10	-15	Organic/Peat	Very Soft
Lacustrine	-15	-35	Clays (CH)	Very Soft
Beach Sand	-35	-45	Sand	
Bay Sound/Estuarine	-45	-75	Clayey (CH)	Stiff to V. Stiff
Pleistocene (Undifferentiated) Prairie Formation	-75		Clays – Generally CH with some sand	Stiff

An additional word about the Marsh deposit may be useful. The marsh is represented as an organic soil and a peat-type material. Examination of the drilling logs suggests that since wood was encountered at the top part of the layer, this layer may be more fibrous near the top and more amorphous at the bottom of the layer. Further investigation of the peat layer may be necessary to better quantify the differences between the top and bottom of the layer.

Transverse Cross Sections through the Breach Site

Three representative transverse cross sections through the levee breach site were prepared from the data at hand. These three sections were developed from Station 8+30, Station 10+00, and Station 11+50. Station 8+30 is the most northerly station of the three. These cross sections were prepared with the intent that they represent the conditions that existed *immediately before* the arrival of Katrina. Data from a pre-Katrina airborne LIDAR (Light Detection and Ranging) survey on the New Orleans Levee System that was conducted during the year 2000 were used to improve the surface topography in the breach area from that presented in the GDM No. 20 and the design documents. The LIDAR data is the best data available for establishing the cross sections before Katrina, because accurate ground survey data were not available during the preparation of this report. The surveys generate points of X, Y, and Z data that are accurate to the nearest foot. A typical LIDAR section is shown in Figure K1-10. The LIDAR surveys were particularly useful in establishing the levee dimensions, slope, and toe elevations on the protected side of the floodwall. Unfortunately, the LIDAR system cannot penetrate through water, so it was not possible to use this technology to acquire the ground topography in the canal. A hydrographic survey was obtained *immediately after* Katrina, on August 31, 2006, to obtain the surface elevations of the canal between the floodwalls on the east and west banks. The data obtained from the hydrographic surveys are reflected in the cross-sections described in the next paragraph.

The three representative cross sections for Station 8+30, Station 10+00, and Station 11+50 are shown in Figures K1-11, K1-12, and K1-13, respectively. Three sections were prepared because the levee dimensions are variable in the

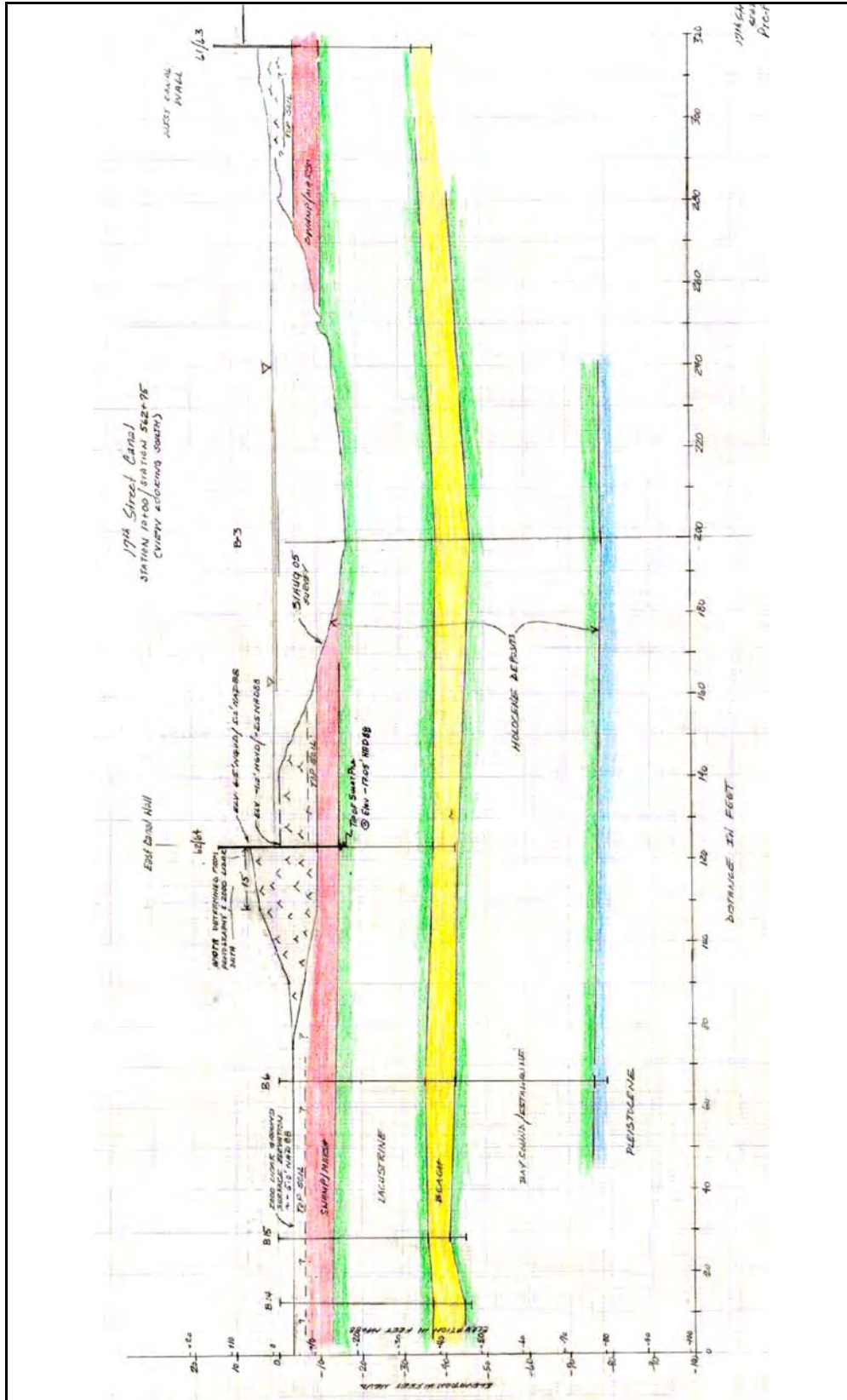


Figure K1-12. Prefailure Cross-Section at Sta 10+00 (New Stationing)/ Sta. 562+75 (GDM Stationing)

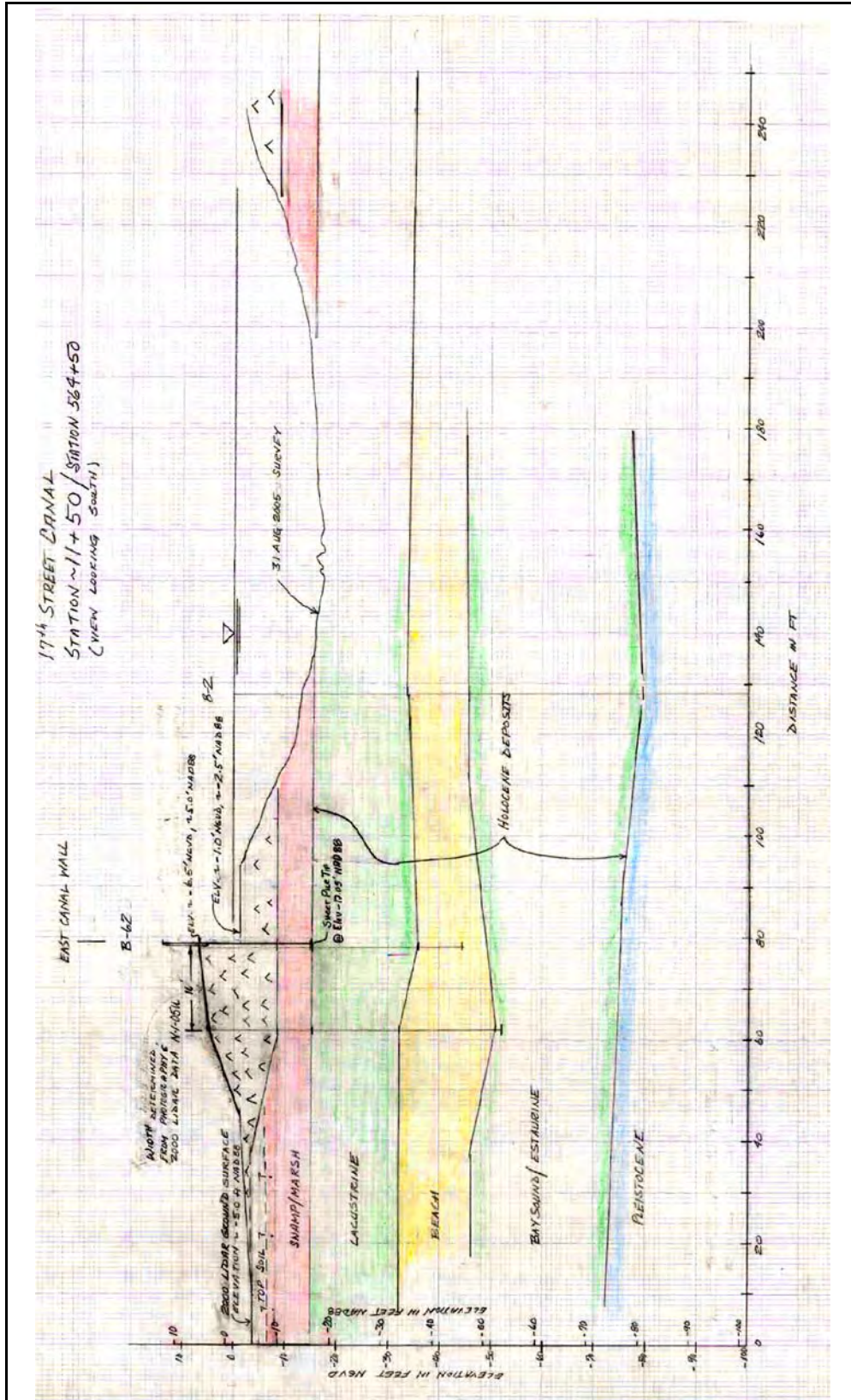


Figure K1-13. Prefailure Cross-Section at Sta. 11+50 (New Stationing)/ Sta. 564+50 (GDM Stationing) (Note: Most scour occurred near this station)

breach area on the east bank. Each cross section shows the conditions across the entire canal from the west bank to the east bank where the breach site is located. A degree of interpretation was necessary, particularly pertaining to the east bank protected side, to complete the cross sections because of the lack of soil boring data in this area. Thus, the marsh/peat layer was interpreted to be thinner under the centerline of the levee than at the toe due to consolidation from the surcharge caused by the weight of the levee. Also, an interpretation was made to include a 2- to 3-ft layer of topsoil over the top of the peat in this area. This effect may be cultural in nature because the protected side of the east bank was located in a residential area with houses having well-kept lawns.

It is also noted that the levee cross section at Station 11+50, the southernmost section of the three and shown in Figure K1-13, is the location where the post-Katrina surveys showed that the most scour occurred while water was flowing through the breach.

Uncertainties

Many uncertainties pertaining to the subsurface in the breach area will be difficult, if not impossible, to resolve because the levee in this area was destroyed and drastically changed due to emergency relief efforts. There was a lack of subsurface information on the protected side of the levee during the 1990 levee raising project described in GDM No. 20. There are efforts planned by the IPET to obtain more information in the vicinity immediately north and south of the breach area to better define soil strengths and thickness of the top soil and peat layers.

Soil Properties

Introduction

The following is a summary of the current soil data available in the breach area of the 17th Street canal. The soil's data for the breach include all borings and cone penetrometer tests (CPT) in the breach area. This area was chosen because the geology and soil types are very similar to the soil types and geology found at the breach area. The breach area and breach location are shown in Figure K1-7. In addition, some soil data from the west levee will be used for the breach area because of similar geology and soil types. This area is shown in Figure K1-8.

The stratigraphy in the breach area is divided into Levee Embankment, Marsh Stratum, Lacustrine Stratum, and Beach Sand Stratum. The data for each stratum are presented below. These data consist of GDM borings, new borings (taken in 2005), and CPTs. Testing is not complete on all of the samples from new borings. In addition, field vane shear tests and CPTs are scheduled to occur in the next couple of weeks, which will provide more data in the breach area.

Levee Embankment

Data on the levee embankment consist of five borings shown in the 1990 General Design Memorandum (GDM) and four cone penetrometer tests (CPT). Of the five GDM borings, four borings collected 3-in. (diameter) undisturbed samples, and one boring collected 5-in. (diameter) undisturbed samples. From the 3-in. samples, four unconfined compression (UC) tests were performed, and five one-point unconsolidated-undrained triaxial compression tests (UU-1), confined at existing overburden pressure, were performed. From the 5-in. samples, four one-point unconsolidated-undrained triaxial compression tests (UU-1), confined at existing overburden pressure, were performed. From these laboratory tests, moisture content and wet unit weights were determined. The moisture contents (%w) in the breach area are shown in Figure K1-14. In addition, these moisture content data were also plotted (Figure K1-15) with the moisture content data collected for the entire east levee on the canal. Also, the moisture content data for the entire west levee on the canal are shown in Figure K1-16.

The wet unit weight data in the breach area are shown in Figure K1-17. Wet unit weight data from the breach area plotted with wet unit weight data for the entire east levee are shown in Figure K1-18. Wet unit weight for the entire west levee on the canal is shown in Figure K1-19.

The undrained shear strength determined from the laboratory tests conducted on samples in the breach area is shown in Figure K1-20. Interpretation of the undrained shear strength from the CPTs using Mayne's method is plotted with laboratory test results in Figure K1-21. Interpretation of the undrained shear strength from the CPTs using the bearing capacity equation ($N_k=15$) is plotted with laboratory test results in Figure K1-22. These interpretations were provided by Dr. Thomas Brandon (Virginia Tech). Undrained shear strength data in the breach area plotted with undrained shear strength data for the entire east levee are shown in Figure K1-23. Undrained shear strength data for the entire west levee are shown in Figure K1-24.

Marsh Stratum

The data for the marsh stratum will be divided into two groups: Data on the marsh stratum under the levee embankment, and data on the marsh stratum at the toe of the levee.

Under the Levee Embankment

Data on the marsh stratum under the levee embankment consist of five borings shown in the 1990 General Design Memorandum (GDM) and four cone penetrometer tests (CPT) taken on the east levee. Of the five GDM borings, four borings collected 3-in. (diameter) undisturbed samples and one boring collected 5-in (diameter) undisturbed samples. From the 3-in. samples, five unconfined compression (UC) tests were performed. From the 5-in. samples, no shear strength data were available. From these laboratory tests, moisture content and wet unit weights were determined. The moisture contents (%w) in the breach

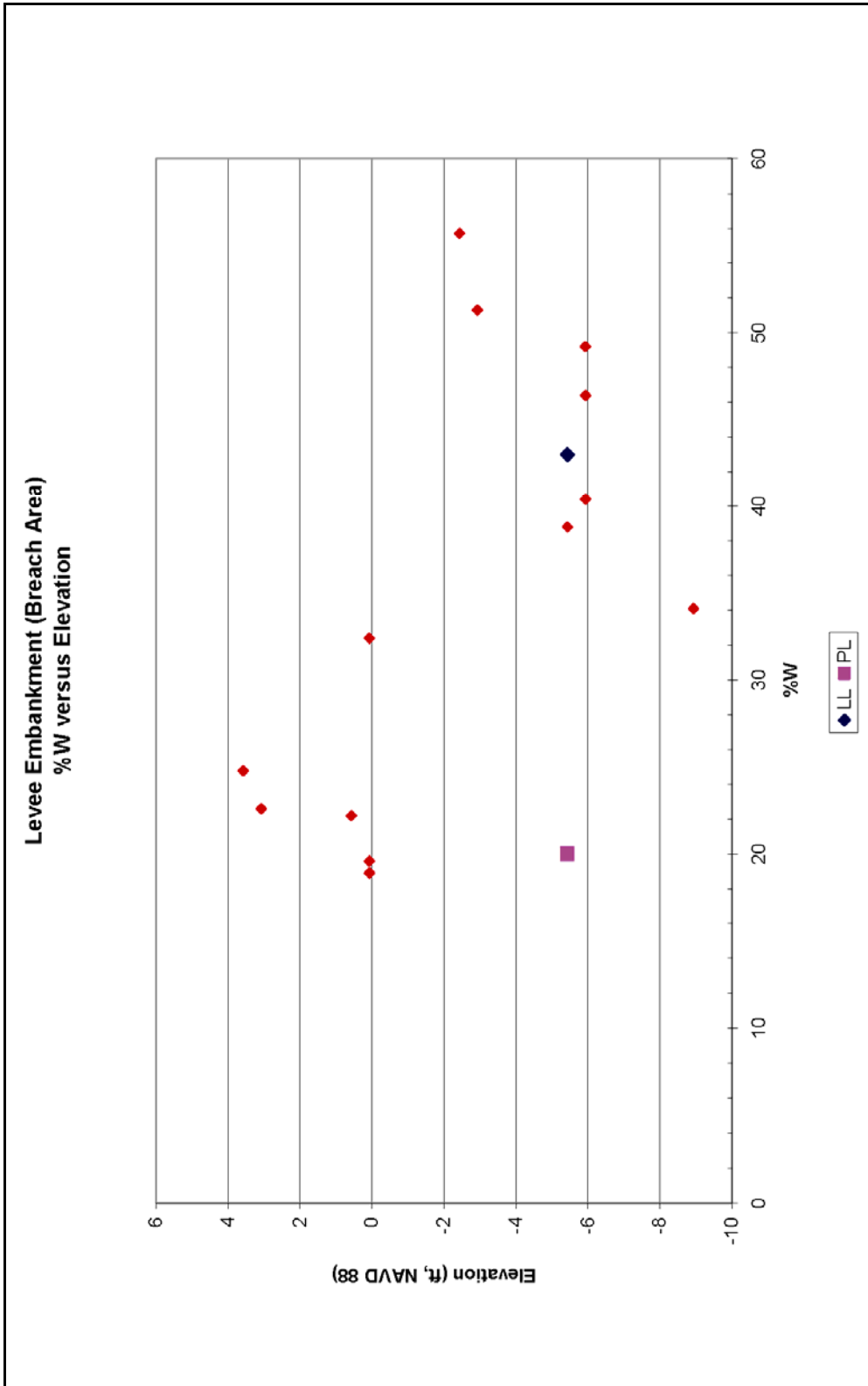


Figure K1-14. Levee Embankment (Breach Area), %w versus Elevation

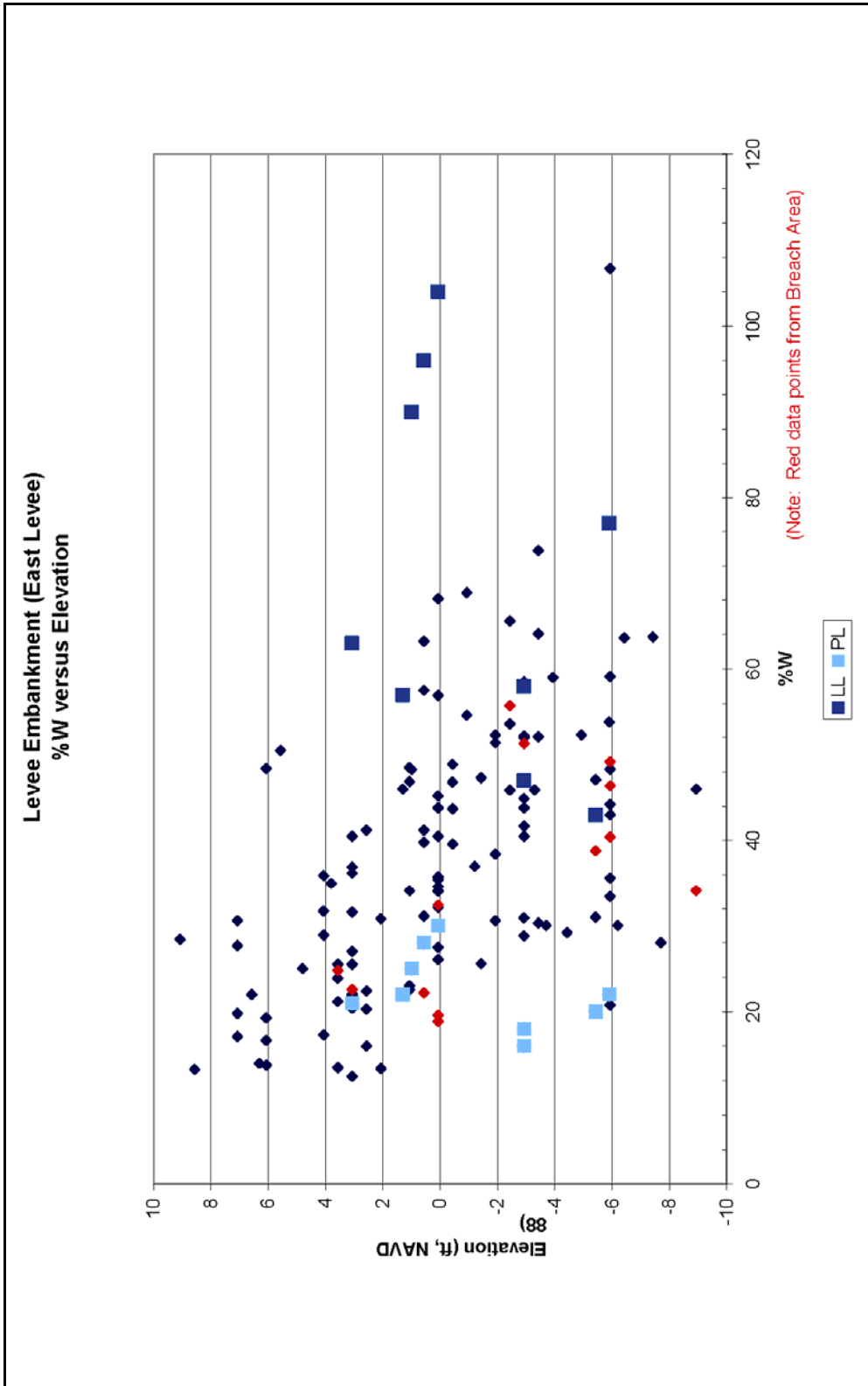


Figure K1-15. Levee Embankment (East Levee), %w versus Elevation

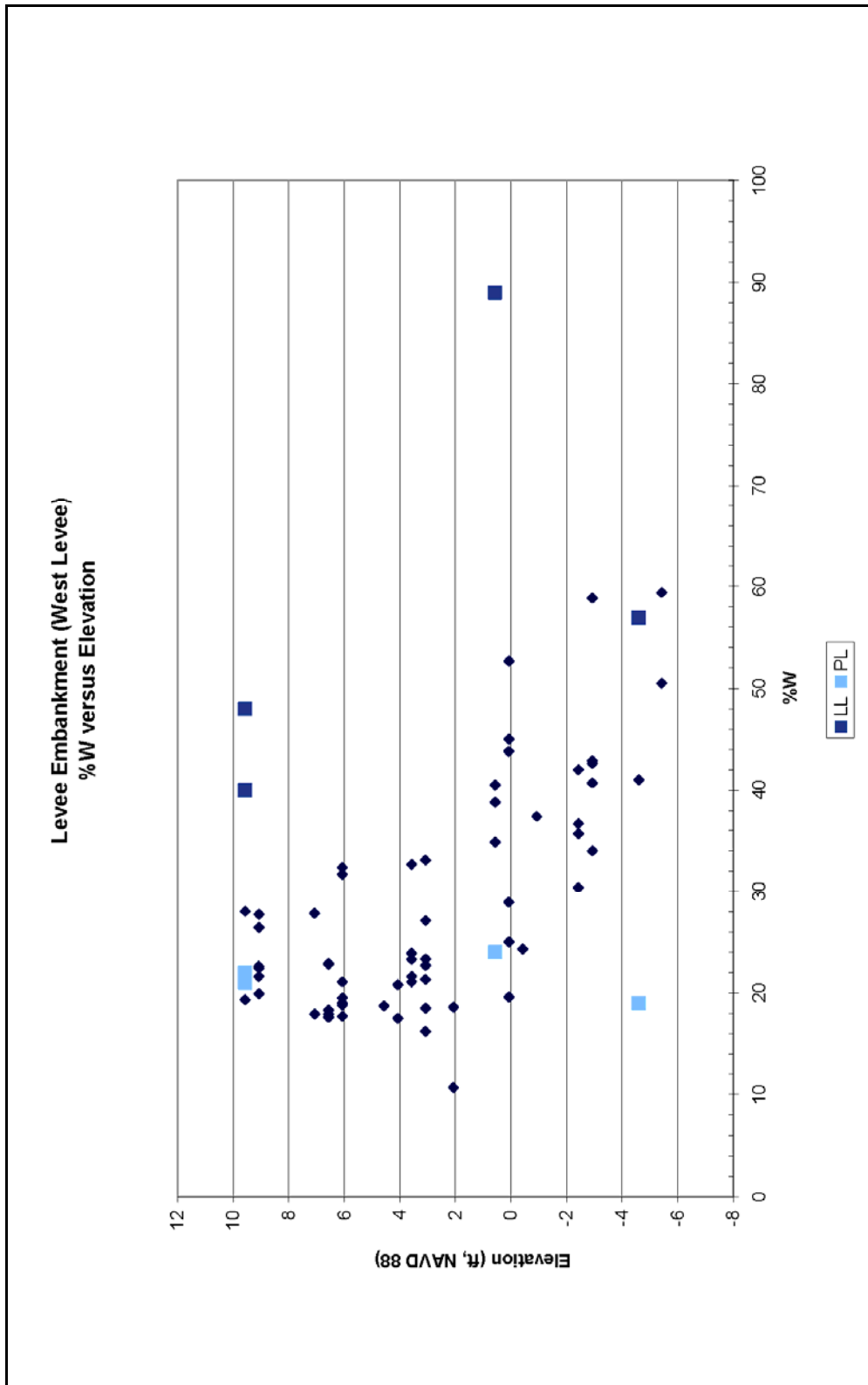


Figure K1-16. Levee Embankment (West Levee), %w versus Elevation

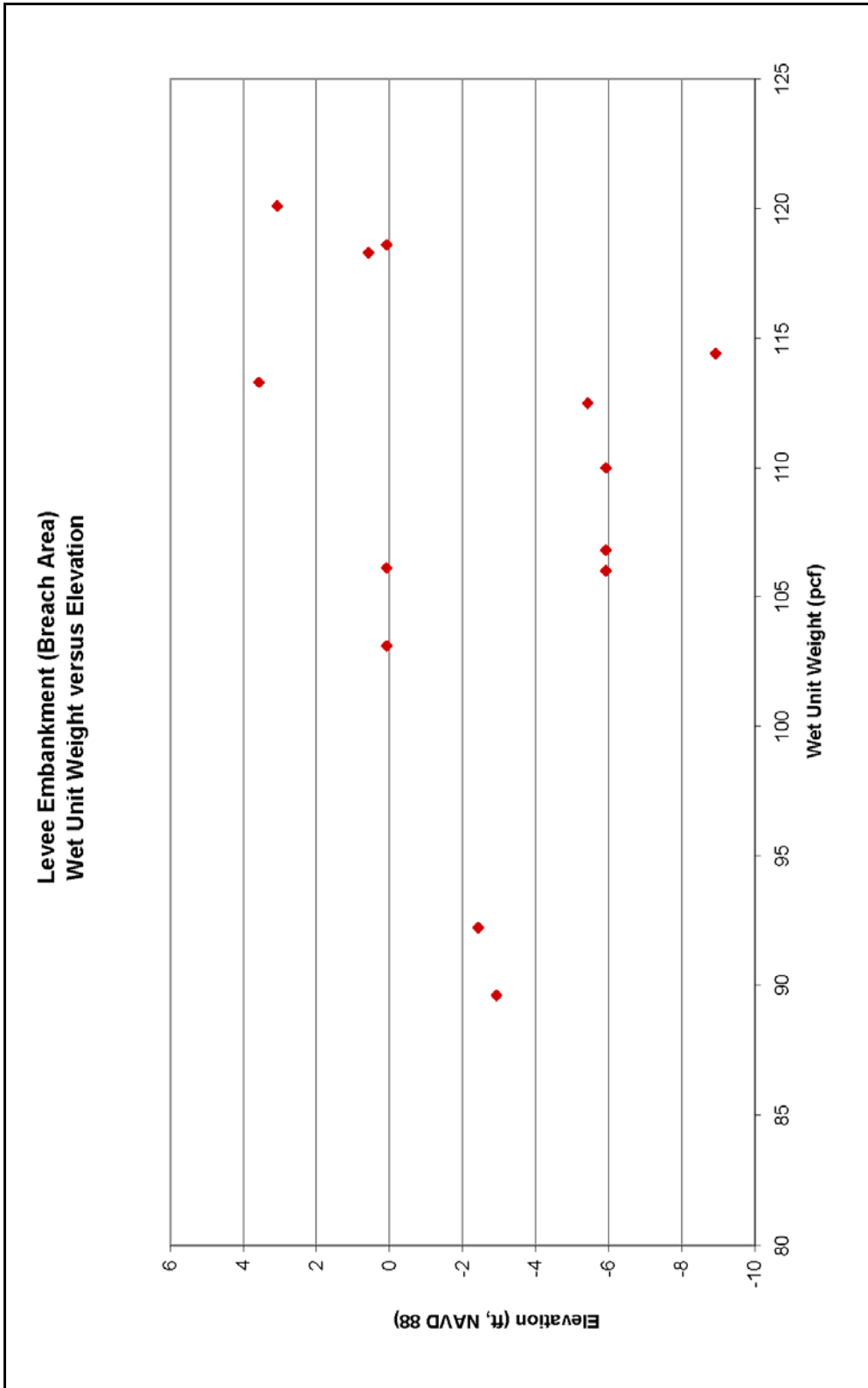


Figure K1-17. Levee Embankment (Breach Area), Wet Unit Weight versus Elevation

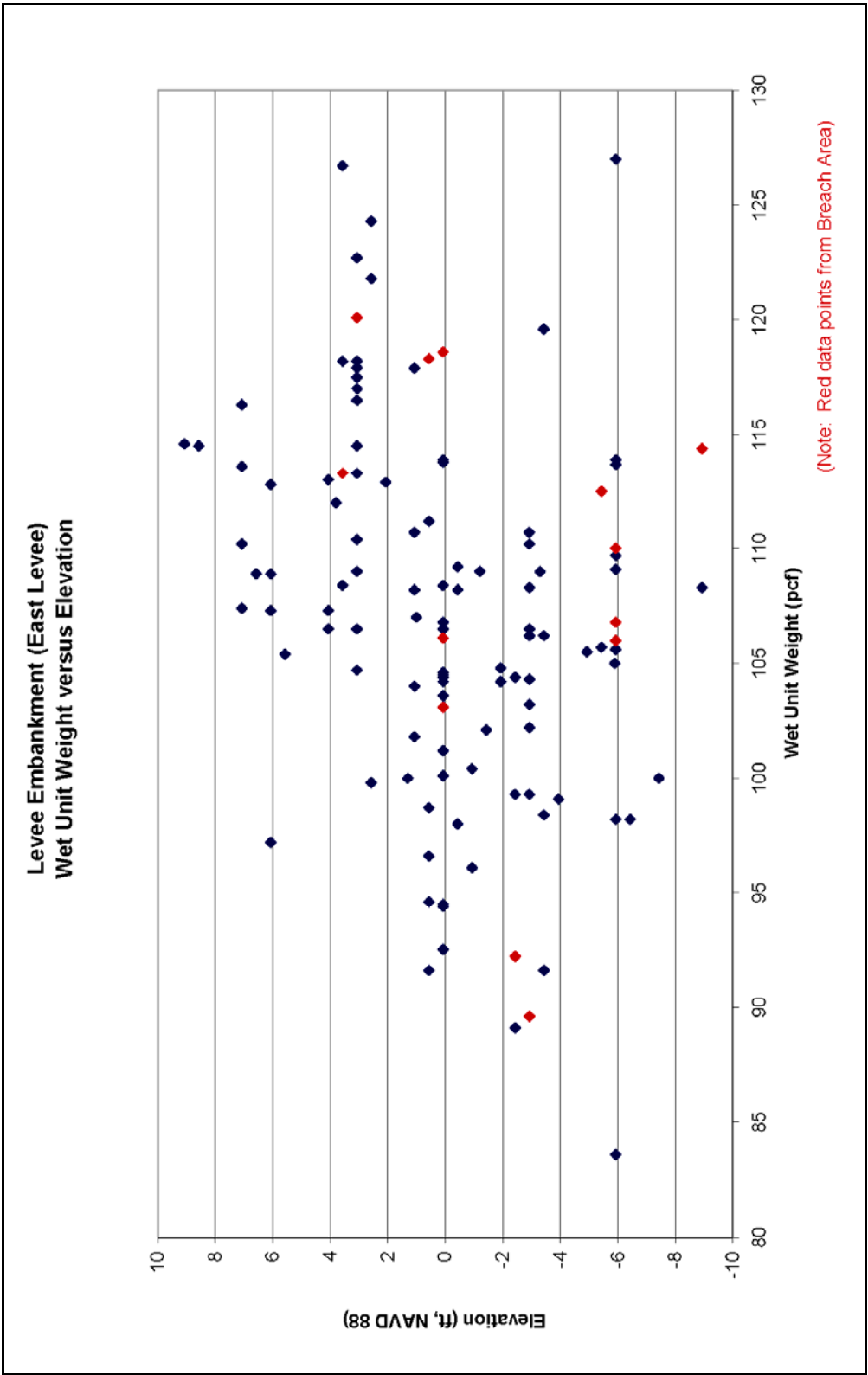


Figure K1-18. Levee Embankment (East Levee), Wet Unit Weight versus Elevation

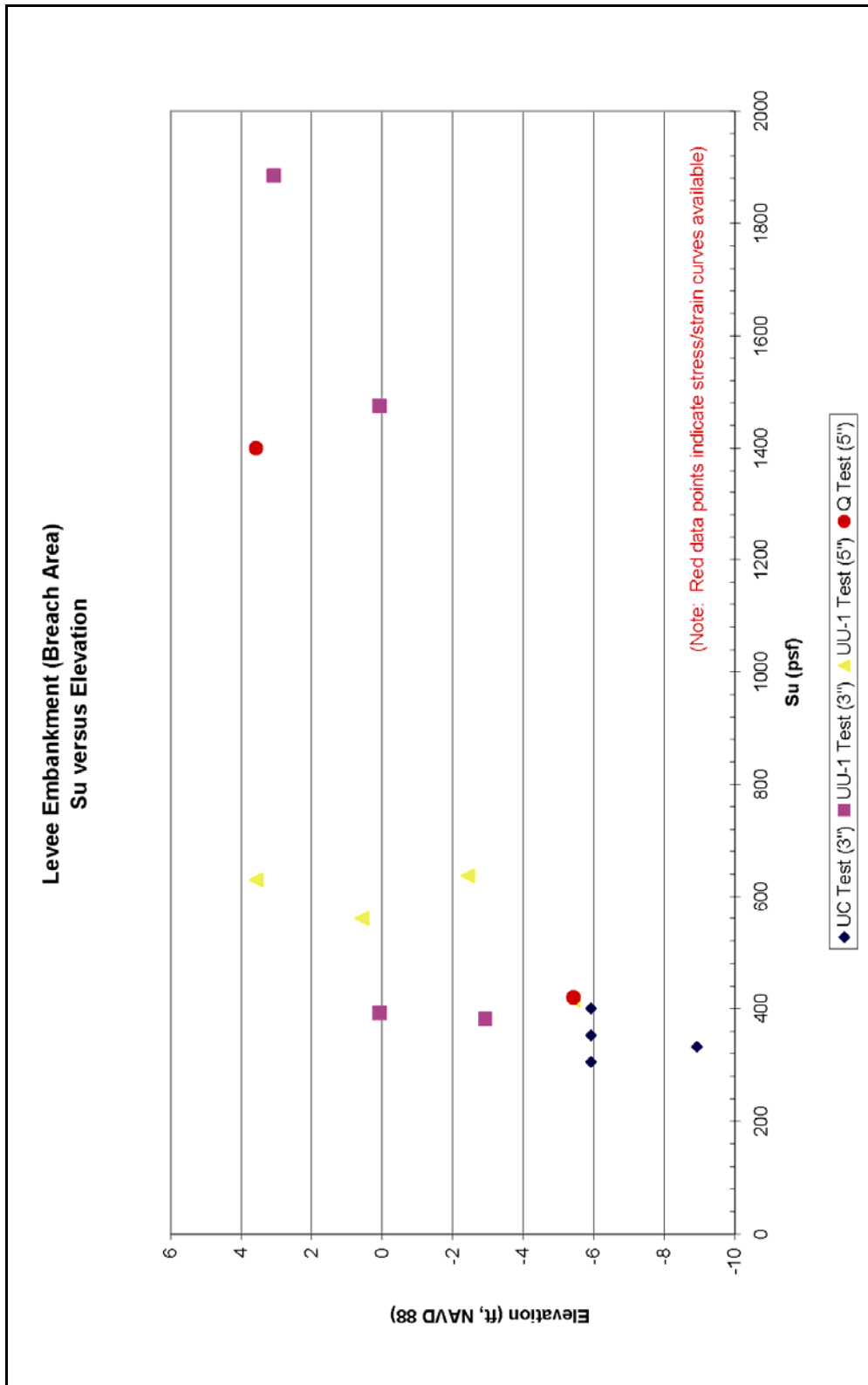


Figure K1-20. Levee Embankment (Breach Area), Su versus Elevation

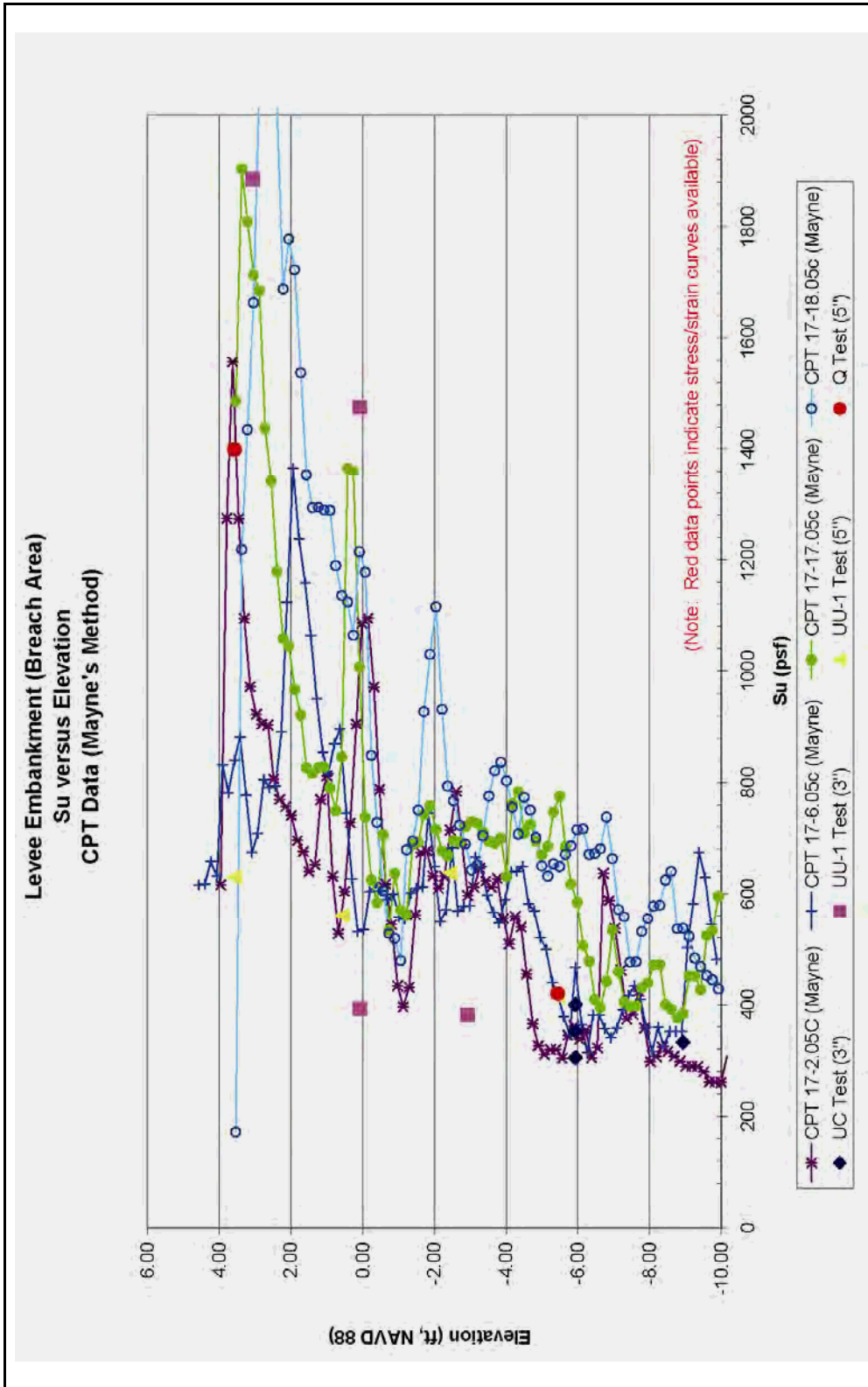


Figure K1-21. Levee Embankment, Su versus Elevation (CPT Data – Mayne's Method)

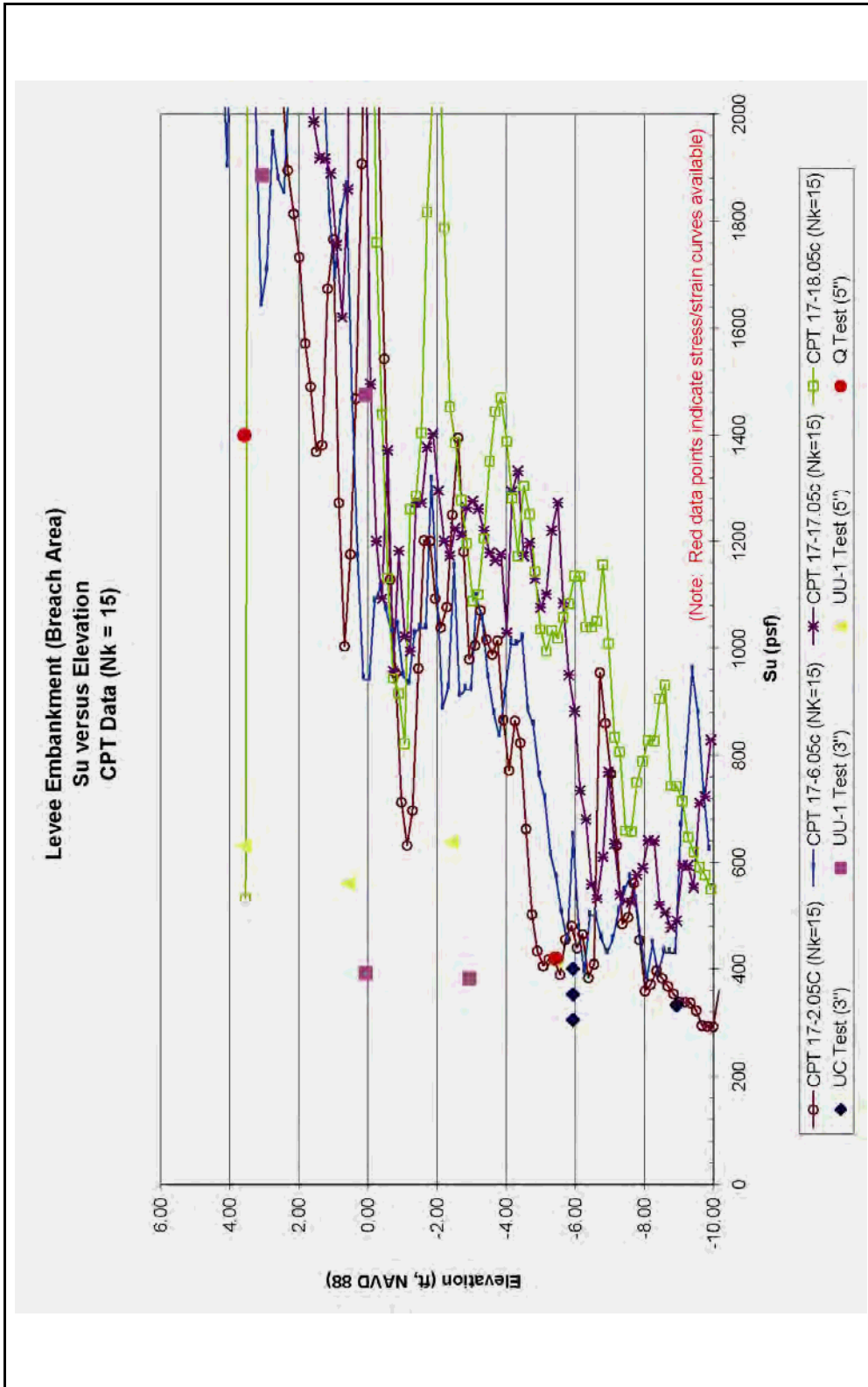


Figure K1-22. Levee Embankment (Breach Area), Su versus Elevation (CPT Data – Nk=15)

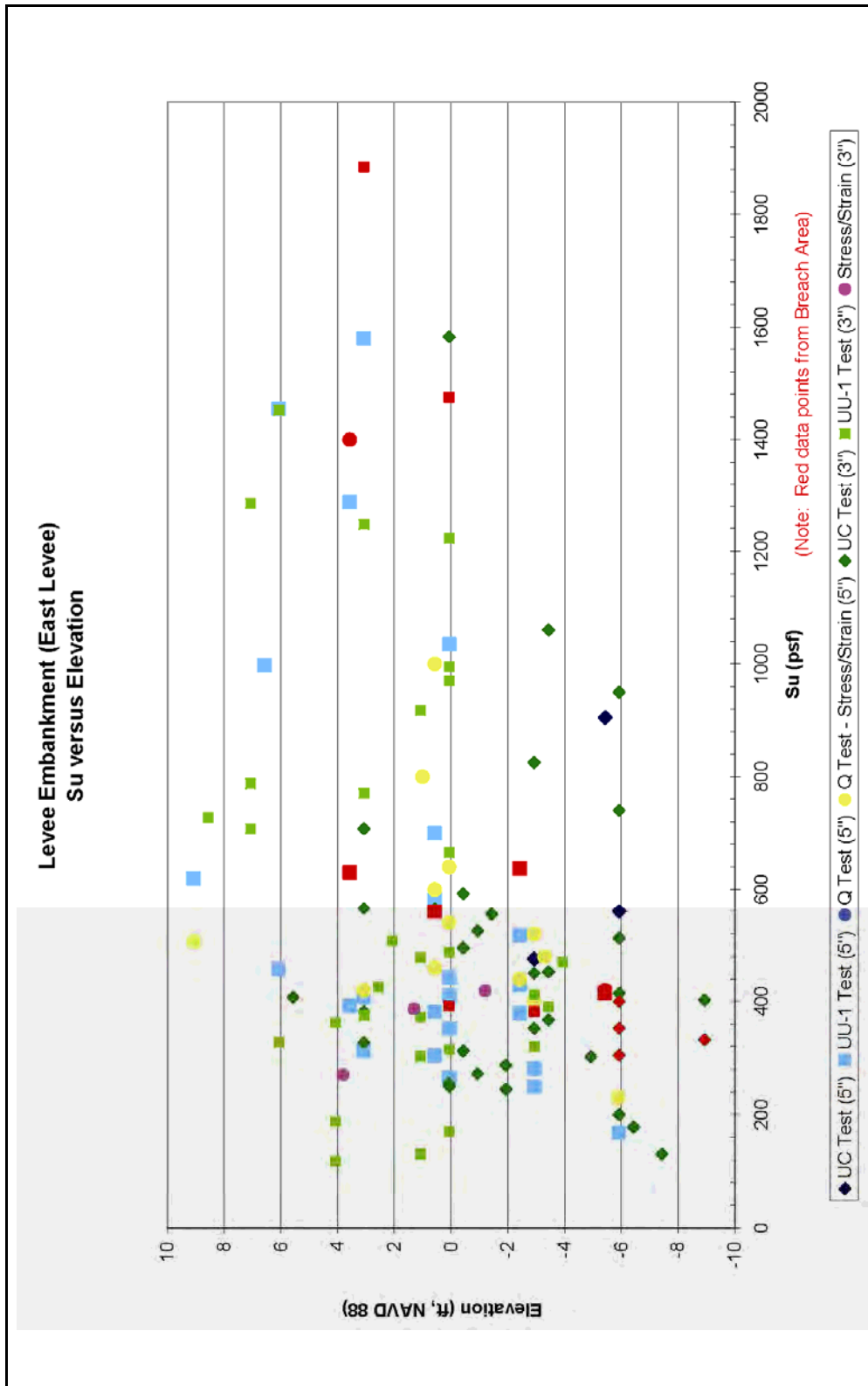


Figure K1-23. Levee Embankment (East Levee), Su versus Elevation

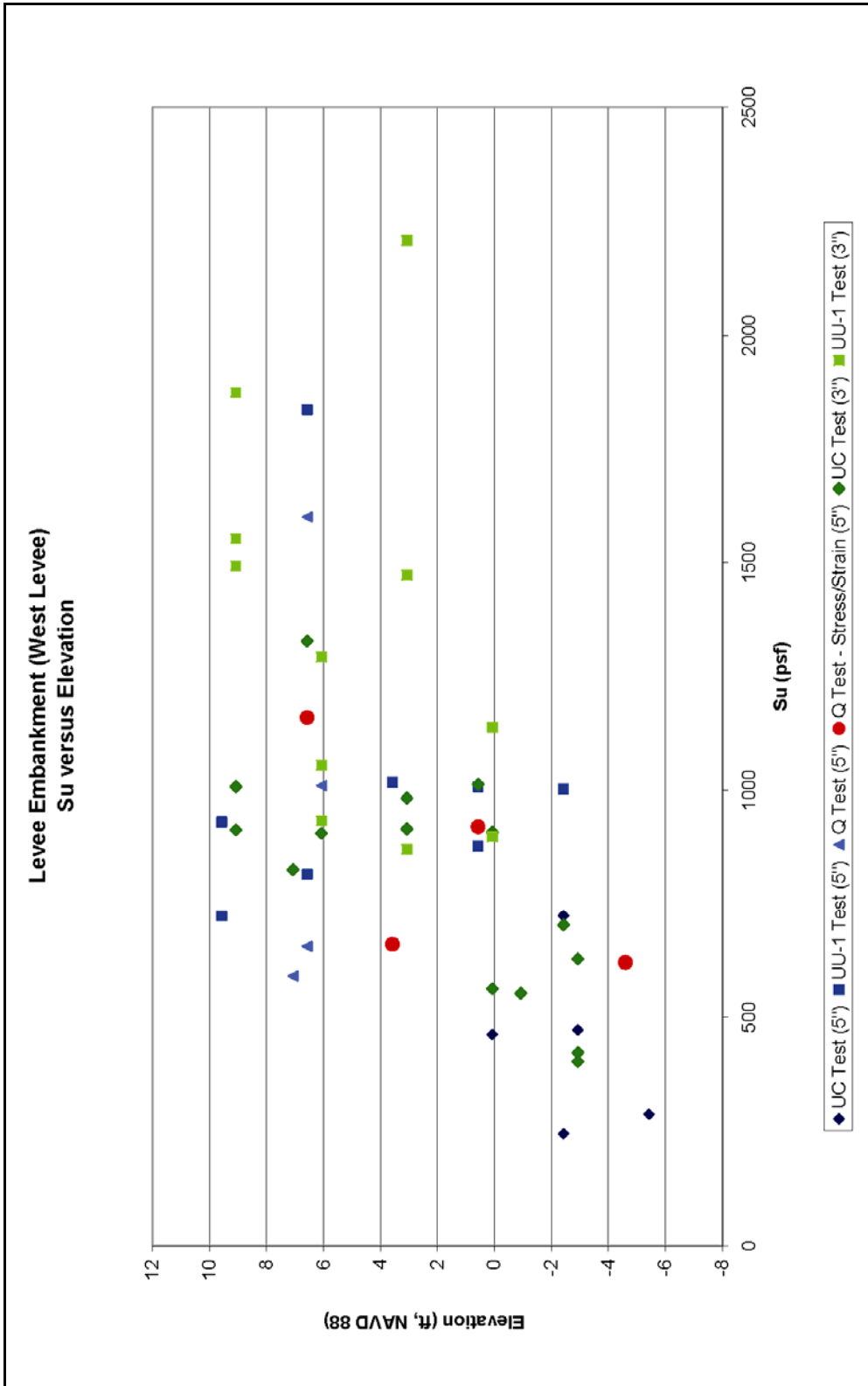


Figure K1-24. Levee Embankment (West Levee), Su versus Elevation

area are shown in Figure K1-25. In addition, this moisture content data were also plotted (Figure K1-26) with the moisture content data collected for the entire east levee on the canal. Also, the moisture content data for the entire west levee on the canal are shown in Figure K1-27.

The wet unit weight data in the breach area are shown in Figure K1-28. Wet unit weight data from the breach area plotted with wet unit weight data for the entire east levee are shown in Figure K1-29. Wet unit weight for the entire west levee on the canal are shown in Figure K1-30.

The undrained shear strength determined from the laboratory tests conducted on samples in the breach area is shown in Figure K1-31. Interpretation of the undrained shear strength from the CPTs using Mayne's method is plotted with laboratory test results in Figure K1-32. Interpretation of the undrained shear strength from the CPTs using the bearing capacity equation ($N_k=15$) is plotted with laboratory test results in Figure K1-33. These interpretations were provided by Dr. Thomas Brandon (Virginia Tech). Undrained shear strength data in the breach area plotted with undrained shear strength data for the entire east levee are shown in Figure K1-34. Undrained shear strength data for the entire west levee are shown in Figure K1-35.

At the Toe of Embankment

Data on the marsh stratum under the toe of the levee embankment consist of five borings taken in 2005 on the protected side, four borings taken in 2005 on the canal side, three borings on the west levee toe shown in the 1990 GDM. Of the borings on the protected side of the east levee, four borings collected 5-in. (diameter) undisturbed samples, and one boring collected 3-in. (diameter) undisturbed samples. Of the borings on the canal side of the east levee, three borings collected 5-in. (diameter) undisturbed samples, and one boring collected 3-in. (diameter) undisturbed samples. Of the three GDM borings taken on the protected side of the west levee, two borings collected 3-in. (diameter) samples, and one boring collected 5-in. (diameter) undisturbed samples. From the 3-in. samples, four unconfined compression (UC) tests were performed, and two one-point unconsolidated-undrained triaxial compression tests (UU-1), confined at existing overburden pressure, were performed. From the 5-in. samples, 14 UC tests were performed, and six unconsolidated-undrained triaxial compression tests (Q) were performed. From these laboratory tests, moisture content and wet unit weights were determined. The moisture contents (%w) in the breach area are shown in Figure K1-36. In addition, this moisture content data were also plotted (Figure K1-37) with the moisture content data collected for the entire east levee on the canal. Also, the moisture content data for the entire west levee on the canal are shown in Figure K1-38.

The wet unit weight data in the breach area are shown in Figure K1-39. Wet unit weight data from the breach area plotted with wet unit weight data for the entire east levee are shown in Figure K1-40. Wet unit weight for the entire west levee on the canal is shown in Figure K1-41.

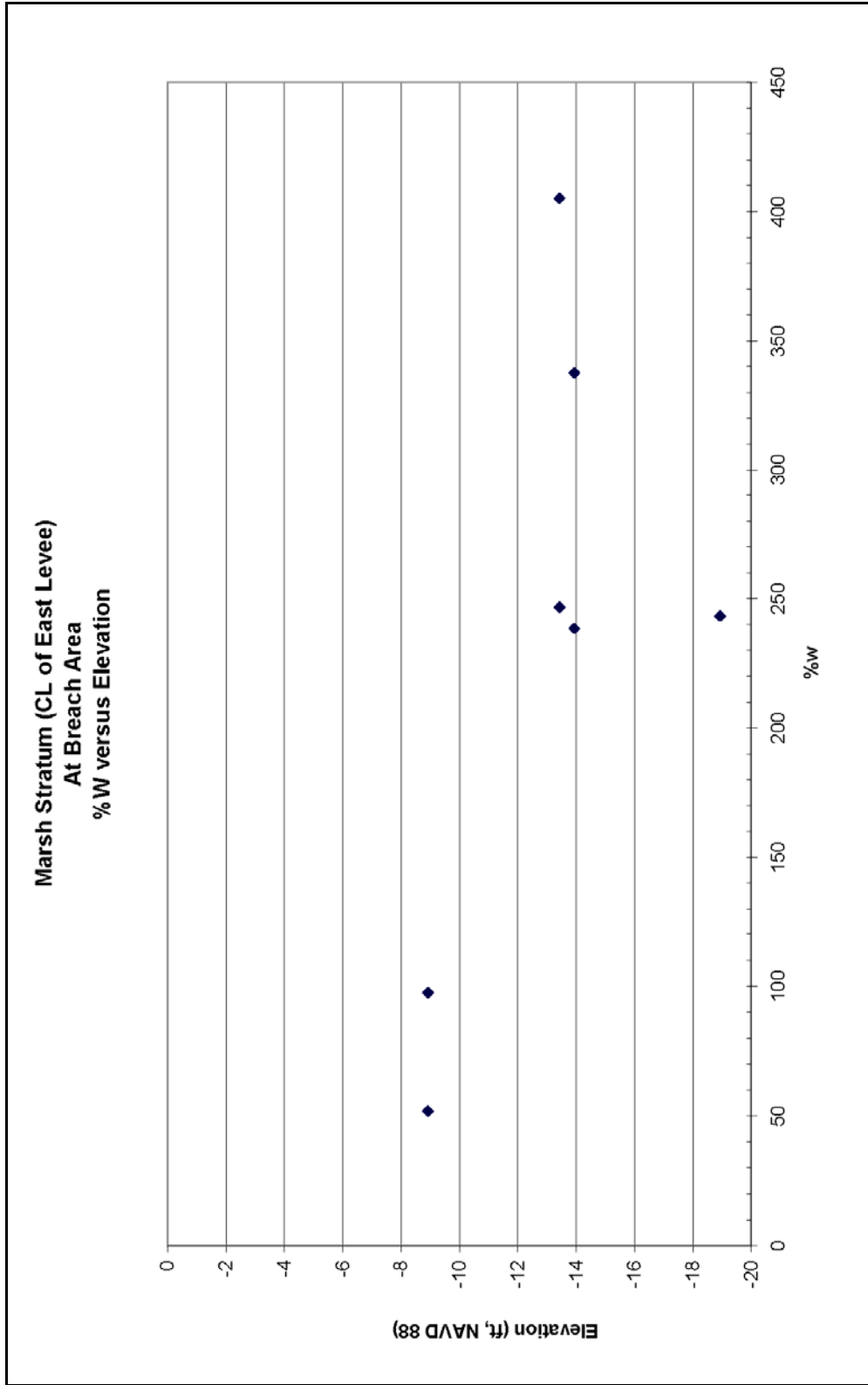


Figure K1-25. Marsh Stratum (CL of East Levee – At Breach Area), %w versus Elevation

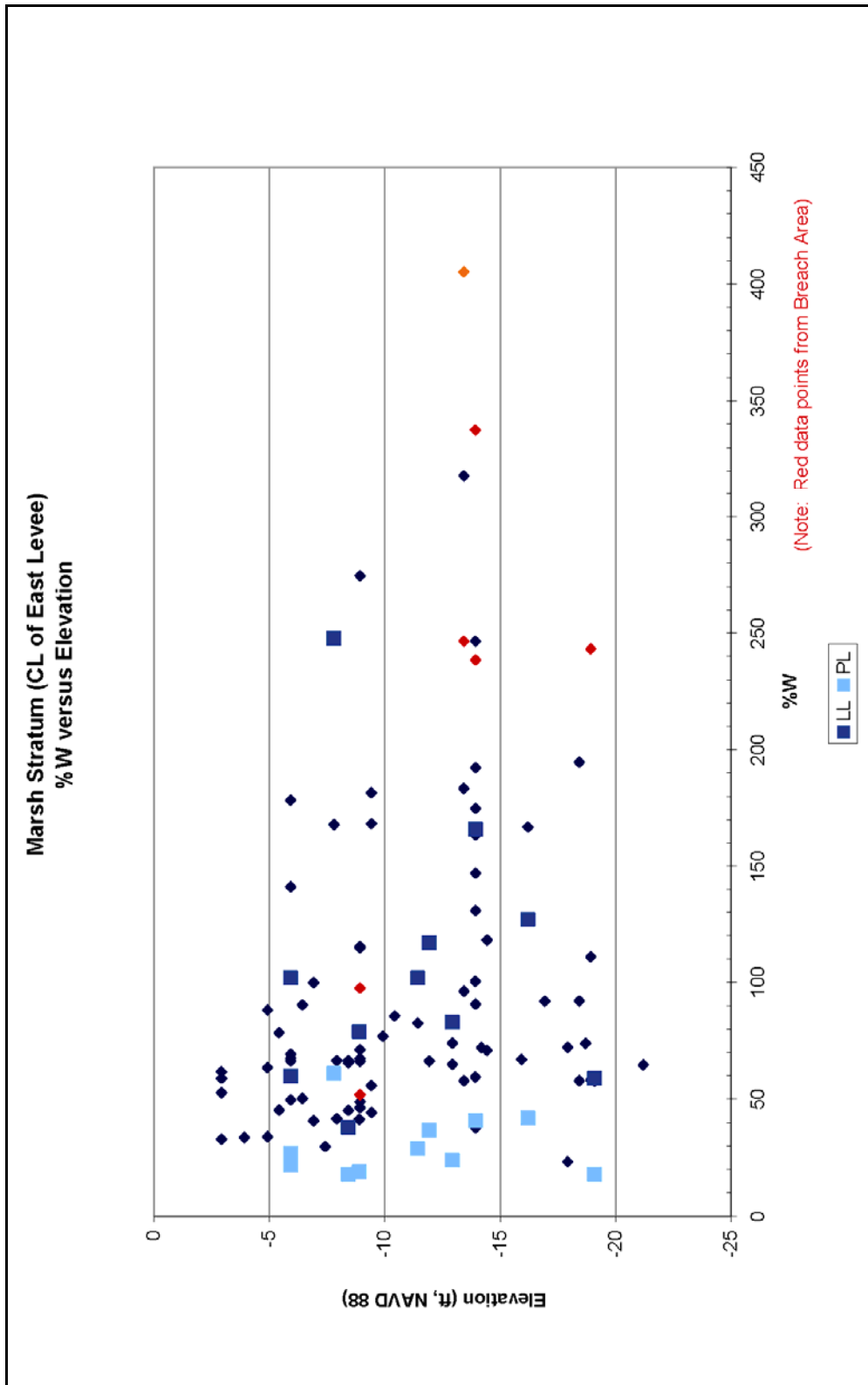


Figure K1-26. Marsh Stratum (CL of East Levee), %W versus Elevation

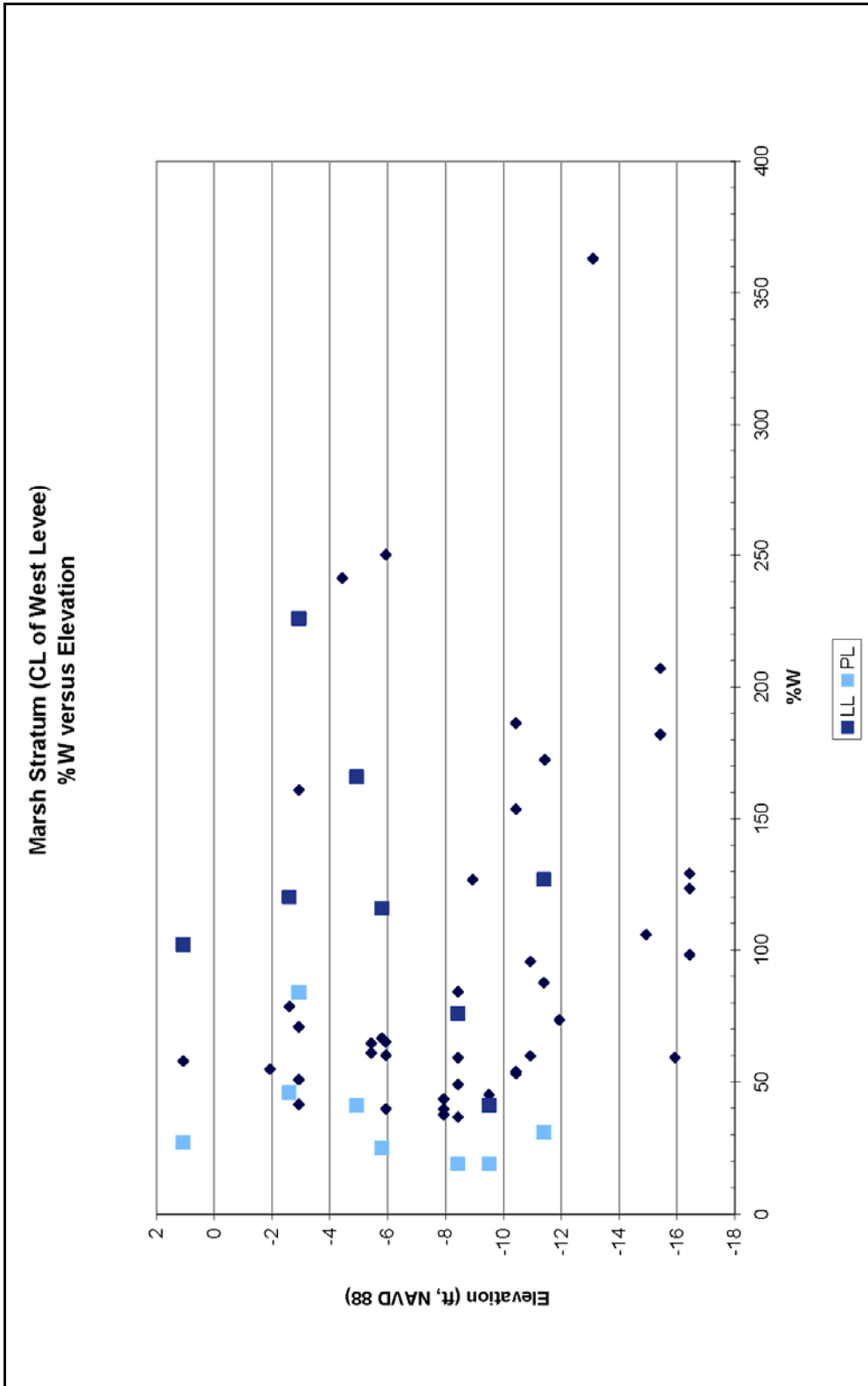


Figure K1-27. Marsh Stratum (CL of West Levee), %w versus Elevation

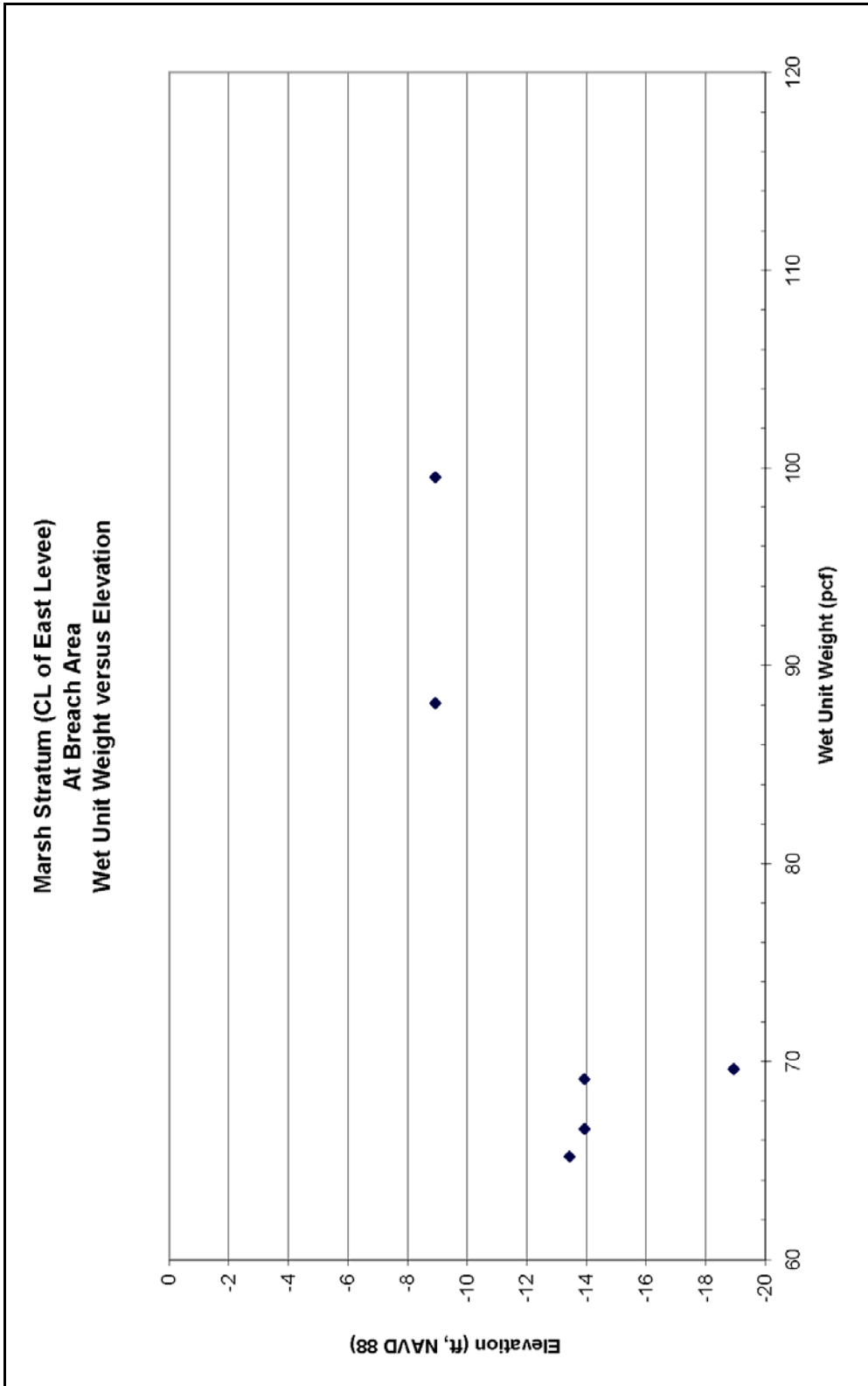


Figure K1-28. Marsh Stratum (CL of East Levee – At Breach Area), Wet Unit Weight versus Elevation

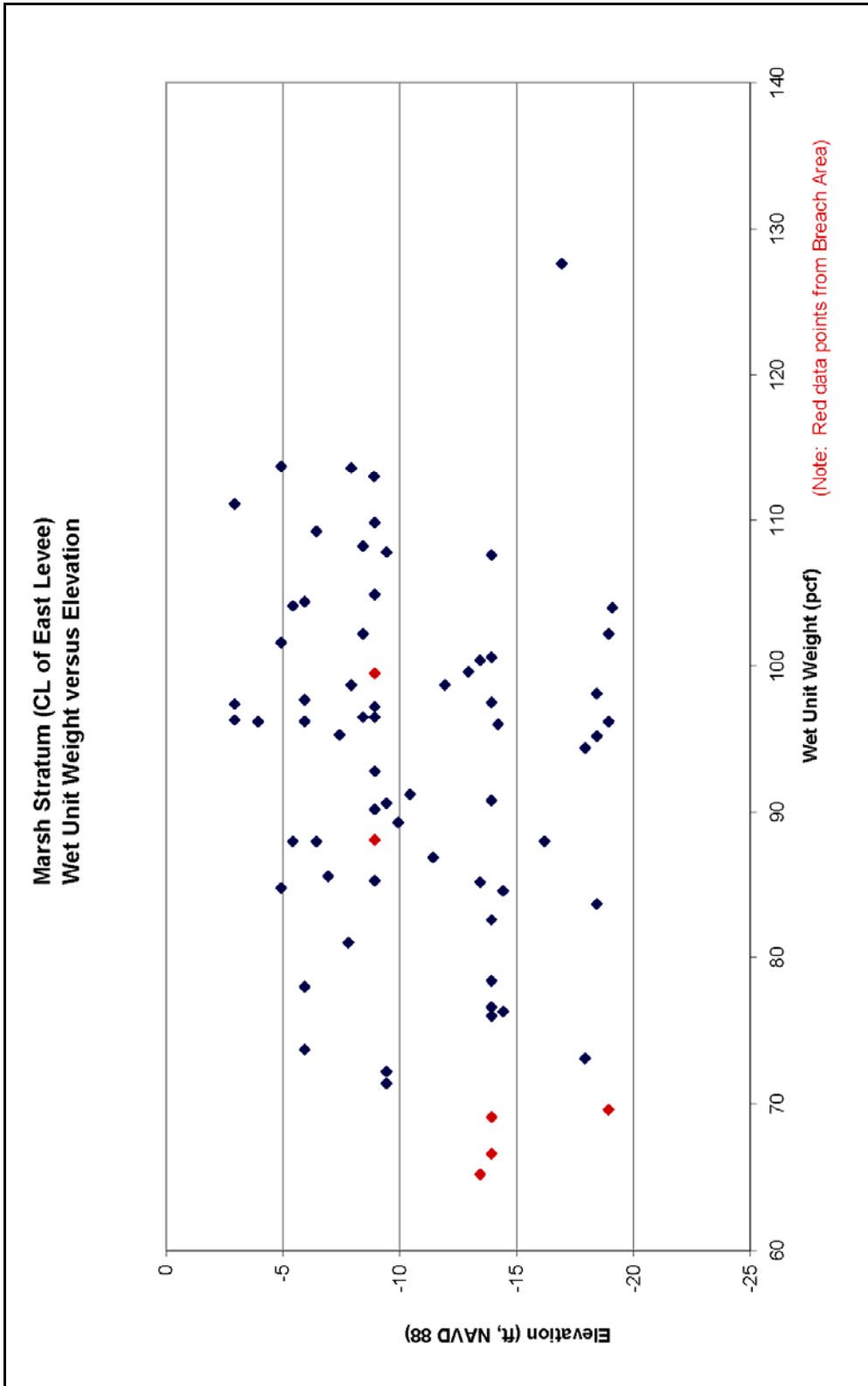


Figure K1-29. Marsh Stratum (CL of East Levee), Wet Unit Weight versus Elevation

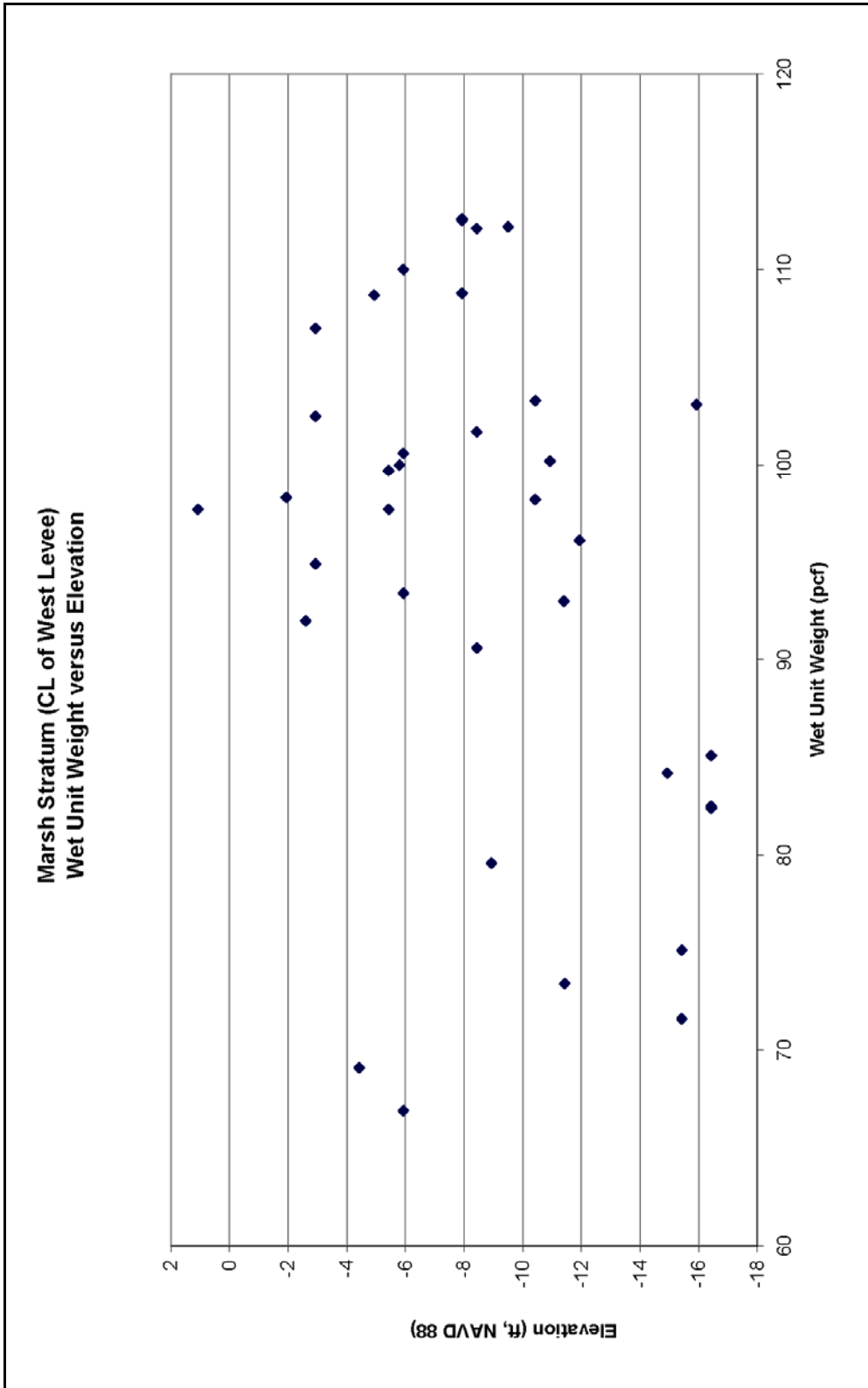


Figure K1-30. Marsh Stratum (CL of West Levee), Wet Unit Weight versus Elevation

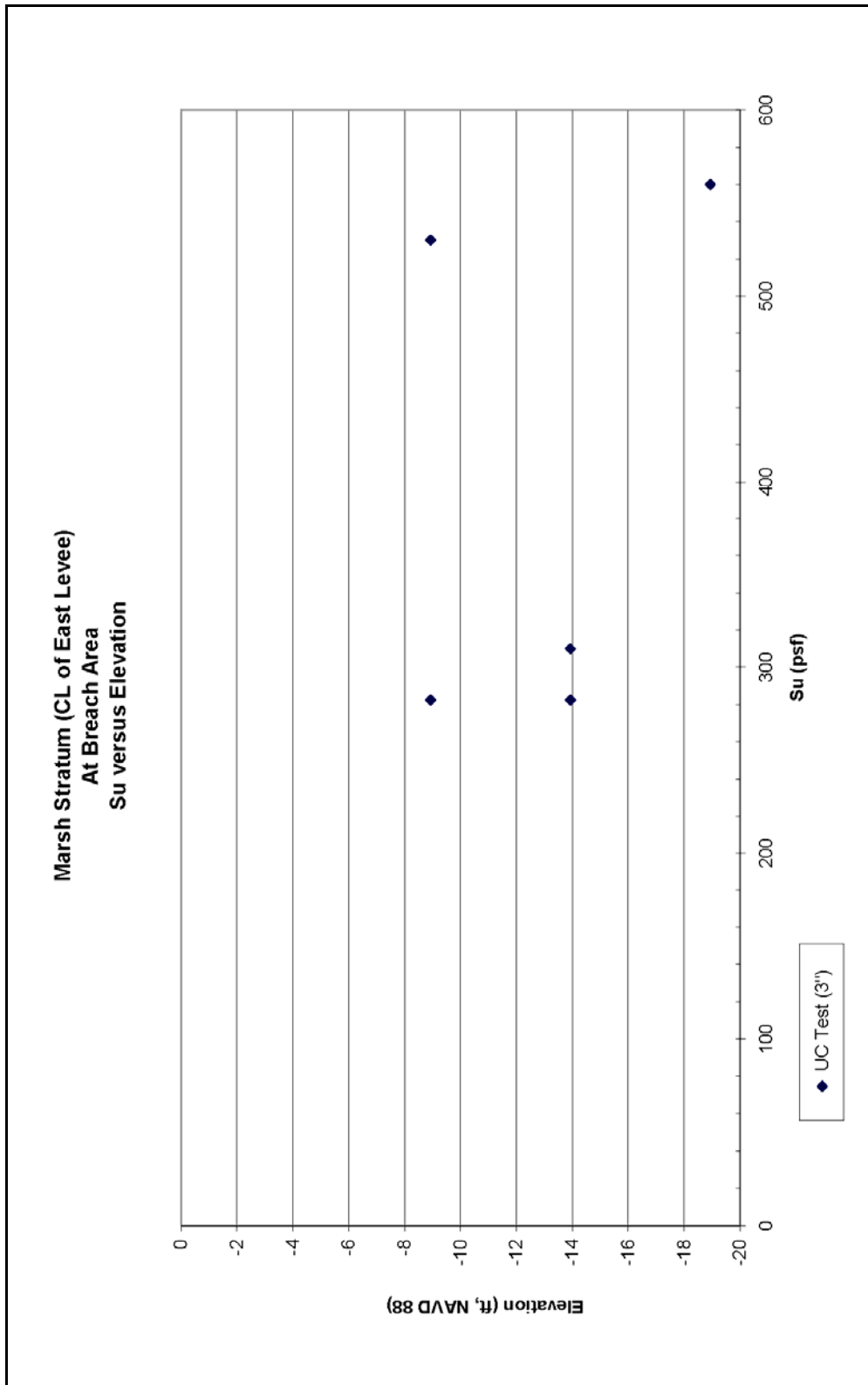


Figure K1-31. Marsh Stratum (CL of East Levee – At Breach Area), Su versus Elevation

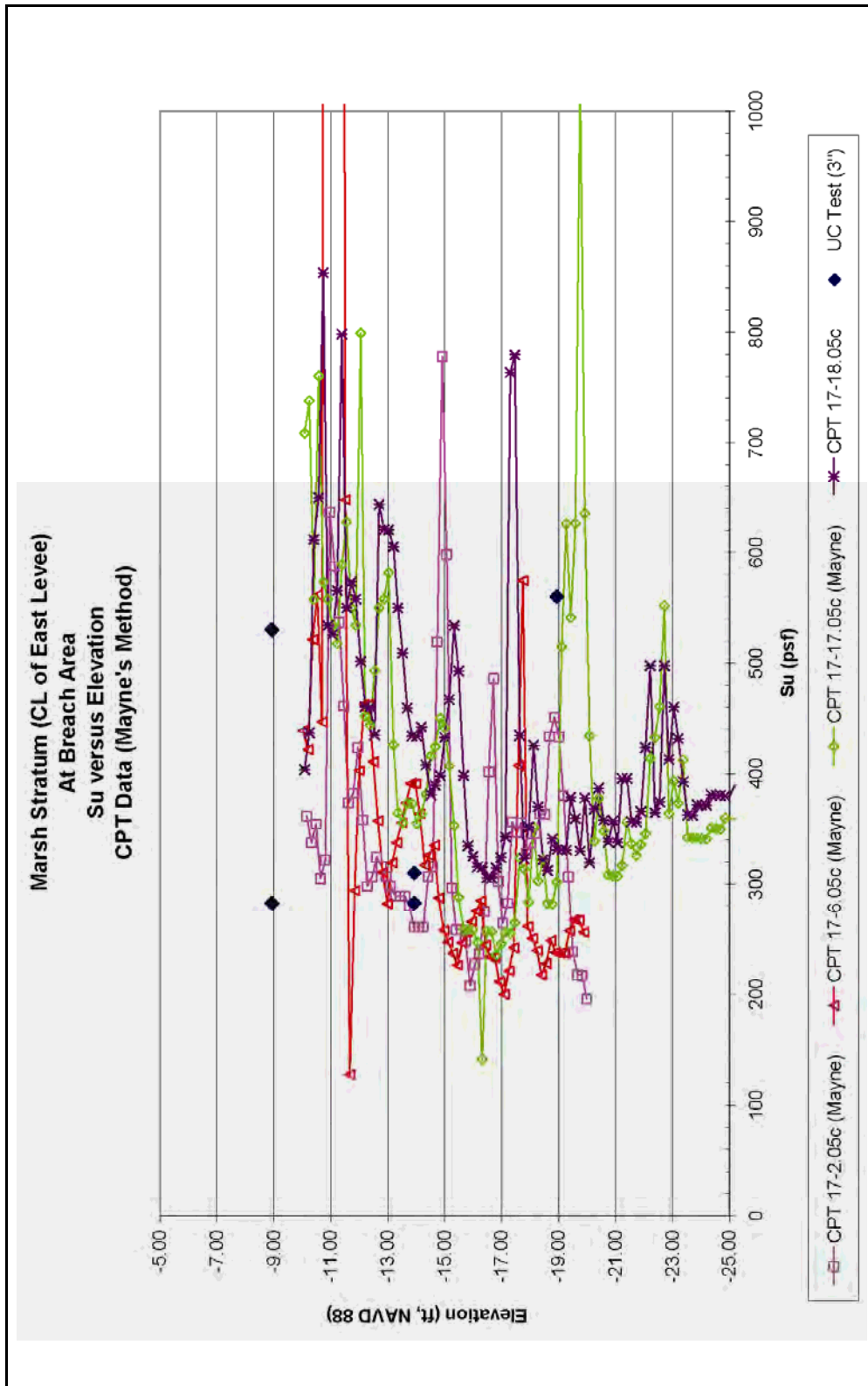


Figure K1-32. Marsh Stratum (CL of East Levee – At Breach Area), Su versus Elevation (CPT Data – Mayne's Method)

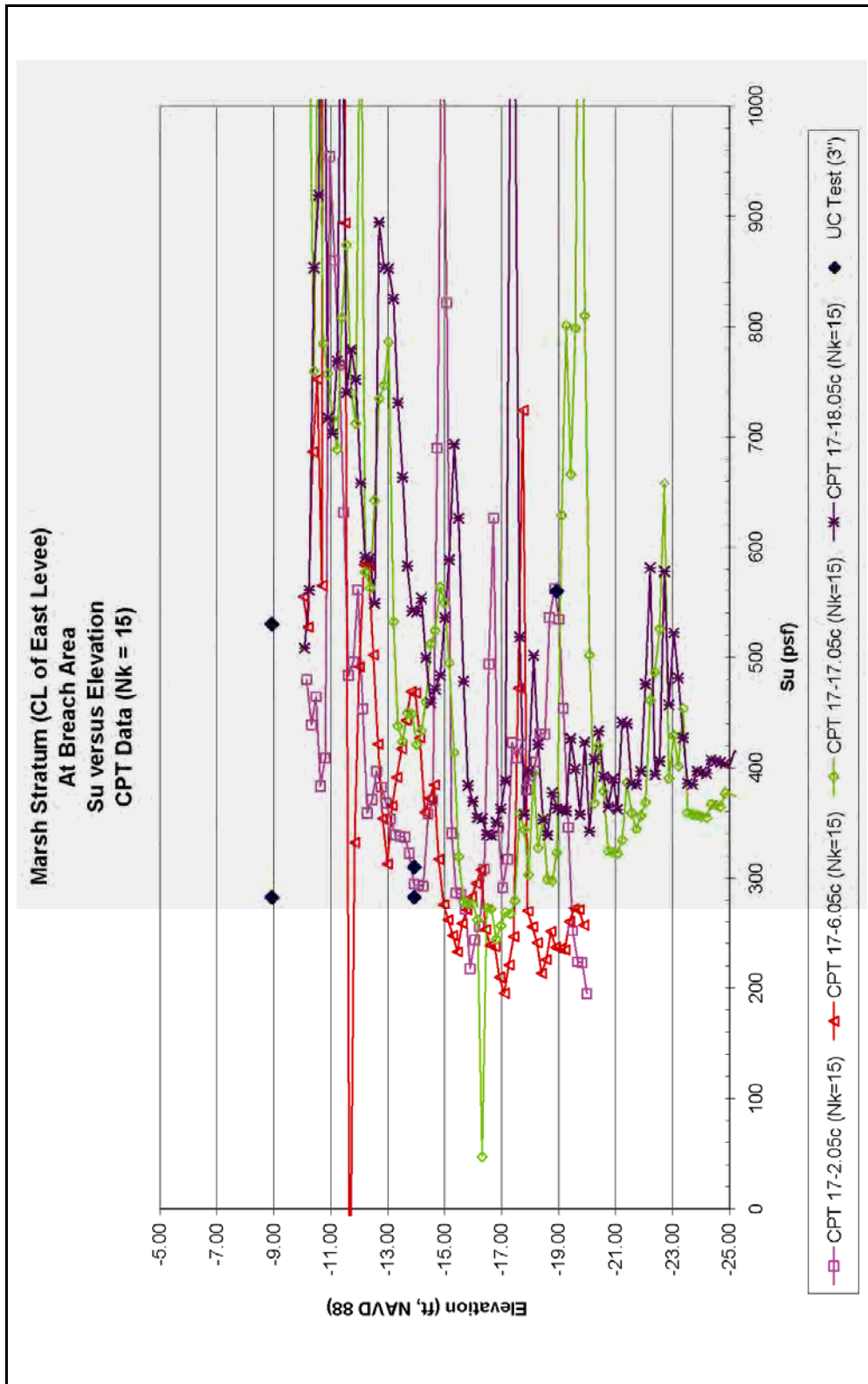


Figure K1-33. Marsh Stratum (CL of East Levee), Su versus Elevation (CPT Data – Nk=15)

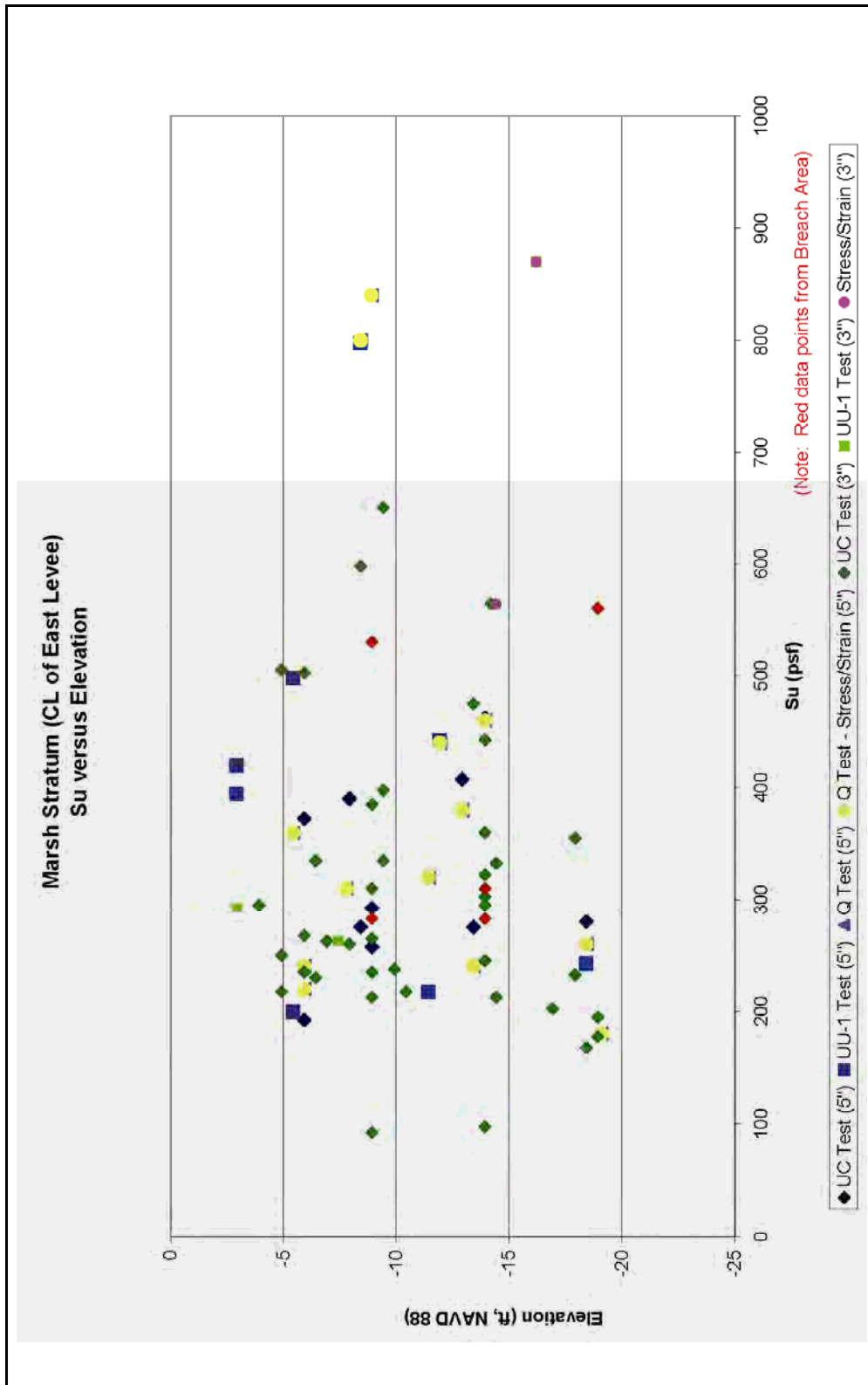


Figure K1-34. Marsh Stratum (CL of East Levee), Su versus Elevation

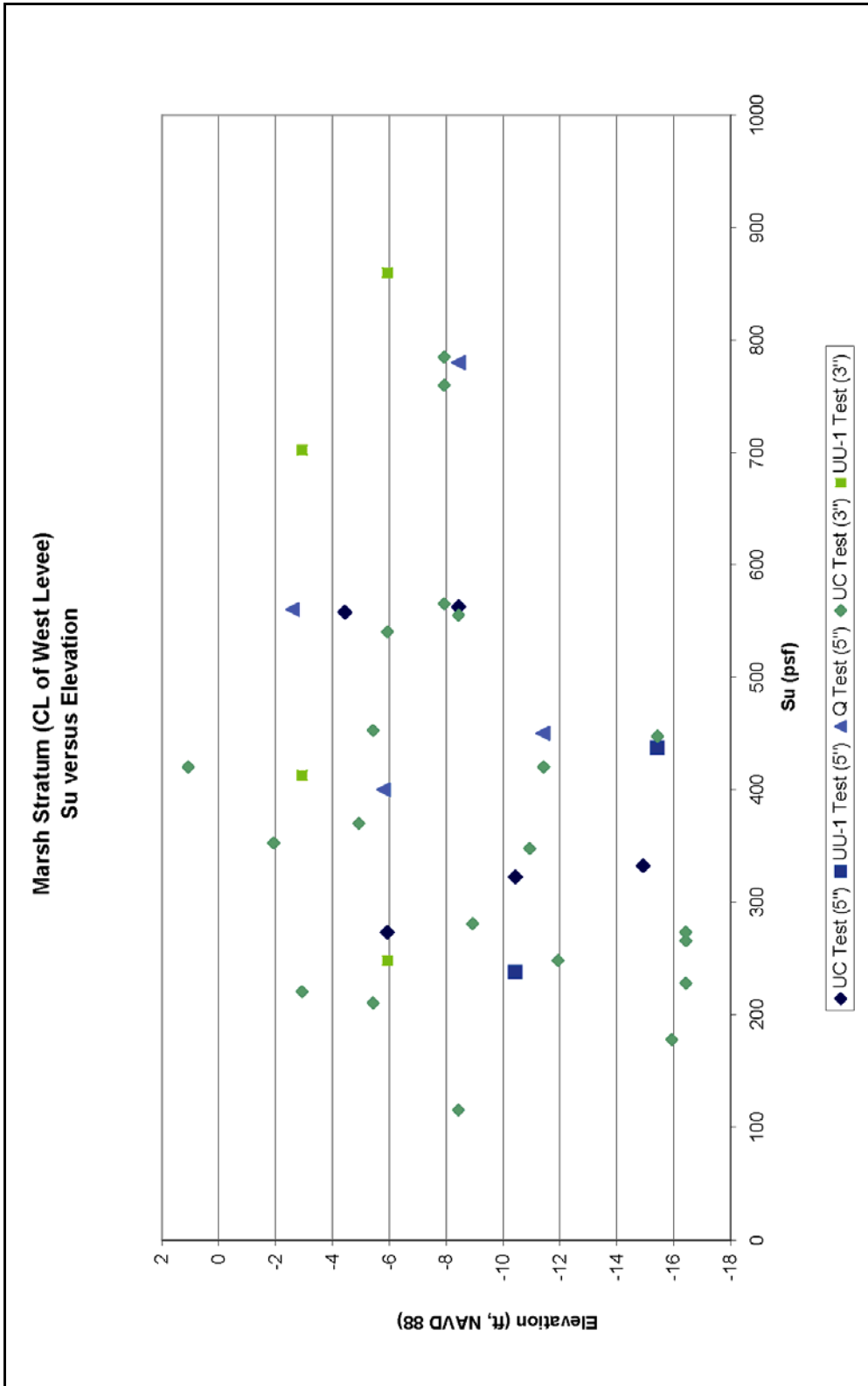


Figure K1-35. Marsh Stratum (CL of West Levee), Su versus Elevation

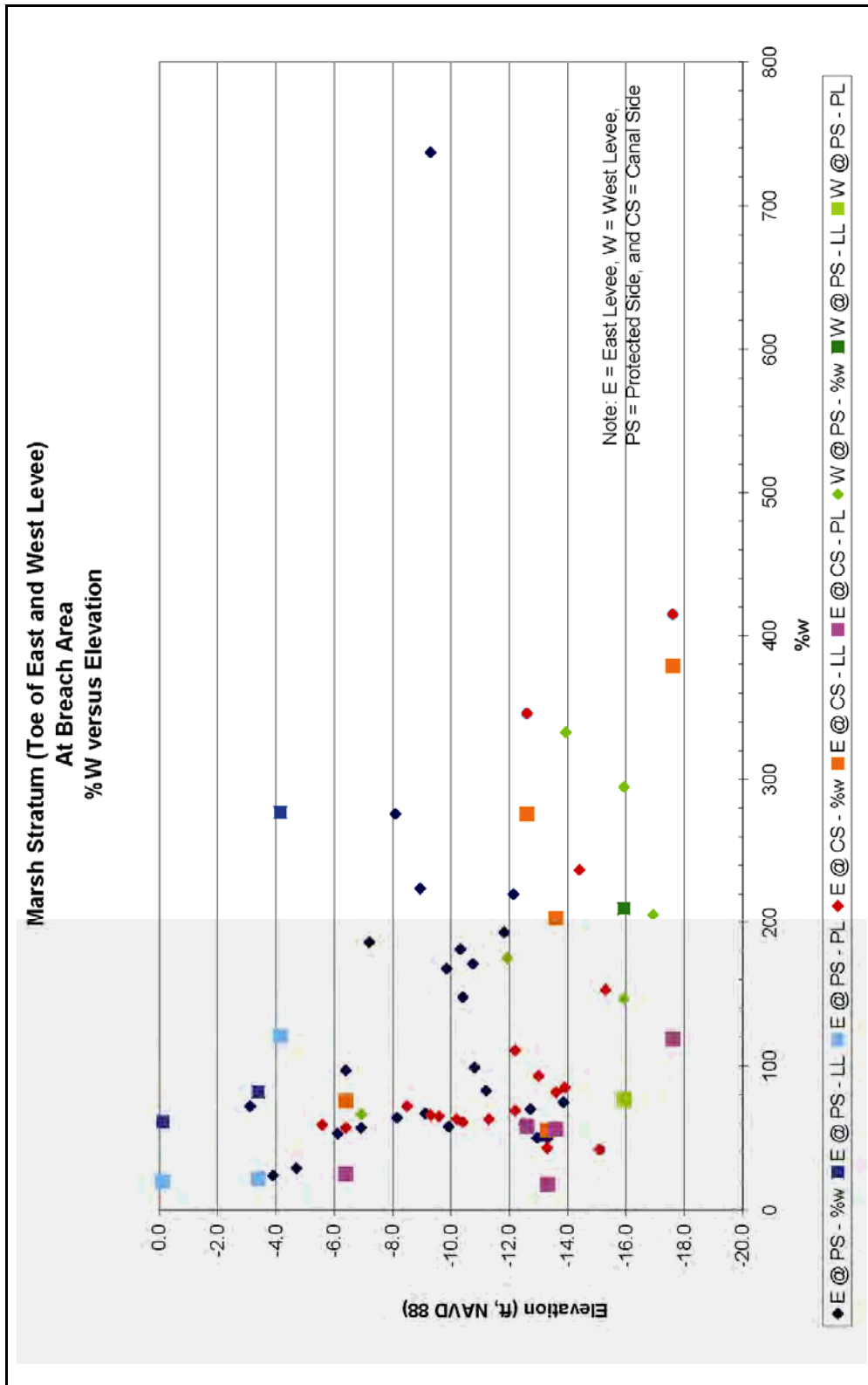


Figure K1-36. Marsh Stratum (Toe of East and West Levee – At Breach Area), %w versus Elevation

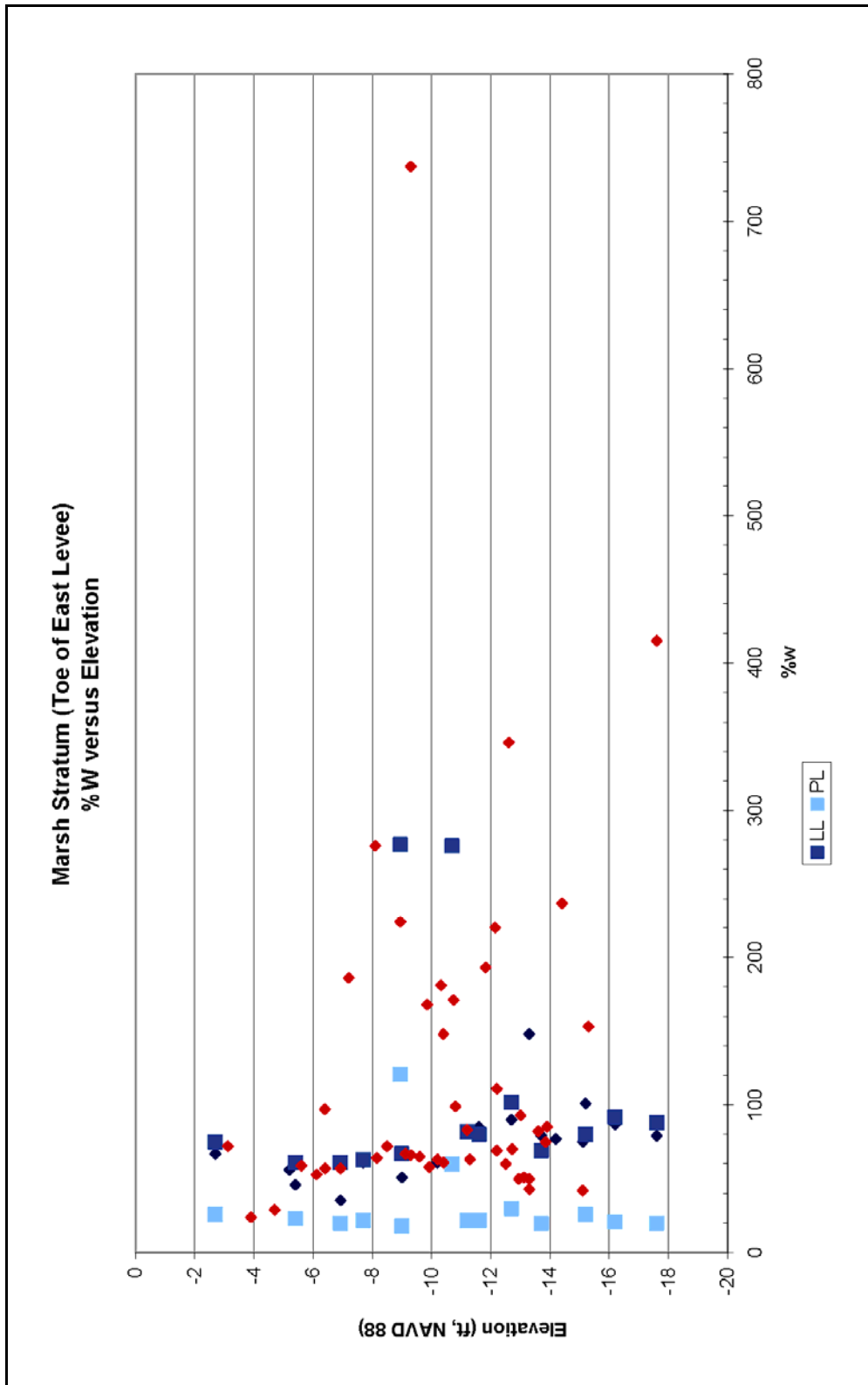


Figure K1-37. Marsh Stratum (Toe of East Levee), %w versus Elevation

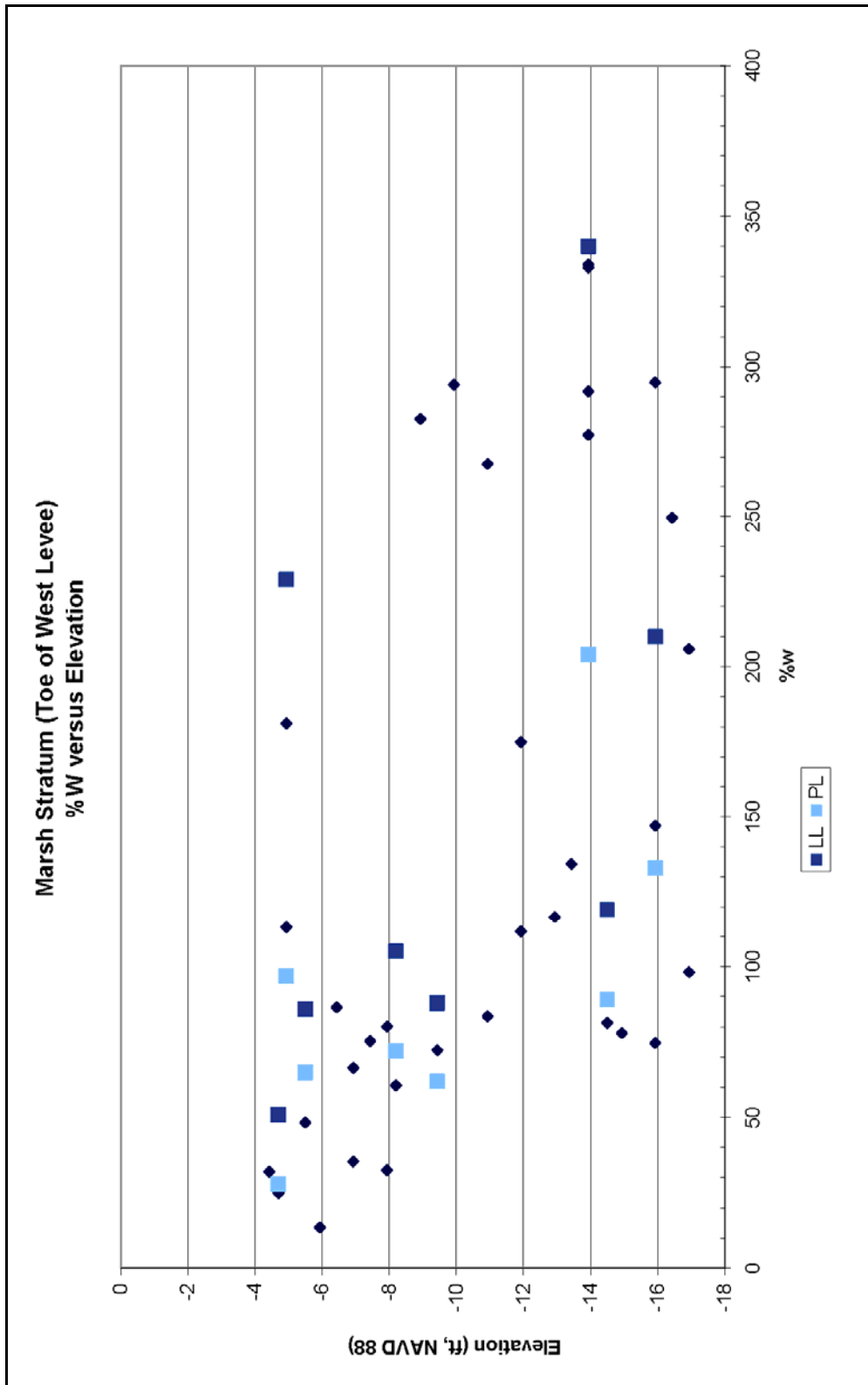


Figure K1-38. Marsh Stratum (Toe of West Levee), %w versus Elevation

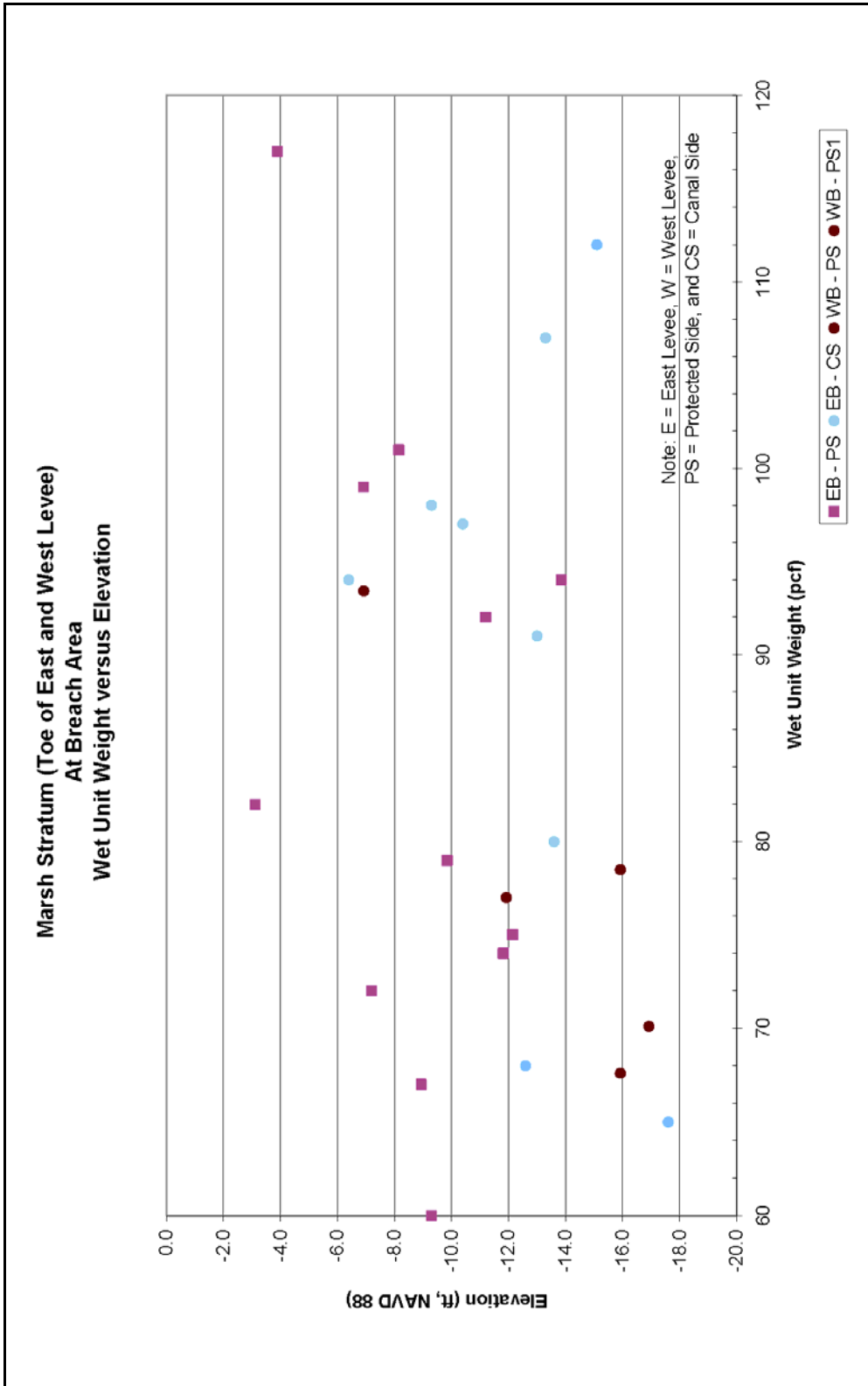


Figure K1-39. Marsh Stratum (Toe of East and West Levee – At Breach Area), Wet Unit Weight versus Elevation

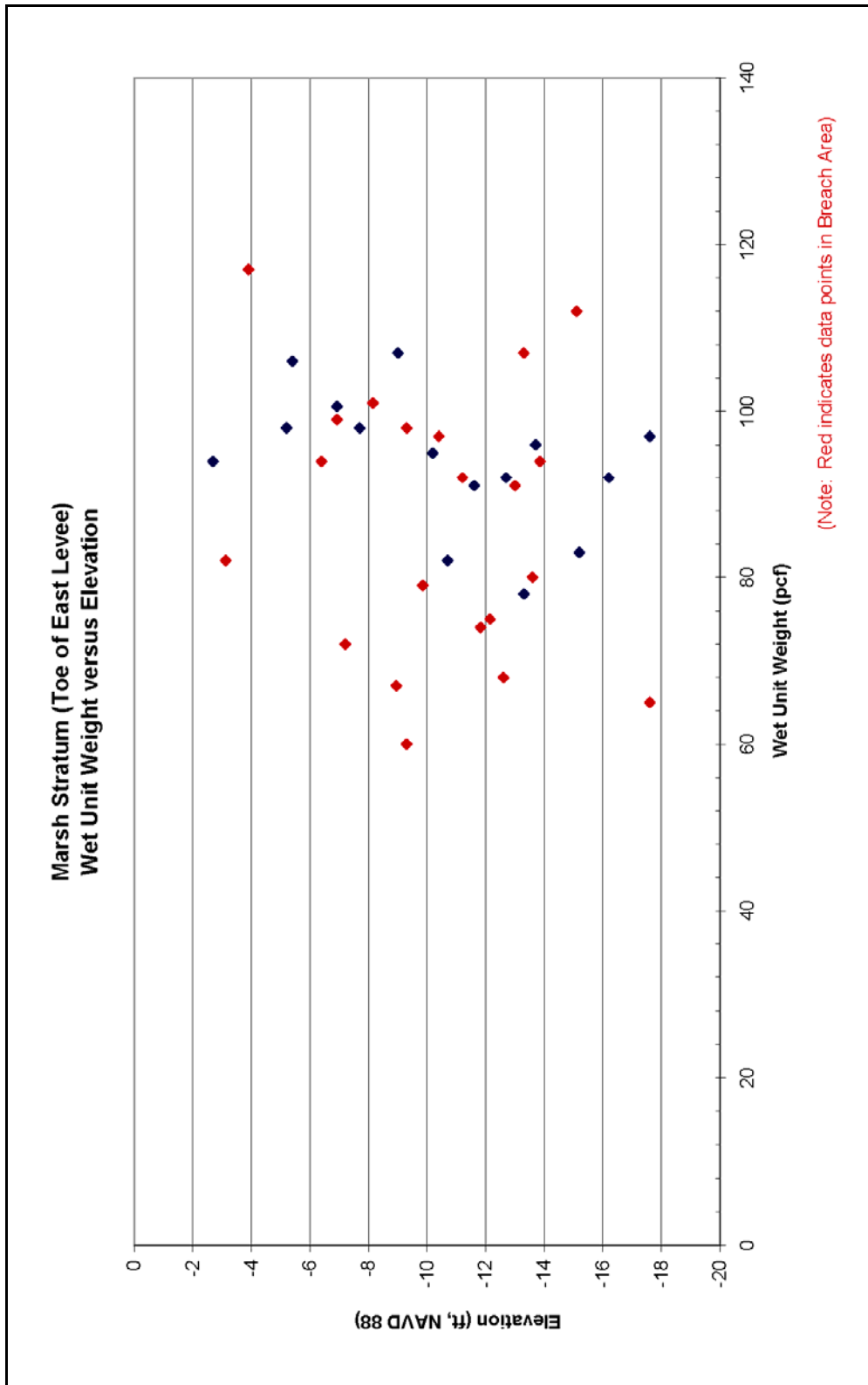


Figure K1-40. Marsh Stratum (Toe of East Levee), Wet Unit Weight versus Elevation

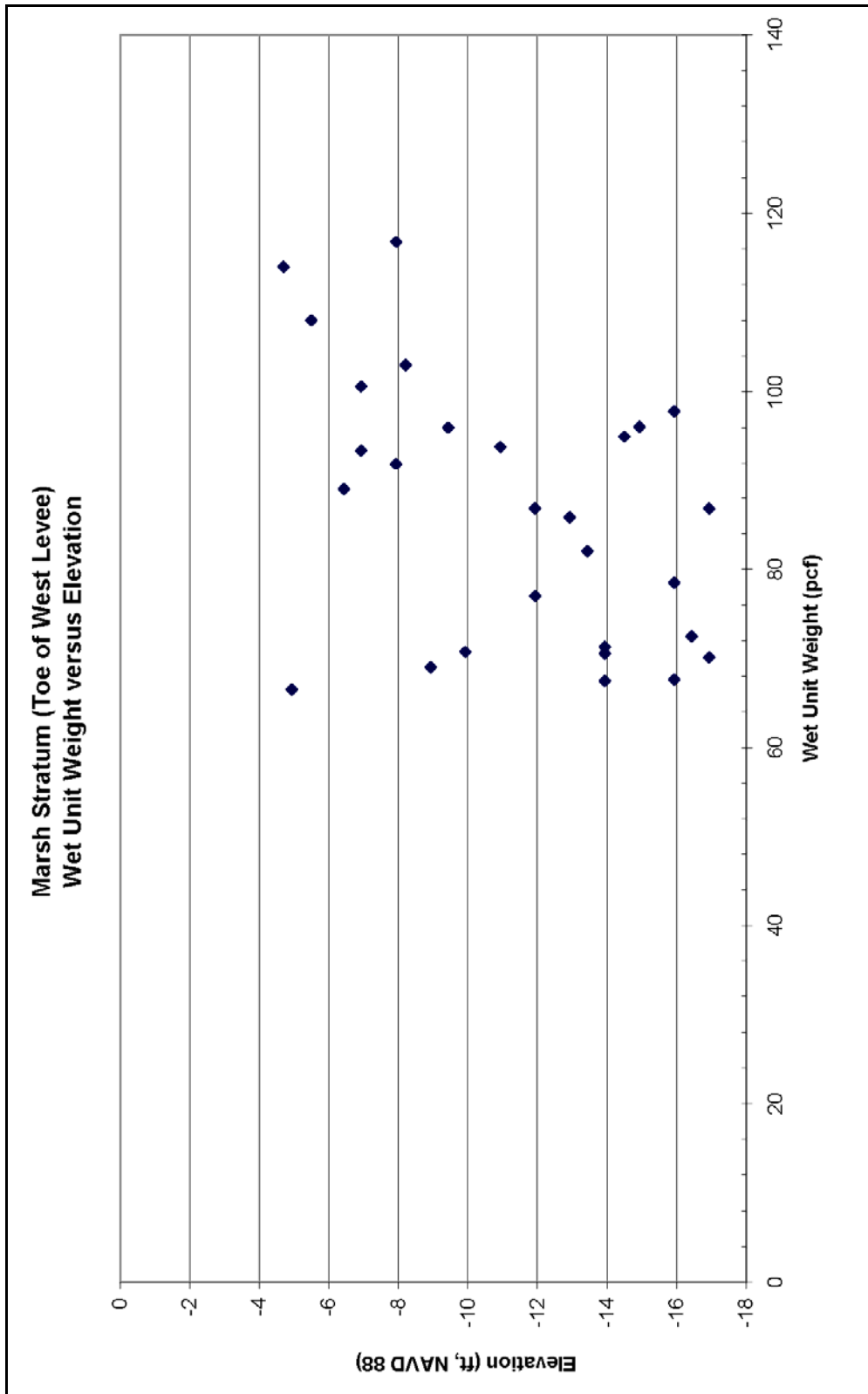


Figure K1-41. Marsh Stratum (Toe of West Levee), Wet Unit Weight versus Elevation

The undrained shear strength determined from the laboratory tests conducted on samples in the breach area is shown in Figure K1-42. Undrained shear strength data in the breach area plotted with undrained shear strength data for the entire east levee are shown in Figure K1-43. Undrained shear strength data for the entire west levee are shown in Figure K1-44.

Lacustrine Stratum

The data for the lacustrine stratum will be divided into two groups: data from under the levee embankment, and data from the toe of the levee.

Under the Levee Embankment

Data on the lacustrine stratum under the levee embankment consist of five borings shown in the 1990 GDM, and four cone penetrometer tests (CPT) taken on the east levee. Of the five GDM borings, four borings collected 3-in. (diameter) undisturbed samples, and one boring collected 5-in. (diameter) undisturbed samples. From the 3-in. samples, ten unconfined compression (UC) tests were performed. From the 5-in. samples, four UC tests were performed, and two one-point unconsolidated-undrained triaxial compression tests (UU-1), confined at existing overburden pressures, were performed. From these laboratory tests, moisture content and wet unit weights were determined. The moisture contents (%w) in the breach area are shown in Figure K1-45. The wet unit weight data in the breach area are shown in Figure K1-46.

Interpretation of the undrained shear strength from the CPTs using the bearing capacity equation ($N_k=15$) is plotted with laboratory test results in Figure K1-47. These interpretations were provided by Dr. Thomas Brandon (Virginia Tech).

At the Toe of Embankment

Data on the marsh stratum under the toe of the levee embankment consist of five borings taken in 2005 on the protected side, four borings taken in 2005 on the canal side, and three borings on the west levee toe shown in the 1990 GDM. Of the borings on the protected side of the east levee, four borings collected 5-in. (diameter) undisturbed samples, and one boring collected 3-in. (diameter) undisturbed samples. Of the borings on the canal side of the east levee, three borings collected 5-in. (diameter) undisturbed samples, and one boring collected 3-in. (diameter) undisturbed samples. Of the three GDM borings taken on the protected side of the west levee, two borings collected 3-in. (diameter) samples, and one boring collected 5-in. (diameter) undisturbed samples. From the 3-in. samples, 14 UC tests were performed, and five one-point unconsolidated-undrained triaxial compression tests (UU-1), confined at existing overburden pressure, were performed. From the 5-in. samples, 25 UC tests were performed, 19 unconsolidated-undrained triaxial compression tests (Q), and 7 one-point unconsolidated-undrained triaxial compression tests (UU-1), confined at existing overburden pressure, were performed. From these laboratory tests, moisture content and wet unit weights were determined. The moisture contents (%w) in the breach area are shown in Figure K1-44. The wet unit weight data in the breach area are shown in Figure K1-49.

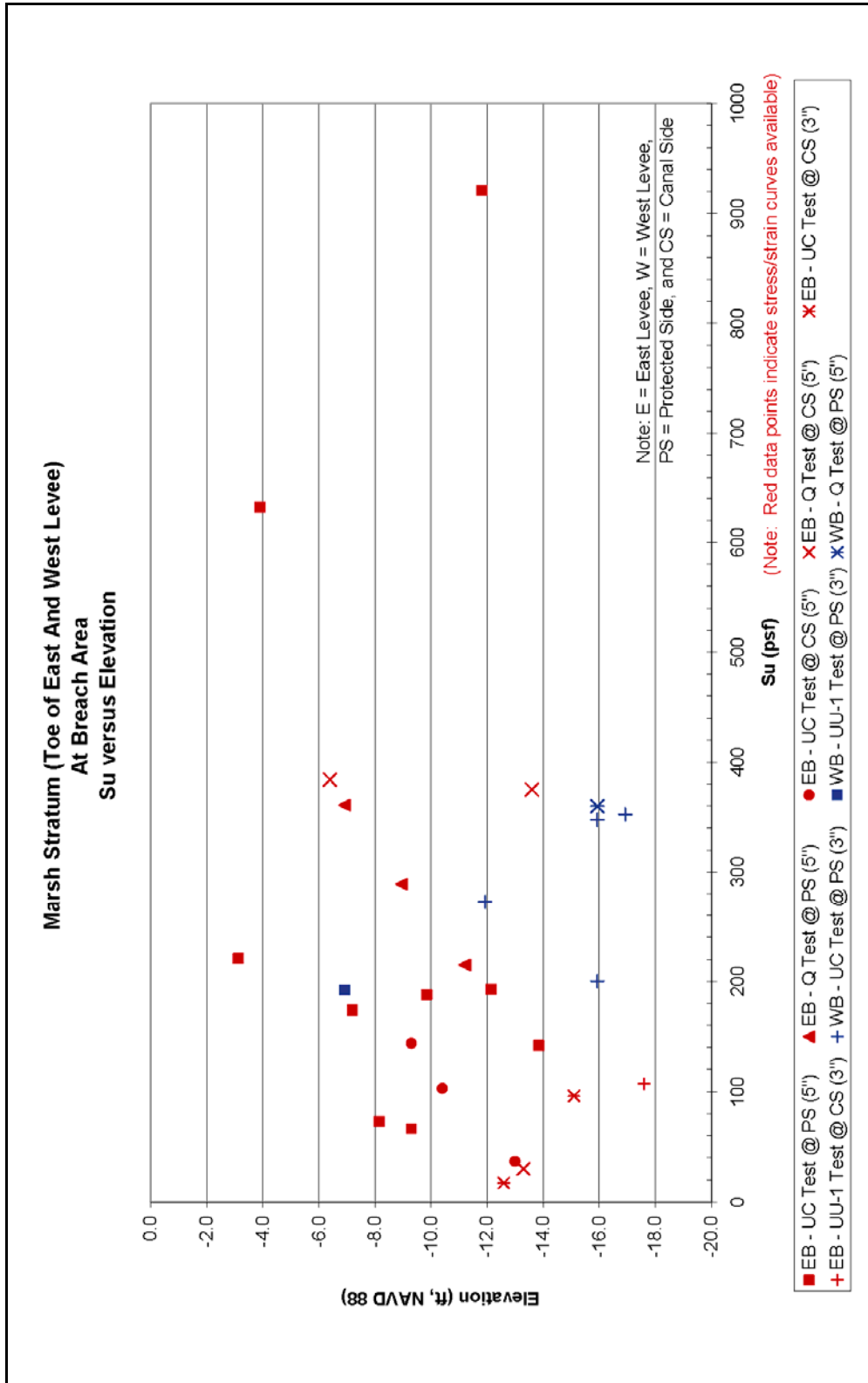


Figure K1-42. Marsh Stratum (Toe of East and West Levee – At Breach Area), Su versus Elevation

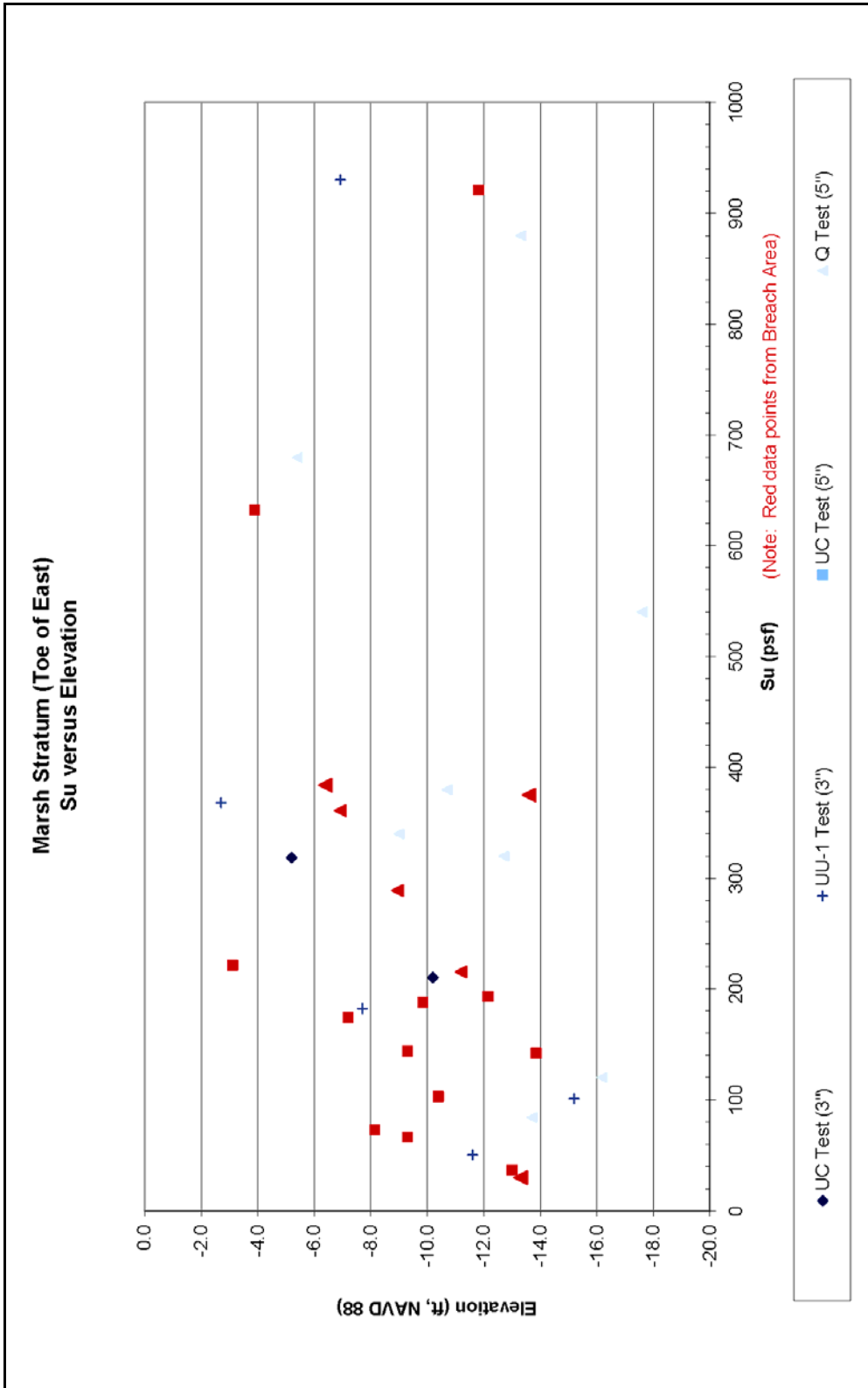


Figure K1-43. Marsh Stratum (Toe of East Levee), Su versus Elevation

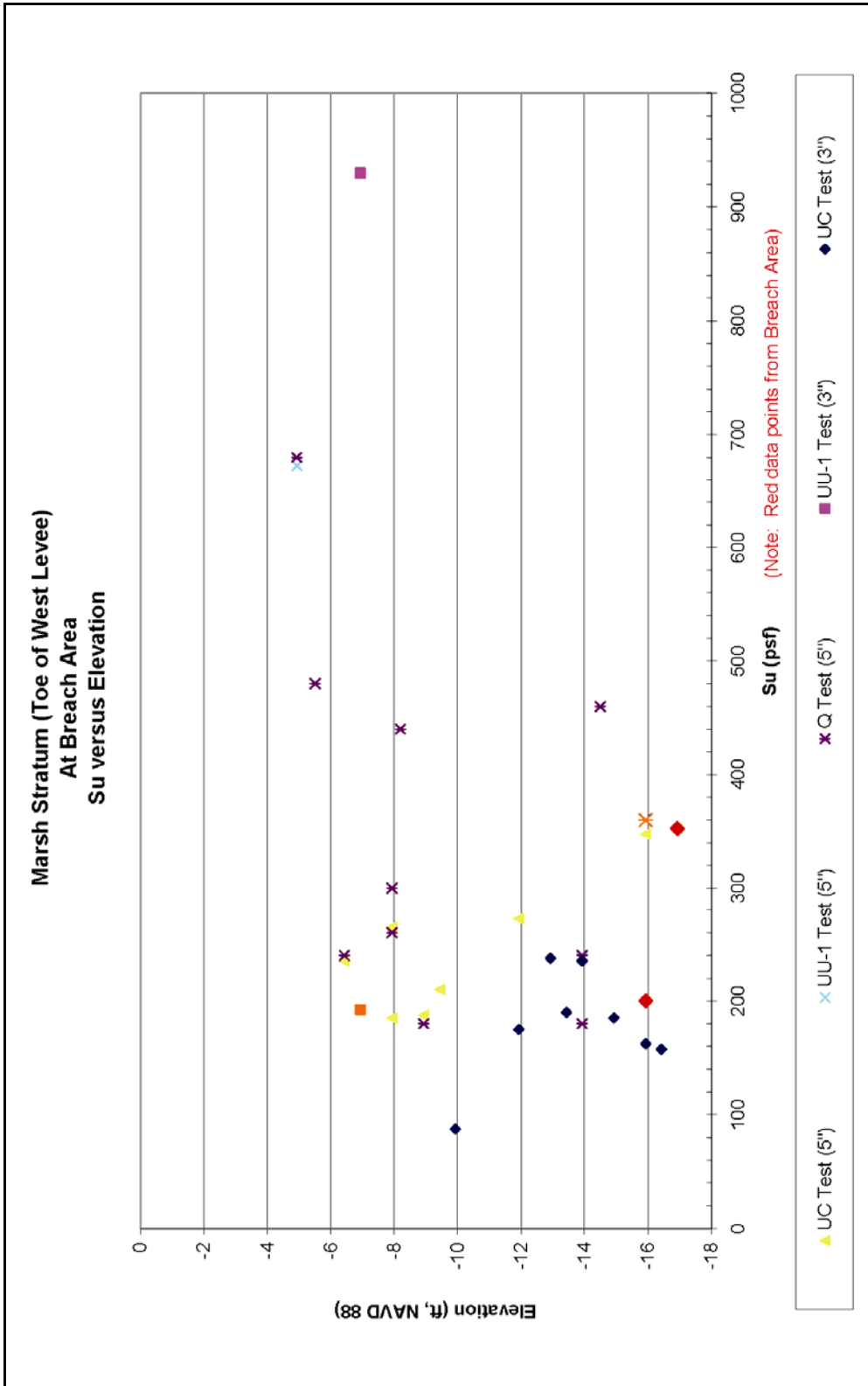


Figure K1-44. Marsh Stratum (Toe of West Levee), Su versus Elevation

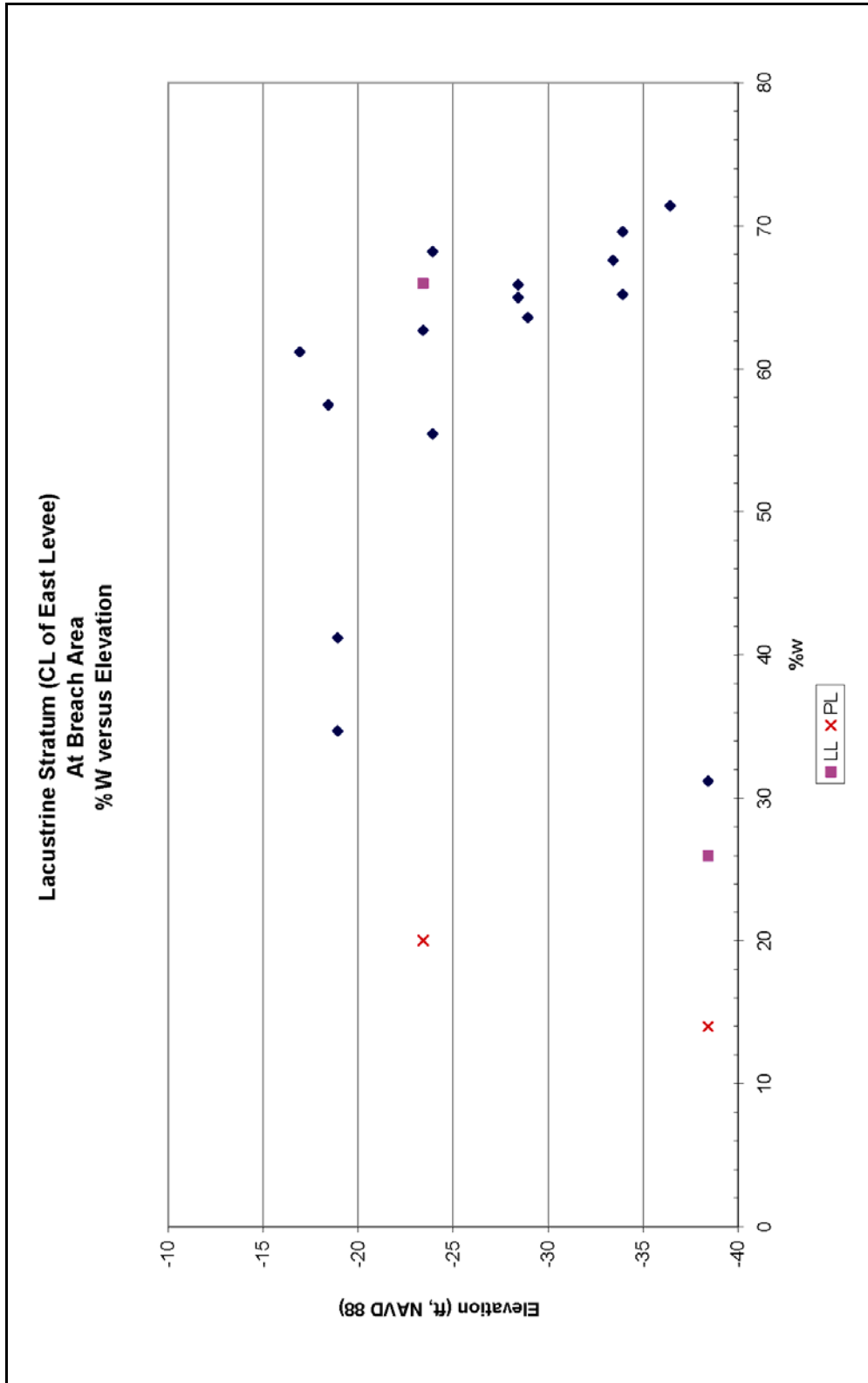


Figure K1-45. Lacustrine Stratum (CL of East Levee – At Breach Area), %w versus Elevation

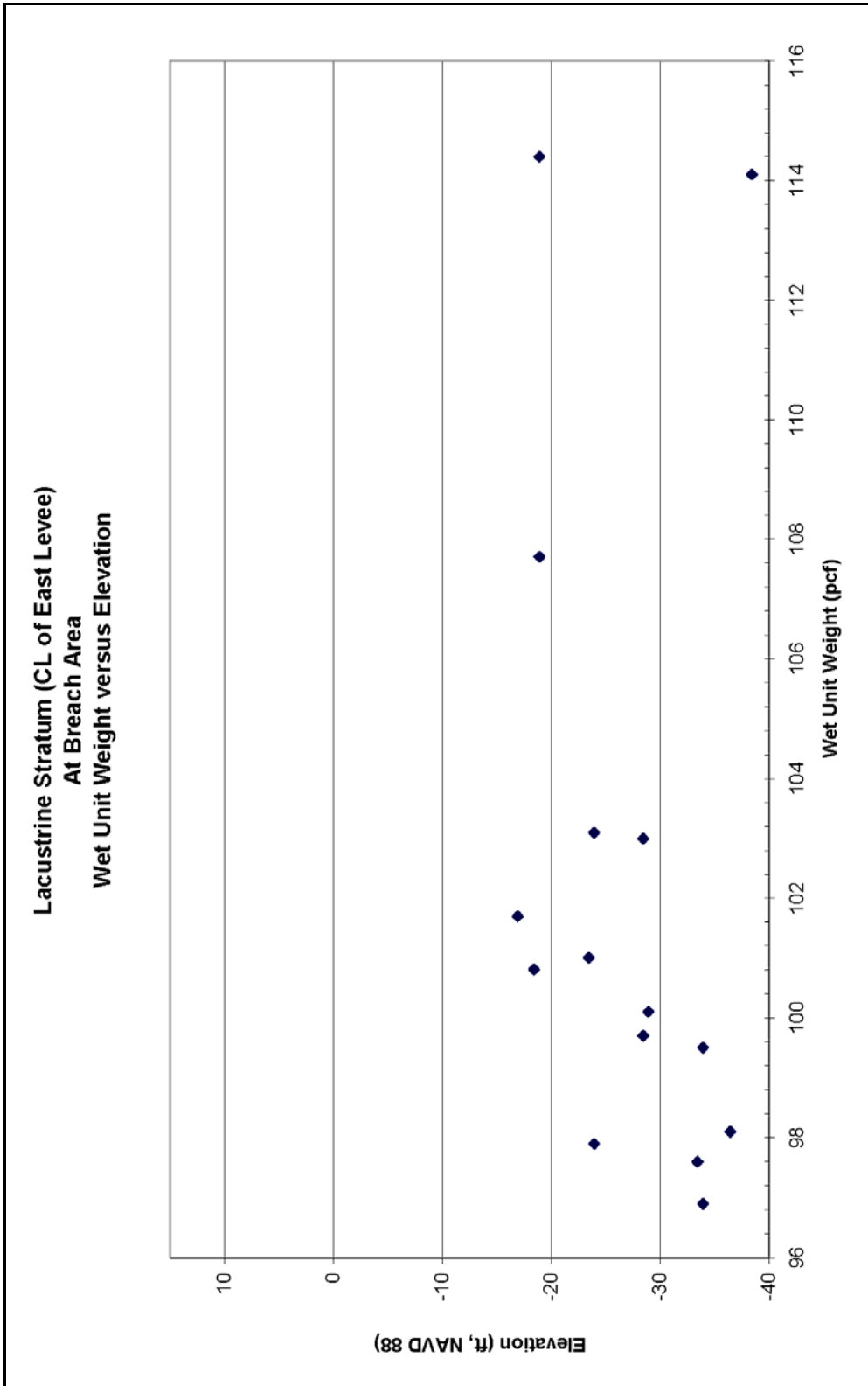


Figure K1-46. Lacustrine Stratum (CL of East Levee – At Breach Area), Wet Unit Weight versus Elevation

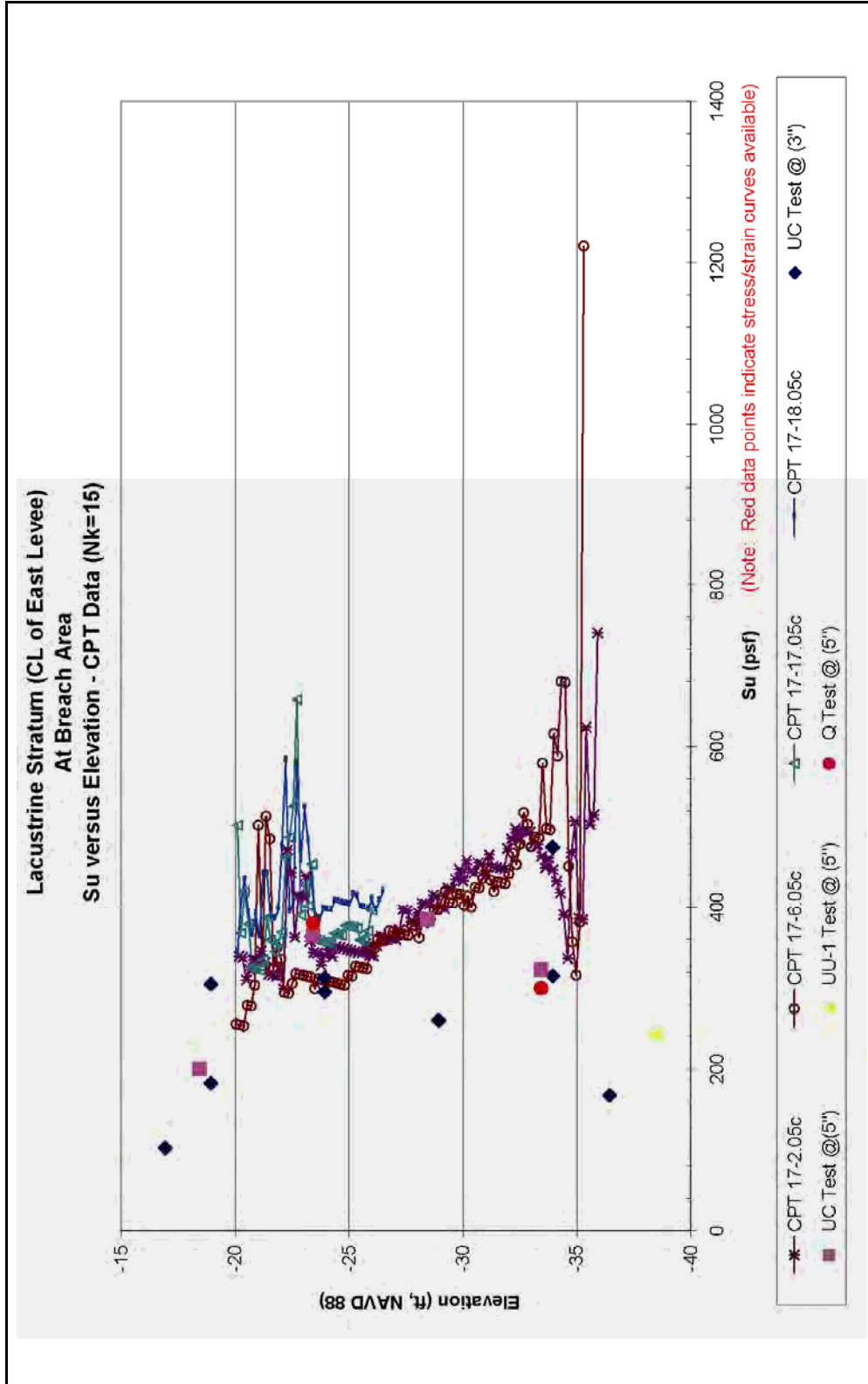


Figure K1-47. Lacustrine Stratrum (CL of East Levee – At Breach Area), Su versus Elevation (CPT Data – Nk=15)

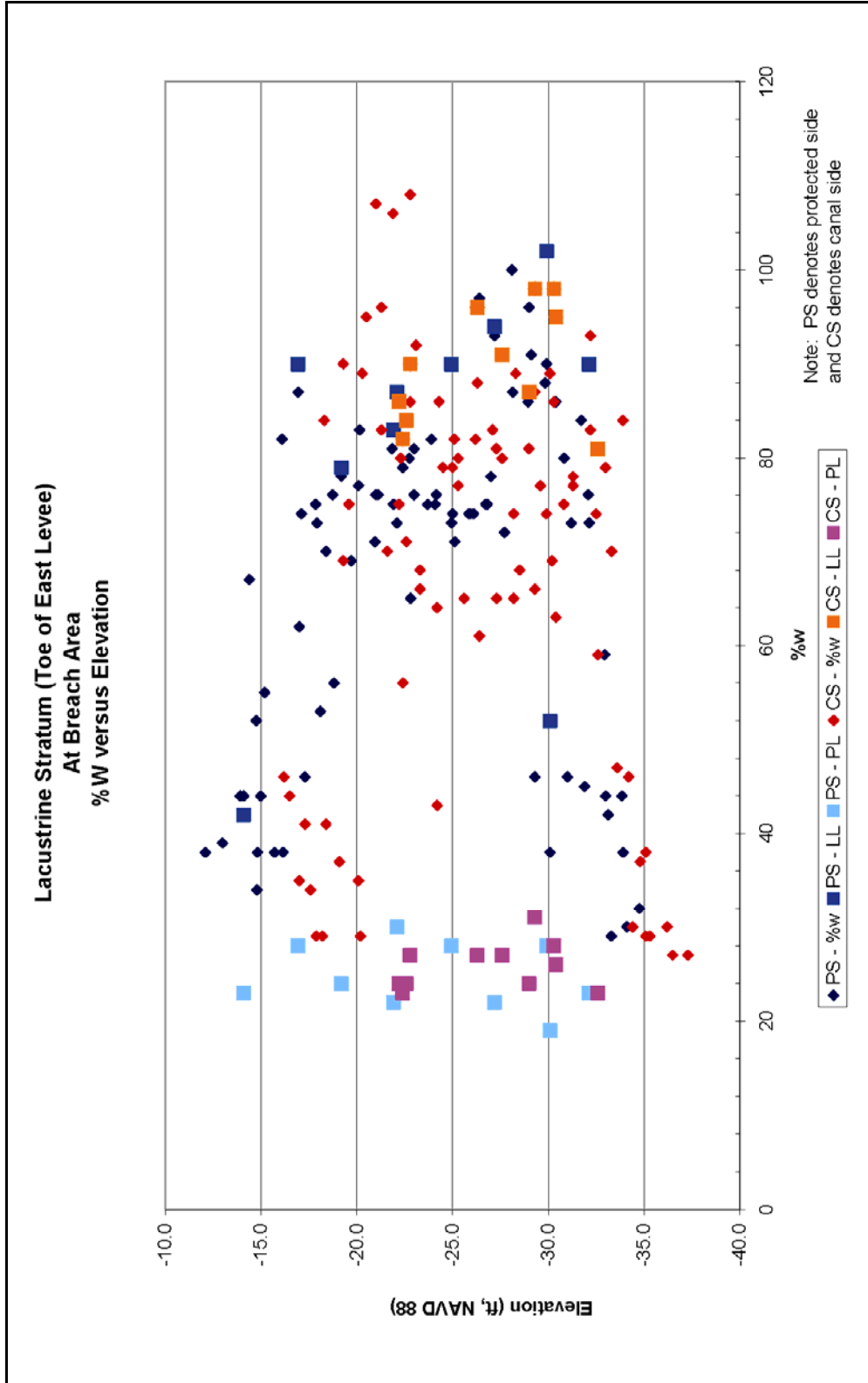


Figure K1-48. Lacustrine Stratum (Toe of East Levee – At Breach Area), %w versus Elevation

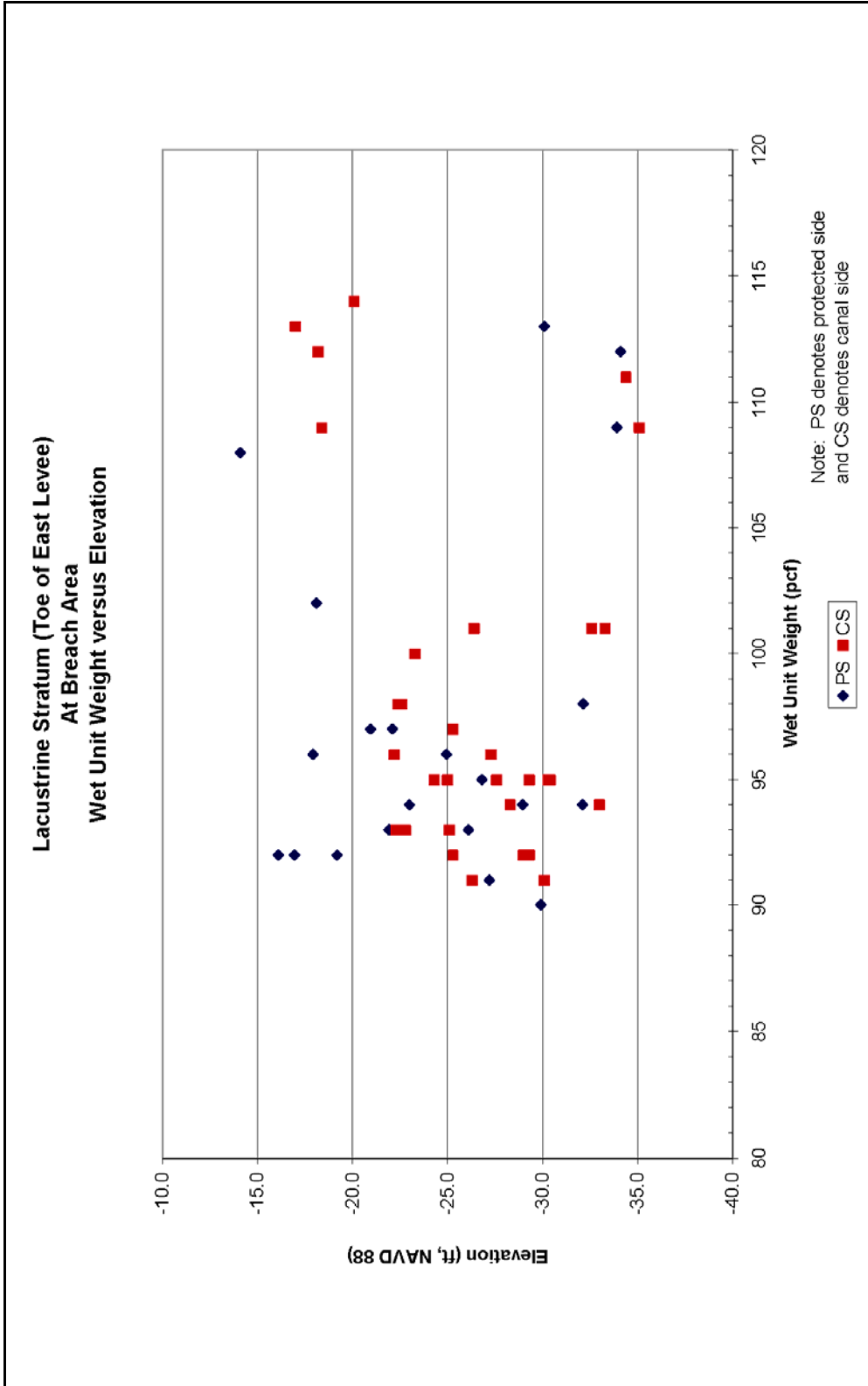


Figure K1-49. Lacustrine Stratum (Toe of East Levee – At Breach Area), Wet Unit Weight versus Elevation

The undrained shear strength determined from the laboratory tests conducted on samples in the breach area is shown in Figure K1-50. The S_u/P ratio for the shear strengths samples is shown in Figure K1-51.

Beach Sand Stratum. Forty standard penetration tests (SPT) were conducted in the beach sand stratum in the breach area. The field (uncorrected) standard penetration number for the beach sand stratum is shown in Figure K1-48. Interpretation of the SPT number from the CPTs will be provided later. Dissipation tests with the CPT were conducted at this stratum at 17-2.05c and 17-6.05c. At 17-2.05c, the head in the sand was about 7.8 ft below the top of the hole or at elevation -3.68 (NAVD 88). At 17-6.05c, the head in the sand was about 6 ft below the top of the hole or at elevation -1.3 (NAVD 88).

Assessment of Shear Strength Data

The assessment of strength data described in the following sections had three objectives:

1. To develop a “shear strength model” for use in stability analyses and soil-structure interaction analyses of the I-walls at the 17th Street Canal, using all data available in February 2006. This strength model includes strengths for the levee fill, the strengths of the peat, the clay, and the sand in the foundation.
2. To compare this strength model to the strength model that was used for design of the I-walls in the area where the breach occurred.
3. To compare the strengths in the breach area with strengths in other sections of the 17th Street Canal I-wall.

Stratigraphy

The northern section of the 17th Street Canal where the breach occurred is shown in the longitudinal sections in Figures K1-7, K1-8, and K1-9, and by the cross sections for Station 8+30 (Figure K1-11), Station 10+00 (Figure K1-12), and Station 11+50 (Figure K1-13).

The levee fill is compacted CL or CH material, with an average Liquid Limit of about 45. The average moist unit weight of the fill is about 110 pcf.

Beneath the fill is a layer of peat or “marsh” 5 ft to 10 ft thick. The peat is composed of organic material from the cypress swamp that occupied the area, together with silt and clay deposited in the marsh. The average moist unit weight of the peat is about 80 pcf. Water contents of the peat are as high as 737%, the average water content is approximately 112%. The peat is fibrous at the top of the layer, and more amorphous near the bottom, indicating more advanced decomposition of the older organic materials at depth.

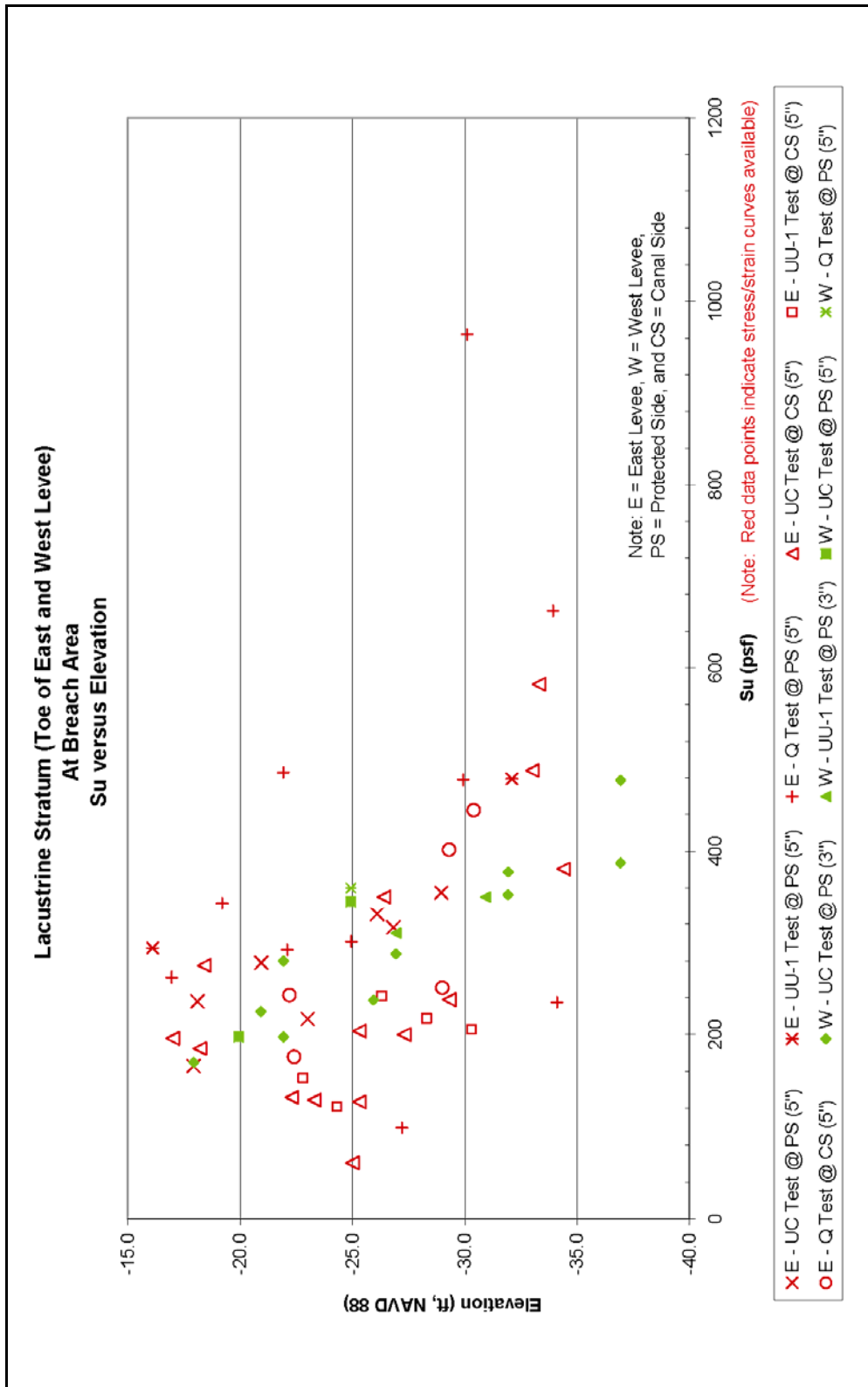


Figure K1-50. Lacustrine Stratum (Toe of East and West Levee – At Breach Area), Su versus Elevation

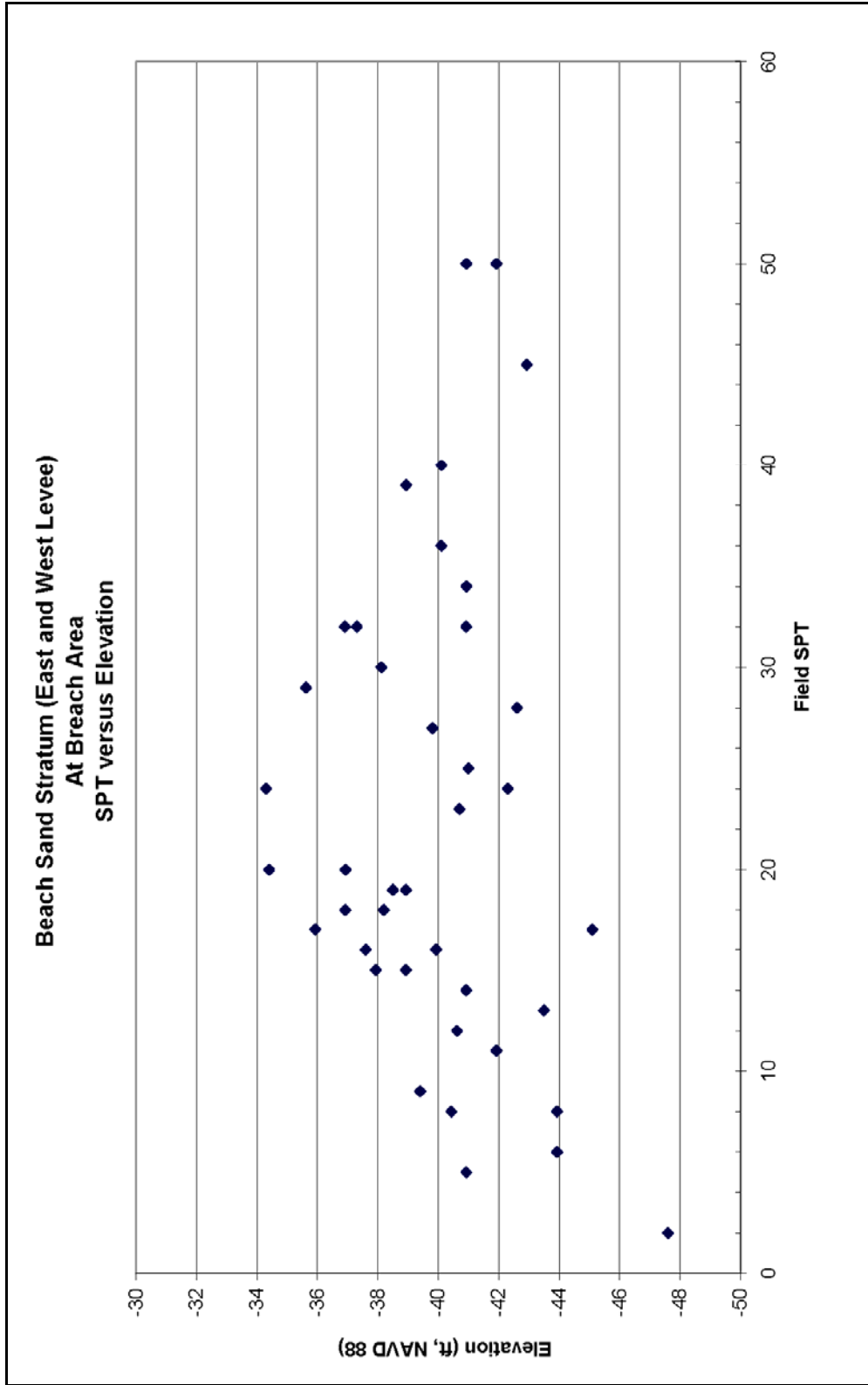


Figure K1-52. Beach Sand Stratum (East and West Levee – At Breach Area), Field SPT versus Elevation

Beneath the peat is a clay or “lacustrine” layer, with an average Liquid Limit of about 95%. The clay is normally consolidated throughout its depth, having been covered and kept wet by the overlying layer of peat. The average moist unit weight of the clay is about 109 pcf, and the average water content is approximately 65%.

Beneath the clay is a layer of Pine Island Beach sand, a silty sand with Standard Penetration blow counts ranging from 2 to 50. This layer is not involved in observed or calculated mechanisms of instability, and its strength is therefore of little importance in stability analyses, except as a more resistant layer beneath the clay.

Sources of information on shear strengths

A considerable number of borings were drilled in the breach area and in neighboring areas before the failure. Additional borings have been drilled, cone penetration tests have been performed, and test pits have been excavated since the failure.

Several hundred unconfined compression tests, UU tests performed using only one confining pressure rather than a range of confining pressures (called UU-1 tests), and conventional UU tests performed using a range of confining pressures have been conducted on the soils at the site. Tests were performed on specimens trimmed from three-inch and five-inch diameter samples. Statistical analyses have been performed on the data from these tests to compute minimum, maximum, and average values of strength, and standard deviations of strength for the levee fill, the peat, and the clay.

Four cone penetration tests with pore pressure measurements (CPTU tests) were performed near the area of the breach after the failure, which have proven to be very useful for evaluating the undrained strength of the clay, and for distinguishing the clay from the overlying peat and the underlying sand.

The evaluation described here focused on undrained shear strengths of the levee fill, the peat and the clay. Because the water loads that resulted in failure of the I-walls increased over a period of hours, there is little doubt that the levee fill and the clay beneath the peat were undrained during the event. Determining whether the peat should be modeled as drained or undrained will require laboratory consolidation tests to determine how quickly it drains when subjected to changes in load. Those tests are being performed at this time. The discussion below considers only undrained strength of the peat. If it is determined that the drained strength, or partially drained strength, is more appropriate for the peat, additional tests will be needed.

Shear strength of levee fill

Data is available from two borings in the breach area (Borings 62 and 64) and several more in the neighborhood of the breach. In all, about 125 strength

tests were performed on the fill materials. Much of the fill is below the static water table, and an $s_u = c$, $\phi_u = 0$ strength interpretation is therefore appropriate. Shear strengths measured in unconfined compression tests are lower than those measured in UU-1 or UU tests.

The measured shear strengths scatter very widely, from about 120 psf to more than 5,000 psf. With such widely scattered values, an average value may not be meaningful, and considerable judgment is needed to select a representative value. Placing greatest emphasis on data from UU tests on five-inch diameter samples, $s_u = 900$ psf appears to be a reasonable value to represent the levee fill. This strength can be compared to a value of 500 psf used in the design analyses.

Shear strength of peat

The peat (or marsh) deposit is stronger beneath the levee crest where it had been consolidated under the weight of the levee, and weaker at the toe of the levee and beyond, where it has not been compressed. The same types of tests were used to measure peat strengths as were used for fill strengths, and samples were performed on three-inch and five-inch diameter samples. Tests were also performed on two-inch diameter samples, but these were not included in the evaluation described here, because it was considered that such small samples would likely be too disturbed to be representative of field conditions.

The measured shear strengths scatter very widely, from about 50 psf to about 920 psf. Values of $s_u = 400$ psf beneath the levee crest, and $s_u = 300$ psf beneath the levee toe appear to be reasonably representative of the measured values. These strengths can be compared to a value of 280 psf used in the design analyses.

Shear strength of clay

The clay is normally consolidated, and its undrained shear strength increases with depth. Figure K1-53 shows variations of undrained shear strength with depth determined using Mayne's method (Mayne 2003)¹. Mayne's method uses the relationship among undrained strength, effective overburden pressure, and preconsolidation pressure that was proposed by Ladd (1991)², and has been found to give more reasonable values of undrained shear strength than use of constant values of the cone factors N_k or N_{kt} .

Whereas other methods of interpreting undrained shear strength from cone results are based on bearing capacity theory, Mayne's method considers tip resistance in relation to pore pressure and overburden pressure. For this reason it does not correspond to a single value of N_{kt} .

¹ Mayne, P. W. (2003). "Class 'A' Footing Response Prediction from Seismic Cone Tests," Proceedings, Deformation Characteristics of Geomaterials, Vol. 1, Lyon, France.

² Ladd, C. C. (1991) "Stability Evaluation During Staged Construction," Terzaghi Lecture, ASCE Journal of Geotechnical Engineering, 117 (4), 540-615.

With Mayne's method, the undrained shear strength is related to cone tip resistance by the equation

$$s_u = 0.091(\sigma'_v)^{0.2} (q_t - \sigma_v)^{0.8} \quad (1)$$

where s_u = undrained shear strength, σ'_v = effective vertical stress, q_t = total cone tip resistance adjusted for pore pressure effects, and σ_v = total vertical stress.

The undrained shear strength calculated with this method is assumed to be equal to that measured using Direct Simple Shear (DSS) tests. This strength is lower than that measured by conventional triaxial compression tests and greater than that measured by triaxial extension tests. Ladd (1991) suggests that this is a reasonable average value for design purposes.

For the soft and very soft clay along the 17th Street Canal, the values of undrained shear strength are very close to values calculated using $N_{kt} = 15$, a value often used for computing undrained strengths of soft clays from CPTU test results.

As shown in Figure K1-53, the variations of undrained strength with depth within the clay computed using Equation (1) are very nearly the same for all four CPTU tests. The straight line representing the average undrained shear strength in the clay has a slope of 11 psf per foot of depth. This rate of strength increase with depth compares to values of 8.4 psf per foot of depth to 13.5 psf per foot of depth determined using laboratory strength test results for samples from borings B-1, B-2, B-3, B-4, and B-6, which appeared to have the most consistent test results.

The rate of increase of strength with depth is directly related to the s_u/p' ratio for the clay, and its buoyant unit weight, as follows:

$$\frac{s_u}{p'} = \frac{\text{rate of increase of } s_u \text{ with depth}}{\text{rate of increase of } p' \text{ with depth}} = \frac{\Delta s_u / \Delta z}{\gamma_{\text{buoyant}}} \quad (2)$$

The value of γ_{buoyant} for the clay is $109 \text{ pcf} - 62.4 \text{ pcf} = 46.6 \text{ pcf}$. Thus the value of s_u/p' is:

$$\frac{s_u}{p'} = \frac{11 \text{ psf per ft}}{46.6 \text{ pcf}} = 0.24 \quad (3)$$

which is a reasonable value for this normally consolidated clay.

These values provide a good basis for establishing undrained strength profiles in the clay. The undrained strength at the top of the clay is equal to 0.24 times the effective overburden pressure at the top of the clay, and the undrained strength increases with depth in the clay at a rate of 11 psf per foot. With this model, the undrained shear strength of the clay varies with lateral position, being greatest beneath the levee crest where the effective overburden pressure is

greatest, and varying with depth, increasing at a rate of 11 psf per foot at all locations.

This model does not consider details of the stress distribution beneath the levee, which would result in “load spread” effects. These effects would result in rotation of principal stresses beneath the levee, and in components of stress due to the levee load decreasing with depth. Including these complex effects would complicate the model considerably. In our opinion, such refinement would make the model impractical, and is not justified. The model described in the previous paragraphs uses a simple stress distribution beneath the levee that satisfies vertical equilibrium, and it reflects the fact that the undrained strength is proportional to consolidation pressure, certainly the most important aspect of the strength of the clay.

The computer program SLIDE¹ uses two-dimensional interpolation to compute strengths that vary in both the horizontal and vertical direction, as is the case with the strength model described above. This feature provides a convenient means for representing the New Orleans levee clay strengths in stability analyses performed with SLIDE.

Shear strength of sand

Correlations with Cone Penetration tip resistance were used to estimate a value of $\phi' = 35$ degrees for the silty sand beneath the clay. As noted previously, the sand layer is not involved in observed or computed failure mechanisms, and the value of ϕ' assigned to it therefore has no influence on computed factors of safety.

Comparison with strengths used in design

The design analyses used undrained strengths for the levee fill, the peat, and the clay, and a drained friction angle to characterize the strength of the sand layer beneath the clay, as does the strength model described above. Thus the strengths are directly comparable.

The values of strength for the levee fill, the peat, and the sand that were used in the design analyses for the 17th Street Canal I-wall, Stations 552+70 to 635+00 (new Stations 0+00 to 82+30) are shown in Table K1-2. This interval includes the breach area, which extends approximately from new Station 7+50 to new Station 12+20.

¹ Available from Rocscience Inc., 31 Balsam Avenue, Toronto, Ontario, Canada M4E 3B5

The design strength values shown in Table K1-2 are taken from Plate 56 of the 17th Street Canal Geotechnical Design Memorandum (GDM)¹. Also shown in Table X are the values of strength from the strength model discussed above.

Table K1-2 Comparison of strengths of levee fill, peat and sand used in design for Stations 552+70 to 635+00 with the strength model based on all data available in February 2006		
Material	Strength uses for design	Strength model based on all data available in February 2006
Levee fill	$s_u = 500 \text{ psf}, \phi = 0$	$s_u = 900 \text{ psf}, \phi = 0$
Peat	$s_u = 280 \text{ psf}, \phi = 0$	$s_u = 400 \text{ psf}, \phi = 0$ beneath levee crest $s_u = 300 \text{ psf}, \phi = 0$ beneath levee toe
Sand	$\phi' = 30 \text{ degrees}$	$\phi' = 35 \text{ degrees}$

It can be seen that the strengths for the levee fill, the peat and the sand used in design are consistently lower than those estimated using all of the data available in February 2006.

The values of strength for the clay vary with depth and laterally, as discussed above. The values of undrained strength used in design are compared with those described above in Figures K1-54, K1-55, and K1-56. These figures show the strengths for the strength model discussed previously as dotted lines, superimposed on photocopies of the GDM figure. Minor variations in the strengths at Stations 8+30, 10+00 and 11+50 occur because the thicknesses of the levee fill and peat are slightly different in the three cross sections, and the effective stresses at the top of the clay are therefore slightly different.

In each of the three cases the rate of increase of strength with depth (11 psf per foot) are essentially the same in the strength model as for the design strengths. Beneath the levee crest, the design strengths are very close to those determined from the strength model. At the toe of the levee, however, the strengths used in design are considerably higher than the strengths from the strength model.

Comparison of strengths within the breach area with strengths elsewhere

Field observations and preliminary analyses show that the most important shear strength is the undrained strength of the clay. Critical slip surfaces intersect only small sections within the peat and the levee fill, and do not intersect the sand layer beneath the clay at all. Therefore the strengths of these materials have small influence on stability, and minor variations in these strengths from section to section would not control the location of the failure.

¹ Design Memorandum No. 20, General Design, Orleans Parish – Jefferson Parish, 17th Street Outfall Canal, U. S. Army Engineer District, New Orleans, March 1990.

For this reason, the comparison of strengths in the breach area with strengths elsewhere has been focused on the undrained strength of the clay.

Within the breach area, only two borings drilled before the failure (Borings 62 and 64) are available. The strengths measured on undisturbed specimens from these borings are listed in Table K1-3.

Table K1-3			
Undrained strengths of clay for specimens from the breach area.			
Boring 62			
Depth	Test type	s_u	Average
24 ft	UC	305 psf	280 psf
34 ft	UC	260 psf	
42 ft	UU-1	178 psf (very loose clayey sand – ignore)	
Boring 64			
Depth	Test type	s_u	Average
22 ft	UC	103 psf	240 psf
33.5 ft	UC	383 psf	
41.5 ft	UC	168 psf (likely disturbed – ignore)	

The strengths summarized in Table K1-3 can be compared with the strengths of specimens from borings to the north and south of the breach, which are summarized in Tables K1-4 and K1-5.

Table K1-4			
Undrained strengths of clay for specimens from borings north of the breach area.			
Boring 66			
Depth	Test type	s_u	Average
28.5 ft	UC	235 psf	317 psf
38.5 ft	UC	398 psf	
Boring 68			
Depth	Test type	s_u	Average
33 ft	UC	340 psf	353 psf
33 ft	UU	360 psf	
39 ft	UU	360 psf	
42.5 ft	UU-1	250 psf (likely sand, not clay – ignore)	
42.5 ft	UU	240 psf (likely sand, not clay - ignore)	

Table K1-5 Undrained strengths of clay for specimens from borings south of the breach area.			
Boring 60			
Depth	Test type	s_u	Average
24 ft	UC	200 psf	326 psf
29 ft	UC	365 psf	
29 ft	UU	380 psf	
34 ft	UC	385 psf	
39 ft	UC	323 psf	
39 UU	UU	300 psf	
44 ft	UU-1	243 psf (loose clayey sand – ignore)	
Boring 58			
Depth	Test type	s_u	Average
24 ft	UC	183 psf	324 psf
29 ft	UC	313 psf	
39 ft	UC	475 psf	
Boring 56			
Depth	Test type	s_u	Average
29 ft	UC	295 psf	305 psf
39 ft	UC	315 psf	

The average strengths from Tables K1-3, K1-4, and K1-5 are compared in Table K1-6 and Figure K1-57.

Table K1-6 Comparison of undrained strengths from breach area borings with strengths from borings north and south of the breach.		
Area	Range of s_u	Average s_u
Breach (Borings 62 and 64)	240 psf to 280 psf	260 psf
North of breach (Borings 66 and 68)	317 psf to 353 psf	335 psf
South of breach (Borings 56, 58 and 60)	305 psf to 326 psf	318 psf

Although the data is sparse, it is fairly consistent, and it appears that the clay strengths in the areas north and south of the breach are higher than those in the breach. Based on the average values shown in Table X4 and Figure X4, the undrained strengths of the clay in the areas adjacent to the breach are 20% to 30% higher than those in the breach area. Strength differences of this magnitude are significant. They indicate that the reason the failure occurred where it did is very likely that the clay strengths in that area were lower than in adjacent areas to the north and south.

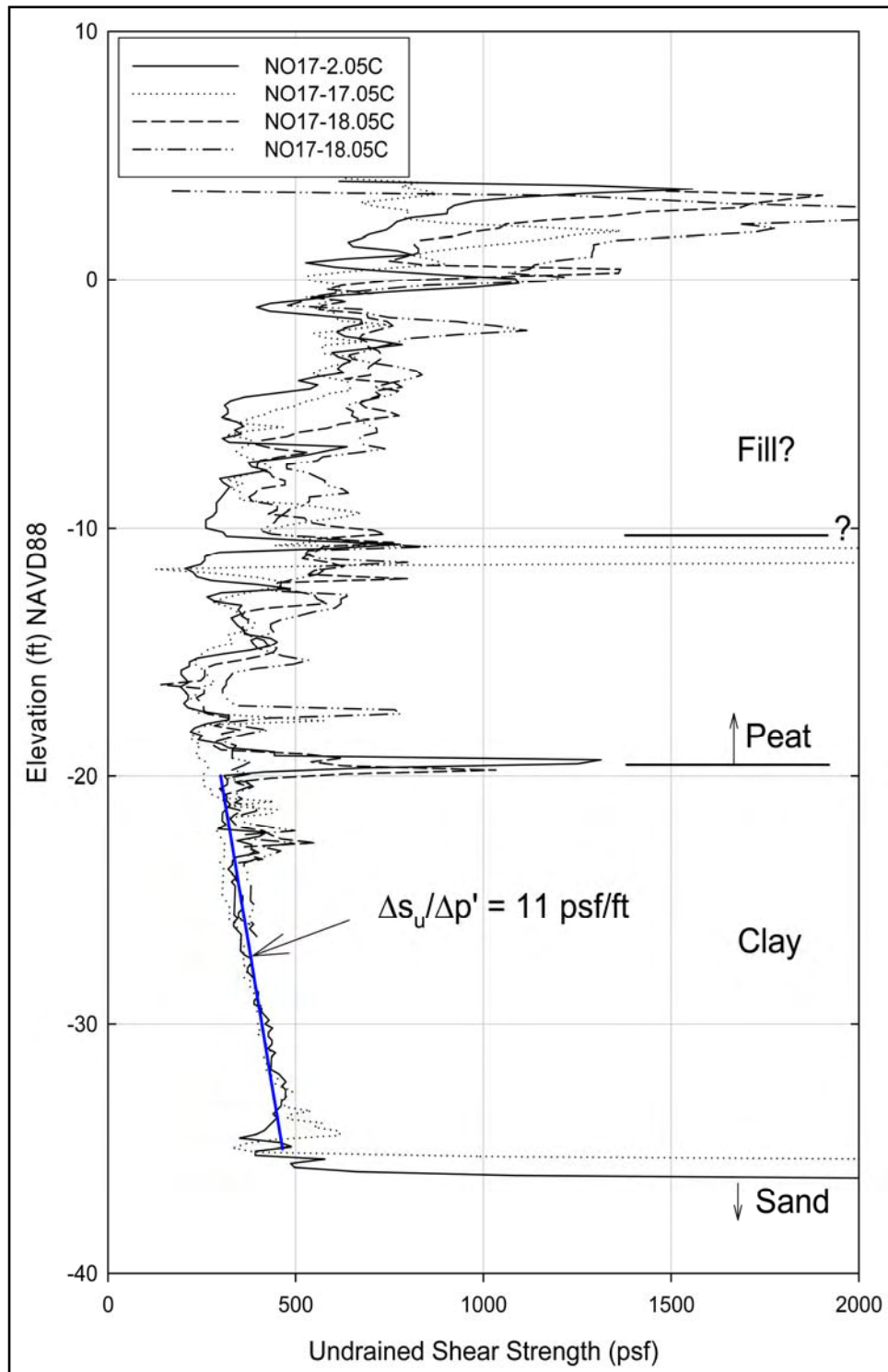


Figure K1-53. Undrained shear strength calculated from CPTU tests using Mayne's method.

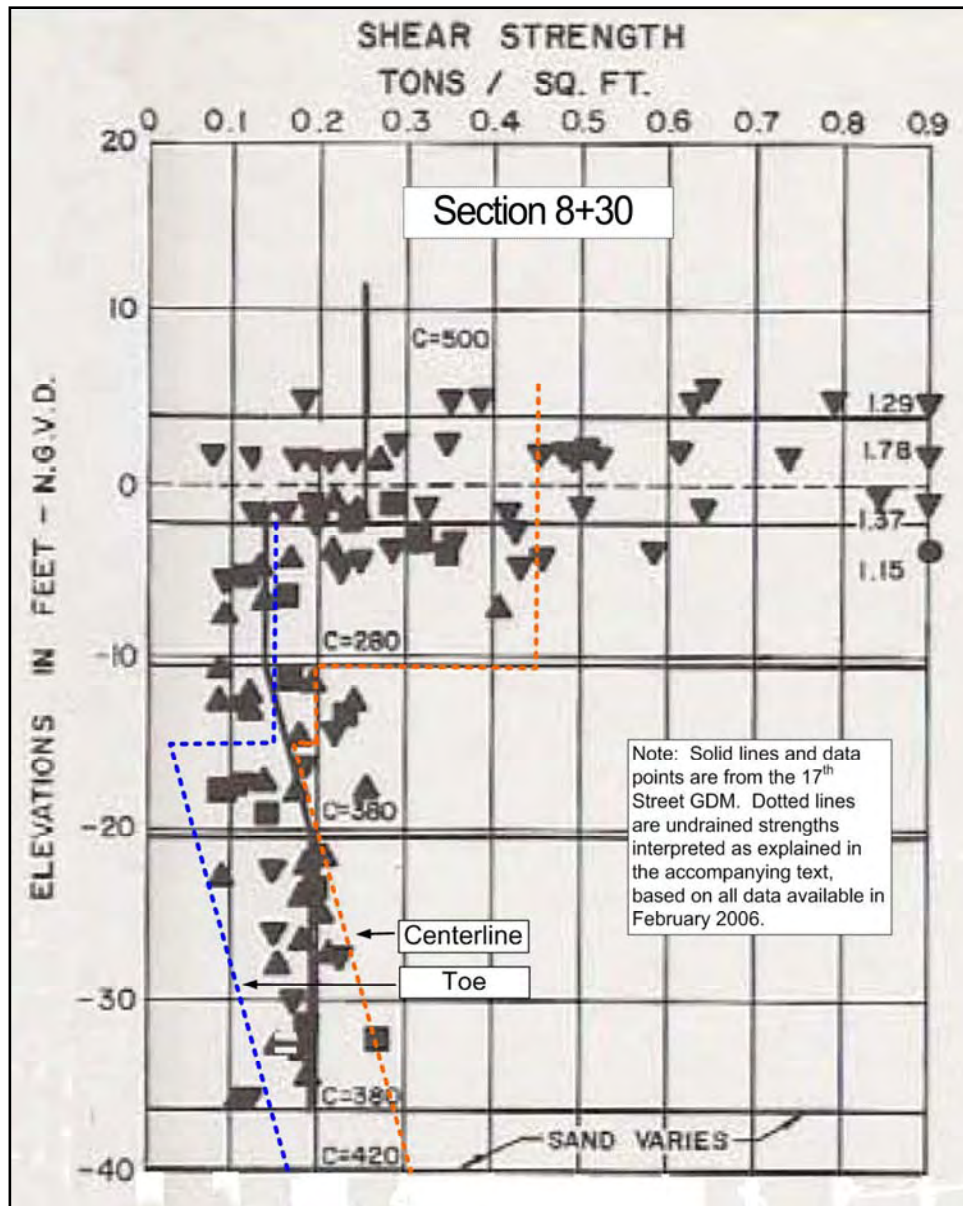


Figure K1-54. Comparison of undrained shear strength profiles used for 17th Street I-wall design with strength profiles interpreted from data available in February 2006, for Section 8+30.

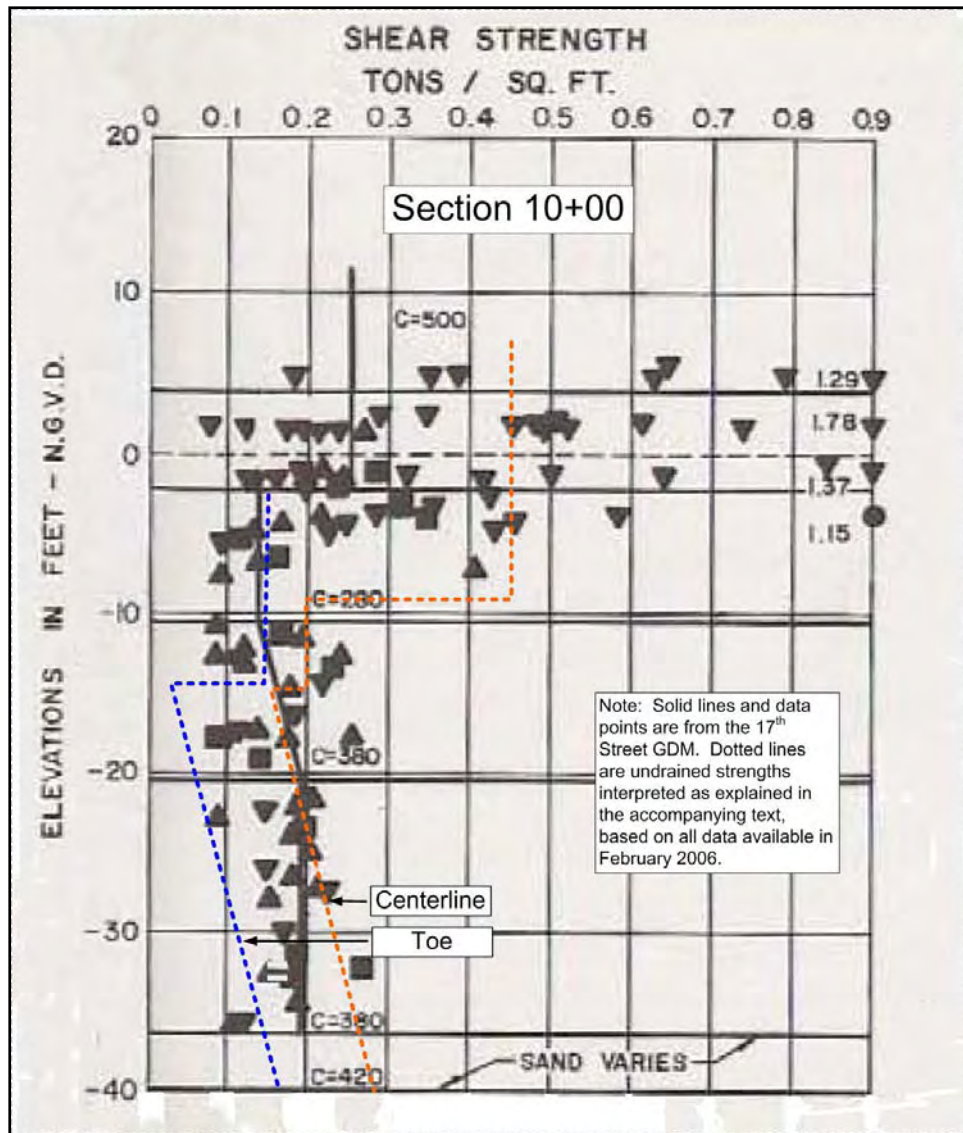


Figure K1-55. Comparison of undrained shear strength profiles used for 17th Street I-wall design with strength profiles interpreted from data available in February 2006, for Section 10+00.

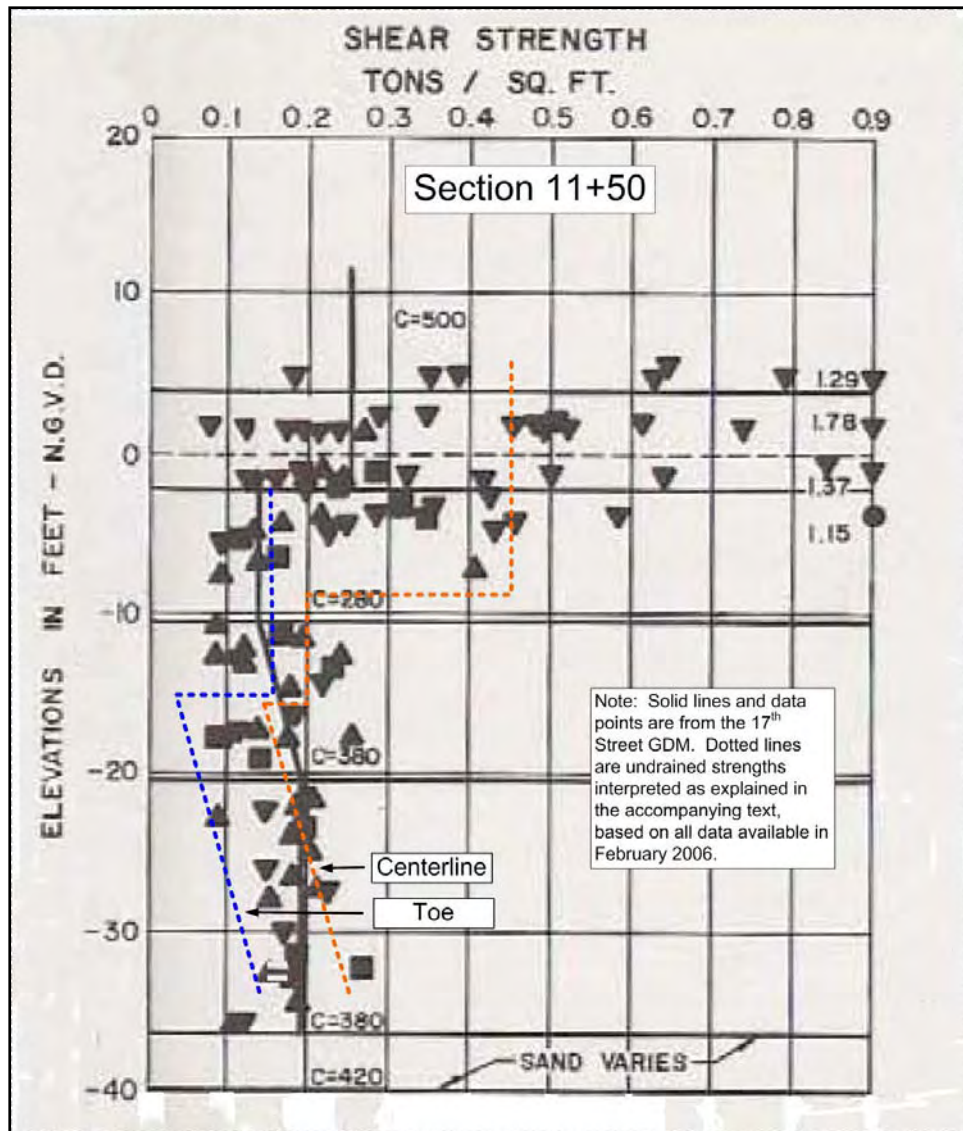


Figure K1-56. Comparison of undrained shear strength profiles used for 17th Street I-wall design with strength profiles interpreted from data available in February 2006, for Section 11+50.

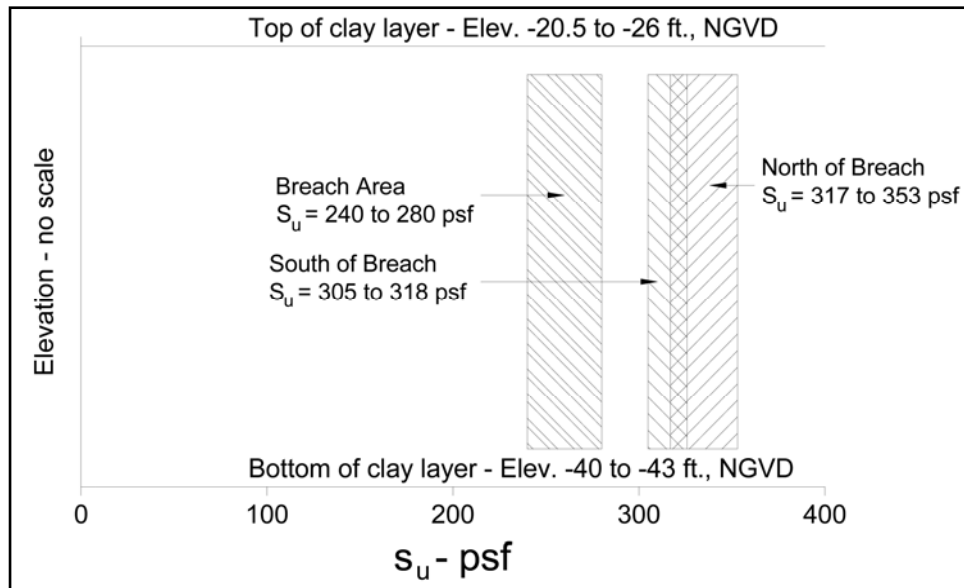


Figure K1-57. Comparison of undrained strengths from breach area borings with strengths from borings north and south of breach.

Appendix A: Description of New Orleans Area Geology, Environments of Deposition, and General Engineer Properties of these Environments

Extracted from

Dunbar, J. B., Torrey, V. H., III, Wakeley, L. D., 1999. "A Case History of Embankment Failure, Geological and Geotechnical Aspects of the Celotex Levee Failure, New Orleans, Louisiana," Technical Report GL-99-11, Engineer Research and Development Center, Waterways Experiment Station, Vicksburg, Mississippi

1 Introduction

The following summary describes the geology and the Holocene history of the New Orleans area, and the relationships between the associated environments of deposition and general engineering properties. This information has been extracted from a technical report on the geological and geotechnical aspects of the Celotex Levee failure, which occurred along the west bank of the Mississippi River in 1985 in the greater New Orleans area (Figure 1). Only the geology sections are presented in this Appendix. This information serves as background information for evaluation of the various canal failures during Hurricane Katrina.

The geologic portions of the Celotex Report were presented in Chapter 2 and Appendix A. Chapter 2 describes the geologic history and geology of the New Orleans area as determined from a review of the technical literature, an evaluation of numerous engineering borings, aerial photo interpretation, and preparation of several detailed cross-sections (Figures 2 through 5 of Chapter 2, see enclosed). Appendix A of this same report provides detailed descriptions and information about the engineering properties of the depositional environments that are present at the surface and in the subsurface. Chapter 2 and Appendix A are presented here in their original order of presentation because of their logical arrangement in the text. The descriptions of the environments are important when examining soil types and physical properties from the respective environments.

Additionally, various references are identified in the text and are presented at the end of this summary appendix. Many of the Corps of Engineer cited publications and maps for the New Orleans area are now presented at the ERDC website on the Geology of the Lower Mississippi Valley (see lmvmapping.erd.usace.army.mil)

A final note, the lacustrine environment is not identified in the summary description and is an important lithostratigraphic unit. This environment is unique to this area because of the protection afforded by the now buried Pine Island beach complex during the filling of the New Orleans area with subsequent sediment by the various Mississippi River distributary channels during the Middle to Late Holocene. The lacustrine environment has been mapped for the back or northern side of the beach ridge in various GDMs, while the front or seaward side has been mapped as being interdistributary. This distinction is primarily a matter of semantics, as opposed to any significant differences between lithology and/or engineering properties of these respective two environments. For purposes of this discussion and overall context, these two environments are nearly identical. The discussion of the interdistributary environment will be representative for the lacustrine environment identified throughout many of the GDMs.

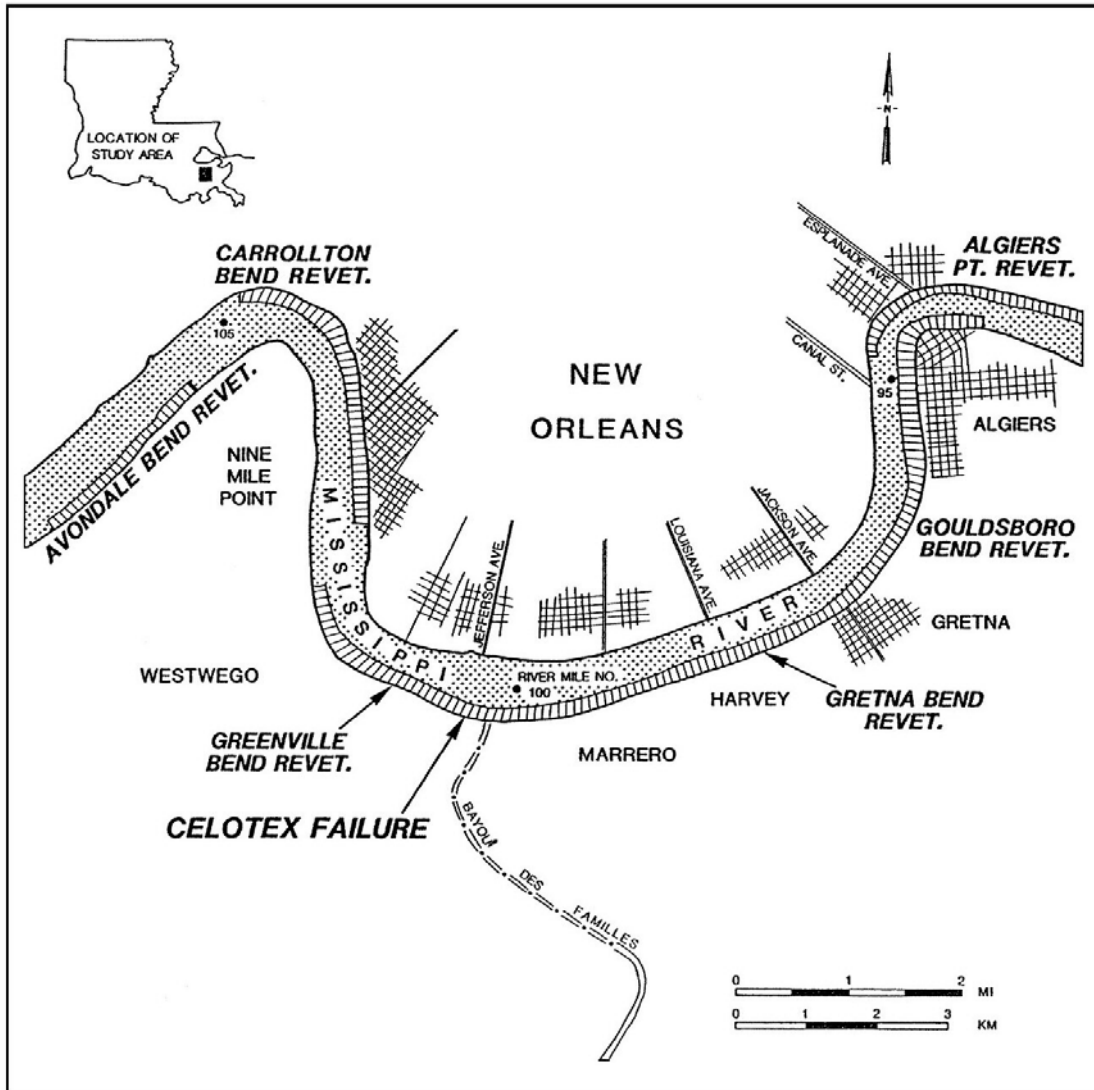


Figure 1. Map of study area showing location of the Celotex levee failure

2 Geology

Physiography

The study area is located in the southern portion of the lower Mississippi Valley and is a part of the Mississippi River's deltaic plain. Broad natural levees associated with the Mississippi River and Bayou des Familles, a prehistoric distributary channel, are the most prominent physiographic features in this area. Surface topography is generally of low relief with surface elevations ranging from approximately 25 ft (7.6 m) NGVD along the levee crests to sea level throughout much of the study area. Over a significant part of the New Orleans Metropolitan area the surface elevation is at or below sea level.

In the New Orleans area, the meander pattern of the Mississippi River is distinctive, making four nearly right angle turns which have changed very little during the past 100 years (Figure 1). The width of the Mississippi River within the study area (river mile 91.0 to 106.0 (146.45 to 170.59 km)) ranges from 1,750 to 2,700 ft (533 to 823 m). The river thalweg elevations through this reach range from -70 ft (-21 m) to about -190 ft (-58 m) NGVD. The top of the bank elevation through the study reach averages about 10 ft (3 m) NGVD. Channel bendways are characterized by deep "permanent" scour pools separated by shallower crossings. Revetment protection along the river corresponds to the deeper scour pools at Avondale, Carrollton, Greenville, Gretna, Gouldsboro, and Algiers (Figure 1).

Geologic Setting and History

The scope of this study permits a summary of the major events to explain the significance of the engineering geology in the study area. The general geologic chronology that has been defined for the Mississippi River's deltaic plain is based upon thousands of engineering borings drilled during the past 50 years, hundreds of radiometric age determinations of organic deltaic sediments, and numerous geologic studies conducted in this region (Fisk 1944; Kolb and Van Lopik 1958a and 1958b; Kolb 1962; Kolb, Smith, and Silva 1975; Autin et al. 1991; Frazier 1967; Saucier 1969 and 1974; May et al. 1984; Dunbar et al. 1994 and 1995; Smith, Dunbar, and Britsch 1986). Boring data identify a diverse surface and subsurface geology that is related to the different course shifts by the Mississippi River and associated deltaic advances during the Holocene (last 10,000 years).

To better understand the geology of the area, it is first necessary to briefly review the geologic history of coastal Louisiana since the late Pleistocene (17,000 to 10,000 years ago). Approximately 17,000 years ago, glaciers covered much of North America and sea level was approximately 300 ft (91 m) below the present level (Kolb, Smith, and Silva 1975). The Gulf shoreline was much farther seaward than at its present location.

The ancestral Mississippi River and its tributaries below Baton Rouge, LA, were entrenched into the underlying Pleistocene surface and had developed a broad drainage basin, approximately 25 miles (40 km) wide, which extended southeasterly beneath the present deltaic plain (Kolb and Van Lopik 1958a). Geologic mapping (Kolb and Van Lopik 1958a and 1958b; May et al. 1984) indicates that the axis of the valley entrenchment occurs in the vicinity of Houma, LA, approximately 45 miles (72 km) southwest of New Orleans.

The underlying Pleistocene surface represents deposits from a much older Mississippi River deltaic plain sequence and associated nearshore environments. These sediments were deposited during the previous interglacial cycle (Sangamon interglacial period), approximately 125,000 to 70,000 years ago. Fisk (1944) collectively called these Pleistocene sediments the Prairie Formation. Sediments of the Prairie Formation outcrop at the surface just north of Lake Pontchartrain.

Sea level began rising approximately 17,000 years ago because of glacial melting and reached its present level between 4,000 and 6,000 years before the present. Rising sea level corresponds to a period of valley-wide aggrading of the ancestral alluvial valley by the existing fluvial systems. Melting glaciers released large quantities of sediment to the Pleistocene drainage system and filled the entrenched valley with coarse sediments (sand and gravel). A dense network of shallow and swiftly flowing braided stream courses formed within the ancestral alluvial valley because of overloading by the massive influx of glacial outwash. Along the length and width of the Lower Mississippi Valley, basal substratum sands are present in the subsurface which represent the relic braided stream or outwash plain sediments from glacial melting (Fisk 1944; Kolb et al. 1968; Krinitzsky and Smith 1969; Saucier 1964 and 1967; Smith and Russ 1974). The change in deposition from a braided system to a meandering Mississippi River system occurred approximately 12,000 years before the present (Saucier 1969; and Krinitzsky and Smith 1969).

Advent of the modern sea level began creation of the modern deltaic plain and led to the present land surface. Present day coastal Louisiana is the product of numerous, but generally short lived, seaward prograding delta systems. These deltas are subsequently reworked by coastal transgressive processes and modified. Five major deltaic systems have been built seaward during the past 6,000 years as shown by Figure 2 (after Frazier 1967). Each delta system consists of several major distributary channels and numerous individual delta lobes (Figure 3). The relative ages of these delta systems are generally well established by radiocarbon dating techniques. Limits of the different delta systems and the chronology of the major distributary channels associated with each system are summarized in Figures 2 and 3 (after Frazier 1967).

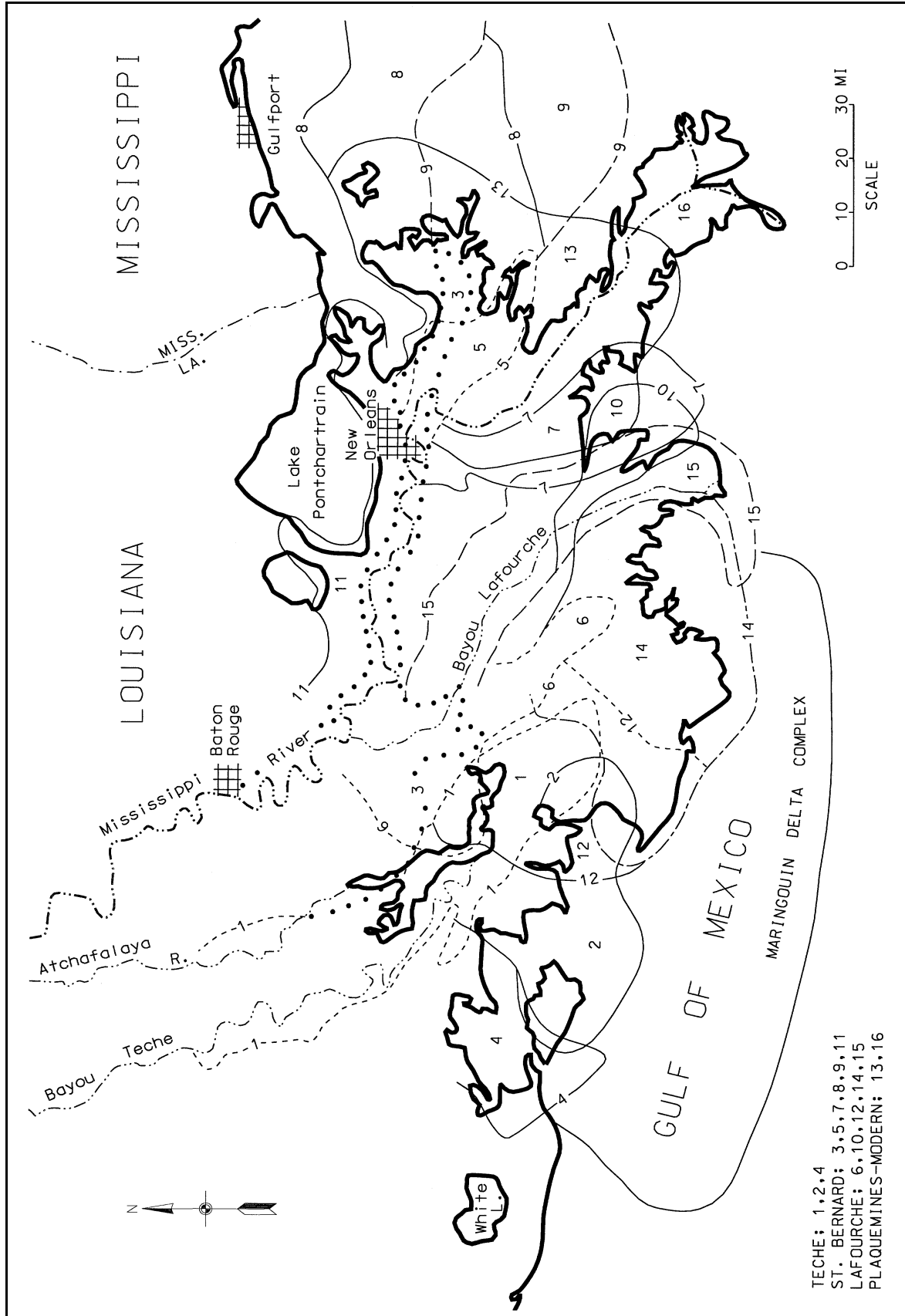


Figure 2. Holocene delta and distributary systems (after Frazier 1967)

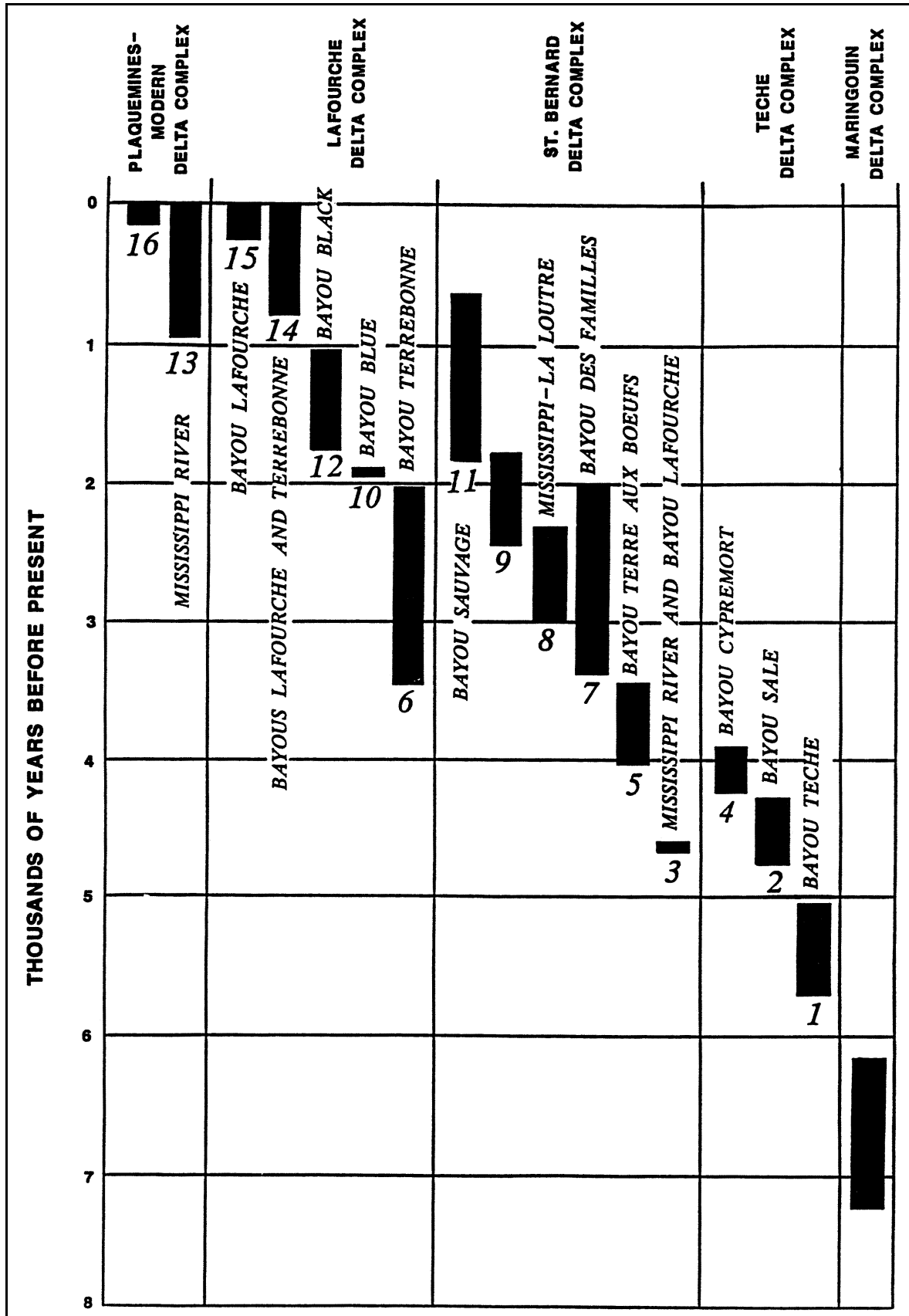


Figure 3. General chronology of Mississippi River delta and distributary systems (after Frazier 1967)

The first advance of a major delta system into the New Orleans area occurred with the St. Bernard system. The present course of the Mississippi River through the New Orleans area was established during the active St. Bernard delta. Partial Mississippi River flow continued to pass through the New Orleans reach following abandonment of the St. Bernard system for the Lafourche delta complex. During the active Lafourche system, the Mississippi River flowed southward at Donaldsonville, through Bayou Lafourche, and to the Gulf of Mexico. After abandonment of the Lafourche system approximately 500 years ago, nearly full Mississippi River flow returned to the present day course.

Geologic Structure

The study area is part of the seaward thickening wedge of Quaternary sediments which dip gently gulfward and fill the Gulf of Mexico geosyncline. Major structures within this sedimentary prism are piercement salt domes and growth faults. In the study area there are no buried salt domes. The vast majority of Louisiana's salt domes are located south and west of the New Orleans area (New Orleans Geological Society 1962 and 1983; and Halbouty 1967).

Faulting has been identified in the subsurface throughout the deltaic plain and in the Pleistocene deposits exposed at the surface north of Lake Pontchartrain (Wallace 1966; and Snead and McCulloh 1984). These faults are not tectonically active. Instead, they are related to sedimentary loading of the Gulf of Mexico basin. Faulting has been identified in the Pleistocene sediments beneath Lake Cataouatche (approximately 8 miles (12.8 km) southwest of New Orleans) and beneath Lake Pontchartrain (Wallace 1966; and Kolb, Smith, and Silva 1975). Fisk (1944) identified several normal faults in the buried Pleistocene sediments beneath New Orleans. He interpreted these faults based on the orientation of stream courses, lake shores, and the Mississippi River. The presence of these faults based solely on this type of evidence is speculative without more detailed stratigraphic evidence to support their existence. Non-tectonic geomorphic and stratigraphic processes can produce these types of linear features without faulting as the underlying mechanism. A detailed engineering study of Pleistocene sediments in the New Orleans area by Kolb, Smith, and Silva (1975) did not identify subsurface faults near the Celotex failure site or for the general New Orleans area. Their study identified only one fault in the New Orleans area (in Lake Pontchartrain) and was based on combined boring and geophysical (subbottom profiling) data.

No faults were identified during this investigation in the study area. Surface faults in Holocene sediments are difficult to detect, because unconsolidated sediments tend to warp rather than shear. Geologic mapping and boring data evaluated during the course of this study did not identify any surface or subsurface faulting in the study area.

Geology and Environments of Deposition

Surface geology

The first objective of this investigation was to map and define the surface and subsurface geology of the study area. Definition of the geology was accomplished by examination and interpretation of historic aerial photography, subsurface data (engineering borings and electrical logs), different hydrographic survey periods, historic maps, and by review of the available geologic literature (Autin et al. 1991; Eustis Engineering Company 1984; Frazier 1967; Kemp 1967; Kolb 1962; Kolb and Van Lopik 1958a and 1958b; Kolb, Smith, and Silva 1975; Kolb and Saucier 1982; Miller 1983; Saucier 1963; Self and Davis 1983). A map of the surface geology for the study area is presented in Figure 4.

Environments of deposition mapped at the surface in Figure 4 include natural levee, point bar, inland swamp, fresh marsh, and several abandoned distributary channels. A complete description of the different environments of deposition present in the study area is contained in Appendix A. Natural levee deposits identified on the geologic map in Figure 4 are shown with the underlying environment of deposition. The surface geology consists primarily of Mississippi River natural levee and point bar deposits, several abandoned distributary channels, and their associated fluvial and deltaic deposits.

Formation of the study area is directly related to the past and present courses of the Mississippi River and its abandoned distributary channels. Abandoned distributary channels within the study area are associated with two major distributary systems, Bayou des Familles-Barataria and Bayou Sauvage-Metarie Bayou (Figure 4). Bayou Des Familles-Barataria is a major St. Bernard distributary channel or Mississippi River course which extends due south from the Mississippi River at the Celotex failure site to Barataria, LA. This distributary system was active from approximately 2,000 to 3,400 years before the present (Frazier 1967).

The second major distributary course mapped in the study area is Bayou Sauvage-Metarie Bayou. According to Frazier (1967), this course was active from about 800 to 1,800 years before the present (Figure 3). However, Saucier (1963) and Kolb and Van Lopik (1958a) indicate that this system may have been active even earlier. Radiocarbon dates from organic sediments beneath the natural levees of Metarie Bayou range from 2,300 to 2,600 years before the present and indicate that a marsh surface was developed within this area. Metarie Bayou intersects the Mississippi River at Kenner and extends eastward, branching into two segments north of Algiers Point. The northern branch extends northeast toward Chef Menteur, Louisiana, as Bayou Sauvage. The southern branch, labeled Unknown Bayou by Saucier (1963), intersects the Mississippi River at Algiers Point (Figures 1 and 4), follows the Mississippi River between Algiers Point and Gretna, and then extends due southeast where it intersects the Mississippi River at 12 Mile Point.

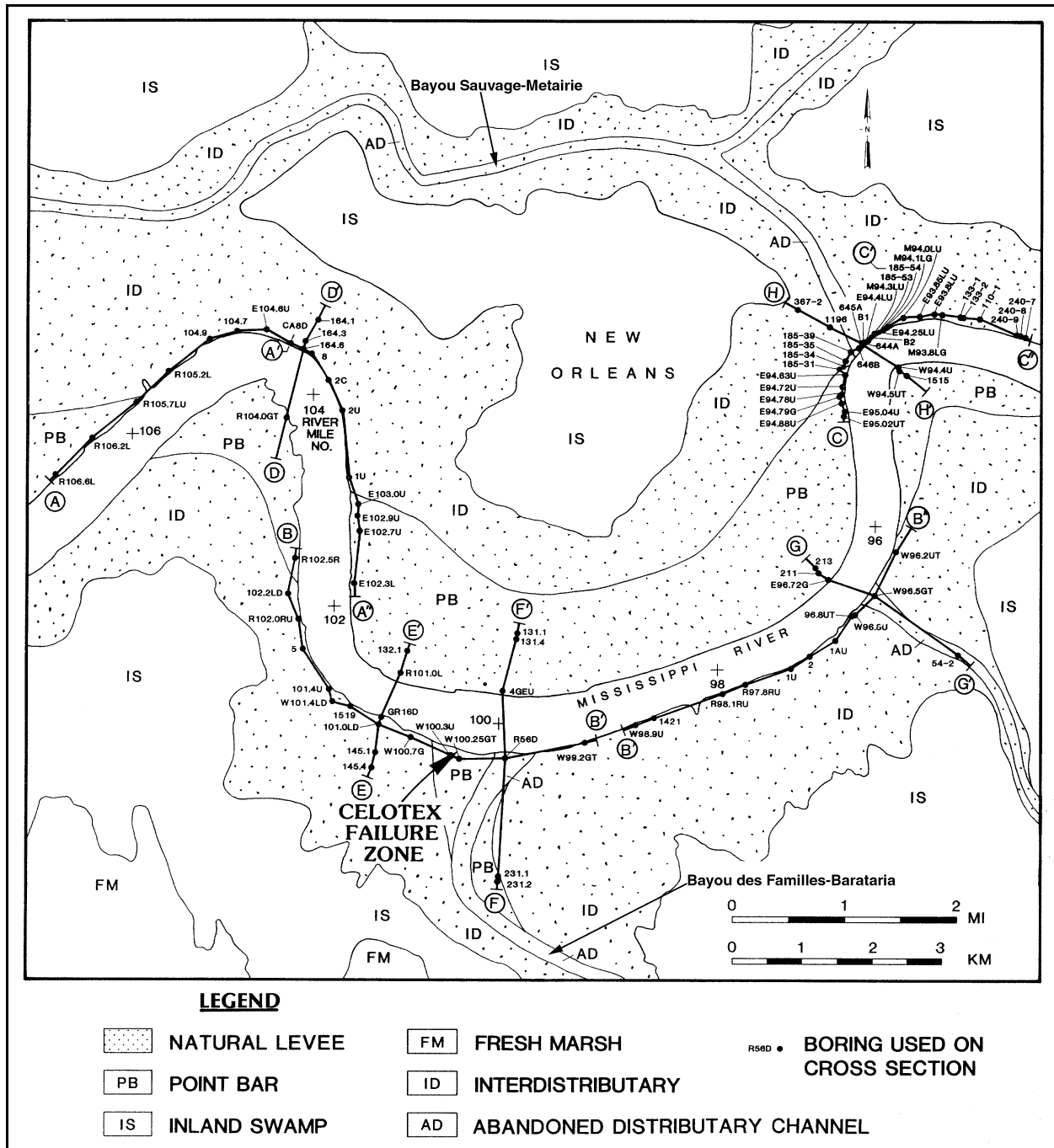


Figure 4. Geologic map of the study area showing boring and cross section locations

Subsurface geology

Eight geologic cross sections were constructed from borings collected and evaluated during this study. The locations of the cross sections are shown on the geologic map in Figure 4. Cross sections A through H are presented as Figures 5a through 5k, respectively. The longer cross sections are presented as

two separate sections or figures for illustration purposes. A legend of symbols and soil types identified on the sections is presented in Figure 51. Sections were constructed such that each revetment reach includes sections parallel and perpendicular to the river bank. Parallel sections were constructed for only the cutbank or concave side as this is the side for maximum erosion and potential bank instability. The majority of soil types shown on the geologic sections are classified according to the Unified Soil Classification System (USCS). Borings not using the USCS (e.g., borings from private engineering companies) are shown with their textural soil types identified. The geologic cross sections show the vertical and horizontal limits of the various environments of deposition adjacent to the river as well as the soil types that form these different environments. Depositional environments present in the subsurface include interdistributary, intradelta, and nearshore gulf. A general description of these environments is contained in Appendix A. For readers desiring further engineering soils data beyond what is presented in this report, a detailed summary of soil engineering properties for the various environments of deposition is presented by Kolb (1962) and Montgomery (1974).

Beneath the nearshore gulf sequence is the Pleistocene surface. The nearshore gulf sediments represent the deposits formed by the transgression of sea level onto the Pleistocene surface. These sediments were deposited under shallow-water conditions, before the advancement of the two major St. Bernard distributary systems into the study area. Establishment of the St. Bernard distributary systems into the study area produced the interdistributary sediments that were deposited into shallow-water, freshwater areas between the active distributary channels. Interdistributary sediments over time filled these shallow areas, and emergent vegetation in the form of fresh marsh began developing when interdistributary filling approached sea level. Closer to the active distributary systems, overbank deposition from the active distributary channels developed well drained natural levees and inland swamps.

A generalized contour map of the Pleistocene surface is presented in Figure 6 (Kolb, Smith, and Silva 1975). In general, the Pleistocene surface throughout the study area dips to the south and southwest at approximately 3 ft per mile (1 m per 1.6 km). Surface elevations on this surface are variable due to erosion by the preexisting Pleistocene drainage system and later Holocene scouring by past and present courses of the Mississippi River and its distributaries. Elevations of the Pleistocene surface range from -50 ft (-15 m) NGVD to greater than -150 ft (-46 m) NGVD in the bendways of the present Mississippi River channel.

Pleistocene deposits are characterized by a significant increase in stiffness and shear strength as compared to the overlying Holocene sediments. Pleistocene soils are fairly resistant to erosion from fluvial scouring. Where these soils occur in the riverbank, they represent a "hard point" which restrains the river's migration and deepening. Pleistocene deposits in the bed and bank of the river have had a significant influence on the river's ability to meander through the study area. There has been very little migration of the channel during the past 100 years as determined from comparison of old hydrographic surveys in Chapter 3 of this report.

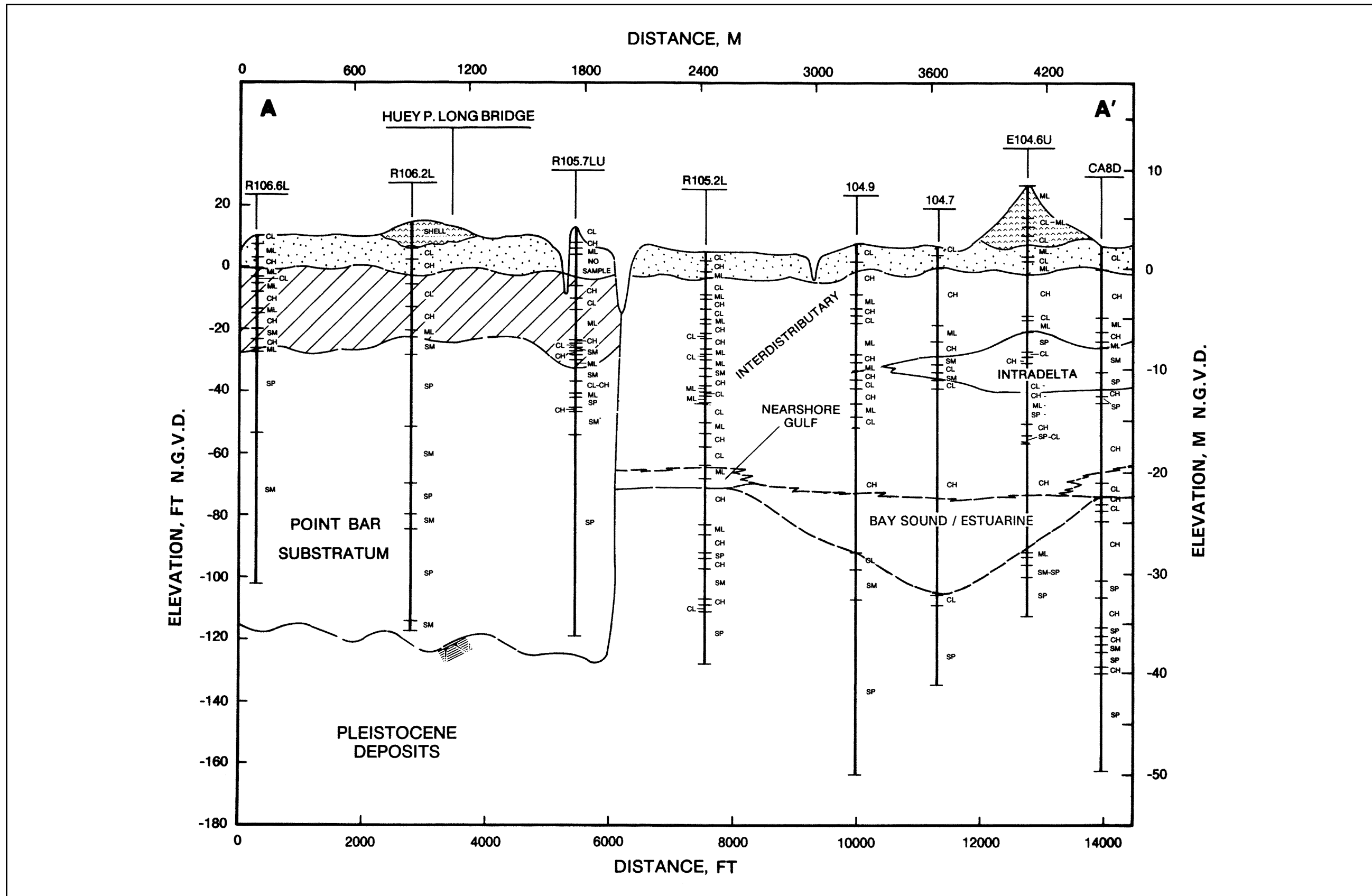


Figure 5a. Geologic cross section A-A' (see Figure 5l for symbol legend)

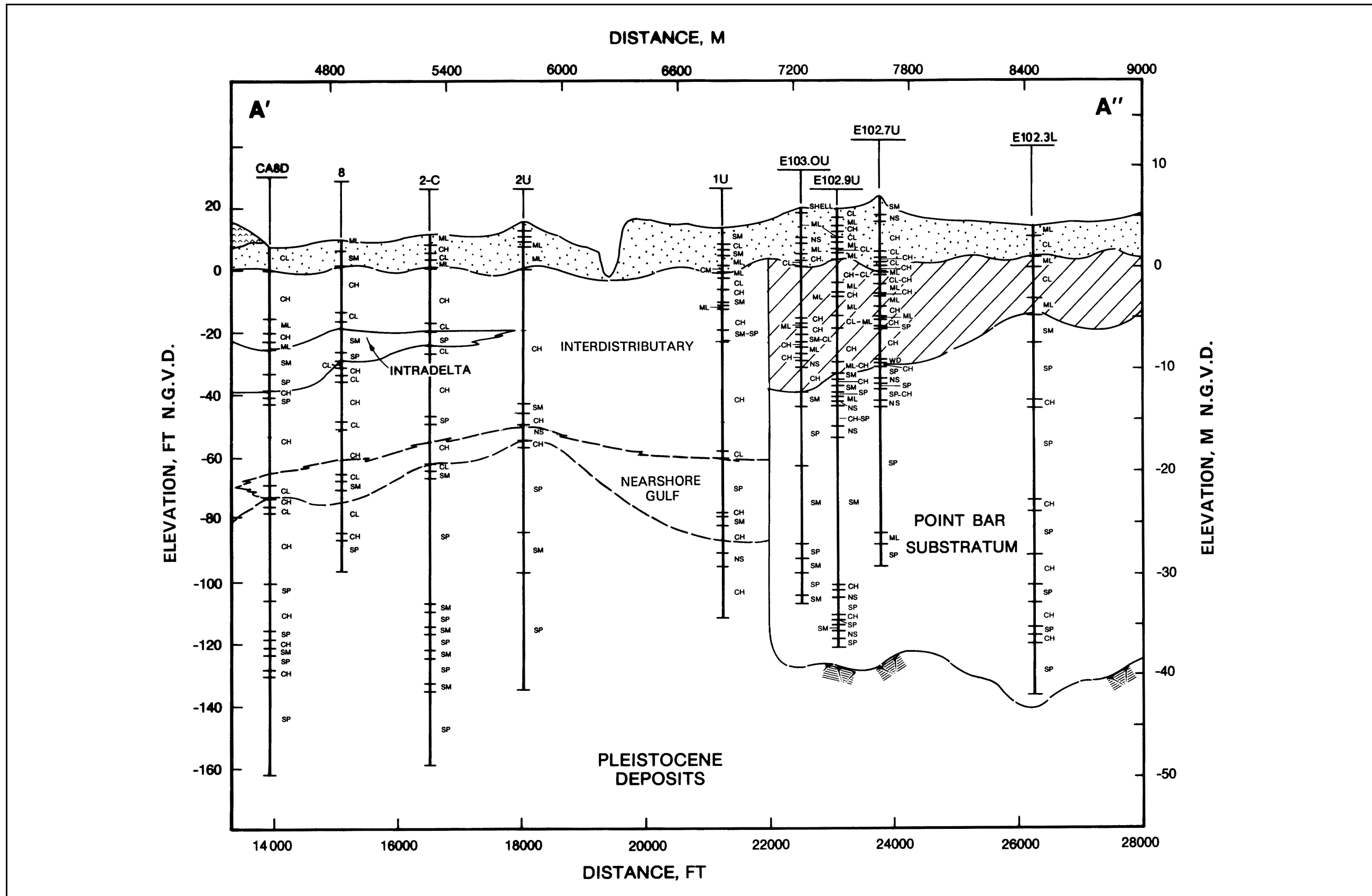


Figure 5b. Geologic cross section A'-A'' (see Figure 5l for symbol legend)

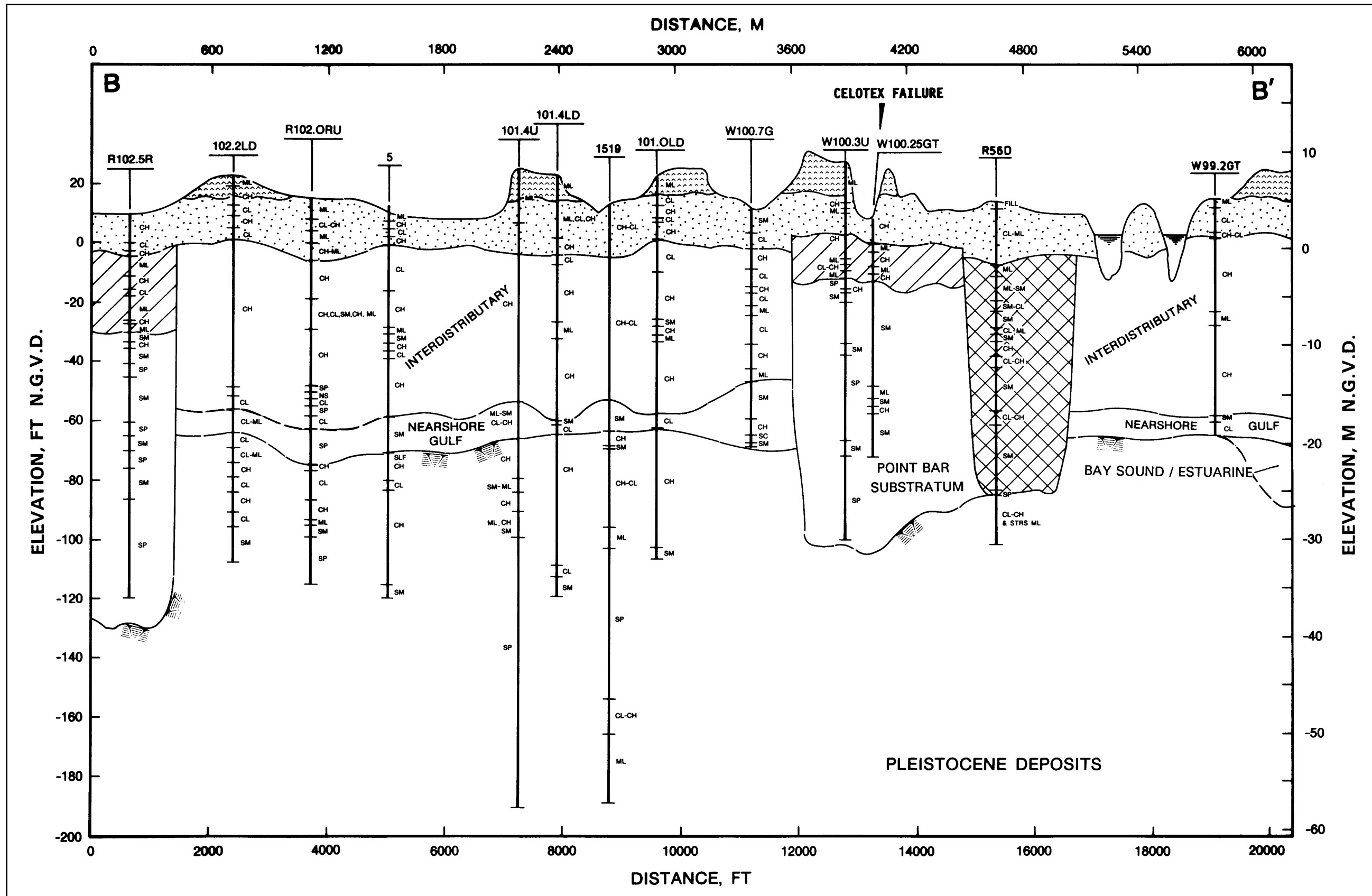


Figure 5c. Geologic cross section B-B' (see Figure 5l for symbol legend)

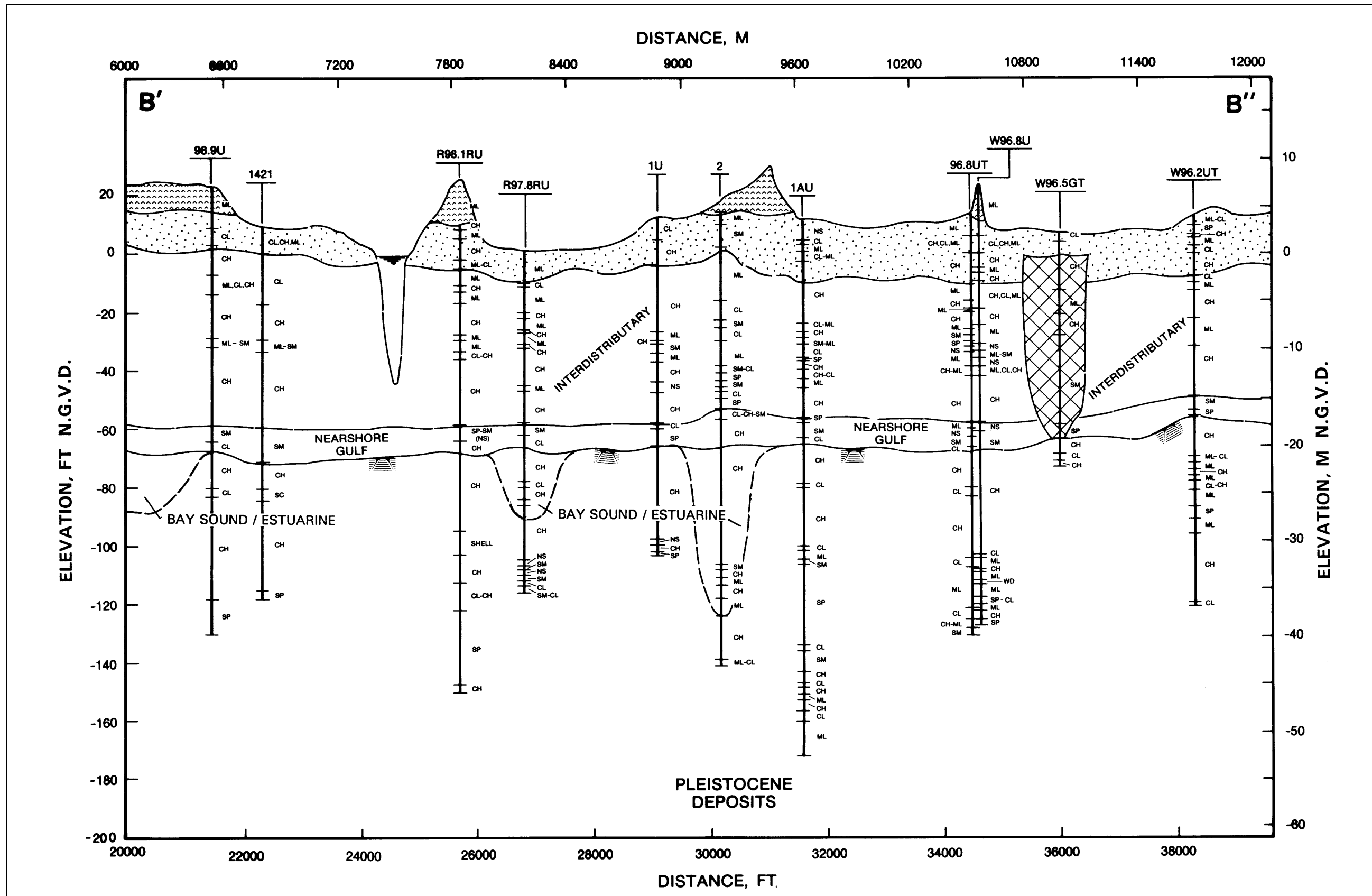


Figure 5d. Geologic cross section B'-B'' (see Figure 5l for symbol legend)

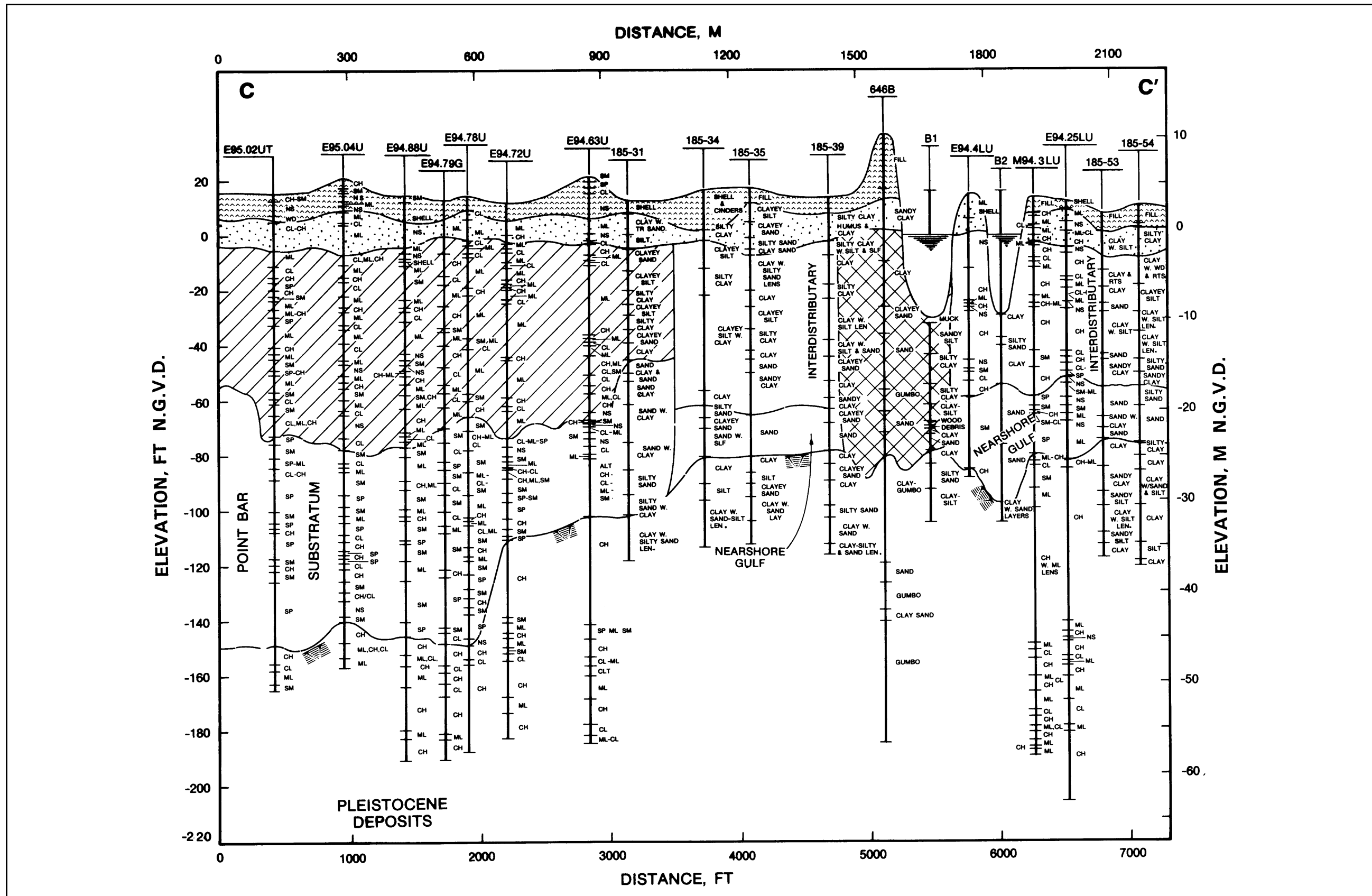


Figure 5e. Geologic cross section C-C' (see Figure 5l for symbol legend)

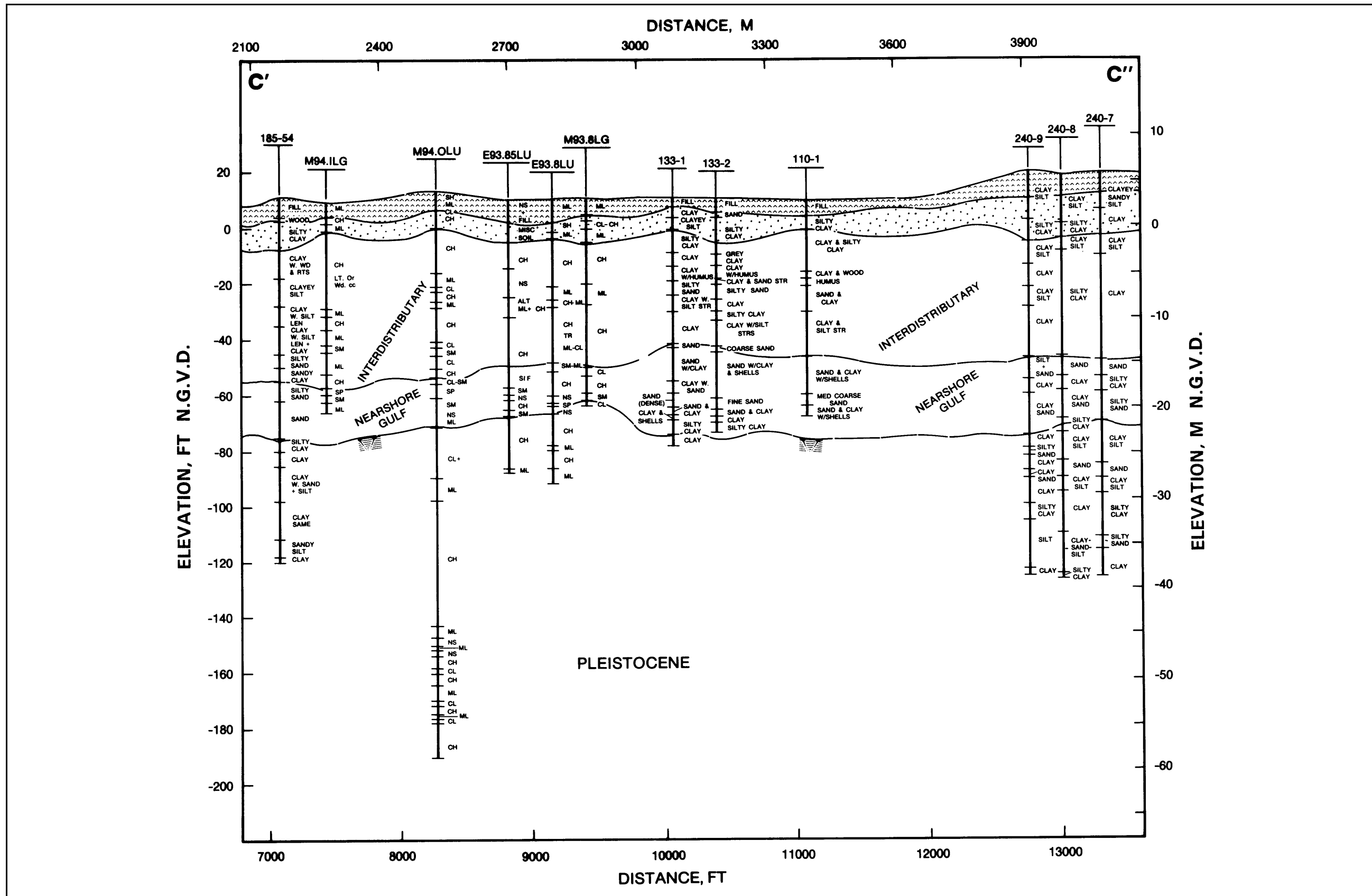


Figure 5f. Geologic cross section C'-C'' (see Figure 5l for symbol legend)

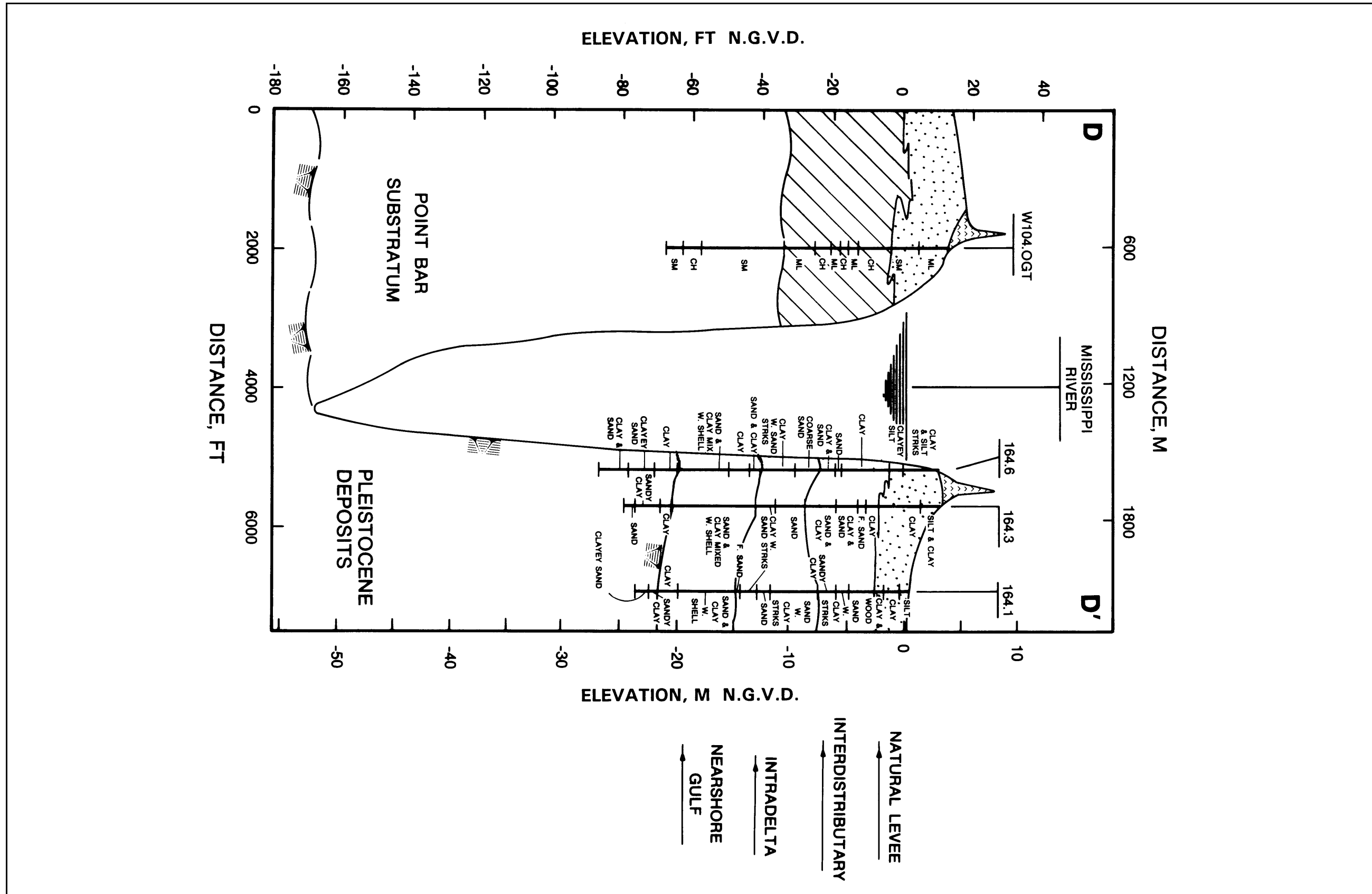


Figure 5g. Geologic cross section D-D' (see Figure 5l for symbol legend)

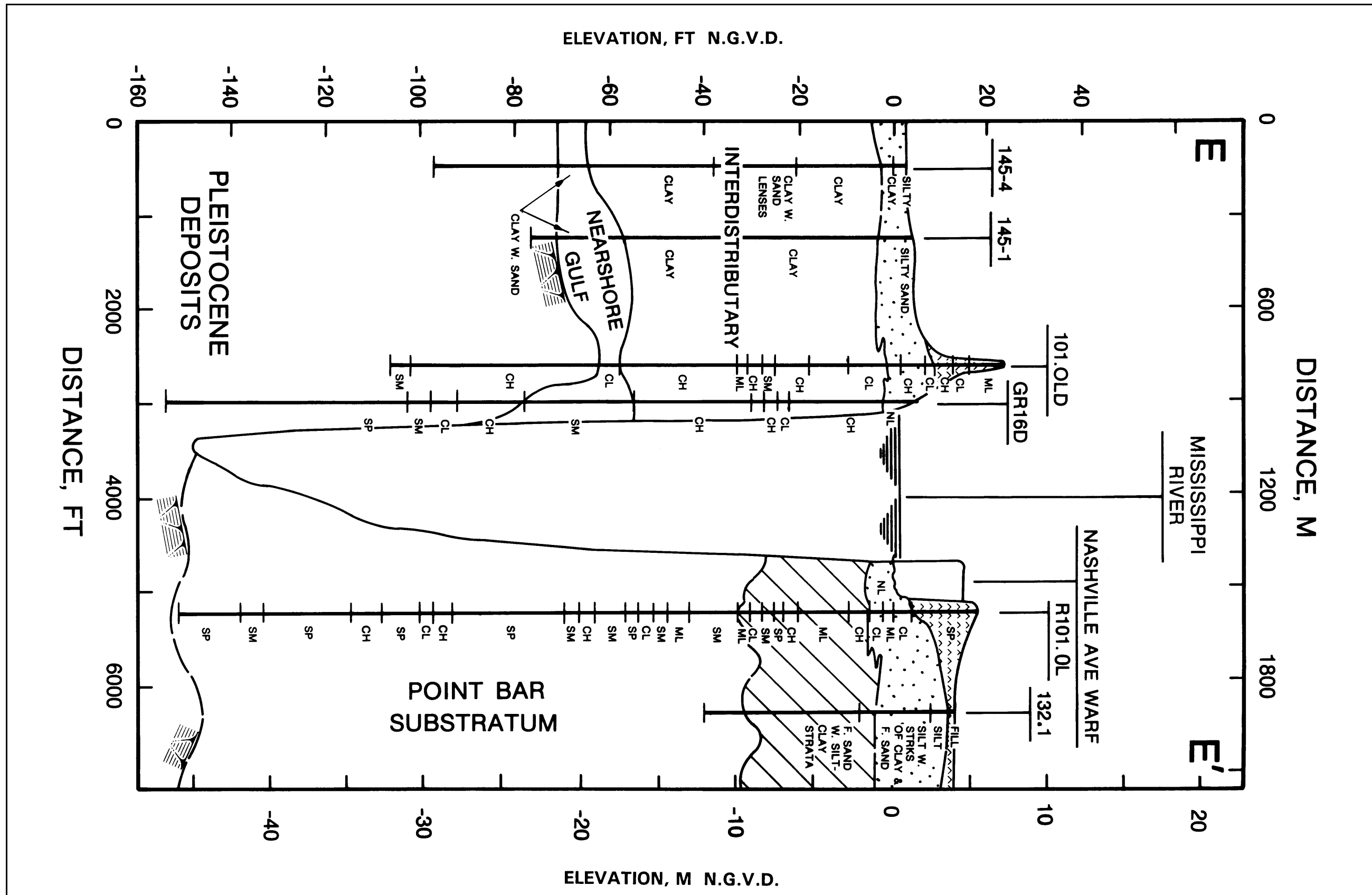


Figure 5h. Geologic cross section E-E' (see Figure 5l for symbol legend)

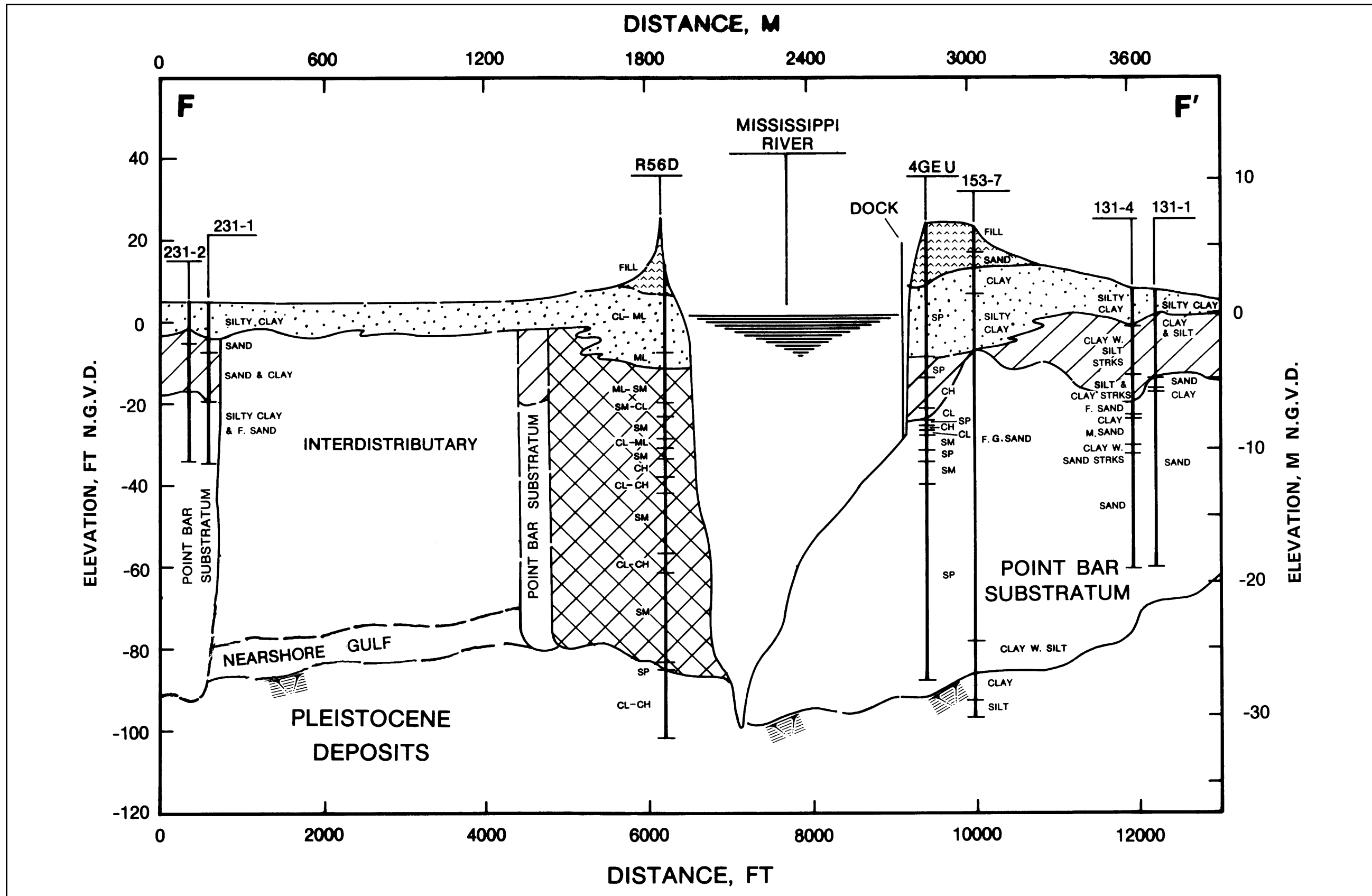


Figure 5i. Geologic cross section F-F' (see Figure 5l for symbol legend)

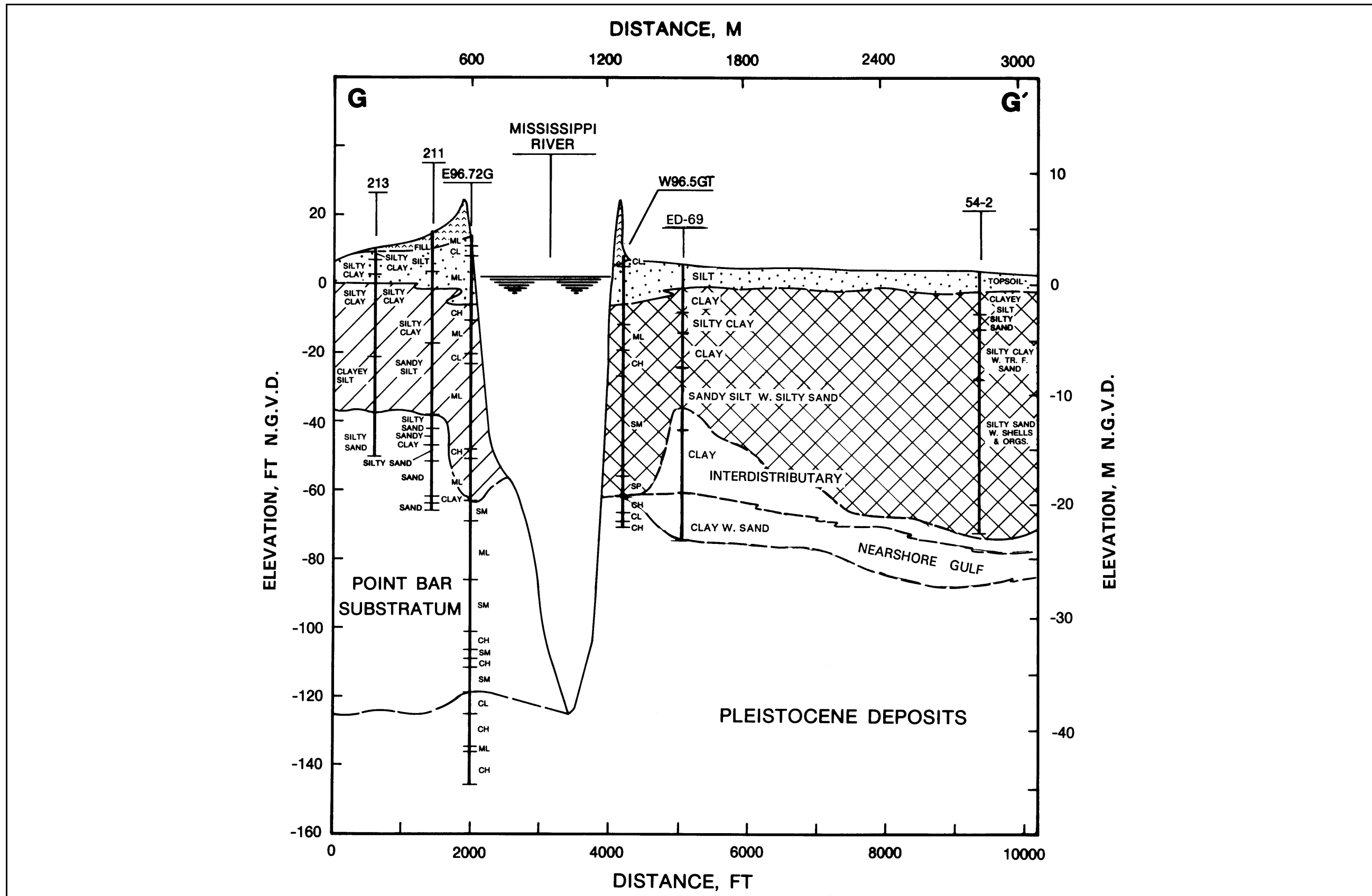


Figure 5j. Geologic cross section G-G' (see Figure 5i for symbol legend)

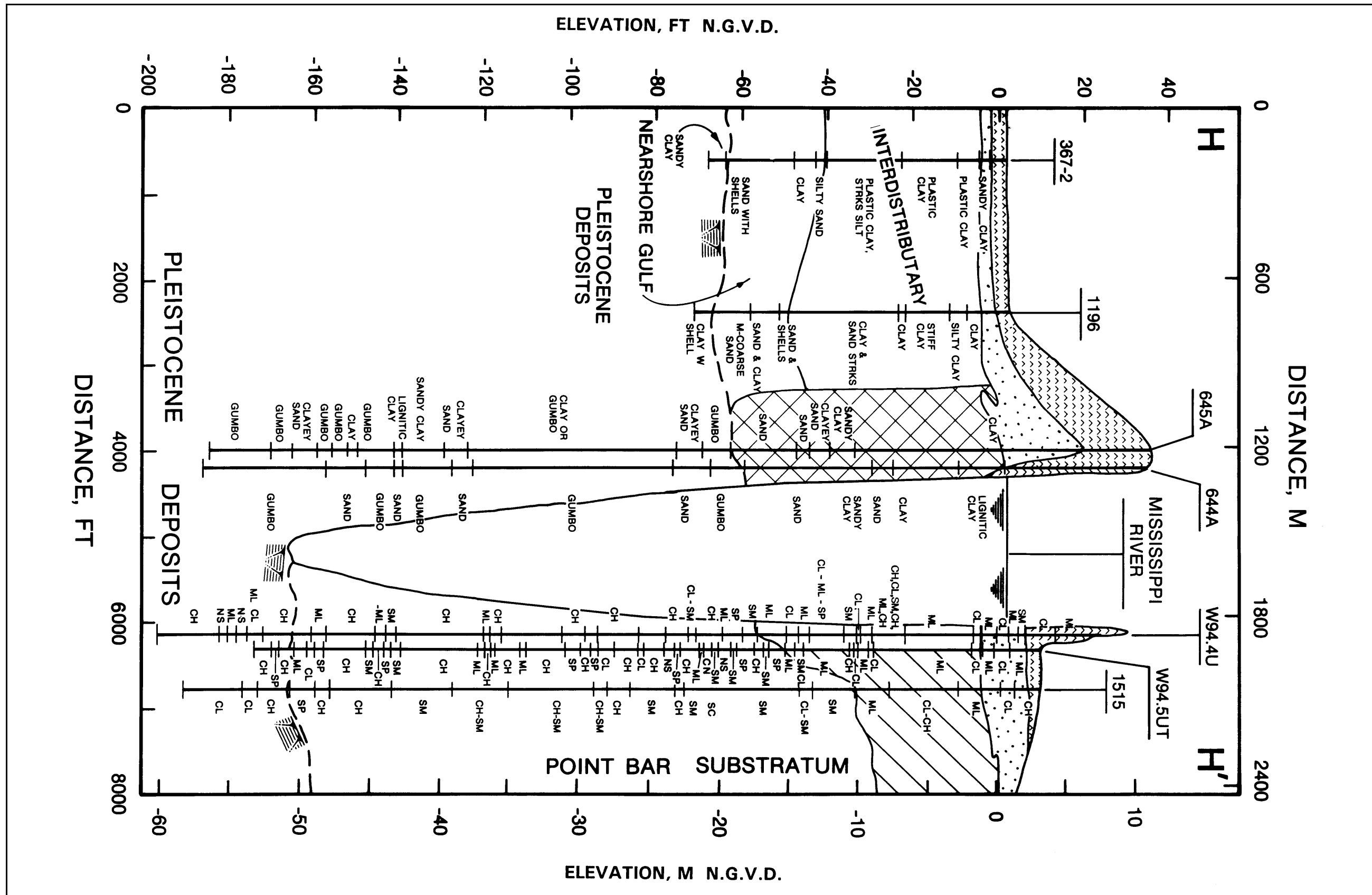
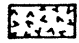
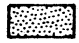
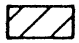
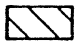



Figure 5k. Geologic cross section H-H' (see Figure 5l for symbol legend)



LEGEND

ENVIRONMENTS OF DEPOSITION

TOPSTRATUM DEPOSITS

-  LEVEE FILL
-  NATURAL LEVEE
-  POINTBAR
-  BACKSWAMP
-  ABANDONED COURSE

SUBSTRATUM DEPOSITS

-  UNDIFFERENTIATED SAND AND GRAVEL
-  UPPER FINE-GRAINED PLEISTOCENE SURFACE

SOIL TYPES (USCS)

- | | |
|-------------------------------------|-----------------------------------|
| CH — CLAY | SP — POORLY GRADED SAND |
| CL — SILTY CLAY,
SANDY CLAY | SW — WELL-GRADED SAND |
| ML — SILT, SANDY SILT,
CLAY SILT | GM — SILTY SAND-GRAVEL |
| SC — CLAYEY SAND | GW — WELL-GRADED
SAND-GRAVEL |
| SM — SILTY SAND | GP — POORLY GRADED
SAND-GRAVEL |

Figure 5l. Legend for the geologic sections of Figures 5a through 5k

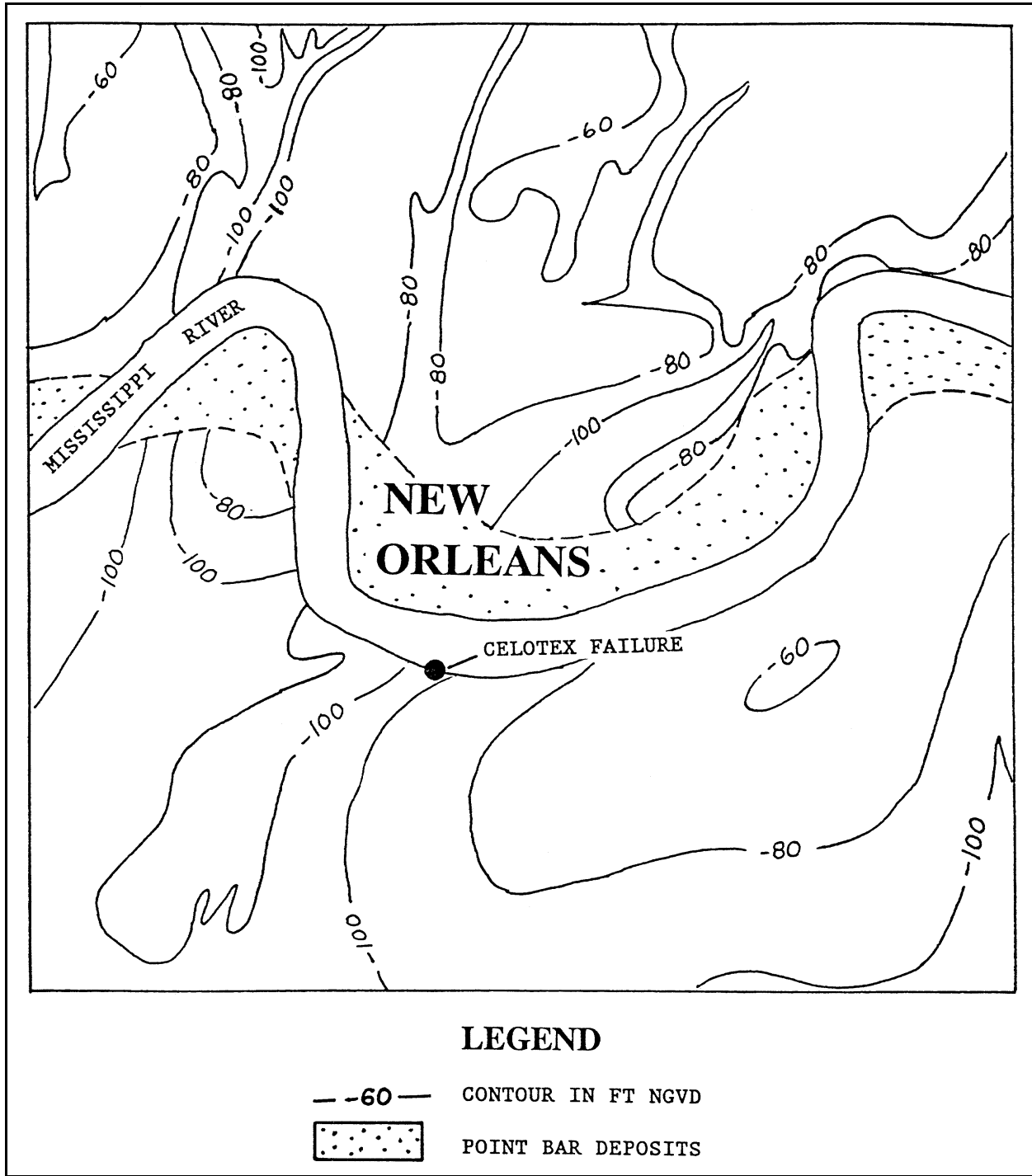


Figure 6. Generalized contour map of the Pleistocene surface (modified after Kolb, Smith, and Silva 1975)

Each of the different depositional environments present in the study area has distinct physical characteristics reflected by differences in soil types and associated engineering properties. Therefore, the geology of the study area will have a major influence on river scouring, lateral migration, and bank stability.

Geology of Selected Revetment Reaches

Celotex failure site and Greenville Bend revetment

This riverbank reach extends from river mile 98.3 to 102.0 (158.2 to 164.1 km) on the right descending bank. The subsurface geology of the Celotex failure site is shown by cross sections B-B' (Figure 5c) and F-F' (Figure 5i). The locations of these sections are shown in Figure 4. Areal photography and boring data identify a point bar sequence (Figure 4 and 5c) associated with Bayou des Familles (Figure 5i). This distributary channel was a major course of the Mississippi River during the active St. Bernard delta complex.

The exact intersection and lateral limits of Bayou des Familles at the Mississippi River are not well defined from areal photography because this area has been extensively developed by industrial and residential construction. The position and lateral extent of the Bayou des Familles channel at the Mississippi River was interpreted from available historic charts, maps, and boring data.

Soil types within the point bar-abandoned distributary sequence are primarily coarse-grained, consisting mainly of silty sands (SM) and well sorted or poorly graded sands (SP). The available boring data indicate that the point bar-abandoned distributary sequence extends approximately 100 ft (30.5 m) below the ground surface before encountering the oxidized and erosion-resistant Pleistocene surface.

The geology immediately upstream and downstream from the Bayou des Familles point bar sequence consists of interdistributary deposits underlain by a generally coarser nearshore gulf sequence (CL, ML, SM, and SC). Soil types are variable within these two depositional environments. Interdistributary sediments consist primarily of clay (CL and CH) with disseminated organics.

Carrollton Bend and Carrollton Bend revetment

This bank reach extends from about river mile 102.0 to 105.0 (164 to 169 km) and encompasses the Carrollton Bend revetment which is on the left descending bank. The subsurface geology of the Carrollton Bend reach is shown on cross sections A-A' (Figure 5a), A'-A'' (Figure 5b), and D-D' (Figure 5g) (see Figure 4 for section locations). The geology consists of natural levee, interdistributary, intradelta, and nearshore gulf sediments. Soil types are variable within the individual environments as shown by the cross sections. The Pleistocene surface ranges between elevations -50 to -75 ft (-15.2 to -22.9 m) NGVD. Where the Mississippi River has entrenched itself into the Pleistocene, the river has formed thick point bar sediments in excess of 120 ft (36.6 m) deep.

Gretna Bend and Gouldsboro revetments

This revetted bank lies between river miles 95.5 and 98.3 (153.6 and 158.2 km). The Gretna Bend and Gouldsboro revetments are contiguous from upstream to downstream, respectively, along the right descending bank. The

subsurface geology of the Gretna Bend and Gouldsboro Revetment reach is shown by cross sections B'-B'' (Figure 5d) and G-G' (Figure 5j) (see Figure 4 for section locations). The geologic sequence is similar to the two upstream revetment reaches already described. The Pleistocene surface ranges between elevations -55 to -70 ft (-16.8 to -21.3 m) NGVD and is overlain by nearshore gulf, interdistributary, and natural levee sediments.

As shown by the surface geology map in Figure 4, there is an abandoned distributary channel which intersects the Mississippi River and extends southeast at approximately river mile 96.5 (155.3 km). The existence of this former distributary channel is indicated by the presence of well-developed natural levees several miles southeast of the Mississippi River. The intersection of this distributary channel with the present Mississippi River is indicated by boring W96.5GT. At this location, a thick sand sequence was encountered in the subsurface.

Algiers Point revetment

This revetment reach lies between river mile 93.7 and 95.5 (150.8 and 153.7 km) on the right descending bank. The subsurface geology of Algiers Point is shown by cross sections C-C' (Figure 5e), C'-C'' (Figure 5f), and H-H' (Figure 5k). The permanent scour pool along Algiers Point is one of the deepest of the Mississippi River entrenchment below Baton Rouge. River thalweg elevations have historically been between -175 and -200 ft (-53.3 and -61 m) NGVD. At Algiers, along the point bar side of the river, fluvial scouring has created a 170-ft (51.8-m) thick point bar sequence (see cross section H-H' of Figure 5k). Soil types are variable within this thick sequence, but are primarily coarse-grained.

Along the concave or left bank of the river, the subsurface geology at Algiers Point consists of interdistributary sediments, separated by point bar deposits and an abandoned interdistributary channel (see Figure 4 and cross section C-C' of Figure 5e). These sediments are underlain by the Pleistocene surface. The lateral and vertical limits of the different depositional environments are shown by the surface geology map and the respective geologic cross sections. Soil types are highly variable as defined by the sections.

The abandoned distributary channel shown in Figure 4 is a former St. Bernard distributary which branches from the main Bayou Sauvage-Metarie Bayou course northwest of Algiers Point. The intersection of this distributary channel at the Mississippi River is defined by coarse-grained sediments in the subsurface in borings located within the former distributary channel (see sections C-C' of Figure 5e and H-H' of Figure 5k).

Appendix A

Environments of Deposition

General

This appendix provides a general description of the environments of deposition which produced the surface and subsurface geology encountered in the study reach. The distribution of surface deposits is shown by the geologic map in Figure 4 of the main text. Subsurface limits of the various depositional environments are shown by the cross sections in Figures 5a through 5k. A geologic legend is presented in Figure 5l that identifies symbols used in the geologic cross sections.

In addition to the general descriptions of the individual environments of deposition, this appendix also provides a very generalized indication of the engineering properties for each environment. Correlation of engineering properties and soil types to the different environments of deposition is based primarily on work by Kolb (1962)¹ and is summarized in Table A1. Additionally, Montgomery (1974) expanded upon Kolb's original work for several of the major depositional environments which form the bulk of the land area in the deltaic plain. Montgomery's work is summarized in Table A2 and provides further engineering data on the following selected environments of deposition: natural levee, point bar, backswamp, prodelta, intradelta, and interdistributary deposits.

In terms of their engineering significance, the biggest contrast occurs between the Pleistocene and Holocene age sediments as shown by the engineering data in Table A1. Pleistocene sediments have higher cohesive strengths, lower water contents, and are much denser than Holocene soils. Holocene deposits in contrast are less consolidated, have higher water contents, and are more variable in density.

The biggest contrast in Holocene soils occurs between the high- and low-energy depositional environments. High-energy environments are generally associated with maximum fluvial and/or wave activity and are mainly composed of coarse-grained sediments. These environments include point bar, substratum, abandoned course, abandoned distributary, beach, nearshore gulf, estuarine/bay

¹ References are listed following the main text.

sound, and intradelta deposits (Table A1). Low-energy environments are composed primarily of fine-grained sediments and include marsh, swamp, natural levee, prodelta, and interdistributary. Only the environments of deposition that are present in the study area are examined in the following section. The environments are presented and described by their order and distribution of occurrence. Deltaic environments not present in the study area but identified in Table A1 are described in further detail by Kolb (1962) or Kolb and Van Lopik (1958a,b) for readers desiring further information.

Surface Environments of Deposition

Natural levee

Natural levees are vertical accretion deposits formed when the river overtops its banks during flood stage and sediment suspended in the flood flow is deposited immediately adjacent to the channel. The resulting landform is a low, wedge-shaped ridge decreasing in thickness away from the channel. The limits of natural levee deposits in the study area are shown in Figure 4 of the main report. Natural levee deposits are mapped in Figure 4 with the underlying environment of deposition (i.e., interdistributary, point bar, or inland swamp). Natural levee deposits cover approximately 40 percent of the study area and involve the Mississippi River and abandoned distributary channels from the active St. Bernard delta complex (i.e., Bayou des Familles-Barataria, Metairie Bayou, Bayou Sauvage, and two unnamed bayous).

Natural levee widths in the study area vary from about 3/4 to approximately 2 miles wide along the Mississippi River, and between 1/4 and 1/2 mile wide along the abandoned St. Bernard distributary channels (Figure 4). Natural levees are thickest adjacent to the main channel, ranging from 10 to 20 ft in thickness (Figures 5a to 5k). Their thickness decreases away from the river, eventually merging with inland swamp deposits.

Natural levee deposits in the study area are composed primarily of clay and silt with minor sand lenses. Soils associated with natural levee deposits are identified in Figures 5a through 5k of the main report. These deposits are generally coarser-grained near the channel, composed of silt (ML) and silty clay (CL), and become finer-grained (i.e., CL and CH) further from the river. Color varies from reddish brown or brown near surface to grayish brown, and medium to dark gray with depth. Darker colored natural levee soils are due to the higher organic content. Organic content is generally low and is in the form of small roots and occasionally disseminated wood fragments. Larger wood fragments are uncommon as oxidation has reduced organic materials to a highly decomposed state. Frequently associated with natural levee deposits are small calcareous nodules, formed as a result of groundwater percolating through the permeable soils and precipitated from solution. Natural levee soils are well-drained, have low-water contents, and generally have a stiff to very stiff consistency (Tables A1 and A2).

	DEPOSITIONAL TYPES	LITHOLOGY PER CENT	PREDOMINANT SOIL TEXTURES ⁽¹⁾	NATURAL WATER CONTENT PER CENT DRY WEIGHT	UNIT WEIGHT LB/CU FT	SHEAR STRENGTH ⁽²⁾		REMARKS	
						COHESIVE STRENGTH LB/SQ FT	ANGLE OF INTERNAL FRICTION IN DEGREES		
RECENT ENVIRONMENTS	NATURAL LEVEES		CH, CL, ML & SM			VALUES RANGE TO APPROXIMATELY 2500 CHARACTERISTIC RANGE 800-1200	ML 20-35	Disposed in narrow bands flanking the Mississippi River and its abandoned courses and distributaries. Consists of interfingering layers of fat and lean clays and sandy silt along the Mississippi River and its abandoned courses. Natural levee materials along abandoned distributaries usually much finer. Thickness varies from 25 ft near Baton Rouge to 0 at sea level. Thickness along distributaries usually on the order of 5 ft or less.	
	POINT BAR SANDY		ML, SM & SP		INSUFFICIENT DATA	INSUFFICIENT DATA	SP 25-35	Usually found flanking the more prominent bends of the present and abandoned courses to a depth of more than 100 ft. Consists of a bedded topstratum 25 to 75 ft thick of silty sand, sandy silt, and sand coarsening with depth. The substratum consists of essentially clean sand.	
	POINT BAR SILTY		CL & ML		INSUFFICIENT DATA	-----	-----	ML 20-30	An unusually fine-grained point-bar deposit consisting almost entirely of silt. Identified just upstream from Donaldsonville and at Laplace.
	PRODELTA CLAYS		CH				-----	0	A homogeneous fat clay in offshore areas and at depth. Contains increasing amounts of lean clay disposed in thin layers near the mouths of active distributaries. Thickness normally varies with depth to Pleistocene. Thicknesses range between 50 and 600 ft.
	INTRADELTA		CH, ML & SM		INSUFFICIENT DATA	INSUFFICIENT DATA	INSUFFICIENT DATA	-----	Relatively coarse sediments bottoming bays and sounds. Thickness ranges from 3 to 20 ft and averages 15 ft. Because of the reworking of bottom sediments by narrowing marine organisms soils have a mottled appearance due to the inclusion of lumps or pockets of coarse material in a fine matrix or fine material in a coarse matrix.
	INTERDISTRIBUTARY		CH				-----	0	Forms clay wedges between major distributaries. Clay sequence interrupted by silty or sandy materials associated with myriad small distributaries. Minor amounts of silt and fine sands typically occur in very thin but distinct layers between clay strata giving deposit a "warved" appearance. Thickness similar to intradelta above.
	ABANDONED DISTRIBUTARY		CH & CL	INSUFFICIENT DATA	INSUFFICIENT DATA	INSUFFICIENT DATA	INSUFFICIENT DATA	-----	Forming belts of clayey sediments from a few feet to more than 1,000 ft in width and from less than 10 to more than 50 ft in depth. A wedge of coarser material is normally found at the upstream end, this wedge of material may range from fine sand for the larger distributaries to silty clays for the smaller.
	ABANDONED COURSE		CH & SP	INSUFFICIENT DATA	INSUFFICIENT DATA	INSUFFICIENT DATA	INSUFFICIENT DATA	-----	Forming belts of fairly coarse sediment in abandoned Mississippi River courses. Average width 2,500 ft. Depth may be 75 to 150 ft. Lower portion of course filled with sandy material which thickens in an upstream direction. Upper portion filled with silts and clays.
	SWAMP		CH			INSUFFICIENT DATA	INSUFFICIENT DATA	-----	Tree-covered organic deposits flanking the inner borders of the marsh and subject to fresh-water inundation; also mangrove-choked areas found landward of the barrier beaches and fringing the mainland. Deposits average 3 to 10 ft thick.
	MARSH		PT	VALUES RANGE TO APPROXIMATELY 800	INSUFFICIENT DATA	VERY LOW	-----	-----	Forms 90 per cent of the land surface in the deltaic plain. Ranges from watery organic ooze to fairly firm organic silts and clays. Maximum thicknesses (30 ft or more) normally associated with areas of greatest subsidence. Average thickness 10 ft.
	SAND BEACH		SP	SATURATED	INSUFFICIENT DATA	0	30-35	Border the open gulf except in areas of active deltaic advance. May be a mile or more in width and more than 10 miles in length. Beach sand may pile as high as 30 ft above gulf level and subside to depths of 30 ft below gulf level. Buried sand beaches reach a thickness of 35 ft in New Orleans area.	
	BAY-SOUND		ML & SM				15-30	Relatively coarse portion of subaqueous delta. Intricately interfingering deposits. Disposed in broad wedges about abandoned courses and major distributaries. Thickness of intradelta associated with present Mississippi on order of 200 ft. Thickness of intradelta associated with abandoned courses much less, averaging between 25 to 100 ft.	
	NEARSHORE GULF		SP	SATURATED	INSUFFICIENT DATA	0	25-35	Found at the borders of the open ocean seaward of the sand or barrier beaches. Thickness appears to increase with distance from shore - maximum thickness believed to be on order of 25 ft. Discontinuous blanket of this material occurs directly above Pleistocene.	
	ESTUARINE		SP	SATURATED	INSUFFICIENT DATA	0	30-40	Sandy facies correlative with nearshore gulf deposits but filling minor valleys entrenched into underlying Pleistocene surface.	
	BACKSWAMP		CH & CL			VALUES RANGE TO APPROXIMATELY 1745 CHARACTERISTIC RANGE 450-1450	0	Thick clays overlying substratum sands upstream from College Point. Occasional lenses of shell are found indicating interfingering fluvial-marine deposits.	
SUBSTRATUM		SP	SATURATED	INSUFFICIENT DATA	0	30-40	Massive sand and gravel deposits filling entrenched valley and grading laterally into nearshore gulf deposits. Material becomes coarser with depth. Maximum thickness on the order of 300 ft in deepest portion of entrenched valley.		
PRE-RECENT	PLEISTOCENE		CH & CL			VALUES RANGE TO APPROXIMATELY 3500 CHARACTERISTIC RANGE 900-1700	0	Ancient former deltaic plain of Mississippi River. Consists of environments of deposition and associated lithologies similar to those found in recent deltaic plain. Depth to this ancient, eroded surface increases in a southerly and westerly direction in southeastern Louisiana.	

LEGEND

GRAVEL (>2.0 MM)
 SAND (2.0-0.05 MM)
 SILT (0.05-0.005 MM)
 CLAY (<0.005 MM)
 ORGANIC MATERIAL
 SHELL
 TYPICAL RANGE OF VALUES INDICATED BY LENGTH OF BAR. BAR WIDTH INDICATES RELATIVE DISTRIBUTION OF VALUES.

(1) SYMBOLS BASED ON UNIFIED SOIL CLASSIFICATION SYSTEM.
(2) SHEARING STRENGTHS OF CLAYS BASED ON UNCONFINED COMPRESSION TESTS.

Table A1. Engineering Properties of Depositional Environments from the Mississippi River Deltaic Plain (from Kolb 1962)

Table A2. Engineering properties of selected depositional environments from the Mississippi River deltaic plain (from Montgomery, 1974)

Deposit	Grain Size and Organic Content	Natural Water Content %	Liquid Limit %	Plasticity Index %	Liquidity Index	Dry Density pcf	Specific Gravity	Void Ratio e	s _v P _v Ratio	Shear Strength	
										Q _c T/sq ft	c _v T/sq ft
Natural levee		18-83 (45)	29-129 (66)	2-90 (42)	0.14-1.18 (0.54)	50-92 (76)	2.62-2.74 (2.69)	0.82-6.16 (1.46)	--	0.08-0.68 (0.20)	8-22 (13)
Point bar (silty)		26-79 (44)	31-87 (54)	7-63 (33)	0.22-1.60 (0.74)	54-98 (78)	2.65-2.77 (2.69)	0.70-2.12 (1.12)	0.14-0.37 (0.27)	0.11-1.24 (0.20)	2-22 (13)
Backswamp (organic)	Insufficient data	42-367 (127)	58-397 (152)	43-218 (106)	0.16-1.41 (0.70)	16-73 (43)	2.10-2.74 (2.46)	1.36-6.73 (3.11)	--	0.03-0.27 (0.14)	7-20 (13)
Backswamp (inorganic)		31-98 (59)	27-148 (83)	19-86 (56)	0.03-1.26 (0.55)	48-91 (65)	2.52-2.75 (2.66)	0.85-2.57 (1.62)	0.07-0.76 (0.26)	0.1-0.72 (0.13)	4-27 (12)
Prodelta		31-70 (53)	39-100 (79)	16-72 (51)	0.12-1.08 (0.51)	49-90 (72)	2.67-2.80 (2.72)	0.84-2.06 (1.32)	0.11-0.39 (0.22)	0.18-0.85 (0.20)	2-22 (13)
Intradelta		24-132 (58)	25-212 (77)	5-164 (52)	0.39-1.52 (0.69)	33-98 (67)	2.57-2.76 (2.70)	0.64-2.84 (1.57)	0.07-0.65 (0.23)	0.01-0.50 (0.20)	2-22 (13)
Inter-distributary		24-113 (57)	38-179 (82)	19-162 (59)	0.13-1.03 (0.61)	45-94 (66)	1.59-2.74 (2.64)	1.01-2.59 (1.58)	0.22-0.85 (0.37)	0.01-0.50 (0.20)	2-22 (13)

LEGEND

Clay (0.005 mm)

Sand (2.0-0.05 mm)

Silt (0.05-0.005 mm)

Organic material

Notes: (1) Numbers in parentheses are average values.
(2) Insufficient consolidated-undrained and drained shear strength data were available for the natural levee, point bar, prodelta, intradelta, and interdistributary deposits. The data shown represent all five deposits.
(3) Insufficient data were available to clearly establish the amount of organic matter typically occurring in each deposit.
(4) Shear strengths are given in cohesion (c), tons per square foot and angle of internal friction (φ) in degrees.
Q denotes unconsolidated-undrained triaxial compression tests.
R denotes consolidated-undrained triaxial compression tests.
S denotes consolidated drained direct shear tests.
(5) Grain-size characteristics based on references 2 and 10.

Inland swamp

Before describing characteristics of inland swamps and their distribution in the study area, a clarification of terminology is in order. Usage of the term inland swamp is restricted to the deltaic plain, whereas the term backswamp is restricted to the Mississippi River alluvial valley. Mapping by May et al. (1984) adopted the usage of the term inland swamp and defined the upvalley margin of this environment. Inland swamps are not bounded by valley margins or older meander belt ridges as in the alluvial valley. Instead, inland swamps in the deltaic plain are areas of high ground and woody vegetation formed because of the high sediment rates from advancing distributary channels.

Kolb (1962) recognized that the term backswamp was inappropriate for the deltaic plain and had reservations about using this term to describe swamp sediments below Donaldsonville, LA. May et al. (1984) have placed the boundary between backswamp and inland swamp near the vicinity of Houma, LA. The boundary separating the two swamp types occurs at the junction of Bayou Teche and Bayou LaFourche, two former Mississippi River courses. Consequently, the summary descriptions and engineering properties in Tables A1 and A2 for backswamp are more appropriate to inland swamp as the samples were derived primarily from inland swamp sediments. The primary distinction here is in process and the ultimate nature of the sediments derived by these processes. In theory, inland swamp sediments are considered to be much finer-grained than backswamp sediments since they are transported by smaller-scale distributary channels to locations on the deltaic plain that are well removed from the main channel. As shown by Figure 3 in the main report, primary Mississippi River flow was not confined to a single main channel during the period of active Holocene delta building but rather was shared by several smaller major distributary courses.

Inland swamps are vertical accretion deposits that receive sediment during times of high-water flow, when the natural levees are crested and suspended sediment in the flood waters is deposited in areas well removed from the main distributary channel. Inland swamp environments are low, often poorly drained, tree-covered areas flanking the main distributary channel. Inland swamps are low areas that are settling basins for flood flow and sediment, and represent one of the final stages in land building by the passing delta front. Sediment supply is sufficient to elevate the land surface to above sea level and allow woody vegetation to develop and become stable.

Inland swamps are the dominant surface environment in the study area and comprise approximately 50 percent of the Holocene deposits depicted in Figure 4. The surface of the inland swamp environment begins at about the 0 ft NGVD elevation. These deposits are approximately 10 to 15 ft thick with the base of this sequence grading into marsh and interdistributary sediments between -10 to -15 ft NGVD (Dunbar et al. 1994).

Inland swamps are composed of uniform, very fine-grained soils, primarily silty clay (CL) and clay (CH). Sand (SM and SP) and silt (ML) may be present but is considered a minor constituent of the total depositional sequence (Table A1 and A2, and Figures 5a through 5k of the main report). These deposits typically contain moderate to high organic contents in the form of

decayed roots, leaves, and wood. Disseminated pyrite is a common but a very minor constituent of these soils and is commonly found in more poorly drained areas which promotes reducing conditions. Inland swamp soils may become well drained during times of low water and undergo short periods of oxidation, lending a mottled appearance to the soil. Inland swamp soils are gray, dark gray, or occasionally black. Inland swamp soils have generally high-water contents, between 30 and 90 percent, as shown by Tables A1 and A2 (backswamp environment).

Point bar

Point bar deposits are lateral accretion deposits formed as a river migrates across its flood plain. River channels migrate across their floodplain by eroding the outside or concave bank and depositing a sandbar on the inside or convex bank. With time the convex bar grows in size and the point bar is developed. Associated with the point bar are a series of arcuate ridges and swales. The ridges are formed by lateral channel movement and represent relic lateral bars separated by low lying swales. The swales are locations for fine-grained sediments to accumulate. Point bar deposits are as thick as the total depth of the river that formed them. These deposits become coarser-grained with increasing depth. Maximum grain size is associated with the river's bedload (coarse sand and fine gravel) while the fine-grained soils occur near the surface. The basal or coarse-grained portion of the point bar sequence is deposited by lateral accretion while the fine-grained or upper portion of the point bar sequence is deposited by vertical accretion.

Point bar deposits in the study area are considered to be young, generally less than 3,500 years old. They began forming along Bayou des Familles-Barataria when the St. Bernard delta system was active but didn't fully develop along the main river until the present Mississippi River course began forming less than 1,000 years before the present.

Soil types in a point bar sequence grade upward from coarse-grained sands and fine gravels near the base to clays near the surface. These deposits are variable, but in the study area are generally composed of at least 50 percent poorly graded fine sand (Figures 5a through 5h and Tables A1 and A2). Point bar deposits are separated into two distinct units, a predominantly fine-grained upper sequence or point bar top stratum, and a coarse-grained lower sequence or point bar substratum. Soil types associated with each unit are identified in the geologic sections in Figures 5a through 5f of the main report.

Abandoned course

An abandoned course as the name implies is a relic fluvial course that is abandoned in favor of a more hydraulically efficient course. An abandoned course contains a minimum of two meander loops and forms when the river's flow path is diverted to a new position on the river's floodplain. This event usually is a gradual process that begins by a break or a crevasse in the river's natural levee during flood stage. The crevasse forms a temporary channel that may, over time, develop into a more permanent channel. Eventually, the new

channel diverts the majority of flow and the old channel progressively fills. Final abandonment begins as coarse sediment fills the abandoned channel segment immediately downstream from the point of diversion. Complete filling of the abandoned course is a slow process that occurs by overbank deposition. The complete filling process may take several hundreds or even thousands of years to complete.

The Bayou des Familles-Barataria abandoned course is a prominent physiographic feature that extends due south from the Mississippi River at approximately river mile 100 (Figures 1 and 4 of the report). The abandoned course extends well beyond the limits of the study area and continues south to Barataria Bay (May et al. 1984, Dunbar et al. 1994). It contains broadly developed natural levees which are easily identified on aerial photography and topographic maps. Well developed natural levees and a meandering plan form distinguish the abandoned course from its short lived predecessor, the crevasse channel.

Boring information from the greater New Orleans area indicates channel fill from the Bayou des Familles abandoned course consists primarily of thick sand deposits capped by a thin layer of silt and clay. Detailed boring information from the abandoned course at its confluence with the Mississippi River is presented in Figures 5c and 5i of the main report. Engineering properties of abandoned course sediments are not sufficiently categorized in Table A1 due to lack of boring data. However, these sediments are considered to be similar in composition to sandy point bar deposits for which data are present.

Abandoned distributary channel

Distributary channels are channels that diverge from the trunk channel dispersing or “distributing” flow away from the main course. By definition, distributary channels do not return flow to the main channel on a delta plain (Bates and Jackson 1987). Distributary channels originate initially as crevasse channels during high flow periods when the main channel is unable to accommodate the larger discharge. If the flood is of sufficient duration, a permanent distributary channel is soon established through the crevasse. Abandonment of a distributary channel or distributary network occurs either as a major course shift upstream or the distributary becomes over extended and loses its gradient advantage in favor of a much shorter distributary channel. Complete abandonment usually occurs because of an improved gradient advantage by the new distributary.

Distributary channel abandonment closely parallels the abandonment of a course. During abandonment, the base of the channel is filled with poorly sorted sands, silts, and organic debris. As the channel continues to fill, the flow velocities are decreased, and the channel is filled by clay, organic ooze, and peats. Abandoned distributaries in the study area are approximately their original width, but only a fraction of their original depth due to infilling. Abandoned distributary channels in the study area are Metairie Bayou, Bayou Sauvage, and two unnamed distributaries that intersect the Mississippi River on the east and west banks (Figure 4). These distributary channels have all been partially or completely filled with sediments.

Often the distal ends of abandoned distributaries have been buried due to subsidence, destroyed by coastal erosion, or closer to the trunk channel, buried by later natural levee deposits (Figure 4). Metarie Bayou in the northern portion of the study area has been buried by later Mississippi River natural levee deposits and altered by the historic activities of man north of the river. Natural levees are ideal for urban development since these areas are topographically higher than the surrounding area.

Abandoned distributaries are recognized on aerial photographs by their natural levees and the urban development associated with these levees. In the subsurface, distributary sediments are recognized by soil types (Table A1) and sedimentary structures characteristic of channel fill deposits. Engineering properties of abandoned distributary sediments are not sufficiently categorized in Table A1 due to lack of boring data. Upper channel fill consists of parallel and wavy laminated silts and silty clays, interbedded with highly burrowed clays with high-water contents. Distorted bedding, slump structures, organic layers, and minor shell material are also common in abandoned distributary deposits.

Freshwater marsh

In the southwestern portion of the study area there is an area of freshwater marsh, a nearly flat expanse where grasses and sedges are the only vegetation. Organic sedimentation plays an important role in the formation of marsh deposits. Peats, organic oozes (mucks), and humus are formed as the marsh plants die and are buried. Decay is largely due to anaerobic bacteria in stagnant water. Vegetative growth and sedimentation maintain the surface elevation at a fairly constant level, and the marsh deposits thicken as a result of subsidence over time. When marsh growth fails to keep pace with subsidence, the marsh surface is eventually inundated by water.

Peats are the most common form of marsh strata remains, and they consist of black fibrous masses of decomposed plants. Detrital organic particles, carried in by marsh drainage, and vegetative tissues form the mucks. Mucks are watery oozes that can support little or no weight. Sedimentation occurs in the marsh when floodwater overtops the natural levees, depositing clays and silts onto the marsh surface. Sediments are also transported to the marsh during lunar tides, wind tides, and hurricane tides when sediment laden marine waters inundate the marsh surface.

Marsh sediments are found in the subsurface as peats (Figures 5b through 5k) and represent a time during the Holocene where the land surface was at sea level and supporting marsh vegetation. Often marsh deposits grade vertically upward in a prograding delta system into inland swamp, followed by natural levee deposits. The reverse sequence is also true (i.e., marsh, natural levee, inland swamp, marsh). Engineering properties of marsh sediments are identified in Table A1.

Subsurface Environments of Deposition

Interdistributary

Interdistributary deposits are sediments deposited in low areas between active distributary channels, usually under brackish water conditions. Sediment laden waters overtop the natural levees of distributary channels during flood stage and deposit the coarsest sediment (silt) near the channel. The finer sediment (silty clay and clay) is transported away from the active distributary channel and settles out of suspension as interdistributary deposits. In this manner, considerable thicknesses of clay are deposited as the distributary builds seaward. Interdistributary clays often grade downward into prodelta clays and upward into the highly organic clays of swamp and marsh deposits.

Interdistributary deposits are found throughout the study area in the subsurface (Figure 5b through 5k of the main report). These deposits range in thickness from 30 to 60 ft and start between 0 to -10 ft NGVD as shown by the cross sections in Figures 5b through 5k. Interdistributary deposits consist of saturated gray clays which are highly bioturbated and contain some silt laminae. Shell fragments and minor amounts of organic debris are also commonly distributed throughout the interdistributary sequence as shown by Tables A1 and A2.

Buried beach

Interdistributary sediments associated with Metairie Bayou, an abandoned St. Bernard distributary in the northern edge of the study area, overlie and grade laterally with buried beach deposits. Buried beach deposits are part of the Pine Island Beach trend, an early Holocene beach trend associated with active sedimentation from the Pearl River (Saucier 1963). Approximately 5,000 years ago, when sea level was slightly lower than the present, longshore drift created a southwest to northeast trending offshore spit or barrier beach complex in the New Orleans area. Sediments forming the spit were derived from sandy fluvial sediments transported by the Pearl River. This spit originated at the river's mouth and extended southwest to the vicinity of New Orleans. This buried beach complex forms the southern shore of Lake Pontchartrain and acted as a natural barrier for filling of Lake Pontchartrain by advancing distributary channels during the active St. Bernard stage of delta growth.

Metairie Bayou (Figure 4) follows the seaward edge of the Pine Island Beach trend and was blocked from entering the main body of Lake Pontchartrain by the higher topography of the relic beach. Instead, Metairie Bayou follows the relic beach trend northeast toward the coastal mainland as the Bayou Sauvage distributary channel. Coastal drainage into Lake Pontchartrain from the Pleistocene uplands breached the beach ridge and formed "The Rigolets," a pass into Lake Pontchartrain at the eastern edge of the deltaic plain (Figure A1 from Saucier 1963).

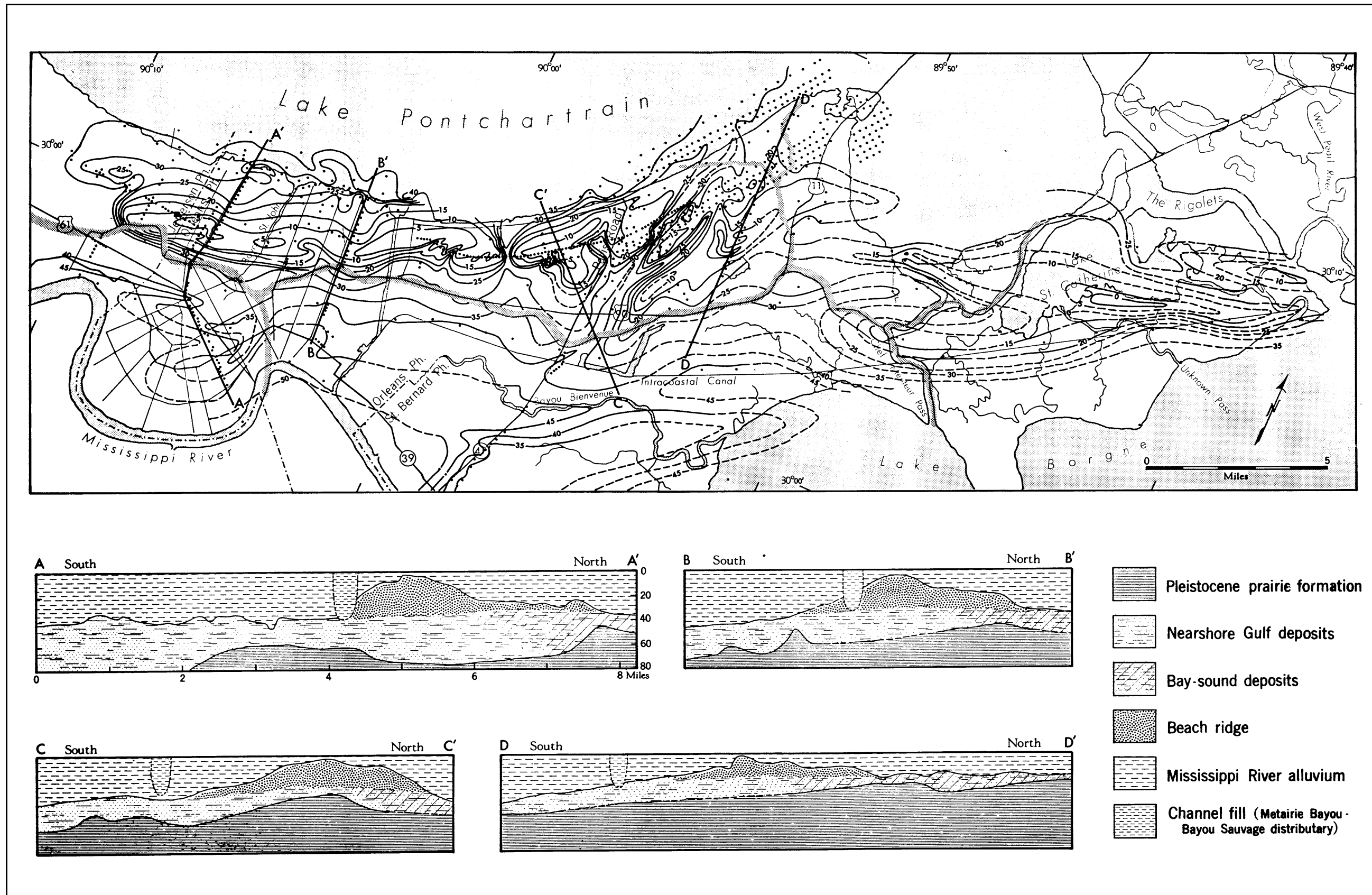


Figure A1. Topography of the buried Pine Island beach trend (Saucier 1963)

The beach trend grades laterally into intradelta and abandoned distributary deposits (Figure A1). Boring data identifies the buried beach deposits as consisting of uniform, fine to medium grained, quartz sand, ranging in color from gray to tan, and white upon exposure at the surface (Saucier 1963). Beach sand is generally well sorted and contains shell fragments.

Intradelta

Intradelta deposits form at the mouth of distributary channels and consist of coarse-grained or sandy sediments. At the mouth of a distributary, the water velocity decreases upon entering open water, depositing coarse-grained sediments from suspension as distributary mouth bars. The coarse sediments are deposited on the bar crest or as fans along the sides of the bars. As the distributary is built seaward, it may cut through or split around the bar. The process is then repeated in each of the smaller, branching distributary channels. These deposits interfinger and merge with interdistributary clays.

Intradelta deposits are identified in the subsurface in borings near the Mississippi River (Figures 5a, 5b, 5e, and 5g). They consist primarily of clean sands and silty sands with some silts. Intradelta deposits are thickest nearer the distributary channels or channel source areas. Engineering properties of intradelta sediments are summarized in Tables A1 and A2.

Nearshore gulf

Nearshore gulf deposits are generally coarse-grained sediments formed by the transgression and interaction of the rising Holocene sea level with the drowned Pleistocene surface. Nearshore gulf deposits represent sediments eroded, transported, and deposited at the land/sea level interface, often at maximum wave energy and under storm conditions. These deposits generally consist of coarse-grained sediments and are primarily characterized by sand and shell hash. Available engineering data is presented in Table A1. The subsurface distribution of this depositional environment is shown by the cross sections in Figures 5a through 5k of the main report. Generally, this environment directly overlies the Pleistocene surface throughout the deltaic plain region.

Estuarine and bay sound

Both of these environments are marine and are a minor environment in the subsurface (see Figures 5a through 5l). Both of these environments directly overlie the Pleistocene surface. These two environments were formed early during the Holocene, or perhaps even Late Pleistocene, when sea level advanced onto the Pleistocene surface. As sea level advanced, it drowned the existing Pleistocene drainage network and created small estuaries and bays.

An estuary is a river valley where fresh water comes into contact with sea water (Bates and Jackson 1987). A bay sound is a partly enclosed brackish water body which is sheltered from direct access to the Gulf and is dominated by both fluvial and marine processes. Since the bay sound is partly restricted from

the Gulf, the depositional energy and associated geomorphic processes are less severe than those associated with the nearshore gulf environment. Sediments deposited within an estuary or bay sound environment have a much greater range in grain size than sediments deposited within the nearshore gulf environment (Table A1). Silt and clay are usually more common within the estuarine and the bay sound environment than the nearshore gulf environment as shown by Table A1.

Substratum

Substratum or “braided stream/outwash plain” deposits related to glacial melting and sea level rise are not present in the study area. Substratum deposits as identified in this report are coarse-grained sediments associated with the point bar environment. The term substratum as used in this report and on the cross sections in Figures 5a through 5k is used in conjunction with and is a modifier of the point bar environment. Point bar substratum deposits are typically the lateral accretion or coarse-grained component of the point bar sequence. The upper boundary occurs at the base of the fine-grained or vertical accretion component of the point bar sequence and is defined by the first nearly continuous silty sand (SM) contact.

Pleistocene

Pleistocene deposits are present only in the subsurface and are correlative to the Prairie Formation. The Prairie Formation is the youngest of Fisk’s (1944) four major interglacial fluvial and deltaic sequences and was deposited during Sangamonian time, approximately 70,000 to 125,000 years ago. The Prairie Formation is similar in origin to the Holocene age deposits which overlie the Prairie. They were both envisioned by Fisk (1944) as fining upward from a coarse-grained substratum to a fine-grained top stratum. Both are products of rising sea level and deposition following continental glaciation. However, detailed analysis of glacial chronology from the midwest, combined with detailed geologic mapping from the Lower Mississippi Valley in recent years, indicates that the four-cycle model of Pleistocene glaciation and the accompanying interglacial deposition are an oversimplification (Autin et al. 1991). Recent studies indicate that the geology of the Prairie Formation in the study area is highly complex (Cullinan 1969; Kolb, Smith, and Silva 1975; Saucier 1977; Dunbar et al. 1994).

Lithologic and stratigraphic data on the Prairie Formation are based on surface exposures north of Lake Pontchartrain in St. Tammy, St. Helena, Tangipahoa, and Washington Parishes, Louisiana, and foundation engineering borings from the greater New Orleans metropolitan area. Pleistocene age soils outcropping on the north shore of Lake Pontchartrain were mapped by Cullinan (1969) as being typically light gray, light brown, or yellowish orange in color and composed of muddy, fine sandstones or fine to very fine sandy siltstones. Beneath the Holocene sediments in the New Orleans area, numerous engineering borings drilled into the Pleistocene surface identify the Prairie as being composed primarily of clay and silty clay and having the following characteristics (Kolb and VanLopik 1958a,b, Kolb 1962): (a) oxidized tan, yellow, or

greenish gray color, (b) a marked decrease in water content, (c) distinctive stiffening in soil consistency and a general increase in shear strength, and (d) the presence of concretions. Pleistocene age soils forming the subsurface in the New Orleans area are usually easily distinguished from Holocene age soils by their sharp contrast in engineering properties, lithology, and stratigraphy. Soil color, water content, and shear strength are the most diagnostic criteria distinguishing Pleistocene from Holocene soils (Table A1).

Between the fine-grained Pleistocene sediments beneath the New Orleans area and the more coarse-grained sediments that outcrop at the surface north of Lake Pontchartrain, there is a transition which may be due to variations within environments of deposition or stratigraphy during the Late Pleistocene. The New Orleans area Pleistocene soils may have formed under several depositional settings, including inland swamp, interdistributary, bay sound, and/or estuarine environments, while the coarser-grained soils north of Lake Pontchartrain are perhaps related to mainland beach and terrestrial fluvial environments draining the Pleistocene uplands. The Prairie surface is a highly complex stratigraphic sequence that consists of multiple depositional facies which formed over a period of several tens of thousands of years, followed by thousands of years of subaerial oxidation and erosion during maximum glacial episodes and lowered sea levels, and then later burial by Holocene sediments.

The Pleistocene surface dips gently to the south and southwest at about 3 to 5 ft per mile (Figure 6 of the main report). Elevations on the Pleistocene surface range from approximately -60 ft NGVD in the northern portions of the study area to more than -100 ft NGVD south of the Mississippi River. The base of the Prairie Formation beneath the Celotex failure site occurs somewhere between elevation -500 and -600 ft NGVD (Cullinan 1969).

References

- Autin, W. J., Burns, S. F., Miller, B. J., Saucier, R. T., and Snead, J. I. (1991). "Chapter 18: Quaternary geology of the Lower Mississippi Valley." Vol K-2, *The Geology of North America*. The Geological Society of North America, Boulder, CO, 547-581.
- Bates, R. L., and Jackson, J. A. (1987). *Glossary of Geology*, 3rd ed., American Geological Institute, Alexandria, VA.
- Clough, G. W. (1966). "Ground water level in silty and sandy Mississippi River upper banks," Mississippi River Commission, Corps of Engineers, Vicksburg, MS. (Mr. F. J. Weaver, Lower Mississippi Valley Division, was a principal assistant in this study).
- Cullinan, T. A. (1969). "Contributions to the geology of Washington and St. Tammy Parishes, Louisiana," U.S. Army Engineer District, New Orleans, LA.
- Dunbar, J. B., Blaes, M., Dueitt, S., and Stroud, K. (1994). "Geological investigation of the Mississippi River deltaic plain, Report 2 of a Series," Technical Report GL-84-15, U.S. Army Engineer Waterways Experiment Station, Vicksburg, MS.
- Dunbar, J. B., Blaes, M., Dneitt, S., and May, J. (1995). "Geological investigation of the Mississippi River deltaic plain, Report 3 of a Series," Technical Report GL-84-15, U.S. Army Engineer Waterways Experiment Station, Vicksburg, MS.
- Dunbar, J. B., and Torrey, V. H. (1991). "Geologic, geomorphological and geotechnical aspects of the Marchand Levee failure, Marchand, Louisiana," Miscellaneous Paper GL-91-17, U.S. Army Engineer Waterways Experiment Station, Vicksburg, MS.
- Eustis Engineering Company. (1984). "Geotechnical investigation: Soil stratification and foundation conditions for residential development," Report for City of New Orleans, Sewerage and Water Board of New Orleans, New Orleans, LA.
- Fisk, H. N. (1944). "Geological investigation of the alluvial valley of the Lower Mississippi River," U.S. Army Corps Engineers, Mississippi River Commission, Vicksburg, MS.

- Frazier, D. E. (1967). "Recent deltaic deposits of the Mississippi River: Their development and chronology." *Gulf Coast Association of Geological Societies. Transactions 17th annual meeting*. San Antonio, TX.
- Halbouty, M. T. (1967). *Salt Domes, Gulf Region, United States and Mexico*. Gulf Publishing Company, Houston, TX.
- Hvorslev, M. J. (1956). "A review of the soils studies," Potamology Investigations Report No. 12-5, U.S. Army Engineer Waterways Experiment Station, Vicksburg, MS.
- Kemp, E. B. (1967). "Geologic setting of New Orleans." *Guidebook New Orleans, LA and vicinity field trip*. The Geological Society of America and Associated Societies, Annual meetings.
- Kolb, C. R. (1962). "Distribution of soils bordering the Mississippi River from Donaldsonville to Head of Passes," Technical Report No. 3-601, U.S. Army Engineer Waterways Experiment Station, Vicksburg, MS.
- Kolb, C. R., and Saucier, R. T. (1982). "Engineering geology of New Orleans," *Geological Society of America, Reviews in Engineering Geology* 5, 75-93.
- Kolb, C. R., Smith, F. L., and Silva, R. C. (1975). "Pleistocene sediments of the New Orleans-Lake Pontchartrain area," Technical Report S-75-6, U.S. Army Engineer Waterways Experiment Station, Vicksburg, MS.
- Kolb, C. R., Steinriede, W. B., Krinitzsky, E. L., Saucier, R. T., Mabrey, P. R., Smith, F. L., and Fleetwood, A. R. (1968). "Geological investigation of the Yazoo Basin, Lower Mississippi Valley," Technical Report 3-480, U.S. Army Engineer Waterways Experiment Station, Vicksburg, MS.
- Kolb, C. R., and VanLopik, J. R. (1958a). "Geology of the Mississippi River Deltaic Plain," Technical Report No. 3-483, Vol 1 and 2, U.S. Army Engineer Waterways Experiment Station, Vicksburg, MS.
- _____. (1958b). "Geological investigation of the Mississippi River-Gulf Outlet Channel," Miscellaneous Paper No. 3-259, U.S. Army Engineer Waterways Experiment Station, Vicksburg, MS.
- Krinitzsky, E. L. (1965). "Geological influences on bank erosion along meanders of the Lower Mississippi River," Potamology Investigations, Report 12-15, U.S. Army Engineer Waterways Experiment Station, Vicksburg, MS.
- Krinitzsky, E. L., and Smith, F. L. (1969). "Geology of backswamp deposits in the Atchafalaya Basin, Louisiana," Technical Report S-69-8, U.S. Army Engineer Waterways Experiment Station, Vicksburg, MS.
- Krinitzsky, E. L., Turnbull, W. J., and Weaver, F. J. (1966). "Bank erosion in cohesive soils of the Lower Mississippi Valley," Vol 92, No. SM1, *Journal of Soil Mechanics and Foundations Division, Proceedings American Society of Civil Engineers*, 121-136.

- May, J. R., Britsch, L. D., Dunbar, J. B., Rodriguez, J. P., and Wlonsinski, L. B. (1984). "Geological investigation of the Mississippi River Deltaic Plain," Technical Report GL-84-15, U.S. Army Engineer Waterways Experiment Station, Vicksburg, MS.
- Miller, W. (1983). "Stratigraphy of newly exposed quaternary sediments, Eastern Orleans Parish, Louisiana," *Tulane Studies in Geology and Paleontology* 17(3, 4), 85-104.
- Montgomery, R. L. (1974). "Correlation of engineering properties of cohesive soils bordering the Mississippi River from Donaldsonville to Head of Passes, LA," Miscellaneous Paper S-74-20, U.S. Army Engineer Waterways Experiment Station, Vicksburg, MS.
- New Orleans Geological Society. (1962). "Salt domes of South Louisiana," Vol 1 and 2, J. C. Stipe and J. P. Spillers, ed., New Orleans, LA.
- _____. (1983). "Salt domes of South Louisiana," Vol 3, S. J. Waguespack, ed., New Orleans, LA.
- Padfield, C. J. (1978). "The stability of riverbanks and flood embankments," Final Technical Report, U.S. Army European Research Office, London, England.
- Saucier, R. T. (1963). "Recent geomorphic history of the Pontchartrain Basin, Louisiana," Technical Report 16, Part A, United States Gulf Coastal Studies, Coastal Studies Institute, Contribution No. 63-2, Louisiana State University, Baton Rouge, LA.
- _____. (1964). "Geological investigation of the St. Francis Basin," Technical Report 3-659, U.S. Army Engineer Waterways Experiment Station, Vicksburg, MS.
- _____. (1967). "Geological investigation of the Boeuf - Tensas Basin Lower Mississippi Valley," Technical Report 3-757, U.S. Army Engineer Waterways Experiment Station, Vicksburg, MS.
- _____. (1969). "Geological investigation of the Mississippi River area, Artonish to Donaldsonville, Louisiana," Technical Report S-69-4, U.S. Army Engineer Waterways Experiment Station, Vicksburg, MS.
- Saucier, R. T. (1974). "Quaternary geology of the Lower Mississippi Valley," Arkansas Archeological Survey, Research Series No. 6, Fayetteville, AR.
- _____. (1977). "The Northern Gulf Coast during the Farmdalian Substage: A search for evidence," Technical Report S-69-4, U.S. Army Engineer Waterways Experiment Station, Vicksburg, MS.
- Saucier, R. T., and Kolb, C. R. (1967). "Alluvial geology of the Yazoo Basin, Lower Mississippi Valley," 1:250,000 map, U.S. Army Engineer Waterways Experiment Station, Vicksburg, MS.

- Self, R. P., and Davis, D. W. (1983). "Geology of the New Orleans area," *The Compass of Sigma Gamma Epsilon* 60(2), 29-38.
- Smith, F. L., and Russ, D. P. (1974). "Geological investigation of the Lower Red River-Atchafalaya Basin area," Technical Report S-74-5, U.S. Army Engineer Waterways Experiment Station, Vicksburg, MS.
- Smith, L. M., Dunbar, J. B., and Britsch, L. D. (1986). "Geomorphological investigation of the Atchafalaya Basin, Area West, Atchafalaya Delta, and Terrebonne Marsh, Vol 1 and 2," Technical Report GL-86-3, U.S. Army Engineer Waterways Experiment Station, Vicksburg, MS.
- Snead, J. I., and McCulloh, R. P. (1984). "Geologic map of Louisiana, scale 1:500,000, Baton Rouge, LA."
- Torrey, V. H., III. (1988). "Retrogressive failures in sand deposits of the Mississippi River, Report 2, Empirical evidence in support of the hypothesized failure mechanism and development of the levee safety flow slide monitoring system," Technical Report GL-88-9, U.S. Army Engineer Waterways Experiment Station, Vicksburg, MS.
- Torrey, V. H., III, Dunbar, J. B., and Peterson, R. W. (1988). "Retrogressive failures in sand deposits of the Mississippi River, Report 1, Field investigations, laboratory studies and analysis of the hypothesized failure mechanism," Technical Report GL-88-9, U.S. Army Engineer Waterways Experiment Station, Vicksburg, MS.
- Torrey, V. H., III, and Weaver, F. J. (1984). "Flow failures in Mississippi riverbanks." *Proceedings IV International Symposium on Landslides*. Vol 2, Toronto, Canada, 355-360.
- Turnbull, W. J., Krinitzky, E. L., and Weaver, F. J. (1966). "Bank erosion in soils of the Lower Mississippi Valley." *Proceedings of the American Society of Civil Engineers, Journal of the Soil Mechanics and Foundation Division*, 92(SM1), 121-136.
- U.S. Army Corps of Engineers. (1909). "Survey of the Mississippi River, Chart Nos. 69 and 70," Mississippi River Commission, Vicksburg, MS.
- U.S. Army Corps of Engineers. (1921). "Survey of the Mississippi River, Chart Nos. 69 and 70," Mississippi River Commission, Vicksburg, MS.
- _____. (1950). "Piezometer observations at Reid Bedford Bend and indicated seepage forces," Potamology Investigations Report No. 5-4, Vicksburg, MS.
- U.S. Army Corps of Engineers. (1975). "Master index, upper and lower Mississippi River surveys for period 1879-80 to 1928 and some historic maps prior to this period," Vol 2, Mississippi River Commission, Vicksburg, MS.
- U.S. Army Engineer District, New Orleans. (1938). "Maps of the Mississippi River, Angola, La., to the Head of Passes," New Orleans, LA.

U.S. Army Engineer District, New Orleans. (1952). "Mississippi River hydrographic survey, 1949-1952, Angola, La., to Head of Passes and South and Southwest Passes and Pass A Loutre," New Orleans, LA.

_____. (1965). "Mississippi River hydrographic survey, 1961-1963, Black Hawk, La., to Head of Passes and South and Southwest Passes and Pass A Loutre," New Orleans, LA.

_____. (1976). "Mississippi River hydrographic survey, 1973-1975, Black Hawk, La., to Head of Passes and South and Southwest Passes and Pass A Loutre," New Orleans, LA.

_____. (1984). "Mississippi River levees, Item M-181.1 to 180.2-L, Marchand Levee setback, final report," New Orleans, LA (internal report, unpublished).

_____. (1986). "Mississippi River levees, Item M-100.4-R, Celotex Levee and Batture restoration, final report," New Orleans, LA (internal report, unpublished).

_____. (1988). "Mississippi River hydrographic survey, 1983-1985, Black Hawk, La., to Head of Passes and South and Southwest Passes and Pass A Loutre," New Orleans, LA (internal report, unpublished).

Wallace, W. E. (1966). "Fault and salt map of South Louisiana," *Gulf Coast Association of Geological Societies*, Vol 16.

K2 – Limit Equilibrium (Slope Stability) Analysis of 17th Street Canal

Limit equilibrium analyses is used to examine stability of the levees and I-wall section of the floodwall, and to examine possible mechanisms of failure at each breach site. The results of these analyses are interpreted in terms of factors of safety and probabilities of failure. This interim report will examine the factors of safety for the 17th Street Canal levee and I-wall section based on the IPET shear strength model described in the Data Report – 17th Street Canal in this Appendix K.

Objectives

The analyses of stability described in the following sections were performed to answer these questions:

- (1) What are the factors of safety for the 17th Street Canal I-wall based on the IPET shear strength model, and how do the factors of safety vary with water level in the canal?
- (2) How are these factors of safety affected by assuming that a crack forms between the canal side of the wall and the levee fill, as the water level rises on the canal side of the wall?
- (3) What water level is needed for a factor of safety equal to 1.0, and how does this differ for Stations 8+30, 10+00, and 11+50?
- (4) How do factors of safety calculated using the New Orleans District Method of Planes compare to factors of safety calculated using Spencer's Method?
- (5) How do factors of safety calculated for design compare with those calculated using the IPET shear strength model and Spencer's Method?
- (6) How do factors of safety calculated for the breach area compare to factors of safety calculated for adjacent reaches of the I-wall, north and south of the breach area?

- (7) What are the probabilities of failure in the breach and adjacent areas?

Conditions Analyzed

Fifteen slope stability analyses (Cases 1 through 15 in Table K4-1) were performed for cross sections at Stations 8+30, 10+00, and 11+50 which are shown in Figures K1-11, K1-12, and K1-13 of the data report. The shear strength profiles for these analyses are shown in Figures K1-54, K1-55, and K1-56 of the shear strength evaluation report. These strengths are identified as “IPET” in Table K2-1.

Five slope stability analyses (Cases 16 through 20 in Table K2-1) were performed using the cross section and strength profile used in the 17th Street Canal design memorandum¹. These are identified as “GDM 20” in Table K2-1.

Average values of moist unit weight were used in the analyses: $\gamma_{\text{sat}} = 109$ pcf for the levee fill, $\gamma_{\text{sat}} = 80$ pcf for the peat, and $\gamma_{\text{sat}} = 109$ pcf for the clay beneath the peat, based on values measured in laboratory tests on undisturbed samples.

The critical slip surfaces found in the analyses did not extend down to the sand beneath the clay, and the sand strength and unit weight therefore did not influence the results of the analyses.

The analyses were performed for undrained conditions in the levee fill, the peat, and the clay beneath the peat. Based on available information, it appears that the permeabilities of all three of these materials were low enough so that dissipation of excess pore pressures during the rise of the water level in the canal would have been negligible, and would have had at most a minor influence on stability.

Analyses were performed for two conditions regarding contact between the I-wall and the adjacent soil on the canal side of the wall. These are indicated by “yes” or “no” in the column labeled “Crack” in Table K2-1.

- For the “no crack” analyses, it was assumed that the soil on the canal side of the wall was in intimate contact with the wall. Water pressures were applied to the surface of the levee fill, and to the I-wall where it projected above the crown of the levee, but were not applied to the face of the wall below the crown of the levee.
- For the “crack” analyses, it was assumed that the I-wall was separated from the levee fill on the canal side of the wall as the water level in the canal rose and caused the wall to deflect away from the canal. Full hydrostatic water pressures were applied to the I-wall, from the water level in the canal to the bottom of the wall.

¹ General Design Memorandum #20 – 17th Street Outfall Canal – Volume 1 (GDM20).

**Table K2-1
Results of Slope Stability Analyses for Stations 8+30, 10+00, and 11+50 of the 17th Street Canal Floodwall.**

Case	Section	Slip Surface	Method	Strength Model	Crack	Water Elev. Ft. NGVD	F
1	8+30	Crit. Circle	Spencer's	IPET	no	8.5	1.75
2	8+30	Crit. Circle	Spencer's	IPET	yes	8.5	1.32
3	8+30	Crit. Circle	Spencer's	IPET	no	11.5	1.41
4	8+30	Crit. Circle	Spencer's	IPET	yes	11.5	1.04
5	8+30	Crit. Circle	Spencer's	IPET	yes	12.1	1.00
6	10+00	Crit. Circle	Spencer's	IPET	no	8.5	1.57
7	10+00	Crit. Circle	Spencer's	IPET	yes	8.5	1.21
8	10+00	Crit. Circle	Spencer's	IPET	no	11.5	1.28
9	10+00	Crit. Circle	Spencer's	IPET	yes	11.5	0.99
10	10+00	Crit. Circle	Spencer's	IPET	yes	11.3	1.00
11	11+50	Crit. Circle	Spencer's	IPET	no	8.5	1.60
12	11+50	Crit. Circle	Spencer's	IPET	yes	8.5	1.21
13	11+50	Crit. Circle	Spencer's	IPET	no	11.5	1.29
14	11+50	Crit. Circle	Spencer's	IPET	yes	11.5	1.03
15	11+50	Crit. Circle	Spencer's	IPET	yes	11.7	1.00
16	GDM 20	Crit. Circle	Spencer's	GDM 20	no	8.5	1.77
17	GDM 20	Crit. Circle	Spencer's	GDM 20	yes	8.5	1.60
18	GDM 20	Crit. Circle	Spencer's	GDM 20	no	11.5	1.45
19	GDM 20	Crit. Circle	Spencer's	GDM 20	yes	11.5	1.24
20	GDM 20	Crit. Circle	Spencer's	GDM 20	yes	13.6	1.00

Analyses were performed for the following canal water levels:

- Elevation 8.5 ft NGVD¹, the approximated water level at the time of failure. As of March 1, 2006 it is estimated that the water level in the 17th Street Canal at the time I-wall began to fail was 7.5 ft to 9.5 ft.
- Elevation 11.5 ft, the water level used as the principal design loading condition.
- The elevations that resulted in computed factors of safety equal to 1.0 at 8+30, 10+00, and 11+50. These were different elevations for the three stations.
- Elevation 13.6 ft, the elevation that resulted in a computed factor of safety equal to 1.0 for the GDM20 cross section and strength. This was analyzed only for the GDM20 cross section and strength model used in design.

¹ All elevations here are referred to NGVD datum. Elevations will be adjusted to NAVD88 when the required information becomes available.

The analyses described here were performed using the computer program SLIDE¹. Critical circular slip surfaces were located for each case, using the search routines available in SLIDE. The analyses were performed using Spencer's method², which satisfies all conditions of equilibrium. Methods that satisfy all conditions of equilibrium have been shown to result in values of factor of safety that are not influenced appreciably by the details of the assumptions they involve³.

In all, 20 cases were analyzed. The conditions analyzed and results of these analyses are summarized in Table K2-1. The critical circles for these cases are shown in Figures K2-1 through K2-15, and K2-17 through K2-21.

Effect of Canal Water Level

The higher the water level in the canal, the lower was the calculated factor of safety, all other things being equal. This can be seen for the no crack condition by comparing Cases 1 and 3, for Station 8+30. Raising the canal water level from elevation 8.5 ft to elevation 11.5 ft results in a decrease in the computed factor of safety of 0.34, from 1.75 to 1.41. For Station 10+00, raising the water level from elevation 8.5 to 11.5 results in a decrease in factor of safety of 0.29 (Cases 6 and 8). For Station 11+50, the reduction is 0.31 (Cases 11 and 13).

Raising the water level also reduces the factor of safety for the cracked condition, as can be seen by comparing Cases 2 and 4, Cases 7 and 9, and Cases 12 and 14. The reduction in the value of F for these cases varies from 0.18 to 0.28.

Effect of a Crack on the Canal Side of the Wall

Assuming that a crack formed on the canal side of the wall, and that hydrostatic water pressure acted through the full depth of the crack, causes a very significant reduction in the value of the calculated factor of safety.

For Station 8+30, with the canal water level at elevation 8.5 ft, the calculated factor of safety for the cracked condition is 1.32, as compared to 1.75 for the uncracked condition. With the water level at 11.5 ft, introducing a crack reduces the factor of safety from 1.41 to 1.04.

For Station 10+00, with the canal water level at elevation 8.5 ft, the calculated factor of safety for the cracked condition is 1.21, as compared to 1.57 for the uncracked condition. With the water level at 11.5 ft, introducing a crack reduces the factor of safety from 1.28 to 0.99.

¹ Available from Rocscience Inc., 31 Balsam Avenue, Toronto, Ontario, Canada M4E 3B5

² Spencer, E. (1967) "A Method of Analysis of the Stability of Embankments Assuming Parallel Inter-Slice Forces," *Geotechnique*, Institution of Civil Engineers, Great Britain, Vol. 17, No. 1, March, pp. 11-26.

³ Duncan, J. Michael, and Wright, Stephen G. (2005), *Soil Strength and Slope Stability*, John Wiley and Sons, New York, 293 pp.

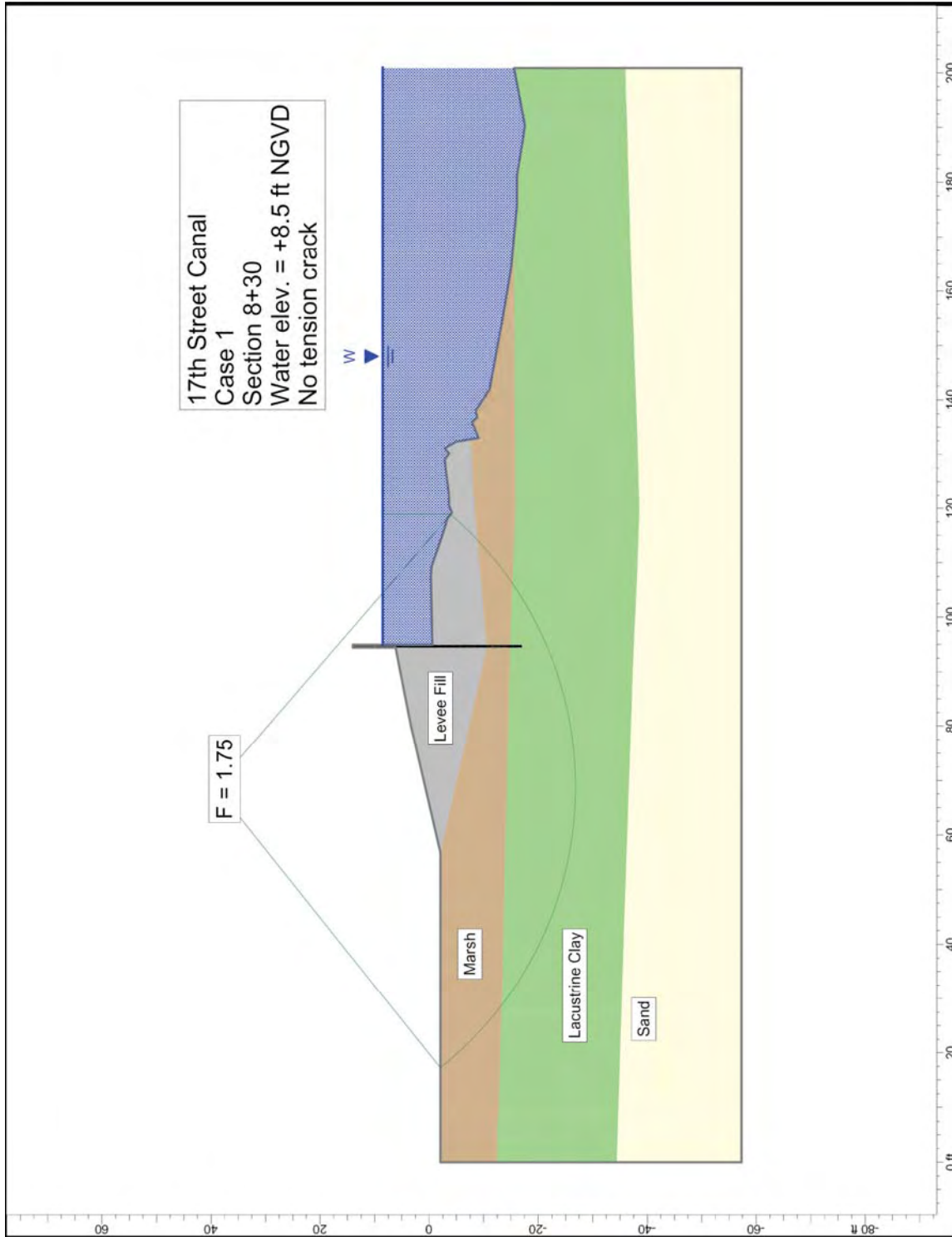


Figure K2-1. Critical circle for 17th Street Canal Station 8+30 – water elevation 8.5 ft, no tension crack.

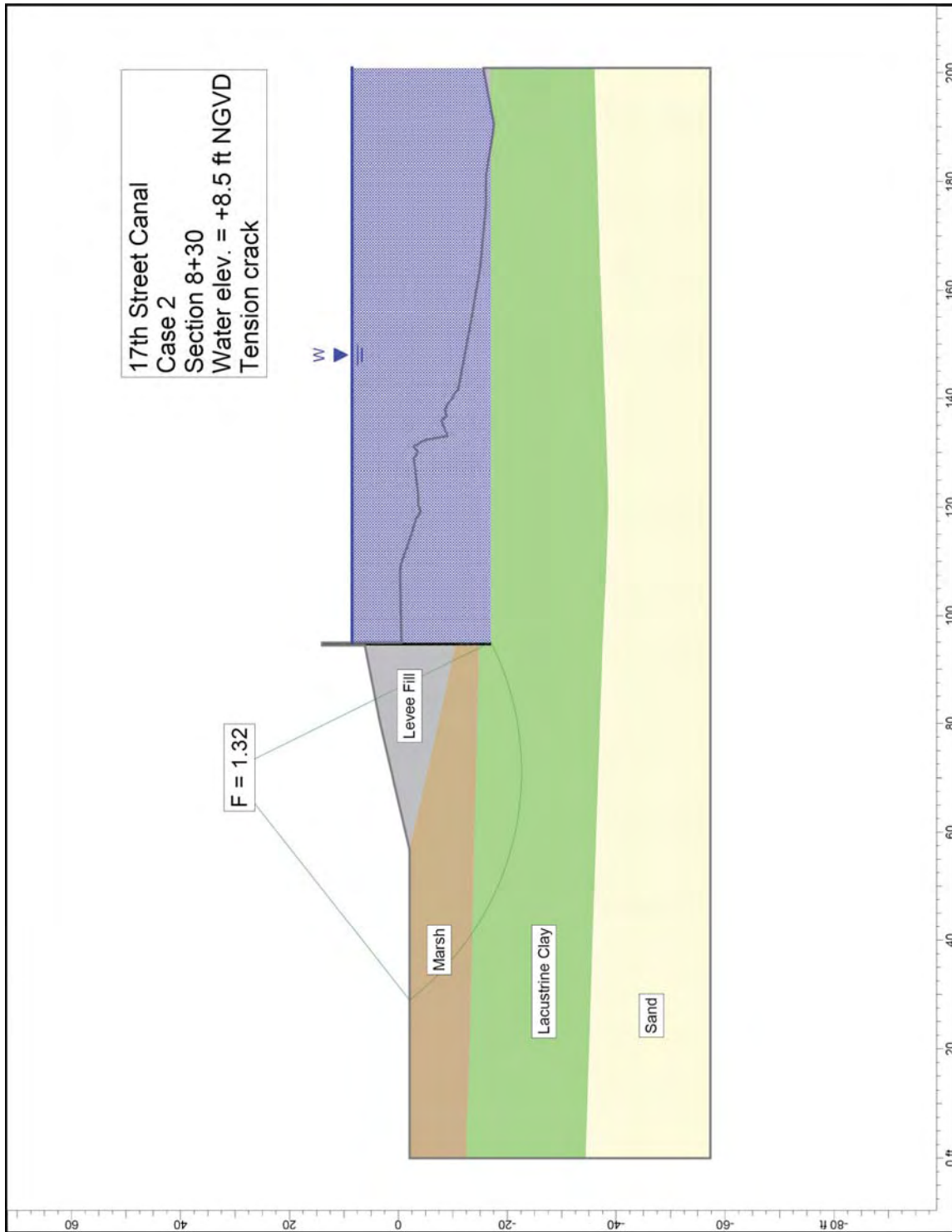


Figure K2-2. Critical circle for 17th Street Canal Station 8+30 – water elevation 8.5 ft, tension crack.

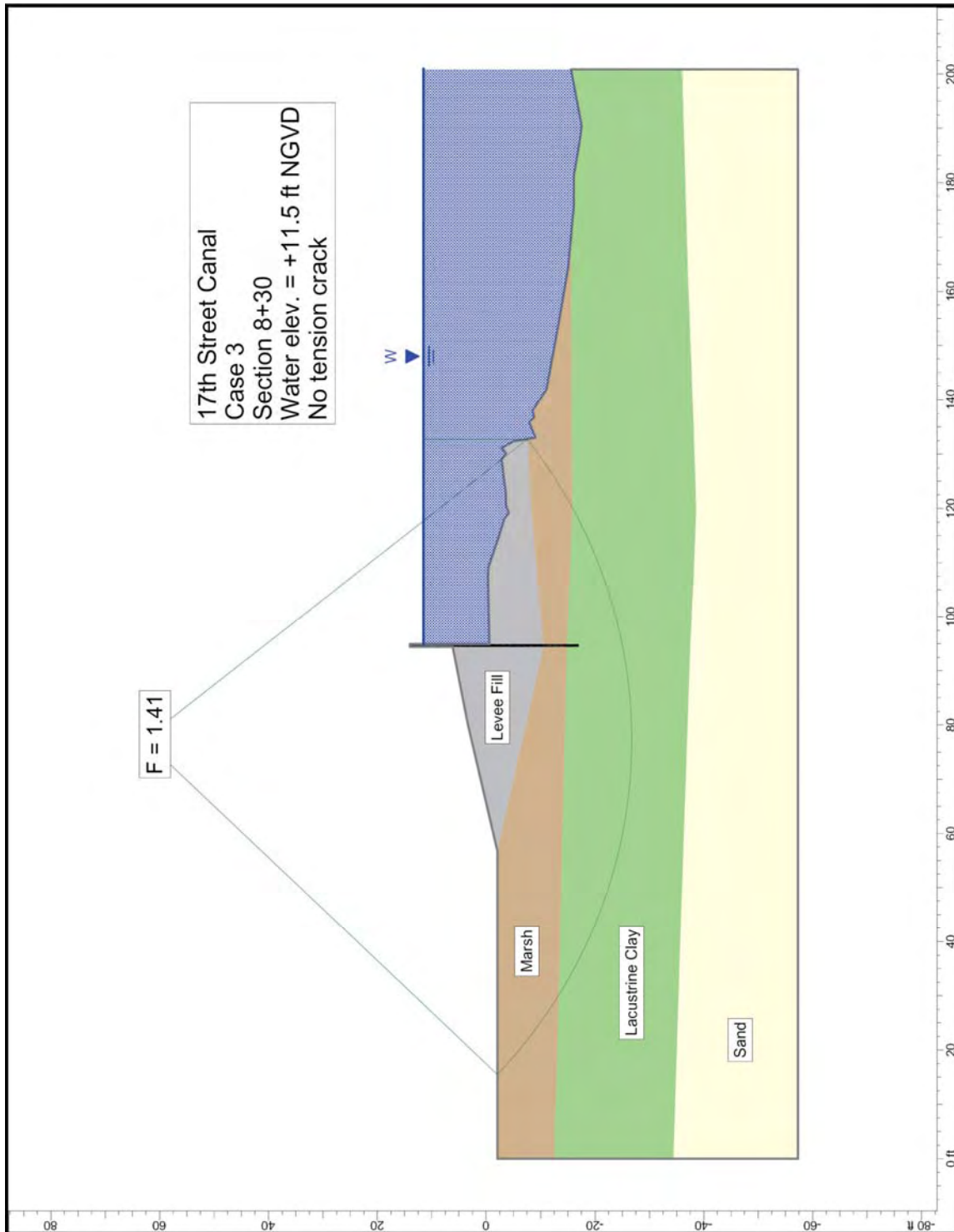


Figure K2-3. Critical circle for 17th Street Canal Station 8+30 – water elevation 11.5 ft, no tension crack.

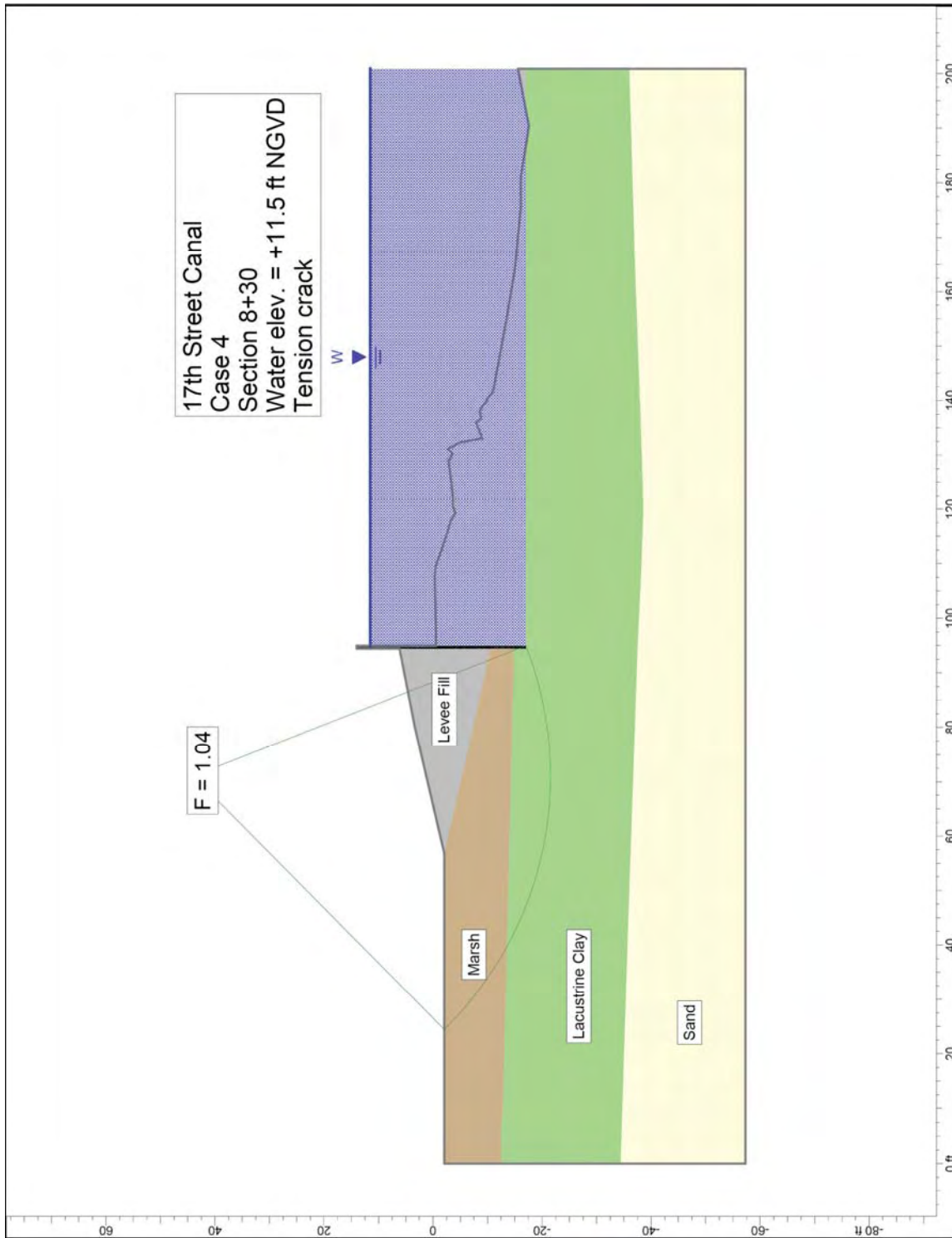


Figure K2-4. Critical circle for 17th Street Canal Station 8+30 – water elevation 11.5 ft, tension crack.

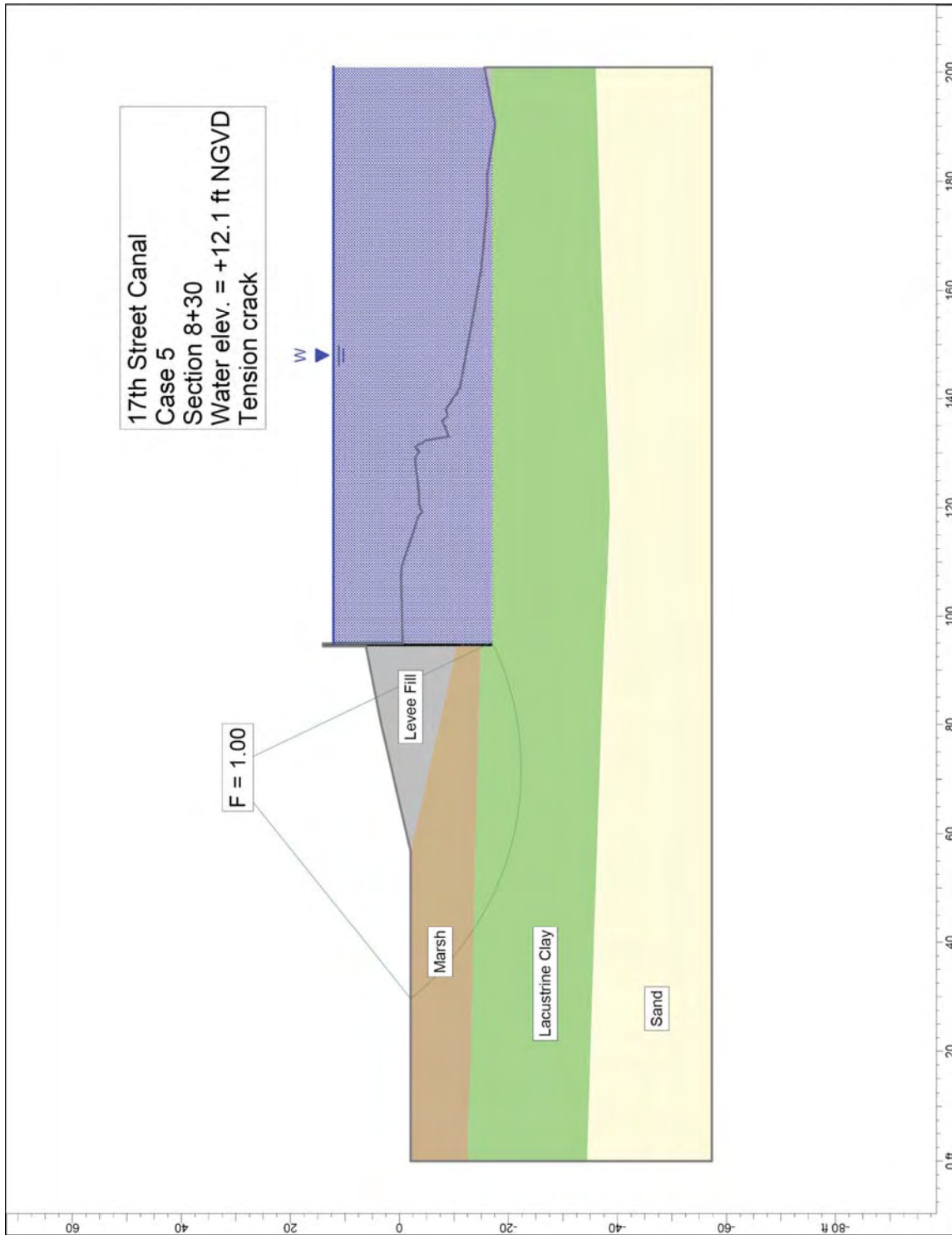


Figure K2-5. Critical circle for 17th Street Canal Station 8+30 – water elevation 5.9 ft, tension crack.

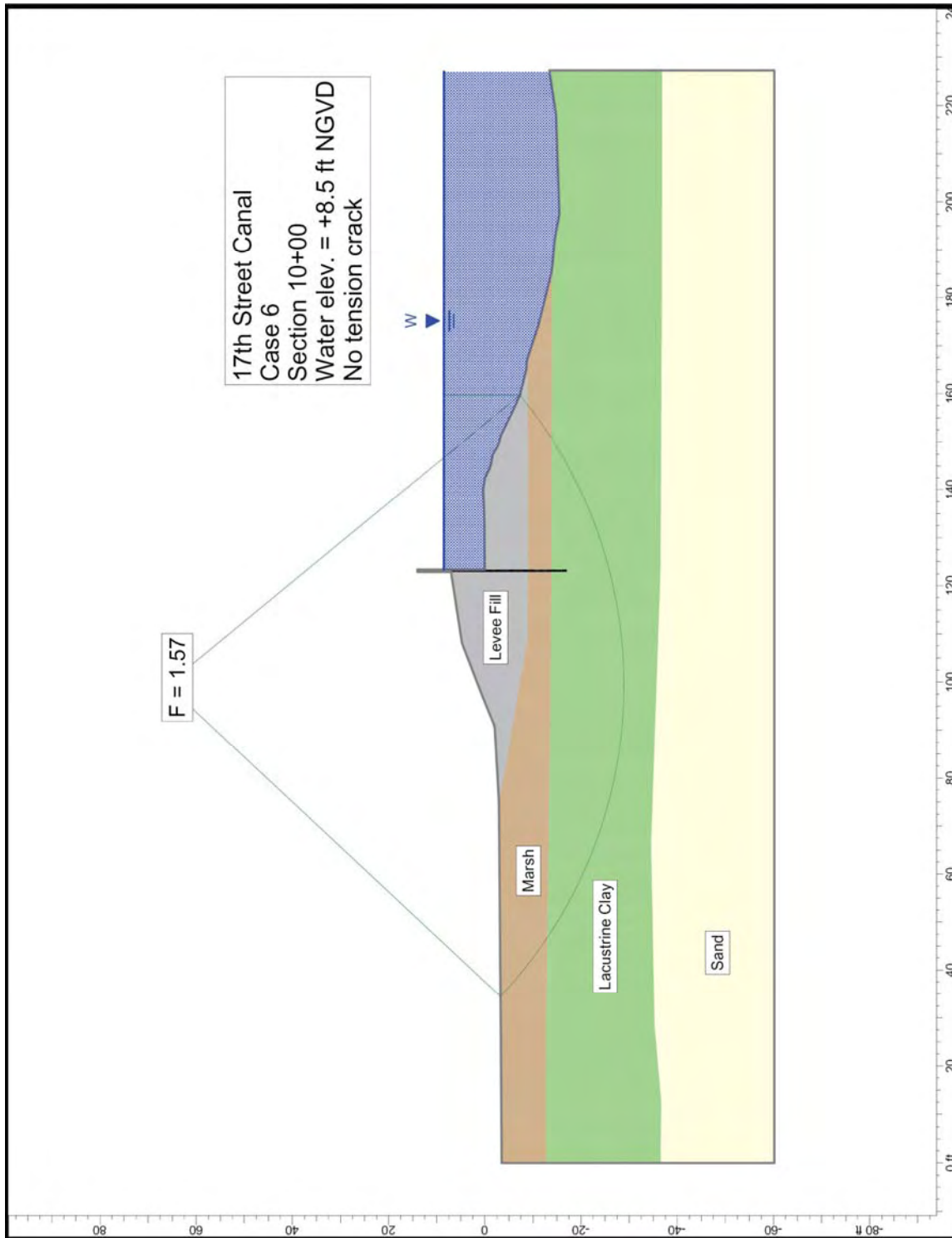


Figure K2-6. Critical circle for 17th Street Canal Station 10+00 – water elevation 8.5 ft, no tension crack.

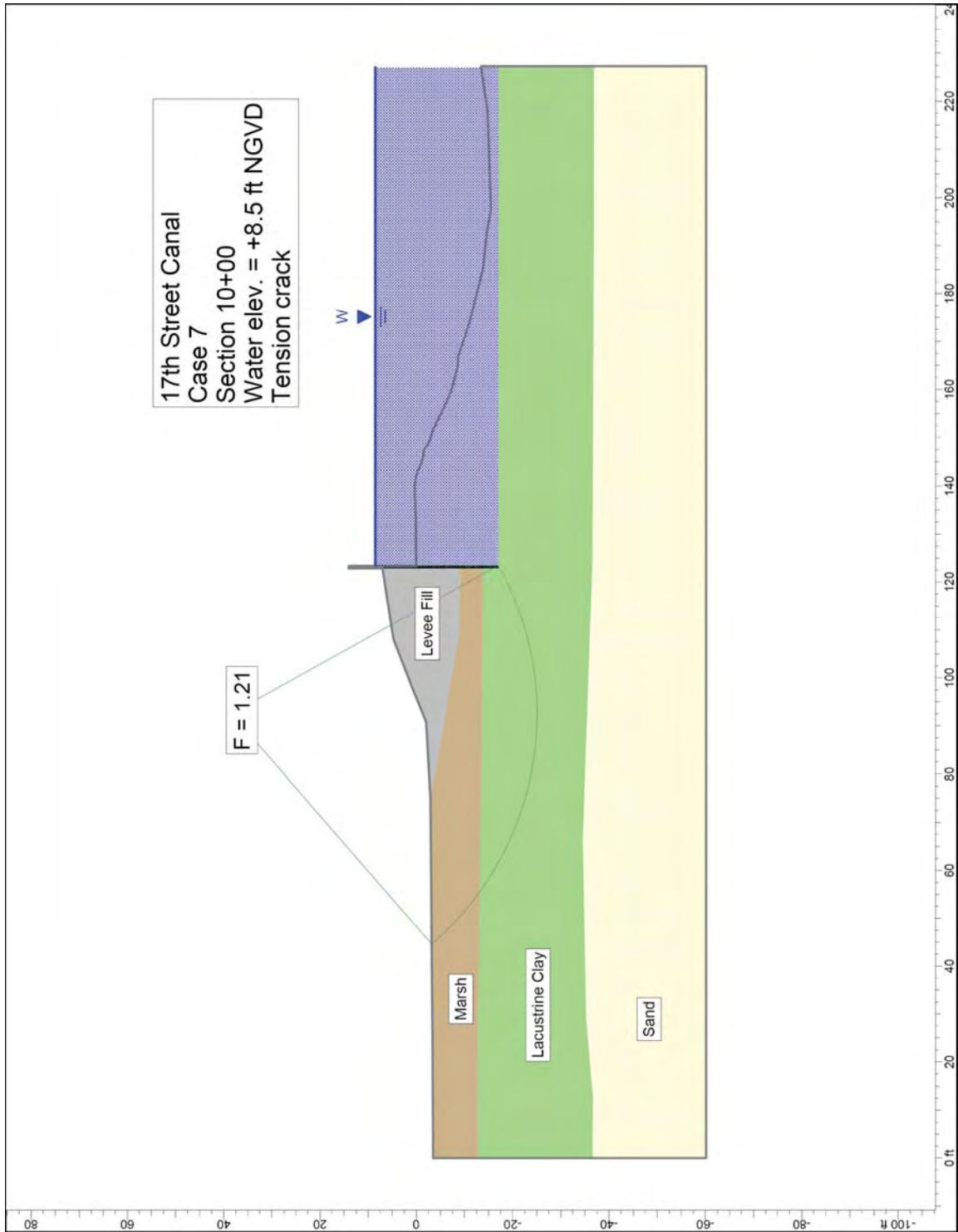


Figure K2-7. Critical circle for 17th Street Canal Station 10+00 – water elevation 8.5 ft, tension crack.

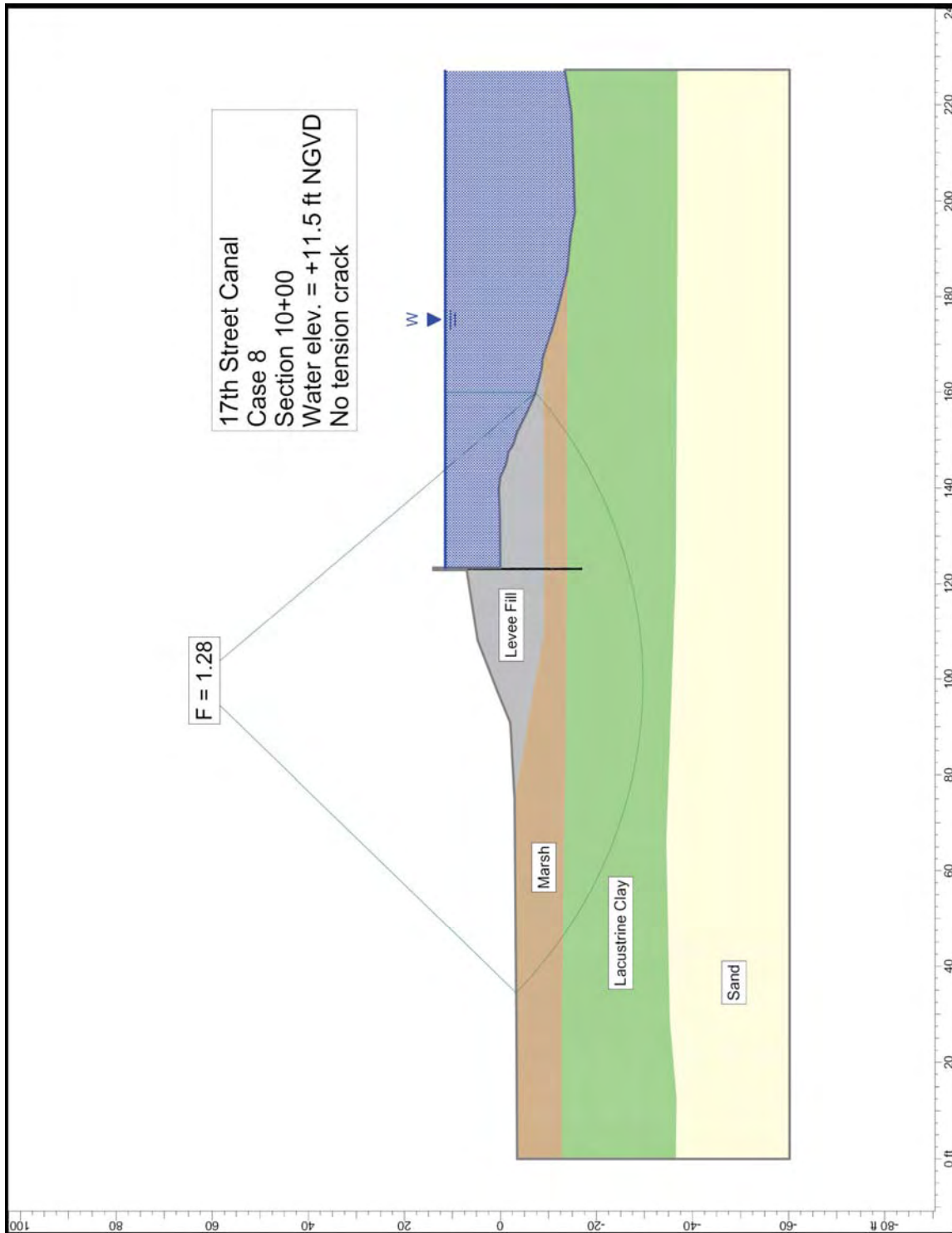


Figure K2-8. Critical circle for 17th Street Canal Station 10+00 – water elevation 11.5 ft, no tension crack.

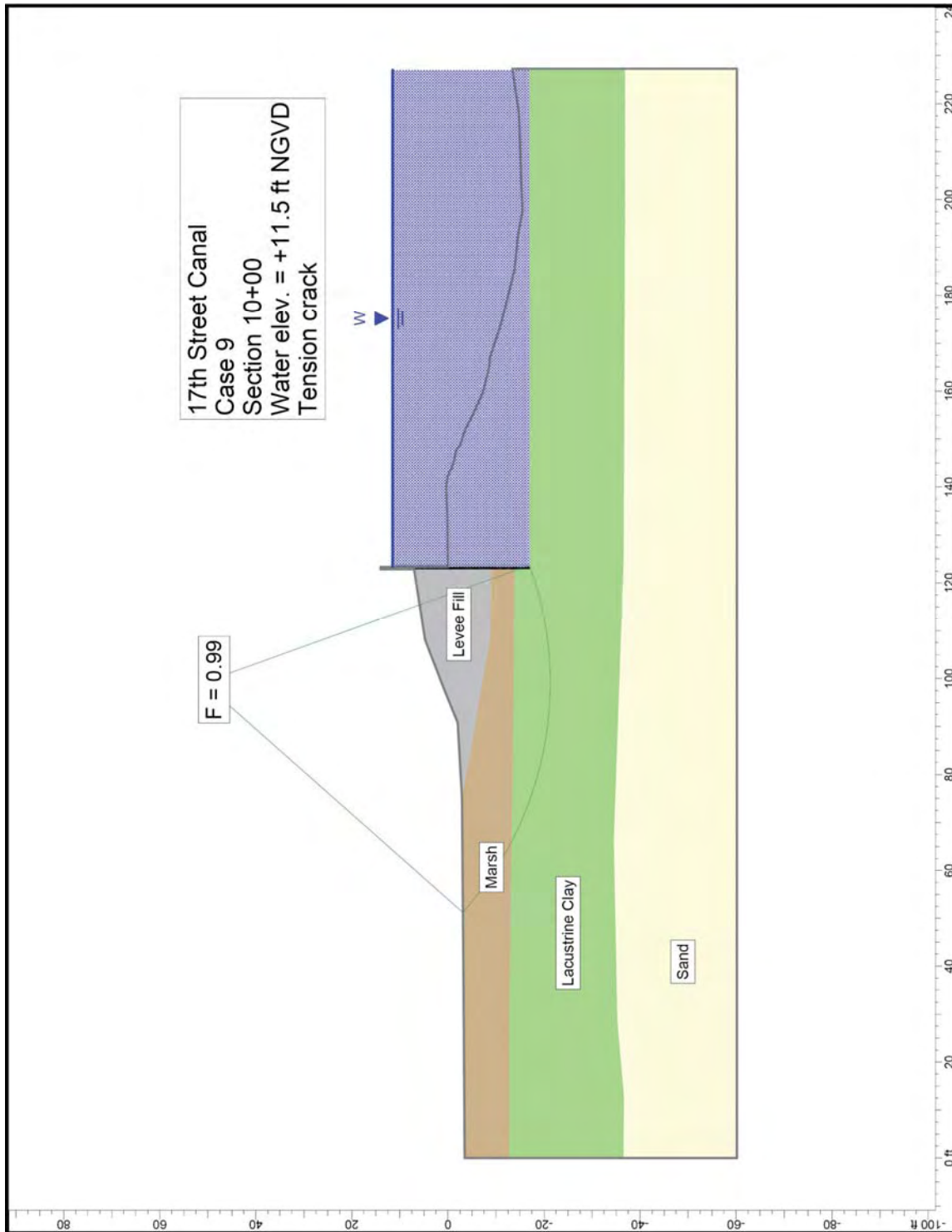


Figure K2-9. Critical circle for 17th Street Canal Station 10+00 – water elevation 11.5 ft, tension crack.

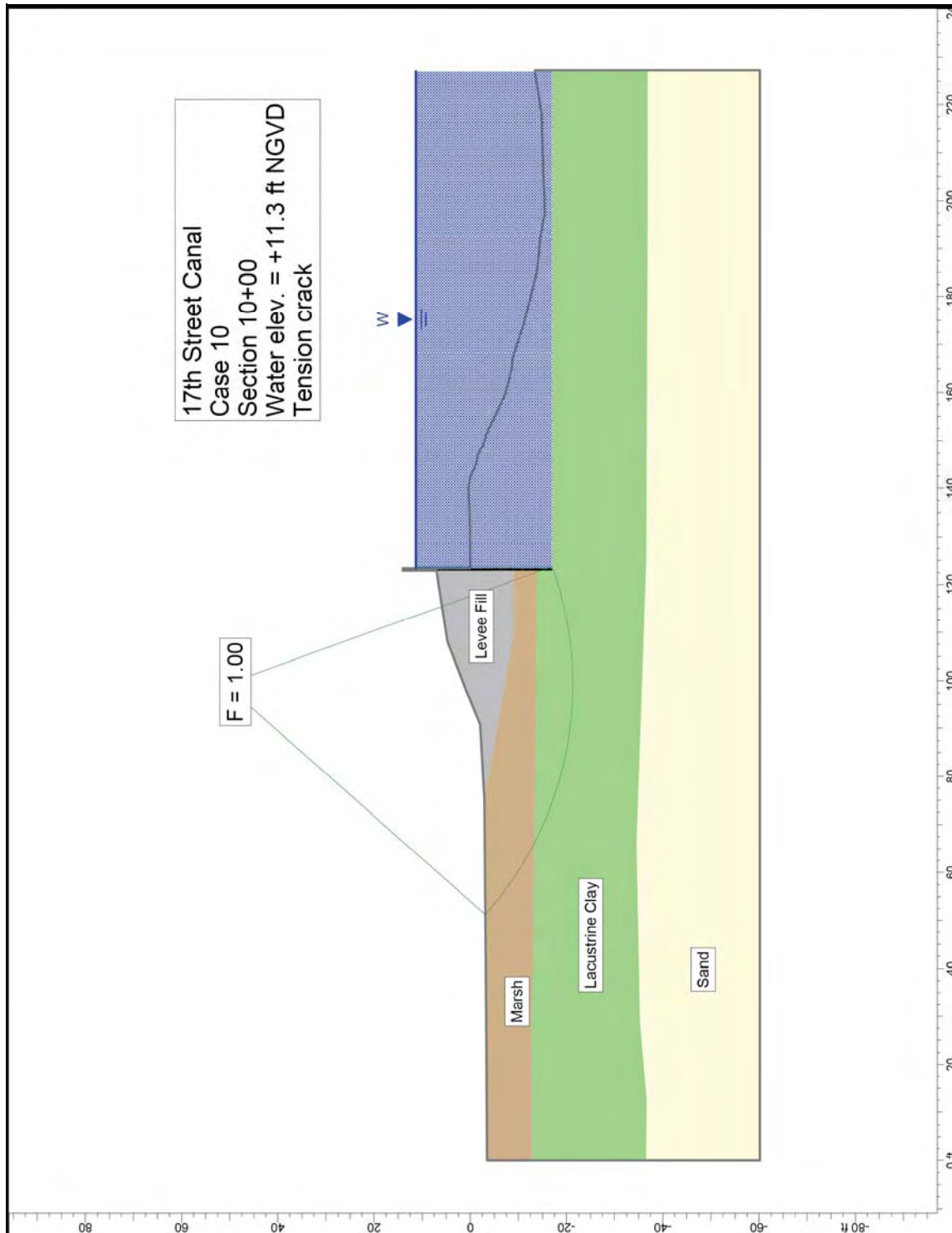


Figure K2-10. Critical circle for 17th Street Canal Station 10+00 – water elevation 11.3 ft, tension crack.

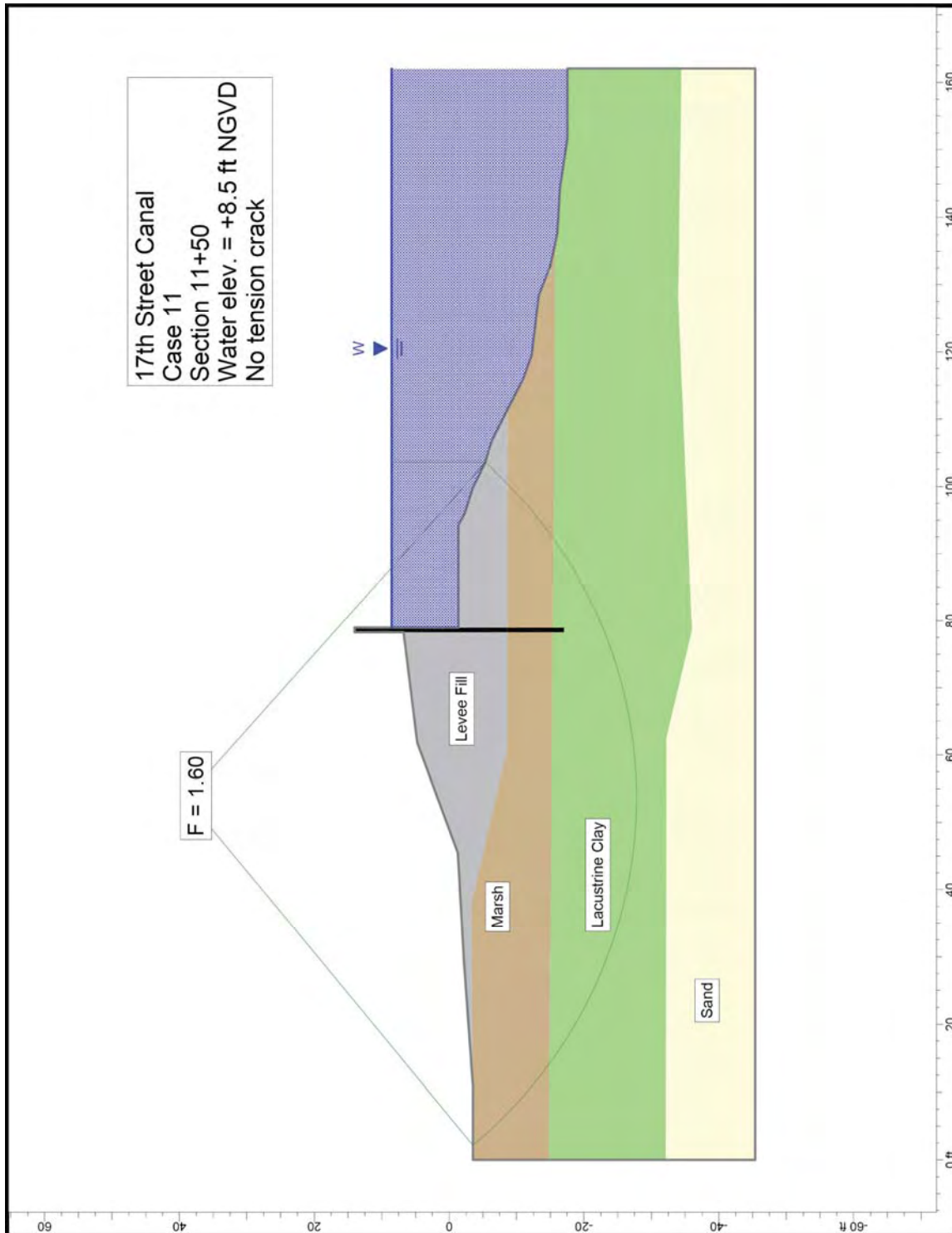


Figure K2-11. Critical circle for 17th Street Canal Station 11+50 – water elevation 8.5 ft, no tension crack.

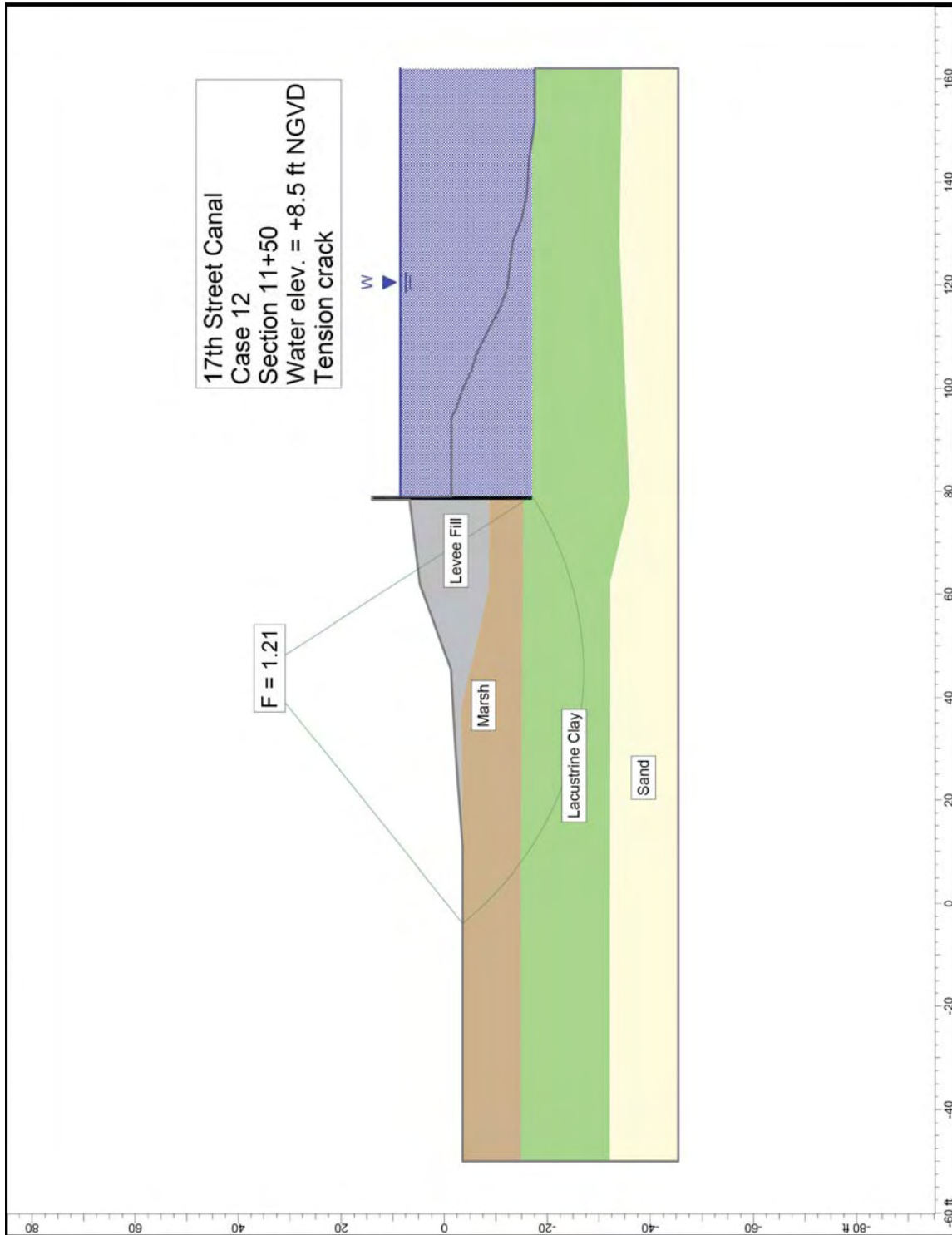


Figure K2-12. Critical circle for 17th Street Canal Station 11+50 – water elevation 8.5 ft, tension crack.

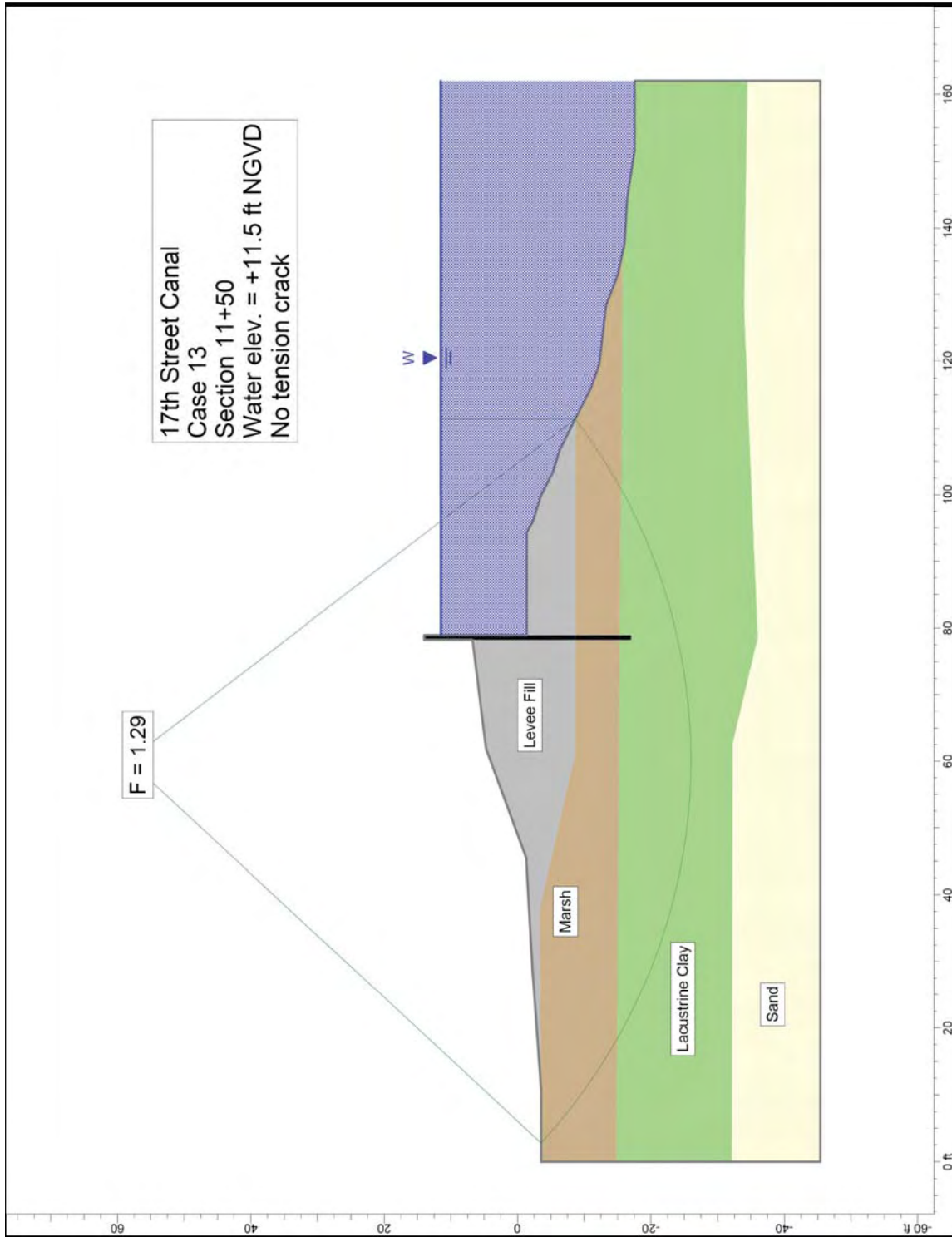


Figure K2-13. Critical circle for 17th Street Canal Station 11+50 – water elevation 11.5 ft, no tension crack.

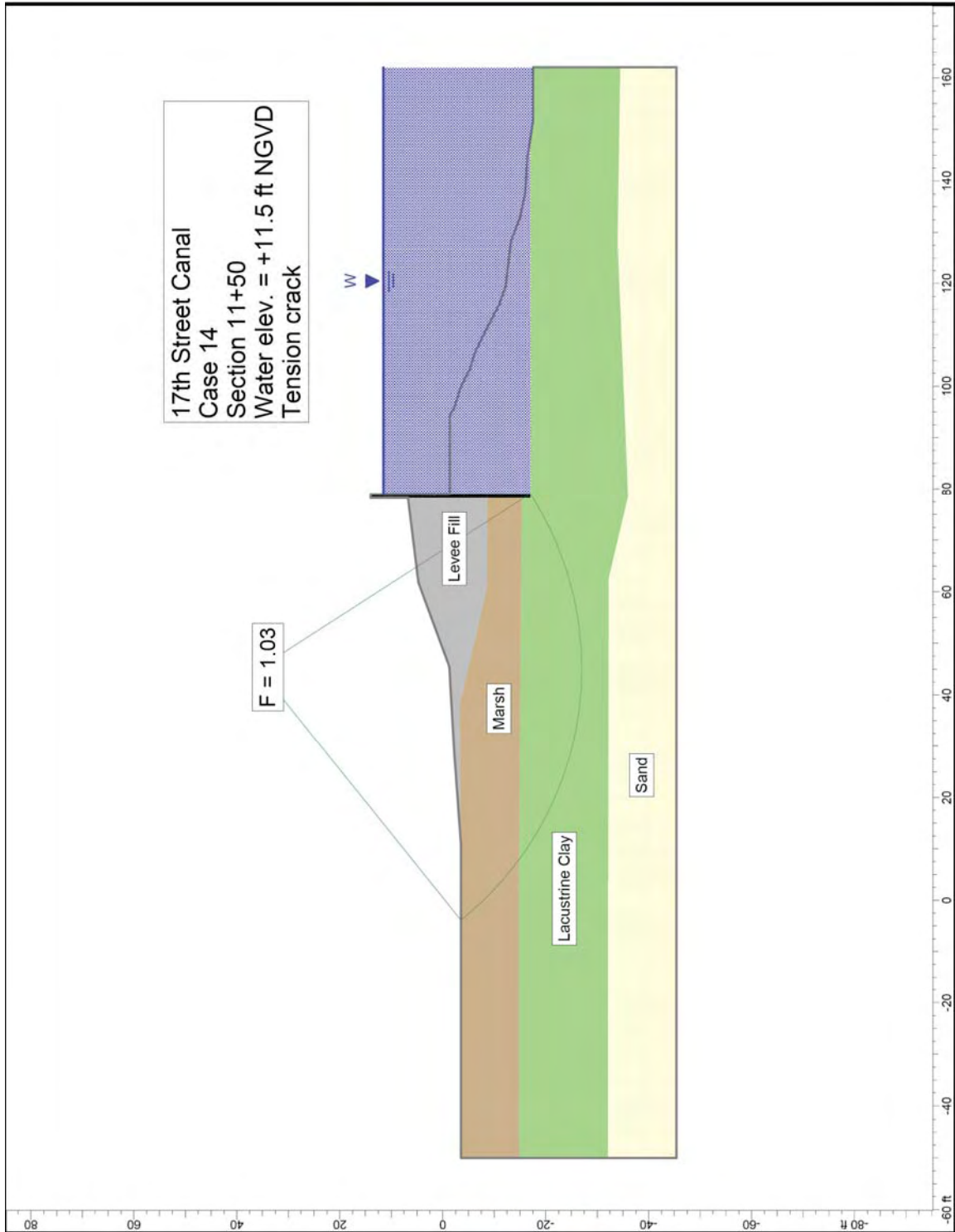


Figure K2-14. Critical circle for 17th Street Canal Station 11+50 – water elevation 11.5 ft, tension crack.

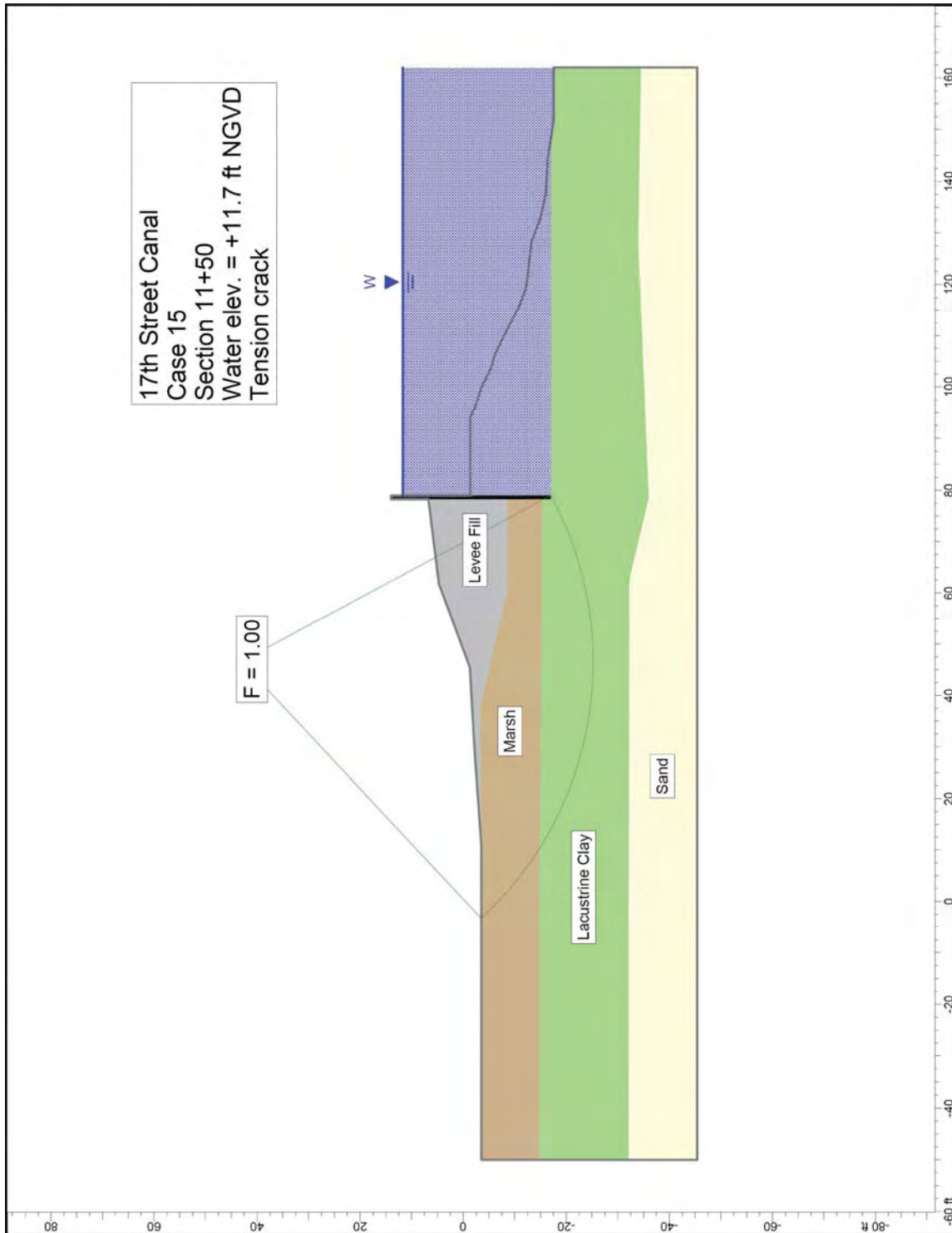


Figure K2-15. Critical circle for 17th Street Canal Station 11+50 – water elevation 11.7 ft, tension crack.

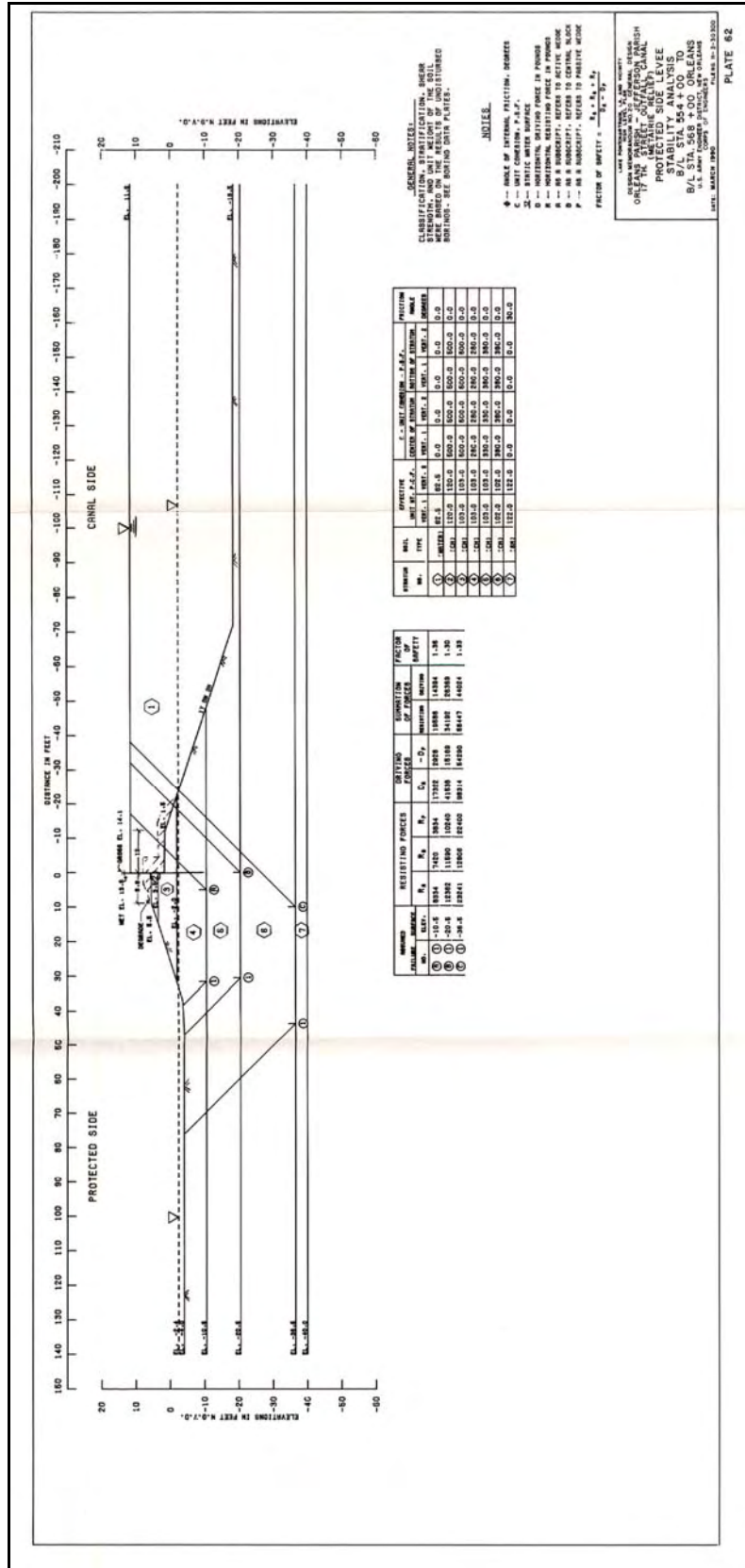


Figure K2-16. Design cross section, from GDM 20, Plate 62.

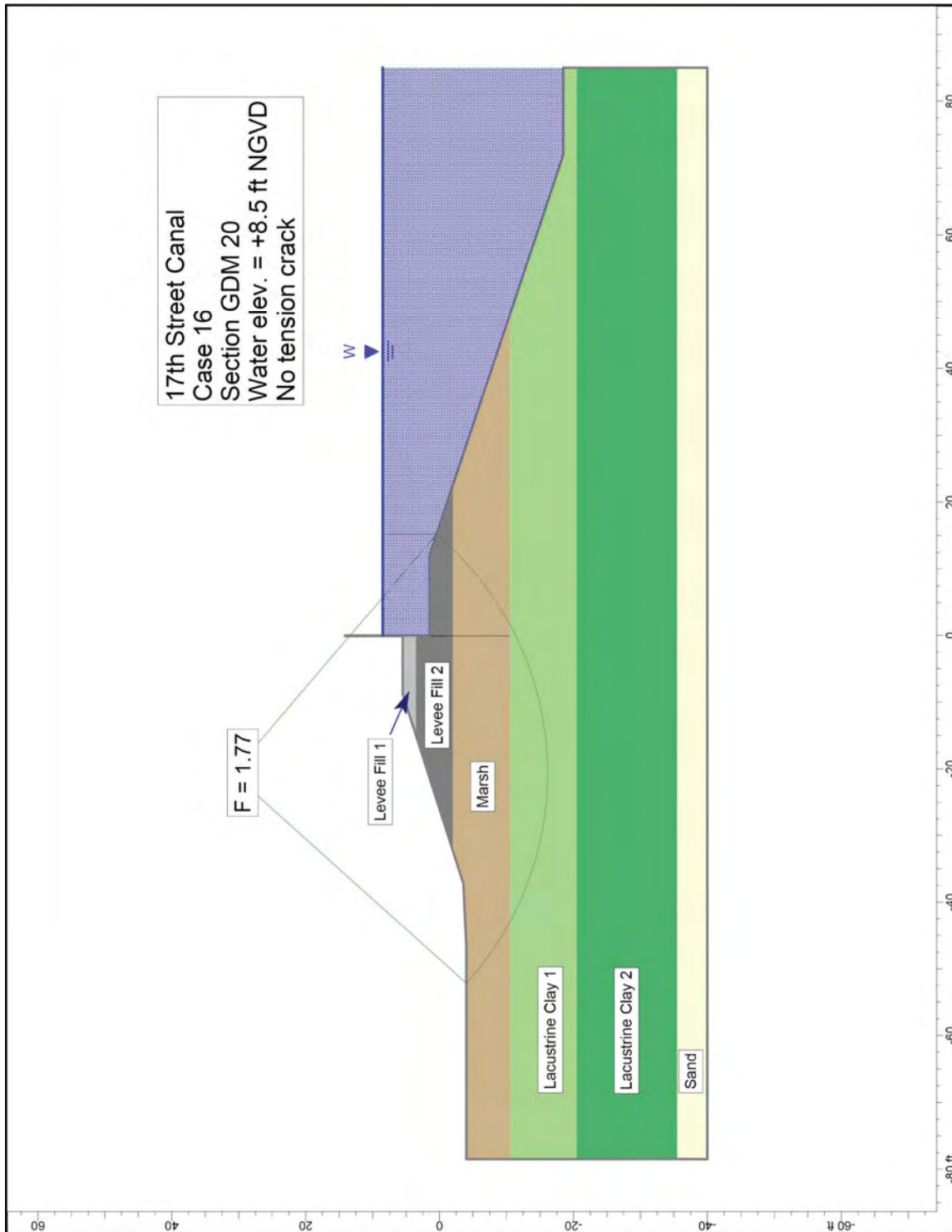


Figure K2-17. Critical circle for 17th Street Canal Design cross section – water elevation 8.5 ft, no tension crack.

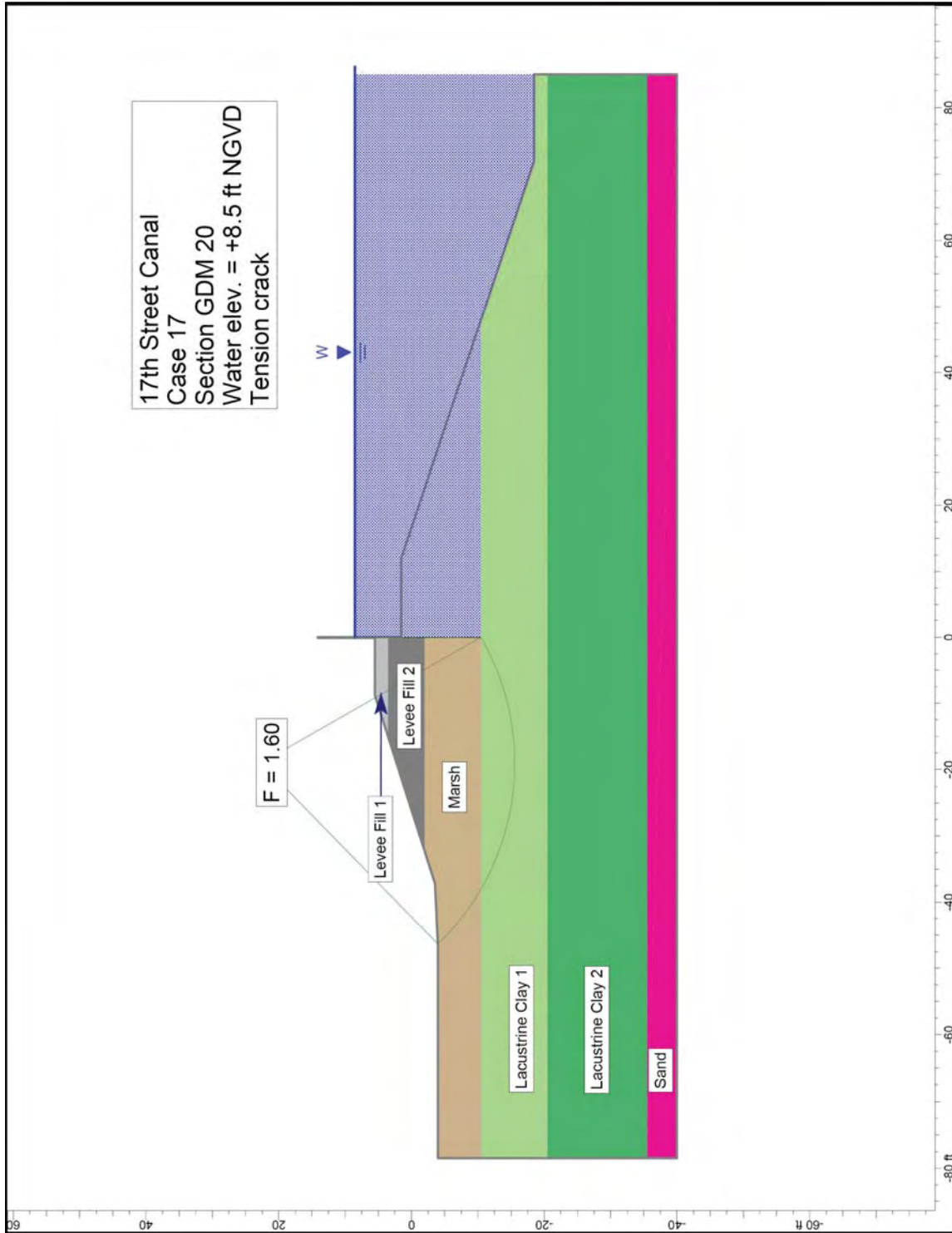


Figure K2-18. Critical circle for 17th Street Canal Design cross section – water elevation 8.5 ft, tension crack.

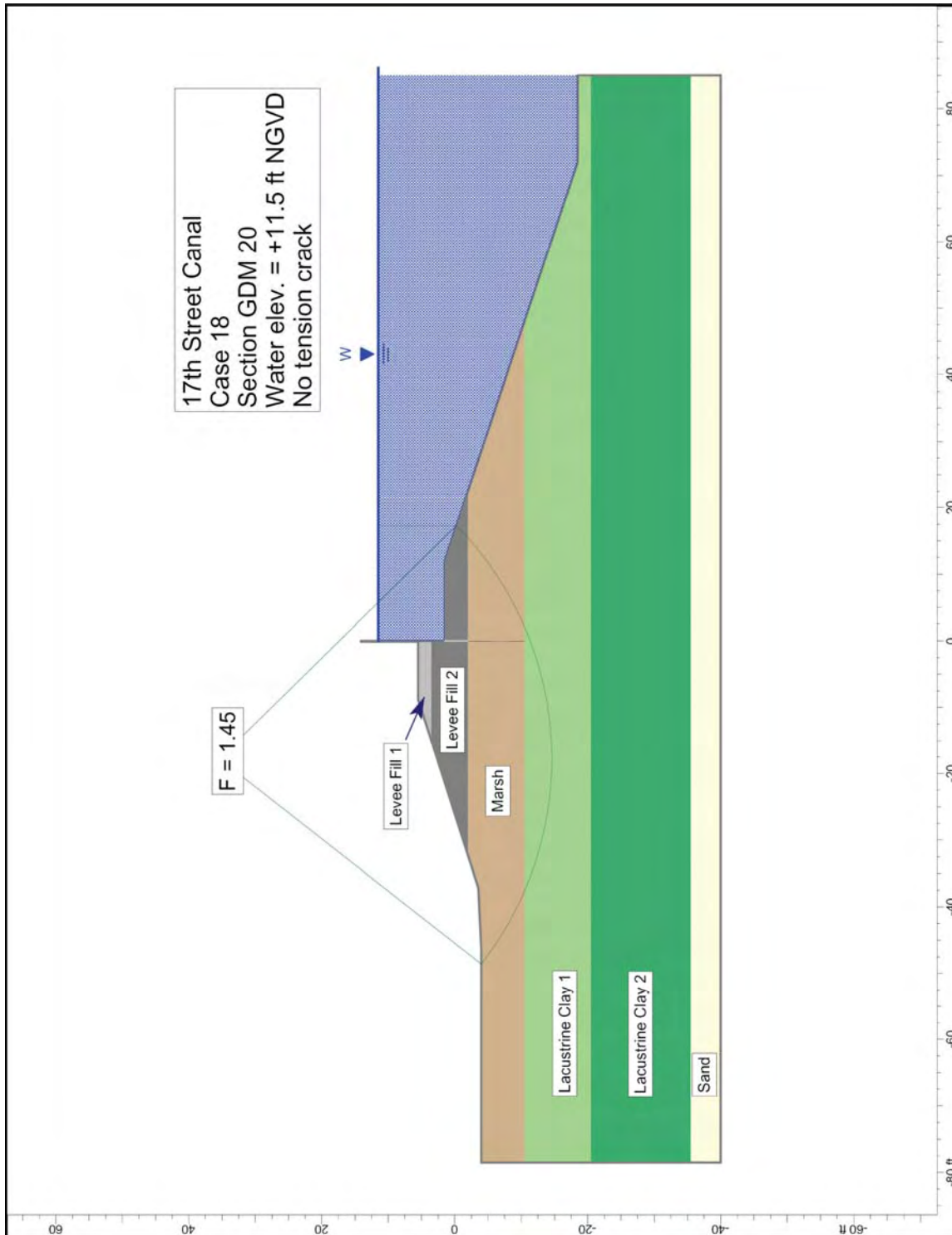


Figure K2-19. Critical circle for 17th Street Canal Design cross section – water elevation 11.5 ft, no tension crack.

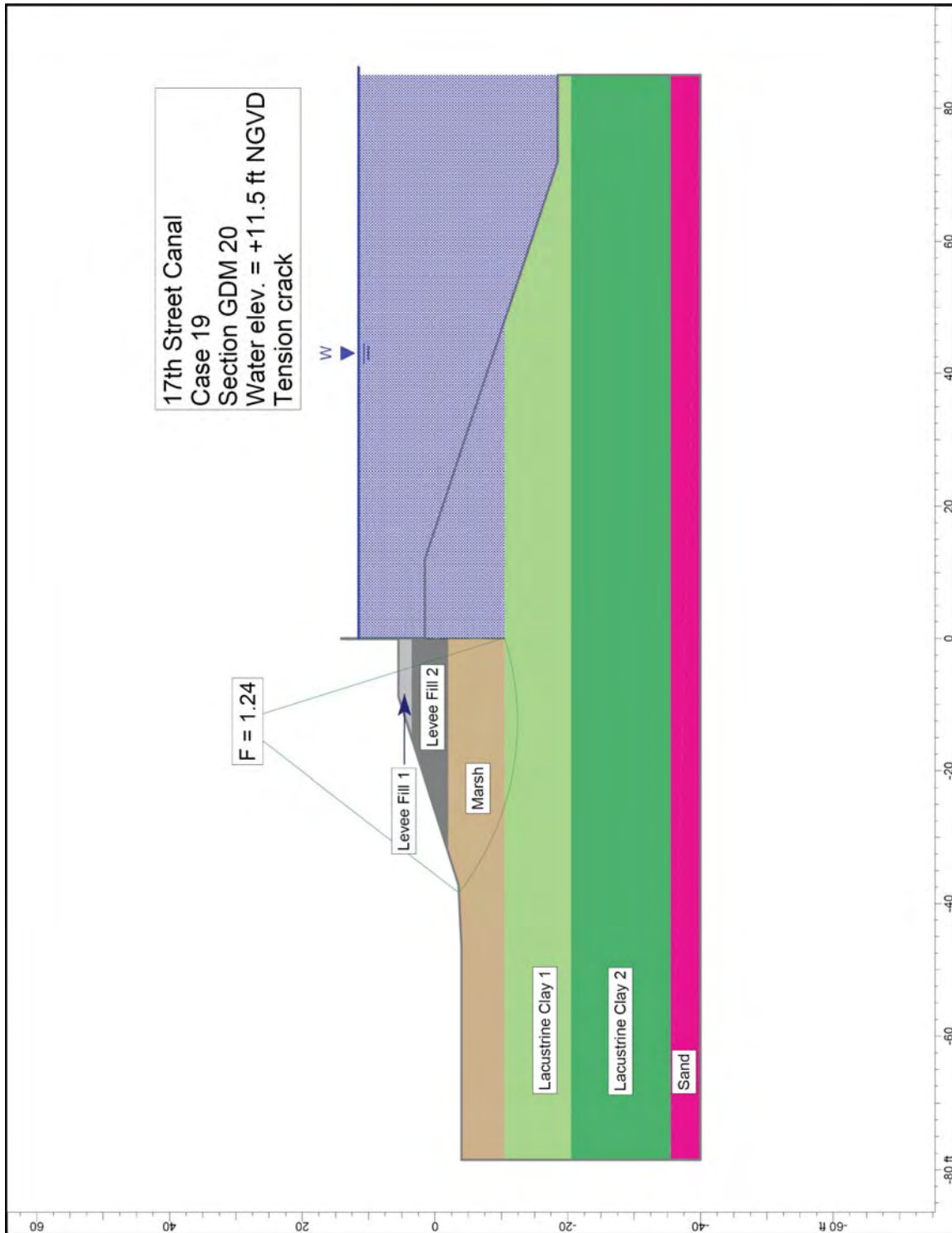


Figure K2-20. Critical circle for 17th Street Canal Design cross section – water elevation 11.5 ft, tension crack.

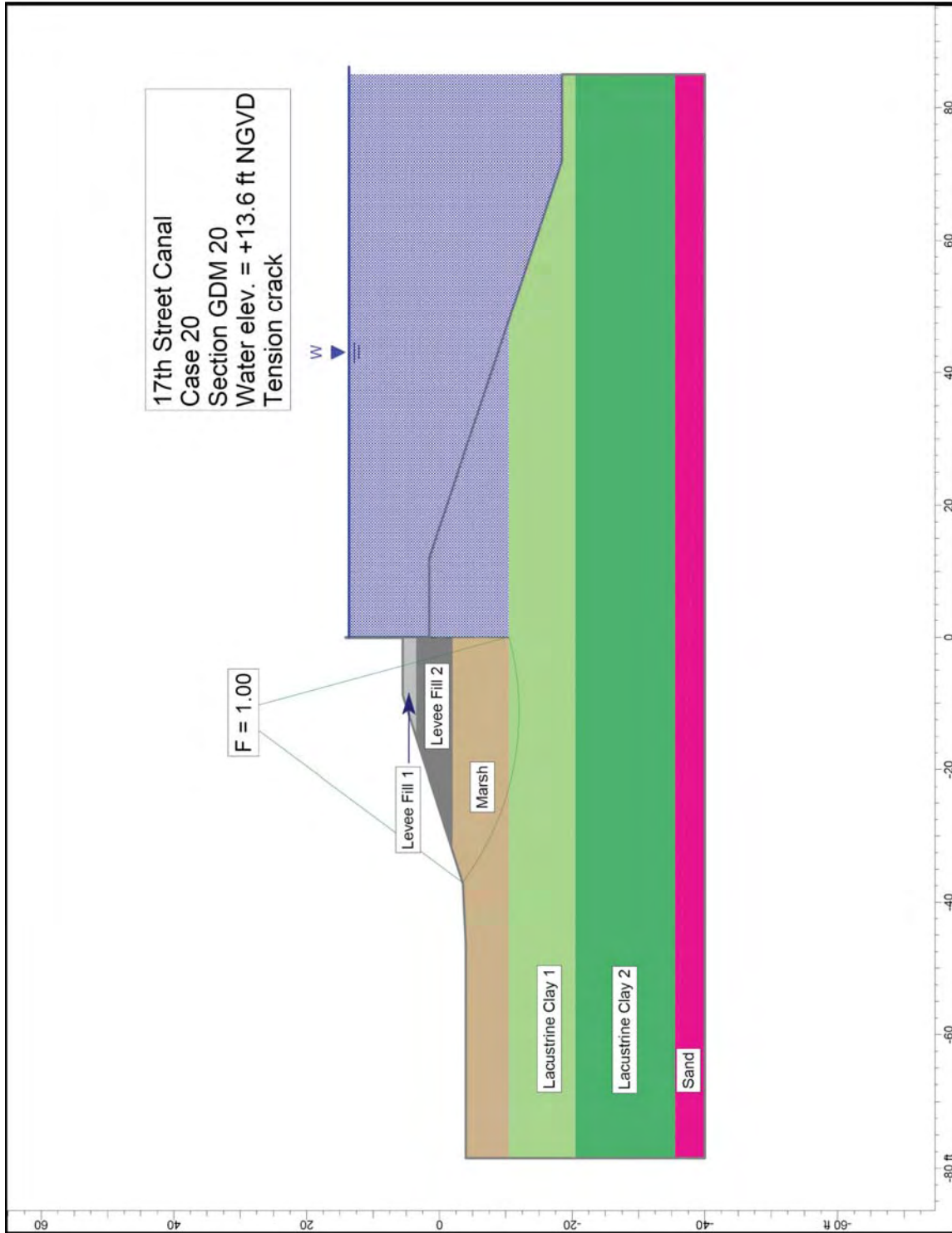


Figure K2-21. Critical circle for 17th Street Canal Design cross section – water elevation 13.6 ft, tension crack.

For Station 11+50, with the canal water level at elevation 8.5 ft, the calculated factor of safety for the cracked condition is 1.21, as compared to 1.60 for the uncracked condition. With the water level at 11.5 ft, introducing a crack reduces the factor of safety from 1.29 to 1.03.

The soil-structure interaction analyses and centrifuge tests yet to be performed may be capable of showing the relationship between water level and the likelihood of development of a crack on the canal side of the wall. These further studies may also show whether the crack extends to the bottom of the wall as assumed here, or only part way. The “no crack” and “full crack” conditions considered here represent the extremes that are possible.

It seems likely that the failure was progressive, with a gradual reduction in factor of safety as the water rose, followed by a more sudden reduction in factor of safety when the crack formed and water filled it. This appears to be a key factor in the mechanism of failure.

For the canal water level at elevation 8.5 ft, the calculated factor of safety is lowest at Station 10+00. This is approximately the same location where an eyewitness report indicates the failure began. The eyewitness report said that failure began at Station 11+00. Subsequently, failure spread to other locations in the breach area.

A sequence of events consistent with the eyewitness report and the calculated results is this:

- As the canal water level rose, a crack did not form until the water reached an average elevation (not accounting for wave effects) of 7.5 ft to 9.5 ft, and the factor of safety before the crack formed was above 1.0.
- When the average water level reached elevation 7.5 ft to 9.5 ft, and the static water pressure force was increased by wave effects, a crack formed between the I-wall and the levee fill on the canal side of the wall, resulting in a reduction in the factor of safety, and the wall began to fail at the location where the factor of safety was lowest.

Static Water Level for Factor of Safety Equal to 1.0

The canal water level was varied to determine the static water level at which the calculated factor of safety would be equal to 1.0, with a crack. Calculated water levels for factors of safety equal to 1.0 for the cracked condition vary from 11.3 ft to 12.1 ft NGVD, as compared with a water level of 7.5 ft to 9.5 ft when failure began based on an eyewitness report. It appears that wave effects might raise the effective water level by 1 to 2 feet, to as much as 11.5 ft. This would reduce the difference between calculated and observed water levels to cause failure to one to two feet. This may indicate that the IPET shear strengths are a little higher than the actual shear strengths.

The difference between calculated and observed water levels causing failure could also be due to the fact that, so far, the stability analyses have only considered circular slip surfaces. Further analyses will be performed using noncircular slip surfaces. While the critical noncircular slip surfaces are assured to have lower factors of safety than the critical circular slip surfaces, it remains to be seen whether the difference is significant or not. Even without this refinement of the analyses, it can be concluded that the IPET strength model is a reasonable representation of the actual conditions in the 17th Street Canal breach area, and that the stability analysis mechanism described here is consistent with the field observations.

Comparison of Spencer’s Method with the Method of Planes

Cases 16 through 20 of Table K2-1 used the design cross section and the shear strengths used in design. The cross section is shown in Figure K2-16, which is taken from Plate 62 of GDM20. The shear strengths are shown in Figures K1-54, K1-55, and K1-56 of the shear strength evaluation report (the design strength profile is the same in all three figures). This cross section and these shear strengths were used as the basis for design of the wall from Wall Stations 554+00 to 568+00, which includes the area where the breach occurred.

The factor of safety computed using the Method of Planes for these conditions was 1.30, with the canal water level at 11.5 ft, and no crack on the canal side of the wall. The factor of safety for this same condition computed using Spencer’s Method (Case 18 in Table K2-1) was 1.45. This shows that the Method of Planes is a conservative method of slope stability analysis.¹

Comparison of Design Analyses With Analyses Performed Using the IPET Strength Model and Spencer’s Method

The design analyses were based on these conditions:

- (1) The analyses were performed for the cross section shown in Figure K2-16.
- (2) The design strength profile shown in Figures K1-54, K1-55, and K1-56 of the shear strength evaluation report were used in the analyses. The same strengths were used under the embankment crest, under the slope, and beyond the toe of the levee.

¹ The Method of Planes is a force equilibrium method. Such methods do not satisfy moment equilibrium, and they require assumptions concerning the orientations of side forces on slices. Depending on the assumed orientations, force equilibrium methods can result in factors of safety that are either higher or lower than factors of safety calculated using methods like Spencer’s Method, which satisfy all conditions of equilibrium.

- (3) The Method of Planes was used to calculate the factor of safety.
- (4) The wall was assumed to be in contact with the levee fill soil on the canal side (the no crack condition).
- (5) The water elevation was assumed to be at 11.5 ft NGVD.

As noted previously, for these conditions a factor of safety equal to 1.30 was calculated using the Method of Planes. Five variations on these conditions were analyzed using Spencer's Method. These are shown in Table K2-1 as Cases 16 through 20.

With the water level at 11.5 NGVD, and a crack between the wall and the soil on the canal side, the factor of safety calculated using Spencer's Method is 1.24. The water level required to reduce the factor of safety to 1.0 is 13.6 ft NGVD.

It appears that the most important difference between the conditions used as the basis for design and the conditions defined in this report is related to the strengths of the peat and clay soils beneath the levee. The design strengths and the IPET strengths are very nearly the same beneath the crest of the levee. However, beneath the levee slopes, and beyond the toe of the levee, the design strengths were higher than the IPET strengths.

Comparison of Factors of Safety in the Breach Area with those in Areas to the North and the South

In order to examine the effect on stability of the higher strengths in the sections north and south of the breach that were discussed in previous sections of this report, stability analyses were performed using shear strengths for the clay and the peat that were 20 percent higher than those estimated for the breach area. This 20 percent higher strength was based on the data available for the area south of the breach. North of the breach a greater difference in clay strength (about 30 percent) was indicated by the available strength data.

The analyses with higher strengths were performed for Station 10+00, with a crack at the canal side of the wall, full hydrostatic water pressure in the crack, and canal water levels at elevations 8.5 ft and 11.5 ft. The results of these analyses are shown in Table K2-2, together with the comparable results from Table K2-1.

For the canal water level at elevation 8.5 ft, a 20 percent increase in clay strength results in a 15 percent increase in factor of safety. A 20 percent increase in peat strength results in 4 percent increase in factor of safety. For the canal water level at elevation 11.5 ft, a 20 percent increase in clay strength results in a 13 percent increase in factor of safety. A 20 percent increase in peat strength results in 5 percent increase in factor of safety.

Case	Section	Slip Surface	Method	Strength Model	Crack	Water Elev. Ft. NGVD	F
7	10+00	Crit. Circle	Spencer's	IPET	yes	8.5	1.21
7A	10+00	Crit. Circle	Spencer's	clay + 20%	yes	8.5	1.40
7B	10+00	Crit. Circle	Spencer's	clay - 20%	yes	8.5	1.02
7C	10+00	Crit. Circle	Spencer's	peat + 20%	yes	8.5	1.26
7D	10+00	Crit. Circle	Spencer's	peat - 20%	yes	8.5	1.16
9	10+00	Crit. Circle	Spencer's	IPET	yes	11.5	0.99
9A	10+00	Crit. Circle	Spencer's	clay + 20%	yes	11.5	1.12
9B	10+00	Crit. Circle	Spencer's	clay - 20%	yes	11.5	0.84
9C	10+00	Crit. Circle	Spencer's	peat + 20%	yes	11.5	1.04
9D	10+00	Crit. Circle	Spencer's	peat - 20%	yes	11.5	0.93

The factors of safety shown in Table K2-2 for increased clay and peat strengths are consistent with the fact that failure did not occur in these areas.

Probabilities of Failure

Probabilities of failure have been estimated using an approximate technique based on the Taylor Series method. The coefficient of variation of the average clay strength and the average peat strength were estimated to be 20 percent. The data available is sparse, and the scatter in measured values is influenced significantly by sample quality as well as variations in properties from one location to another. The estimate values of COV = 20 percent is thus largely based on judgment. Even so, it is valuable to examine what probabilities of failure would be associated with this level of uncertainty concerning shear strengths.

The Taylor Series numerical method¹⁻⁵ was used to estimate the standard deviation (σ_F) and the coefficient of variation of the factor of safety (COV_F), using these formulas:

¹Wolff, T. F. (1994). "Evaluating the reliability of existing levees." Report, Research Project: Reliability of Existing Levees, prepared for U.S. Army Engineer Waterways Experiment Station Geotechnical Laboratory, Vicksburg, Miss.

$$\sigma_F = \sqrt{\left(\frac{\Delta F_{\text{clay strength}}}{2}\right)^2 + \left(\frac{\Delta F_{\text{peat strength}}}{2}\right)^2} \quad (1)$$

$$\text{COV}_F = \frac{\sigma_F}{F_{\text{MLV}}} \quad (2)$$

where $\Delta F_{\text{clay strength}}$ = difference between the values of the factor of safety calculated with the clay strength increased by one standard deviation and decreased by one standard deviation from its most likely value. $\Delta F_{\text{peat strength}}$ is determined in the same way. F_{MLV} is the “most likely value” of factor of safety, computed using the IPET shear strengths.

Using the factors of safety listed in Table K2-2 for water level = 8.5 ft, $\Delta F_{\text{clay strength}} = 1.40 - 1.02 = 0.38$, and $\Delta F_{\text{peat strength}} = 1.26 - 1.16 = 0.10$. Substituting these values in Eq (1) leads to $\sigma_F = 0.39$. With $F_{\text{MLV}} = 1.21$, the value of COV_F calculated using Eq (2) = $0.39/1.21 = 0.32$.

For water level = 11.5 ft, $\Delta F_{\text{clay strength}} = 1.12 - 0.84 = 0.28$, and $\Delta F_{\text{peat strength}} = 1.04 - 0.93 = 0.11$. Substituting these values in Eq (1) leads to $\sigma_F = 0.30$. With $F_{\text{MLV}} = 0.99$, the value of COV_F calculated using Eq (2) = $0.30/0.99 = 0.30$.

With both F_{MLV} and COV_F known, the probability of failure (p_f) can be determined using Table K2-3. For water level = 8.5 ft ($F_{\text{MLV}} = 1.21$, $\text{COV}_F = 0.32$), the probability of failure is about 30 percent. For water level = 11.5 ft ($F_{\text{MLV}} = 0.99$, $\text{COV}_F = 0.30$), the probability of failure is out of range of the values in Table K4-3, and exceeds 50 percent.

For areas north and south of the breach, where strengths and most likely values of factor of safety are higher, the probabilities of failure are lower. For water level = 8.5 ft ($F_{\text{MLV}} \approx 1.45$ and $\text{COV}_F \approx 30$ percent), the probability of failure would be between 10 percent and 15 percent. For water level = 11.5 ft ($F_{\text{MLV}} \approx 1.15$ and $\text{COV}_F \approx 30$ percent), the probability of failure would be between 30 percent and 40 percent.

Summary

The results of the analyses described in the preceding sections are reasonably consistent with the performance of the I-wall in the breach area. Calculated water levels for factors of safety equal to 1.0 for the cracked condition vary from 11.3 ft to 12.1 ft NGVD, as compared with a water level of 7.5 ft to 9.5 ft at the time failure began based on an eyewitness report. It appears that wave effects might raise the effective water level by 1 to 2 feet, to as much as 11.5 ft. This would reduce the difference between calculated and observed water levels to cause failure to one to two feet. This may indicate that the IPET shear strengths are a little higher than the actual shear strengths.

Table K2-3 Probabilities of Failure Based on Lognormal Distribution of F⁴									
F_{MLV}	COV_F = Coefficient of Variation of Factor of Safety								
	10%	12%	14%	16%	20%	25%	30%	40%	50%
1.05	33.02%	36.38%	38.95%	41.01%	44.14%	47.01%	49.23%	52.63%	55.29%
1.10	18.26%	23.05%	26.95%	30.15%	35.11%	39.59%	42.94%	47.82%	51.37%
1.15	8.83%	13.37%	17.53%	21.20%	27.20%	32.83%	37.10%	43.24%	47.62%
1.20	3.77%	7.15%	10.77%	14.29%	20.57%	26.85%	31.76%	38.95%	44.05%
1.25	1.44%	3.54%	6.28%	9.27%	15.20%	21.68%	26.98%	34.95%	40.66%
1.30	0.49%	1.64%	3.49%	5.81%	11.01%	17.30%	22.75%	31.26%	37.48%
1.35	0.15%	0.71%	1.86%	3.53%	7.83%	13.66%	19.06%	27.88%	34.49%
1.40	0.04%	0.29%	0.95%	2.08%	5.48%	10.69%	15.88%	24.80%	31.70%
1.50	0.00%	0.04%	0.23%	0.67%	2.57%	6.38%	10.85%	19.49%	26.69%
1.60	0.00%	0.01%	0.05%	0.20%	1.15%	3.71%	7.29%	15.21%	22.40%
1.70	0.00%	0.00%	0.01%	0.06%	0.49%	2.11%	4.84%	11.81%	18.75%
1.80	0.00%	0.00%	0.00%	0.01%	0.21%	1.18%	3.18%	9.13%	15.67%
1.90	0.00%	0.00%	0.00%	0.00%	0.08%	0.65%	2.07%	7.03%	13.08%
2.00	0.00%	0.00%	0.00%	0.00%	0.03%	0.36%	1.34%	5.41%	10.91%
2.20	0.00%	0.00%	0.00%	0.00%	0.01%	0.10%	0.56%	3.19%	7.59%
2.40	0.00%	0.00%	0.00%	0.00%	0.00%	0.03%	0.23%	1.88%	5.29%
2.60	0.00%	0.00%	0.00%	0.00%	0.00%	0.01%	0.09%	1.11%	3.70%
2.80	0.00%	0.00%	0.00%	0.00%	0.00%	0.00%	0.04%	0.66%	2.60%
3.00	0.00%	0.00%	0.00%	0.00%	0.00%	0.00%	0.02%	0.39%	1.83%

F_{MLV} = factor of safety computed using most likely values of parameters

The difference between calculated and observed water levels causing failure could also be due to the fact that, so far, the stability analyses have only considered circular slip surfaces. Further analyses will be performed using noncircular slip surfaces. While the critical noncircular slip surfaces are assured to have lower factors of safety than the critical circular slip surfaces, it remains to be seen whether the difference is significant or not. Even without this refinement of the analyses, it can be concluded that the IPET strength model is a reasonable representation of the actual conditions in the 17th Street Canal breach area, and that the stability analysis mechanism described here is consistent with the field observations.

The calculated factors of safety are about 25 percent lower when it is assumed that a crack develops between the wall and the levee fill on the canal side of the wall. The results calculated assuming that a crack formed, and that full hydrostatic water pressure acted in the crack, are consistent with field observations, indicating that it is highly likely that a crack did form in the areas where the wall failed. It seems likely that when a crack formed and the portion of the wall below the levee crest was loaded by water pressures, the factor of safety would have dropped quickly by about 25 percent. Soil structure

interaction analyses and centrifuge model tests will likely provide further understanding of crack formation and its relation to wall stability.

The New Orleans District Method of Planes is a conservative method of slope stability analysis. All other things being equal, the factor of safety calculated using the Method of Planes was about 10 percent lower than the factor of safety calculated using Spencer's method, which satisfies all conditions of equilibrium.

The factors of safety calculated in the design analyses were higher than the factors of safety calculated for the conditions that are believed to best represent the actual shear strengths, geometrical conditions, and loading at the time of failure. The principal differences between the design analyses and the conditions described in this report relate to (1) the assumption that a crack formed between the wall and the levee soil on the canal side of the wall, and (2) the fact that the design analyses used the same strength for the clay and the peat beneath the levee slopes, and for the area beyond the levee toe, as for the zone beneath the crest of the levee. The IPET strength model has lower strengths beneath the levee slopes and beyond the toe.

Factors of safety for areas adjacent to the breach, where clay strengths are higher, were about 15 percent higher than those calculated for the breach area. These differences in calculated factor of safety are not large, and it thus appears that the margin of safety was small in areas that did not fail. It is possible that areas adjacent to the breach remained stable primarily because cracks did not form in those areas, and the wall was therefore less severely loaded.

Estimates of probability of failure for a water level of 8.5 ft NGVD are about 30 percent in the breach area, and 10 percent to 15 percent in the areas north and south of the breach. For a water level of 11.5 ft, the estimated probability of failure is about 50 percent in the breach area and 30 percent to 40 percent north and south of the breach. If stability analyses considering noncircular slip surfaces result in appreciably lower factors of safety, the corresponding probabilities of failure will be higher.

K3 – Physical Modeling

Drainage Canals – Physical Centrifuge Modeling

Scale modeling using large geotechnical centrifuges at RPI and at ERDC has commenced with trial models of London Avenue and 17th Street canal levees and floodwalls based on the available site characterization and performance analyses. The conceptual design of the scale models and development of the experimental procedures has been based on established international practice, drawing upon the combined expertise and experience of the centrifuge modeling groups at ERDC, RPI, GeoDelft and Steedman & Associates. The experiment plan has been developed in close collaboration with numerical work being performed as part of the Levee Analysis, to ensure that the models can meet their primary objective of providing qualitative insight and independent validation of the numerical analyses. Bulk samples of peat from the field have been taken for direct use in the models. A kaolin clay and fine sand has been used to replicate the clay and sand layers in the field. In common with standard geotechnical centrifuge model practice, the models are designed to be geometrically similar, reduced scale models with all significant engineering parameters (dimensions, permeability, density, strength and stiffness) correctly reproduced. Custom built chambers have been constructed to contain the models with windows to facilitate video imagery of the onset of failure in the levee and foundations. The first trial models have been completed. The results are encouraging, showing that failure mechanisms consistent with the field observations can be realistically reproduced. Instrumental data from the model tests, particularly of the development of pore water pressure in the soil layers beneath the levee, are being examined and compared with numerical analyses. A full series of model tests will be carried out during March and April, using both centrifuge facilities as appropriate.

Simulation of Field Conditions

The design of the scale models has benefited from the extensive data collection and analysis in the field and from the site investigation and characterization activity under the levee performance analysis task. Collaboration with all members of the levee performance analysis group and subsequent exchange of cross-sections, long sections and soil properties have ensured that for each of the drainage canal sections investigated, the scale model design has proceeded with the best available information.

As the scale models are subject to a steady high acceleration field during a centrifuge ‘flight’, they are constructed within a strongbox that must be designed to resist the full field pressure from the free water (in the canal), ground water and soil acting on the side walls and base. For these experiments, new strongboxes have been designed and built specifically to accommodate the particular geometry and depths of the levees and their foundations. Based on the field observations and the Dutch experience of levee failures, it was considered important to include a substantial length of ground behind levees within the model to ensure that any failure mechanism had the freedom to extend ‘landward’ if it desired. Several boxes have been constructed to facilitate the model making process and provide duplication. The boxes were constructed from aluminum alloy plate, with a stiff, plexiglass window on one side for viewing. A schematic diagram of the model chamber is shown in Figure K3-1 showing the transparent window and water reservoir below the floor of the strongbox. The long walls of the strongbox are restrained from bowing outwards by their fixings along the end and base of the chamber, and by a frame bolted across the top prior to flight (not shown in the figure for clarity).

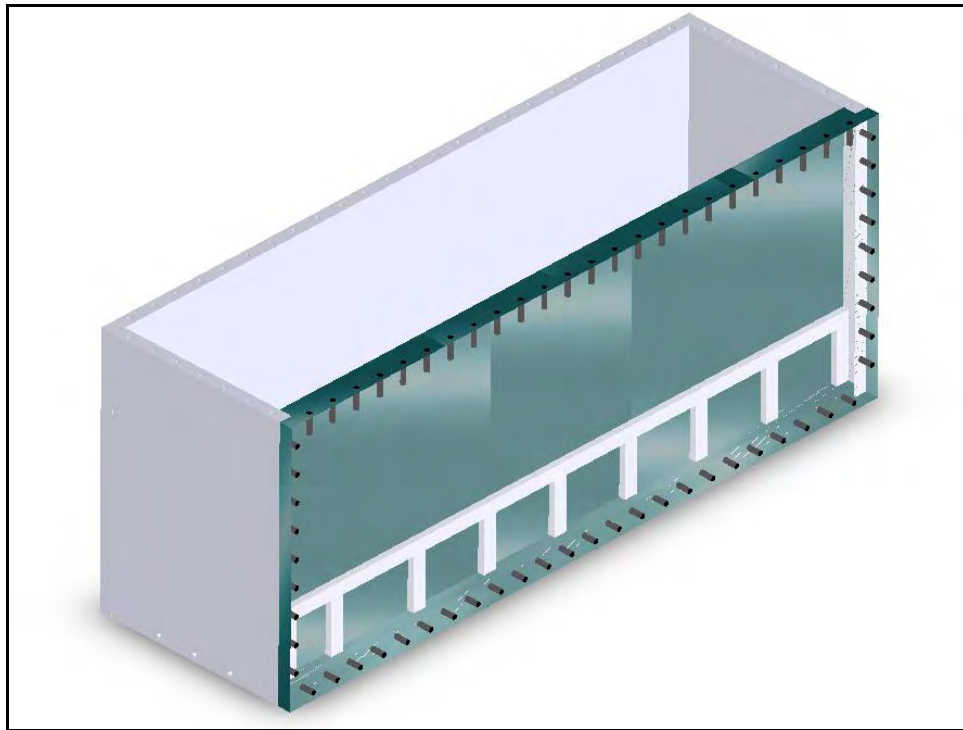


Figure K3-1. Diagram of the model chamber with top bracing omitted

Simulation of field conditions requires that all relevant mechanical properties of the engineered structures and natural ground conditions are accurately reproduced in the model. In the case of the structures, the significant elements are the levee itself and the sheet pile wall with concrete capping beam.

For the sheet pile wall, it is straightforward to scale the bending stiffness of the wall. Expressed simply, any deflection or bending of the wall under pressure from the water or soil should be geometrically the same in the scale model and in

the field. If the sheet pile wall in the field was to bend so that the top deflected one twentieth of its overall height, for example, it would be expected that the scale model wall would also deflect one twentieth of its height. From this requirement, it is easily deduced that for a 1/N scale model subject to a steady acceleration field of N times earth's gravity, the bending stiffness of the wall should be reduced by N^3 per unit length. A steel sheet pile wall such as the PMA-22 section with a moment of inertia of 22.4 in⁴ will then be correctly scaled by a steel plate 0.129" thick at 50g. Alternatively, the steel sheet pile section could be correctly represented at 50g by a solid aluminum alloy plate, with thickness of 0.18". The unit weight of the steel sheet pile wall and its plastic moment capacity are not relevant to the study, as there is no evidence that dynamic movement of the wall or plastic hinges in the wall (none of the sheet piles recovered from any of the levee failures show any sign of local plastic bending) contributed to the observed performance. Similarly, in the early stages of failure, no evidence has yet been put forward that water flow through the clutches of the sheet piles, separation of the clutches or fracture of the concrete capping beam contributed to the failure. It is therefore concluded that the sheet pile wall may be realistically represented by a metal plate (steel or aluminum alloy) with the correct bending stiffness.

Natural soils and constructed fill in the field have an inherent variability which is impossible to reproduce at a microscopic scale whether in analytical, numerical or physical models of performance, for design or for assessment. It is standard practice, therefore, to use site investigation techniques to measure soil properties and then to deduce an equivalent profile of strength and permeability that is appropriate to the situation under consideration. Using the currently available soil data, representative pre-Katrina cross-sections for the drainage canal levees, including undrained soil strength profiles and stratigraphy have been developed. These profiles have been adopted for the physical scale models also and, with the exception of the peat layer, reconstituted laboratory soils are being used for the clay and sand layers. Laboratory soils provide the same characteristics as field soils in terms of strength and compressibility, but may be handled more easily and reliably. The use of reconstituted, remoulded soils as equivalent field soils is well established and common practice.

The levees were constructed over many decades from compacted clay. Analysis has provided values for the strength of the levee to be used in the numerical models, and the same strength was therefore adopted for the physical scale models. For the first trial models, the strength of the clay in the levees was selected to be 500 psf, being the strength used for design. Later models will adopt a strength value of 900 psf, based on the assessment of site investigation data available at February 2006.

The foundations of the levee comprise layers of peat, clay and sand. Each of the three drainage canal breach sites have a different profile and each have been or will be modeled accordingly. The natural clay beneath the peat is normally consolidated throughout its depth, with an average unit weight of 109 pcf and average water content of approximately 65 percent. The properties of the natural clay have been adopted from analysis of design documents and field data, and reconstituted kaolin clay selected to represent the material in the scale model.

Kaolin clay is coarse grained clay used extensively in centrifuge model studies to represent natural clays. The beach sand stratum that underlies the lacustrine clay and/or peat stratum is fine medium dense sand, with typical strength and permeability characteristics. For the purposes of the scale model tests, the important parameters to model are the density and the permeability, which is controlled by the fine fraction in the soil. A fine laboratory sand (Nevada Sand with $D_{10} = 0.08\text{mm}$) has been used to reproduce this stratum. Full details of these materials may be found in Appendix K3-1.

The characteristics of the peat or marsh stratum have been assessed and determined to be comprised of two groups: the peat stratum under the levee embankment, and the peat stratum at the toe of the levee. Undisturbed samples taken from borings have provided laboratory samples from which compression tests, moisture content and unit weights have been determined. Close examination of the peat shows that it is relatively free of fibers and is similar in character to organic clay. In these circumstances, the appropriate course of action is to use the field material, cut from block samples and reconsolidated in the centrifuge to its original condition.

To create conditions in the scale model which are as realistic as possible, careful consideration must be taken in the construction of the model specimen. Two workshops have been held to review the experimental methods and model design, at GeoDelft and at RPI. The workshops addressed equipment, instrumentation, material and procedures for standardizing the model tests.

The generic model configuration is shown below, for London North. The sand layer was placed in the chamber first by raining it slowly from a hopper. The rate of pouring and height are calibrated to ensure that the appropriate density is achieved. Miniature instruments were positioned in the sand layer during the pouring process, as were markers in the sand against the window, to form a grid. The wall is placed into position, held by a temporary brace. Once the sand layer is completed, the chamber is evacuated, flushed with carbon dioxide and then the sand is saturated by slowly introducing de-aired water. The vacuum is released.

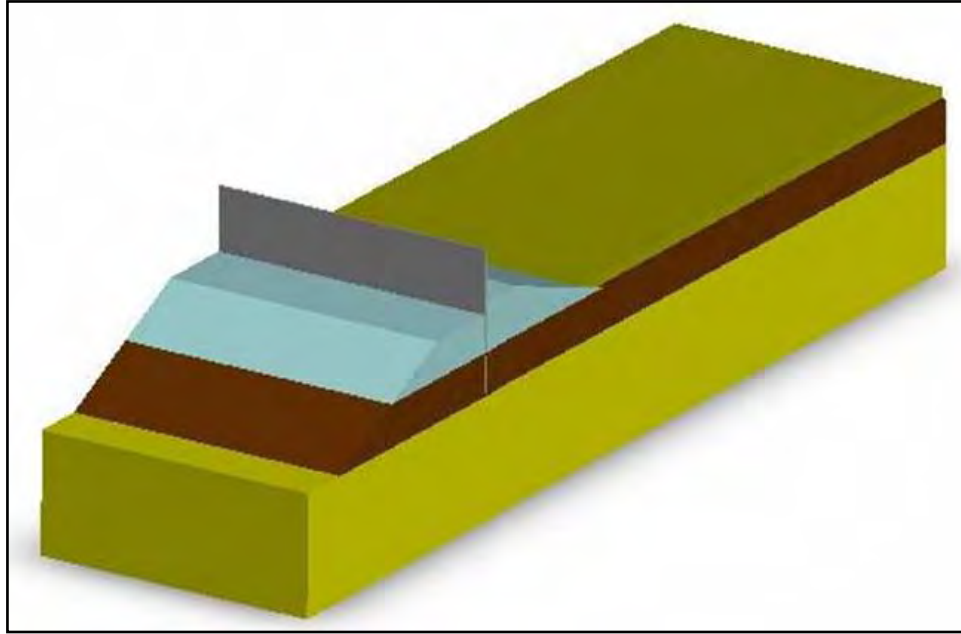


Figure K3-2. Schematic diagram of the model geometry (London Avenue North)

The peat layer, cut from the blocks of natural soil is placed on the sand bed on either side of the wall. A surcharge of gravel equivalent to the weight of the final levee and of similar profile is placed on the peat layer (temporarily protected by a geotextile membrane) and the specimen accelerated on the centrifuge until the weight of the gravel has consolidated the peat layer. This process will create a depression under the gravel mimicking the additional consolidation of the peat by the levee over time and satisfying the observation of varying strength in the peat layer under the levee and under the toe.

The levee is formed by consolidating a block of clay in two pieces, representing the flood side and protected side of the sheet pile wall. The blocks of clay for the levee were formed by consolidating the reconstituted kaolin clay to the required strength upside down in a wooden mould. The moulds have the form of the levee profile. The blocks were then trimmed to their final shape, the gravel (and protective membrane) removed and the two sections of the clay embankment placed in position against the wall. The temporary brace can now be removed and the specimen again accelerated on the centrifuge, water introduced and a steady flow regime established below the levee. Finally, the water level is brought up to the flood level and the performance of the levee observed.

For the physical model of 17th Street canal, the main elements are similar, except that the peat layer overlies a layer of clay, representing the lacustrine clay stratum in the field. To form this layer in the model, the reconstituted kaolin clay is placed at high water content and consolidated using the centrifuge before placing of the peat layer above. The advantage of the centrifuge consolidation process is that this will correctly reproduce the process of normal consolidation as in the field, resulting in a profile of strength of the clay increasing with depth that can be matched to the field profile. The process takes many hours before the clay layer is fully consolidated and is monitored by measuring the decay of the

excess pore water pressure in the clay over time. Determining the strength of the clay after placement in the model is achieved by calculation and laboratory testing based on correlations between density and moisture content versus resultant strength. Reconstituted kaolin clay has been used in centrifuge model tests since the 1960s and there is long experience of the accurate prediction of strength following mixing and consolidation.

The workshops also discussed the optimum acceleration level (expressed in multiples of earth's gravity, g) at which the experiments should be conducted. This 'g' level dictates the linear scale in geotechnical centrifuge scale modeling, such that for example the reduction in depth in the model is precisely compensated by the increase in self weight of the layers above, resulting in identical stresses in the model as in the prototype. The model tests will be carried out at 50g, sufficiently high to provide a model of sufficient size to replicate the field structure with negligible boundary effects from the model container and sufficiently low to provide reasonable detail in the layering and soil profile.

Miniature instrumentation is used both inside and outside the model container to capture information on the performance of the specimen during the model test. For these experiments, the main instrumentation will be pore pressure transducers, displacement transducers and video and still photography of the model and sheet pile wall. Consideration has also been given to the hydraulic arrangements for the control of water supply, and the optimum orientation of the model box on the centrifuge platform to minimize any errors associated with the radial acceleration field in the centrifuge.

The generic description of the model test process above is intended to provide a general overview of the experimental procedure. A more detailed discussion of centrifuge modeling, sources of error and limitations is provided in Appendix K3-1, together with additional information on the materials, equipment and typical data from the initial model tests carried out at RPI to confirm the proposed methodology.

Design of Trial Models for Drainage Canals

Prior to initiation of any physical modeling efforts, two workshops were held to discuss in detail the model design and test procedure based on the team's prior experience of physical modeling of levee structures and experience of model testing with very soft clays. These workshops were held in December 2005 and January 2006 at GeoDelft in the Netherlands and at RPI, NY. Both institutes operate internationally recognized centrifuge research facilities and are important centers of expertise. Both meetings reviewed the current information available on the pre and post-hurricane conditions of the levee systems (17th Street, London Avenue, and Industrial Canal). The design of the models requires consideration of possible failure mechanisms and the workshops therefore discussed a wide range of alternative mechanisms, based on post-failure observations and prior experience in the Netherlands of similar levee designs, including flow of water around the pile generating uplift pressures in the downstream material, and movement of the wall due to the relatively weak clay of the levee. The

workshops then discussed and agreed on the design of the trial models, selection of materials and test procedures, as described in detail below. The trial models were intended to test alternative model arrangements and methods of construction prior to the final models. In January at the second workshop, detailed planning of the test program and experimental methods (model preparation, boundary conditions, instrumentation, data acquisition and reporting) were reviewed and agreed in detail to ensure that a standard approach was adopted at ERDC and RPI during the model testing.

London Avenue Canal levee model

Cross sections of the levees on London Avenue drainage canal (London North failure and London Mirabeau failure) with the currently known soil layering and properties were reviewed. The London Avenue breach sites consist of, in general, a clay levee founded on a foundation of peat and fine sand, as shown in Figure K3-2 above. For the purposes of the trial models, the sheet pile wall was modeled using an aluminum plate, the sand using a Nevada Sand at 60 percent Relative Density, the levee using a reconstituted kaolin clay and the peat layer using the natural peat, cut from block samples from the field. Following the modeling principles discussed above, the design cross section through the 1/50 scale trial model is shown in Figure K3-3 below.

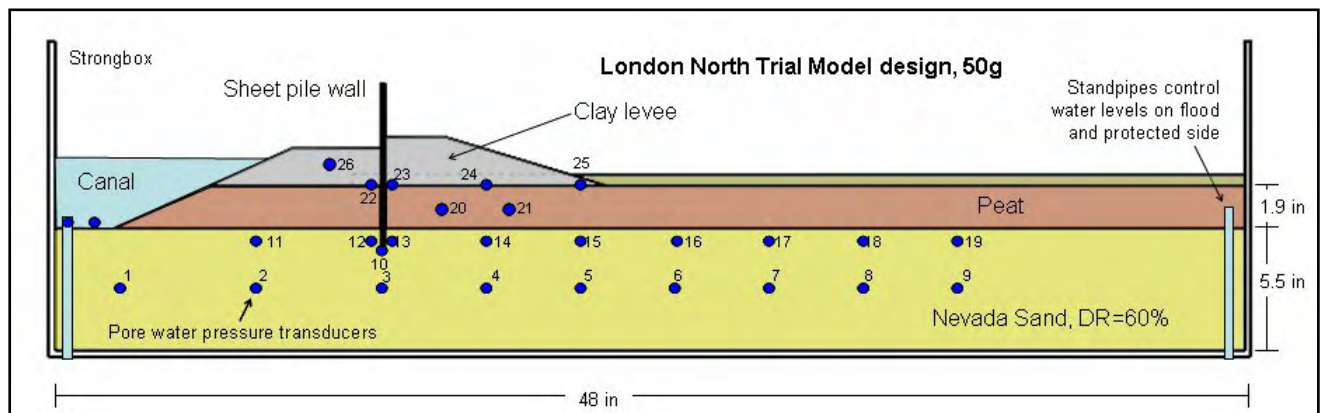


Figure K3-3. Diagram of London North Trial Model Design (model units)

The clay levee in the trial model had strength after consolidation of 500 psf (based on the original design values). For kaolin clay, this is equivalent to a saturated density of around 110 pcf. Future models will use an increased strength of 900 pcf (kaolin saturated density of 113 pcf), based on the latest assessment of all information. The geometry of the clay levee was based on information available from design documents, as-built documents, LIDAR surveys, and field reconnaissance. The peat layer will be formed from the natural peat samples taken from the field. The sheet pile wall will be modeled using a solid steel plate of thickness 0.125", such that the bending stiffness of the wall is a correct representation of the sheet pile wall in the field (based on the PMA-22 section), as discussed above.

Pore pressure transducers are located along the mid depth of the sand stratum and near the top of the sand, below the peat. As the canal fills with water, the

excess pore pressure in these transducers will rise, with the greatest rise occurring closest to the canal. If the wall rotates and a crack opens down the front of the wall, then transducers under the centerline of the levee will also experience a full head of water pressure.

17th Street Canal levee model

As with the London Avenue breaches, the 17th Street breach site was reviewed. The cross section here consists broadly of a clay levee on a foundation of peat and lacustrine clay. Following the procedures discussed above, the selection of materials for the trial model comprised speswhite kaolin clay for the levee and lacustrine clay stratum, and natural peat for the peat layer. The sheet pile wall was modeled using an aluminum plate. A cross section through the trial model is shown in Figure K3-4 below.

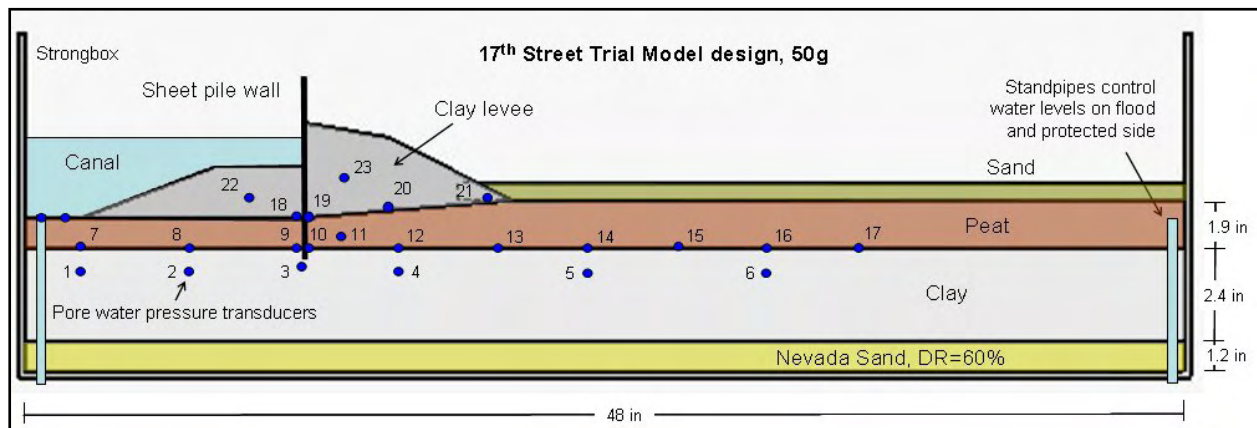


Figure K3-4. Diagram of 17th Street Trial Model Design (model units)

The clay levee in the trial model had strength after consolidation of 500 psf (based on the original design values). For kaolin clay, this is equivalent to a saturated density of around 110 pcf. Future models will use an increased strength of 900 pcf (kaolin saturated density of 113 pcf), based on the latest assessment of all information. The geometry of the clay levee was based on information as described above for the London North section. The peat layer will be formed from the natural peat samples taken from the field. As with the London North Model design, the steel sheet pile wall will be modeled for the 17th Street model using a solid steel plate of thickness 0.125", such that the bending stiffness of the wall is a correct representation of the sheet pile wall in the field (based on the PMA-22 section), as discussed above.

The underlying clay layer has strength after consolidation increasing from 280 psf to 390 psf at the base (an increase of 11 psf per foot depth). Constructed using reconstituted kaolin clay, the saturated density of the clay will again be around 110 pcf.

Pore pressure transducers are located on the interface between the peat and the clay stratum and within the clay layer and the clay levee. Once steady state conditions are established at the start of the model, the precise rate of rise of the

flood in the canal is immaterial as the performance of the foundation and levee will be undrained.

Interim Results

The results from the trial models have been encouraging. The model making process has been tested through the construction of the two trial models, one of which involved a sand bed beneath the peat and one of which involved a clay layer. Techniques for placing the sand and peat and for consolidating the clay have proved satisfactory and resulted in a layered model with densities and strengths close to the target density/strength profile based on the current available information. The approach, developed during the workshops, towards the sequence and method of construction of the levee and sheet pile wall has also proved successful. The hydraulic system to control water levels in the ground and the canal has permitted steady state conditions to be developed prior to the flood stage, and then for the water in the canal to be raised progressively until large scale movements of the levee and flood wall were initiated, as may be seen after the trial model test in Figure K3-5 for London Avenue North. Data from the miniature transducers buried in the soil beneath the levee have provided valuable information on the change in water levels (water pressure) as the canal floods. In the London North example below, Figure K3-6, the trend of increasing water level is seen in the sand layer beneath the levee as the water level in the canal rises. As expected, the rise is proportionately less further away (landward) from the canal. In this trial model the wall was seen to lean over as the water rose and there is an increase in the rate of rise of water level in the sand as this occurs. The rate increases as the wall starts to lean over landward.



Figure K3-5. Rotation of the sheet pile wall in the London Avenue Trial Model

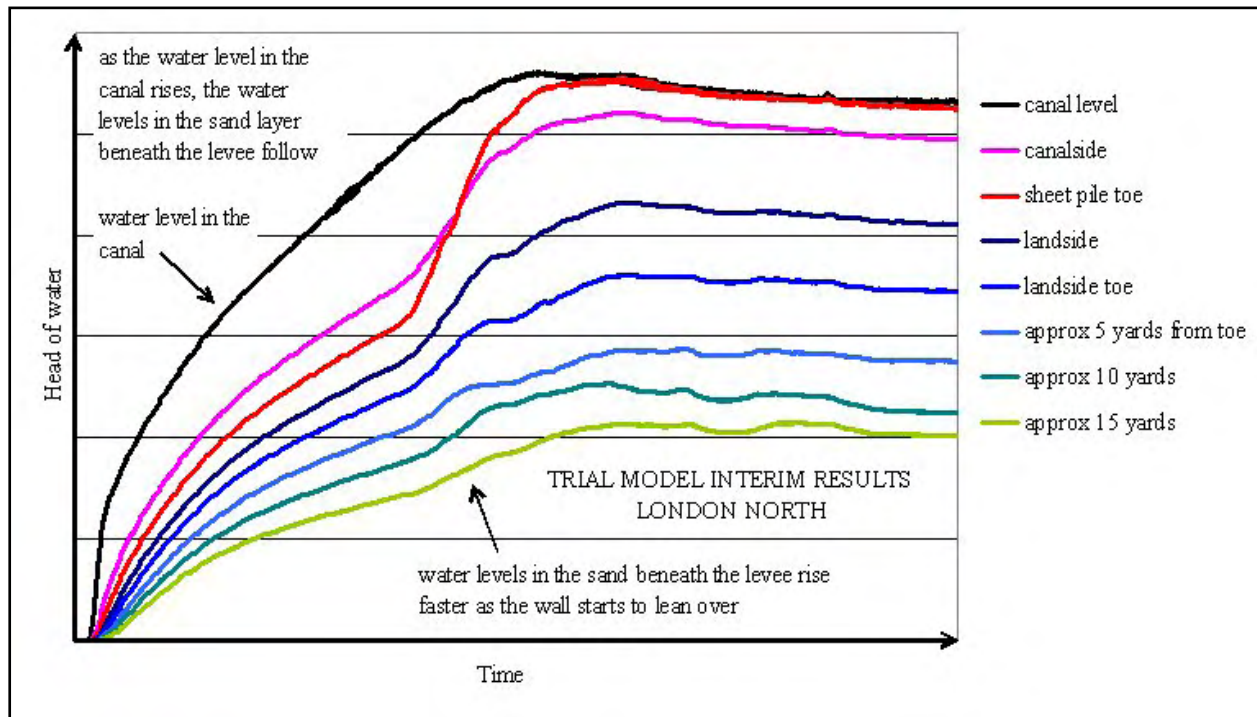


Figure K3-6. Rising water pressures in the sand in the London Avenue Trial Model

The second trial model, of 17th Street, has also provided good results, confirming the model process and design. Figure K3-7 shows the movement of the levee landward after the model test was completed and the water had been drained from the canal side (left).



Figure K3-7. Sliding movement of the levee landward (to the right) observed at the completion of the 17th Street trial model test

In this case, as the water rose in the canal the wall again started to lean over, which resulted in a sliding failure in the clay layer immediately below the peat. Data from both the trial models are being assessed in detail prior to the initiation of the main model test phase, planned to commence at ERDC in March.

Planned Work

The intention of the physical modeling work is to contribute to and support the overall analysis of the levee performance system. Particular strengths of the physical modeling are in exploring failure mechanisms and providing key information and insights to the numerical modeling work. The efforts that have been completed thus far and reported in this 60 percent report have already provided valuable information to the numerical modelers and clearly demonstrated the possibility of modeling realistic failure mechanisms. It should be noted that the geometry of the levee sections and material properties used in the physical modeling were those as understood from available information at the time of the modeling work. Future efforts for the physical modeling work will be as described following.

- Further refinement of the levee geometries, material properties, sheet pile characteristics and other relevant factors will be performed such that the final models will represent as accurately as possible the actual field levees.
- Continued improvements in the testing procedures and data collection procedures will be performed to insure that the quantity and quality of collected data are the highest quality.
- Perform a thorough analysis of the data collected from the London North and 17th Street models. The intention of this analysis will be to understand the failure mechanisms and improve all future models.
- Hold a meeting of the physical modeling team (ERDC, Steedman & Associates, RPI, GeoDelft) to review all data collected thus far and analysis performed to give careful consideration to future models.
- Complete duplicate physical models for each of the failures at London North, London Mirabeau, and 17th Street.
- Provide detailed data of pore pressure and displacement measurements to numerical modeling team for use in that analysis.
- Perform any additional physical models that are deemed necessary by the full team responsible for the levee performance analysis work.

Appendix K3-1

Levee Performance Analysis, Physical Modeling

Background and scaling principles

It is well known that the behavior of most geomechanical materials, such as soil and rock, is very dependent on stress level. In conventional small scale model tests, performed in the earth's gravitational field, it is not always possible to maintain similarity with prototype situations, and to ensure that stress levels in areas of interest reach field values. A geotechnical centrifuge can subject small models to centripetal accelerations that are many times the earth's gravitational acceleration. By selecting a suitable acceleration level the unit weight of the model being tested can be increased by the same proportion by which the model dimensions have been reduced. Thus stresses at geometrically similar points in the model and prototype will be the same. Three assumptions must be satisfied to provide a realistic representation in the model of the field performance. These are firstly, that the model is a correctly scaled version of the prototype, secondly that the $1/N$ scaled model when subjected to an ideal gravity field behaves like the prototype at $1g$; and thirdly that the centrifuge produces this ideal gravitational field. These assumptions are briefly examined below.

To satisfy this first assumption, that the model is an exactly scaled version of the prototype, requires that the scaling relationships between the model and prototype are met. These scaling relationships can be derived from either analysis of the relevant variables, or from consideration of the governing equation which describes the phenomenon being modeled. The establishment of correct scaling relationships is crucial if the prototype response is to be correctly modeled and any given specific problem may have a unique set of scaling relationships that may be derived by either of the two methods outlined above. Some of the more common relationships are given below in Table K3-1.

Table K3-1 Useful Scaling Relationships for Centrifuge Models Subject to a Steady Acceleration Field Equivalent to Ng (N times earth's gravity, g)	
Parameter	Scaling factor
Acceleration	N
Seepage velocity (laminar)	N
Length	$1/N$
Mass	$1/N^3$
Stress	1
Strain	1
Force	$1/N^2$
Time (diffusion events)	$1/N^2$
Time (inertial events)	$1/N$

To illustrate how the scaling relations may be used to advantage in the centrifuge, consider the time scale of $1/N^2$ for diffusion processes. Consolidation occurs very slowly in the field, but as a laminar flow process, will occur N^2 times

faster in a reduced scale centrifuge model. For a model 1/N times the prototype dimensions, and if both model and prototype materials have the same properties, then the excess pore pressure dissipation will occur N^2 times faster in the model than in the corresponding prototype. This permits the re-consolidation of soil samples in the centrifuge to take place in a matter of hours, when in the field or at full scale this process would take years.

The second assumption that the 1/N scale model under an ideal Ng gravity field will perform exactly as in the field at full scale will be satisfied if the material properties of the model and prototype are the same. Consequently, the use of in-situ materials is often preferred, but in many cases is not necessary provided that the mechanical properties of the material can be effectively reproduced in an alternative. Thus it is common practice to use laboratory sand or reconstituted kaolin clay to substitute for block samples from the field, particularly when plastic deformation and remolding of the soil under high stress ratios will dominate the expected outcome.

The third assumption, that the centrifuge can supply an ideal Ng gravity field, cannot be completely satisfied. This condition would require that the acceleration at any point throughout the model would not change in magnitude or direction. However, since the acceleration at a point in the model is directly proportional to the radius of that point from the centre of rotation, there must be a variation in imposed acceleration from the surface to the base of the model. This variation in acceleration level also leads to a non-linear stress gradient through the model. From consideration of the stress gradient, it is found that the error is minimized by designing the model based on a gravity scale equivalent to the steady acceleration field calculated at a depth one third the depth below the model surface. The error in any event is negligible provided that the depth of the model is small relative to the radius of the model surface.

There will also be a variation in the acceleration field along flat horizontal surfaces of the model due to the radial nature of the acceleration field, which generates a small component parallel to the model's surface. The effect of this radial divergence of the acceleration field is easily imagined by considering the concave profile (aligned along a line of constant radius) that will be adopted by any free surface water in the model chamber. Again, by ensuring that the orientation of the model chamber on the platform is such that the long dimension is parallel to the axis of rotation, then any effect caused by the radial divergence of the acceleration field can be easily minimized. The most common issue to be addressed in this respect is the design of standpipes and calculations of the depth of free water at different locations on the model.

Finally, as in any rotating reference frame, there is a potential for the movement of particles to be distorted relative to the reference frame of the model chamber depending on the velocity of the particle and the direction of travel relative to the centrifuge platform. This error is caused by Coriolis accelerations and is particularly significant for fast moving particles, such as ejecta. For slow moving particles the effect is not noticeable.

Centrifuge facilities at ERDC and RPI

The centrifuge facility at ERDC is an Acutronic Model 680-1 balanced beam centrifuge used primarily for modeling geotechnical engineering field problems and also for studying other gravity related engineering phenomena in the fields of environmental, structures, blast, cold regions, hydraulics and coastal engineering. The centrifuge has a large capacity (1200 g-ton) and is capable of carrying a payload (such as a soil model) of 2 tons to 350g or 8 tons to 143g mounted on a swinging platform. The platform radius is 6.5 m and platform area is 1.3 m by 1.3 m. The centrifuge center has been operational since 1996.

The centrifuge facility at RPI is an Acutronic Model 665 balanced beam geotechnical centrifuge. This is a medium sized (150 g-ton) machine which has been in operation at RPI since August 1989. The machine has a radius of 3 m and for these purposes can carry a payload of up to 0.8 tons. The radius of the models is around 2.8m and hence the depth of the model is less than 1/10 of the radius of the centrifuge. A maximum acceleration level of 200g (265 rpm) can be achieved from rest in approximately 10 minutes. Details of the centrifuge specification and testing facility can be found at <http://www.nees.rpi.edu>.

Model chamber

The centrifuge model tests were performed in a rectangular strong box of internal dimensions 48 inches long x 13 inches wide x 14 inches deep. The intent of the long, narrow chamber is to create a plane strain model, which is appropriate to studying a two dimensional 'slice' through the levee running from the canal landward. In contrast with laboratory element tests typical field tests, the centrifuge can reproduce the performance of a very large area (and depth) of ground. At a steady acceleration of 50g, the design of the model chamber reproduces an area in the field some 54 feet wide by 200 feet long, or 10,800 square feet (1/4 acre). The mass of equivalent soil in the field contained within the model exceeds 40 million pounds. One long side of the strong box comprises a 2 inch thick Perspex window (48 inches long x 14 inches high) through which deformations of the plane model can be observed while the model is in flight.

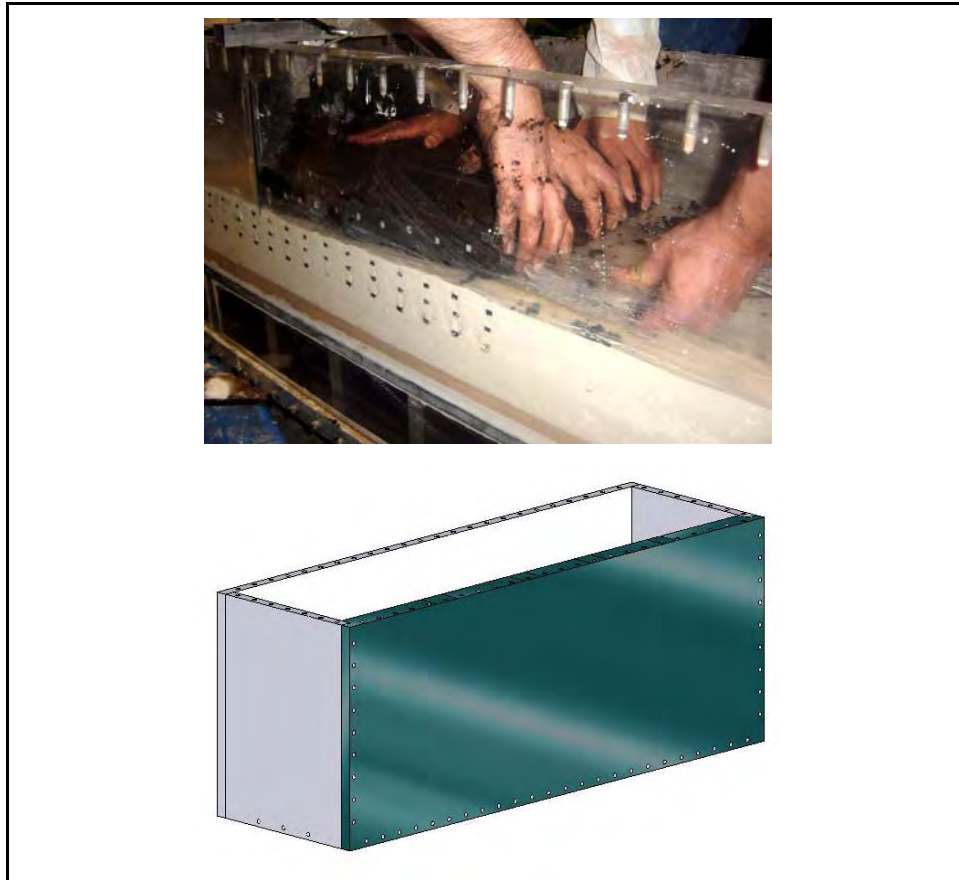


Figure K3-8. View of model chamber with perspex window

Instrumentation

Pore pressure transducers

Pore water pressures will be measured at various locations with the models by miniature pore pressure transducers manufactured by Druck Ltd. These transducers (PDCR81) are 6.35 mm in diameter and 11.3 mm in length. The transducer consists of a thin circular diaphragm machined from a silicon crystal and clamped to a supporting ring. Strain gauge circuits integrated into the back of the silicon diaphragm enable resistivity changes in the crystal to be correlated with applied pressures on the crystal diaphragm. A de-aired porous stone is fitted to protect the diaphragm and to ensure that pore pressures and not total stresses are measured. The wires from the strain gauge circuits are carried via a plastic sleeve out of the model, and this plastic sleeve also acts as an air passage to provide an atmospheric pressure behind the silicon diaphragm. Some versions of this miniature device are sealed and do not require to be vented.

The transducers are calibrated over their full working range and produce a linear response over the range of pressures experienced in the tests. Errors in pore pressure measurement due to temperature effects and flow of water into and

out of the porous stones have been discussed in the literature and can be considered to have no significant effect for the centrifuge model tests reported here.

Displacement transducers

The vertical displacements at various locations of the model will be measured using LVDTs (Linear Variable Differential Transformers). The LVDTs are manufactured by Schaevitz Engineering (Models MHR-500 and MHR-1000).

These LVDTs consist of a stationary coil assembly and a movable core. The coil assembly houses a primary and two secondary windings. The core is a steel rod of high magnetic permeability, smaller in diameter than the internal bore of the coil assembly; this contact free configuration eliminates measurement errors due to friction. When an AC excitation voltage is applied to the primary winding, a voltage is induced in each secondary winding through the magnetic core. The position of the core determines how strongly the excitation signal couples to each secondary winding. When the core is in the center, no signal is created. As the core travels to the left or to the right of center, an output voltage proportional to the displacement is created. The nominal linear ranges of the LVDTs to be used in this study are ± 12.7 mm and ± 25.4 mm.

Non-contact laser transducers will also be used to monitor the movement of the sheet pile walls and potentially to monitor the settlement of the downstream side of the levee. The laser transducers are manufactured by Keyence (Model LB70), and have the advantage (compared to LVDTs) that displacements can be accurately monitored without physical contact being maintained during movement (for example of the sheet pile wall).

Model Materials: Sand and Clay

Sand

The sand being used in this study is a standard laboratory sand known as Nevada sand, purchased from Gordon Sand Company of Compton, California. This sand has been used extensively by researchers to study a wide range of geotechnical problems. The sand is well characterized; as part of a major multi-laboratory investigation in the early 1990s, EARTH Technology Corporation carried out general laboratory tests on the sand which included sieve analyses, specific gravity tests, maximum and minimum density tests, and constant-head permeability tests (Arulmoli et al. 1992). The specific gravity of Nevada sand was determined to be 2.67 and the maximum and minimum dry densities were estimated as 17.33 kN/m^3 and 13.87 kN/m^3 respectively. The corresponding minimum and maximum void ratios were $e_{\min} = 0.511$ and $e_{\max} = 0.887$. Tables K3-2 and K3-3 summarize the results from the EARTH Technology laboratory tests and Figure K3-9 shows a typical grain size distribution for Nevada sand. Constant-head permeability tests were performed using reconstituted samples (Arulmoli et al. 1992). The permeability corresponding to a relative density of $D_r = 40$ percent, was $k = 6.6 \times 10^{-5} \text{ m/sec}$. The hydraulic conductivity versus

relative density is plotted in Figure K3-10, and Table K3-4 summarizes these results.

Table K3-2 General test results for Nevada sand (Arulmoli et al. 1992)	
D ₁₀	0.08 mm
D ₅₀	0.15 mm
Specific gravity, G _s	2.67
Max. void ratio, e _{max}	0.887
Min. void ratio, e _{min}	0.511
Max. dry density	17.33 kN/m ³
Min. dry density	13.87 kN/m ³

Table K3-3 Sieve analysis for Nevada sand (Arulmoli et al. 1992)						
Sieve number	10	20	40	60	100	200
Sieve size (mm)	2	0.84	0.42	0.25	0.15	0.075
Percent passing through sieve	100	100	99.7	97.3	49.1	7.7

Table K3-4 Constant-Head Permeability Tests Results for Nevada sand (Arulmoli et al. 1992)				
Test No.	Dry density (kN/m ³)	Void ratio	Relative density (%)	Permeability (m/sec)
1	16.95	0.55	91	2.3 x 10 ⁻⁵
2	15.08	0.742	40.2	6.6 x 10 ⁻⁵
3	15.76	0.667	60.1	5.6 x 10 ⁻⁵

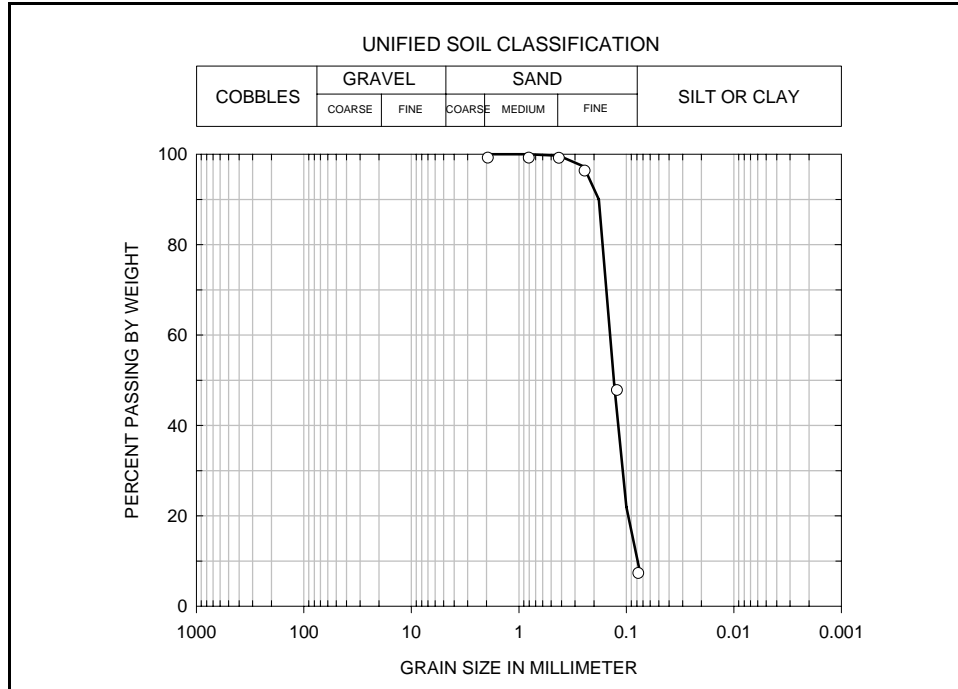


Figure K3-9. Grain size distribution for Nevada sand (after Arulmoli et al. 1992)

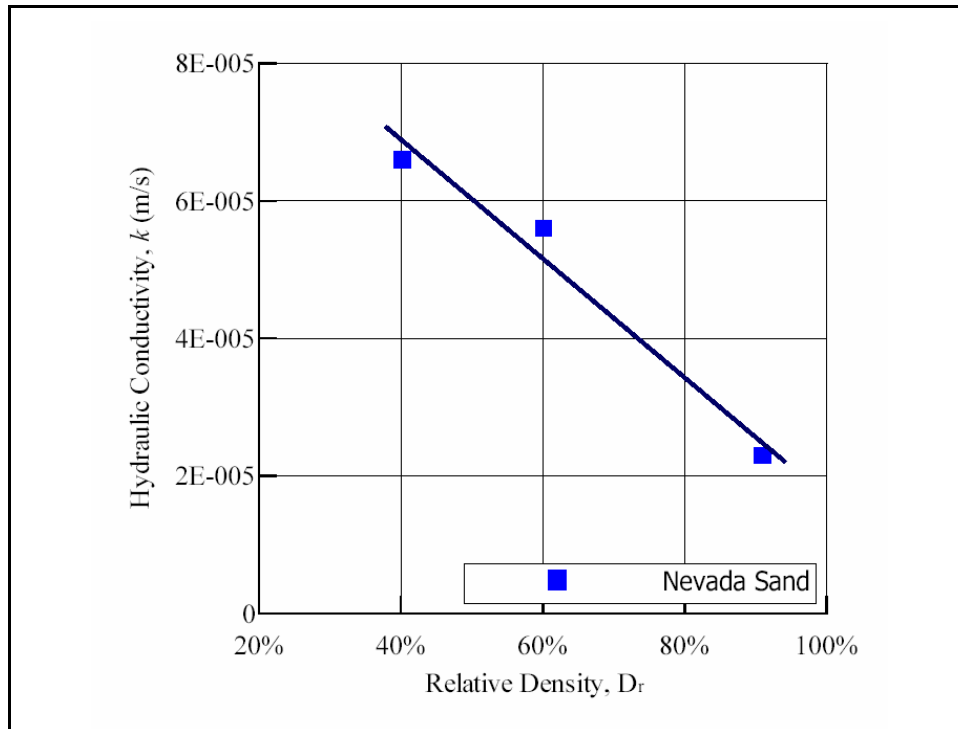


Figure K3-10. Hydraulic conductivity versus relative density for Nevada sand (after Arulmoli et al. 1992)

Dry Nevada sand is pluviated through air into the centrifuge container in a number of sub-layers (typically six). Each sub-layer may also be compacted by dropping an aluminum block to achieve the desired relative density. The dry pluviation and compaction procedure is calibrated in advance of the experiment to ensure that the target Relative Density of the sand can be reliably achieved (typically 60 percent RD). In the trial model, three layers of colored sand were also placed at intermediate depths to reveal mechanisms of piping or large scale movement.

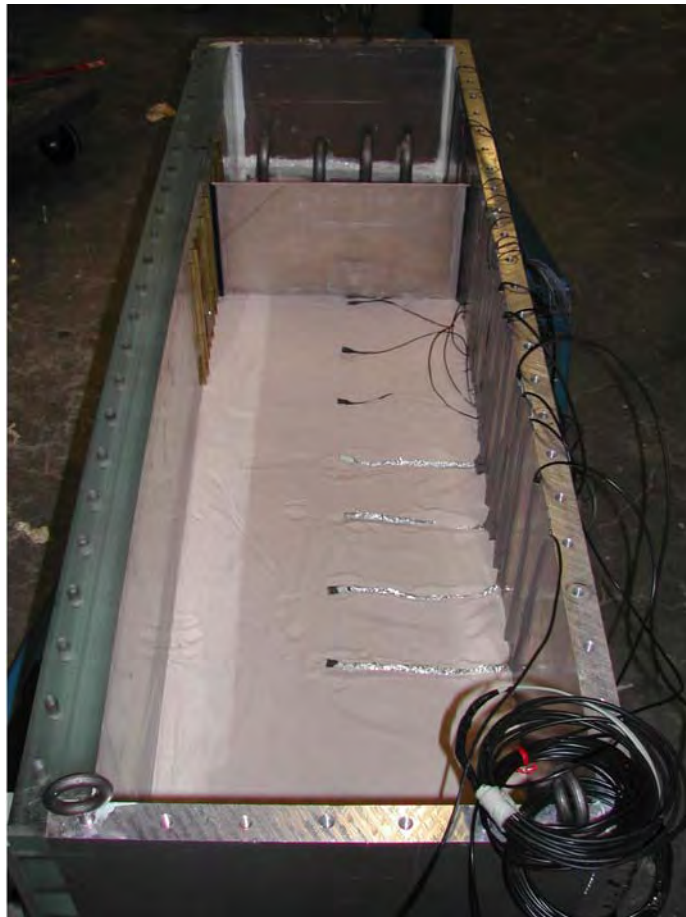


Figure K3-11. Positioning of pore pressure transducers in the sand layer

A number of pore pressure transducers were positioned installed at a height of 7 cm and 12 cm above the base of the Nevada sand. Once the thickness of the Nevada sand layer has reached exactly 14 cm and the whole layer is compacted to the target density, the sand will be saturated. The saturation process requires flushing with carbon dioxide prior to introduction of de-aired, de-ionized water under vacuum onto the surface of the sand until the whole layer is saturated. This saturation process may take as much as 24 hours. These procedures for saturating sand specimens in large centrifuge chambers have been developed over many years and are standard practice. Independent testing by use of p wave measurements in similar specimens has shown that the method achieves complete saturation.

Clay

The material selected to model the soft normally consolidated 'laucustrine' clay stratum was a speswhite kaolin clay (ASP 600) supplied by Engelhard Corporation, New Jersey. The main geotechnical properties of the kaolin are presented below in Table K3-5. Kaolin is a coarse grained clay which has the advantage of further accelerating consolidation of samples. It is widely used in geotechnical laboratory investigations and its properties and performance have been thoroughly researched and are widely documented.

Table K3-5 Geotechnical Properties of Speswhite Kaolin	
Specific gravity g/cm^3	2.58
Liquid limit (percent)	58
Plastic limit (percent)	27
Plasticity index (percent)	31

Preparation of speswhite kaolin to a predetermined profile of consolidation is achieved by exploiting the relationship between Specific Volume, V and mean effective stress, p' for normal consolidation. Figure K3-12 illustrates the typical log-linear relationship found between specific volume and mean stress from which the consolidation characteristics of the clay can be deduced. The slope of the consolidation curve is commonly known as λ in $V - \ln p'$ space. The Specific Volume is defined as the total volume of void and solid assuming a unit volume of solid.

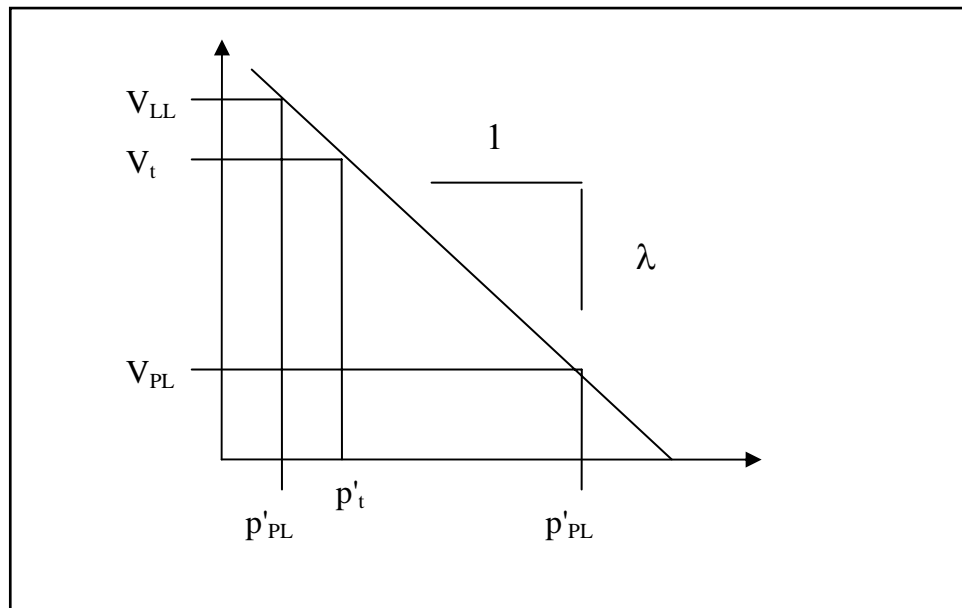


Figure K3-12. Log-linear relationship between Specific Volume and mean effective confining stress, p' for normally consolidated clay

By knowing the Specific Volume at the liquid limit (LL) and at the plastic limit (PL) of the clay, and the relationship between the strength of the normally consolidated clay and the moisture content (related to Specific Volume) between

these two limits (a factor of 100) then an estimate of the overburden load can be made to achieve any desired strength in the clay, following mixing from slurry. By this means, the clay levee can be constructed to a defined normally consolidated strength, which may then be tested by measurement of water content.

Once the target moisture content has been determined, the clay layer is pre-consolidated to its target strength profile from slurry placed in the centrifuge strong box or in the case of the levee block, by placing the slurry in a mold. Dry powdered kaolin clay is mixed with de-aired water to slurry at around 100 percent moisture content. The slurry was then carefully placed by hand into the strongbox to a depth of 13 cm or into the mold. An overburden load (sand) is placed over the slurry by first placing a layer of geotextile fabric on the slurry surface and then pluviating a sand surcharge (of calculated weight) to a depth of 10 cm. The sand was then saturated and the model chamber placed on the centrifuge, to use its own self weight to provide a gradient of effective stress through the specimen. The advantage of this process is the precise control of the gradient of stress in the clay layer, which is similar to the geological process that takes place over millennia as clay layers are laid down in the natural ground. The disadvantage is the time that the process may take, which can last many hours. The centrifuge is slowly accelerated at slew rate of 0.25 g/min to 10g, 20g, 30g, 40g and 50 g, being held at each g-level for approximately 30 minutes while consolidation of the clay is monitored through records of the vertical settlement and excess pore pressure dissipation. The target strength profile for the clay layer in the 17th Street trial model was 280 – 380 psf (13 – 18kPa). Once the consolidation process is completed, the centrifuge is stopped and the rest of the model assembled.

K4 – Concrete I-Wall and Sheet Piling Material Recovery, Sampling and Testing: 17th Street Canal Levee Breach

Introduction

On Monday and Tuesday, 12-13 December 2005, samples of the concrete I-wall and sheet piling were taken at or adjacent to the 17th Street Canal levee breach. The objectives of this exercise were a:) to verify conformance of material properties of the I-wall concrete and reinforcing steel, and the sheet piling with their respective specifications; b:) to verify the as driven length of the of the sheet piling and c:) potentially validate the Parallel Seismic testing that was performed in an attempt to determine, in situ, the sheet piling tip elevation

The 17th Street Canal breach is located on the east side of the canal just south of Hammond Highway. Figure K4-1 shows the breach shortly after Hurricane Katrina. The material samples were obtained from the (relatively) undisturbed I-wall sections at the north and south end of the breach. Concrete and rebar samples were obtained on Monday, 12 December and sheet piling were extracted on Tuesday, 13 December 2005.

The I-wall is comprised of a series of concrete wall panels separated by expansion joints and is founded on sheet piling driven through the levee. A typical cross section is shown in Fig. K4-2.

Material Sample Recovery

The material samples recovered from the site included two four foot square by 12 inch thick wall panel samples, two nominally six inch diameter cylindrical cores, one each from the wall panel samples, six samples of reinforcing steel from the wall panels and 14 sheet piles. All samples were marked and tagged and placed into a controlled and documented chain of custody.



Figure K4-1. 17th Street canal breach

The I-wall panels immediately north and south of the breach were designated H22 and H38, respectively. A four foot by four foot section was sawcut from the top of the north end of the I-wall section H38 and from the top of the south end of I-wall section H22. The contractor first drilled a six inch diameter core from the designated four foot square sample at the north end of wall panel H38.. The core drill and saw are shown mounted to the wall at panel H38 at the south end of the breach in Fig K4-3. Figure K4-4 shows the core being removed from panel H38. It was marked and tagged MH38C1C01 as shown in Fig. K4-5.

Prior to drilling, the cores were considered as potential compressive strength test specimens. However the core contained rebar and was not a valid test specimen. The resulting holes were used to for rigging to support and remove the four foot by four foot wall samples as shown in Figs. K4-6 and K4-7.

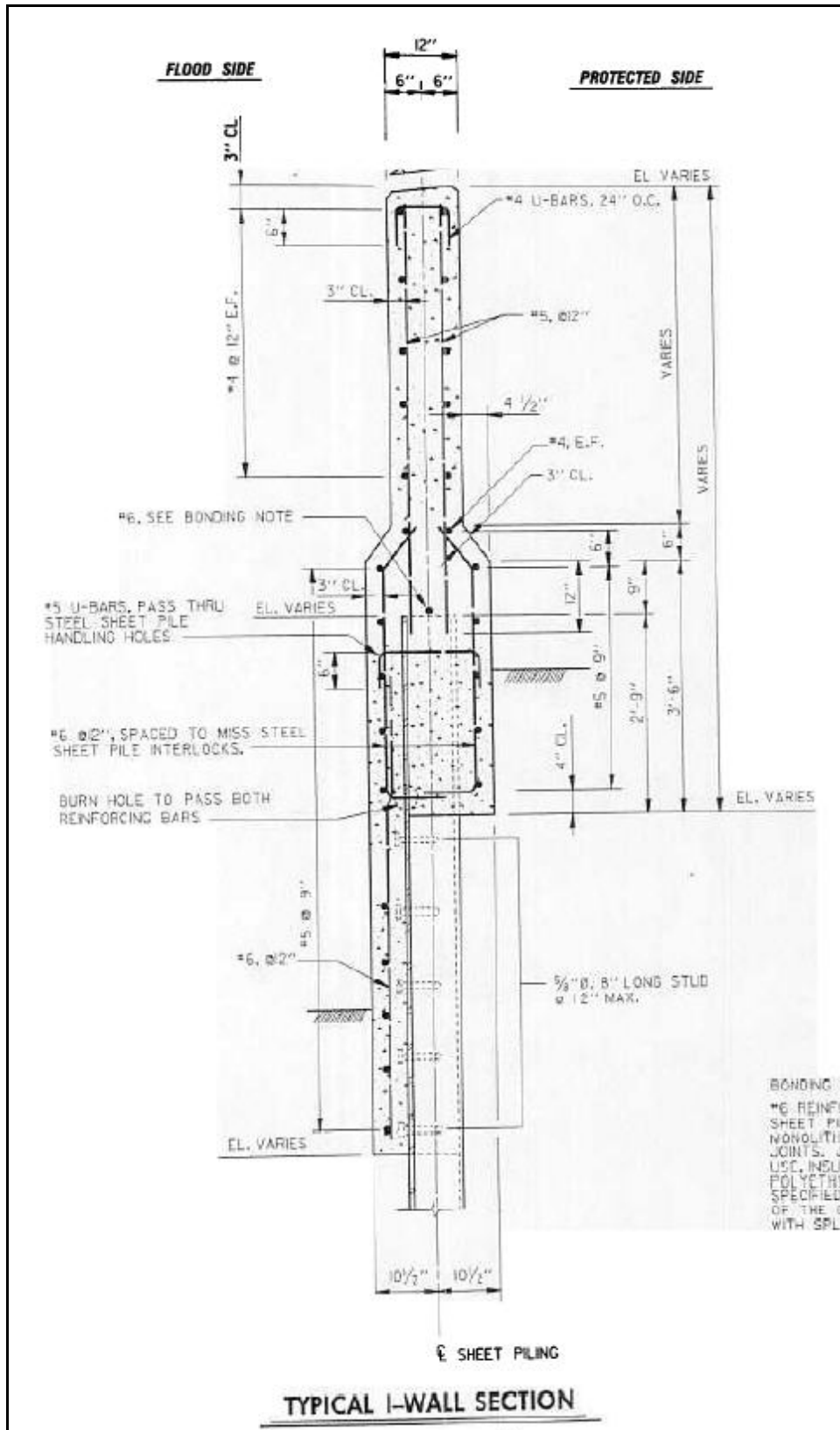


Figure K4-2. Typical I-wall section



Figure K4-3. Core drill and saw mounted to wall panel H38



Figure K4-4. core being removed from panel H38



Figure K4-5. Core from wall panel H38

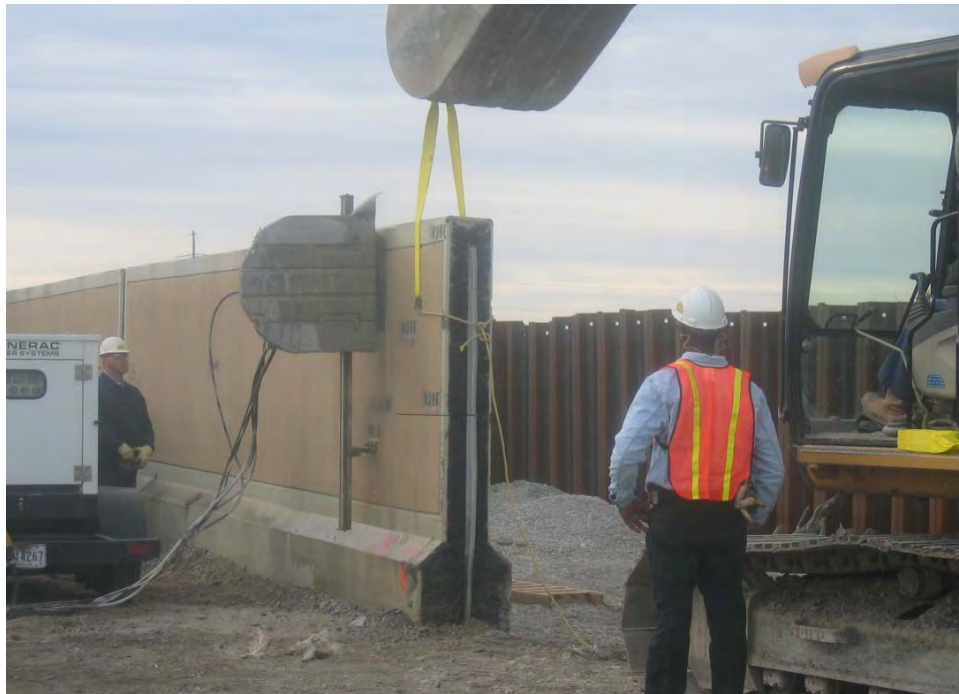


Figure K4-6. Sawing of sample from wall panel H38



Figure K4-7. Removal of sample from wall panel H38

A similar procedure was used to obtain a four foot square sample from the south end of wall panel H22 at the north end of the breach as shown in Figs. K4-8 and K4-9. The concrete core was marked and tagged MH22C1C01 as shown in Fig. K4-10. This core also contained rebar and was not suitable for

testing. The wall panel sample was marked and tagged MH22C1 as shown in Fig. K4-11.



Figure K4-8. Core drill and saw mounted at panel H22



Figure K4-9. Sample being removed from wall panel H22



Figure K4-10. Cylindrical core from wall panel H22



Figure K4-11. Wall sample MH22C1

Rebar samples were then removed from the remaining sections of wall panels H38 and H22. A hoe ram was used for controlled demolition of wall panels in order to expose the rebar samples as shown in Fig. K4-12. Some of the demolition of the concrete around the rebar samples was done with a small hand

held jack hammer as shown in Fig. K4-13. A portable electric bandsaw was used to cut the rebar samples as shown in Fig K4-14.



Figure K4-12. Demolition of concrete for rebar sampling at panel H22



Figure K4-13. Demolition of concrete around rebar sample at panel H38



Figure K4-14. A portable electric bandsaw is used to cut rebar samples

At wall panel H38 a two foot long sample of the following rebar were obtained: 1) A #4 horizontal bar from the east face of the wall approximately 29 inches down from the top of the wall. The north end of the sample terminated at the vertical sawcut for the wall sample MH38C1. 2) A #5 vertical approximately 76 inches from the north end of panel H38. 3) A #6 vertical from the west face of the lower section of the wall. This #6 bar was approximately 8 inches from the north end of panel H38. (This sample has the orange paint shown in Fig. K4-15.) These rebar samples were marked and tagged MH38R1, MH38R2 and MH38R3, respectively.



Figure K4-15. Number 6 rebar sample being taken from panel H38

At wall panel H22 a two foot long sample of the following rebar were obtained: 1) A #4 horizontal bar from the west face of the wall, approximately six inches down from the top of the wall 2) A #5 vertical bar from the west face of the wall approximately 74 inches from the south end of the wall pane. 3) A #6 vertical from the west face of the lower end of the wall approximately 16 inches from the south end of the wall panel. These samples were marked and tagged MH22R1, MH22R2 and MH22R3, respectively.

Figure K4-16 shows the wall panel samples, cores, and rebar samples collected on Monday, 12 December 2005. Note that the cores were placed in sealed plastic bags and each core and the 3 rebar samples from each of the two wall panels were placed in individual latching boxes. These samples were transported to a secure area at a warehouse at the Corps of Engineers' New Orleans District Office.



Figure K4-16. Wall panel samples, cores and rebar samples

After the cores, wall panel and rebar samples were obtained the contractor began demolition of the wall panels to expose the top of the sheet piles for extraction. A scissor concrete crusher was used to demolish the upper portion of the wall panels as shown in Fig. K4-17. A hoe ram was then used to remove the lower portion of the of the wall panel around the sheet piling (Reference the wall cross section in Fig. K4-2.) as shown in Fig. K4-18. The same procedure was used for both wall panels H38 and H22.



Figure K4-17. Demolition of top portion of wall panel H38



Figure K4-18. Hoe ram demolishing lower portion of wall panel H38

On Tuesday, 13 December 2005, sheet piles were extracted. The location of the sheet piles extracted at or adjacent to wall panel H38 is schematically shown in Fig. K4-19. Starting from the north end of panel H38, the piles are designated MH38SP1, MH38SP2, ..., MH38SP16 (the last number of the designation is incremented going from north to south).

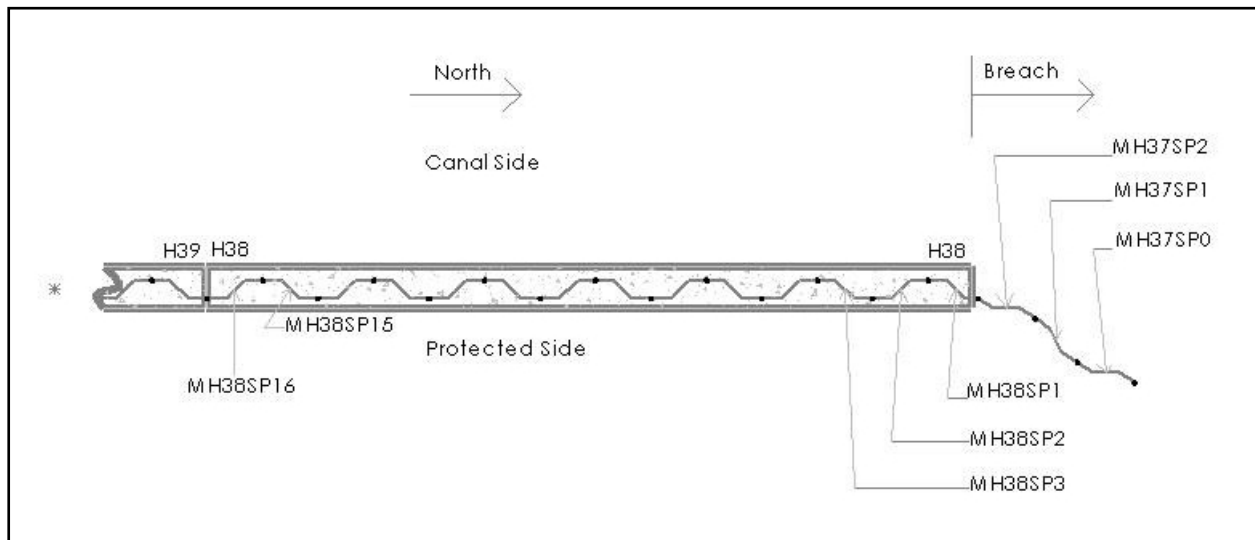


Figure K4-19. Sheet pile designations at wall panel H38

Sheet piles MH38SP2, MH38SP3 were extracted as a pair. Their lengths were approximately 23'-7" and 23'-8", respectively. MH38SP1 and MH37SP2 were then extracted as a pair. Their lengths were approximately 23'-3". The contractor then moved to the south end of wall panel H38 and extracted MH38SP15 and MH38SP16. Their lengths were approximately 23'-5". MH38SP15 and MH38SP16 were at a location corresponding to a soil boring hole where Parallel Seismic tests were conducted in an attempt to determine the length of the sheet pile in situ. The contractor then attempted to extract sheet pile MH37SP1 as a single pile, but MH37SP0 came with it. Their lengths were approximately 23'-6". Extraction of sheet piles at the south end of the breach is shown in Figs. K4-20 and K4-21. The out-of-plumb orientation (from displacement of the piling in the breach) of piles MH37SP1 and MH37SP0 is clearly evident in Fig. K4-21. Figure K4-22 shows measuring and tagging of sheet piling.



Figure K4-20. Extraction of sheet piles MH38SP2 and MH38SP3



Figure K4-21. Extraction of sheet piles MH37SP1 and MH37SP0

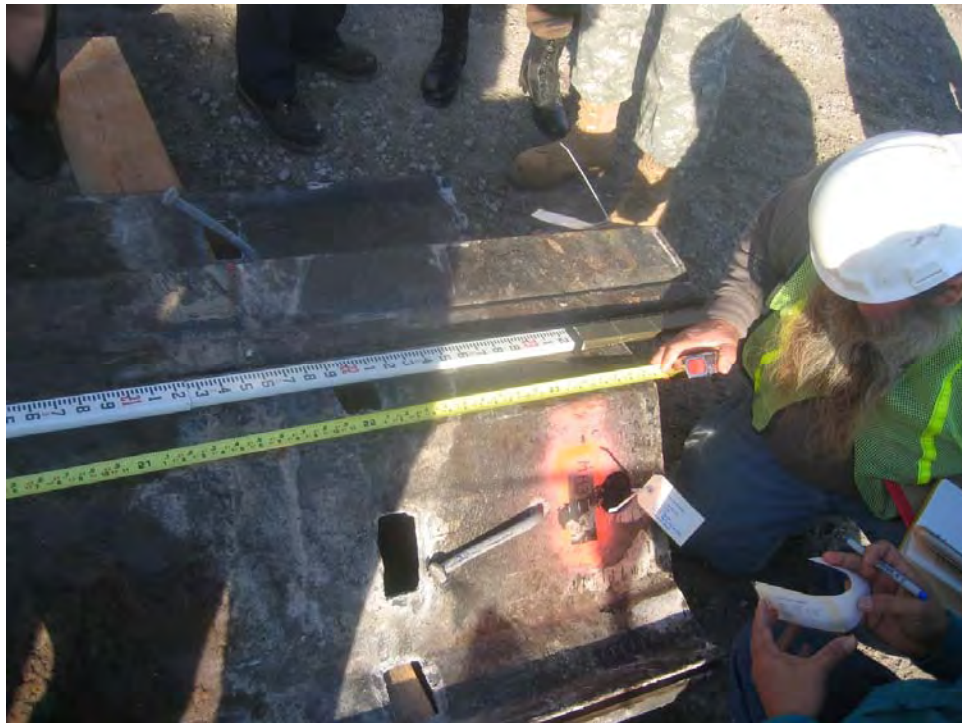


Figure K4-22. Measuring and tagging of sheet piles

Sheet piles were then extracted at the location of wall panel H22, immediately north of the breach. Four sheet piles at the south end of wall panel H22 were designated MH22SP1, MH22SP2, MH22SP3 and MH22SP4. (The last number of the designation was incremented going from south to north.) Sheet piles MH22SP1 and MH22SP2 were extracted as a pair as shown in Fig. K4-23. These piles had a length of approximately 23'-7" and 23'-6", respectively. Sheet piles MH22SP3 and MH22SP4 were extracted as a pair and had a length of approximately 23'-7" and 23'-6", respectively. The contractor then pulled a pair of piles from just north of the north end of wall panel H22 at a location coincident with a boring hole where Parallel Seismic testing had been performed. These piles were designated MH21SP1 and MH21SP2. Both of these sheet piling had a length of approximately 23'-6".



Figure K4-23. Extraction of sheet piling MH22SP1 and MH22SP2

Figures K4-24 and K4-25 show the sheet piling extracted from the south and north ends of the breach, respectively. The sheet piles were loaded on a truck and transported to a secure location within a warehouse at the Corps of Engineers' New Orleans District Office.



Figure K4-24. Sheet piling extracted from south end of breach



Figure K4-25. Sheet piling extracted from north end of breach

Sheet Piling Length and Tip Elevation

The sheet piling extracted from the 17th Street Canal breach site ranged in length from 23'-3" to 23'-8". The top of the pilings were at approximately elevation 6.25 ft. (The pilings adjacent to the expansion joints between wall panels were driven slightly lower as can be seen in Fig. K4-26. This was done to improve the performance and effectiveness of the expansion joint.) A 23'-3"

piling length provides for a tip elevation of -17.0 ft. Obviously, piling driven with a lower top elevation have a correspondingly lower tip elevation.



Figure K4-26. Lower top elevation of sheet piling at expansion joint

Material Testing

On Friday, 16 December 2005, three each, nominally six inch diameter, concrete cores were drilled from the wall panel samples MH22C1 and MH38C1.

These cores were marked and tagged MH22C1-01, MH22C1-02, MH22C1-03, MH38C1-01, MH38C1-02, and MH38C1-03. A sample of steel was also flame cut from each of four sheet piling. The six cores, four steel samples and the previously obtained six samples of rebar were transferred to Beta Testing & Inspection, LLC of Gretna, LA (BTI) for testing.

The concrete cores were obtained and tested for compressive strength by BTI in accordance with ASTM C 42 and C 39. As can be seen in Table K4-1, all of the cores had a compressive strength in excess of the specified 3000 psi compressive strength. More comprehensive details of the testing are in BTI's report in Appendix A.

Table K4-1 Concrete Compressive Strength		
Core	Specified Compressive Strength (psi)	Compressive Strength As Tested (psi)
MH22C1-01	3000	4000
MH22C1-02	3000	3190
MH22C1-03	3000	3940
MH38C1-01	3000	3960
MH38C1-02	3000	4360
MH38C1-03	3000	4100

Tensile tests of the sheet piling material samples were performed, in accordance of ASTM A 370, by a subcontractor to BTI. A summary of the test results and the tensile requirements of the material specification, ASTM A 328 are provided in Table K4-2. More comprehensive details of the testing are in BTI's report in Appendix A.

Table K4-2 Sheet Piling Tensile Requirements and Tests Results			
Sample	Yield Strength (ksi)	Tensile Strength (ksi)	Elongation in 2 in. (%)
MH21SP1-01	58.5	80.9	33.0
MH22SP2-01	55.4	80.1	29.9
MH 37SP1-01	55.5	82.1	32.1
MH38SP16-01	57.0	80.0	32.7
ASTM A 328 Tensile Requirements	39	70	20

Tensile tests of the rebar samples, in accordance of ASTM A 370, were also performed. A summary of the test results and tensile requirements for the specified ASTM A 615 Grade 60 reinforcement is provided in Table K4-3. More comprehensive details are included in BTI's report in Appendix A.

Table K4-3 Reinforcing Steel Tensile Requirements and Test Results				
Sample	Bar Size Designation No.	Yield Strength (ksi)	Tensile Strength (ksi)	Elongation in 8 in. (%)
MH22R1	4	65.0	107.5	11.7
MH22R2	5	62.9	104.5	13.2
MH22R3	6	65.9	108.1	9.3
MH38R1	4	91.0	107.5	16.2
MH38R2	5	61.3	99.7	9.8
MH38R3	6	79.5	97.7	11.4
ASTM A 615 Grade 60 Tensile Requirements	3, 4, 5 or 6	60	90	9

Appendix A: Test Report from Beta Testing & Inspection, LLC



Beta Testing & Inspection, LLC
Forensic Engineering Division

February 14, 2006

Paul F. Mlakar, Ph.D., P.E.

US Army Corps of Engineers
Engineer Research and Development Center
3909 Halls Ferry Road
Vicksburg, MS 39180

**RE: Testing of 17th Street Canal Floodwall Materials
Final Report
BTI Report No.: 1047-ES121605**

Dear Mr. Mlaker:

On December 16, 2005, specimens were sampled at the US Army Corps of Engineers New Orleans District warehouse and transported to Beta Testing & Inspection, LLC (BTI) laboratory for testing. All specimens were labeled, tagged, and secured prior to transporting. BTI cut a total of six concrete cores from two wall sections. Three cores were cut from each section. Mark Cheek, P.E. of BTI witnessed the removal of 12"x 6" sections from four different sheet piles and assumed responsible possession of six reinforcing bars; two No.4, two No.5, and two No.6. Representatives of BTI were informed by the Corps of Engineers that the material samples provided to BTI or obtained by BTI were portions of existing components taken from the 17th Street Canal Floodwall Project. Also, Mr. Bob Brooks of the USACE provided BTI with material data sheets and project specifications for the sampled materials. BTI has completed testing of concrete cores, steel sheet pile sections, and steel reinforcing bars.

Concrete Cores

Three cores were cut from the west face of sample panel MH22C1 and three from the east face of sample panel MH38C1. The cores were obtained in accordance with procedures defined by ASTM C-42. Prior to compression testing each core was prepared in accordance with ASTM C-42, C-617, and C-39. Each core was then tested in compression to failure and the results recorded in accordance with ASTM C-39. See Tables C.1 and C.2 for results of the concrete core testing.

P.O. Box 2203 • Gretna, LA 70054 • (504) 227-2273 • fax (504) 227-2274
13801 Old Gentilly Road Suite #17 New Orleans, Louisiana 70129

Table C.1

Sample panel MH38C1						
Core ID	Capped Length (in.)	Diameter (in)	Area (in ²)	l/d	Correction factor	Maximum load (lbs.)
MH38C1-01	11.9	5.67	25.25	2.09	1	100,000
	Compressive strength (psi)	Fracture type	Age (days)	Load application	Test date/time	Sample date/time
	3960	C	NA	vertical	12/21/05 10:00am	12/16/05 11:00am
Core ID	Capped Length (in.)	Diameter (in)	Area (in ²)	l/d	Correction factor	Maximum load (lbs.)
MH38C1-02	9.19	5.65	25.12	1.62	0.97	113,000
	Compressive strength (psi)	Fracture type	Age (days)	Load application	Test date/time	Sample date/time
	4360	A	NA	vertical	12/21/05 10:00am	12/16/05 11:00am
Core ID	Capped Length (in.)	Diameter (in)	Area (in ²)	l/d	Correction factor	Maximum load (lbs.)
MH38C1-03	11.8	5.66	25.15	2.08	1	103,000
	Compressive strength (psi)	Fracture type	Age (days)	Load application	Test date/time	Sample date/time
	4100	D	NA	vertical	12/21/05 10:00am	12/16/05 11:00am

Table C.2

Sample panel MH22C1						
Core ID	Capped Length (in.)	Diameter (in)	Area (in ²)	l/d	Correction factor	Maximum load (lbs.)
MH22C1-01	11.9	5.66	25.12	2.10	1	100,500
	Compressive strength (psi)	Fracture type	Age (days)	Load application	Test date/time	Sample date/time
	4000	D	NA	vertical	12/21/05 10:00am	12/16/05 11:00am
Core ID	Capped Length (in.)	Diameter (in)	Area (in ²)	l/d	Correction factor	Maximum load (lbs.)
MH22C1-02	11.8	5.66	25.22	2.08	1	80,500
	Compressive strength (psi)	Fracture type	Age (days)	Load application	Test date/time	Sample date/time
	3190	B	NA	vertical	12/21/05 10:00am	12/16/05 11:00am
Core ID	Capped Length (in.)	Diameter (in)	Area (in ²)	l/d	Correction factor	Maximum load (lbs.)
MH22C1-03	11.9	5.67	25.25	2.09	1	99,500
	Compressive strength (psi)	Fracture type	Age (days)	Load application	Test date/time	Sample date/time
	3940	A	NA	vertical	12/21/05 10:00am	12/16/05 11:00am

The average compressive strength of cores from panel MH38C1 is 4140psi and 3710psi for panel MH22C1. Section C3D-7.2.1 of the provided project specifications requires a minimum compressive strength of 3000psi @ 28 days. The average compressive strength of each set of cores exceeded the project minimum requirements.

Steel Sheet Piling

A welder provided by the Corps of Engineers cut one 12"x 6" specimen from each of the four-sheet pile using an acetylene cutting torch. Mandina's Inspection a subcontractor of BTI then prepared and tested each specimen in tension to failure in accordance with ASTM A-370. The provided material data sheets reference ASTM A328 in which a minimum tensile strength of 70,000psi is required. The average tensile strength of the sheet pile samples was 80,755psi, which exceeds the minimum project requirements. See enclosure SHEET PILE TENSILES for tests results.

Testing of 17th Street Canal
Floodwall Materials

February 14, 2006

Steel Reinforcing Bars

Six pieces of steel reinforcing bars each measuring 2' in length were secured and transported to BTI's laboratory. The steel reinforcing bar samples ranged in size from No. 4 to No. 6 bars. Mandina's Inspection a subcontractor of BTI tested the rebar specimens to failure in accordance with ASTM A-615 & A370. Section C3B-6.1.1 of the project specifications references ASTM A-615. ASTM A-615 requires a minimum tensile strength of 90,000psi for Grade 60 steel. The specimens tested tensile strength exceeds the minimum project requirements. See enclosure STEEL REINFORCING BAR TENSILES for test results.

Upon completion and acceptance of the testing program, all of the materials, tested and untested, will be sealed and returned to the New Orleans District Office of the US Army Corps of Engineers. Enclosed are copies of our laboratory accreditations and equipment calibration reports associated with the test performed. Should you have any questions regarding this letter or require additional information, please do not hesitate to contact us.

Sincerely,

Beta Testing & Inspection, LLC



Mark A. Check, P.E.
Vice-President

Enclosures

SHEET PILE TENSILES

MECHANICAL TESTING LABORATORY DIVISION

MTL JOB NO. _____

TENSILE NO. _____

SPECIMEN ID	WIDTH INCHES	THICKNESS SQ. IN.	AREA SQ. IN.	YIELD STR. POUNDS	YIELD STR. PSI	TENSILE STR. POUNDS	TENSILE STR. PSI	ELONGATION IN 2" GAGE PERCENT
MH 215 P1-01	.493	.363	.188	11000	53510	15200	80951	2.661 33.0 %

TENSILE NO. _____

SPECIMEN ID	WIDTH INCHES	THICKNESS SQ. IN.	AREA SQ. IN.	YIELD STR. POUNDS	YIELD STR. PSI	TENSILE STR. POUNDS	TENSILE STR. PSI	ELONGATION IN 2" GAGE PERCENT
MH 225 P2-01	.500	.373	.186	10300	55370	14900	80107	2.598 29.9 %

TENSILE NO. _____

SPECIMEN ID	WIDTH INCHES	THICKNESS SQ. IN.	AREA SQ. IN.	YIELD STR. POUNDS	YIELD STR. PSI	TENSILE STR. POUNDS	TENSILE STR. PSI	ELONGATION IN 2" GAGE PERCENT
MH 375 P1-01	.497	.371	.184	10200	55434	15100	82065	2.642 32.1 %

TENSILE NO. _____

SPECIMEN ID	WIDTH INCHES	THICKNESS SQ. IN.	AREA SQ. IN.	YIELD STR. POUNDS	YIELD STR. PSI	TENSILE STR. POUNDS	TENSILE STR. PSI	ELONGATION IN 2" GAGE PERCENT
MH 385 P16-01	.493	.406	.200	11400	57000	16000	80000	2.655 32.7 %

G:\WORDDATA\SI FORMS\TTFY.LAB

STEEL REINFORCING BAR TENSILES MH-22

MH22

MECHANICAL TESTING LABORATORY DIVISION

MTL JOB NO. _____

TENSILE NO. _____

8" Gage

SPECIMEN ID	DIA. INCHES	AREA SQ. IN.	YIELD LOAD POUNDS	YIELD STR. PSI	ULTIMATE LOAD POUNDS	TENSILE STR. PSI	ELONGATION IN 8" GAGE PERCENT	REDUCTION IN AREA PERCENT
R1	.500	.20	13,000	65,000	21500	107,500	8.935 11.68	.358 .100 50%

TENSILE NO. _____

SPECIMEN ID	DIA. INCHES	AREA SQ. IN.	YIELD LOAD POUNDS	YIELD STR. PSI	ULTIMATE LOAD POUNDS	TENSILE STR. PSI	ELONGATION IN 8" GAGE PERCENT	REDUCTION IN AREA PERCENT
R2	.624	.31	19,500	62,903	32400	164516	9.052 13.5%	.481 .181 41.6%

TENSILE NO. _____

SPECIMEN ID	DIA. INCHES	AREA SQ. IN.	YIELD LOAD POUNDS	YIELD STR. PSI	ULTIMATE LOAD POUNDS	TENSILE STR. PSI	ELONGATION IN 8" GAGE PERCENT	REDUCTION IN AREA PERCENT
R3	.750	.44	29,000	65,909	45800	104,090	8.746 9.25%	.626 .307 30.2%

TENSILE NO. _____

SPECIMEN ID	DIA. INCHES	AREA SQ. IN.	YIELD LOAD POUNDS	YIELD STR. PSI	ULTIMATE LOAD POUNDS	TENSILE STR. PSI	ELONGATION IN 8" GAGE PERCENT	REDUCTION IN AREA PERCENT

G:\WORDDATA\MSIFORMS\TT505.LAB

p-2

88916961888

David Mandina

Steel Reinforcing Bar Tensiles MH-38

MH 38

MECHANICAL TESTING LABORATORY DIVISION

MTL JOB NO. _____

TENSILE NO. _____

8" Gage

SPECIMEN ID	DIA. INCHES	AREA SQ. IN.	YIELD LOAD POUNDS	YIELD STR. PSI	ULTIMATE LOAD POUNDS	TENSILE STR. PSI	ELONGATION IN 8" GAGE PERCENT	REDUCTION IN AREA PERCENT
R-1	.500	.20	18,200	91,000	21,500	107,500	9.292 16.15%	.377 .111 44.5%

TENSILE NO. _____

SPECIMEN ID	DIA. INCHES	AREA SQ. IN.	YIELD LOAD POUNDS	YIELD STR. PSI	ULTIMATE LOAD POUNDS	TENSILE STR. PSI	ELONGATION IN 8" GAGE PERCENT	REDUCTION IN AREA PERCENT
R-2	.624	.31	19,000	61,240	30,200	99,677	9.785 9.81%	.443 .154 50.3%

TENSILE NO. _____

SPECIMEN ID	DIA. INCHES	AREA SQ. IN.	YIELD LOAD POUNDS	YIELD STR. PSI	ULTIMATE LOAD POUNDS	TENSILE STR. PSI	ELONGATION IN 8" GAGE PERCENT	REDUCTION IN AREA PERCENT
R-3	.750	.44	35,000	79,545	43,000	97,725	8.912 11.4%	.539 .228 48.18%

TENSILE NO. _____

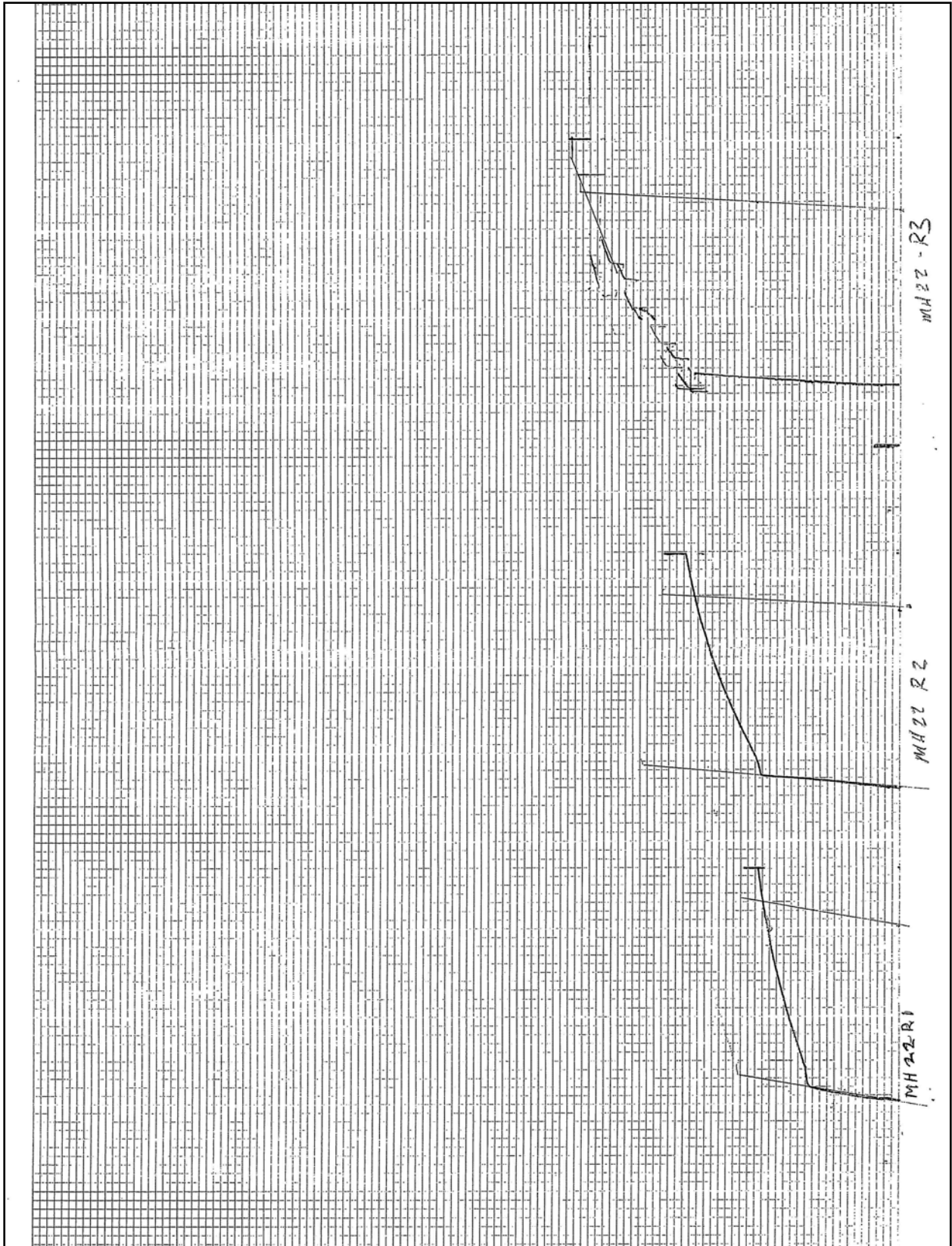
SPECIMEN ID	DIA. INCHES	AREA SQ. IN.	YIELD LOAD POUNDS	YIELD STR. PSI	ULTIMATE LOAD POUNDS	TENSILE STR. PSI	ELONGATION IN 8" GAGE PERCENT	REDUCTION IN AREA PERCENT

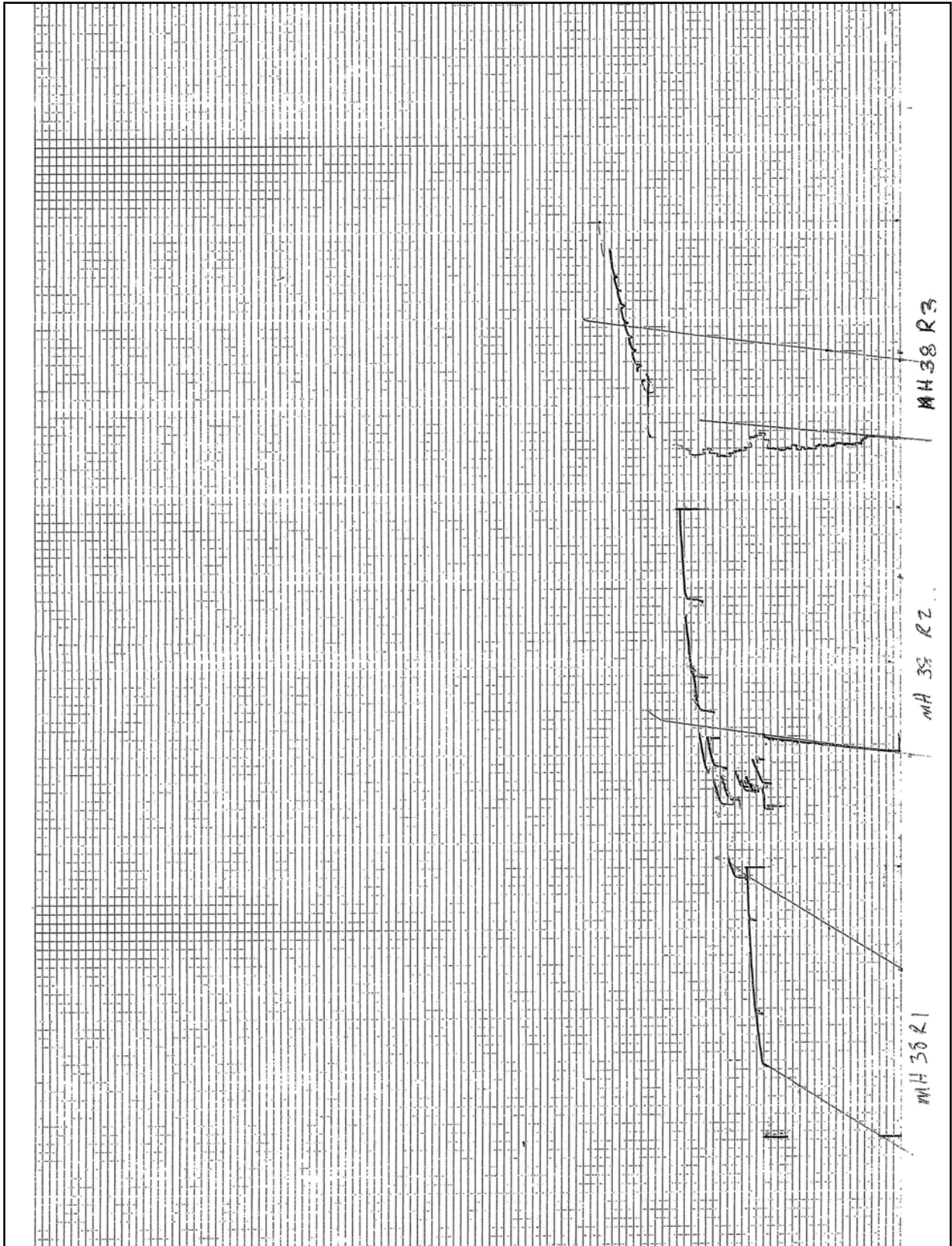
G:\WORD\DATA\MSFORMS\TT505.LAB

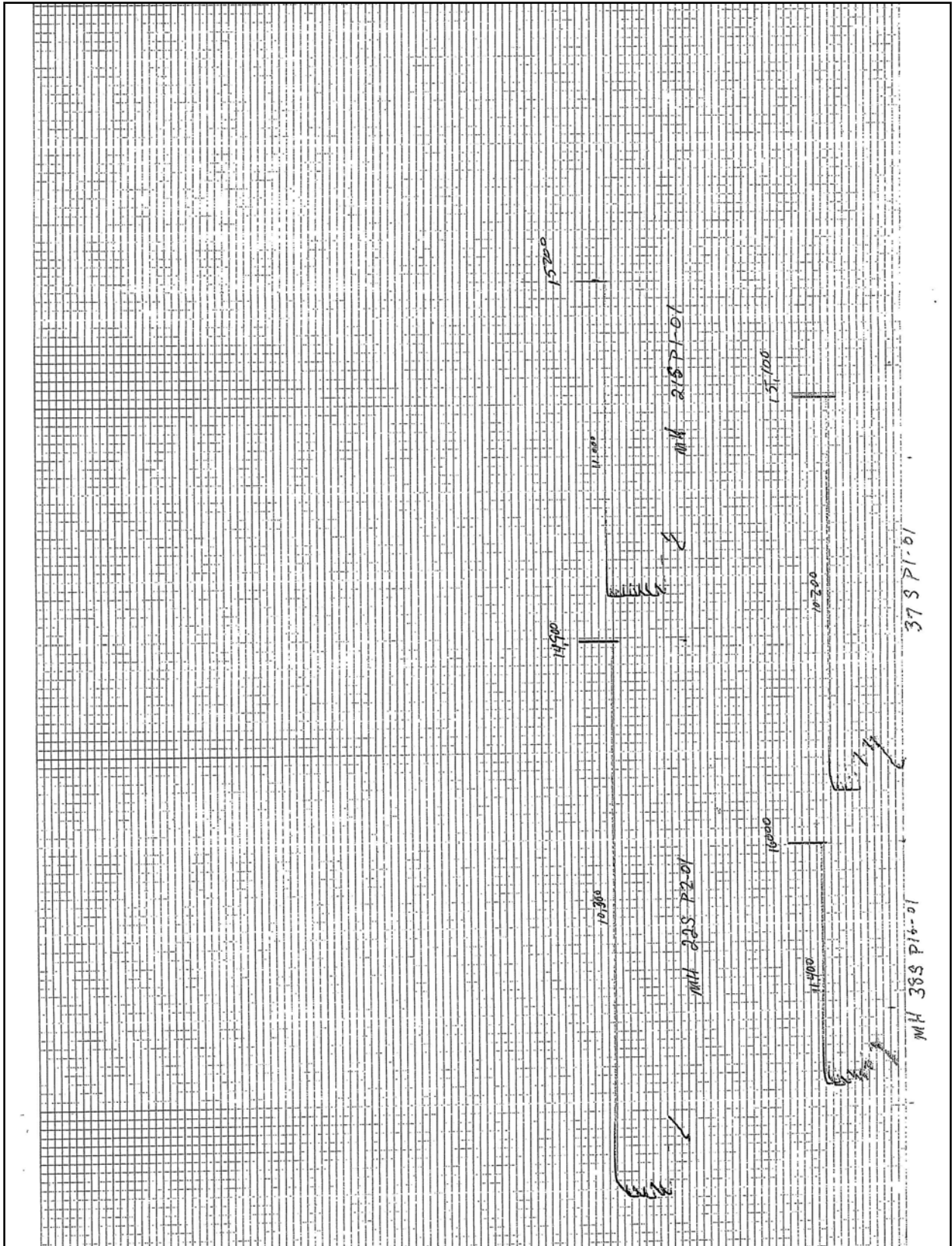
P. 1

5043661688

David Mandina







**American Association of State Highway and Transportation Officials
AASHTO Accreditation Program - Certificate of Accreditation**

This is to signify that

Beta Testing & Inspection, LLC

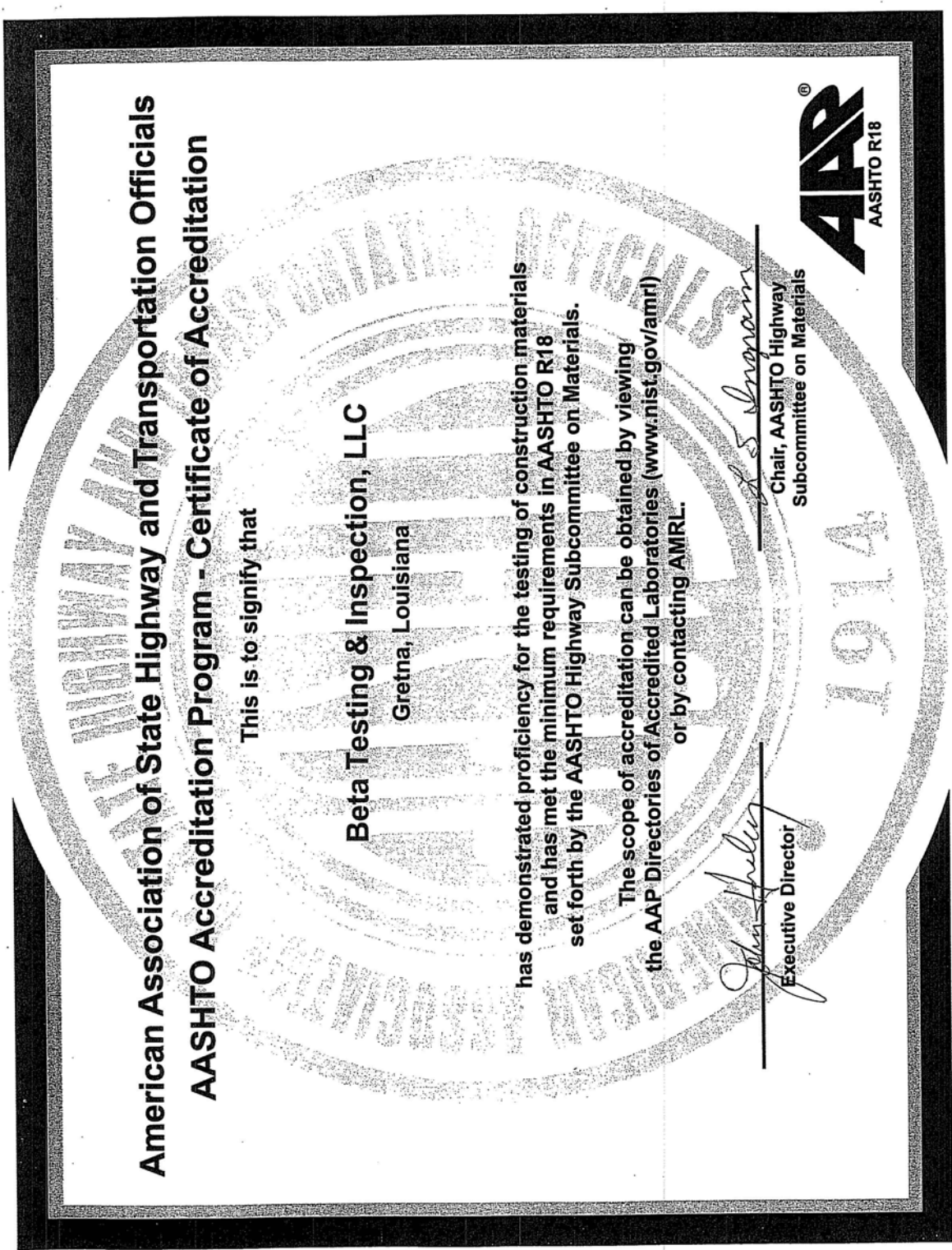
Gretna, Louisiana

has demonstrated proficiency for the testing of construction materials and has met the minimum requirements in AASHTO R18 set forth by the AASHTO Highway Subcommittee on Materials.

The scope of accreditation can be obtained by viewing the AAP Directories of Accredited Laboratories (www.nist.gov/amrl) or by contacting AMRL.


Executive Director


Chair, AASHTO Highway
Subcommittee on Materials





DEPARTMENT OF THE ARMY
ENGINEER RESEARCH AND DEVELOPMENT CENTER, CORPS OF ENGINEERS
GEOTECHNICAL AND STRUCTURES LABORATORY
WATERWAYS EXPERIMENT STATION, 3909 HALLS FERRY ROAD
VICKSBURG, MISSISSIPPI 39180-6199

REPLY TO
ATTENTION OF:

CEERD-GS-E (1110-1-8000c)

22 Aug 05

Memorandum For Commander, USAE District, New Orleans, ATTN: CEMVN-CD-QS/Mr. Geoff Laird,
PO Box 60267, New Orleans, LA 70160-0267

SUBJECT: Validation of Beta Testing and Inspection, LLC, Gretna, LA

1. In reference to Military Interdepartmental Purchase Request No. W42HEM51322885, dated 13 May 05, an inspection of the materials testing laboratory of Beta Testing and Inspection, Gretna, LA was performed on 13 Jun 05. The results of that inspection were reported to the Commander, USAE District, New Orleans on 20 Jun 05. The laboratory reported their deficiency corrections to the Materials Testing Center (MTC) on 19 Jul and 09 Aug 05. These corrections were compared to the ASTM Standards for compliance and were found to be satisfactory. We also examined AMRL Inspection Report No. 994F, Dated 01 Jul 04, CCRL Inspection Report No. J-71, dated 18 Aug 04, and the AASHTO Accredited Laboratory List dated 18 Aug 05.

2. The Quality System of the laboratory is satisfactory and we are granting a validation of the lab to perform material tests for the U.S. Army Corps of Engineers. The material test methods that the laboratory is validated to perform are:

a. **Aggregate Tests:** ASTM C40, C117, C127, C128, C136, C29, C88, C131, C535, C566, C702, D75, and D4791.

b. **Bituminous Tests:** ASTM D2726 and D3666.

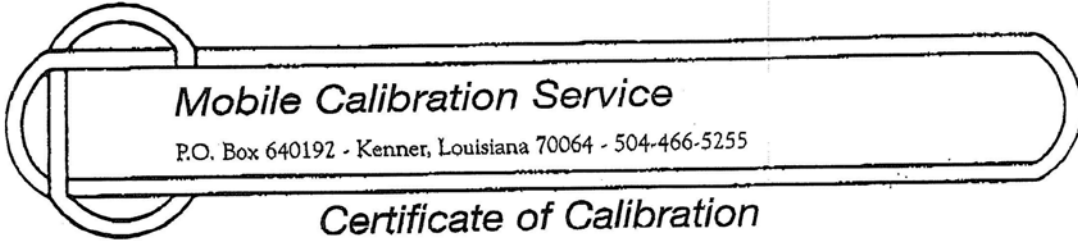
c. **Concrete Tests:** ASTM C31, C39, C138, C143, C172, C173, C231, C1064, C42, C78, C157, C174, C192, C293, C470, C511, C617, C1077, and C1231.

d. **Soil Tests:** ASTM D421, D422, D558, D698, D1140, D1556, D1557, D2168, D2216, D2217, D2487, D2488, D2922, D3017, D3740, and D4318.

3. We will add Beta Testing and Inspection, Gretna, LA to the list of commercial laboratories qualified to conduct material tests for the U.S. Army Corps of Engineers, see the MTC homepage at <http://www.wes.army.mil/SL/MTC/mtc.htm>. All Corps offices will be notified of this decision and will have the opportunity to use their services. The laboratory will remain on our list of laboratories qualified to conduct material tests until **13 Jun 08**, three (3) years from the date of the inspection.

DANIEL A. LEAVELL
Director, Materials Testing Center

CF:
Mr. Mark Cheek / Beta Testing and Inspection, Gretna, LA



Certificate of Calibration

This is to certify that the following described testing machine has been calibrated in accordance with ASTM E4 and found to be within a tolerance of 1%. Method of verification and pertinent data are in accordance with ASTM E-4. The testing device(s) used have been verified per ASTM E 74 and are traceable to the National Institute of Standards & Technology (N.B.S.)

CLIENT: Beta Testing & Inspection Co.
P.O.Box 203
Gretna, Louisiana 70054

DATE: August 1, 2005
Recal: August, 2006
Last Cal: August, 2004

MACHINE IDENTIFICATION: Soiltest Concrete Tester #9003

MACHINE RANGE: 0-250000 Pounds
0-30000 Pounds

CALIBRATED RANGE: 25000-250000 Pounds
3000-30000 Pounds

CALIBRATION APPARATUS
Strainsense Load Cell 860916A
Strainsense Load Cell 880305A

CLASS A RANGE
8400-500000 Pounds
960-12000 Pounds

CALIBRATED TO NIST
8-04
10-04

CALIBRATION RESULTS

MACHINE READING	ACTUAL LOAD LBS RUN #1	DIFFERENCE POUNDS	PERCENT ERROR	ACTUAL LOAD LBS RUN #2	DIFFERENCE POUNDS	PERCENT ERROR
LOW PRESSURE GAUGE						
3000	2985	15	+0.50	2990	10	+0.33
5000	4980	20	+0.40	4975	25	+0.50
10000	9965	35	+0.35	9970	30	+0.30
15000	14955	45	+0.30	14945	55	+0.37
20000	19930	70	+0.35	19940	60	+0.30
25000	24920	80	+0.32	24910	90	+0.36
30000	29880	120	+0.40	29900	100	+0.33
HIGH PRESSURE GAUGE						
25000	25100	100	-0.40	25050	50	-0.20
50000	50150	150	-0.30	50200	200	-0.40
75000	75190	190	-0.26	75270	270	-0.36
100000	100230	230	-0.23	100280	280	-0.28
125000	125210	210	-0.17	125220	220	-0.18
150000	149840	160	+0.11	149790	210	+0.14
175000	174610	390	+0.22	174670	330	+0.19
200000	199480	520	+0.26	199350	650	+0.33
250000	249260	740	+0.30	249060	940	+0.38

The above are as found readings.

MOBILE CALIBRATION SERVICE

Warren A. Meyn Jr.
Warren A. Meyn Jr.

Certificate of Calibration

and Traceability to the

United States National Institute of Standards & Technology

MODEL: SS504C
STRAINSENSE LOAD CELL, SERIAL NO. 860916A/M-8/96(LO)
50,000 LBF CAPACITY, COMPRESSION
ADMET-DC-16 INDICATOR, SERIAL NO. P16-0008081

The above identified instrument was calibrated in accordance with section 7 of the American Society for Testing and Materials (ASTM) Specification E74-02, entitled "Standard Practice of Calibration of Force-Measuring Instruments...". This calibration is in conformance with the requirements of Morehouse QAM Rev. 7, dated 12/04/00.

Calibration was performed at the following indicator settings:

Load Cell 1
Channel 1

The result of this calibration as determined by statistical analysis according to section 8 of ASTM E74-02, is as follows:

<u>Uncertainty</u>	<u>Resolution</u>
20.4 Lbf	12.0 Lbf

Class A Loading Range according to ASTM E74-02:

8,160.0 Lbf to 50,000 Lbf

Calibration was performed for a temperature of 23 degrees C.

This calibration is certified traceable to the United States National Institute of Standards & Technology according to the following documentation and calibration apparatus used:

Dead Weight Force Machine S/N M-7471 NIST Lab No. 822/268391-03

Uncertainty of Force Standard used did not exceed +/-0.002% of applied load

Calibrated by:

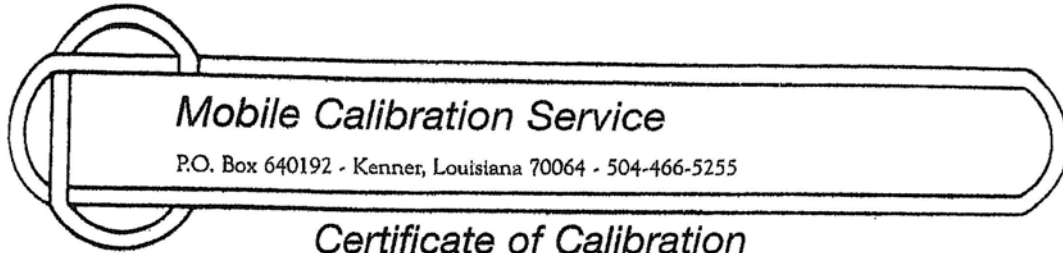


Date Calibrated:
August 18, 2004

Report No:860916A/M-8/96(LO)H1804

MOREHOUSE INSTRUMENT COMPANY, INC.
FORCE CALIBRATION LABORATORY
1742 SIXTH AVENUE
YORK, PA 17403-2675 U.S.A.
PHONE: 717 / 843-0081
FAX: 717 / 846-4193
WEB: www.morehouseinst.com

This Certificate shall not be reproduced except in full, without written approval from Morehouse Instrument Company, Inc.
PAGE 04 12/16/2005 14:48 5044662825 WMEYN MOBILE CAL



Certificate of Calibration

This is to certify that the following described testing machine has been calibrated in accordance with ASTM E4 and found to be within a tolerance of 1%. Method of verification and pertinent data are in accordance with ASTM E-4. The testing device(s) used have been verified per ASTM E 74 and are traceable to the National Institute of Standards & Technology (N.B.S.)

CLIENT: Mandina Inspection Service
3861 Peters Road
Harvey, La.

DATE: June 9, 2005

MACHINE IDENTIFICATION: Tinius Olsen Universal Testing Machine

MACHINE RANGE: 0-120000 Pounds

CALIBRATED RANGE: 10000-120000 Pounds

CALIBRATION APPARATUS

Strainsense Load Cell 050106
Morehouse Ring 5-4537

CLASS A RANGE

5000-50000 Pounds
25000-250000 Pounds

CALIBRATED TO NIST

1-05
5-04

CALIBRATION RESULTS						
MACHINE READING	ACTUAL LOAD LBS	DIFFERENCE POUNDS	PERCENT ERROR	ACTUAL LOAD LBS	DIFFERENCE POUNDS	PERCENT ERROR
	RUN #1			RUN #2		
10000	10030	30	-0.30	10025	25	-0.25
20000	20060	60	-0.30	20050	50	-0.25
40000	40100	100	-0.25	40060	60	-0.15
60000	60120	120	-0.20	60150	150	-0.25
80000	80190	190	-0.24	80160	160	-0.20
100000	100290	290	-0.29	100220	220	-0.22
120000	120330	330	-0.28	120290	290	-0.24

The above are as found readings. No calibration adjustments required.

MOBILE CALIBRATION SERVICE

[Signature]
K. Kevin Wehr
TECHNICIAN



**OLSON
ENGINEERING, Inc.**

SPECIALIZING IN CONDITION EVALUATION OF THE
CIVIL STRUCTURE & INFRASTRUCTURE



www.olsonengineering.com

January 6, 2006

U. S. Army Corps of Engineers
Engineering Research and Development Center
3909 Halls Ferry Rd.
Vicksburg, MS. 39180

Attn: Mr. Richard W. Haskins, ERDC-ITL-MS
Ofc: (601)634-2931
Fax: (601)634-2873
E-Mail: Richard.W.Haskins@erdc.usace.army.mil

Re: Nondestructive Testing Investigation Report No. 2
Parallel Seismic Re-Testing Results for Sheet Pile Lengths
New Orleans 17th Street and IHNC Levees
New Orleans, LA
Olson Engineering Job No. 1875C

Dear Sirs,

We are pleased to report herein the results of re-testing with the Parallel Seismic method of one sheet pile location at each of the 17th Street and Inner Harbor Navigational Canal (IHNC) levees. This additional work was conducted as a result of the initial incorrect prediction of sheet pile lengths at the North and South ends of the break at the 17th Street Levee (report dated December 5, 2005, Olson Job No. 1875). Actual sheet pile lengths were revealed to be about 23.5 ft in USACE excavations of sheet piles conducted on December 13, 2005 (the sheet piles were incorrectly predicted to be about 7 ft shorter in our initial report).

Discussion of Initial Sheet Pile Depth Predictions

When we learned that the USACE removal of sheet piles at the North and South ends of the 17th Street Levee breach for revealed actual total sheet pile lengths of about 23.5 ft, we immediately reviewed the PS data for ground-truthing purposes to examine the data and see if there was an indication of the actual sheet pile tips in the data or not. Our review of the data found that there was evidence of possible weaker diffraction events in the bottom 3 ft or so of the initial PS data that corresponded to the actual sheet pile tip depths.

As discussed in our draft report addendum letter of December 13th, 2005 which was



transmitted to the USACE at that time, we attribute our mis-interpretation of the data to the following three factors:

1. the PS data sets contained misleading apparent ground/tube vibrations that showed apparent slower velocity and weaker signals at the incorrectly predicted 7ft short sheet pile depths. This energy is now attributed to strong energy emitting from the concrete walls in to the ground due to the horizontal impacts to the concrete walls just below the chamfers;
2. the different shape of the now apparent sheet pile diffraction events due to the spreading out of energy for the wall-shaped steel sheet piles versus our experience with previous arrowhead diffraction events measured for rod-shaped steel H-piles in research and consulting by our firm; and,
3. the single biggest problem that led to the misinterpretation of the initial data was the lack of data available to clearly identify the weak diffraction of wave energy emitting from the pile tips. This was due to the fact that the borehole casings only extended a few feet beyond the actual pile tip depths. The desired typical cased borehole depth would extend 10-15 ft beyond the suspected/hoped for maximum sheet pile depths and this was recommended in our proposal of October 22, 2005 (Olson Proposal No. 2005169.1) for the project.

Borings were also recommended to be drilled as close as practical to the foundation to be tested preferably within 3-5 ft or less horizontally of the foundation, but generally no more than 10 ft away from a foundation to be tested with the PS method. We understand that the USACE borings were initially drilled in to the levees for geotechnical sampling purposes only and that PS testing was decided upon after the borings were drilled. The 4 inch diameter PVC casings that were subsequently grouted in-place in the boreholes for the PS tests were shorter than the drilled boreholes and extended only to depths of 25 ft below the levee ground surface. Such borehole casing depths would have been deep enough for successful PS tests if the sheet piles were around 16 ft in length, but the 25 ft long casings resulted in there only being about 3 feet of casing at or below the 23.5 ft long sheet pile tips. Thus there were only 3-4 PS test records from which hydrophone PS data could be obtained at or below the pile tips. As discussed above and in the report addendum, we feel that the limited PS data from below the sheet pile tips contributed significantly to our incorrect interpretation of the weak diffraction events.

A conference call about the PS results and our draft report addendum was held with Messrs. Richard Haskins and Paul Mlakar of the USACE and Larry Olson and Dennis Sack of Olson Engineering, Inc. on December 16th. As requested by Mr. Mlakar at that time, we have updated the draft addendum letter to include not only a review of the data from the PS tests at the 17th Street Levee, but also the PS data from the London Avenue and IHNC levees that was also presented in our initial report. The final report addendum is being provided as a separate letter.

Parallel Seismic Re-Test Field Investigation Overview

We were quite concerned about the initial incorrect sheet pile length predictions and this led to our decision to gather more data on the weak diffraction events that were apparently indicative of the actual sheet pile tips for the two USACE cased boreholes at the 17th Street Levee North and South breach ends. Consequently, we decided to conduct additional PS tests at the South End of the breach at Station 20+78 which was only about 7 ft from the USACE PS boring in this area. The testing was also at the South End of the 17th Street levee breach immediately adjacent to the area where the USACE excavated sheet piles and found their total lengths to be nominally 23.5 ft on December 13, 2005. We also conducted tests at the IHNC levee adjacent to the North end of the south breach at Station 17+11 within about 10 ft north of where a cased borehole PS test had been done earlier.

This additional nondestructive investigation was conducted at no cost by Olson Engineering to the USACE with the field support of Southern Earth Sciences, Inc. (SESI) of Baton Rouge, Louisiana who also provided their services at no cost. SESI had used their Seismic Cone Penetrometer (SCPT) Geoprobe rig with a biaxial geophone to investigate sheet pile tests in PS/SCPT tests of the 17th Street and London Avenue Levees for the state of Louisiana levee investigation team and their field tests were conducted after our initial field PS tests. A photograph of the Geoprobe rig is shown in Photo 1 and the SCPT tool is shown in Photo 2.



Photo 1 - Geoprobe Rig for PS/SCPT testing at South End of Breach of 17th Street Levee at Station 17+78 where sheet piles were exposed by USACE PS Cased Borehole (white PVC cap visible)



Photo 2 - Seismic Cone Penetrometer Tool with Bearing pressure at tip followed by pore pressure ring followed by skin friction sleeve followed by bi-axial horizontal geophones

The initial SESI PS/SCPT tests were able to be conducted to greater depths and much closer horizontally (typically within 3 ft of the concrete walls) without drilling borings. As discussed with USACE, we also provided consulting services to SESI in the analysis of their initial PS/SCPT results. Analyses of their initial bi-axial geophone results showed similar sheet pile depths to our initial hydrophone PS results with their findings presented in the SESI report to the State of Louisiana.

In our joint efforts with SESI at the IHNC and 17th Street Levees on December 21 and 22, 2005, respectively, SESI conducted PS/SCPT tests with their bi-axial (two perpendicular, horizontal geophones) seismic cone penetrometer tool (Photo 2). For our comparison PS testing with a small diameter hydrophone receiver, they pushed a non-retrievable dummy tip into the levee soils. Next, SESI installed a temporary 1 inch PVC casing inside the Geoprobe hollow steel push rods which were then retrieved to leave the PVC casing in the ground. Then the hole annulus and inside of the PVC casing were filled with water so we could conduct hydrophone-based Parallel Seismic (PS) tests.

The joint effort with SESI allowed for a comparison of the data obtained from the two different types of PS test transducers, ie., the more omni-directional hydrophone receiver vs. the bi-axial horizontal geophones. In our National Cooperative Highway Research Program 21-5 and 21-5(2) research projects for Determination of Unknown Bridge Foundation Depths for scour safety studies, we compared hydrophones and tri-axial geophones in Parallels Seismic tests. Generally, the hydrophone was found to be the more sensitive receiver to the arrival of initial weak direct energy in PS tests of bridge foundations, particularly for diffraction events due to its more all-around or "omni-directional" response to wave energy emitting from the impacted bridge substructure foundation system.

Parallel Seismic Re-Test Results

The joint Olson/SESI PS re-test program was planned to evaluate both bi-axial geophones (results to be reported by SESI) and hydrophone receivers and investigate PS data results quality for impacts applied directly to sheet piles, and from horizontal to vertical impacts to the concrete walls in which the levee sheet piles are embedded. The PS re-test results of the 17th Street re-tests are presented first below followed by the IHNC results. The field effort was also made possible by USACE personnel and their subcontractors who also contributed significantly to the re-test program and assisted in the field by providing site access, excavation assistance to expose sheet piles, and testing assistance. The State of Louisiana levee investigation team also contributed their input to the re-test program and observed the field PS re-test effort as well.

17th Street PS Re-Test Results at South End of Breach - Station 20+78

Based on the stickup of the sheet piles of about 1.25 ft above the levee ground surface, the 23.5 ft long sheet piles extend to about 22.25 ft below existing grade at the south end of the 17th Street levee breach at Station 20 +78 where the 1 inch PVC casing was installed to about 30

ft deep by SESI at about 2.5 ft from the wall edge on the protected side. The locations of the impacts with a 3-lb impulse hammer with a black hard plastic tip to the sheet pile and concrete levee wall at various positions are shown in Photos 3-7 and the PVC casing is shown in Photo 8.



Photo 3 (Fig. 1) - Horizontal impact to sheet pile at 0.5 ft below concrete wall - protected levee side



Photo 4 (Fig. 2) - Horizontal impact to side of concrete wall at el. 5 about 0.5 ft below chamfer



Photo 5 (Fig. 3) - Angled downward impact to chamfer of wall at ~ el. 5.75



Photo 6 (Fig. 4) - Vertical downward impact to top of wall



Photo 7 (Fig. 5) - Angled impact to 1 inch diameter, 6 ft long steel rod held at an angle on sheet pile side at 0.5 ft below concrete - protected levee side

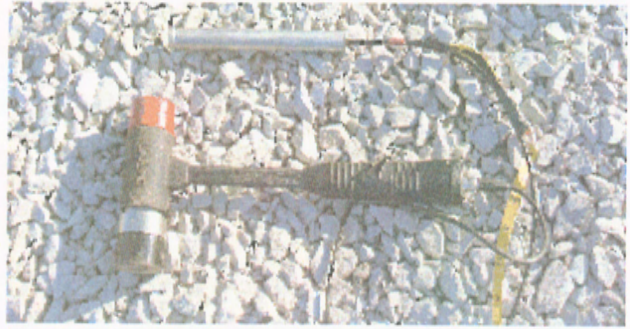


Photo 8 - 3-lb Impulse Hammer with black hard plastic tip and small diameter hydrophone used in PS re-tests

The PS re-test results for the impact positions shown in Photos 3-7 are respectively presented in Figures 1-5 below. The expected diffraction event should occur at a depth of about 22.25 ft from the sheet pile tip in these hydrophone-based PS results. Review of the figures shows that the weak diffraction events are now clearly evident for all of the impact locations. This is due to the increase in PS test depth 30 ft for the 1 inch diameter casing installed by the geoprobe vs. the initial grouted casing depth of only 25 ft.

The PS data presented in Figures 1-5 were produced by 5 impacts which were averaged at each 1 ft test depth interval, filtered and normalized to the largest signal strength (global maximum display) to optimize the display of the diffraction events. Review of Figure 1 shows the diffraction event at 23.0 ft deep due to direct horizontal sheet pile impacts. There is also some energy occurring in advance of the diffraction event at shallower depths. In Figure 2 the horizontal impacts to the concrete wall also show a diffraction event at 22.7 ft deep, but a little less clear with more energy emitting from the concrete wall. By comparison, the diffraction event is clear at 21.8 ft deep for the angled downward impact to the chamfer in Figure 3. Apparently the more vertical impact to the chamfer put more energy down the sheet pile with less energy emitting from the wall. In Figure 4, the impacts to the top of the wall were further away from the ground and the sheet pile, so the diffraction event is quite clear at 21.5 ft. The impacts to the angled steel rod also produced a diffraction event at 22.6 ft as shown in Figure 5, but it was comparatively weaker, likelier due to less energy being imparted by the rod impacts.

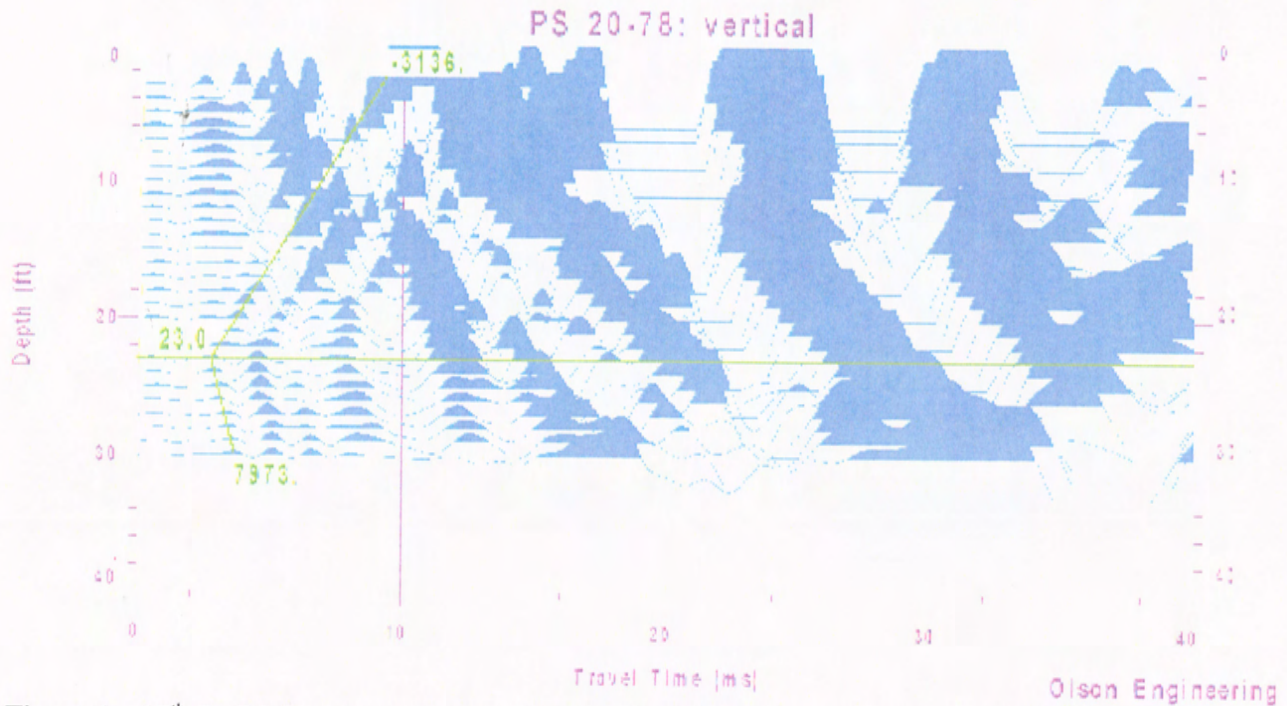


Figure 1 - 17th St. PS Results at Station 20+78 - Sheet Pile impacted at ~ el. 1.5 (0.5 ft below bottom of levee concrete wall on protected side)

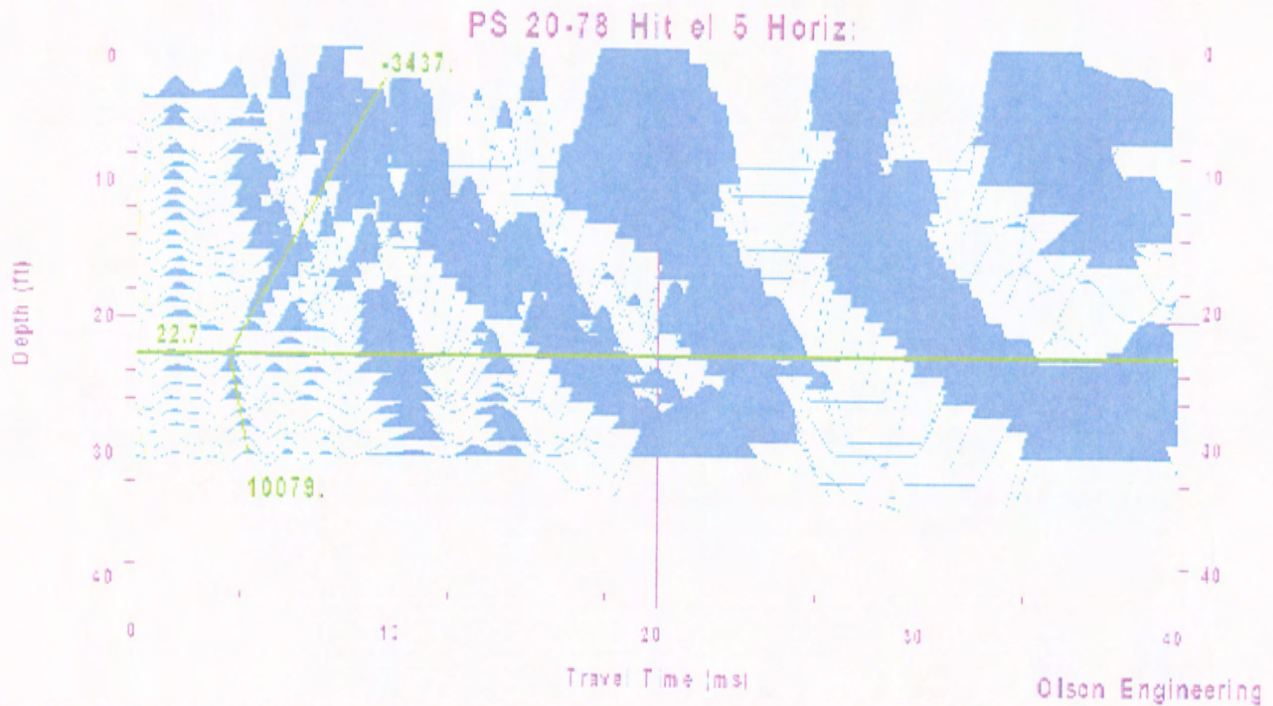


Figure 2 - 17th St. PS Results at Station 20+78 - Concrete Wall impacted horizontally at ~ el. 5 (~0.5 ft below chamfer edge on protected side)

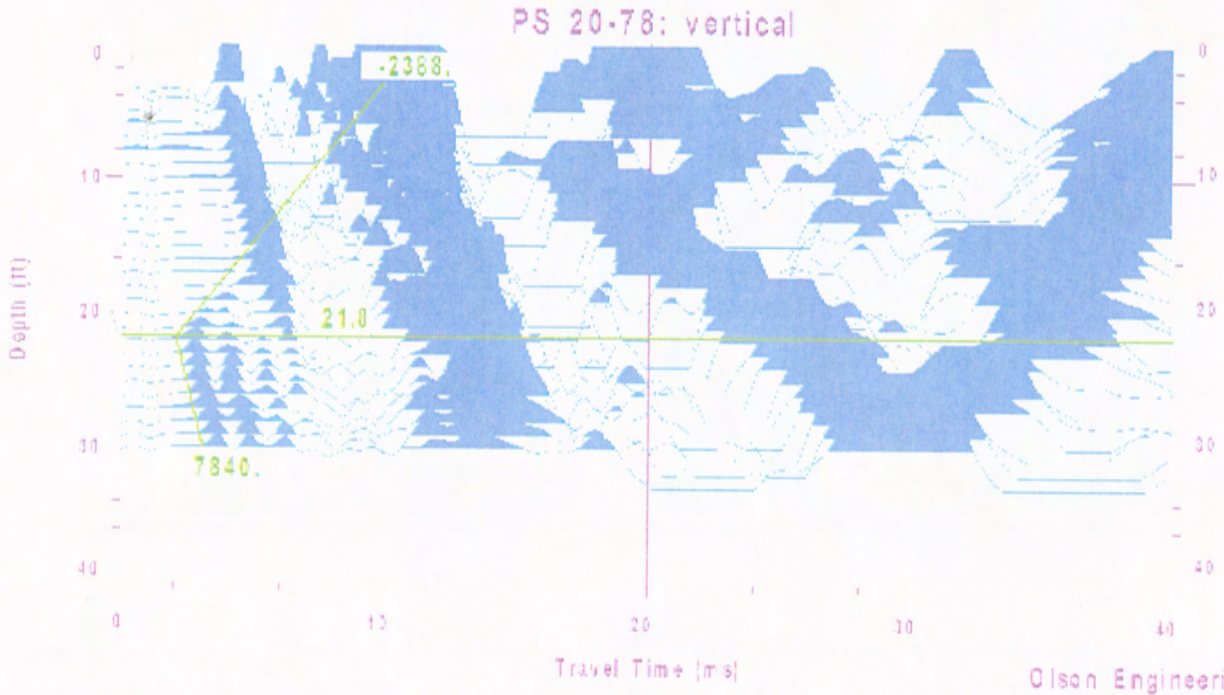


Figure 3 - 17th St. PS Results at Sta. 20+78 - Angled Impacts to Chamfer of Concrete Wall at Sta. 20+78 (~el. 5.75 on protected side)

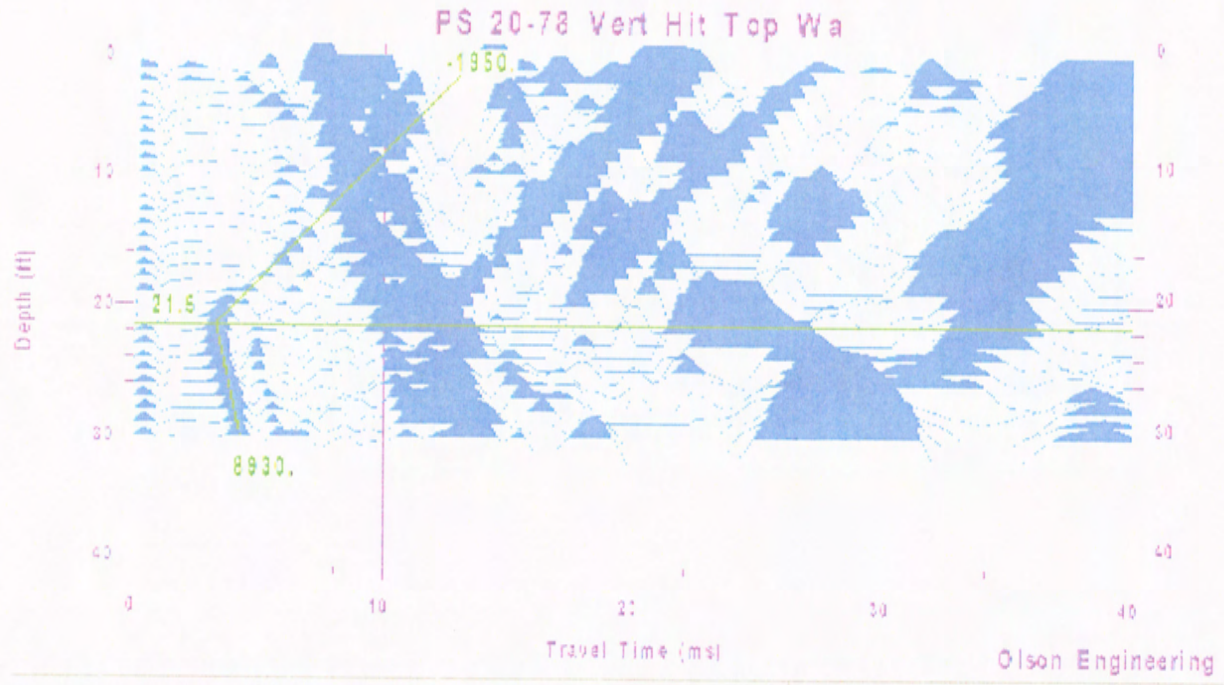


Figure 4 - 17th St. PS Results at Sta. 20+78 - Vertical Impacts to Top of Concrete Wall at Sta. 20+78

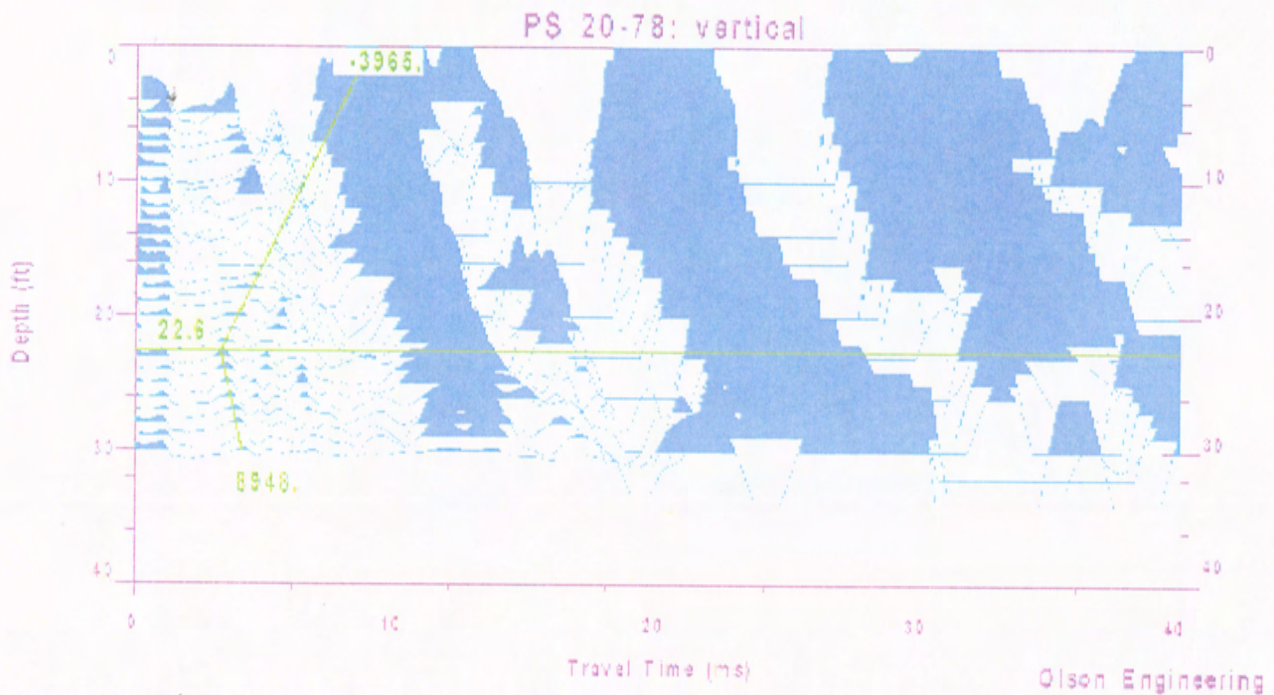


Figure 5 - 17th St. PS Results at Sta. 20+78 - Angled Impacts to 1 inch diameter, 6 ft long rod held against steel sheet pile at ~ el. 1.5 at 0.5 ft below concrete wall

IHNC PS Re-test Results at North End of South Breach - Station 17+11

The IHNC re-tests were performed in an area of the wall that had been pushed back and the levee soils dropped down to expose a sheet pile on the canal side at Station 17+11 which was about 10 ft north of the USACE cased boring in this area. Shovels were used to expose enough of the sheet pile to impact it with the 3 lb impulse hammer as shown in Photo 9. The PS tests were done using a hydrophone in the 1 inch PVC casing installed by SESI with the Geoprobe rig as shown in Photo 10.



Photo 9 - IHNC 3-lb Impulse hammer impacts to sheet pile on canal side at Station 17+11



Photo 10 - Small Hydrophone receiver on tape in 1 inch PVC casing installed by Geoprobe Rig at IHNC

Sonic Echo testing was conducted from end to end of a nearby exposed sheet pile and a compression wave velocity of about 17,000 ft/second was measured which is essentially the theoretical velocity of a steel rod of 16,600 ft/s. The Sonic Echo results did show a single clear echo from the pile tip in air, but not the multiple echoes normally measured on H-piles in air. Impulse Response analyses in the frequency did not show clear resonant echo peaks from the exposed pile tip. This is due to the spreading out of the energy in to the rest of the interlocked sheet pile wall and the lack of a resonant, rod-like shape for a sheet pile wall. When similar Sonic Echo/Impulse response tests were attempted from the exposed top of an embedded 23.5 ft long sheet pile at the South end of the 17th Street breach, no echo from the pile tip was apparent. This result was expected as the attenuation of the compression wave energy is high due to the large surface area of a steel sheet pile.

The exposed sheet pile at the north end of the south IHNC breach showed a total length of 19 ft - 6.5 inches. Of this, about 4 ft - 7 inches of the piles had been embedded in the 8 ft tall concrete wall. Thus, about 15 ft of the sheet piles are typically embedded in the levee soils. Given the 1 ft higher elevation of the top of the PVC casing on the levee soils versus the bottom of the concrete wall, the sheet pile tip is expected to be at a depth of about 16 ft in the PS hydrophone signal versus depth results which are presented below in Figures 6-8. Horizontal impacts were applied just below the concrete wall to the canal side of the exposed sheet pile (Fig. 6) and to the concrete wall at 6.5 ft below the top of the wall (Fig. 7) which was 1.5 ft above the bottom of the concrete wall while vertical impacts were applied to the top of the wall (Fig. 8).

Review of Figure 6 for the case of direct horizontal impacts to the sheet pile shows a weak direct arrival wave front that is slower below the 16 ft depth of the sheet pile. However, no diffraction events are evident in this PS-based hydrophone test data. This may be due to the evident separation of the levee soil from the canal side of the wall due to the wall being pushed back by the breach forces. This apparent lack of tight contact between the sheet pile and the levee soils may have resulted in the diffraction event energy not being well coupled into the surrounding saturated soils.

Review of Figures 7 and 8 for horizontal and vertical impacts to the concrete wall does not show clear direct arrivals when the apparent weak energy was picked as shown in the figures. No diffraction events are clearly evident in the figures either. These results further support the possibility that there is poor soil contact to the sheet pile on the canal side that diminished the diffraction effect in the IHNC re-tests.

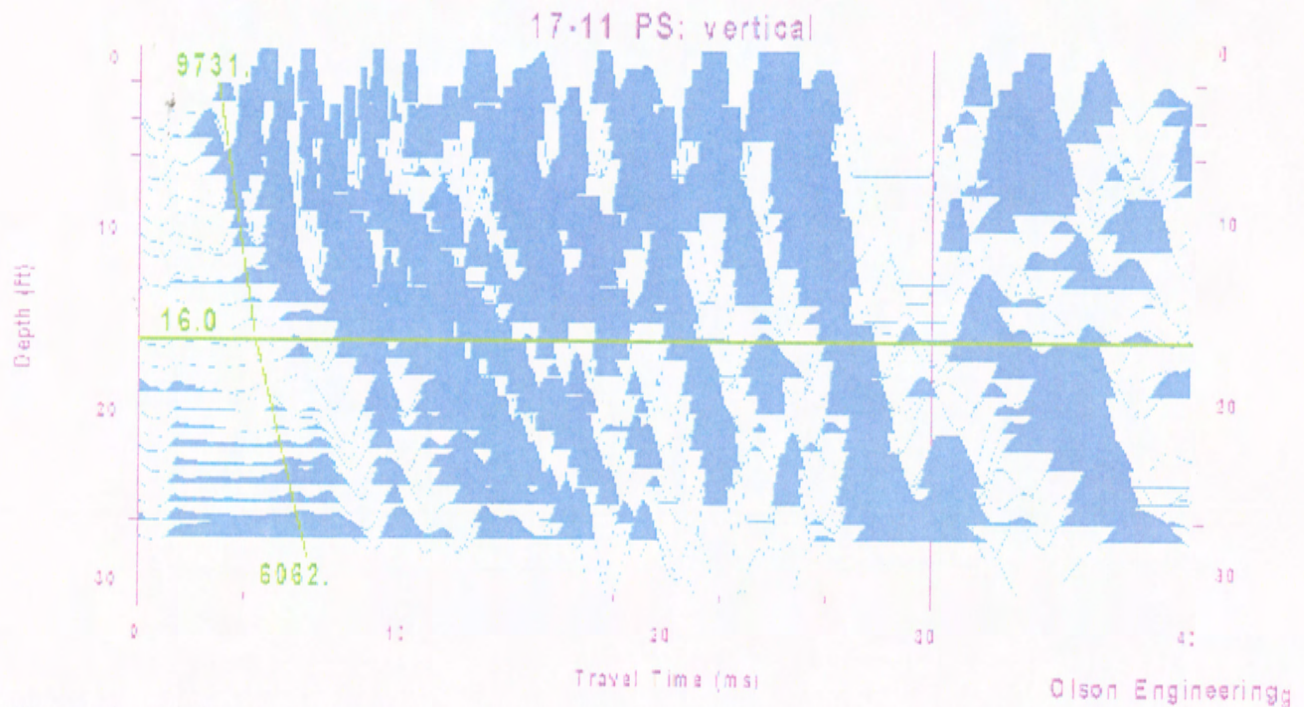


Figure 6 - PS Results at IHNC Sta. 17+11 - Impact to Sheet Pile at ~ 0.5 ft below bottom of Concrete Wall on Canal Side

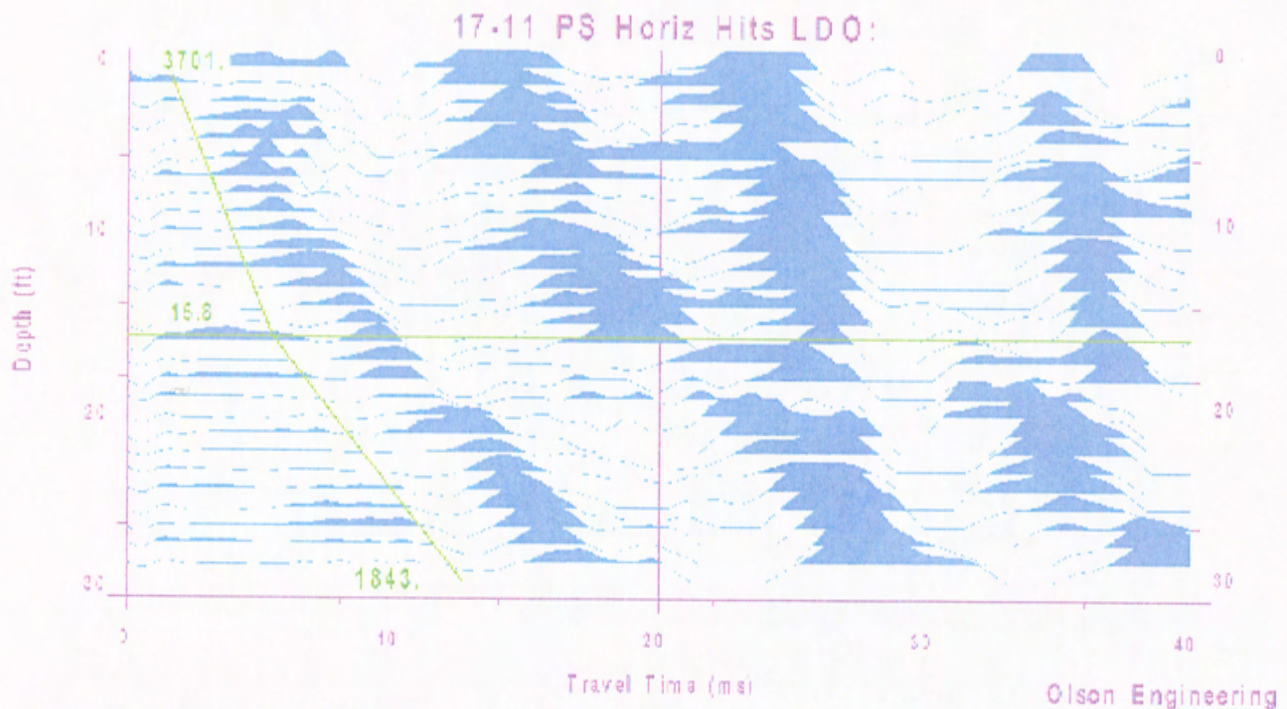


Figure 7 - PS Results at IHNC Sta. 17+11 - Horizontal Impact to Concrete Wall at ~ 6.5 ft below top of Wall on Canal Side

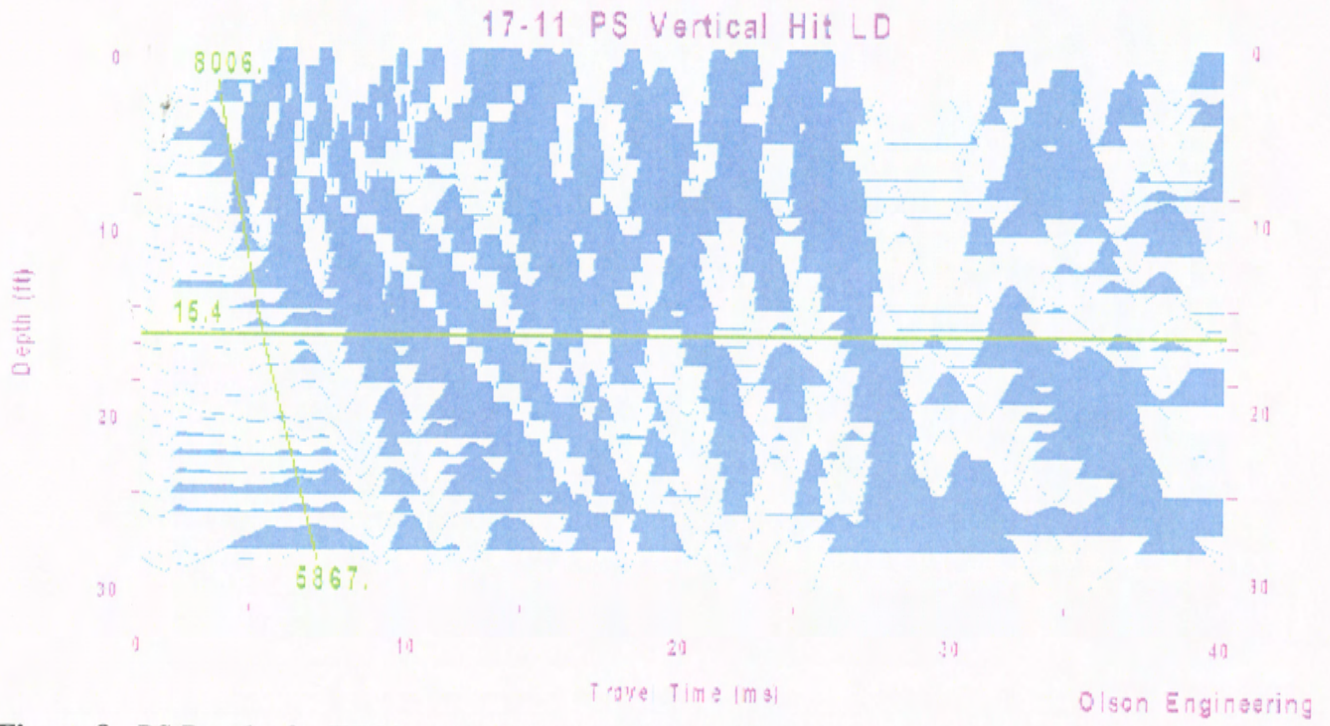


Figure 8 - PS Results for IHNC at Sta. 17+11 for Vertical Impacts to top of 8 ft tall Concrete Wall

Summary of Conclusions and Findings

17th Street Parallel Seismic (PS) Re-Test Results at Station 20+78. The hydrophone-based PS re-test results at the South End of the 17th Street breach clearly identified the pile tips within about 1 ft of the actual sheet pile depth of ~22.25 ft based on clear diffraction events at the sheet pile tip for impacts to the pile side, wall side, chamfer, wall top and even a rod held against the pile side. The results were clearest for the vertical hits on top of the wall, chamfer impacts and direct sheet pile impacts.

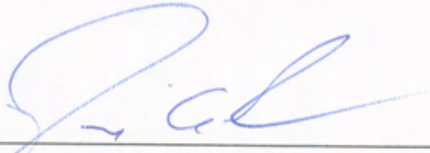
IHNC PS Re-Test Results at Station 17+11. The hydrophone-based PS re-test results at the North End of the south IHNC breach showed a weak direct arrival for impacts directly to the sheet pile that predicted the actual depth of 16 ft. However, only very tentative identifications of such direct arrivals were evident in PS results for either horizontal or vertical impacts to the levee concrete wall. None of the PS results at IHNC showed the clear diffraction arrival events at the pile tip depth found in all of the 17th Street PS re-test results. The lack of the diffraction arrival events may be due to the apparent lack of tight soil contact between the IHNC wall on the canal side as a result of the breach force pushing the wall back. Clear separation of the soil and wall was still evident at the surface in this area. Such lack of contact may have diminished the coupling of energy in to the soils from the diffraction event at the pile tip.

CLOSURE

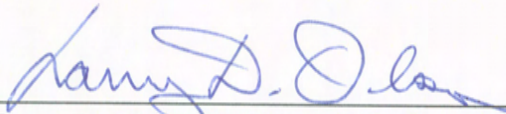
The field NDT investigation was performed in accordance with generally accepted testing procedures. If there are any questions, or further information is required, please do not hesitate to call. If any additional information is developed pertinent to this study, please contact our office.

Respectfully submitted,

OLSON ENGINEERING, INC.



Dennis A. Sack
Associate Engineer



Larry D. Olson, P.E.
Principal Engineer

(1 copy e-mailed and 2 copies mailed)

e-mail cc: Mr. Paul F. Mlakar (Paul.F.Mlakar@erdc.usace.army.mil)



**OLSON
ENGINEERING, Inc.**

**SPECIALIZING IN CONDITION EVALUATION OF THE
CIVIL STRUCTURE & INFRASTRUCTURE**



www.olsonengineering.com

**NONDESTRUCTIVE TESTING INVESTIGATION
SHEET PILE FOUNDATION LENGTHS
NEW ORLEANS LEVEES
NEW ORLEANS, LOUISIANA**

Prepared for:

U. S. Army Corp of Engineers
Engineering Research and Development Center
3909 Halls Ferry Rd.
Vicksburg, MS. 39180

Attn: Mr. Richard W. Haskins, ERDC-ITL-MS
Ofc: (601)634-2931
Fax: (601)634-2873
E-Mail: Richard.W.Haskins@erdc.usace.army.mil

Olson Engineering Job No. 1875

December 5, 2005

This is a preliminary report subject to revision; it does not contain final conclusions of the United States Army Corps of Engineers.

K-226

12401 W. 49th Ave., Wheat Ridge, CO 80033-1927 USA

PHONE: 303.423.1212



FAX: 303.423.6071

TABLE OF CONTENTS

1.0 INVESTIGATION SCOPE AND SUMMARY OF FINDINGS	1
2.0 PARALLEL SEISMIC METHOD	2
3.0 INVESTIGATION RESULTS AND SUMMARY	4
4.0 CLOSURE	6

Table I: Summary of Sheet Pile Tip Depths and Elevations
From Parallel Seismic Testing of New Orleans Levees

Appendix A - Parallel Seismic (PS) Data

1.0 INVESTIGATION SCOPE AND SUMMARY OF FINDINGS

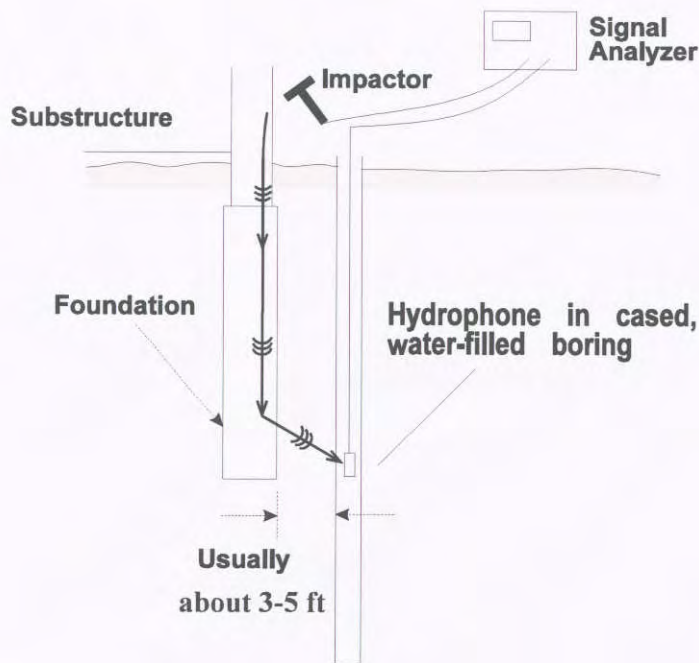
This report presents the Nondestructive Testing (NDT) investigation results for the determination of the unknown lengths of sheet piles below concrete walls of the New Orleans levee system. The levee sheet piles were tested with the Parallel Seismic (PS) method to determine their depths. The PS tests were conducted at the 17th Street, London Avenue, and the Inner Harbor Navigational Canal (IHNC) levees in 8 cased borehole locations at undamaged levee wall locations next to breaches.

The PS results indicate the presence of piles under the concrete wall, and showed that they extended to approximately 13-15 ft below the casing top for all of the sites tested as summarized in Table I. These sheet pile depths translate to elevations of approximately 10 feet below mean sea level (range of 9.3 to 11.8 feet below mean sea level). A discussion of the PS method and the investigation results are presented below.

2.0 PARALLEL SEISMIC METHOD

The Parallel Seismic (PS) method was used to estimate the depth of the foundations. The PS test equipment used in this investigation included a 3-lb instrumented impulse hammer, single hydrophone receiver, and a dynamic signal analyzer (Olson Instruments Freedom Data PC), as illustrated in Fig. 1. When the instrumented hammer directly impacted the supported concrete wall, it (or a nearby accelerometer) triggered the PC- based signal analyzer to capture the time records. A 16-channel National Instruments digital card was used to acquire the data in an Olson Instruments portable Freedom Data PC. Photographs of the field testing are shown in Figure 2.

The PS method involves impacting the exposed portion of the foundation or substructure attached to the foundation or a location which when impacted couples sufficient energy to the pile to generate a sound or stress wave which travels down the foundation. The wave energy is tracked by a hydrophone receiver suspended in a water-filled, cased and sometimes grouted borehole drilled



**Foundation Depth Determination
with the Parallel Seismic Test**
Figure 1 - PS test schematic

typically within 3-5 feet of the foundation edge. Note that for this investigation, the boreholes were found to be located as far as 21.1 feet from the levee wall, resulting in poorer quality data for some tests. The PS tests typically involve lowering the hydrophone(s) to the bottom of the borehole, impacting the exposed portion of the foundation structure and recording the hydrophone(s) responses. Then the hydrophone receiver(s) is raised to the next test elevation. This test sequence is repeated until the top of the casing (or the top of the water level in the casing) is reached. The pile depth is determined by plotting the hydrophone(s) response from all depths on a single display or page. For soils of constant velocity surrounding the piles, a break in the slope of the line occurs below the bottom of the piles indicating the pile depth. For soils with varying velocities, a break often cannot be identified from the slope of the lines, but the bottom of the piles can be identified by observing the traces of the hydrophone plot to identify changes in the response, such as a reduction in signal amplitude, change in signal frequency, or diffraction/reflection of tube wave energy from the foundation bottom.



Figure 2 - Photographs of impacting Wall of IHNC Levee at South Borehole of South Breach and Freedom Data PC at Cased Borehole with Hydrophone Receiver Downhole

3.0 INVESTIGATION RESULTS AND SUMMARY

The investigation was performed on October 27, 2005 and October 28, 2005 using the Parallel Seismic (PS) method by Mr. Larry D. Olson and Ms. Hunter Yarbrough of Olson Engineering, Inc., with assistance from U. S. Army Corps of Engineers personnel Mr. Richard Haskins and Mr. Don Yule. The 3 levee locations tested were at the 17th Street, London Avenue, and Inner Harbor Navigational Channel (IHNC). The PS test site at each test area was designated by the breach location and the position of the borehole. Hammer impacting was done horizontally on the levee wall face and vertically on the wall top where possible. The Parallel Seismic tests were performed with 5 impacts (horizontal and/or vertical) to the concrete walls at each of the hydrophone receiver depth intervals of nominally 1 ft for the entire water-filled length of the boreholes, starting typically 25 ft below the top of the borehole and continuing up to the top of the borehole casing at each site.

The Parallel Seismic tests were performed using a 3-lb hard-plastic tipped instrumented impulse hammer as a source and a single Olson Instruments hydrophone as a receiver. The pile locations were chosen to obtain a length measurement at the locations adjacent to levee breaks which occurred following Hurricane Katrina. Note that the reported data in Appendix A are pile tip depths measured from top of casing and that the PS predicted pile tip depths in true elevation as well as from the bottom wall chamfer can be found in Table I. Review of this table indicates sheet pile depths of 13-15 ft below the tops of the cased boreholes which corresponds to about 10 ft below mean sea level. Given the 1 ft hydrophone receiver measurement depth intervals, the PS results are believed to be accurate to within about 1 ft of the reported depths where data quality is high.

The Parallel Seismic data and results for the 17th Street Site can be found in Figures A-1 and A-2 in the Appendix. The Parallel Seismic data and results for the London Avenue Sites can be found in Figures A-3 to A-5, where Figures A-3 and A-4 are from the North breach and Figure A-5 is from the South breach. The Parallel Seismic data and results for the IHNC can be found in Figures A-6 to A-8, where Figure A-6 is from the breach near Florida Street and Figures A-7 and A-8 are

from the South breach. The exposed parts of all locations consisted of concrete retaining walls which had embedded sheet piles underneath. For the eight tested sites, PS tests were performed to a depth of 25 feet below the top of the grouted, 5 inch PVC casings which were filled with water.

The PS results presented in Appendix A are from typically horizontal hammer hits (data quality was better in one location using a vertical hammer hit as presented in Figure A-3). The horizontal hammer hits were located on the thicker wall sections just below the bottommost chamfer corner and the vertical hammer hits were located on top of the approximately 7 foot concrete retaining wall. The vertical axis in Figures A-1 and A-2 represents depth below casing top, with each waveform at 1 foot intervals starting at 25 feet at the bottom of each casing. The horizontal axis represents acoustic wave travel time in milliseconds (ms).

The generally faster compressional wave velocities of the sheet piles are represented by the shallow, usually more negatively sloped data in the figures at depths near the apparent pile tips. The more gentle, usually less negatively sloped data of the first breaks of the deeper traces represent the slower soil velocities below the pile tips. This is not the case in several of the data sets due to higher soil layer velocities at depth, likely associated with the presence of ground water which results in velocities of about 5,000 ft/second. Where the boreholes could be drilled less than ten feet away from the wall/pile (preferred), such saturated faster soil layers did not have as significant of an impact on data quality.

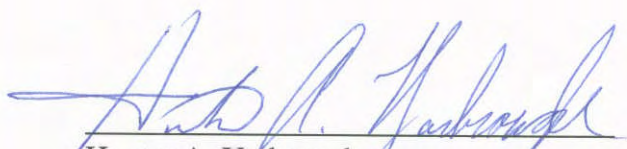
The PS measured pile tip depths for the eight locations indicate that there are piles present underneath the concrete retaining walls. Some of the results are of lower quality data due to a significant distance (17 to 22 ft) between the wall impact points to the boreholes as indicated in Table I. This is evidenced by the relatively weak signals from the piles compared to the signals from the impacted concrete walls on top of the piles, and from the relatively great depth at which the high-velocity pile signals finally start to arrive sooner than the low velocity signals being carried down the water-filled boreholes (tube waves). Accordingly, data quality was rated as high, medium and low (H, M and L) in Table I based on the distance between the wall-borehole and the signal quality.

4.0 CLOSURE

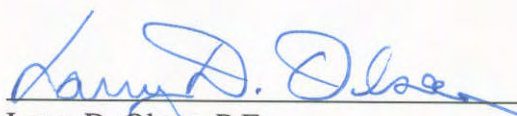
The field NDT investigation was performed in accordance with generally accepted testing procedures. If there are any questions, or further information is required, please do not hesitate to call. If any additional information is developed pertinent to this study, please contact our office.

Respectfully submitted,

OLSON ENGINEERING, INC.



Hunter A. Yarbrough
Geophysical Project Engineer



Larry D. Olson, P.E.
Principal Engineer

(1 copy faxed and 2 copies mailed)

**Table I: Summary of Sheet Pile Tip Depths and Elevations
From Parallel Seismic Testing of New Orleans Levees**

Levee Site	Sheet Pile Tip Depth From Top of Casing (ft) – (Data Quality)	Sheet Pile Tip Depth From Bottom Concrete Wall Chamfer (ft)	Sheet Pile Tip Elevation (ft above sea level)*	Distance Between Borehole and Levee Wall
17 th Street North End	14.4 - H	15.5	-10.6	5.5 ft
17 th Street South End	14.0 - H	15.0	-9.3	6.2 ft
London Avenue North Break North End	14.6 - L	16.1	-11.2	17.8 ft
London Avenue North Break South End	13.1 - M	14.9	-9.7	7 ft
London Avenue South Break	14.3 - M	15.3	-10.6	17.2 ft
IHNC Florida Street Break	14.8 - M	16.5	-10.3	21 ft
IHNC South Break North End	13.7 – H	16.6	-10.4	9.5 ft
IHNC South Break South End	14.4 – M	16.1	-11.8	21.1 ft

H – Indicates areas where the data quality is high and the borehole is positioned within 10 feet of the sheet pile.

M – Indicates areas where the data quality is medium and/or the borehole is positioned greater than 10 feet away from the sheet pile.

L – Indicates areas where the data quality is low and/or the bore hole is positioned greater than 10 feet away from the sheet pile.

* The elevations of the borehole casing tops were provided by the US Army Corps of Engineers and are NAVD 88 Format.

**APPENDIX A
PS DATA AND RESULTS**

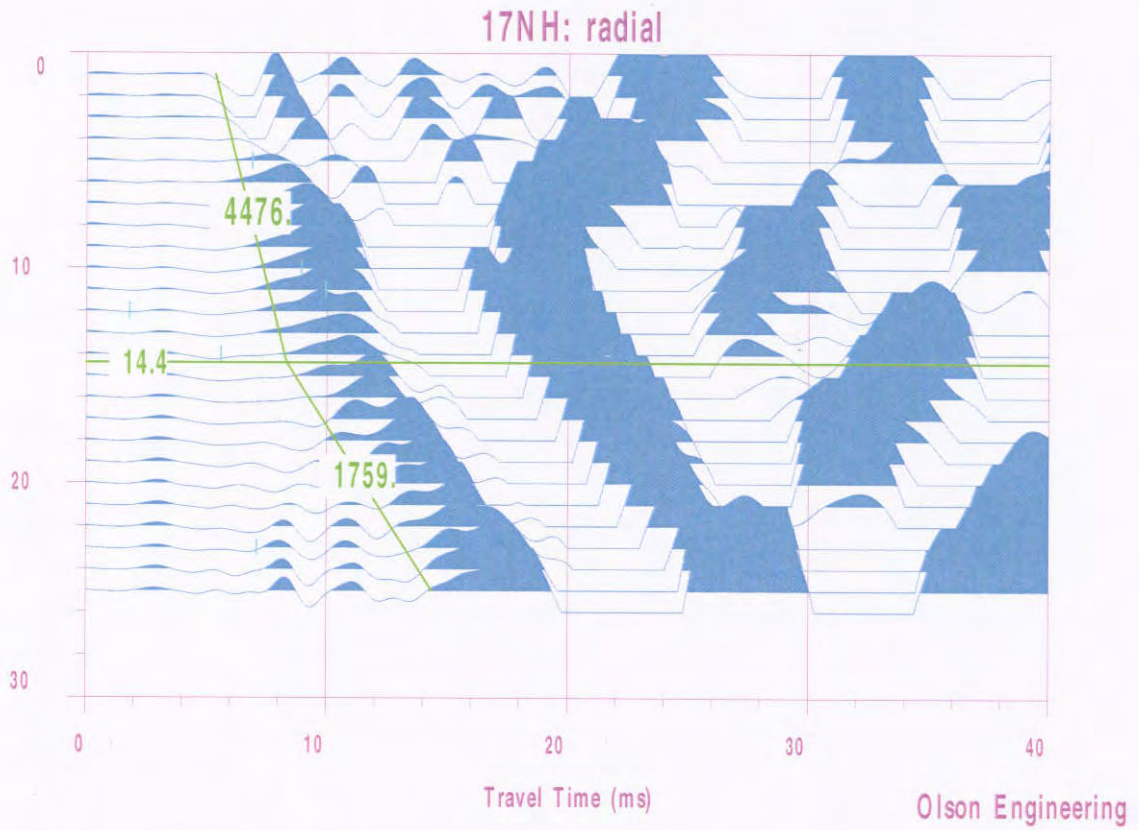


Figure A-1: 17th Street site, North borehole, depth is referenced to top of casing

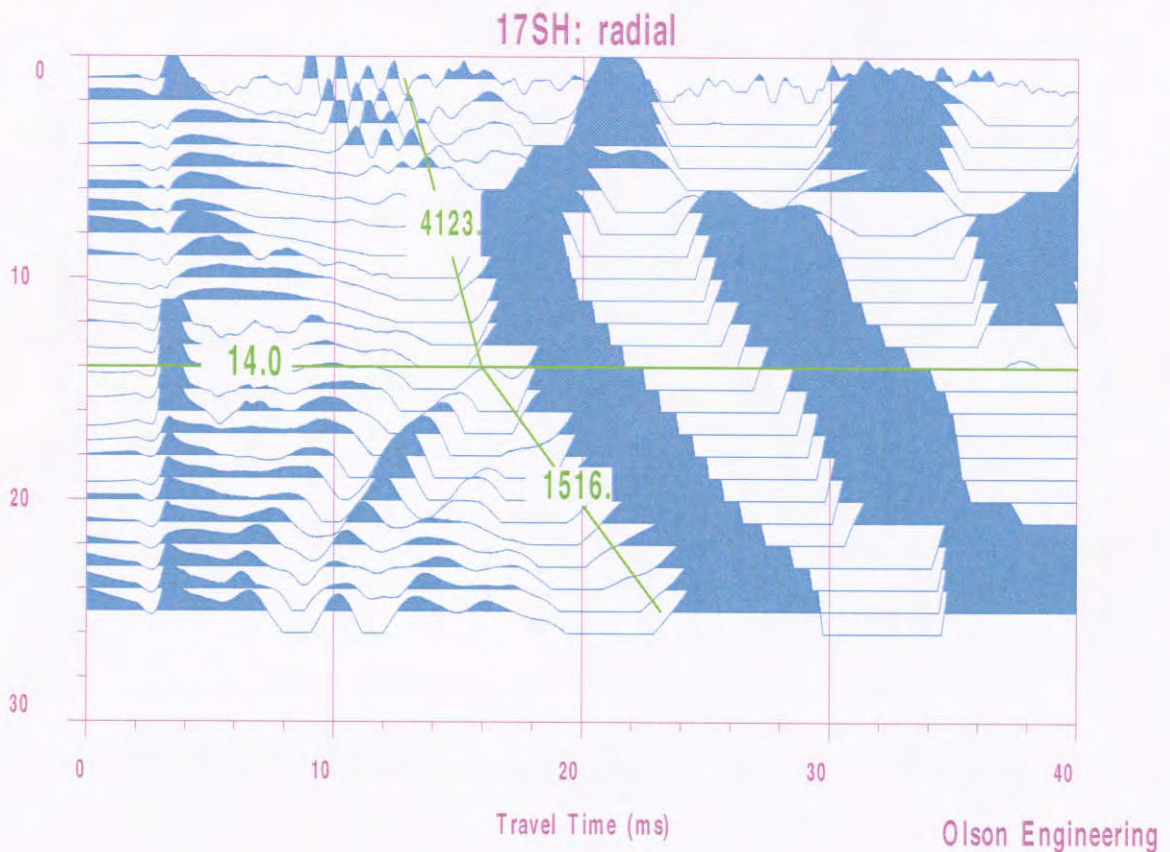


Figure A-2: 17th Street Site, South borehole, depth is referenced to top of casing

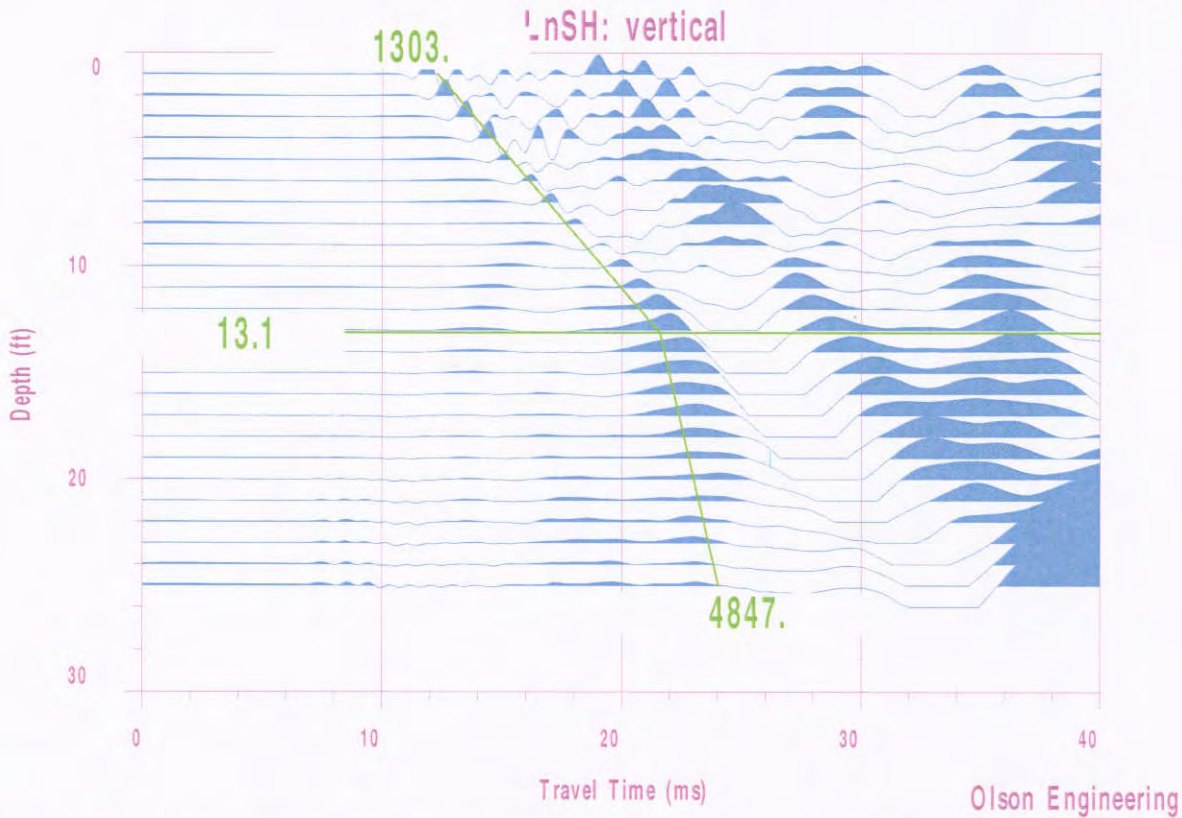


Figure A-3: London Avenue North site, North borehole, depth is referenced to top of casing

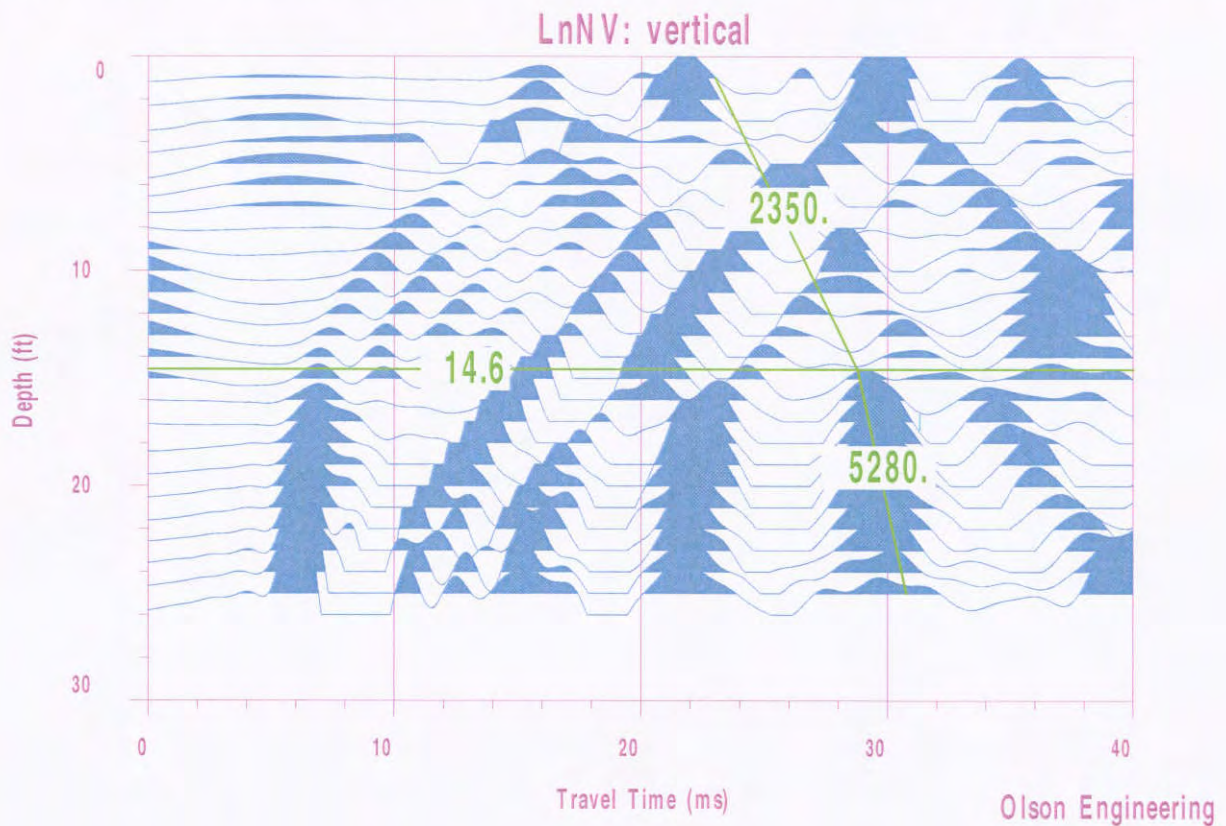


Figure A-4: London Avenue North site, South borehole, depth is referenced to top of casing K-237
 This is a preliminary report subject to revision; it does not contain final conclusions of the United States Army Corps of Engineers.

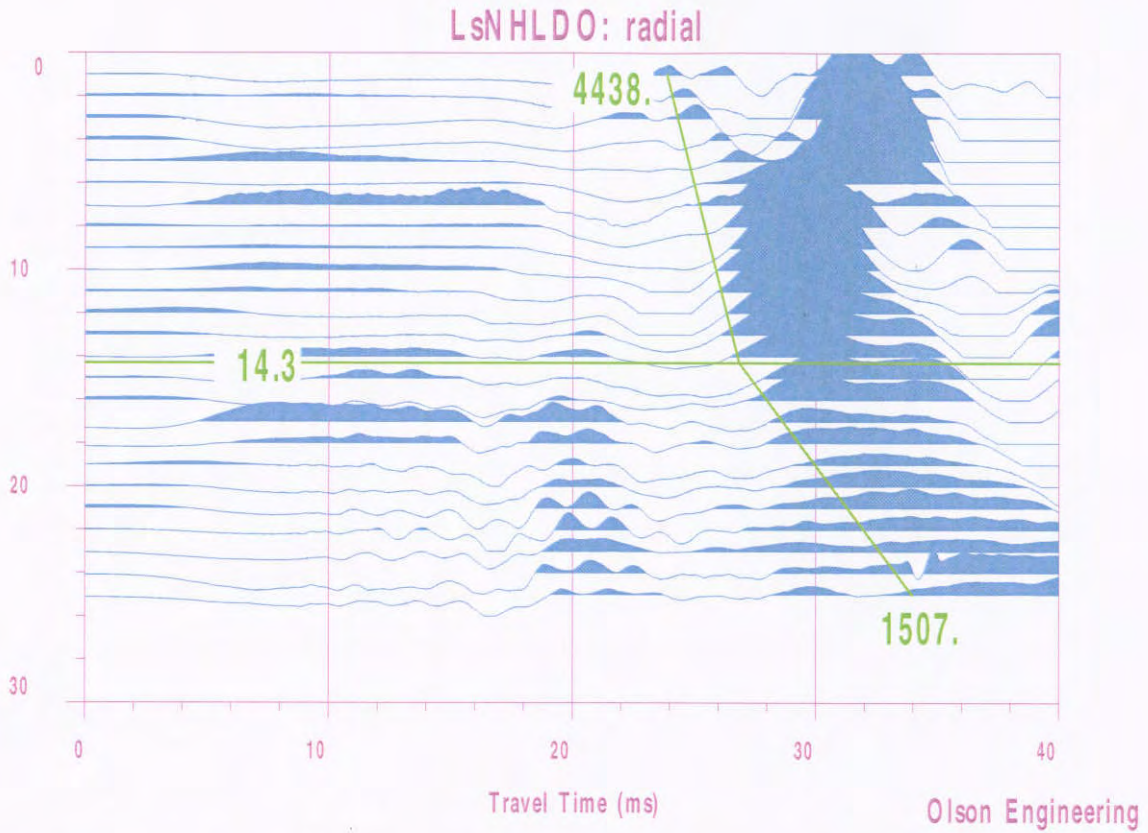


Figure A-5: London Avenue South site, North borehole, depth is referenced to top of casing

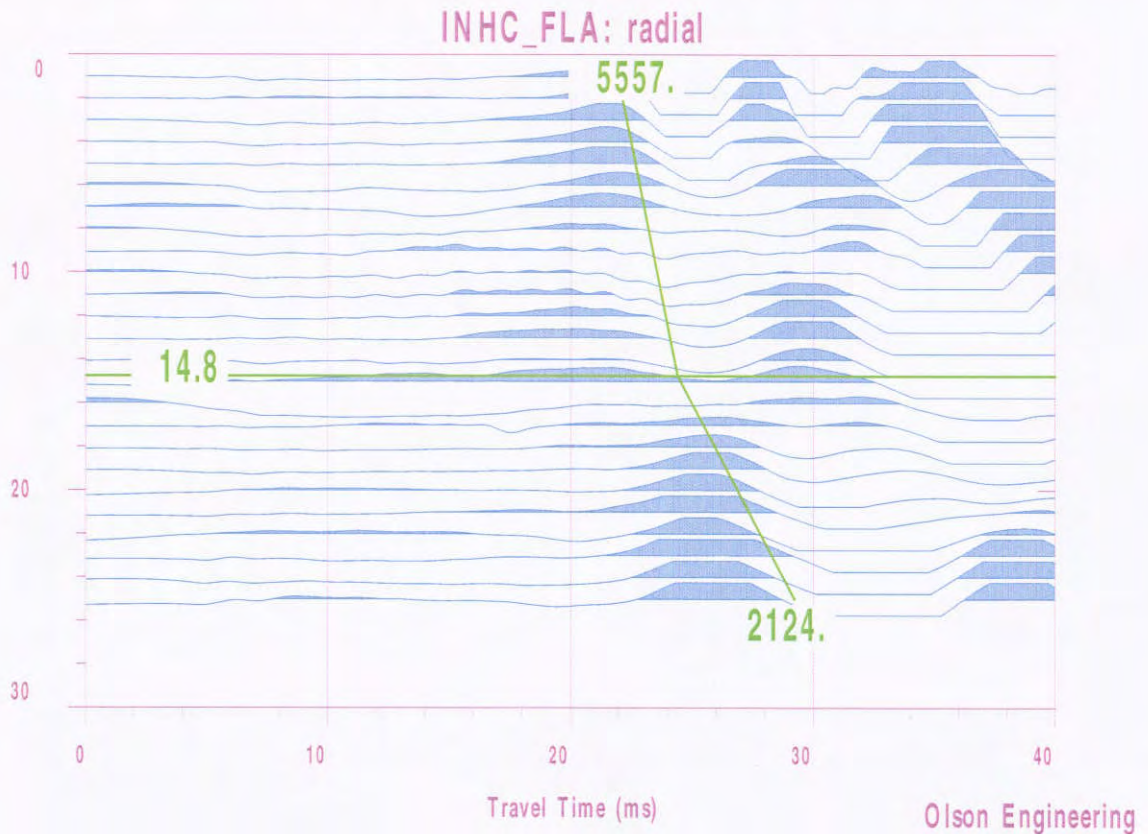


Figure A-6: IHNC Florida Street site, depth is referenced to top of casing

This is a preliminary report subject to revision; it does not contain final conclusions of the United States Army Corps of Engineers.

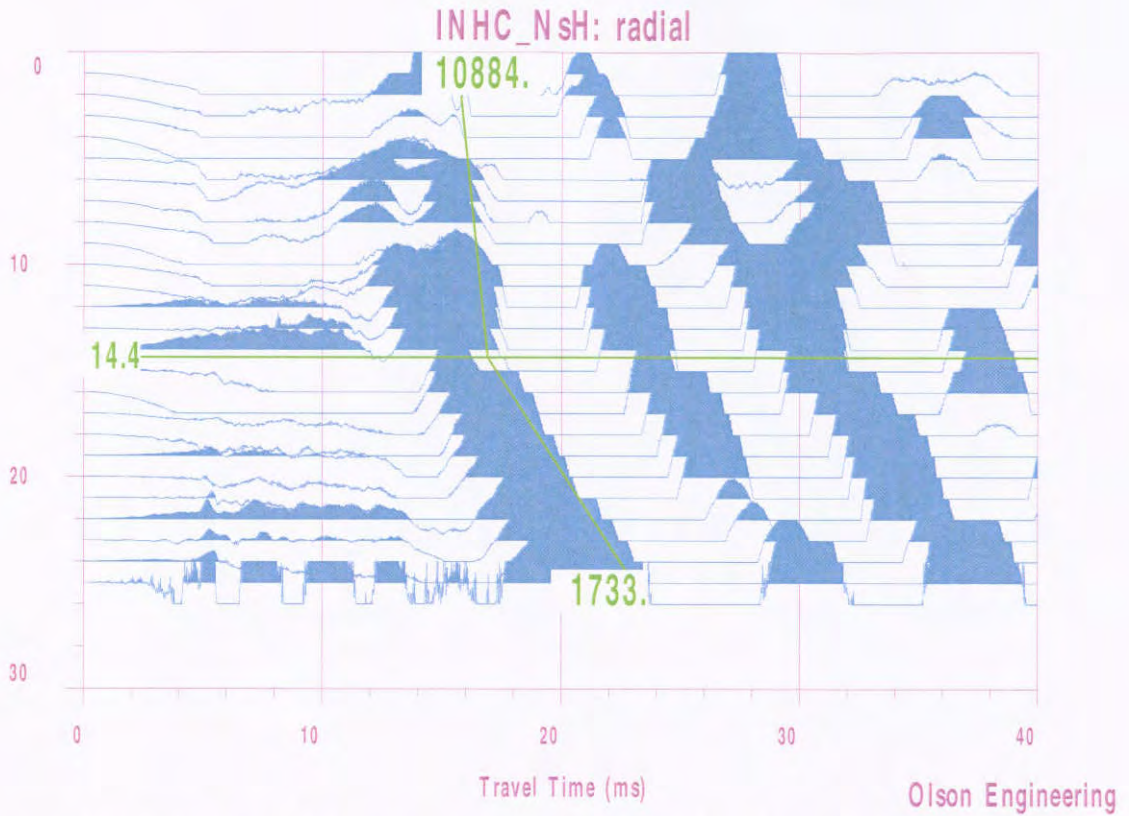


Figure A-7: IHNC South site, North borehole, depth is referenced to top of casing

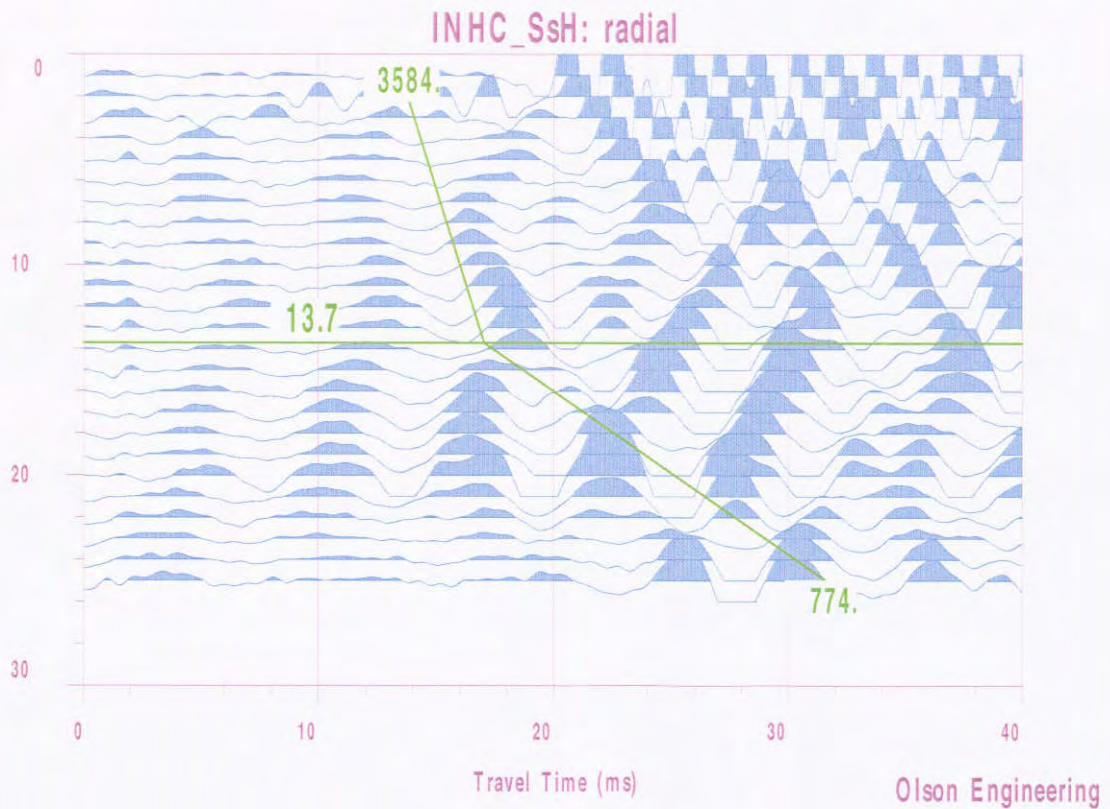


Figure A-8: IHNC South site, South borehole, depth is referenced to top of casing

This is a preliminary report subject to revision; it does not contain final conclusions of the United States Army Corps of Engineers.



**OLSON
ENGINEERING, Inc.**

**SPECIALIZING IN CONDITION EVALUATION OF THE
CIVIL STRUCTURE & INFRASTRUCTURE**



www.olsonengineering.com

January 9, 2006

U. S. Army Corp of Engineers
Engineering Research and Development Center
3909 Halls Ferry Rd.
Vicksburg, MS. 39180
Attn: Mr. Richard W. Haskins, ERDC-ITL-MS
Ofc: (601)634-2931
Fax: (601)634-2873
E-Mail: Richard.W.Haskins@erdc.usace.army.mil

Re: Addendum to Nondestructive Testing Investigation Report
Sheet Pile Lengths
New Orleans Levees
New Orleans, LA
Olson Engineering Job No. 1875

Dear Sirs:

This letter is being sent as an addendum to a report issued to the USACE by our office on December 5, 2005 (Olson Job No. 1875) which reported the results of an investigation conducted by our firm into the determination of the unknown length of steel sheet piles which were located beneath concrete walls and formed part of the levee structure at a number of locations in the New Orleans area. The levee sheet piles were tested with the Parallel Seismic (PS) method to determine their depths. The PS tests were conducted at the 17th Street, London Avenue, and the Inner Harbor Navigational Canal (IHNC) levees in 8 cased borehole locations at undamaged levee wall locations next to breaches.

The initially reported PS test results indicated the presence of piles under the concrete wall, and were interpreted by our firm to show that they extended to approximately 13-15 ft below the casing top for all of the sites tested. These sheet pile depths translated to elevations of approximately 10 feet below mean sea level (range of 9.3 to 11.8 feet below mean sea level).

It is our understanding that four sheet piles at the north end and 4 sheet piles at the south end of the 17th Street levee breach area have been pulled, and that our data interpretation of nearby PS results in north and south cased borings was shown to be incorrect. The actual embedded lengths were found to be approximately 17 feet below mean sea level (20-22 feet below the casing top elevation used in our investigation) with total sheet pile lengths of 23.5 ft.



This addendum to our initial report discusses our review of the initial analyses in light of the ground-truth findings for the pulled sheet pile. It also includes our recommendations for any future nondestructive test programs to determine the unknown sheet pile lengths.

Results of PS Data Review

Since our initial data interpretation is apparently incorrect for PS tests near the north and south ends of the 17th Street levee breach, we decided to re-analyze the data to try to determine why. We used the reported actual sheet pile tip elevations of about -17 ft below mean sea level and the 23.5 foot nominal excavated total pile lengths reported to us by Mr. Haskins of the USACE as a known quantity, and reviewed both the raw data as well as the processed data plots presented in our initial report for all sites tested. What we found was that the error was not due to problems with the actual test method, but rather due to a misinterpretation of the data on our part as discussed below.

17th Street Site PS Data Review

Figure 1 presents the data plot presented in our initial report for the north side location at the 17th Street site. As seen, our interpretation indicated a pile tip depth of about 14 feet, based on the typical "break" in the slope of the lower-frequency signal arrivals at that depth. For most foundations, this would indicate the tip depth quite well, and thus this break was selected as the indicated pile tip depth. However, as seen in both this plot in Fig. 1 and in Fig. 2, which is a re-processed plot of the same data set, there is also a clear set of faster signal arrivals apparent at an earlier time which start to appear at about 20-21 feet deep. These signals are apparently diffracting (reflecting up and transmitting down) from the tip of the sheet pile wall acting as a signal source. Data from the south side of the 17th Street site is presented in Fig. 3 (from the original report) and Fig. 4 (re-processed plot) and these figures also show the high-frequency energy emitted from the apparent sheet pile tip at 21 feet below top of casing. The 21 ft depth corresponds to a mean sea level elevation of about -17 ft for the sheet pile depths.

Our misinterpretation resulted at least partly from the fact that the sheet pile did not emit any significant energy from the side at shallower depths, but rather acted as a point source of energy from the tip. This type of response is unusual, but not unheard of as we have observed it in PS tests of steel H-piles below pilecaps with left-pointing "arrowheads" indicating the H-pile tips in front of the larger wave energy emitting from impacting footings/pilecaps/columns/walls of bridge substructure. The interpretation was also made more difficult in hindsight in that apparently due to the wall shape of the sheet piles, the normally expected arrowhead shape indicating a tip diffraction was bent back to near-vertical (vs. an H-pile with a full arrowhead shape). The interpretation was particularly complicated by there only being about 3 ft of data that could be obtained below the sheet pile tips due to the casing depth of 25 ft. Normally a casing depth of 10 to 15 ft below the expected pile tip depth is recommended for PS tests in order to obtain a clearer pile tip identification.

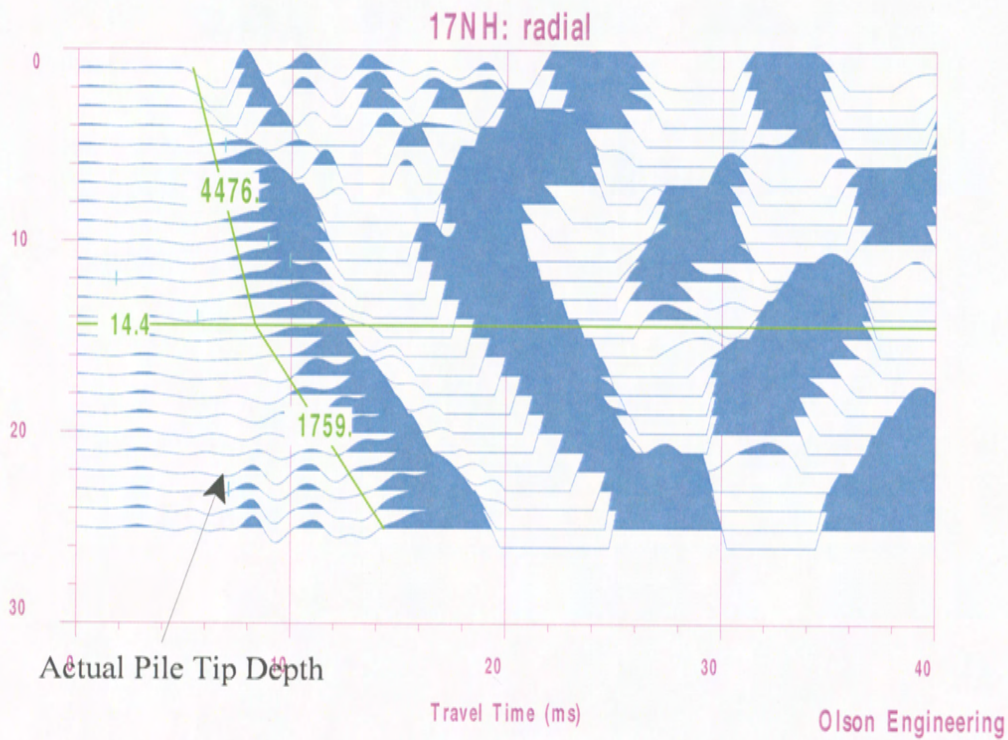


Figure 1 17th Street Levee North Site, Initial PS Data Interpretation

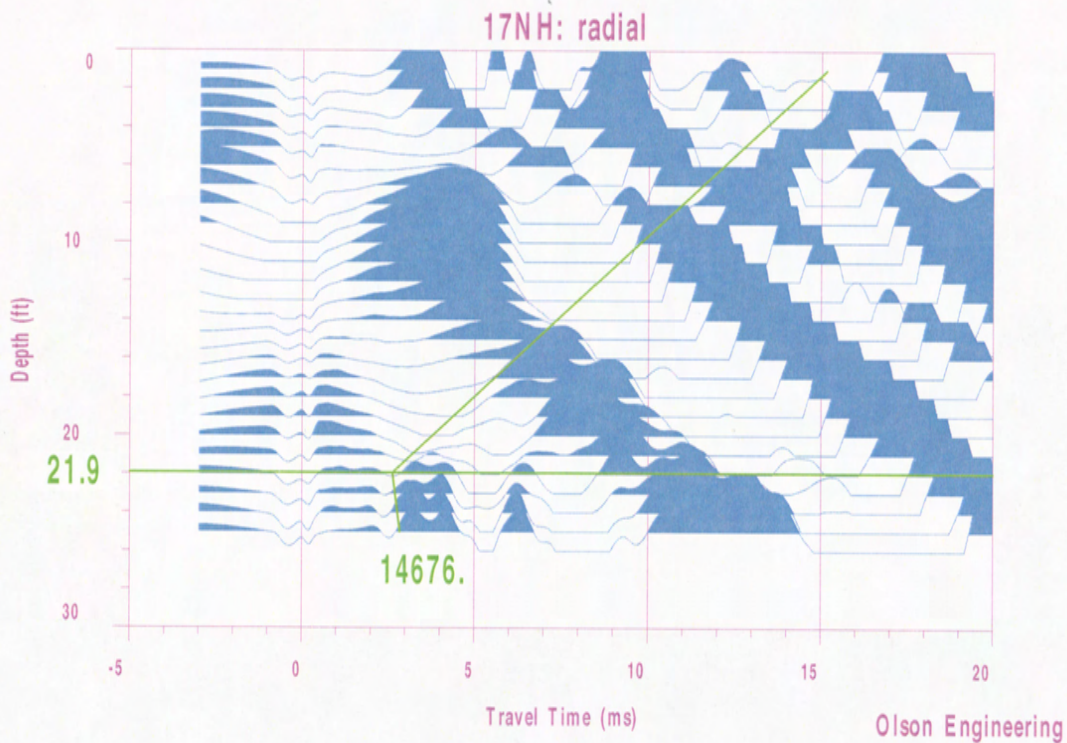


Figure 2 17th Street Levee North Site, Re-interpretation of PS Results

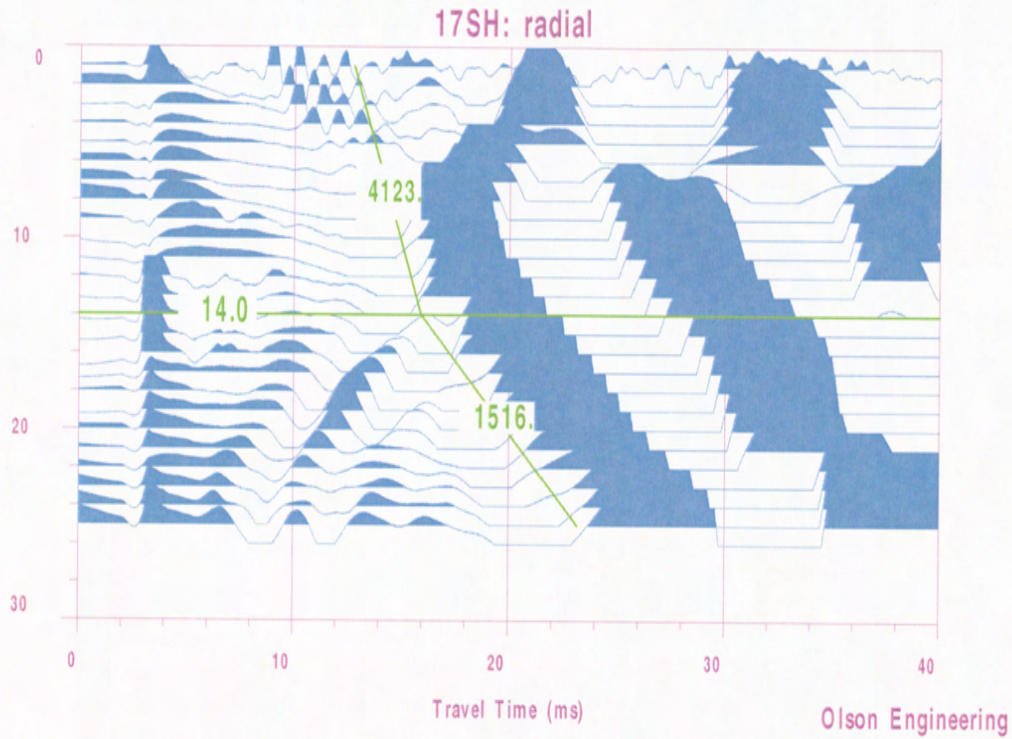


Figure 3 17th Street Levee South Site, Initial PS Data Interpretation

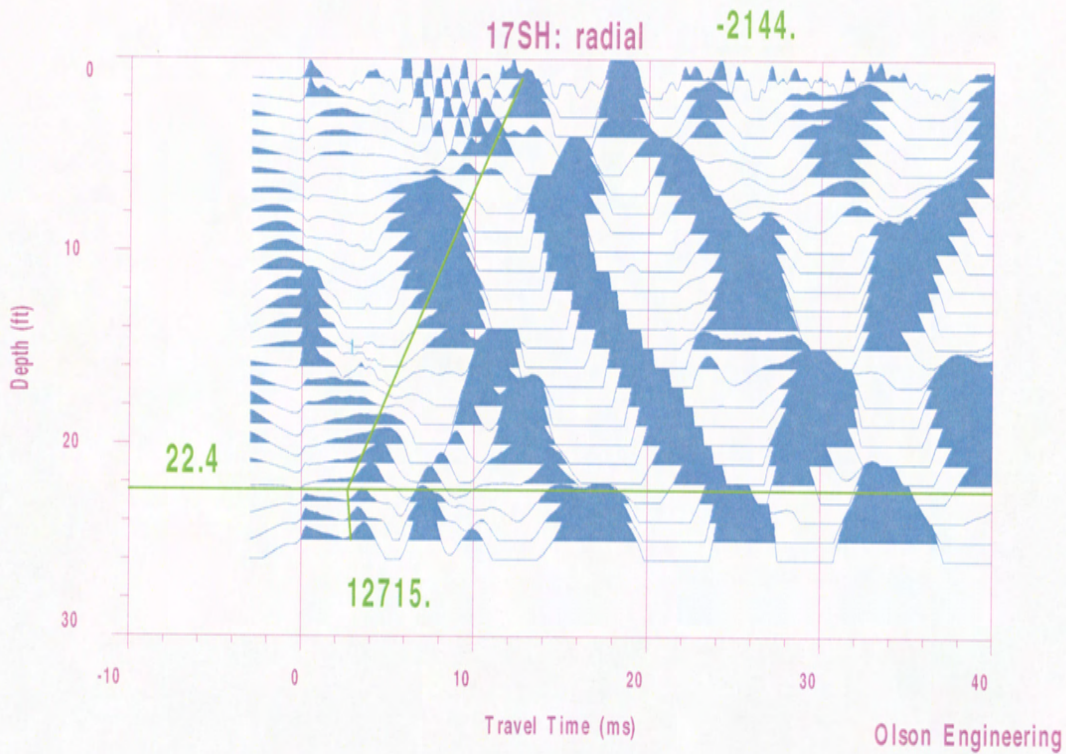


Figure 4 17th Street Levee South Site, Re-interpretation of PS Results

London Avenue North Break Data Review

The data collected from the London Ave. North site was reexamined to look for tip diffraction events similar to those seen for the 17th Street site data sets. Close examination of the data sets (Figs. A-3 and A-4 in our original report on this testing) show that there is a clear but vertical diffraction event for data at the South borehole, which was located at about 7 feet from the levee wall. The diffraction event in this figure, however, appears as a near-vertical line, with no clear "break" in the slope which would be indicative of a tip depth. It would appear likely that a break would have been seen if the casing went down the recommended 10-15 feet deeper than the expected pile tip depth, since there is a small possible indication of a break visible in the very bottom data trace for this location (at about 24 feet below casing top).

The data set from the North borehole shows a very weak set of possible diffraction events, with a similar shape as the south borehole. The diffraction events in the data from this borehole, however, are very weak. This is presumably due to the almost 18 ft horizontal separation between the borehole and the levee wall at this site. This large separation would attenuate the high-frequency diffraction energy, as well as decrease the resolution of the data that is seen.

London Avenue South Break Data Review

The data set from the South Break site borehole (Fig. A-5 in our original report) shows a very weak and distorted set of possible diffraction events, but with no clear slope change in the data indicative of a tip depth. Close examination of the data shows the first arrivals of the possible diffraction energy to be nearly vertical versus depth down to the last recorded record. Again, this is likely due to the limited depth of the casing in the borehole, which limited the test range to just a few feet deeper than the pile tip. In addition, this borehole was located 17.2 feet from the levee wall, which results in attenuated, distorted, low resolution diffraction energy from the pile tip.

IHNC Florida Street Break Data Review

The data set from the IHNC Florida Street Break site borehole (Fig. A-6 in our original report) shows no indication of tip diffraction energy. Note that this borehole was located about 21 feet from the levee wall, which is a distance greater than the expected pile tip depth. This large separation would be expected to greatly distort and attenuate any energy radiating from the pile tip. Thus, it is not unexpected that there is no visible tip diffraction energy in this data set.

IHNC South Break Data Review

The data set from the two tests conducted at the IHNC South Break site were presented in Figs. A-7 and A-8 in our original report. Figure A-7 is from the north borehole, which was located 9.5 feet from the levee wall. Figure A-8 is from the south borehole, which was located 21.1 feet from the levee wall. Examination of both data sets shows no clear indication of diffraction energy from the pile tip. This may be due to the distances between the boreholes and the wall, as well as possible separation between the sheet piles and the soil in the areas near the break.

Recommendations for Future Nondestructive Testing of Sheet Pile Lengths

The data presented in our original report does show the energy emitted by the sheet pile tips for most of the tests done in boreholes close to the levee walls, and can be made even clearer by re-processing the data from the 17th Street site to emphasize the higher frequency energy from the sheet piles as presented in Figs. 2 and 4 above. Based on this knowledge of how the PS test data behaves when testing these types of sheet piles in this environment, we have prepared these recommendations for any future NDT investigations of sheet pile lengths.

1. Drill Cased Borings Closer to Walls and Deeper. In our opinion, the PS method can be effectively used to measure unknown sheet pile depths with good confidence, as long as the boreholes are located and at least within 7 feet or less of the edge of the levee wall. Even closer borings will further improve the accuracy of the PS results. The borings should also be drilled and cased with PVC casings to at least 10 and preferably 15 ft below the expected pile tip depths.
2. Impact Sheet Pile Sides Directly. The PS data quality would be further enhanced by impacting the sheet piles at their exposed top just below the concrete wall directly. This will input significantly more energy in to the sheet pile and less into the concrete wall that was impacted in the initial investigation. This could be done with shallow excavations with a small backhoe in advance of the NDT. Alternatively, we have found that vertical impacts on the wall top or on the chamfer produce clearer diffraction energy traces than do horizontal impacts as discussed in our Report No. 2 for the re-test results.
3. Confirmation with complimentary NDT Methods. Magnetic metal detectors for boreholes may also be able to detect the sheet pile presence if borings are cased with plastic and able to be drilled close enough for this approach to be effective. The practicality of this can be further explored, if desired. We have already gathered some information on available equipment.

CLOSURE

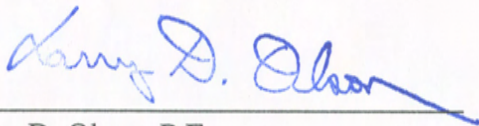
The field NDT investigation was performed in accordance with generally accepted testing procedures. If there are any questions, or further information is required, please do not hesitate to call. If any additional information is developed pertinent to this study, please contact our office.

Respectfully submitted,

OLSON ENGINEERING, INC.



Dennis A. Sack
Associate Engineer



Larry D. Olson, P.E.
Principal Engineer

(1 copy e-mailed and 2 copies mailed)

e-mail cc: Mr. Paul F. Mlakar (Paul.F.Mlakar@erdc.usace.army.mil)